THE JOURNAL
OF
CHEMICAL PHYSICS

VOLUME 18, NUMBER 5 MAY, 1950

Editorial

THE Journal of Chemical Physics is a research journal intended to provide a medium for the publication of research results in the field of chemical physics. The Journal is published by the American Institute of Physics. The only income of the Journal is from subscriptions, from the page charge levied on institutions supporting the research which is published in the Journal, provided they wish to honor the charge, and minor income from the sale of back numbers, etc. The amount of material which can be accepted in the Journal is, in the long run, limited by the subscription income.

Recent increases in the cost of printing and a very considerable increase in the number of manuscripts submitted to the editor's office have resulted in this limitation becoming very real. Individuals who are interested in the health and growth of the Journal will aid this by subscribing to the Journal or by bringing the opportunity to subscribe to the attention of others who may be interested in the Journal.

The Surface Tension of Liquid Metals and the Excess Binding Energy of Surface Atoms

R. A. ORIANI
Research Laboratory, General Electric Company, Schenectady, New York
(Received July 28, 1949)

By assuming that the cohesive energy of a liquid metal can be expressed as the sum of the pairwise interaction energies of nearest neighbors, and by obtaining the number of effective nearest neighbors for atoms on the surface and in the interior from simple considerations, it is shown that the pairwise bonding energy of surface atoms is greater than that for atoms in the interior of liquid metals. With mercury as the sole exception, this excess bonding energy is a nearly constant 2 percent of the cohesive energy when the liquids are taken as close-packed, but greater variation of this proportion is obtained when the liquids are taken as solid-like in structure.

INTRODUCTION

SKAPSKI[1] has pointed out that the total molar surface energy, σ_0, of a liquid metal is roughly a constant fraction of L_0 its molar heat of evaporation at absolute zero, and shows that this fraction should be $\frac{1}{4}$ for close-packed liquids if the pairwise binding energy of surface atoms is taken as equal to that for atoms in the interior of the liquid. He further points out that for sodium, tin, lead, and silver the proportionality is less than $\frac{1}{4}$, whereas for the non-metallic liquids, benzene and carbon tetrachloride, it is $\frac{1}{4}$, and for mercury it is about $\frac{1}{2}$. In Fig. 1 we present a much amplified and corrected version of Skapski's diagram for all liquid metals for which reliable data exist.

Because of uncertainty in the experimental data, it is hard to know what significance may be attached to the fact that the points for benzene and carbon tetrachloride lie nearer to the dashed line of slope $\frac{1}{4}$ than to the line of slope $\frac{1}{6}$ for all the metallic liquids, with the exception of mercury. Indeed, considering the method of computing σ_0 (see below) and L_0, one may well take the two carbon compounds as falling on the line of the liquid metals. Nevertheless, Skapski takes this small disparity as meaning that "the metallic character of a liquid contributes a negative term to its surface energy . . . ;" (from this point of view one would conclude that mercury is the most non-metallic of all the liquids shown in Fig. 1). He then proceeds to compute this negative contribution on the basis of the Thomas-Fermi assumption of perfectly free electrons, and on the

[1] A. S. Skapski, J. Chem. Phys. **16**, 389 (1948).

TABLE I.

Lattice	Plane of minimal $n\Delta Z$	Z_i (effective)	Z_s	ΔZ
Hexagonal close-packed	$(10\bar{1}0)$	12	8	4
Fcc	(111)	12	9	3
Bcc (sodium)	(100)	13.5	8.6	4.9

assumption that the ratio of electron densities in the surface layer and in the interior is determined by the ratio of the number of atoms in the configuration volume unit. Skapski obtains excellent agreement between the σ_0's for silver and sodium thus computed and those calculated from the experimental surface tensions and their temperature coefficients. However, this appears to be fortuitous since G. W. Sears* of this laboratory has applied Skapski's method to the calculations of the surface tensions of eight liquid metals with the result that no agreement with experimental values is at all evident, and in fact, four of the calculated surface tensions are negative values. Such a situation comes about because the calculation depends on the algebraic sum of the two large terms, of which one is the negative contribution from the metallic character of the liquid, and the other the positive value $\frac{1}{4}L_0$.

In the present paper no attempt is made to explain whatever difference may exist between metallic and nonmetallic liquids. Attention is directed solely to the metallic liquids, in which there can be no entropy contribution from internal degrees of freedom; by the use of empirical data and of simple assumptions, it is shown that the surface atoms are bound differently from the atoms in the interior of the liquid, and that this difference is correlatable with the energy of cohesion of the liquids.

METHOD OF ANALYSIS

The total molar surface energy, σ_0, of a liquid metal is defined as

$$\sigma_0=A[\sigma-T(d\sigma/dT)]=fN^{\frac{1}{3}}(M/\rho)^{\frac{2}{3}}[\sigma-T(d\sigma/dT)], \quad (1)$$

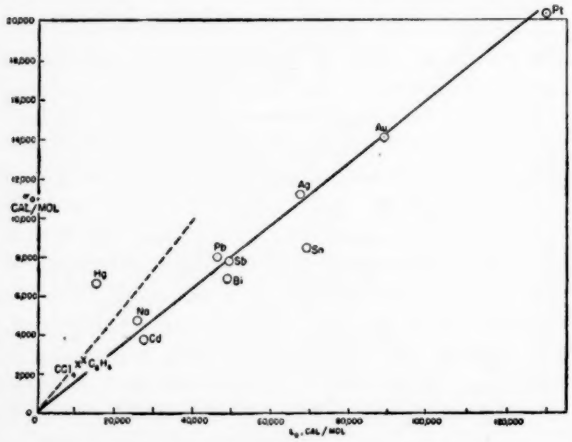

FIG. 1. Plot of σ_0 against heat of vaporization.

* G. W. Sears, private communication.

in which all the terms refer to experimentally determined quantities.

In Eq. (1) σ and ρ are, respectively, the surface tension and density of the liquid metal at the temperature T. A is the area occupied by one mole of surface atoms and is computed as shown from the Avogadro number, N, the atomic weight, M, and a factor, f, due to the packing of the liquid (f is 1.09 for close-packed structures and 1.12 for b.c.c.).[1] Since σ_0 is practically independent of temperature,[1] it is clear that σ_0 is the energy required to bring N atoms from the interior of the liquid to its surface at 0°K and to increase the area of the latter by A. But this energy is equal to the difference between the potential energy of the atoms in the bulk and that of the atoms on the surface, and hence may be termed ΔU. If we let u= the pairwise energy of interaction among the atoms in the bulk of the liquid, computed on a molar basis, and v= the pairwise interaction energy among the atoms of the surface layer, then assuming only nearest-neighbor interactions, and that the surface is only one atomic layer in thickness, one can write

$$\Delta U=\tfrac{1}{2}Z_iu-\tfrac{1}{2}Z_sv=\sigma_0, \quad (2)$$

where Z_i and Z_s are the coordination numbers in the interior and at the surface of the liquid, respectively. The interaction energy v, represents an average of the pair-wise interaction energies ϵ_{11} and ϵ_{12}, where the subscripts 1 and 2 refer to atoms in the first (i.e., surface) layer and in the second layer, respectively. It is felt that the small difference that probably exists between ϵ_{11} and ϵ_{12} should be neglected in view of the other approximations in this treatment. If we designate by ϕ the difference $(v-u)$, and express the heat of evaporation at 0°K, L_0, by $\frac{1}{2}Z_iu$, then Eq. (2) can be transformed to

$$\phi=2/Z_s[(\Delta Z/Z_i)L_0-\sigma_0], \quad (3)$$

in which σ_0 is evaluated by relation (1) from experimental quantities, and $\Delta Z=Z_i-Z_s$.

In order to carry out calculations of the excess binding energy, ϕ, it is necessary to evaluate Z_i and Z_s for the liquid metals. The work of Prins[2] and Stewart[3] justifies using the coordination number Z_i of the close-packed solid metals for those of the corresponding liquids. The case of the more complex lattices will be considered below. No ambiguity in Z_i arises for the *fcc* and hexagonal close-packed arrangements, for which it is 12. However, in the *bcc* system any one atom has eight nearest and six next-nearest neighbors; in order to give proper weight to the next-nearest neighbors in this and more complicated lattices, we have calculated the variation of internal energy of sodium with small changes in the interatomic spacing by means of the applicable Morse function.[4] As may be shown by actual computation, the

[2] J. A. Prins and H. Petersen, Physica **3**, 147 (1936).
[3] G. W. Stewart, Phys. Rev. **46**, 706 (1934).
[4] J. C. Slater, *Introduction to Chemical Physics* (McGraw-Hill Book Company, Inc. New York, 1939), Chapter 27.

TABLE II. Experimental data and calculated values of ϕ.

Metal	Structure	Z_i	Z_s	ΔZ	A, cm²/mol	T(°K)	σ, ergs/cm²	$d\sigma/dT$	σ_0, $\frac{\text{cal}}{\text{mole}}$	L_0, $\frac{\text{cal}}{\text{mole}}$	ϕ $\frac{\text{cal}}{\text{mole pairs}}$
Gold	*fcc*	12	9	3	4.69×10^8	1393	1128[a]	−0.10	14,200	88,900	1780
Platinum	*fcc*	12	9	3	4.2	2273	1820[b]	(−0.1)	20,600	130,000	2660
Silver	*fcc*	12	9	3	4.59	1323	916[a]	−0.13	11,300	67,460	1240
Lead	*fcc*	12	9	3	6.66	639	442[c,d]	−0.10	8070	46,000	765
Sodium	*fcc*	12	9	3	8.00	373	222[e,h]	−0.07	4750	25,800	380
Mercury	*fcc*	12	9	3	5.1	273	465[c]	−0.22	6700	15,000	−655
Cadmium	*fcc*	12	9	3	5.6	640	616[e]	(−0.1)	3810	27,500	680
Antimony	*fcc*	12	9	3	8.14	913	350[f]	−0.06	7860	49,000	970
Bismuth	*fcc*	12	9	3	6.95	593	375[e,d]	−0.07[j]	6940	48,600	1160
Tin	*fcc*	12	9	3	6.0	635	530[e,d,g]	−0.08[i]	8510	69,000	1920

[a] See reference 7.
[b] L. L. Bircumshaw, Phil. Mag. **3**, 1286 (1927).
[c] See reference 8.
[d] See reference 9.
[e] Krause, Sauerwald, and Michalke, Zeits. f. Anorg. Chem. **181**, 353 (1929).
[f] See reference 10.
[g] See reference 11.
[h] F. E. Poindexter, Phys. Rev. **27**, 820 (1926).
[i] Drath and Sauerwald, Zeits. f. anorg. allgem. Chemie **162**, 301 (1927).

variation can be approximated by $(r_1/r_2)^m$, where r_1 is the distance between nearest neighbors, r_2 that between next-nearest neighbors, and $m=\frac{1}{2}$. This, then, is the weighting factor by which the number of next-nearest ligands is to be multiplied to convert it to the effective number of nearest neighbors. The same exponent has been used for the other metals as for sodium, being appropriate within the order of approximation contemplated in this treatment. Following Pauling,[5] we shall not consider as ligands, from which to compute effective nearest-neighbors, atoms removed from the sum of the single-bond radii by a distance greater than about 0.8A.

In order to obtain Z_s, it is not sufficient merely to take the coordination number of an atom in the most densely populated plane. The plane that the lattice presents to the surface is that one which makes possible the least increase in internal energy for an atom going from the interior of the liquid to the surface. This means the smallest value of the product $n\Delta Z$, where n = number of surface atoms per unit area, and $\Delta Z = Z_i - Z_s$, since the smaller the decrement in coordination number, the smaller the change in pair-wise energy of interaction, but the larger the number of atoms per unit area. This product has been evaluated for the various planes of the hexagonal close-packed, face-centered, and body-centered cubic lattices, (second-nearest neighbors included in the *bcc* case), and the planes having minimal $n\Delta Z$ are, in the same order, $(10\bar{1}0)$, (111), and (100). The values of Z_s and ΔZ corresponding to these planes are listed in Table I. The situation is much less well defined for the more irregular lattices. The Z_s corresponding to the plane of minimal $n\Delta Z$ for the distorted cubic closed-packed lattices was taken the same as for the hexagonal close-packed, though Z_i, and hence ΔZ, was adjusted for second-neighbor interactions. The case of white tin, with its tetragonal lattice, was worked out as a special case. The lattice structures and parameters were taken from Wyckoff[6] and from Pauling.[5]

Because of the uncertainty that exists with respect to the packing in liquid metals whose solid phases do not exhibit close packing, the quantity, ϕ, has been calculated in two ways. Table II presents the data, sources of the data, and the results when the assumption is made

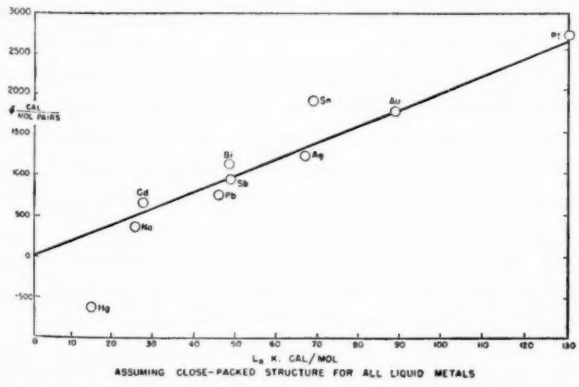

FIG. 2. Plot of ϕ against the heat of vaporization at 0°K.

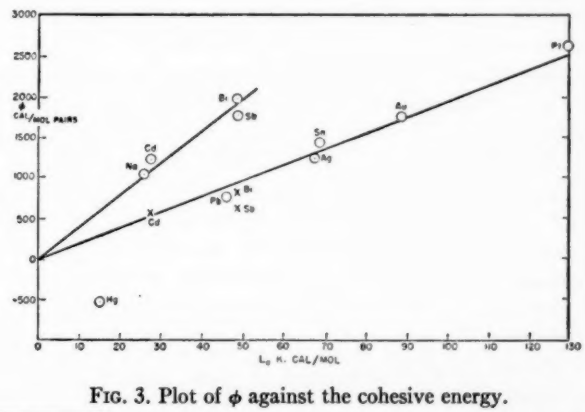

FIG. 3. Plot of ϕ against the cohesive energy.

[5] L. Pauling, J. Am. Chem. Soc. **69**, 542 (1947).

[6] R. W. G. Wyckoff, *Crystal Structures* (Interscience Publishers, Inc., New York, 1948.)

TABLE III. Values of ϕ computed by assuming solid-like structure for the liquid metals.

Metal	Structure	Z_i	Z_s	ΔZ	ϕ cal./mole pairs
Sodium	*bcc*	13.5	8.6	4.9	1070
Mercury	Rhombohedral	11.5	8	3.5	−535
Cadmium	Rhombohedral	11.7	8	3.7	1220
Cadmium	Rhombohedral	11.7	9*	2.7	565
Antimony	Rhombohedral	11.5	8	3.5	1760
Antimony	Rhombohedral	11.5	9*	2.5	615
Bismuth	Rhombohedral	11.5	8	3.5	1965
Bismuth	Rhombohedral	11.5	9*	2.5	810
Tin	Tetragonal	5.9	4.9	1	1300

* Computed on the basis of next-lowest $n\Delta Z$.

that all the metallic liquids are face-centered cubic, irrespective of the structure of the solid state. The heat of vaporization at 0°K is approximated by using the heat of sublimation. Figures in parentheses are estimated values for lack of experimental data, and the source of the data is indicated. Data for gallium[7] were not used, because there is some evidence that the liquid consists partly of diatomic molecules, and also the $d\sigma/dT$ was not measured; molecular complexity similarly ruled out data for selenium.[8] The data for copper[9] give a large positive value for the temperature coefficient of surface tension that is almost certainly due to experimental error, so that the value of σ is not considered reliable. The data for potassium,[10] zinc[11] and aluminum[9] are very incomplete and of indeterminate reliability. Figure 2 is a plot of ϕ *vs.* the heat of vaporization at 0°K for the liquid metals considered as close-packed.

The second way of computing ϕ is to consider that the liquid retains a blurred copy of the solid structure, even in the case of the more complex lattice. Hence, it is necessary to take into account next-nearest neighbors as effective nearest neighbors, as described above. Table III presents the results for the metals whose solid phases are not *fcc*, and Fig. 3 is the corresponding plot of ϕ against the cohesive energy. There is some doubt as to which is the proper Z_s to use for the irregular lattices of cadmium, antimony, and bismuth, so that other planes of very similar $n\Delta Z$, and thus of only slightly larger energy, might be considered. These atoms have six nearest and six next-nearest neighbors in the lattice, and so may be considered as having modified hexagonal packing; since the hexagonal close-packed arrangement has a plane having $Z_s=9$, for which the value of $n\Delta Z$ is near that for the plane listed in Table I for which $Z_s=8$, the quantity ϕ for these atoms was calculated using both values of Z_s. In all cases, the circles in Fig. 3 represent values computed on the basis of minimal $n\Delta Z$ for the idealized lattices, giving proper weight to the second-nearest neighbors. The crosses, for cadmium, antimony and bismuth represent values computed on the basis of next-lowest $n\Delta Z$ for the prototypic lattice. These latter values fall on the same curve as those for the face-centered metals.

DISCUSSION

The total molar surface energy is roughly one-sixth of the heat of evaporation of a metal; this means that the energy required to put an atom into a liquid-vapor interface is about $\frac{1}{6}$ of that needed to place that atom in the vapor phase. The present calculations show that the pairwise bonding energy of atoms on the surface of a liquid metal is, with the exception of mercury, greater than that for atoms in the interior of the liquid.* On the average, this disparity is 13 percent of the pairwise bonding energy of the interior atoms. Furthermore, independently of the type of packing assumed in the liquid, the excess binding energy is approximately a constant fraction of the cohesive energy of the liquid, about 2 percent. The correlation between the excess binding energy, ϕ, and the cohesive energy is simpler when all the liquid metals are taken as close-packed. When a solid-like structure is adopted for the liquids, there seems to be a separation into two families, the *fcc*, and the complex lattices, only if the lattice plane for minimal $n\Delta Z$ is used. If the plane having the next-lowest $n\Delta Z$ is used, then a single curve is obtained, as shown in Fig. 3; this is of interest since a small difference in $n\Delta Z$ means only a small and negligible difference in energy, and this implies little or no preference between the two planes. Sodium can be made to fall on this same curve if, as was done for cadmium, antimony, and bismuth, one uses the Z_s corresponding to the next-to-lowest value of $n\Delta Z$. The case of mercury is an irreducible anomaly; it is difficult to understand the reason for the negative value of ϕ, though one might point out that it may be related to the anomalously large surface energy that mercury displays relative to its small cohesive energy. The result that the surface atoms have a greater pairwise bonding energy than that of the bulk atoms is consistent with the usual view of surface tension of liquids. It may be remarked that, because of the nature of the treatment, nothing can be deduced from this result about the geometric relations on the surface; that is, whether this excess energy can be correlated with a smaller or larger average separation of the atoms on the surface. Whether or not the correlation here presented is of real significance and may be extended to consider the variation of the $\phi(L_0)$ relation with structure type, depends on the results obtained with new and more precise surface tension data on other metals, coupled with better calculation of the effect of second-nearest neighbors.

[7] Richards and Boyer, J. Am. Chem. Soc. **43**, 274 (1921).
[8] Astakhov, Penin, and Dobkina, J. Phys. Chem. U.S.S.R. **20**, 403 (1946).
[9] Smith, J. Inst. Metals **12**, 168 (1914).
[10] Quincke, Ann. d. Physik **135**, 261.
[11] T. R. Hogness, J. Am. Chem. Soc. **43**, 1621 (1921).

* It is interesting that this is the conclusion reached by Udin, Shaler, and Wulff [J. Metals Tech. **1**, 18 (1949)] from the results of their work on the surface tension and viscosity of solid copper, as well as by Benedicks [Pittsburgh International Conference on Surface Reactions, p. 196 (1948)].

Reactions of Recoil Atoms in Liquids*

J. M. Miller, J. W. Gryder, and R. W. Dodson
Chemistry Department, Columbia University, and Chemistry Department, Brookhaven National Laboratory

(Received June 29, 1949)

The reactions in liquid phase of the recoil atoms formed in the (n, γ) process are discussed in terms of a model involving energy loss by elastic collisions, dissociation of solvent molecules by impact, and eventual reaction in a liquid cage. Expressions are derived which relate the fraction of the recoil atoms ultimately found in a given molecular species to the composition and properties of the liquid. Previously published data are interpreted in terms of this model.

INTRODUCTION

THE radiative capture of neutrons by nuclei produces energetic recoil atoms as a consequence of the substantial momentum of the emitted gamma-rays. The recoil energy (order of magnitude a few hundred ev) is generally sufficient to rupture chemical bonds; and the recoiling atom is hence believed to move as a free atom through the system, losing energy by impact with the molecules of the system. This effect is the basis of the Szilard-Chalmers method for concentrating and isolating the radioactive atoms produced by neutron capture. Complete separation is rarely attained because of subsequent reactions in which the recoil atom may resubstitute in a molecule of the parent type or may synthesize other molecules of a type not separated by the procedure employed. As a result, a certain fraction of the radioactive atoms formed is not separated by the usual extraction methods (e.g., aqueous phase extraction of irradiated organic halides). This fraction often has a value of about one-half, and has sometimes been termed the "retention."

The reactions of such recoil atoms have been discussed by Libby,[1] who has emphasized the role played by their high energy and has given reasons for believing that the predominant reaction which occurs is resubstitution in a molecule of the parent species. With the aid of certain simplifying assumptions he has derived expressions for the yield of radioactive parent species in a one component system and in systems in which the component of interest is present in very low concentration. With similar assumptions we have treated less restricted cases. Our treatment leads to prediction of the yields of various molecular species into which the recoil atoms are incorporated, for all concentrations. In some cases the results differ from those of Libby.

We make the following assumptions:

(1) Every (n, γ) process produces a free recoil atom. The kinetic energy of this atom is such that it cannot participate in stable chemical combination until it has lost energy. In any given system under discussion it will be considered that all recoil atoms are produced with the same initial kinetic energy E_0.

(2) Energy loss occurs predominantly by elastic collisions with the solvent atoms and essentially not at all by ionization. These collisions are "billiard ball" type. Indeed, until chemical combination occurs, the recoil atoms behave as if they were traveling through an assemblage of free atoms and colliding with one atom at a time.

(3) If sufficient energy is transferred in a given collision the struck molecule will be dissociated into free radicals. In case the recoil atom has a kinetic energy less than a critical amount ϵ, after this impact, it will be trapped in a liquid cage and react with a radical trapped with it; otherwise it will escape the cage and fail to combine in that collision. It is by such processes that the activity is incorporated into a non-separable form.

THEORY

Consider a system (e.g., an organic halide irradiated with a constant flux of neutrons) that is in a steady state in which a constant number of radioactive recoil atoms are being produced per unit time and a constant number are experiencing any specified reaction per unit time. The range of energy in which the recoil atoms can produce the reactions of interest extends from some upper limit (which may equal E_0 or be less than E_0, depending on the reaction considered) down to a minimum energy, ν, which the recoil atom must have in order to break the bond by collision. In the steady state the energy spectrum of the atoms undergoing collision per unit time has some distribution independent of time. We represent this by $N(E)$, where $N(E)dE$ is the number of atoms with energy between E and $E+dE$ making collisions per unit time.

It is a convenient property of billiard ball collisions that the probability distribution for energy after impact is constant between the appropriate extreme limits. Thus if we consider the elastic impact of a recoil atom of kinetic energy E with a stationary atom, the probability that the recoil atom has an energy below ν after collision is $(\nu-\gamma_i E)/(E-\gamma_i E)$ for $E \leqslant \nu/\gamma_i$, and is zero for greater E. Here γ_i is the minimum fraction of the energy which can be retained after impact (i.e., the fraction retained after head-on collision), and is equal to $(M-m)^2/(M+m)^2$, where M and m are the masses of the impact partners. For generality we call a collision with an atom of type i in molecular species j a collision of type ij, and denote the probability that a particular collision is of this type by p_{ij}.

With the above assumptions, a recoil atom is in-

* Part of the research covered in this paper was done at the Brookhaven National Laboratory under the auspices of the AEC.

[1] W. F. Libby, J. Am. Chem. Soc. 69, 2523 (1947), ample references to the literature are given in this paper.

corporated into a stable compound whenever* it falls to an energy below ϵ from an energy above ν in a collision, it being assumed that ϵ is less than ν. To calculate the yield of a particular radioactive molecular species, we write an expression for the number of recoil atoms falling below ν per unit time, a corresponding expression for the number falling from an energy greater than ν to an energy below ϵ per unit time in collisions of the type of interest, and take their ratio. We shall denote this yield by R, with appropriate subscripts.

The total number of recoil atoms falling below ν per unit time is given by the expression

$$\sum_{ij}\int_{\nu}^{\nu/\gamma_i} p_{ij}N(E)\frac{(\nu-\gamma_i E)}{(E-\gamma_i E)}dE, \tag{1}$$

where the double sum is taken over all different types of atoms in all different molecular species. In the steady state this is, of course, also equal to Q, the number of active atoms being formed per unit time. The upper limit of the integral is written as ν/γ_i, since from greater energies it is impossible to reach the region below ν in a single collision of type ij. In cases where $\gamma_i E_0<\nu$, the upper limit may be replaced by E_0 since $N(E)$ is zero above E_0. By the same reasoning the number of active atoms falling below ϵ per unit time as a result of collisions with like atoms ($\gamma_i=0$) in a particular molecular species is

$$\int_{\nu}^{E_0} pN(E)\frac{\epsilon}{E}dE, \tag{2}$$

where p is the probability of a collision of this variety. The yield of the reaction of interest, i.e., the ratio of the number of radioactive atoms which are incorporated into the given molecular species to the total number of radioactive atoms is then given by

$$R=\frac{\displaystyle\int_{\nu}^{E_0} pN(E)\epsilon/EdE}{\displaystyle\sum_{ij}\int_{\nu}^{\nu/\gamma_i} p_{ij}N(E)[(\nu-\gamma_i E)/(E-\gamma_i E)]dE}. \tag{3}$$

The properties of this expression are illustrated in the following special cases.

Case I

Pure compound in which only collisions with like atoms need be considered, as for example CCl_4 when collisions with carbon atoms are neglected. In this case the denominator of (3) becomes

$$\int_{\nu}^{E_0} N(E)\frac{\nu}{E}dE$$

and we obtain in agreement with Libby[1]

$$R=\epsilon/\nu. \tag{4}$$

Case II

Like Case I, but with compound of interest diluted with isotopic atoms in a different state of chemical combination, as for example CCl_4 diluted with $SiCl_4$ when collisions with carbon and silicon are neglected. In this case the denominator of (3) becomes

$$\int_{\nu}^{E_0} pN(E)\frac{\nu}{E}dE+\int_{\nu}^{E_0}(1-p)N(E)\nu/EdE$$

and the fraction found in the compound of interest is

$$R=p\epsilon/\nu. \tag{5}$$

In the example considered, R is the yield of carbon tetrachloride molecules combining radioactive chlorine, and p is the probability that the impact partner in any given collision is a chlorine atom in a CCl_4 molecule. It should be noted that p will vary with the composition of the system and that ϵ may also be a function of composition.

Case III

Effectively a two component system in which active recoil atoms can collide only with their isotopes or with other atoms for which $\gamma E_0<\nu$ i.e., a diluent of mass comparable to that of the recoil atom so that this atom can reach the energy range below ν in the first collision. Here, and subsequently, γ refers to collisions with diluent. An example of this case would be carbon tetrachloride diluted with carbon disulfide, if only collisions between active chlorine atoms and sulfur atoms or other chlorine atoms are considered. For this case there results

$$R=\frac{\displaystyle\int_{\nu}^{E_0} pN(E)\frac{\epsilon}{E}dE}{\displaystyle\int_{\nu}^{E_0} pN(E)\frac{\nu}{E}dE+\int_{\nu}^{E_0}(1-p)N(E)\frac{(\nu-\gamma E)}{(E-\gamma E)}dE} \tag{6}$$

which reduces to

$$\frac{1}{R}=\frac{\nu}{\epsilon}+\frac{(1-p)}{(1-\gamma)}\frac{\nu}{p\epsilon}-\frac{(1-p)\gamma}{(1-\gamma)p\epsilon(\bar{1}/E)}, \tag{7}$$

where

$$\frac{\bar{1}}{E}\equiv\frac{\displaystyle\int_{\nu}^{E_0}[N(E)/E]dE}{\displaystyle\int_{\nu}^{E_0}N(E)dE}$$

is an average value of $1/E$ in the energy range ν to E_0.

* This treatment neglects the fact that some collisions can occur which bring the recoil energy below ϵ but in which insufficient energy is transferred to cause bond rupture.

Case IV

Like Case III except that $\gamma E_0 > \nu$ so that a single collision with a diluent atom cannot bring the recoil atom from E_0 to below ν in this collision, as for example carbon tetrachloride diluted with bromine when collisions with carbon are neglected. In this case the expression for the yield of the compound resulting from isotopic substitution will be identical with (6) except that the upper limit of the second integral in the denominator will be ν/γ and the integrals will not cancel. It should be noted that a system such as liquid C_2H_5Br falls more nearly into this case than into Case I.

The Distribution on Function $N(E)$

The last two cases indicate the desirability of obtaining an explicit expression for $N(E)$. We can do this by arguments analogous to those employed in neutron slowing down theory.[2] Since a steady state is under consideration, it is evident that the number of recoil atoms leaving an energy interval dE_1, which is given by $N(E_1)dE_1$, must equal the number entering the same interval. Hence, for any system, such as Case I or Case II, in which collisions occur only between impact partners of equal mass,

$$N(E_1)dE_1 = Q\delta(E_1 - E_0)dE_1 + \int_{E_1}^{E_0} N(E)\frac{dE_1}{E}dE. \quad (8)$$

The first term on the right, which represents the number of the newly formed atoms undergoing collision per unit time at energy E_0, employs the Dirac delta-function, which has the property of vanishing at all points except $E = E_0$ where it goes to infinity in such a manner that the integral of the function is unity. The second term gives the number which enter the interval dE_1 per unit time as a result of collisions above E_1. The solution of this integral equation is

$$N(E) = Q\delta(E - E_0) + Q/E. \quad (9)$$

For Case III consideration of the steady state gives

$$N(E_1)dE_1 = Q\delta(E_1 - E_0)dE_1 + \int_{E_1}^{E_0} pN(E)\frac{dE_1}{E}dE + \int_{E_1}^{E_0} (1-p)N(E)\frac{dE_1}{E - \gamma E}dE, \quad (10)$$

where the last two terms refer to collisions with like and unlike atoms respectively. The solution of Eq. (10) is

$$N(E) = Q\delta(E - E_0) + \frac{1-p\gamma}{1-\gamma}\frac{Q}{E_0}\left(\frac{E_0}{E}\right)^{(1-p\gamma)/(1-\gamma)}. \quad (11)$$

It is now possible to evaluate $\bar{1}/E$ for Case III. The result, after simplification, is

$$\frac{\bar{1}}{E} = \frac{\gamma(1-p)}{\nu(1-p\gamma) - \nu(1-\gamma)(\nu/E_0)^{(\gamma-p\gamma)/(1-\gamma)}}. \quad (12)$$

When this is used in Eq. (7), one obtains

$$R = p\frac{\epsilon}{\nu}\left(\frac{E_0}{\nu}\right)^{(\gamma-p\gamma)/(1-\gamma)}. \quad (13)$$

For Case IV the equation for $N(E)$ becomes

$$N(E_1)dE_1 = Q\delta(E_1 - E_0)dE_1 + \int_{E_1}^{E_0} pN(E)\frac{dE_1}{E}dE + \int_{E_1}^{E_1/\gamma} (1-p)N(E)\frac{dE_1}{E - \gamma E}dE. \quad (14)$$

In principle one could solve Eq. (14) in intervals (i.e., $E_0 - \gamma E_0$, $\gamma E_0 - \gamma^2 E_0$, $\cdots$, $\gamma^{n-1}E_0 - \gamma^n E_0$) making use of the solution in preceding intervals to obtain the solution in a given interval. A rigorous solution can also be obtained by the method outlined by Placzek[2] for the logarithmic energy distribution in the identical case. However, both of these procedures are very laborious, and for simplicity we shall use the approximate solution

$$N(E) = Q\delta(E - E_0) + \frac{Q}{[(1-p)(1-\gamma) + p]E} \quad (15)$$

which is applicable for $E \ll E_0$. Employing Eqs. (15) and (3) we obtain

$$R = \frac{p\epsilon/\nu}{1 + [(1-p)/(1-\gamma)]\gamma \ln\gamma} \quad (16)$$

when terms of the order of ν/E_0 are neglected.

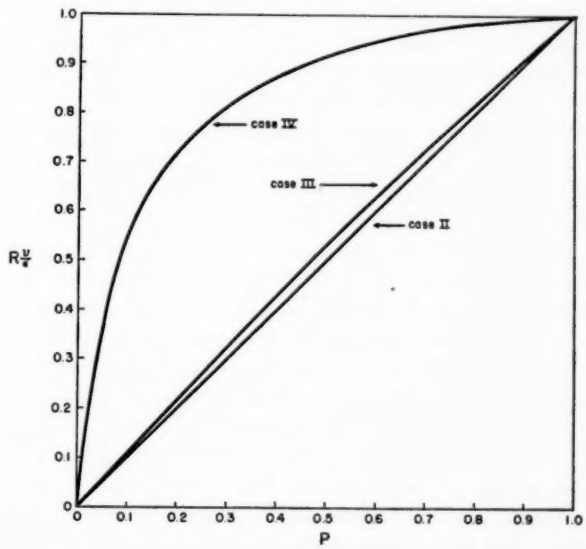

FIG. 1. The effect upon yield caused by diluting with equal mass atoms (Case II, $\gamma = 0$), nearly equal mass atoms (Case III, $\gamma = 0.03$), and significantly different mass atoms (Case IV, $\gamma = 0.9$).

[2] G. Placzek, Phys. Rev. **69**, 423 (1946).

DISCUSSION

It is of interest to compare the above results with the expression obtained by Libby[1] for the yield of the radioactive compound resulting from isotopic substitution at high dilution, namely

$$R=p\frac{\epsilon}{\nu}\left[\frac{1-\gamma}{1-\gamma(1-\ln\gamma)}\ln\frac{E_0}{\nu}\right], \tag{17}$$

where the term in brackets gives** the average number of collisions necessary to reduce the energy of the recoil atom from E_0 to ν. Expression (17) is to be compared with Eqs. (5), (13), and (16) as p becomes small relative to unity:

$$R=p\frac{\epsilon}{\nu}, \tag{5'}$$

$$R=p\frac{\epsilon}{\nu}\left(\frac{E_0}{\nu}\right)^{\gamma/(1-\gamma)}, \tag{13'}$$

$$R=p\frac{\epsilon}{\nu}\left[\frac{1-\gamma}{1-\gamma(1-\ln\gamma)}\right]. \tag{16'}$$

It is seen that each result gives R proportional to $p(\epsilon/\nu)$, but that the several expressions differ by a factor of the order of $\ln E_0/\nu$ in the slope with which they approach the origin.

In Fig. 1 the quantity $R\nu/\epsilon$ has been plotted against p in order to illustrate the nature of the general solutions given above. For Case III we have chosen as representative values $E_0/\nu=30$ and $\gamma=0.03$, and for Case IV γ has been taken to be 0.90, which is approximately the case for atomic collisions between chlorine and hydrogen. The form of the curves in Fig. 1 is to be expected from the physical nature of the problem since if $N(E)$ is constant with respect to p the chance of reaction will decrease directly with p; but if $N(E)$ increases on dilution, as it must be for all diluents whose atoms have a different mass from that of the radioactive recoil atom, the chance of reaction will decrease more slowly than p because of the increased number of collisions per unit energy interval per unit time. When the concentration of the species into which recoil atom is substituting is very low, one would expect the relative yield in two systems, such as CCl_4 in $SiCl_4$ and CCl_4 in cyclohexane, to be determined principally by the average number of collisions required to cool the hot atom. The ratio of the required number of these collisions when γ equals zero to the number required for any other value of γ is, from the expression included in Eq. (17) indeed equal to the ratio of Eq. (5') to Eq. (16').

It should be emphasized that the above considerations apply only to a system consisting of "unbound billiard ball atoms," and that the assumptions made in the calculations certainly are not valid for collisions taking place at energies slightly above those involved in chemical binding. At these energies phenomena become important which tend to make the theoretical considerations inapplicable. Elastic and inelastic interactions with the whole molecule will take place, and these will affect the energy distribution. Furthermore, the probability that both the hot atom and the displaced atom will have insufficient energy to escape the liquid cage will become large; and consequently the inactive atom may recombine with the radical, thereby reducing the substitution yield.* Other factors which would cause a divergence between the theoretical considerations and physical systems are the change of ϵ with composition of the solution and the fact that collisions with partially shielded atoms, such as the carbon atom in CCl_4, have been neglected in the above treatment.

Although realizable physical systems differ in these several aspects from the assumptions made in the foregoing treatment, it seems plausible that the physical mechanism discussed can play a significant role in the reactions of recoil atoms. This type of process is to be distinguished from chemical reactions of a more familiar nature in which the recoil atoms react, after substantial energy loss, with chemical compounds in a highly specific manner. The relative importance of the two kinds of mechanism will undoubtedly depend on the system considered.

The only published results of an investigation of the chemical reactions of recoil atoms with which foregoing analysis can be compared are those of Bohlman and Willard[3] in which the substitution of active bromine in

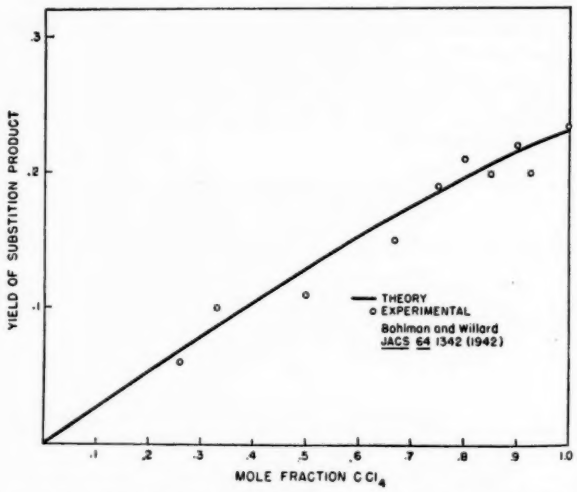

FIG. 2. A comparison of the calculated and experimental values of the yield of organic radiobromine substitution product(s) in carbon tetrachloride-bromine solutions.

** Note that the γ employed here is defined differently from that used in reference 1; the sum of the two is unity.

* When one considers Case I, taking into account both the probability that the bond is broken and that two atoms are trapped in the liquid cage, the result is $R=\frac{1}{2}\ln[1+2(\epsilon/\nu)]$ which reduces to $R=\epsilon/\nu$ for small values of ϵ/ν. Application of this refinement to the other cases does not change the form of the dependence of R on concentration.

[3] Bohlman and Willard, J. Am. Chem. Soc. 64, 1342 (1942).

carbon tetrachloride after neutron bombardment was studied. These investigators found significant quantities of active CCl_2Br_2 in addition to CCl_3Br; but in the following discussion we shall assume that the primary process in the formation of the dibrom compound is entirely analogous to the formation of the monobrom compound and that in both cases reaction results from a mechanism similar to that supposed in the general theory given above. The occasional formation of a dibrom derivative can be explained either by the assumption that the initial process leaves the CCl_3 radical in such an energy state that it sheds another chlorine becoming a CCl_2 radical which then reacts with the active bromine atom and a bromine molecule in the side of the cage to form CCl_2Br_2, or that the newly formed active monobrom compound has enough excitation energy to react with a bromine molecule in the cage wall to form the dibrom material. Our treatment of the system will not distinguish between the two products obtained experimentally.

If p is the probability that the impact partner in a collision of an active bromine atom is another bromine atom, then $N(E)$ is given by Eq. (15) with $\gamma=0.15$. The yield of CCl_3Br can be obtained by the same reasoning used in deriving Eq. (3) and is

$$R_{CCl_3Br}=\frac{(1-p)\int_{\nu}^{\epsilon/\gamma}N(E)\frac{\epsilon-\gamma E}{E-\gamma E}dE}{(1-p)\int_{\nu}^{\nu/\gamma}N(E)\frac{\nu-\gamma E}{E-\gamma E}dE+p\int_{\nu}^{E_0}N(E)\frac{\nu}{E}dE}. \quad (18)$$

When $N(E)$ is inserted in (18) and the indicated operations performed, one obtains

$$R=\frac{(1-p)}{0.85(0.67+0.33p)}\left[\frac{\epsilon}{\nu}-0.15-0.15\ln\frac{\epsilon}{0.15\nu}\right]. \quad (19)$$

In order to compare this expression with the experimental results, it is necessary to express p in terms of N, the mole fraction of carbon tetrachloride in the system. If S is the ratio of the impact cross section of a chlorine atom to that of a bromine atom, then

$$p=\frac{1-N}{1-N+2NS},$$

and (19) becomes

$$R=\frac{2SN}{0.85(1-N+1.34SN)}\times\left[\frac{\epsilon}{\nu}-0.15-0.15\ln\frac{\epsilon}{0.15\nu}\right]. \quad (20)$$

When N is equal to one, S does not appear in Eq. (20); and consequently ϵ/ν can be obtained from the extrapolated experimental value of 0.23 for the yield in pure carbon tetrachloride. The value thus obtained is 0.45.*** An approximate value of S can be calculated from the bond radii of 0.99A for chlorine and 1.11A for bromine.[4] The result is 0.90. Using the above values for S and ϵ/ν, one can calculate yield as a function of mole fraction of carbon tetrachloride from Eq. (20). A comparison of experimental and calculated results is given in Fig. 2.

It is gratifying that the relatively simple analysis presented here is in such close agreement with experiment. However, it is not impossible that the data can be explained on other bases and consequently experiments have been undertaken further to characterize reactions of this type. The results of these investigations will be published subsequently.

*** In this calculation it has been assumed that ϵ is independent of concentration. While a rigorous justification of this assumption is not evident, it is interesting to note that the molecular mass and impact cross section, both of which might be expected to be pertinent to the value of ϵ, are closely similar for carbon tetrachloride and bromine. Likewise, the intermolecular forces, as reflected in the heat of vaporization, boiling point, and viscosity are closely similar for the two components. It seems therefore not unlikely that ϵ is essentially composition independent in this system.

[4] Bond radii are from Pauling, *Nature of the Chemical Bond* (Cornell University Press, Ithaca, 1940), p. 179. It is not obvious that the value of S obtained in this manner applies to the case at hand because of the very great energies with which the collisions occur.

Isotope Effect in the Vibrational Frequency Spectra and Specific Heats of Sodium Hydride and Deuteride*,†

EDWARD V. SAYRE‡ AND JACOB J. BEAVER
Department of Chemistry, Columbia University, New York, New York

(Received July 1, 1949)

The prediction by the Born and von Karman lattice dynamics theory of the effect of isotopic substitution on crystal vibration frequencies has been determined by calculation of frequency spectra of sodium hydride and sodium deuteride. In each case 6690 of the lattice frequencies have been calculated with the aid of I.B.M. punched card computers. They have been chosen and weighted in such a way that the whole frequency spectra of the crystals are uniformly sampled. Both spectra exhibit acoustical branches which are nearly identical and optical branches, the frequencies of which are essentially in the ratio of the square root of two. In both cases, the optical branches extend somewhat uniformly over very broad ranges of frequencies, in marked contrast to the estimation of optical frequencies as a few monochromatic lines.

The molar heat capacities of these two compounds have been determined experimentally between 60 and 90°K with an adiabatic calorimeter and compared to corresponding curves calculated from the frequency spectra. The theoretical and experimental sets of curves possess the same general form. In both cases the deuteride values are higher than the hydride values, with the curves of the two substances diverging with increasing temperature. The theoretical curves, however, are nearly uniformly displaced from the experimental curves by about ten percent, an effect which could have arisen from an error in the repulsive force constants.

DURING approximately the last decade, there has been increasing interest in the application of the lattice dynamic theory of Born and von Karman[1] to the more exact calculation of vibrational spectra and specific heats. Sparking this interest were the extensive series of calculations by Blackman[2] determining vibrational spectra for linear ionic lattices and regular two-dimensional and cubic lattices. These showed marked deviation from the simple Debye distribution. Blackman assumed in these calculations only quasi-elastic forces operative between nearest and next nearest neighboring atoms. Later Fine[3] calculated, in a similar manner, the vibrational spectrum for a body centered cubic lattice using force constants in agreement with the elastic constants of tungsten. He was able to calculate the specific heat curve of tungsten from this spectrum with fair accuracy. Montroll, and Montroll and Peaslee[4] have applied special matrix methods to the calculation of frequency distributions in simple two-dimensional and cubic lattices and body-centered cubic lattices.

In the case of ionic crystals, however, close approximations to the true force constants can be made assuming they arise from the central force fields, Coulombic, van der Waals and repulsive, from which crystal energies have been calculated. Difficulty arose, however, from the slow convergence in summing long-range Coulombic forces over the lattice. Born and Thompson[5] converted these sums into a more convergent form by adapting the procedure by which Ewald[6] obtained lattice sums of Coulombic potentials. Lyddane and Herzfeld[7] proposed instead an extension of Madelung's[8] method and carried their procedure through to the calculation of several of the vibrational frequencies of sodium chloride. Kellermann,[9] using the summation procedure stemming from Ewald, calculated a detailed vibration spectrum for sodium chloride and from it calculated a specific heat curve that was in excellent agreement with experimental values. Distributions of vibrational frequencies for the simpler case of potassium chloride (atomic masses assumed equal) were calculated by Foldy[10] and by Iona.[11] Here again specific heat calculations were in good agreement with experiment.

Recently Raman[12] has objected to the entire lattice dynamic theory, proposing instead that the frequency spectra of even simple crystals are composed of relatively few discrete lines, some of which may be measured directly in Raman and infra-red spectra, and some of which must be assumed from a best fit to specific

* From a dissertation by Edward V. Sayre submitted to the Graduate Faculty of Pure Science of Columbia University in partial fulfillment of the requirements for the degree of Doctor of Philosophy.

† Published with the assistance of the Ernest Kempton Adams fund of Columbia University.

‡ Present address, Research Laboratories, Eastman Kodak Company, Rochester, New York.

[1] M. Born and Th. von Karman, Physik. Zeits. **13**, 297 (1912); **14**, 15 (1913).

[2] M. Blackman, Zeits. f. Physik **86**, 421 (1933); Proc. Roy. Soc. **148A**, 365 (1934), **148A**, 384 (1935), **159A**, 416 (1937), **164A**, 62 (1938), **181A**, 58 (1942); Phil. Trans. Roy. Soc. **236A**, 103 (1936); Proc. Camb. Phil. Soc. **33**, 94 (1937); Rept. Progress Phys. **8**, 11 (1941).

[3] P. C. Fine, Phys. Rev. **56**, 355 (1939).

[4] E. W. Montroll, J. Chem. Phys. **10**, 218 (1942), **11**, 481 (1943); E. W. Montroll and D. C. Peaslee, *ibid.* **12**, 98 (1944).

[5] M. Born and S. H. C. Thompson, Proc. Roy. Soc. **147A**, 594 (1934); S. H. C. Thompson, *ibid.* **149A**, 487 (1935).

[6] P. P. Ewald, Ann. d. Phys. **64**, 253 (1921).

[7] R. H. Lyddane and K. F. Herzfeld, Phys. Rev. **54**, 846 (1938).

[8] E. Madelung, Phys. Zeits. **19**, 524 (1918).

[9] E. W. Kellermann, Phil. Trans. Roy. Soc. **238A**, 513 (1940); Proc. Roy. Soc. **178A**, 17 (1941).

[10] L. S. Foldy, Phys. Rev. **60**, 64 (1941).

[11] M. Iona, Phys. Rev. **60**, 822 (1941).

[12] C. V. Raman, Proc. Indian Acad. Soc. **14A**, 459 (1941).

heat data. Opponents of Raman's theory point particularly to the close agreement between experimental specific heat data and the calculations of Kellermann and Iona where no arbitrary constants needed to be assumed.

The Born and von Karman theory can be checked more rigorously, however, by studying the effect of isotope substitution upon specific heat. An isotope exchange will alter interatomic distances and forces only to a very slight extent and will alter the equations of motion of the atoms essentially only in factors of mass. Sodium hydride and sodium deuteride are crystals well suited for such a check. It has been shown conclusively by neutron diffraction study[13] that they have simple sodium chloride structure. Sodium is essentially a pure isotope, and both hydrogen and deuterium can be obtained as nearly pure isotopes. The relative difference in mass between these two isotopes is the greatest available.

In this research vibration spectra of sodium hydride and sodium deuteride have been calculated in the manner of Kellermann.[9] Specific heat curves have been calculated from these frequencies for a critical region, then checked by physical measurement.

THE FREQUENCY DISTRIBUTION

The Secular Equation

Kellermann's equations[9] inherit their basic form and notation from that of Born and Born and Goeppert-Mayer.[14] Through them the vibration frequencies of a sodium chloride lattice are calculated from the characteristic roots of sixth-order secular matrices, developed in the following manner. Upon the assumption that an arbitrarily chosen central atom vibrates with harmonic motion, its equations of motion may be written in the form

$$m_k\frac{\partial^2 u_{kx}{}^0}{\partial t^2}=-\sum_y\sum_l\sum_{k'}{}'K_{xy}{}^{kk'}(l)u_{k'y}{}^l+\sum_y\sum_l\sum_{k'}{}'K_{xy}{}^{kk'}(l)u_{ky}{}^0, \quad (1)$$

where m_k is the mass of the central atom under consideration (type k in lattice cell o), $u_{ky}{}^0$ its displacement in the y direction, $u_{k'y}{}^l$ the y component of displacement of a type k' atom in lattice cell l and $K_{xy}{}^{kk'}(l)$ the Hooke's law constant of x component of force on the undisplaced central atom resulting from the outer atom's displacement $u_{k'y}{}^l$. The summation, as indicated by the prime, should not extend to $l=0$, $k=0$. Assuming these atomic displacements occur in unidirectional waves whose periodicities are integral multiples of the unit cell dimensions, i.e., waves satisfying the Born boundary conditions, the equations of motion of all atoms of the same type become identical. The simultaneous solution of the six residual equations necessary to describe the displacements in the three coordinate directions of the two types of molecules in a sodium chloride lattice for a given wave vector leads to the secular equation. These displacement wave functions may be written:

$$\mathbf{u}_{k'}{}^l=\mathbf{U}_{k'}\exp[(-i\omega t+2\pi i[\mathbf{s}\cdot\mathbf{r}_{kk'}{}^l])] \quad (2)$$

where the two vectors $\mathbf{r}_{kk'}{}^l$ and $\mathbf{s}$ are, respectively, the vector describing the lattice position of atoms and the wave number vector of the advancing wave front, i.e., a vector of the reciprocal lattice. In this lattice these vectors can be represented by integer coordinate numbers in the following way: the equilibrium vector between like atoms,

$$\mathbf{r}_{kk}{}^l=r_0\begin{bmatrix}l_x\\ l_y\\ l_z\end{bmatrix}, \quad \sum_y l_y \text{ even}; \quad (3)$$

the equilibrium vector between unlike atoms,

$$\mathbf{r}_{kk'}{}^l=r_0\begin{bmatrix}m_x\\ m_y\\ m_z\end{bmatrix}, \quad \sum_y m_y \text{ odd}; \quad (4)$$

and the reciprocal lattice vector,

$$\mathbf{s}=\frac{1}{2r_0n}\begin{bmatrix}h_x\\ h_y\\ h_z\end{bmatrix}, \quad (5)$$

where h_x, h_y, and h_z are either all even or all odd, r_0 is the distance between nearest atomic centers, and n is the number of times the linear dimensions of the theoretical macro crystalline block considered, usually one mole, exceeds those of the unit cell, in this case a single molecule.

Combination of Eqs. (1) and (2) results in

$$-m_k\omega^2U_{kx}=\sum_y\sum_l\sum_{k'}{}'(-K_{xy}{}^{kk'}(l)U_{k'y}\times\exp[2\pi i[\mathbf{s}\cdot\mathbf{r}_{kk'}{}^l]+K_{xy}{}^{kk'}(l)U_{ky}). \quad (6)$$

And if the further substitution

$$(kk';xy)=\sum_l{}'K_{xy}{}^{kk'}(l)\exp(2\pi i[\mathbf{s}\cdot\mathbf{r}_{kk'}{}^l]) \quad (7)$$

$$[kk';xy]=\sum_l K_{xy}{}^{kk'}(l)$$

is made, the equations of motion become

$$-m_k\omega^2U_{kx}=\sum_y\sum_{k'}-(kk';xy)U_{k'y}+[kk';xy]U_{ky}=\sum_y\sum_{k'}-\{kk;xy\}U_{k'y}. \quad (8)$$

[13] Shull, Wollan, Morton, and Davidson, Phys. Rev. **73**, 842 (1948).

[14] M. Born, *Dynamik der Kristallgitter* (Leipzig, 1915); *Atomtheorie des Festen Zustandes*. (Leipzig and Berlin, 1923), second edition; M. Born and M. Goeppert-Mayer, *Handbuch der Physik* (1933), second edition, Vol. 24, Part 2.

Combination of these equations in a matrix array, together with a unitary transformation of the mass elements, result in a symmetric matrix with elements of form $\{kk';xy\}/(m_k)^{\frac{1}{2}}(m_{k'})^{\frac{1}{2}}$ whose six characteristic roots for a given wave vector are the real values ω^2.

Assuming that the central and an outer atom interact through central field forces, the potential between them when the outer atom is displaced may be expressed in a Taylor's series expansion as

$$\psi(|\mathbf{r}_{kk'}{}^l|)+\sum_y \left.\frac{\partial\psi(|\mathbf{r}|)}{\partial u_y}\right|_{r=r_{kk'}{}^l} u_y+\cdots. \tag{9}$$

Since the x component of force of this field on the central atom is the partial derivative of this function with respect to x, the Hooke's law constant of the force resulting from the displacement becomes

$$K_{xy}{}^{kk'}=\frac{\partial^2\psi(r)}{\partial x\partial y}=\frac{xy}{r^2}\frac{\partial^2\psi(r)}{\partial r^2}-\left(\frac{xy-r^2\delta_{xy}}{r^3}\right)\frac{\partial\psi(r)}{\partial r}, \tag{10}$$

in which $r=|r_{kk'}|$ and δ_{xy} is Kronecker's delta. Therefore

$$[kk';xy]=\sum_l\left[\frac{xy}{r^2}\frac{\partial^2\psi(r)}{\partial r^2}-\left(\frac{xy-r^2\delta_{xy}}{r^3}\right)\frac{\partial\psi(r)}{\partial r}\right],$$

$$(kk';xy)=\sum_l\left[\frac{xy}{r^2}\frac{\partial^2\psi(r)}{\partial r^2}-\left(\frac{xy-r^2\delta_{xy}}{r^3}\right)\frac{\partial\psi(r)}{\partial r}\right]$$

$$\times\exp(2\pi i(\mathbf{s}\cdot\mathbf{r}_{kk'}{}^l)). \tag{11}$$

Kellermann had excellent success assuming the simple potential function,

$$\psi(|\mathbf{r}|)=\frac{e_ke_{k'}}{r}+\frac{Ae^2{r_0}^{n-1}}{6nr^n}, \tag{12}$$

and summing the Coulombic interaction over the entire lattice, and the latter, repulsive term only between nearest neighbors. In this function an e is the charge on one of the univalent ions, A the Madelung constant, and n an experimental constant. Substituting the Coulombic portion of this potential into Eqs. (11)

$$[kk';xx]^c=\sum_l\left(\frac{3x^2-r^2}{r^5}\right)e_ke_{k'},$$

$$[kk';xy]^c=\sum_l\frac{3xy}{r^5}e_ke_{k'},$$

$$(kk';xx)^c=\sum_l\left(\frac{3x^2-r^2}{r^5}\right)e_ke_{k'}\exp(2\pi i(\mathbf{s}\cdot\mathbf{r})),$$

$$(kk';xy)^c=\sum_l\frac{3xy}{r^5}e_ke_{k'}\exp(2\pi i(\mathbf{s}\cdot\mathbf{r})). \tag{13}$$

From this it may be seen that quantities $v_a/e^2[kk';xy]^c$ and $(v_a/e^2(kk';xy)^c$, v_a being the volume per molecule, are dimensionless sums equally applicable to all crystals of sodium chloride structure. In a cubic lattice where for each atom at lattice position $\mathbf{r}_k{}^l$ there corresponds an identical atom at position $-\mathbf{r}_k{}^l$, it follows from the form of Eqs. (13) that

$$[kk';xx]^c=[kk';xy]^c=0. \tag{14}$$

Kellermann calculated $v_a/e^2(kk';xy)^c$ to an accuracy of one to two percent for many wave vectors, and with one exception these were used here.

From Eqs. (11) it may be seen that $\sum_x(kk';xx)^c$ represents the divergence of the field at the position of the central atom. Through an analysis of the lattice vibrations as electromagnetic waves, Kellermann[9] has shown that this function should satisfy La Place's equation for all wave vectors except $\mathbf{s}=0$ in which case the expression becomes Poisson's equation, i.e.,

$$\sum_x(kk';xx)^c{}_{\mathbf{s}\neq 0}=0,$$

$$\sum_x(kk';xx)^c{}_{\mathbf{s}=0}=4\pi\frac{e_ke_{k'}}{v_a}. \tag{15}$$

Hence for a cubic lattice

$$(kk';xx)^c{}_{\mathbf{s}=0}=\frac{4}{3}\pi\frac{e_ke_{k'}}{v_a}. \tag{16}$$

Substituting of the repulsive potential into Eqs. (19) and summating over the six nearest neighbors only gives

$$\frac{v_a}{e^2}[kk';xx]^R=\tfrac{2}{3}A(n+1)-\frac{4}{3}A,$$

$$\frac{v_a}{e^2}[kk';xy]^R=0,$$

$$\frac{v_a}{e^2}(kk';xx)^R=\tfrac{2}{3}A(n+1)\cos 2\pi s_xr_0-\tfrac{2}{3}A\cos 2\pi s_yr_0$$

$$-\tfrac{2}{3}A\cos 2\pi s_zr_0,$$

$$\frac{v_a}{e^2}(kk';xy)^R=0. \tag{17}$$

Unfortunately compressibility data is not available for sodium hydride, for the calculation of n. However, it is possible to determine n by a Born-Haber cycle.

	ΔH	
$Na(c)+H_2(g)\rightarrow NaH(c)$	− 12.8 kcal.	[15]
$Na(g)\rightarrow Na(c)$	− 25.9	[16]
$Na^+(g)+e\rightarrow Na(g)$	−118.0	[16]
$H(g)\rightarrow\frac{1}{2}H_2(g)$	− 51.9	[16]
$H^-(g)\rightarrow H(g)+e$	16.5	[17]
$Na^+(g)+H^-(g)\rightarrow NaH(c)$	−192.1	
PV correction	1.2	
$\Delta E=$	−190.9	

[15] H. Hagen and A. Seiverts, Zeits. f. anorg. allgem. Chemie **185**, 239 (1930).

[16] F. R. Bichowsky and F. D. Rossini, *The Thermochemistry of the Chemical Substances* (New York, 1936).

[17] E. A. Hylleraas, Zeits. f. physik **63**, 291 (1930).

TABLE I. Frequencies of the sodium hydride lattice.

Wave vector			Frequencies ($\omega \times 10^{-13}$ sec.$^{-1}$) Optical branch			Acoustical branch			
			Longi-			Longi-			
p_x	p_y	p_z	tudinal	Transverse		tudinal	Transverse†		Weight
10	5	0	16.30	16.30	12.24	2.94	2.94	2.56	0
10	4	0	17.76	14.79	12.15	3.08	2.77	2.54	12
10	2	2	19.25	14.34	10.33	3.23	2.88	2.13	12
10	2	0	20.07	12.18	11.51	3.30	2.45	2.39	12
10	0	0	20.94		11.10*	3.38		2.29*	3
9	5	1	17.54	15.72	11.23	3.35	2.83	2.12	24
9	3	3	18.82	15.47	9.40	3.51	2.81	1.94	12
9	3	1	19.34	13.76	11.05	3.29	2.64	2.33	48
9	1	1	20.66	11.88	10.79	3.31	2.45	2.23	24
8	6	0	17.05	16.93	10.33	3.24	3.01	2.11	24
8	4	2	19.86	14.01	9.55	3.61	2.55	2.00	48
8	4	0	19.15	14.20	10.68	3.33	2.69	2.18	24
8	2	2	20.44	12.92	9.94	3.41	2.52	2.06	24
8	2	0	20.79	11.69	10.75	3.30	2.37	2.22	24
8	0	0	21.43		10.65*	3.28		2.20*	6
7	7	1	18.89	15.47	9.32	4.00	2.39	1.91	12
7	5	3	21.85	11.58	8.40	4.07	2.14	1.74	24
7	5	1	19.87	14.29	9.12	3.61	2.64	1.85	48
7	3	3	21.58	11.83	8.80	3.85	2.19	1.83	24
7	3	1	21.10	12.06	9.69	3.42	2.65	1.63	48
7	1	1	21.78	10.65	9.94	3.21	2.18	2.07	24
6	6	2	21.23	12.76	8.26	3.97	2.33	1.70	24
6	6	0	19.54	15.12	8.45	3.59	2.78	1.73	12
6	4	4	23.17	9.12	7.76	4.41	1.75	1.62	24
6	4	2	22.02	11.33	8.38	3.85	2.22	1.68	48
6	4	0	21.40	12.59	8.20	3.52	2.47	1.64	24
6	2	2	22.45	10.19	8.87	3.45	1.96	1.86	24
6	2	0	22.38	10.34	8.95	3.14	2.14	1.82	24
6	0	0	22.65	9.40*		2.92	1.97*		6
5	5	5	23.84		7.35*	4.99		1.54*	4
5	5	3	23.26	9.25	7.38	4.43	1.82	1.52	24
5	5	1	21.90	12.21	7.40	3.75	2.36	1.49	24
5	3	3	23.53	8.36	7.78	4.04	1.63	1.59	24
5	3	1	23.05	10.02	7.46	3.41	2.06	1.44	48
5	1	1	23.33	8.72	8.48	2.83	1.70	1.64	24
4	4	4	24.01	7.18*		4.70	1.49*		8
4	4	2	23.69	8.86	6.71	4.10	1.71	1.32	24
4	4	0	23.16	10.45	6.51	3.38	2.14	1.22	12
4	2	2	24.11	7.42	7.38	3.29	1.52	1.35	24
4	2	0	23.97	8.51	6.84	2.75	1.78	1.26	24
4	0	0	24.01	7.68*		2.19	1.57*		6
3	3	3	24.44	6.70*		3.90	1.33*		8
3	3	1	24.35	8.02	5.98	3.08	1.62	1.02	24
3	1	1	24.69	6.76	6.59	2.25	1.30	1.12	24
2	2	2	24.95	6.07*		2.75	1.04*		8
2	2	0	24.98	6.76	5.45	2.06	1.29	0.59	12
2	0	0	25.11	6.04*		1.21	0.95*		6
1	1	1	25.35		5.51*	1.41		0.59*	8
0	0	0	(25.50)		5.28*	0	0	0	1

† Many waves listed have only a quasi-longitudinal or transverse nature.
* These values to be counted twice.

TABLE II. Frequencies of the sodium deuteride lattice.

Wave vector			Frequencies ($\omega \times 10^{-13}$ sec.$^{-1}$) Optical branch			Acoustical branch			
			Longi-			Longi-			
p_x	p_y	p_z	tudinal	Transverse		tudinal	Transverse†		Weight
10	5	0	11.60	11.60	8.66	2.92	2.92	2.56	0
10	4	0	12.65	10.51	8.60	3.06	2.76	2.54	12
10	2	2	13.72	10.16	7.31	3.20	2.88	2.13	12
10	2	0	14.32	8.63	8.15	3.28	2.44	2.39	12
10	0	0	14.94		7.86*	3.35		2.29*	3
9	5	1	12.46	11.20	7.95	3.33	2.82	2.12	24
9	3	3	13.36	11.02	6.65	3.45	2.82	1.93	12
9	3	1	13.67	9.98	7.73	3.26	2.63	2.33	48
9	1	1	14.74	8.41	7.63	3.29	2.44	2.22	24
8	6	0	12.14	12.02	7.31	3.25	2.99	2.09	24
8	4	2	14.09	9.97	6.83	3.57	2.54	2.00	48
8	4	0	13.63	10.08	7.57	3.30	2.68	2.18	24
8	2	2	14.57	9.18	7.03	3.38	2.51	2.06	24
8	2	0	14.84	8.28	7.61	3.26	2.36	2.22	24
8	0	0	15.31		7.53*	3.25		2.20*	6
7	7	1	13.42	10.91	6.60	4.08	2.52	1.91	12
7	5	3	15.47	8.36	5.94	4.00	2.13	1.74	24
7	5	1	14.07	10.37	6.26	3.58	2.63	1.86	48
7	3	3	15.32	8.51	6.23	3.78	2.18	1.83	24
7	3	1	15.04	8.57	6.87	3.41	2.66	1.54	48
7	1	1	15.57	7.55	7.03	3.17	2.18	2.07	24
6	6	2	15.04	9.14	5.85	4.00	2.28	1.70	24
6	6	0	13.89	10.75	5.98	3.57	2.77	1.72	12
6	4	4	16.41	6.67	5.49	4.32	1.73	1.62	24
6	4	2	15.65	8.09	5.97	3.78	2.21	1.68	48
6	4	0	15.26	8.93	5.81	3.53	2.46	1.62	24
6	2	2	16.02	7.28	6.28	3.39	1.95	1.86	24
6	2	0	16.02	7.32	6.35	3.11	2.14	1.81	24
6	0	0	16.24	6.65*		2.88	1.97*		6
5	5	5	16.87		5.20*	4.99		1.54*	4
5	5	3	16.47	6.62	5.23	4.44	1.82	1.52	24
5	5	1	15.59	8.70	5.25	3.71	2.35	1.48	24
5	3	3	16.73	6.08	5.50	3.93	1.63	1.58	24
5	3	1	16.47	7.12	5.30	3.36	2.05	1.45	48
5	1	1	16.74	6.21	6.02	2.76	1.72	1.63	24
4	4	4	17.03	5.08*		4.69	1.49*		8
4	4	2	16.88	6.23	4.76	4.13	1.70	1.32	24
4	4	0	16.57	7.40	4.62	3.34	2.14	1.22	12
4	2	2	17.26	5.30	5.25	3.21	1.52	1.35	24
4	2	0	17.21	6.02	4.87	2.69	1.78	1.26	24
4	0	0	17.28	5.44*		2.15	1.57*		6
3	3	3	17.45	4.75*		3.86	1.33*		8
3	3	1	17.46	5.67	4.26	3.06	1.61	1.01	24
3	1	1	17.76	4.80	4.69	2.22	1.30	1.10	24
2	2	2	17.92	4.33*		2.71	1.04*		8
2	2	0	17.98	4.80	3.92	2.03	1.29	0.59	12
2	0	0	18.12	4.32*		1.19	0.94*		6
1	1	1	18.28		3.96*	1.39		0.58*	8
0	0	0	(18.41)		3.82*	0	0	0	1

† Many waves listed have only a quasi-longitudinal or transverse nature.
* These values to be counted twice.

Therefore, since

$$\Delta E = -\frac{N_0 A e^2}{r_0}\left(1-\frac{1}{n}\right)$$

$$n = 5.08.$$

The error in the resulting repulsive force constants should not in general be greater than the error in n. Therefore since an error in ΔE of a kilocalorie is required to produce an error of 2 percent in n, the repulsive force constants will have about the same order of accuracy as the previously calculated Coulombic force constants, on the assumption that the simple repulsive potential function is valid for sodium hydride.

The Lattice Frequencies

There will be $6N_0$ normal modes of vibration for these crystals determined by the N_0 wave vectors $\mathbf{s}$ within the first Brillouin zone. These are the waves characterized by all even and all odd integer values of h_x, h_y, h_z bounded by the equations

$$\frac{h_x}{n}=\pm 1,\quad \frac{h_y}{n}=\pm 1,\quad \frac{h_z}{n}=\pm 1;\quad \frac{h_x}{n}\pm\frac{h_y}{n}\pm\frac{h_z}{n}=\pm\tfrac{3}{2}. \qquad (20)$$

New wave vector coefficients

$$p_y=\frac{10h_y}{n} \qquad (21)$$

define, for all odd and all even integer values of p_x, p_y, and p_z a lattice within the reciprocal lattice, with identical symmetry to it. There are 1115 such **p** vectors within the first zone. However, for an isotropic lattice all vectors differing only by permutation of p_x, p_y, and p_z or by changes of their signs have degenerate frequencies. Therefore one need consider only the vectors with positive coefficients

$$0\leq p_z\leq p_y\leq p_x\leq 10, \quad p_x+p_y+p_z\leq 15. \tag{22}$$

There are 48 such vectors. Kellermann calculated Coulombic force constant sums for all of these vectors except one, $p_x=p_y=7$, $p_z=1$, apparently overlooked. The Coulombic sums for this vector are:

$$\begin{aligned}
&\frac{v_a}{e^2}(11;xx)^c=\frac{v_a}{e^2}(11;yy)^c=0.778\\
&\frac{v_a}{e^2}(11;zz)^c=-1.600\\
&\frac{v_a}{e^2}(12;xx)^c=\frac{v_a}{e^2}(12;yy)^c=5.759\\
&\frac{v_a}{e^2}(12;zz)^c=-11.573\\
&\frac{v_a}{e^2}(11;xz)^c=\frac{v_a}{e^2}(11;yz)^c=-0.859\\
&\frac{v_a}{e^2}(11;xy)^c=-2.145\\
&\frac{v_a}{e^2}(12;xz)^c=\frac{v_a}{e^2}(12;yz)^c=-0.246\\
&\frac{v_a}{e^2}(12;xy)^c=0.829.
\end{aligned} \tag{23}$$

The lattice frequencies listed in Tables I and II were calculated using the force constants described above and the value of 2.440A for r_0 of sodium hydride.[18] The force constants were assumed identical for sodium hydride and sodium deuteride, the only difference in the two calculations being the mass change. The calculations were performed with punched card machines at the Watson Scientific Computing Laboratory of Columbia University. Major operations were done on an Aberdeen Relay Calculator upon which matrix multiplication could be performed directly. Irreducible sixth-order matrices were first rotated until all elements in the off-diagonal quadrants were negligible. Characteristic roots were extracted from the resulting third-order matrices, and from all irreducible fourth-order matrices by the iteration methods described by Aitken.[19] The frequencies of vector of shortest wave length, $p_x=10$, $p_y=5$, $p_z=0$, were calculated, although this vector does not fall within the group described above. These frequencies, therefore, were not considered in the calculation of the frequency distributions and specific heats. The vector of longest wave-length, $p_x=0$, $p_y=0$, $p_z=0$, requires special consideration. Kellermann's deduction that the Coulombic force constants obey Poisson's rather than La Place's equation for this particular vector (Eq. (16)) results in a cubic crystal in three triply degenerate second-order matrices

$$\begin{pmatrix} \dfrac{K}{m_1} & -\dfrac{K}{(m_1)^{\frac{1}{2}}(m_2)^{\frac{1}{2}}} \\ -\dfrac{K}{(m_1)^{\frac{1}{2}}(m_2)^{\frac{1}{2}}} & \dfrac{K}{m_2} \end{pmatrix}$$

$$K=\frac{e^2}{v_a}\left[-\frac{4\pi}{3}+\frac{2}{3}A(n+1)-\frac{4}{3}A\right] \tag{24}$$

with roots

$$\omega^2=0, \quad K/\mu,$$

where μ is the reduced mass.

Lyddane and Herzfeld[7] had previously derived the same Coulombic force constant for transverse waves of this vector. In their purely electrostatic argument they identified the Coulombic force with the Lorentz-Lorenz field $4/3\pi\mathbf{P}$, **P** equals the polarization. However, in order to consider displacements uniform over the entire crystal, the wave-length must be infinite compared to the length of crystal to which it is applied. This means the crystal must be finite in the direction of the wave vector. Lyddane and Herzfeld, therefore, pictured the crystal as an infinite slab, and added a further term, $-4\pi\mathbf{P}\cdot\mathbf{s}/s$, for the field of the polarization changes on the surfaces of the slab. They, therefore, arrived at degenerate transverse waves of the same frequency as Kellermann and a longitudinal wave of frequencies

$$\omega^2=0, \quad \frac{e^2}{\mu v_a}\left[\frac{8\pi}{3}+\frac{2}{3}A(n+1)-\frac{4}{3}A\right]. \tag{25}$$

However, in any true physical picture the crystal is finite in all dimensions, and thus an internal field should result from surface polarization charges, no matter what the direction of displacement. This field would be independent of the size of the crystal so long as all relative proportions were constant. If the finite crystal were assumed to have macroscopic cubic symmetry, the 0, 0, 0 vibration would, of course, be calculated as triply degenerate. Nevertheless, both of Lyddane and Herzfeld's frequencies for $s=0$ are given in Tables I and II, the longitudinal frequency being placed in

[18] E. Zintl and A. Harder, Zeits. f. physik. Chemie **B14**, 265 (1931).

[19] A. C. Aitken, Proc. Roy. Soc. Edinburgh **57**, 269 (1937).

brackets to indicate its doubtful nature. The extremely low weight given this frequency (1 in 6000) in the calculation of the distribution spectrum means the uncertainty of its value has negligible effect upon subsequent calculations made here.

Each vector of Table I or II is degenerate to all other vectors whose coefficients differ only by permutation of order or changes of sign. Each of these vectors determines the center position of cells of equal volume in the reciprocal lattice. If the vector ends on the first zone boundary the cell it describes will lie only partially within the first zone. The vectors of Tables I and II, therefore, were weighted by the number of above permutations, this normal weighting number being divided by two when the vector ended on the zone surface. The sum of these weights, being proportional to the volume of the zone, is equal to exactly 1000. A single frequency given a weight of one in these tables may be considered an average value for $N_0/1000$ modes of vibration.

In order to avoid meaningless fluctuation in the frequency distribution arising from considering too few frequencies in a given range, the range needed to be of the order of 10 percent of the frequency values. Such a range has only about twice the spread of the accuracy of the calculations. Specifically, for the acoustical branches of both the hydride and deuteride spectra the frequencies were summed in ranges of $\Delta\omega=0.3\times10^{13}$ sec.$^{-1}$; for the deuteride optical branch $\Delta\omega=1.0\times10^{13}$ sec.$^{-1}$, and for the hydride optical branch $\Delta\omega=1.5\times10^{13}$ sec.$^{-1}$. The frequency distributions so derived are shown in Fig. 1.

It is apparent from these results that: (1) the spectra break nicely into acoustical and optical branches, resulting from vibrations that differ only in whether unlike atoms are in phase or 180° out of phase, (2) that the acoustical frequencies are nearly identical for the two compounds, (3) that the optical frequencies for the hydride are all greater than the corresponding frequencies of the deuteride by approximately the square root of two, and (4) that the optical branch spectra of both are far from monochromatic, that of the hydride being even less so than that of the deuteride. The first three of these conclusions are in agreement with concepts extrapolated from previous, less detailed calculations. The last conclusion is in marked disagreement with many previous predictions. The effective mass in optical vibrations varies from the mass of the lighter atom to the reduced mass of the molecule. These limits, of course, become more nearly identical as the ratio of the atomic weights of the two elements of the crystal increases. In the case of a linear lattice, where there is a single force constant, this results in the optical frequencies becoming more monochromatic as the mass of one element is made progressively lighter. This has led many to assume that the specific contribution of the optical vibrations of a sodium chloride lattice compound should be approximated by three Einstein functions. In the three-dimensional case, however, there exists a range of force constants. Hence even for a group of vibrations for which the effective mass is essentially constant, the frequencies will still cover a range. This range will become broader as the effective mass is decreased in the same proportion as the frequencies will increase. Consideration of Kellermann's distribution for sodium chloride, where the two atomic weights were of the same order of magnitude, and of these distributions, where the atomic masses are greatly unequal, show that in no general case for this lattice should one expect a monochromatic optical branch spectra from these calculations.

The relatively great breadth of the optical branch of

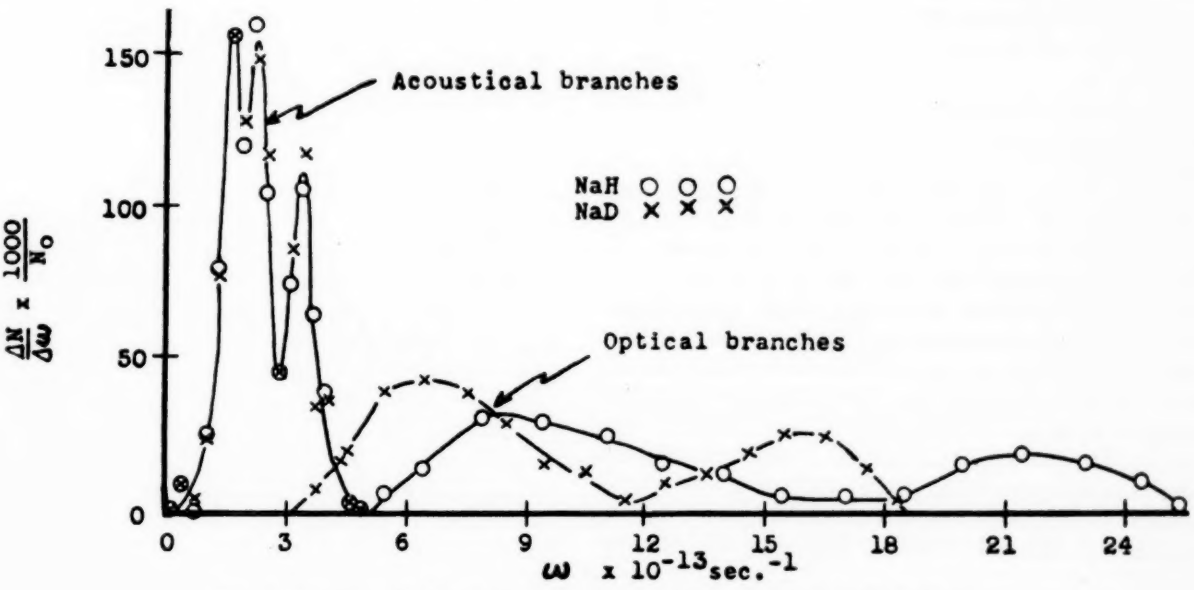

FIG. 1. Frequency distributions of sodium hydride and sodium deuteride lattices.

sodium hydride in these calculations suggests the alkali hydrides may be particularly well adapted for experiments verifying a selection between Born and Raman's concepts.

EXPERIMENTAL

The Calorimeter

Specific heat measurements were made with an adiabatic calorimeter of the type described by Southard and Brickwedde.[20] The calorimeter itself was a platinum cylindrical can 5 cm by 2.5 cm O.D. In it's center, extending upward from the bottom, was a 0.5-cm diameter platinum well housing a platinum resistance thermometer. To promote good conduction of heat throughout the calorimeter, eight radial and two annular vertical gold vanes were set in the annular space between the thermometer well and outer wall. The outer wall was wound with a constantan wire heating element (approximately 21 ohms). This wire winding was painted with picein to insure good thermal contact and covered with "Dutch metal" leaf to minimize heat loss by radiation. The lid had a small open platinum tube, 0.5 cm by 0.5 cm diameter, extending upward from its center, to which a soft glass tube was sealed. Through this tube the calorimeter could be filled. The calorimeter was closed, containing one-third of an atmosphere of helium, by sealing off the soft glass tube as near as possible to the lid itself.

The calorimeter was suspended by three nylon threads within a copper shield, which was maintained continuously throughout runs at the same temperature as the calorimeter. The shield, made of 0.1 cm copper sheet, was a 4.5 cm diameter cylinder 6.5 cm in length with 1.4 cm deep conical caps at top and bottom. The top, bottom and sides were wound externally with constantan wire so that they could be heated separately. Differential thermocouples read temperature differences between the top, bottom and sides of the shield and the calorimeter.

The shield was suspended by Nylon threads from a floating heavy copper ring, which in turn was suspended similarly from a fixed copper ring. The fixed ring was attached directly inside the lid of a copper can (16.5 cm by 6.5 cm diameter) within which the rings and shield were sealed. This can was immersed directly into the cryostating fluid, and held in position on the end of a one half inch steel tube, which was soldered into its lid. Through this tube an insulating vacuum could be pumped within the can. All electric wires were brought into the can through this tube, then wrapped around the fixed ring to insure their being brought to the temperature of the cryostat. They were next wrapped around the floating ring, where they were brought to the same temperature as the shield before leading to it. To maintain its temperature, the floating ring was wound internally with an independent heating element, and a differential thermocouple read the temperature difference between it and the side of the shield. Except for lags at the beginning and end of calorimeter heating periods, the floating ring, the parts of the shield, and the calorimeter could all be maintained within 0.02°C of the same temperature.

The cryostating liquid, liquid nitrogen, was held in an inclosed Dewar flask in which the vapor pressure of nitrogen could be controlled.

The exact temperature of the calorimeter was determined to ±0.002°C by the platinum resistance thermometer, whose resistance was determined by a calibrated, thermostatted Mueller bridge. The resistance thermometer was calibrated at the National Bureau of Standards and its resistance at the ice point checked in this laboratory.

The heating current was measured by determining the potential drop it produced across a Leeds and Northrup precision ten ohm resistance. The resistance was thermostatted and recently had been calibrated at the National Bureau of Standards. This potential and the potential drop across the calorimeter heating winding was measured by a calibrated Leeds and Northrup Type K-2 potentiometer. The potentiometer was set against an Eppley unsaturated standard cell, which also was thermostated and whose potential was occasionally checked against those of similar cells. The wires leading to the potentiometer tapped the wires carrying heating current to the calorimeter at the point halfway between the shield and the calorimeter. In this way all of the measured potential drop would be a contribution to the heating of the calorimeter except for one half of the heat conducted to the shield by the potential measuring leads. To minimize this loss the heating leads were made short (2 cm from shield to calorimeter) and the potential measuring leads long (10 cm from midpoint

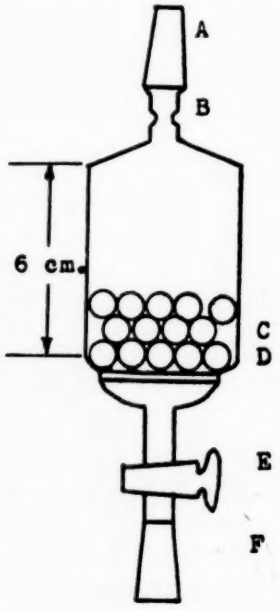

FIG. 2. Filter and drying chamber. *A*—14/35 ground glass joint—inner section. *B*—Restriction in neck to hold glass beads. *C*—½ cm glass beads. *D*—Sintered glass plate (3.5 cm diameter). *E*—Stopcock. *F*—14/35 ground glass joint—outer section.

[20] J. C. Southard and F. G. Brickwedde, J. Am. Chem. Soc. 55, 4378 (1933).

of heating leads to shield). Both were of A. W. G. No. 40 copper wire doubly wound with cotton. Under these conditions this heat loss would be less than 0.01 percent of that delivered to the calorimeter, a negligible amount. Current was supplied from a six cell, low discharge lead storage battery, which was brought to a steady state by drawing current from it through a dummy load for at least an hour before making measurements.

Timing was controlled by electric impulses received via telephone lines from a precision pendulum clock in the Department of Astronomy. This clock was checked periodically by astronomic measurement and found to be accurate to the order of 0.001 percent. The impulses were used to activate an electronic scaling unit of two, similar to those commonly employed in radioactivity counting. Impulses reaching this scaling unit alternately would cause the opening and closing of a double throw, double pole switch. When open this switch directed the heating current through the dummy load. An impulse at the beginning of the run would close the switch which then directed the current through the calorimeter winding. A second impulse at the end of the run again would open the switch. Measurement with an oscilloscope showed a time lag of 0.025 sec. between the arrival of an impulse and switch closing and 0.019 sec. between impulse and switch opening. The time loss of 0.006 sec. could be neglected in the usual eight minute heating period.

The calorimeter and measuring instruments all rested on an interconnected metal shielding sheet. The shielding was joined electrically to the heating circuit at the negative side of the standard resistance used in measuring current.

Typical operating conditions were a current of 0.06 international amperes, potential drop across heater of 1.2 international volts, for a heating period of 480 sidereal seconds. This resulted in approximately 4°C temperature rise.

Potassium chloride was measured as a standard for checking the calorimeter. The specific heat curve of this salt had been measured carefully by Southard and Nelson[21] and their values checked by Feodos'ev.[22] The potassium chloride was recrystallized and fused in the manner described by Southard and Nelson. A comparison between values taken from their curve and ones determined in this laboratory is given in Table III. The agreement there is somewhat better than the precision of measurement. Repeated blank measurements on the calorimeter showed a possible error of 0.5 percent. The major contribution to this error seemed to arise from the lack of precision with which the calorimeter could be sealed. The use of this tube was necessary, however, in order that sodium hydride could be loaded into the calorimeter in the complete absence of air. Since the heat content of the sodium hydride samples was in general only half as great as the blank, this uncertainty might result in a 1 percent error in the measured molar heat contents of sodium hydride or deuteride.

TABLE III. Molecular heat capacity of potassium chloride.

Temperature (°K)	C_p (cal./mole) Southard and Nelson	This laboratory
80.04	8.230	8.222
76.65	7.945	7.946
73.46	7.670	7.687
69.19	7.290	7.298

Preparation of Materials

Numerous attempts to prepare sodium hydride by passing hydrogen over or through hot sodium (400 to 600°C) and collecting the salt as a condensate on cooler portions of the apparatus resulted only in yields of a few milligrams per day. The proper filling of the calorimeter and analysis of the products, however, required the preparation of about a half mole of material. Resort was made, therefore, to a procedure patented by Muckenfuss,[23] the hydrogenation at moderately high temperature and pressure of sodium dispersed in a hydrocarbon oil in a rocking autoclave. This procedure had the serious disadvantages: (1) the hydride formed as a very fine powder and therefore was unusually reactive; (2) the highly reactive hydride could not be handled continuously within a single vacuum sealed apparatus, but had to be transferred from hydrogenation to purification and loading apparatus with resulting danger of oxidation; and (3) in the preparation of sodium deuteride, exchange between the deuterium gas and hydrocarbon solvent was to be feared. The method, however, yielded conveniently the large amount of product required.

Selection of the proper hydrocarbon was surprisingly critical. To minimize isotopic exchange only fully saturated hydrocarbons were tried. The hydrogenation proceeded readily in long chain petroleum fractions of the kerosene to heavy mineral oil range, but removal of these oils from the hydride required extra steps of repeated washings with more volatile solvents. Hydrogenation proceeded too slowly in such volatile solvents as hexanes, heptanes, or octanes, presumably because of their lower viscosity. After periods of as long as two days reaction would still not be complete in them. A petroleum cut of about the decane range proved just adequate in both reaction rate and volatility. Standard Oil Company commercial naptha No. 4 was used. It was washed repeatedly with fuming sulfuric acid, then with a sodium hydroxide solution, dried, allowed to stand for a period of several days over sodium, then distilled from sodium directly into a hydrogenation bomb liner. About 300 ml of the fraction boiling between 167 and 180°C were used in the 600 ml capacity

[21] J. C. Southard and R. A. Nelson, J. Am. Chem. Soc. **55**, 4865 (1933).

[22] N. Feodos'ev, J. Phys. Chem. (U.S.S.R.) **12**, 291 (1938).

[23] A. W. Muckenfuss, U. S. Patent 1,958,012, May 8, 1934.

TABLE IV. Milliequivalents of sodium in test samples.

From titration of base	From volume of hydrogen
0.4180	0.4188
1.121	1.120
1.093	1.096

TABLE V. Chemical analysis of hydrides.

	Milliequivalents per sample of		
Sample	Base[a]	H[b]	NaH and/or NaD[c]
NaH–I	0.997	0.999	
	2.260	2.262	
	5.014		5.057
NaH–II	1.133	1.136	
	1.720	1.699	
	7.764		7.835
NaD–I	0.816	0.813	
	0.502	0.498	
	11.83		11.92
NaD–II	1.897	1.888	
	1.320	1.300	
	6.085		6.097

[a] From titration of aqueous solution of sample.
[b] From hydrogen liberated from sample by water.
[c] From weight of sample.

Pyrex glass bomb liner. A single piece of C. P. sodium metal was cut beneath dry decane then transferred immediately to beneath the purified solvent. Hydrogenation was carried out in a bomb[24] rocking in an autoclave at 240°C and 400 p.s.i. initial (cold) pressure for about ten hours. Tank hydrogen and deuterium were used directly after the bomb had been thoroughly flushed or evacuated.

Following hydrogenation, the bomb liner, containing the sodium hydride under a protective decane layer, was transferred to a nitrogen filled dry box. In the dry box the hydride slurry was syphoned into an enclosed fritted glass funnel—drying chamber, shown diagrammatically in Fig. 2. Slurry entered the chamber through joint A, and all possible filtrate was sucked off through joint F. Joint A was then covered by a short connecting tube which had a stopcock at its center. This tube was connected to a high vacuum system, and all residual solvent pumped off through it as vapor. Periodically throughout this drying, the stopcock in this connecting tube was closed, the sealed drying chamber detached and shaken. The glass balls in the drying chamber then effectively broke up any packed hydride allowing uniform and complete evaporation of the solvent. When evaporation was complete the chamber was filled with helium, which was dried by passing through two liquid air traps in one of which the gas was filtered through a sintered glass plug. The connecting tube was then replaced quickly by the short soft glass tube leading into the calorimeter, also filled with dry helium. A high vacuum was then pumped in the drying chamber and calorimeter through joint F. Sodium hydride was shaken down into the calorimeter, one-third of an atmosphere of dry helium admitted, and the soft glass tube leading into the calorimeter sealed off as close to the calorimeter as possible.

Sample tubes were then filled in a manner similar to the filling of the calorimeter. Approximately 40 mg samples were sealed into 3-cm lengths of 6-mm tubing, one end of which had been blown into a thin-walled bulb.

The purity of the products was determined by analysis. The sodium to hydrogen (or deuterium) ratio was determined by decomposing a sample in water in a hydrogen atmosphere. The amount of hydrogen liberated was compared to the basicity of the resulting solution. The analytical procedure was checked by running similar samples of freshly distilled sodium metal. The results of these check analyses, given in Table IV, show the method to be good to a few parts per thousand. The absence of inert contaminates was proved by the decomposition of a weighted sample in water and titration of the resulting alkalinity.

The hydrogen to deuterium ratio in sodium deuteride was determined by decomposing a sample by heat and analyzing the liberated gas on a mass spectrometer.[25] This isotopic analysis showed sample NaD–I to be 71.5 percent deuteride and sample NaD–II to be 71.2 percent deuteride.

Irregularities in taking hydride samples, such as slight thermal decomposition upon sealing in glass break seal tubes, lowered the precision of analysis of the hydrides. The analytical results in Table V, however, show that in all the samples measured the chemical impurities were never greater than the order of one per cent. Since the effect of the most expected impurities, e.g., sodium hydroxide and decane, would be to change the heat capacity and the calculated number of moles per sample roughly by the same fraction, the resulting error in the molar heat contents would be considerably below the precision of measurement.

The Molar Heat Capacities

Molar heat capacities were calculated from the distribution curves of Fig. 1, by multiplying each distribution point by its appropriate Einstein function, integrating beneath the curve so derived, and multiplying this area by $N_0/1000$. Specifically, for the frequency of each of the points plotted in Fig. 1 the heat capacity per mol was interpolated from the table of Wilson, Johnson and others in the Taylor-Glasstone treatise.[26] This molar heat capacity contribution per point then was multiplied by the sum of the weights of all fre-

[24] A 406–22B American Instrument Company stainless steel bomb was used through the courtesy of Professor Robert C. Elderfield.

[25] Professor D. Rittenberg of the Department of Biochemistry of Columbia kindly undertook the mass spectrographic analyses.

[26] H. S. Taylor and S. Glasstone, *Treatise on Physical Chemistry* (New York, 1942), 3rd Ed., page 654.

quencies contributing to it. The sum of these products divided by 1000 was the calculated molar heat capacity.

Consideration of the frequency distribution curves would indicate that the contribution of the acoustical frequencies to heat capacity would be essentially the same for sodium deuteride as for sodium hydride. At very low temperatures, therefore, the molar heat capacity curves of the two substances should nearly coincide. At higher temperatures, however, contributions from the optical frequencies of the deuteride would appear sooner than from the optical frequencies of the hydride. The two curves should, therefore, separate over a broad temperature range, and rejoin only at relatively high temperatures. In the temperature range conveniently reached by a liquid nitrogen filled cryostat, 60 to 90°K this separation is first becoming experimentally apparent. Thus, this range was chosen for measurement. Calculated heat capacities for this temperature range are given in Table VI, and are plotted in Fig. 3.

The experimentally determined heat capacity data are listed in Tables VII and VIII, and are also plotted in Fig. 3. They are reported in terms of the calorie defined by Bichowsky and Rossini[27] and the temperature scale of Hoge and Brickwedde.[28] The deuteride samples were corrected for their hydride content by subtracting the heat capacity of hydride contained, as determined from the experimental hydride curve, from the total heat capacity of the sample. On both compounds duplicate sets of data were determined. Each set was run on an independently prepared sample, and was composed of about nine points taken at intervals averaging three and one half degrees. The two sets of data on sodium hydride were in close agreement, the derivation of the mean of the sets being 0.17 percent. One of the sodium deuteride sets lies slightly below the other. The derivation of the mean of these sets is, therefore, somewhat greater, i.e., 0.48, percent but still within the anticipated experimental error.

TABLE VI. Calculated molar heat capacities of sodium hydride and deuteride.

Temperature	C_v of hydride			C_v of deuteride		
	Acoustical	Optical	Total	Acoustical	Optical	Total
60	2.933	0.014	2.947	2.961	0.107	3.068
65	3.213	0.024	3.237	3.244	0.153	3.397
70	3.436	0.038	3.474	3.464	0.209	3.673
75	3.649	0.055	3.704	3.678	0.274	3.952
80	3.839	0.077	3.916	3.868	0.340	4.208
85	4.014	0.105	4.119	4.041	0.417	4.458
90	4.162	0.136	4.298	4.188	0.500	4.688

The calculated curves at all points are nearly 10 percent higher than the corresponding experimental curves. This is well beyond the experimental error and the error of calculation, subject to the assumption that the interatomic potential functions were correctly selected. The calculated and observed curves show many similarities, however. They are nearly parallel throughout the range studied. The deuteride curve in both the real and theoretical case is higher than the hydride curve by about the same amount, and in each case the curves are diverging at about the same rate. In fact, if the theoretical curves were transposed along the abscissa by 10°K the two sets of curves would come close to coincidence. This could lead one to assume that the frequencies of Tables I and II were all to small by the order of 10 percent.

An error of this magnitude and kind could have entered into the calculations in the repulsive force constants. For these repulsive force constants a potential function of the type, b/r^n, was used, which served to average the potential of true repulsive forces with attractive van der Waals and dipole-quadripole forces. Such a force function was used very successfully in the case of sodium chloride where the van der Waals forces are small compared to the repulsive forces. It is not surprising, however, that it would be less applicable to sodium hydride in which forces of the van der Waals

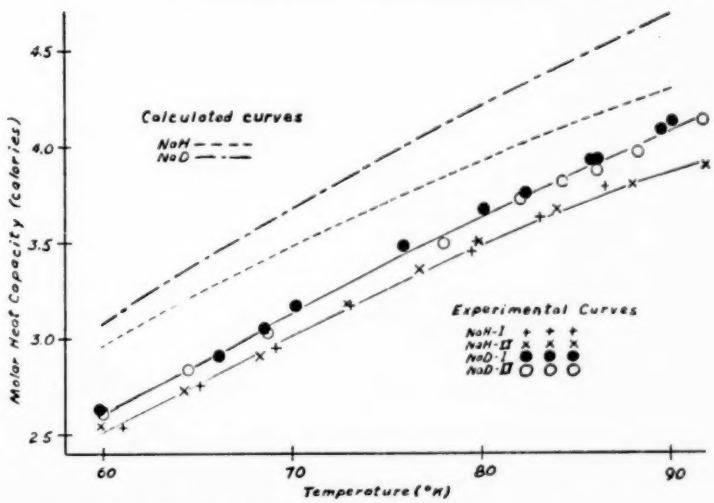

FIG. 3. Molar heat capacities of sodium hydride and sodium deuteride.

[27] F. R. Bichowsky and F. D. Rossini, *The Thermochemistry of Chemical Substances* (New York, 1936), p. 9.
[28] H. J. Hoge and F. G. Brickwedde, J. Research Nat. Bur. Stand. **22**, 351 (1939).

TABLE VII. Experimental molar heat capacities of sodium hydride.

Weight of sample NaH–I 5.2599 grams Weight of sample NaH–II 5.5412 grams Temperature (°K)	C_p (cal./mole)	Sample
59.94	2.543	II
61.02	2.537	I
64.22	2.733	II
65.10	2.752	I
68.23	2.915	II
69.09	2.953	I
72.89	3.180	II
73.07	3.167	I
76.77	3.357	II
79.51	3.446	I
79.71	3.500	I
79.95	3.487	II
83.05	3.624	I
84.06	3.665	II
86.47	3.783	I
88.01	3.795	II
91.84	3.899	II

TABLE VIII. Experimental molar heat capacities of sodium deuteride.

Weight of sample NaD–I 4.7990 grams Weight of sample NaD–II 7.0841 grams Temperature (°K)	C_p (cal./mole)	Sample
59.85	2.635	I
60.17	2.605	II
64.59	2.838	II
66.17	2.903	I
68.55	3.054	I
68.73	3.024	II
70.10	3.164	I
75.87	3.480	I
78.04	3.495	II
80.15	3.673	I
82.08	3.710	II
82.33	3.756	I
84.31	3.812	II
85.79	3.928	I
86.14	3.868	II
86.19	3.935	I
88.28	3.966	II
89.52	4.093	I
90.07	4.127	I
91.75	4.129	II

type would be expected to be more important. Further error could have occurred in this term because it was calculated from the difference between the crystal energy and energy of Coulombic interaction. This energy difference may be further below the true "repulsive energy" in the sodium hydride crystal than it would in a more truly ionic crystal. One would expect from the above derivation that sodium hydride would have a greater coefficient of compressibility than is calculated from a Born-Haber cycle, and that when such compressibility data is available a better calculation of lattice frequencies could be made. It is also possible that a recalculation using the more detailed separate van der Waals, dipole-quadripole, and exponental repulsive potential functions of Born and Mayer[29] would produce results in closer agreement with the experimental results.

Certainly, in the majority of their aspects, however, the data and predictions of this paper are already in substantial agreement.

Although this research in no way provides a clear-cut experimental decision between the Born and von Karman and the Raman theories of specific heats, it shows that the two theories are in remarkable disagreement in their predictions of the distributions of optical branch vibration frequencies in sodium hydride and deuteride crystals. For this reason these substances seem particularly to offer opportunities for further study.

[29] M. Born and J. E. Mayer, Zeits. f. Physik **75**, 1 (1932): J. E. Mayer, J. Chem. Phys. **1**, 279 (1933).

I. The Infra-Red Spectrum of Tetramethyl Lead and the Force Constants of $M(CH_3)_4$ Type Molecules*

RAYMOND K. SHELINE** AND KENNETH S. PITZER***
Department of Chemistry, University of California, Berkeley, California

(Received August 22, 1949)

The infra-red absorption of tetramethyl lead has been measured in the region 2–23μ. A frequency assignment has been proposed. A partial normal coordinate analysis has been made using the fundamental frequencies of this investigation and the data of previous investigators of tetramethyl compounds. Thereby M−C valence-type force constants of all the Group IV tetramethyl derivatives and the analogous tetramethyl ammonium ion have been determined. These force constants are compared with those predicted by the rules of Badger and Gordy and the relationship between bond force constants and atomic parameters is briefly considered.

INTRODUCTION

THE Raman and infra-red spectra of the Group IV tetramethyl alkyls and the analogous tetramethyl ammonium ion have been reported in a number of papers.[1–12] Recently a reasonably complete assignment has been proposed.[12]

This study was directed at three objectives: first, to observe the infra-red spectrum of tetramethyl lead in the region 2μ–23μ, to propose an assignment for the tetramethyl lead, and to calculate the M−C force constants of the tetramethyl compounds; second, to calculate an effective methyl mass (i.e., the mass a methyl group would necessarily have in order to give the correct force constant in a simplified calculation) for stretching and bending frequencies; third, to compare the force constants derived in the normal coordinate treatment with those predicted by the rules of Badger[13,14] and Gordy,[15] and conversely to compare with standard electronegativities those derived by assuming Gordy's Rule and substituting the true force constants.

EXPERIMENTAL

Sample

The tetramethyl lead was obtained from the Republic Laboratories. It was purified by redistilling and collecting a middle fraction. The product had a boiling point of 110.0°C at 725-mm Hg pressure.

Infra-Red Spectrum

Since the infra-red work of Kettering and Sleator[8] on tetramethyl lead does not cover the range from 660 to 450 cm^{-1}, it seemed advisable to reexamine the infra-red spectrum of this substance with particular attention to the 660–450 cm^{-1} region. Accordingly, measurements were made on the gas in a 9.4-cm glass cell with KBr windows using the Perkin-Elmer 12B automatic

TABLE I. The infra-red spectrum of $Pb(CH_3)_4$, gas and liquid.

Gas ν(cm^{-1}) Kettering and Sleator*	Gas ν(cm^{-1}) This research	Liquid ν(cm^{-1}) This research
	476 s.	475 v.s. (unresolved)
658 w.		
774 v.s.	769 v.s.	771 v.s. (unresolved)
937 w.	933 v.w.	931 w.
1032 w.	1022 v.w.	1022 w.
		1051 v.w.
	1076 w.	1067 w.
		1122 s.
	1140 / 1147 s.	1152 s.
1169 s.	1162 sh.	1164 sh.
1305 m.	1306 w.	1296 m.
1381 w.	1392 m.	1390 s. (unresolved)
1462 s.	1453 m.	1440 s. (unresolved)
	1621 w.	1618 m.
1925 w.	1925 w.	1922 m.
2170 w.		2108 v.w.
	2292 w.	2290 m.
	2910 s.	2905 s. (shoulder)
2980 s.	2982 / 2992 s.	3000 v.s. (unresolved)
		3380 v.w.
3700 w.	3760 v.w.	3770 w.
		4050 w.
		4100 w.
4400 w.	4350 v.w.	4360 w.

w.=weak m.=medium s.=strong v.=very sh.=shoulder

* See reference 8.

* Based on a thesis submitted by Raymond K. Sheline in partial fulfillment of the requirements for the Ph.D. degree at the University of California. This research was aided by the ONR under N7 ONR-295 Task Order X as Project No. NR-058-097.

** Present address: Institute for Nuclear Studies, University of Chicago, Chicago, Illinois.

*** On leave of absence from the University of California as Director of Research of the AEC, Washington, D. C.

[1] K. W. F. Kohlrausch and Barnes, Anales Soc. Espan. Fis. Quim. **30**, 733 (1932).
[2] K. W. F. Kohlrausch and F. Köppl, Zeits. f. physik. Chemie **B26**, 209 (1934).
[3] D. H. Rank and E. R. Bordner, J. Chem. Phys. **3**, 248 (1935).
[4] D. H. Rank, J. Chem. Phys. **1**, 572 (1933).
[5] N. G. Pai, Proc. Roy. Soc. (London) **149**, 29 (1935).
[6] A. B. Duncan and J. W. Murray, J. Chem. Phys. **2**, 146, 642 (1934).
[7] J. T. Edsall, J. Chem. Phys. **5**, 225 (1937).
[8] C. F. Kettering and W. W. Sleator, Physics **4**, 39 (1933).
[9] F. T. Wall and C. R. Eddy, J. Chem. Phys. **6**, 107 (1938).
[10] S. Silver, J. Chem. Phys. **7**, 1113 (1939); **8**, 919 (1940).
[11] T. F. Anderson, J. Chem. Phys. **4**, 161 (1936).
[12] Young, Koehler, and McKinney, J. Am. Chem. Soc. **69**, 1410 (1947).
[13] R. M. Badger, J. Chem. Phys. **2**, 128 (1934).
[14] R. M. Badger, J. Chem. Phys. **3**, 710 (1935).
[15] W. Gordy, J. Chem. Phys. **14**, 305 (1946).

prism spectrometer. All spectral data were obtained at room temperature. Pressures of 63, 32, and 6.5 mm were used. In order to determine whether certain bands were missing in the gas, where the maximum pressure at room temperature was 63 mm, the liquid was run in the Perkin-Elmer liquid cell using amalgamated lead spacers of thickness 0.127 and 0.051 mm. The absorption curves are given in Figs. 1 and 2, respectively, and the frequencies are summarized in Table I along with the data of Kettering and Sleator. The liquid of course contains certain bands which are so intense as to be unresolved. The frequency corresponding to the center of these bands is listed in Table I. The calibration of the Perkin-Elmer spectrometer was checked several times during the period of operation and the data from it are probably accurate to ± 1 cm^{-1} at 625 cm^{-1}, ± 5 cm^{-1} at 2000 cm^{-1} and ± 15 cm^{-1} at 3000 cm^{-1}.

FREQUENCY ASSIGNMENTS

There is unanimity of opinion among the previous investigators that the tetramethyl compounds belong to the point group T_d. This is confirmed by both the electron diffraction and molecular vibrational analysis.[9,10] Therefore, a tetrahedral T_d point group is assumed in all subsequent discussion.

The band notation of Young, Koehler, and McKinney is used throughout. The Raman data of Duncan and Murray[6] are used in the assignment. Considering first the fundamental frequencies, the polarized lines at 2918, 1170, and 460 cm^{-1} can be only A_1 vibrations. The high intensity and sharpness of these bands is in

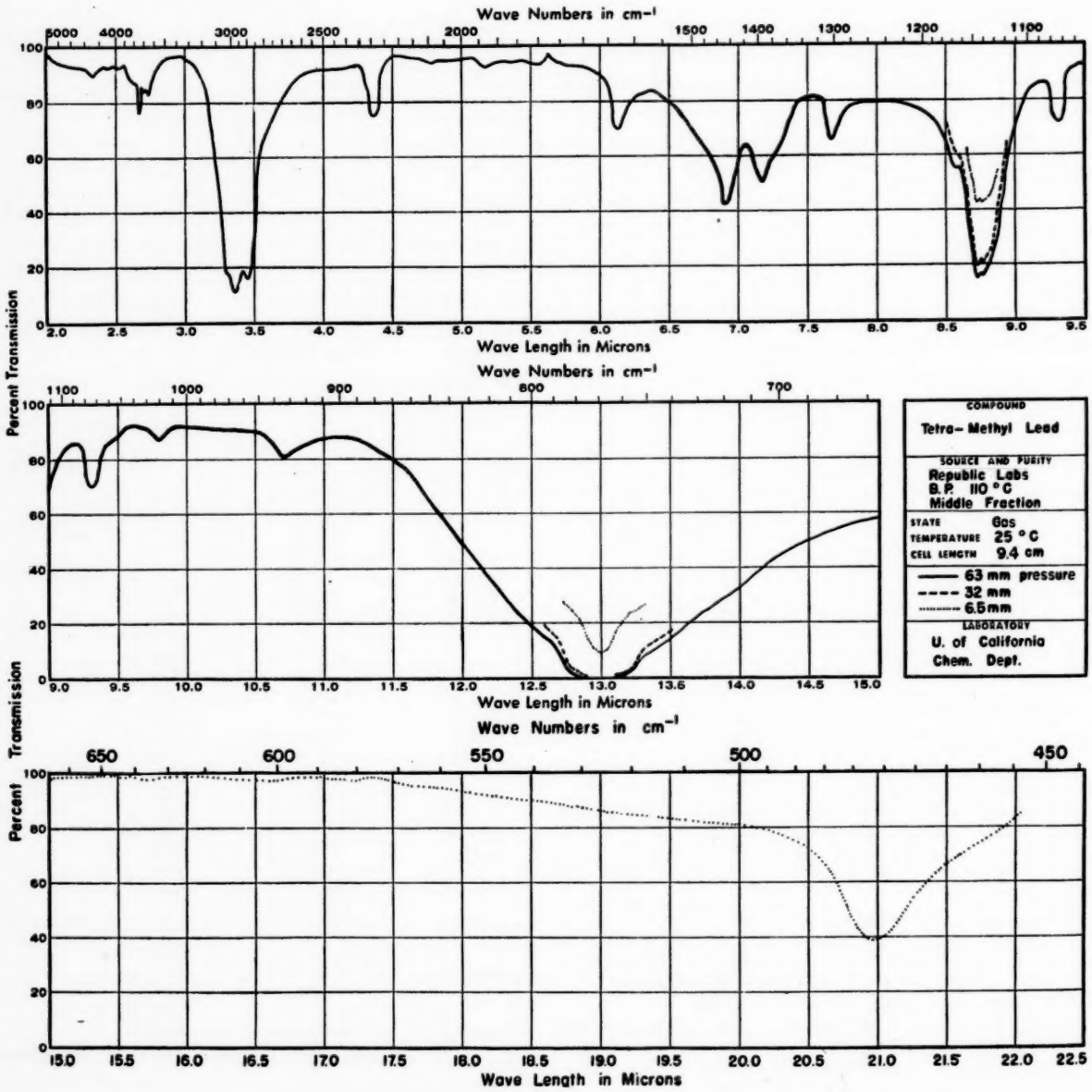

FIG. 1. Infra-red absorption of gaseous tetramethyl lead.

keeping with this assignment. Their designation as ν_1, ν_2, and ν_3 seems unambiguous since ν_1 and ν_2 are typical methyl stretching and deformations respectively whereas ν_3 is in the range expected for skeletal stretchings. Seven coincidences are expected in the Raman and infra-red spectra for F_2 vibrations. ν_{13} is undoubtedly the line at 2982 cm^{-1} as suggested by the partial resolution of its $\perp$ contour in the infra-red. ν_{14} is the line at 2910 cm^{-1}, the expected coincidence in the Raman being obscured by the strong A_1 vibration at 2918 cm^{-1}.

ν_{15} is assigned as 1453 cm^{-1} because it appears as such a strong band in the infra-red in spite of the fact that it does not appear in the Raman spectrum. The coincidence of a depolarized Raman line at 1155 cm^{-1} with an infra-red band of $\perp$ structure at 1147 cm^{-1} suggests strongly the assignment ν_{16} which agrees well with the assignment of ν_2 at 1170 cm^{-1}, since both are methyl symmetrical deformations. The coincidence at 769 and 767 cm^{-1} in the infra-red and Raman in the region of methyl rocking suggest 769 cm^{-1} as ν_{17}. ν_{18} is unambiguously 475 cm^{-1} since the value is in the expected skeletal stretching range and the KBr infra-red region of this research shows a strong band at 476 cm^{-1} in coincidence with a fairly strong depolarized band at 473 cm^{-1} in the Raman. This leaves the strong depolarized Raman band at 130 cm^{-1} to be the skeletal bending mode, ν_{19}.

There are left, then, 4 bands of symmetry type E, active and depolarized in the Raman, to be assigned. The CH_3 non-symmetrical stretching, ν_5, is assigned as 2999 cm^{-1}. ν_6 is assigned as 1453 cm^{-1}. Thus ν_6 lacks confirmation in the Raman. ν_7 is assigned as 767 cm^{-1}

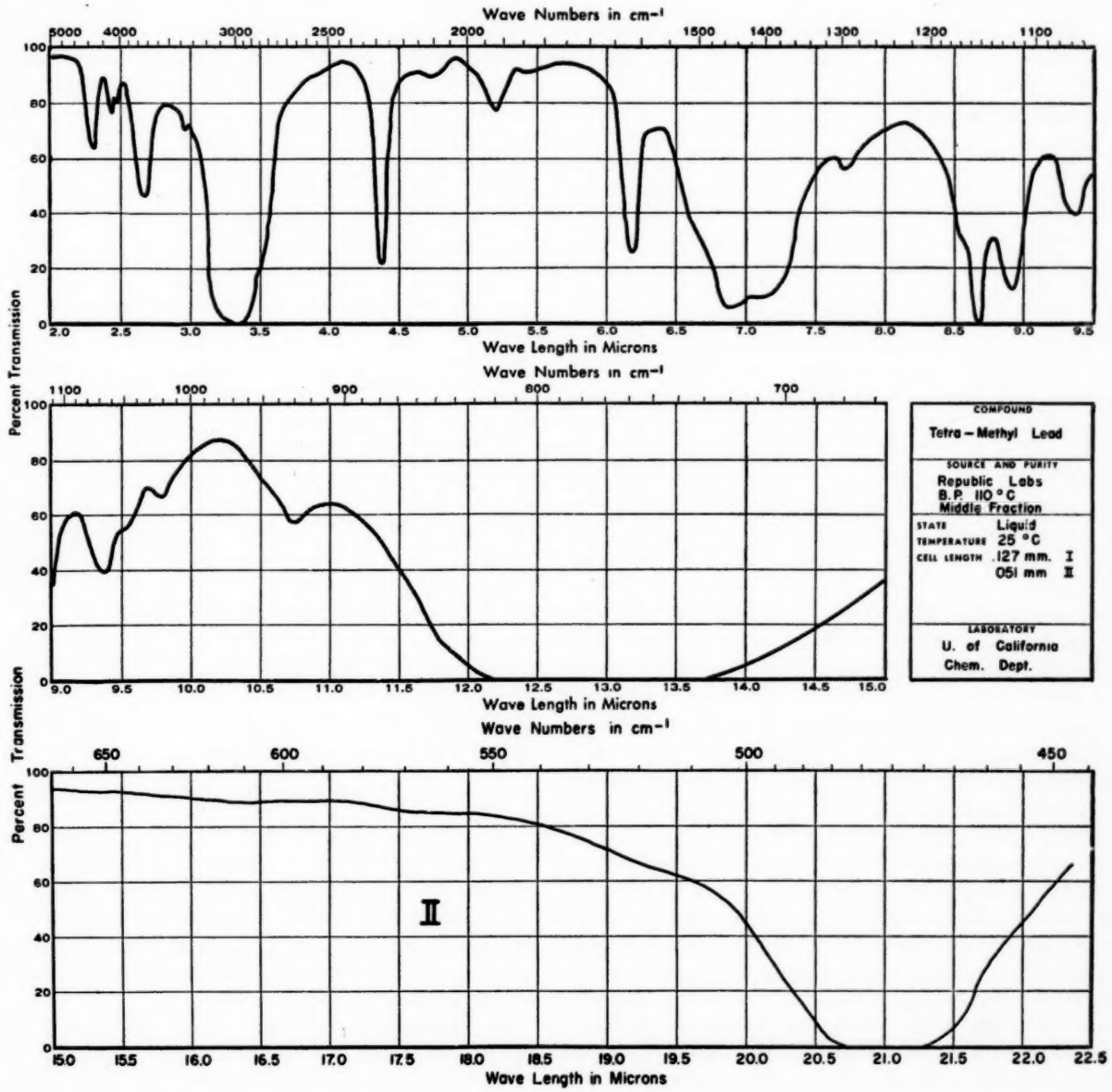

FIG. 2. Infra-red absorption of liquid tetra-methyl lead.

TABLE II. Observed frequencies, assignments, and calculated frequencies for combination bands in $Pb(CH_3)_4$.

Infra-red (gas and liquid) ν cm^{-1}	Raman (liquid)[a] $\Delta\nu$ cm^{-1}	Assignment	Species	Calculated frequency ν cm^{-1}
	(102)[a]	ν_8	E	
	130 s. (depol.)	ν_{19}	F_2	
	460 v.s. (pol.)	ν_3	A_1	
476 s. (gas)	473 m. (depol.)	ν_{18}	F_2	
	577 v.w.	$\nu_8+\nu_{18}$	F_1+F_2	575
769 v.s. (gas)	767 w.	ν_7, ν_{17}	E, F_2	
931 w.	930 v.w.	$\nu_3+\nu_{18}$	F_2	933
1022 w.		$\nu_{16}-\nu_{19}$	$A_1+E+F_1+F_2$	1022
1051 v.w.		$\nu_{16}-\nu_8$	F_1+F_2	1050
1067 m.		$\nu_3+\nu_{18}+\nu_{19}$	$A_1+E+F_1+F_2$	1063
1140, 1147, 1162 s. (gas)	1155 m. (depol.)	ν_{16}	F_2	
	1170 m. (pol.)	ν_2	A_1	
1296 m.		$\nu_2+\nu_{19}$	F_2	1300
1392 m. (gas)		$2\nu_3+\nu_{18}$	F_2	1393
1453 m. (gas)	(1453)[a]	ν_6, ν_{15}	E, F_2	
1618 m.		$\nu_{16}+\nu_{18}$	$A_1+E+F_1+F_2$	1625
1922 m.		$\nu_{16}+\nu_{17}$	$A_1+E+F_1+F_2$	1919
2108 v.w.		$2\nu_{18}+\nu_{16}$	$A_1+E+2F_1+3F_2$	2098
2290 m.	2292 w.	$2\nu_{16}$	A_1+E+F_2	2304
2910 s. (gas)	2918 s. (pol.)	ν_{14}, ν_1	F_2, A_1	
2982, 2992 s. (gas)	2999 s.	ν_{13}, ν_5	F_2, E	
3380 v.w.		$\nu_{14}+\nu_{18}$	$A_1+E+F_1+F_2$	3383
	3679 v.w.	$\nu_{14}+\nu_{17}$	$A_1+E+F_1+F_2$	3677
3770 w.	3755 v.w.	$\nu_{13}+\nu_{17}$	$A_1+E+F_1+F_2$	3749
4050 w.		$\nu_{14}+\nu_{16}$	$A_1+E+F_1+F_2$	4062
4100 w.		$\nu_2+\nu_{14}$	F_2	4080
4360 w.		$\nu_{14}+\nu_{15}$	$A_1+E+F_1+F_2$	4363

[a] These lines do not appear in the Raman.

the same as ν_{17}. Finally ν_8 is assigned as 102 cm^{-1} because as both Young, Koehler, and McKinney and Duncan and Murray have suggested, the depolarized line at 130 cm^{-1} appears as a broad line, and there is an indication that it is actually a super-position of two bands.[12] The value 102 cm^{-1} was chosen so as to obtain the best fit with combination bands. The inadequacy of the assignment of the type E vibrations suggests that a careful re-examination of the Raman spectrum of $Pb(CH_3)_4$ would be a valuable experiment. All other observed bands with the exception of the band observed in the liquid at 1122 cm^{-1} have readily been assigned as combinations or overtones. The 1067 cm^{-1} line seems too intense for a ternary combination band unless one supposes that it gains intensity by resonance with the ν_{16} fundamental. The calculated frequencies of these combinations and overtones agree well with the experimental values as listed in Table II. The assignment of the fundamentals is also listed in Table II.

The infra-red bands listed are those of the liquid except where resolution of the liquid is so poor that the gas is used. This is done so that comparison with the liquid Raman spectrum will be more valid. The band at 1122 cm^{-1} in the liquid is quite strong. It is interesting to note that it is not observed in the gas spectrum although other bands less intense in the liquid are observed in the gas. This, together with the fact that it is not readily assignable as a combination or overtone, leads one to suspect a liquid effect. In this regard it is to be observed from the spectra of the liquid and the gas that the entire contours of ν_{16} seem different in the liquid and in the gas. The fivefold concentration effect in the liquid does not produce the increase in absorption which is seen elsewhere in the spectrum. The change in band contour is not the usual liquid effect of narrowing the width of the over-all band. Since there is only one band in which this effect is observed, it would not appear to be a tendency toward association in the liquid which causes this band, but rather a liquid interaction with the specific symmetrical methyl deformation, ν_{16}. Except for the location of ν_{14} and the assignment of certain of the combination bands, this assignment agrees with the assignment of Young, Koehler, and McKinney. The substantiation of ν_{18} with the KBr infra-red was, however, gratifying.

CALCULATIONS AND APPLICATIONS

In order to ascertain the degree of approximation involved in considering methyl groups to be single masses, a normal coordinate treatment has been undertaken on the A_1 and E vibrations of $N^+(CH_3)_4$, $C(CH_3)_4$, $Si(CH_3)_4$, $Ge(CH_3)_4$, $Sn(CH_3)_4$ and $Pb(CH_3)_4$ and the force constants so derived are compared to those of a simple methane-like calculation.

In general the assignment of the A_1 and E frequencies of Young, Koehler, and McKinney[12] appears to be correct. However, the assignment of 1252 cm^{-1} and 1289 cm^{-1} as the CH_3 symmetrical deformation fre-

TABLE III.

Compound	Wave number of CH_3 symmetrical deformation
Ethane	1375 cm^{-1} (calculated)
Propane	1370
Butane	1374
Isobutane	1377
2,2 dimethyl butane	1376
Average	1374±2 cm^{-1}

quency, ν_2, of $C(CH_3)_4$ and $N^+(CH_3)_4$ respectively should be questioned. In case of neopentane it is not consistent with the other saturated hydrocarbons for which it is possible to find CH_3 symmetrical deformation assignments. They always occur in the 1360–1380 cm^{-1} range as will be seen from the following Table III: Accordingly the estimate of Pitzer and Kilpatrick[16] of 1360 cm^{-1} as the methyl deformation is used in these calculations. Very often the symmetrical deformation is too weak to be observed. This is true in the case of ethane where the value of 1375 cm^{-1} in Table III is inferred from combination bands. Therefore the fact that no band appears in the Raman spectrum of neopentane at 1360 cm^{-1} does not invalidate the assignment of Pitzer and Kilpatrick. For $N^+(CH_3)_4$ the band at 1418 cm^{-1} is chosen as the CH_3 symmetrical deformation, ν_2, rather than the band at 1289 cm^{-1}. This choice agrees with the general trend and has the advantage of being a weaker band than the fairly strong one at 1289 cm^{-1}. As explained in the previous paragraph, we expect the symmetrical deformation to be weak.

The frequencies used for the calculations are listed in Table IV. First a calculation was made assuming the CH_3 groups were single atoms of mass 15.0028. This calculation for a methane-like penta-atomic molecule give *C*-Central atom stretching force constants which are listed in the second column of Table V. Interaction force constants were neglected in computing the bending force constants which are listed in Table VI. In computing the force constants for the general $M(CH_3)_4$, 17-atom molecule, the methods developed by Wilson[17] were used to derive a secular equation for the A_1 vibrations. This equation can be shown to check the equation of Silver[10] who derived his equation by other methods. Then the secular determinantal equation of Silver for the E vibrations is used with certain modifications to determine the C−M bending force constants using values for the other force constants already derived from the A_1 secular equation.

The internal coordinates α, β, r, and R are defined as small displacements in the H−C−H or H−C−M, C−M−C bond angles and C−H and C−M bond distances. Symmetry coordinates, normalized, orthogonal, linear combinations of these internal coordinates transforming according to the appropriate irreducible representations of the Group T_d were obtained. The F and G matrices together with the determinantal and expanded secular equations for the A_1 symmetry group are given in Table VII.

TABLE IV. Frequencies used in calculating $M(CH_3)_4$ force constants.

Molecule	A_1 frequencies ν_1 (cm^{-1})	ν_2 (cm^{-1})	ν_3 (cm^{-1})	E frequencies ν_5 (cm^{-1})
$N^+(CH_3)_4$	2930	1418	752	372
$C(CH_3)_4$	2910	1360	733	335
$Si(CH_3)_4$	2919	1254	598	202
$Ge(CH_3)_4$	(2917)	(1244)	(540)	(110)
$Sn(CH_3)_4$	2915	1200	506	(103)
$Pb(CH_3)_4$	2918	1170	460	(102)

TABLE V. The approximate and exact stretching force constants and effective methyl masses for $M(CH_3)_4$ type molecules.

Molecule	Approximate force const. in 10^5 dynes/cm	Exact force const. in 10^5 dynes/cm	Effective methyl mass[a]
$N^+(CH_3)_4$	5.01	5.50	16.50
$C(CH_3)_4$	4.76	5.28	16.67
$Si(CH_3)_4$	3.17	3.38	16.04
$Ge(CH_3)_4$	(2.58)	(2.72)	15.83
$Sn(CH_3)_4$	2.27	2.37	15.71
$Pb(CH_3)_4$	1.87	1.94	15.56

[a] The effective methyl mass is the point mass which a methyl group must have to give the correct force constant.

The determinantal secular equation for E vibrations is that of Silver[10] except that the notation is changed to that used in the A_1 vibrations. Also the force constants for H−C−H and H−C−M are assumed equal so that both k_β and k_γ in the Silver notation become k_α in the new notation. With these changes the secular equation for the E vibrations is that given in Table VIII. In computing the numerical values of the G matrix tetrahedral bond angles were assumed for the H−C−H angles in the methyl groups as well as for the skeletal structures. Dumond and Cohen's 1947 Table of Fundamental Constants[18] were used. Isotopic masses were used where there is a single predominant isotope.

There are insufficient data to evaluate the interaction force constants explicitly. Therefore all off-diagonal elements in the F matrices have been disregarded. The force constants for the A_1 vibrations were determined by successive approximations, until the computed frequencies agreed with the observed values. By assuming that the H−C−H and the H−C−M bending force constants are equal, and by transferring f_α and f_d (see Table IX) from the A_1 secular equation, the fourth order E secular equation was reduced to a first order equation in the C−M bending force constant. It may thus be determined explicitly.

[16] K. S. Pitzer and J. E. Kilpatrick, Chem. Rev. **39**, 435 (1946).
[17] E. B. Wilson, Jr., J. Chem. Phys. **7**, 1047 (1939); J. Chem. Phys. **9**, 76 (1941).
[18] J. W. M. Dumond and E. R. Cohen, Rev. Mod. Phys. **20**, 82 (1948).

TABLE VI. The approximate and exact bending force constants and effective methyl masses for $M(CH_3)_4$ type molecules.

Molecule	Approximate force constant in 10^5 dynes/cm	Exact force constant in 10^5 dynes/cm	Effective methyl mass
$N^+(CH_3)_4$	0.408	0.503	18.53
$C(CH_3)_4$	0.331	0.400	18.16
$Si(CH_3)_4$	0.120	0.135	17.03
$Ge(CH_3)_4$	(0.0357)	(0.0394)	(16.60)
$Sn(CH_3)_4$	(0.0313)	(0.0343)	(16.47)
$Pb(CH_3)_4$	(0.0307)	(0.0334)	(16.35)

TABLE VII. Matrices and secular equations for A_1 vibrations in $M(CH_3)_4$ molecules. (The symbol μ indicates the reciprocal mass.)

F matrix

$$\begin{vmatrix} f_d & 0 & 0 \\ & d^2 f_\alpha & 0 \\ & & f_D \end{vmatrix}$$

G matrix

$$\begin{vmatrix} \mu_H+\frac{\mu_C}{3} & -\frac{4\mu_C}{3d} & -\frac{\sqrt{3}\mu_C}{3} \\ & \frac{2\mu_H}{d^2}+\frac{16\mu_C}{3d^2} & \frac{4\sqrt{3}\mu_C}{3d} \\ & & \mu_C \end{vmatrix}$$

Secular Equation:

$$\begin{vmatrix} f_d\left(\mu_H+\frac{\mu_C}{3}-\lambda\right) & -\frac{4}{3}f_d\frac{\mu_C}{d} & -\frac{\sqrt{3}}{3}f_d\mu_C \\ -\frac{4d}{3}f_\alpha\mu_C & 2f_\alpha\mu_H+\frac{16}{3}f_\alpha\mu_C-\lambda & \frac{4\sqrt{3}}{3}df_\alpha\mu_C \\ -\frac{\sqrt{3}}{3}f_D\mu_C & \frac{4\sqrt{3}}{3}f_D\frac{\mu_C}{d} & f_D\mu_C-\lambda \end{vmatrix}=0$$

Simplified expanded Secular Equation:

$$\lambda^3-\left(f_d\left[\frac{\mu_C}{3}+\mu_H\right]+f_D\mu_C+f_\alpha\left[\frac{16}{3}\mu_C+2\mu_H\right]\right)\lambda^2$$
$$+\left(f_\alpha f_D\mu_C\mu_H+f_d f_\alpha\left[2\mu^2{}_H+\frac{18}{3}\mu_H\mu_C\right]+2f_\alpha f_D\mu_H\mu_C\right)\lambda$$
$$-2f_d f_\alpha f_D\mu^2{}_H\mu_C=0$$

Three of these molecules $N^+(CH_3)_4$, $C(CH_3)_4$ and $Si(CH_3)_4$ have been treated earlier. Comparison of the force constants of Wall and Eddy,[9] and those of Silver[10] with those of this research is made in Table X.

DISCUSSION

The differences between the force constants of Wall and Eddy and those of Silver may be attributed entirely to differences in assignment. However, the differences between these two investigations and the present research must be attributed not only to differences in assignment, but also to the fact that these authors assumed constant C−H bending and stretching force constants, the force constants of Crawford and Brinkley,[19] whereas we have evaluated all constants from the data. Interaction constants would be required if a constant C−H bending force constant were to hold. Both the frequencies and the calculated force constants of this research indicate a definite trend to lower values as the size of the central atom increases and the distance between the central atom and the carbon atom increases. This trend is indicative of the lessening of interaction between the hydrogen bendings and the M−C stretching frequencies as the stretching force constants and vibrational frequencies lessen. As the frequencies and interactions decrease, the effective methyl mass should decrease, finally approaching the normal methyl mass of 15.028 grams. This is exactly the trend observed in Tables V and VI.

The correlation of bond force constants with atomic parameters such as bond distance, electronegativity of the atoms associated in the bond and bond order requires a considerable range of data to test the relationships which have been proposed. The values for the various M−C stretching force constants calculated

[19] B. L. Crawford, Jr. and S. R. Brinkley, Jr., J. Chem. Phys. 9, 71 (1941).

TABLE VIII. Secular equation for *E* vibrations in $M(CH_3)_4$ molecules.

$$\begin{vmatrix} a-M\lambda & e & f & g \\ e & b-m\lambda & h & j \\ f & h & c-m\lambda & k \\ g & j & k & d-m\lambda \end{vmatrix}=0$$

where M = carbon mass, m = hydrogen mass, $r_0 = C-H$ distance, $R_0 = M-C$ distance, and

$$a=3f_\beta+\frac{4}{3}f_d+f_\alpha\left(\frac{17}{6}+\frac{r_0}{R_0}+\frac{3}{2}\frac{r_0^2}{R_0^2}\right)$$
$$b=\frac{4}{9}f_d+\frac{17}{18}f_\alpha$$
$$c=\frac{1}{9}f_d+\frac{10}{9}f_\alpha$$
$$d=\frac{4}{9}f_d+\frac{13}{9}f_\alpha$$
$$e=-\frac{4}{3\sqrt{3}}f_d-\frac{f_\alpha}{\sqrt{3}}\left(\frac{17}{6}+\frac{r_0}{2R_0}\right)$$
$$f=\frac{2}{3\sqrt{3}}f_d+\frac{4}{\sqrt{3}}f_\alpha\left(\frac{1}{6}-\frac{r_0}{2R_0}\right)$$
$$g=\frac{4}{3\sqrt{3}}f_d+\frac{f_\alpha}{\sqrt{3}}\left(\frac{19}{6}-\frac{r_0}{2R_0}\right)$$
$$h=-\frac{2}{9}(f_d+f_\alpha)$$
$$j=\frac{4}{9}f_d-\frac{19}{18}f_\alpha$$
$$k=-\frac{2}{9}f_d+\frac{7}{9}f_\alpha$$

TABLE IX. Numerical values used in solving A_1 and *E* secular equations.

Molecule	M−C Distance, R_0	C−M Distance, r_0	Mass M_m	$f_d\times10^5$ (dynes/cm) from A_1 vib.	$f_\alpha\times10^5$ (dynes/cm) from A_1 vib.
$N^+(CH_3)_4$	1.47	1.093	14.007	4.887	0.4423
$C(CH_3)_4$	1.55	1.093	12.004	4.836	0.4024
$Si(CH_3)_4$	1.93	1.093	27.987	4.867	0.3551
$Ge(CH_3)_4$	1.98	1.093	72.6	4.865	0.3551
$Sn(CH_3)_4$	2.18	1.093	118.70	4.860	0.3316
$Pb(CH_3)_4$	2.29	1.093	207.21	4.870	0.3180
		Hydrogen mass = 1.0081			
		Carbon mass = 12.0038			

TABLE X. Comparison of the force constants of $M(CH_3)_4$ molecules by various investigators.

Investigators		Molecules		
		$N^+(CH_3)_4$	$C(CH_3)_4$	$Si(CH_3)_4$
Silver	f_d 10^5 dynes/cm	(4.76)	(4.76)	(4.76)
	f_α 10^5 dynes/cm	(0.468)	(0.468)	(0.468)
	f_D 10^5 dynes/cm	5.51	5.20	3.31
	f_β 10^5 dynes/cm	0.501	0.399	0.137
Wall and Eddy	f_d 10^5 dynes/cm		(4.76)	(4.76)
	f_α 10^5 dynes/cm		(0.468)	(0.468)
	f_D 10^5 dynes/cm		4.71	3.14
This research	f_d 10^5 dynes/cm	4.887	4.836	4.867
	f_α 10^5 dynes/cm	0.4423	0.4024	0.3551
	f_D 10^5 dynes/cm	5.50	5.28	3.38
	f_β 10^5 dynes/cm	0.503	0.400	0.135

TABLE XI. Atomic parameters used in calculating the force constants by the rules of Gordy and Badger.

	Gordy's parameters			Badger's parameters	
Molecules	χ_A	χ_B	d	d_{ij}	$c_{ij}\times10^5$
$N^+(CH_3)_4$	3.29[a]	2.55	1.47	0.68	1.86
$C(CH_3)_4$	2.55	2.55	1.55	0.68	1.86
$Si(CH_3)_4$	1.8	2.55	1.93	0.94	1.53
$Ge(CH_3)_4$	1.7	2.55	1.98	1.06	1.25
$Sn(CH_3)_4$	1.7	2.55	2.18	1.18	1.176
$Pb(CH_3)_4$	1.5	2.55	2.29	1.26	1.176

[a] By rule of Pauling which states that a unit positive formal charge increases the electronegativity of an atom by about ½ of the distance to the next atom to the right in the periodic table.

TABLE XII. Comparison of calculated and experimental force constants.

Molecule	Calc. f_D Badger's rule 10^5 dynes/cm	Calc. f_D Gordy's rule 10^5 dynes/cm	Obs. f_D 10^5 dynes/cm
$N^+(CH_3)_4$	3.77	8.69	5.50
$C(CH_3)_4$	2.83	4.81	5.28
$Si(CH_3)_4$	1.58	3.44	3.38
$Ge(CH_3)_4$	1.57	3.16	(2.72)
$Sn(CH_3)_4$	1.18	2.67	2.37
$Pb(CH_3)_4$	1.08	2.20	1.94

in this research are useful in this connection. The most prominent relationships between force constants and atomic parameters are those of Badger[13,14] and Gordy.[15] Badger's relationship expresses the force constant as follows:

$$k_0=\frac{C_{ij}}{(d-d_{ij})^3}, \tag{1}$$

where

k_0 = stretching force constant in dynes/cm,
d = interatomic distance in A, and
C_{ij} and d_{ij} = constant depending on the row in the periodic table in which the bonded atoms occur (see Table X).

Gordy's semi-empirical formula appears to have a somewhat wider range of applicability. The stretching force constant in 10^5 dynes/cm is given by:

$$k=aN\left(\frac{\chi_A\chi_B}{d^2}\right)^{\frac{3}{4}}+b, \tag{2}$$

where a and b are empirical constants having the values $+3.29$ and -0.40 respectively for tetrahedral molecules except neopentane in which case a and b are $+2.94$ and -1.40, respectively. N is the bond order and χ_A and χ_B are the electronegativities of the bonded atoms and d the bond distance in angstroms. The bond order is assumed to be 1.0 in all the cases with which we will deal. This assumption in the case of $N^+(CH_3)_4$ is justified by the fact that the electronegativities of the bonded atoms are not widely different so that "no bond" mesomeric forms of zero bond order do not contribute very much to the bond character. The other atomic parameters used in the calculations according to the relations proposed by Badger and Gordy are listed in Table XI. The values of the stretching force constants as obtained by the rules of Badger and Gordy (Eqs. 1 and 2) are compared with the experimental values in Table XII.

The values computed by Badger's Rule are consistently low whereas those computed by Gordy's Rule are consistently high, except in the case of neopentane which was treated with different constants. Although the agreement of Gordy is decidedly better that that of Badger, the fit between experimental and predicted force constants still leaves much to be desired. The extremely high value which obtains from Gordy's Rule for $N^+(CH_3)_4$ might be avoided by a different correction of electronegativity for formal charge.

If the electronegativity of carbon is assumed to be 2.55 [20] and the experimental force constants are used in Gordy's Rule (Eq. 2), the electronegativities of Si, Ge, Sn, and Pb are 1.76, 1.40, 1.37, and 1.13 respectively. These compare with the values of Gordy of 1.80, 1.70, 1.70, and 1.50.

[20] W. Gordy, Phys. Rev. **69**, 604 (1946).

II. The Effective Methyl Mass and Its Use in Determining the Force Constants and Character of Metallo-Organic Bonds*

RAYMOND K. SHELINE**
Department of Chemistry, University of California, Berkeley, California
(Received September 28, 1949)

The "effective methyl masses" of the Group IV tetramethyl derivatives and the analogous tetramethyl ammonium ion are shown to give a linear relationship when plotted against their respective stretching and bending frequencies. The linear relationships are used to determine "effective methyl masses" from Group V trimethyl stretching and bending frequencies and from some Group VI dimethyl stretching frequencies. Then the "effective methyl masses" so determined are used in simplified calculations to predict stretching and bending force constants for Groups V and VI methyl derivatives. This procedure is shown to give stretching force constants for dimethyl mercury and dimethyl zinc which are in good agreement with those obtained by Gutowsky on the basis of a less approximate normal coordinate treatment, the average deviation being 1 percent. Finally this large number of new metallo-organic force constants is summarized with existing metallo-organic force constants and the nature of the metallo-organic bond is discussed.

INTRODUCTION

As normal coordinate treatments are undertaken on ever more complex molecules, the need for approximation methods, knowledge of their realm of application and their refinement becomes increasingly necessary. This need is particularly evident in the development of accurate metallo-organic force constants because the average simple metallo-organic molecule is anywhere from a nine-atom to a seventeen-atom system. In spite of the simplifications which Wilson introduced into normal coordinate analysis, calculations on these metallo-organic compounds become prohibitively difficult to do for large numbers of molecules without the aid of an electronic or mechanical secular equation computer.

In all molecular vibrational treatments there are some approximations; therefore it has been natural for numerous investigators[1–3] to consider a recurring group of atoms, like a methyl group, a single rigid sphere. The expediency of such an approximation on any particular molecule will depend on the degree of approximation which is introduced in comparison to the approximations and labor necessary to carry out a complete normal coordinate analysis.

PROCEDURE

In order to ascertain the degree of approximation involved in considering methyl groups as single masses and with the hope of being able to correct for this approximation in certain types of molecules, the force constants derived from a normal coordinate analysis of the A, and E vibrations of $N^+(CH_3)_4$, $C(CH_3)_4$, $Si(CH_3)_4$, $Ge(CH_3)_4$, $Sn(CH_3)_4$ and $Pb(CH_3)_4$ were used in the preceding article in simplified calculations to determine the magnitude of methyl masses assuming they were point masses. The numerical values of these masses were defined as "effective methyl masses." When the effective methyl masses are plotted against their respective stretching and bending frequencies, a linear relationship obtains. This plot is shown in Figs. 1 and 2. These figures indicate that the C—H interaction is a continuous function of the C—M stretching and bending frequencies.

The continuity of the points in Figs. 1 and 2 indicates that it might be possible to use these figures with the appropriate stretching and bending frequencies to determine an effective methyl mass which in turn could be used in a simplified calculation (methyl group considered a single rigid sphere) to get an accurate force constant. Accordingly algebraic expressions relating the effective methyl mass and their respective stretching and bending frequencies have been derived; they are:

$$M_{(CH_3\,Eff.)} = 0.003574\nu(\text{cm}^{-1}) + 13.916$$
(for stretching modes in the region 450–850 cm^{-1}), (1)

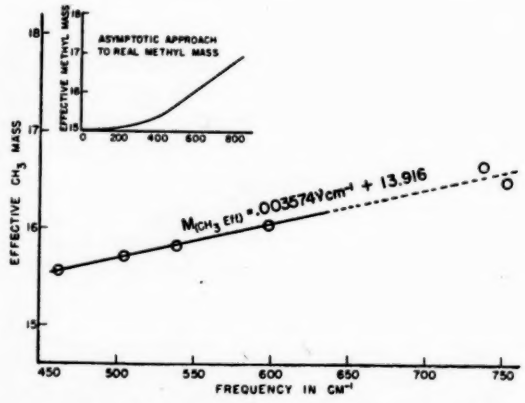
ASYMPTOTIC APPROACH TO REAL METHYL MASS
EFFECTIVE METHYL MASS
EFFECTIVE CH3 MASS
FREQUENCY IN CM-1
M(CH3 Eff) = .003574ν cm-1 + 13.916

FIG. 1. The effective methyl mass *versus* the stretching frequency.

* Based on a thesis submitted by Raymond K. Sheline in partial fulfillment of the requirements for the Ph.D. degree at the University of California. This research was facilitated by support extended the University of California by the Navy Department, ONR, under N7 ONR-295, Task Order X as Project No. NR-058-097.

** Present address: Institute for Nuclear Studies, University of Chicago, Chicago, Illinois.

[1] F. T. Wall and C. R. Eddy, J. Chem. Phys. **6**, 107 (1938).
[2] F. T. Wall, J. Am. Chem. Soc. **60**, 71 (1938).
[3] K. S. Pitzer, J. Chem. Phys. **8**, 711 (1940).

TABLE I.[a] Force constants of $Hg(CH_3)_2$ and $Zn(CH_3)_2$ accurately and by approximation.

	$Hg(CH_3)_2$		$Zn(CH_3)_2$	
Numerical values	stretching	bending	stretching	bending
Frequency (cm^{-1})	515	156	504	144
Effective methyl mass	15.756	16.658	15.717	16.556
Central atom mass	200.61		65.38	
Method	stretching force Const. in 10^5 dynes/cm	bending force Const. in 10^5 dynes/cm	stretching force Const. in 10^5 dynes/cm	bending force Const. in 10^5 dynes/cm
Normal coordinate analysis (Gutowsky)	2.45	0.0944	2.39	0.0657
Approximation using effective methyl mass	2.461	0.102	2.352	0.0671
Approximation using normal methyl mass 15.028	2.348	0.0936	2.249	0.0629

[a] Since this manuscript was completed, H. S. Gutowsky, J. Am. Chem. Soc. **71**, 3194 (1949) has reported the force constants of dimethyl cadmium. Cd--C stretching and bending are 2.05×10^5 and 0.0796×10^5 dynes/cm respectively. Using an effective methyl mass for stretching and bending of 15.578 and 16.607 respectively, force constants of 1.983×10^5 and 0.0849×10^5 dynes/cm are obtained. Using a methyl mass of 15.00, 1.910×10^5 and 0.0784×10^5 dynes/cm are obtained.

and

$$M_{(CH_3Eff.)}=0.008526\nu(cm^{-1})+15.328$$

(for bending modes in the region 100–400 cm^{-1}).

Both the idea and the practical use of effective methyl masses are essentially empirical. Therefore, although the concept is useful in practical calculations, it is unwise to attach undue physical significance to it. However, certain considerations are justified. From the slopes of the lines in Figs. 1 and 2, it is observed that the rate of change of effective methyl mass with change in frequency is much greater in the case of C−M bending vibrations than in the case of C−M stretchings. This is equivalent to concluding that the sum of the rate of change of moment of inertia with respect to C−M distance and the rate of change of interaction of C−H vibrations with C−M vibrations is greater in the case of bendings than in stretchings. It is substantiated by simple mechanical considerations and by the fact that the ratio of bending interaction force constants to bending force constants is generally much greater than the ratio of stretching interaction force constants to stretching force constants. Indeed the necessity of neglecting bending interaction force constants which are not negligible accounts to a large extent for the much greater unreliability of bending force constants. It is to be further noted that in the region 450–850 cm^{-1} for stretching vibrations and in the region 100–400 cm^{-1} for bending vibrations the straight line relationship means that the rate of change of interaction is approximately equal to the rate of change of the decrease of frequency.

In order to test the use of the effective methyl mass in determining force constants, a search, for fairly simple methyl derivatives on which normal coordinate analyses were available, was undertaken. This search yielded only the dimethyl derivatives of mercury and zinc.[4] Data were available on the skeletal normal coordinate analysis of all the trimethyl derivatives of the Group V[5] elements and on the dimethyl derivatives of oxygen, sulfur, and selenium. Therefore, it was decided to test the approximation on dimethyl mercury and dimethyl zinc and on the basis of this limited knowledge of the realm of applicability to predict those force constants of the Groups V and VI methyls for which there appears to be a reasonable chance for success. Confirmation of the success or failure of this approximation of the Groups V and VI methyl derivatives must await a complete assignment and normal coordinate analysis which is at the present beyond the scope of this work.

CALCULATIONS, FORCE CONSTANTS, AND DISCUSSION

1. Dimethyl Mercury and Dimethyl Zinc,

Gutowsky[4] has recently summarized the available infra-red and Raman data on dimethyl mercury and dimethyl zinc, completed the necessary molecular spectra to make possible a complete assignment and executed a complete normal coordinate analysis on these compounds. The C−M−C skeletons of both dimethyl mercury and dimethyl zinc are shown to be linear.

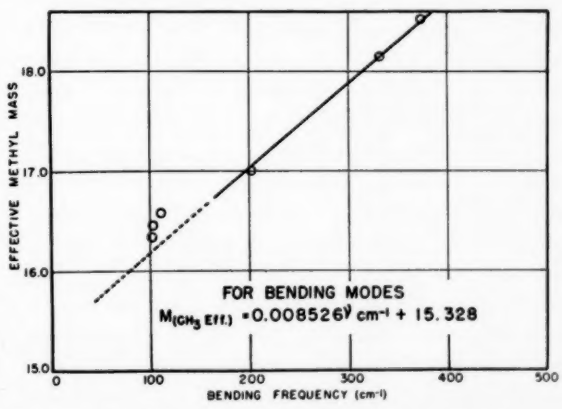

FIG. 2. The effective methyl mass *versus* the bending frequency.

[4] H. S. Gutowsky, J. Chem. Phys. **17**, 128 (1949).

[5] Rosenbaum, Rubin, and Sandburg, J. Chem. Phys. **8**, 366 (1940).

TABLE II. Force constants for Group V trimethyl molecules.

	Molecule				
	$N(CH_3)_3$	$P(CH_3)_3$	$As(CH_3)_3$	$Sb(CH_3)_3$	$Bi(CH_3)_3$
Stretching force const. in 10^5 dynes/cm (Rosenbaum *et al.*)	3.97	2.78	2.44	2.09	1.75
Bending force const. in 10^5 dynes/cm (Rosenbaum *et al.*	0.382	0.214	0.182	0.136	0.119
Stretching force const. in 10^5 dynes/cm (this research)	4.25	2.93	2.57	2.19	1.82
Bending force const. in 10^5 dynes/cm (this research)	0.427	0.240	0.201	0.152	0.132
Observed ν_3 (cm^{-1})	1036	708	583	513	460
Observed ν_4 (cm^{-1})	423	305	239	188	171
Calculated (Rosenbaum) ν_3 (cm^{-1})	1078	710	584	517	454
Calculated (Rosenbaum) ν_4 (cm^{-1})	380	256	220	185	170
Calculated (this research) ν_3 (cm^{-1})	1091	711	583	519	462
Calculated (this research) ν_4 (cm^{-1})	368	250	216	185	169

Therefore, if the methyl groups are assumed to be single rigid spheres, these nine-atom molecules become linear triatomic CO_2-like molecules. Using the stretching and bending frequencies assigned by Gutowsky to calculate effective methyl masses for stretching and bending and then using these masses in a simple CO_2 calculation the stretching and bending force constants are derived. They are compared in Table I with the stretching and bending force constants obtained by assuming a simple CO_2 type molecule with mass 15.028 for the methyl groups. In Table I are included also the various numerical values of the molecular constants used in the calculation.

The agreement of the effective methyl mass approximation with normal coordinate analysis in the case of stretching force constants is striking and is probably within the experimental accuracy of the spectra. The mean deviation is 1.0 percent whereas Gutowsky has a root mean square deviation of 1 percent on his calculated frequencies. It should be noted that both in the work of Gutowsky and in this research the interaction force constant, f_{dd}, has been neglected in computing the stretching force constant.

The agreement of bending force constants is not so good. In each case the effective methyl mass approximation gives bending force constants which are too high, whereas the normal methyl mass gives approximations which are too low. This relationship is easy to understand. The normal methyl mass does not take into account interactions within the methyl groups which affect the skeletal bending whereas the effective methyl mass approximation includes not only this effect but also methyl-methyl repulsion in an arrangement in which the angle between methyls was tetrahedral. Since in linear dimethyl mercury and dimethyl zinc there should be little methyl-methyl repulsion, it is not surprising that the calculation on the basis of tetrahedral methyl-methyl repulsion gives too high a bending force constant for dimethyl molecules.

Accordingly, we may conclude from the data on dimethyl mercury and dimethyl zinc that the effective methyl mass approximation is a good approximation for totally symmetric stretching force constants and that the shape of the molecule especially when it determines methyl-methyl repulsion is an important consideration in applying the effective methyl mass to bending force constants.

TABLE III. Molecular constants of some Group VI dimethyl molecules.

Constants	Molecules		
	$CH_3-Se-CH_3$	CH_3-S-CH_3	CH_3-O-CH_3
B_2 frequency (cm^{-1})	1098	742	602
Angle between methyl groups (degrees)	116	105	99
Effective Me mass	17.840	16.568	16.067
Kohlrausch's stretching force const. (Methyl mass 15)$\times 10^5$ dynes/cm	2.59	3.05	4.53
Stretching force const. (this research) $\times 10^5$ dynes/cm	2.78	3.25	4.87

2. The Trimethyl Derivatives of N, P, As, Sb, and Bi

Rosenbaum, Rubin, and Sandburg[5] reviewed and summarized the available molecular spectra on the trimethyl Group V compounds. After completing the necessary spectra to give comprehensive enough data to make skeletal assignments for each of these molecules, they used the formulas of Kohlrausch[6] to determine bending and stretching force constants for the A_1 frequencies assuming ammonia-like structures and single atom methyl masses of 15. Then they used the force constants calculated to compute the $2E$ frequencies. Their agreement was excellent considering the approximations involved. Since the angles between the methyl groups in all of the trimethyl Group V molecules is approximately tetrahedral, it seemed probable that it would be possible using effective methyl masses to derive both stretching and bending force constants which are more accurate than those of Rosenbaum *et al.*

In computing the force constants for the MR_3 molecule the methods developed by Wilson were used to derive secular equations for the A_1 and E vibrations using a pure valence force potential function with no cross terms. These equations can be shown to check the equations of Kohlrausch. The composite chemical atomic weight was used for Sb whereas the rest are physical atomic weights of the 1942 International Committee on Atomic Weights.

The bending and stretching force constants of Rosenbaum *et al.* are compared with those of this research in Table II. Table II also shows the results of the calculation of the E vibrations by transferring force con-

[6] K. W. F. Kohlrausch, Der Smekal-Raman-Effekt (1939), p. 70.

stants and effective methyl masses from the A_1 secular equation by both the methods of Rosenbaum and this research.

The calculation approximation based on a methyl mass of 15.0 gives better agreement for the E frequencies than the effective methyl mass approximation of this research. This may indicate that the effective methyl mass approximation is not good for vibrations of other than class A (symmetric vibrations).

3. Dimethyl Oxygen, Sulfur and Selenium

Use of the effective methyl mass to predict the stretching force constants in dimethyl ether, dimethyl sulfide, and dimethyl selenide is also indicated. The skeletal structure of these molecules has definitely been established as a non-linear three-atom symmetric chain. Since the methyl-methyl repulsion would be expected to be very different in these molecules from the methyl-methyl repulsion in the tetramethyl molecules from which the effective methyl masses for bending were derived, it does not seem advisable to predict bending force constants. The molecular constants of these molecules are listed in Table III along with the stretching force constants (based on a methyl mass of 15.0) and the force constants of this research (using effective methyl masses).

Recently, D. W. Scott[7] has made a somewhat more complete calculation on dimethyl sulfide in which the force constants for the carbon-hydrogen stretching and methyl bending were set equal to infinity. These coordinates were then factored out of the secular equation by Wilson's method. His value for the stretching force constant was 3.13×10^5 dynes/cm.

In summary the effective methyl mass has been shown to apply to A_1 vibrations where the central atom is at the center of mass and therefore acts like an infinite mass. The shape of the molecule in determining methyl-methyl repulsion is shown to be an important consideration in determining bending force constants. In the case of bending force constants, it is probable that only methyl derivatives in which the methyls are separated by approximately tetrahedral angles are susceptible to this approximation. Finally, the stretching and bending force constants of all the Group V trimethyl molecules and the stretching force constants of dimethyl ether, dimethyl sulfide, and dimethyl selenide are predicted. The validity of the use of the effective methyl masses to calculate these force constants must await a more accurate normal coordinate analysis of these molecules.

FORCE CONSTANTS AND CHARACTER OF METALLO-ORGANIC BONDS

Table IV lists the known metallo-organic force constants together with the force constants derived in the preceding article and those derived in this article using the effective methyl mass. Some molecules are listed in this table which are not metallo-organic for the purpose of considering vertical periodic table trends and molecular shape effects. The stretching and bending force constants for the Ni—C bond are from the data of Crawford and Cross[8] on $Ni(CO)_4$. The ratio of stretching and bending force constants and the bond electronegativity (i.e., the difference in electronegativity between the metal atom and the carbon atom) also are included in the table. The electronegativity differences are calculated from the values of Gordy.

TABLE IV.[a] Atomic parameters and force constants for metallo-organic compounds.

Molecule	Bonds	f_{st}[b]	f_B[c]	$\frac{f_{st}}{f_B}$	Bond electronegativity $x_M - x_C$
$N^+(CH_3)_4$	N^+—C	5.50	0.408	13.48	0.75
$C(CH_3)_4$	C—C	5.28	0.331	15.95	0.00
$Si(CH_3)_4$	Si—C	3.38	0.120	28.16	−0.75
$Ge(CH_3)_4$	Ge—C	2.72	(0.0357)	(76.19)	−0.85
$Sn(CH_3)_4$	Sn—C	2.37	(0.0313)	(75.72)	−0.85
$Pb(CH_3)_4$	Pb—C	1.94	(0.0307)	(63.19)	−1.05
$N(CH_3)_3$	N—C	4.25	0.427	9.95	0.43
$P(CH_3)_3$	P—C	2.93	0.240	12.21	−0.45
$As(CH_3)_3$	As—C	2.57	0.201	12.79	−0.55
$Sb(CH_3)_3$	Sb—C	2.19	0.152	14.41	−0.75
$Bi(CH_3)_3$	Bi—C	1.82	0.132	13.79	−0.75
$Ni(CO)_4$	Ni—C	2.52	0.089	28.31	
$Zn(CH_3)_2$	Zn—C	2.39	0.0657	36.38	−1.35(?)
$Hg(CH_3)_2$	Hg—C	2.45	0.0944	25.75	−1.55(?)
$O(CH_3)_2$	O—C	4.87			
$S(CH_3)_2$	S—C	3.25			
$Se(CH_3)_2$	Se—C	2.78			
$Al_2(CH_3)_6$	Al—C	2.91			
$Fe(CO)_5$	Fe—C	3.36			

[a] Since this manuscript was completed, H. S. Gutowsky, J. Am. Chem. Soc. **71**, 3194 (1949) has reported the force constants of dimethyl cadmium as $f_{st}=2.05\times10^5$ dynes/cm and $f_B=0.0796\times10^5$ dynes/cm. Therefore f_{st}/f_B is 25.75.
[b] f_{st} = stretching force constant in units of 10^5 dynes/cm.
[c] f_B = bending force constant in units of 10^5 dynes/cm.

1. Numerical Values of the Force Constants

The accuracy of the tetramethyl Group IV, dimethyl mercury, dimethyl zinc, and $Ni(CO)_4$ stretching and bending force constants is in general probably good. The accuracy of the trimethyl Group V and dimethyl Group VI force constants must be tested by a more complete normal coordinate analysis to determine its accuracy, whereas the Al—C and Fe—C stretching force constants are only approximate force constants.

2. Degree of Covalent Character in Metallo-Organic Bonds

Smyth[9] in a summary of dipole measurements on metallo-organic molecules concludes that metallo-organic bonds are essentially covalent. He draws this conclusion because it leads to the fact that the bonds connecting the metal atoms to halogens in halogen containing metallo-organic molecules are as ionic in char-

[7] D. W. Scott, Petroleum Experimental Station, Bartlesville, Oklahoma (private communication).

[8] B. L. Crawford, Jr. and P. C. Cross, J. Chem. Phys. **6**, 523 (1938).

[9] C. P. Smyth, J. Org. Chem. **6**, 421 (1941).

TABLE V. Distances between methyl groups.

Molecule	M—C dist.	α	r	r^3
$N^+(CH_3)_4$	1.45	109°28′	2.368	13.28
$C(CH_3)_4$	1.54	109°28′	2.515	15.91
$Si(CH_3)_4$	1.93	109°28′	3.152	31.32
$Ge(CH_3)_4$	1.98	109°28′	3.233	33.79
$Sn(CH_3)_4$	2.18	109°28′	3.560	45.12
$Pb(CH_3)_4$	2.29	109°28′	3.740	52.32
$N(CH_3)_3$	1.47	108°	2.378	13.45
$P(CH_3)_3$	1.87	100	2.865	23.52
$As(CH_3)_3$	1.98	96	2.942	25.46
$Sb(CH_3)_3$	2.13	94½	3.129	30.63
$Bi(CH_3)_3$	2.23	93	3.234	33.82

M—C Dist. = M—C distance in angstrom units.
α = angle between bonds (degrees).
r = distance between methyl groups in angstrom units.

acter as the bonds in some typical salt molecules. For the purpose of learning something about the degree of covalent character in metallo-organic bonding the ratio of stretching to bending force constants was determined. Ionic bonding is central force bonding, whereas covalent bonding is directed valence force bonding. Therefore, if repulsion between like atoms or radicals in different molecules is kept constant, the ratio of stretching to bending force constants would provide a quantitative measure of the amount of ionic character in a bond. The ideal of constant repulsion between like atoms or radicals in different molecules is of course unattainable. However, the ratio of stretching to bending force constants should still provide a qualitative measure of the ionic character in a bond. Table IV indicates that the ionic character of the metallo-organic bond varies over a considerable range, and that it varies in most cases qualitatively as the electronegativity difference on the atoms which make up the bond. It would appear from Table IV that the ratio of stretching to bending force constants in the Zn—C and Hg—C bonds does not agree with the bond electronegativities. However, as Gutowsky has already pointed out, Gordy's values for the electronegativities of Zn and Hg are not in agreement with Haissinsky,[10] the magnitude of the electronegativities being reversed. This reversal of magnitude is to be anticipated if the bond electronegativities and the ratio of stretching to bending force constants are to agree qualitatively for $Hg(CH_3)_2$ and $Zn(CH_3)_2$.

There is considerable ionic character in some metallo-organic bonds as is indicated by the extremely intense infra-red absorption bands observed in the spectra of $Fe(CO)_5$ and $Al_2(CH_3)_6$ and assigned as Fe—C and Al—C stretchings. The intensity of these bands indicates a large dipole moment in the metal-carbon bond.

Since our measure of the ionic character of a bond using the stretching to bending force constant ratio was rendered only qualitative by the repulsions of like atoms or groups in different molecules, it is desirable to study these repulsions. The effects of the repulsion of the groups attached to a given atom on the ratio of stretching to bending force constants is indicated in Table IV and Table V. The effect of increasing the repulsion between these groups would be to decrease the ratio of stretching to bending force constant. This is true because the effect of increasing the repulsion between adjacent groups would not affect the stretching force constant to a first approximation, whereas the bending force constant would be increased thus lowering the ratio. Therefore, the spatial arrangement of the groups attached to a given atom is important in considering the stretching to bending force constant ratio. This may be seen by noting how large this ratio is in the case of the linear metallo-organics, $Hg(CH_3)_2$ and $Zn(CH_3)_2$, where the methyl repulsion is at a minimum. This is also brought out in Table V. The distance (r) between the methyl groups attached to a given atom is calculated. Since the repulsive force decreases as the reciprocal of the third power of r for a pure ionic bond this distance is very critical. For a covalent bond the function is more complicated than a reciprocal power function, but is also very critical to changes in r.

Accordingly, we see (Table V) that the third power of this repulsive distance varies over a large range in the tetrahedral Group IV molecules. This variation is due to the fact that the C central atom bond distance is increasing continuously as the periodic table is descended vertically. However, in the Group V trimethyl molecules the variation of the third power of the repulsive distance is considerably less because the increase in C central atom bond distance is partially compensated by a lessening of the angle between the bonds as the periodic table is descended vertically. This trend is also reflected by the ratio of stretching to bending force constants in these two groups of molecules. That is, in the Group IV tetramethyls there is a large increase in the ratio whereas in the Group V trimethyls the increase is considerably less.

Consequently, it is to be concluded that, if compensation for the effects of the methyl-methyl repulsion is included, the metallo-organic bond varies in degree of covalency over a considerable range approximately as would be expected from the bond electronegativities. Since all metallo-organic bonds have a carbon atom in common and since the electronegativity of carbon falls about in the middle of the scale of electronegativity, the extremes of ionic character observed in the bonds of salt molecules are not possible in metallo-organic bonds.

The author wishes to acknowledge the inspiration and guidance of Professor K. S. Pitzer in the preparation of this paper.

[10] M. Haissinsky, J. phys. rad. 7, 7 (1946).

Molecular Motion in Certain Solid Hydrocarbons

E. R. ANDREW*
Lyman Laboratory of Physics, Harvard University, Cambridge, Massachusetts
(Received October 3, 1949)

An investigation has been made of the variation of the nuclear resonance absorption line width with temperature for four long chain aliphatic compounds and eight aromatic hydrocarbons. The aliphatic compounds are dimorphous; in the lower temperature modification it is concluded that the molecules are rigid at the lowest temperatures, but that an increasing number of molecules rotate about their length as the temperature increases; in the upper temperature modification all the molecules rotate. The naphthalene crystal lattice is found to be rigid up to the melting point. Benzene and anthracene, however, show sharp line-width transitions at about 110° and 190°K, respectively. It is suggested that in benzene this is due to tunnelling or rotation of the molecules about their hexagonal axes. The explanation for anthracene is less clear, but it is suggested that each molecule rotates about its long diad axis. The xylenes, mesitylene, and hexamethylbenzene show internal rotation of the CH_3 groups at all temperatures above 95°K. In addition, hexamethylbenzene has a line-width transition over the range 135–210°K, attributed to tunnelling or rotation of the molecules about their hexagonal axes.

A calculation is made of the reduction of the intramolecular contribution to the resonance line second moment caused by rotational oscillation of molecules in a crystal lattice. The effects of certain types of molecular motion on the intermolecular contribution are also calculated.

I. INTRODUCTION

GUTOWSKY and Pake[1] have shown that the magnetic dipolar broadening of nuclear resonance absorption lines in solids is reduced by molecular motion in the crystal lattice. For a number of compounds such motion was found to set in as the temperature was increased, and by a quantitative analysis of the resonance lines they obtained information concerning the nature of the molecular motion encountered. The present paper gives the results of an investigation by this method, of molecular motion in certain hydrocarbons and in a related alcohol.

The twelve compounds studied were:

Long chain paraffins:
- *n*-Octadecane
- *n*-Octacosane
- Dicetyl

Long chain alcohol:
- Lauryl alcohol

Aromatic hydrocarbons:
- Benzene
- *o*-, *m*- and *p*-Xylene
- Mesitylene
- Hexamethylbenzene
- Naphthalene
- Anthracene

All the materials were supplied by Eastman Kodak (highest purity grade).

The apparatus was that used by Gutowsky and Pake, and the experimental technique was essentially the same. The temperature range of measurement, which in their experiments had been from 90°K to room temperature, was extended upwards by use of an oil bath and immersion heater. The samples under investigation were powdered solids occupying about 1 cc volume. Proton resonances were used throughout this investigation in the applied field of 6774 gauss from a permanent magnet (resonance frequency 28.8 Mc/sec.). The apparatus did not enable the shape of the resonance line to be plotted out directly; a phase-sensitive amplifier, which serves to give a good signal to noise ratio, together with a small sinusoidal modulation of the applied field, yields the first derivative of the resonance line-shape. The line-shape itself may be obtained, if required, by direct integration of the measured derivative. For comparison with theory the second moment of the resonance line-shape about its center has to be computed; this, however, can be done directly from the derivative curve. Values of second moment quoted later in this paper are the mean of those obtained from about three sets of derivative measurements. The probable error of the mean ranged from 0.2 gauss^2 for the narrowest lines to about 0.8 gauss^2 for the broadest lines. A subtraction of 0.2 gauss^2 from the mean computed values has been made to allow for field inhomogeneity over the sample. The line-shape could be completely plotted only at steady temperatures; in the intervals 100–200°K and 210°–270°K the sample warmed up continuously, giving only time enough at each temperature to measure the width between the stationary points of the derivative curve. This, however, was sufficient to indicate the temperature range in which changes in line-shape occurred, and their order of magnitude; the complete line-shape and second moment could be obtained at fixed temperatures on both sides of the change.

Before proceeding to an account of the experimental results and their detailed explanation, some general remarks will be made concerning the information which the theory allows us to deduce from the experimental results. It may be said at once that unless the reorien-

* Commonwealth Fund Fellow. Now at the Department of Natural Philosophy, University of St. Andrews, Scotland.

[1] H. S. Gutowsky and G. E. Pake, J. Chem. Phys. **18**, 162 (1950); see also earlier experiments by N. L. Alpert, Phys. Rev. **75**, 398 (1949).

tation frequency[1] characteristic of a type of motion in the crystal lattice exceeds that represented by the half-width of the resonance line, the second moment of the line will be unaffected by the motion; this type of experiment is therefore unable to detect such motion. (The half-width is of the order of 30 kc/sec. for the solids considered here.) Therefore, whenever the statement is made later in this paper that a reduction in line-width is to be explained by a certain type of motion, it should not be assumed that the motion was altogether absent before the reduction took place (although this *may* have been the case), but merely that the motion took place too infrequently to be effective in these measurements.

The various types of molecular motion about a rotational axis which may be encountered in a crystal include:

(i) Rotation.
(ii) Quantum mechanical tunnelling through the potential barrier. The rotational axis must also be a symmetry axis if this motion is to be possible.
(iii) Rotational oscillation.

Provided the frequency of rotation, tunnelling or oscillation exceeds the minimum reorientation frequency, all these forms of motion cause a reduction of line width and of second moment. Moreover, if the axis of rotation is an axis of three-, four-, or sixfold symmetry, the rotation in (i) need not be maintained all the time, provided the necessary number of reorientations are made per second. Thus a small fraction of the time may be spent in excited states of high rotational frequency and the remainder of the time in the various equivalent fixed positions. This type of motion is almost equivalent in results to tunnelling, merely providing a different mechanism for the angular changes.

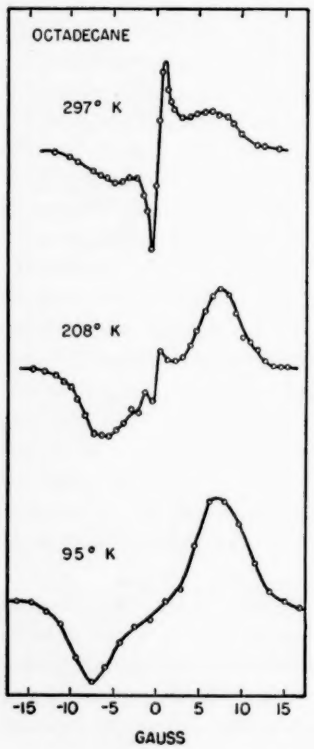

FIG. 1. Resonance line derivatives for octadecane.

The effect of rotation (including the non-continuous form just mentioned) on the second moment is identical with that of tunnelling about a three-, four-, or sixfold axis[1] (except insofar as there may be a slight difference in the intermolecular contributions). Second moment data are therefore unable to distinguish between these forms of motion. A distinction can, however, usually be made from rotational oscillation, and in principle from tunnelling about a twofold axis, although the difference in the expected reduction of second moment from that for higher symmetry tunnelling is not always very large.

A further piece of evidence which may be used in determining the type of motion encountered comes from x-ray structural determinations. If the structure of the crystal has been successfully determined at temperatures where the motion is found to occur, then we may rule out uniform or nearly uniform continuous rotation of the heavier atoms in the crystal. In molecular crystals this will usually imply that such motion for the hydrogen atoms is also ruled out.

II. LONG-CHAIN PARAFFINS

Experimental Results

(i) *n*-Octadecane, *n*-$C_{18}H_{38}$. At the lowest temperature of measurement, 95°K, the derivative of the resonance line, shown in Fig. 1, indicated no fine structure in the line itself. The mean second moment was 23.9 gauss^2. There was evidence of fine structure, however, at 208°K, Fig. 1, where the second moment was 20.3 gauss^2. This fine structure became more pronounced at higher temperatures, the second moment decreasing to 16.2 gauss^2 at 297°K, a few degrees below the melting point (300°K). The second moment is plotted against temperature in Fig. 2. It decreased smoothly until the melting point was reached, at which temperature the narrow line characteristic of liquids was obtained.

(ii) *n*-Octacosane, *n*-$C_{28}H_{58}$. At 99°K and at 205°K there was no evidence of fine structure; the second moment was 26.6 gauss^2. At 228°K fine structure of the kind found for octadecane began to appear; the second moment decreased smoothly until a temperature of 326°K was reached, as indicated in Fig. 2. Here a discontinuity in second moment occurred, and the line narrowed rapidly over the last seven degrees before the solid melted.

(iii) Dicetyl, *n*-$C_{32}H_{66}$. The behavior was similar to that of octacosane. At the lowest temperatures the second moment was 27.1 gauss^2. Fine structure of the kind encountered in octadecane and in octacosane appeared at 235°K, and as shown in Fig. 2, the second moment decreased continuously until 318°K where it remained steady at 14 gauss^2 until 336°K. At this temperature the second moment fell rapidly over the last six degrees before reaching the melting point at 342°K.

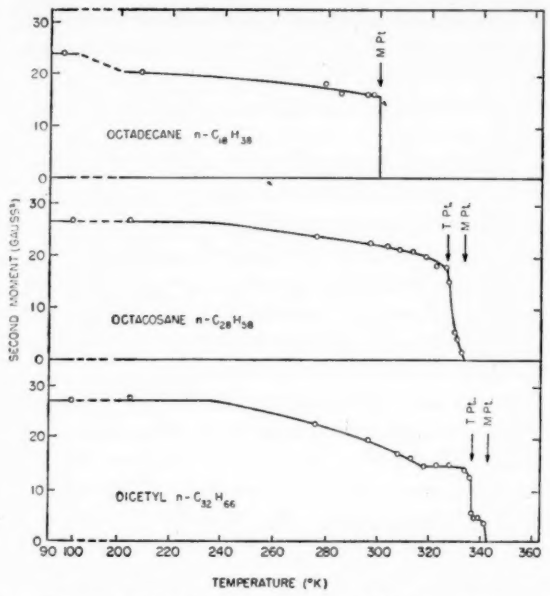

FIG. 2. The variation with temperature of the second moment of the resonance line for three long chain paraffins.

Discussion

The structures of the normal paraffins have been investigated by Müller[2] using x-rays; for one member of the series, $C_{29}H_{60}$, the structure has been completely determined. The molecule consists of a plane zig-zag chain of carbon atoms with the characteristic tetrahedral interbond angle of $109\frac{1}{2}°$. The carbon chains are all arranged parallel to the *c*-axis of an orthorhombic unit cell as the projection on the basal plane shown in Fig. 3 indicates. Other members of the series studied less completely show the same kind of molecular structure and parallel packing, but with differences in detail. Several members of the series are polymorphous showing structural changes about 6° below the melting point. The structural transition temperatures have been measured for the whole series by Piper *et al.*[3]

If the structure of a crystal is known and the lattice can be assumed rigid, Van Vleck's formula[4] makes possible the calculation of the second moment of the proton resonance line.[5] For the paraffins the intramolecular contribution to the second moment predominates. The x-ray analysis does not give the position of the hydrogen atoms, but it may be reasonably assumed that the C−H bonds are tetrahedrally distributed with respect to the C−C bonds of the chain; the C−C bond length is taken as 1.54A from Müller's work, and the C−H distance as 1.094A from spectroscopic data.[6]

For the general member C_nH_{2n+2} the intramolecular contribution is found to be $[18.5+19.1/(n+1)]$ gauss². For the smaller intermolecular contribution, it is good enough to use Müller's structure for $C_{29}H_{60}$ despite the slight differences in packings for the various members of the series. The intermolecular contribution is then found to be 7.8 gauss², the total second moment thus becoming $[26.3+19.1/(n+1)]$ gauss². For $n=28$ (octacosane), the calculated second moment is 27.0 gauss², which is in good agreement with the experimental value of 26.6 gauss² for temperatures below 228°K. For $n=32$ (dicetyl), the calculated second moment is 26.9 gauss², which is in good agreement with the experimental value of 27.1 gauss² for temperatures below 235°K. Thus at the lower temperatures the molecules are effectively stationary for these two paraffins. For $n=18$ (octadecane), the calculated second moment is 27.3 gauss², which is appreciably higher than the experimental value of 23.9 gauss² at 95°K. This suggests that the molecules are not quite stationary and there there is still some motion of the kind to be discussed, which is found at higher temperatures in all three paraffins.

Müller found that as the temperature increased the axial ratio a/b changed progressively toward that of a higher symmetry hexagonal form. (In Fig. 3 this means that the angle ψ tends to 30°.) For $21 \leqslant n \leqslant 29$, members of the series C_nH_{2n+2} reached hexagonal symmetry before melting. For $n \leqslant 23$ the change in axial ratio was continuous, but for $n \geqslant 24$ an abrupt transition took place about 6° below the melting point.

Müller explained the higher symmetry hexagonal form by supposing that all the molecular chains were in rotation about their lengths at this temperature; the structure was then that of close-packed cylindrical molecules. At the lower temperatures he assumed that there would be rotational oscillation of the molecules; an increasing number would have sufficient energy to surmount the potential barrier as the temperature increased, thus causing the progressive transition of axial ratios. As a result of later work on the dielectric

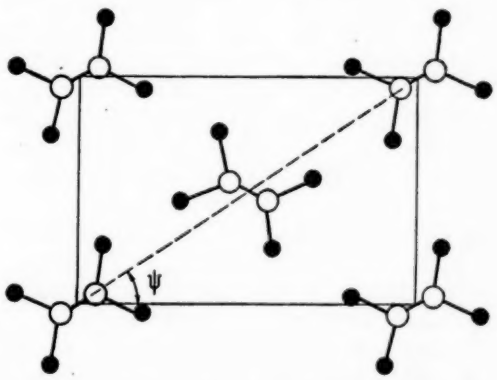

FIG. 3. Diagram illustrating the packing of the long chain paraffins in the unit cell. The molecules are shown projected on the base of the unit cell. The open circles represent carbon atoms; the solid circles represent hydrogen atoms.

[2] A. Müller, Proc. Roy. Soc. **A120**, 437 (1928); **127**, 417 (1930); **138**, 514 (1932).
[3] Piper, Chibnall, Hopkins, Pollard, Smith, and Williams, Biochem. J. **25**, 2072 (1931).
[4] J. H. Van Vleck, Phys. Rev. **74**, 1168 (1948).
[5] Gutowsky, Kistiakowsky, Pake, and Purcell, J. Chem. Phys. **17**, 972 (1949).
[6] G. Herzberg, *Infrared and Raman Spectra of Polyatomic Molecules* (D. Van Nostrand Company, Inc., New York, 1945), p. 440.

constant of long chain di-ketones, Müller[7] concluded that the chains had considerable torsional flexibility, and that torsional oscillations might, at least in part, be the cause of the increase in symmetry.

In comparing the present results with the work of Müller, it may first be noted that the discontinuous changes in second moment found for octacosane and dicetyl correspond to the structural changes found by him; for octadecane he found that the axial ratio changed continuously, and in fact no discontinuity in second moment was found.

To further test the compatibility of the present results with Müller's conclusions, it is necessary to calculate the reduction in second moment caused by rotation or oscillation of the molecules. Gutowsky and Pake[1] have given formulas for the reduction of the intramolecular contribution to the second moment caused by rotation or quantum-mechanical tunnelling between equivalent positions. (Tunnelling is not a possibility here, however, since the axis of rotation is not an axis of symmetry.) Using these formulas, it is found that this contribution is reduced from the rigid lattice value of $[18.5+19.1/(n+1)]$ gauss^2 to $[6.8-11.6/(n+1)]$ gauss^2 if all the molecules rotate. The values are 6.2, 6.4, 6.4 gauss^2 for $n=18$, 28, 32, respectively. Gutowsky and Pake assumed for the purpose of their calculations that the intermolecular contribution would not be appreciably affected by the rotation. In Appendix II the effects of certain kinds of motion on this contribution are calculated, and as an example, it is shown there that for the paraffins, the intermolecular contribution is, however, reduced by a factor of three from 7.8 gauss^2 to 2.6 gauss^2. Intra- and intermolecular contributions are thus reduced by about the same factor. The total second moments to be expected if all the molecules rotate are therefore 8.8, 9.0, 9.0 gauss^2 for octadecane, octacosane, and dicetyl, respectively.

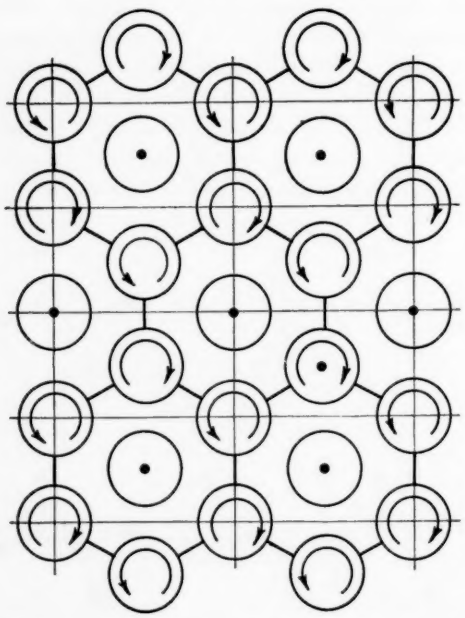

FIG. 4. A suggested arrangement of rotating molecules for dicetyl, shown projected on the basal plane of the unit cell.

[7] A. Müller, Proc. Roy. Soc. **A174**, 137 (1940).

A comparison of these values with the experimental second moment values shown in Fig. 2 indicates that for octadecane up to the melting point, and for the other two paraffins up to their transition points, the second moments are too great for all the molecules to be rotating. It seems reasonable to suppose, therefore, that the progressive reduction of second moment is due to the rotation of some, but not all, of the molecules. Those molecules which do not rotate presumably oscillate; we must, therefore, find what reduction of second moment is caused by rotational oscillation in order to know how much of the observed reduction can be ascribed to this cause. The necessary calculation is carried out in Appendix I, where the reduction factor is given as a function of the amplitude of oscillation. As an approximation in applying these results to the paraffins, it will be assumed that the intermolecular contribution is reduced by the same factor; this was almost exactly the case for uniform rotation. It is found that for angular oscillation amplitudes of 30°, 45° and 60° that the reductions in second moment below the rigid lattice values for the paraffins are 6.2, 10.8 and 13.9 gauss^2, respectively. For octadecane the second moment was 11 gauss^2 below the rigid lattice value at the melting point, while for octacosane and dicetyl at their transition points the corresponding reductions were 10 and 12 gauss^2. If the experimental reductions are to be accounted for on the basis of oscillation alone, it is necessary to assume oscillatory amplitudes of at least 45°. Without a detailed knowledge of the shape and size of potential barrier we cannot make a definite pronouncement, but it seems more likely that at lower temperatures the molecules occupy oscillatory energy levels and that as the temperature rises the amplitude of oscillation increases with an increasing number of molecules occupying rotational levels. It should be noted in this connection that for $C_{29}H_{60}$, whose structure Müller determined completely, only a small fraction of the molecules could have been rotating at the temperature of his investigation, 293°K. The reduction of second moment for octacosane, the next member in the series, is in fact quite small at this temperature (see Fig. 2).

In the case of dicetyl, the second moment appears to maintain a steady value of 14.5 gauss^2 over a 15° range below the transition point. As we have noticed, this value is greater than the 9.0 gauss^2 which would be expected if all the molecules rotated. If this effect is real, it suggests a stable arrangement with about two-thirds of the molecules rotating and one-third merely oscillating. A possible explanation of such an arrangement is as follows. The molecules in plan pack together in an almost hexagonal array. The molecules themselves are far from having circular symmetry about their axes,

and would tend to rotate like a set of meshed gearwheels. However, a closed train of identical gears will only rotate if it contains an even number of members, and it will be seen on examination that it is not possible for the whole hexagonal array of molecules to rotate in this manner since it is made up of a set of almost equilateral triangular groups containing three members. If, however, one-third of the molecules do not rotate, one can imagine satisfactory systems of meshing molecules such as that indicated schematically in Fig. 4.

We now have to account for the much lower values of second moment which were found for octacosane and dicetyl above their transition temperatures. The values are rather lower than those calculated for uniform rotation of all the molecules. Presumably the structural change at the transition point lowers the potential barriers hindering rotation to an extent permitting all the molecules to rotate. It is likely that other forms of motion will also be present such as torsional oscillations, lateral and longitudinal motion and flexing. These motions, which would also be present to some extent below the transition point, would cause the second moment to be still lower than that calculated for rotation alone.

Finally, an attempt should be made to explain the nature of the fine structure of the resonance line. Only a qualitative explanation will be attempted since the molecular proton system is a complicated one. The characteristic features are the sharp positive and negative peaks on the derivative curve, which reflect a sharp central peak in the resonance line itself. Because it is sharp, this peak only represents a small fraction of the total energy of the resonance line.

The paraffin chain may be grouped as a set of CH_2 groups with a CH_3 group at each end. Taken separately, only the CH_3 groups give a central peak. As shown by Andrew and Bersohn[8] the resonance line for an equilateral triangular group of protons has a central component, which for a rigid lattice and a powdered sample, contains a fraction 0.19 of the line intensity of the whole group. When the triangle rotates about the paraffin chain axis, which makes an angle 35° 16′ with the normal to the plane of the three protons, this fraction is slightly enhanced to 0.25. In the rigid lattice this central line is presumably not visible as fine structure owing to the considerable broadening caused by protons of other molecules and of adjacent groups in the same molecule. When the molecule rotates or oscillates with large amplitude, the broadening due to neighbors becomes several times smaller as we have seen, thus perhaps allowing this central component to be resolved. This hypothesis could be tested by substituting some other nucleus for one of the protons in each end group.

III. LAURYL ALCOHOL

Lauryl alcohol, n-$C_{12}H_{25}OH$, like several other members of the normal primary alcohol series is dimorphous.[9,10] In both structural forms the carbon chain has the same form and dimensions as in the paraffins, and the chains are arranged parallel to each other in the unit cell. Bernal[11] found that lauryl alcohol solidified at 297°K into a hexagonal form, with the parallel chains normal to the base of the unit cell. On cooling to 289°K this transformed to a monoclinic structure with the chains inclined at an angle of 57° to the cell base. The transition was found to be irreversible, however, since the hexagonal structure could not be reproduced without first melting. Bernal suggested that the hexagonal structure followed from rotation of the molecules about their chain lengths.

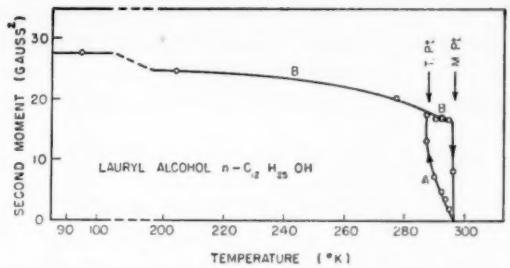

FIG. 5. The variation with temperature of the second moment of the resonance line for lauryl alcohol.

The mean experimental values of second moment are plotted against temperature in Fig. 5, and a series of resonance line derivatives for various temperatures is shown in Fig. 6. At the lowest temperature, 95°K, the mean second moment 27.7 gauss² is in good agreement with the calculated value 27.1 gauss² for a rigid lattice. In obtaining this calculated value it was assumed that the intermolecular contribution was the same as that for the corresponding paraffin since the detailed structure of lauryl alcohol is not known.

On raising the temperature, the second moment decreased continuously until the melting point was reached as with octadecane, sharp peaks appearing in the derivative curve (Fig. 6). On solidifying again the hexagonal form was first obtained with a much narrower line than that for the monoclinic form, giving the hysteresis loop in Fig. 5. Below 287°K the same resonance lines were obtained as when heating up.

These results find the same explanation as that for the paraffins. For the monoclinic form, the motion is the same as for octadecane up to the melting point; for the hexagonal form, the motion is the same as for octacosane and dicetyl above their transition points.

IV. BENZENE, NAPHTHALENE, AND ANTHRACENE

Benzene, C_6H_6

At 94°K the mean second moment was 11.4 gauss². At this and higher temperatures the resonance line was single-humped showing no fine structure. At both

[8] E. R. Andrew and R. Bersohn, J. Chem. Phys. **18**, 159 (1950).

[9] T. Malkin, J. Am. Chem. Soc. **52**, 3739 (1930).
[10] D. A. Wilson and E. Ott, J. Chem. Phys. **2**, 231 (1934).
[11] J. D. Bernal, Zeits. f. krist. **83**, 153 (1932).

205°K and 273°K the line was much narrower, with second moment values 2.1 and 2.0 gauss², respectively. In Fig. 7 the line width (reckoned between the stationary points of the derivative curve) is plotted against temperature, and it will be seen that a sharp drop occurs over the range 100–118°K.

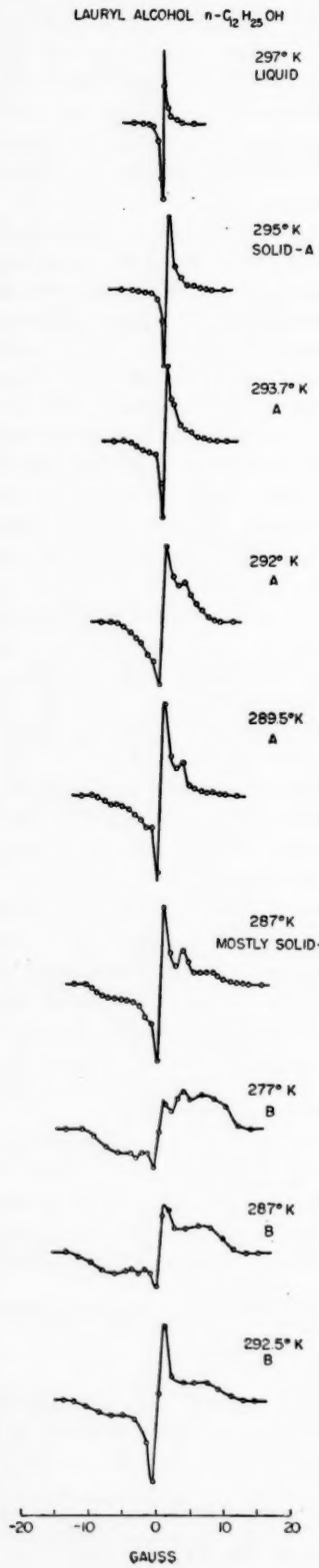

FIG. 6. Resonance line derivatives for lauryl alcohol, illustrating the hysteresis loop shown in Fig. 5.

The benzene molecule is known to be a plane hexagon of carbon atoms each with a side-bond hydrogen atom in the plane, thus producing a plane hexagon of protons. In calculating the theoretical intramolecular contribution to the second moment, Brockway and Robertson's[12] value 1.39A has been taken for the carbon-carbon bond length; for the carbon-hydrogen bond length we have taken the value 1.08A, intermediate between 1.09A for $-C-H$ and 1.07A for $=C-H$.[6] The contribution is 3.3 gauss². Using the structure of benzene determined by Cox,[13] the intermolecular contribution is found to be 5.3 gauss² for the temperature of Cox's determination, 251°K, and approximately 6.4 gauss² at 94°K, assuming the contraction of solid benzene at the lower temperature is not very different from that of naphthalene for which a value of the contraction is available. The total calculated second moment for a rigid lattice is therefore 9.7 gauss² at 94°K. The experimental value is 1.7 gauss² larger than this; the discrepancy is probably due to the use of a rather larger modulating field than usual on account of the very weak signal obtained at this temperature. The lattice can therefore be treated as rigid at 94°K.

The sharp drop in line-width over the range 100–118°K must indicate the commencement of some considerable motion in the lattice; the reduction is more than can be accounted for by mere rotational oscillation or vibration. An examination of the lattice structure suggests that rotation or tunnelling of the benzene molecules about their hexagonal axes is the motion likely to require the least energy. The evidence of the x-ray analysis (see Section 1) suggests that of these forms of motion, the more likely are tunnelling and non-uniform rotation.

This rotational motion would reduce the intramolecular contribution by a factor of four. The effect on the intermolecular contribution is not covered by the cases considered in Appendix II, but if we assume that this contribution is reduced by the same factor as the intramolecular contribution, as was the case for the paraffins, the total theoretical second moment would be 2.4 gauss² at 120°K and 2.1 gauss² at 273°K in good agreement with the experimental values. This agreement should not, however, be interpreted as ruling out other forms of motion such as rotation or tunnelling about the diad axes, which though less likely (since the potential barrier is probably much greater) would give roughly the same theoretical values of second moment. By studying line-width changes in substituted benzene compounds it may be possible to make a more definite decision between these forms of motion.

[12] L. O. Brockway and J. M. Robertson, J. Chem. Soc. 1934 (1939).
[13] E. G. Cox, Proc. Roy. Soc. **A135**, 491 (1932).

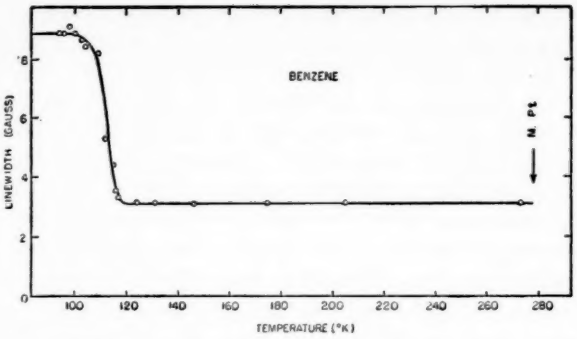

FIG. 7. The variation with temperature of the resonance line width for benzene.

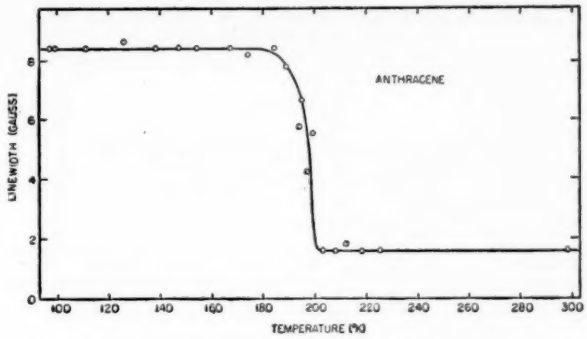

FIG. 8. The variation with temperature of the resonance line width for anthracene.

The specific heat of benzene[14] shows no anomaly in the region of 100°K. The motion does not, therefore, accompany a structural change. An explanation of the breadth of the temperature range over which the line narrows is given by Purcell, Sachs, and Turner[15] in conjunction with their measurements of relaxation times for benzene and other solids exhibiting similar line-width changes.

Naphthalene, $C_{10}H_8$

The line-width did not change appreciably over the whole range of measurement from 96°K to the melting point 353°K. There appeared to be a decrease of the order of 10 percent in line width at the higher temperatures, but the accuracy was not good because the signal was weak. The resonance line was a single-humped curve showing no fine structure; the mean experimental second moment was 9.1 gauss^2. The structure of naphthalene has been determined by Robertson.[16] Using a carbon-hydrogen bond length of 1.08A as for benzene, the intramolecular contribution is found to be 3.2 gauss^2. Together with an intermolecular contribution of 6.9 gauss^2, the total theoretical second moment is 10.1 gauss^2. Thus the naphthalene lattice is essentially rigid at all temperatures; the slight reduction of line width at higher temperatures, if real, can be explained as due to lattice expansion and to some vibrational motion.

Anthracene, $C_{14}H_{10}$

At 97°K the mean experimental second moment was 11.4 gauss^2; the resonance line was again a single-humped curve at all temperatures. As Fig. 8 indicates, the line width remains unchanged until about 184°K, when it suddenly narrows by a factor of five over a temperature range of about 16°. Above 200°K the line width remains at this narrow value. At 203°K and 298°K the mean experimental second moments were 0.75 and 0.65 gauss^2, respectively.

The structure of anthracene has been determined by Robertson.[16] For a rigid lattice the intra- and intermolecular contributions are 3.2 and 7.1 gauss^2, respectively, making a total of 10.3 gauss^2. This indicates that the lattice is effectively rigid below 184°K.

The line-width change was a surprise in view of the lack of motion shown by naphthalene, which has a similar structure. Moreover, the magnitude of the reduction of the second moment, namely by a factor of 16, is difficult to explain. Rotation about the two diad axes normal to the length of the hexagon chain seems to be ruled out by lack of room in the lattice for the molecule to turn end over end. Rotation or tunnelling about the third diad axis lying along the length of the hexagon chain seems a possibility. However, tunnelling merely reduces the theoretical intramolecular component from 3.2 gauss^2 to 2.5 gauss^2, while the *total* observed value is only 0.75 gauss^2; even uniform rotation about this axis only reduces this contribution to 2.0 gauss^2. It seems necessary, therefore, to assume other motions besides tunnelling or rotation involving bending, twisting, and side-bond deformation, in order to account for such a low, almost liquid-like, value. This explanation cannot be regarded as entirely convincing, and it is possible that more radical ideas should be considered, such as motion or tunnelling of the protons about a rigid carbon skeleton. The size of the potential barriers involved seems, however, to render this explanation improbable. There is, of course, the possibility that the resonance line has very wide skirts whose energy is too low to detect, but whose contribution to the second moment is quite finite. It is clear that more experiments, particularly on related compounds, are needed before a satisfactory explanation can be put forward.

From the results of this section, the general remark may be made that line-width transitions are to be found in substances for which there are no obvious reasons to expect them.

V. THE XYLENES AND MESITYLENE

There were no important changes in the resonance lines of these compounds from 95°K to their melting

[14] Huffman, Parks, and Daniels, J. Am. Chem. Soc. **52**, 1547 (1930).
[15] Sachs, Turner, and Purcell, Bull. Am. Phys. Soc. **24**, 21 (1949).
[16] J. M. Robertson, Proc. Roy. Soc. **A142**, 674 (1933); **140**, 79 (1933).

TABLE I. Mean experimental second moment values for the xylenes and mesitylene.

Substance	Molecular formula	Melting point °K	Mean second moment (gauss²) 95°K	205°K	277°K	Theoretical rigid lattice second moment (gauss²)
o-Xylene	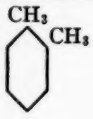	245	9.8	8.8	Liquid	21.1
m-Xylene	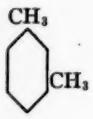	219	9.8	8.9	Liquid	20.7
p-Xylene		288	9.9	8.9	7.7	20.7
Mesitylene	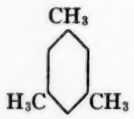	220	9.8	7.6	Liquid	23.8

points. The mean experimental second moments are given in Table I. For the most part the resonances were single-humped curves, although for *m*-xylene and mesitylene there was some evidence of a central peak being resolved at 205°K.

In calculating the rigid lattice second moments, which are also given in Table I, the following assumptions have been made:

(a) that the six bonds were coplanar with the benzene ring, adjacent bonds subtending angles of 60°;
(b) C−H bond lengths in CH_3 groups of 1.094A as in Section II;
(c) C−H side bond lengths of 1.08A as in Section IV;
(d) C−C side bond lengths of 1.53A and C−C ring bond lengths of 1.39A;[11]
(e) that as the lattice structure of these compounds has not been determined, the intermolecular contribution is 5.4 gauss² since it is 5.3 gauss² for benzene and 5.6 gauss² for hexamethylbenzene (Section VI); these are related compounds and all have apolar molecular structures;
(f) that the orientation of the CH_3 groups is that which maximizes the shortest distance between a hydrogen atom of the CH_3 group and any other hydrogen atom elsewhere in the molecule.

It will be seen from Table I that the experimental second moment is less than the calculated rigid lattice value by more than a factor two for all four substances from 95°K to their melting points. Since the molecules are all of different shape and symmetry the most obvious explanation of the low second moment value common to all four is to assume there is rotation or threefold tunnelling of the CH_3 groups about the direction of the C−C sidebond. Such motion reduces the second moment contribution of the protons of the CH_3 groups, which is, in all cases, the predominant contribution, by a factor four. Since the molecule as a whole is not rotating, the intermolecular contribution will probably only be reduced slightly by the motion, and in fact it will be assumed not to change. The remaining intramolecular contributions are small anyway; if they too are assumed not to change, the theoretical second moment values for *o*-, *m*-, *p*-xylene, and mesitylene are respectively 11.2, 10.8, 10.8, 11.5 gauss². If, however, these remaining intramulecular contributions were reduced even as much as to zero, the values are only slightly lower, namely 9.3, 9.3, 9.3, 9.5 gauss². The experimental values at 97°K do all lie between these limiting calculated values, and lend support to the internal rotational motion suggested. The slightly lower values of second moment at higher temperatures are probably caused by the combined effects of lattice expansion and vibrational motion.

VI. HEXAMETHYLBENZENE

Resonance line derivatives taken at 96°K and 280°K are shown in Fig. 9(a). The line-width is plotted against temperature in Fig. 9(b). It is seen to have a steady value from 95°K to 135°K and to decrease gradually over a range 135–210°K to another steady value which remains unchanged at 380°K, the highest temperature of measurement. The mean experimental second moment at 96°K was 13.0 gauss² and above 210°K was 2.5 gauss².

The structure of hexamethylbenzene has been determined by Lonsdale,[17] and confirmed with slightly more accurate bond lengths by Brockway and Robertson.[12] In calculating the theoretical intramolecular contribution to the rigid lattice second moment it has been assumed that each CH_3 group lies symmetrically with respect to the plane of the benzene ring, with one proton in the plane and the other two equally spaced on either side. By arranging all the CH_3 groups in the same sense round the ring, the closest approach of hydrogen atoms from different groups was a maximum. The intra- and intermolecular contributions were found to be 27.1 gauss² and 5.6 gauss² respectively, giving a total of 32.7 gauss².

Since the observed second moment in the range 95°–135°K is less than half the rigid lattice value, it is natural to look for the explanation in terms of rotation or tunnelling of the CH_3 groups about the C−C sidebonds, since this was found to be an adequate explanation of the results for the other polymethylbenzenes in Section V. The effect of such motion is to reduce the contribution of the CH_3 groups by a factor four. If it be assumed that all other contributions are unaltered, the calculated second moment becomes 16.4 gauss². By assuming instead that the other contributions are reduced by a factor 0.7, the calculated value

[17] K. Lonsdale, Proc. Roy. Soc. **A123**, 494 (1929).

can be made to agree with the experimental value of 13.0 gauss^2. Such a reduction factor seems quite reasonable in the light of the previous sections and of the fact that the molecule as a whole is not moving.

It is now necessary to seek an explanation of the still lower second moment (2.5 gauss^2) found at temperatures above 210°K. Uniform rotation of the molecule as a whole is ruled out by the evidence of the x-ray analysis. Moreover, if there were such rotation of the whole molecule, one might expect to find a structure of higher symmetry than the triclinic structure actually found. Sixfold tunnelling or nonuniform rotation of the molecule about the hexagonal axis seem the most likely possibilities therefore. If the CH_3 groups were fixed, such molecular motion would reduce the rigid second moment by a factor of about three. No attempt has been made to calculate the expected second moment for the very complicated case of the two superimposed forms of motion, but it is clear that the observed second moment is of the order of magnitude to be expected, and we may therefore adopt this explanation.

The specific heat of hexamethylbenzene has been measured by Huffman, Parks, and Daniels,[14] and is shown as a function of temperature in Fig. 9. The authors explained the specific heat discontinuity at 108°K in terms of a structural change; since the structure is triclinic above this temperature, it is presumably also triclinic below, but with different lattice constants. The change does not, however, affect the resonance line. The authors could offer no explanation of the specific heat hump at 135–165°K. The present work suggests that this hump may be associated with the onset of rotational motion of the molecules about their hexagonal axes.

ACKNOWLEDGMENTS

The author wishes to thank Professor E. M. Purcell for his interest and helpful advice. He is greatly indebted to Dr. G. E. Pake and Dr. H. S. Gutowsky for the use of their former apparatus.

APPENDIX I

The Effect of Rotational Oscillation on Second Moment

For a rigid pair of like nuclei Van Vleck's formula for the second moment of the resonance line contains the geometrical factor $[(3\cos^2\theta-1)/r^3]^2$ which we will call y^2, where θ is the angle between the applied field and the pair direction, and r is the internuclear distance. Gutowsky and Pake[1] have shown that when the nuclei are in sufficiently rapid motion, y must be replaced in the above factor by its mean value over the motion.

We may express $\cos\theta$ in terms of other angles of the system:

$$\cos\theta=\cos\theta'\cos\gamma+\sin\theta'\sin\gamma\cos(\phi-\phi_0) \qquad (1)$$

where θ' is the angle between the applied field and the axis of rotational oscillation, γ is the angle between the pair direction and the axis of rotational oscillation, ϕ_0 is the azimuth of the plane containing the field direction and the axis of oscillation, ϕ is the azimuth of the pair direction.

We shall assume that the oscillation is simple harmonic so that we may write $\phi=\phi_1+\alpha\sin\omega t$, where ϕ_1 is the azimuth of the mean position of the pair direction and α is the angular amplitude.

The mean value of y over the motion merely requires the evaluation of $\langle\cos^2\theta\rangle_{Av}$ since r remains constant. Performing the necessary integration, this is found to be

$$\langle\cos^2\theta\rangle_{Av}=\cos^2\theta'\cos^2\gamma+2\sin\theta'\cos\theta'\sin\gamma\cos\gamma\cos\delta J_0(\alpha)+\tfrac{1}{2}\sin^2\theta'\sin^2\gamma(1+\cos2\delta J_0(2\alpha)),$$

where $\delta=\phi_1-\phi_0$.

The ratio of second moments for the oscillatory and rigid cases is then given by $\bar{y}^2/y^2$. For a powdered

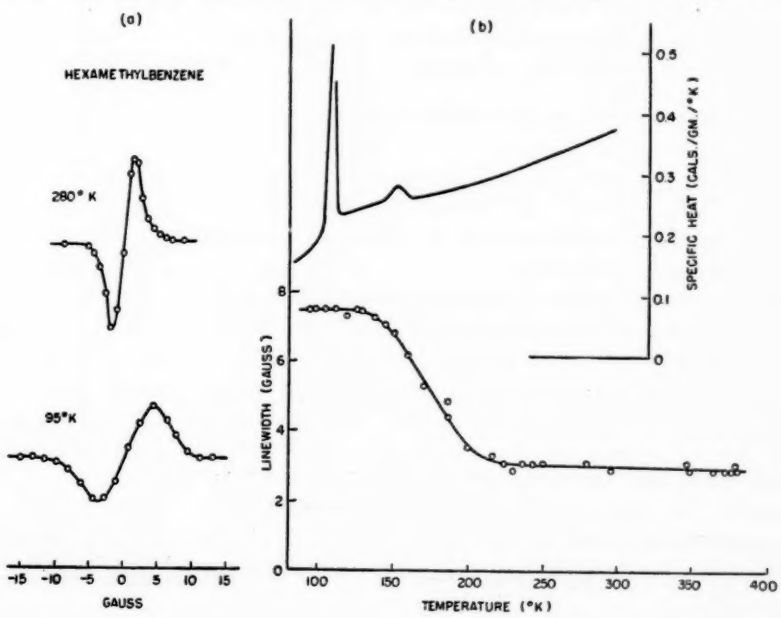

FIG. 9. (a) Resonance line derivatives for hexamethylbenzene; (b) the variation with temperature of the resonance line width and of the specific heat for hexamethylbenzene.

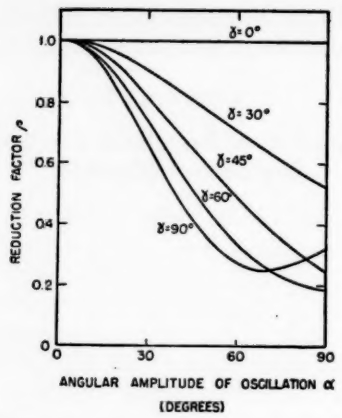

FIG. 10. The variation of the second moment reduction factor ρ with amplitude of angular oscillation α, for various orientations γ of the oscillation axis with respect to the nuclear pair direction.

sample, it is now necessary to average this result for: (i) all values of ϕ_0 over a circle; (ii) all values of θ' over a sphere. After averaging it is found that the ratio of second moments is

$$\rho=1-\tfrac{3}{4}[(1-J_0^2(\alpha))\sin^2 2\gamma+(1-J_0^2(2\alpha))\sin^4\gamma]. \quad (2)$$

For small angles α, this gives the approximate result

$$\rho=1-\tfrac{3}{2}\alpha^2\sin^2\gamma. \quad (3)$$

Values of ρ from Eq. (2) are plotted in Fig. 10.

APPENDIX II

The Change of Contribution to Second Moment Due to Coplanar Motions

We shall consider only the case where the two nuclei are confined to a single plane. The procedure and notation of Appendix I will be used. If angles of azimuth are measured in the plane, then $\gamma=90°$, and

$$\cos\theta=\sin\theta'\cos(\phi-\phi_0). \quad (4)$$

We need the mean value of y over the motion, where $y=(3\cos^2\theta-1)/r^3$; that is, we require

$$\bar{y}=\tfrac{3}{2}\sin^2\theta'(A\cos 2\phi_0+B\sin 2\phi_0+C)-C$$

where

$$A=\langle[\cos 2\phi/r^3]\rangle_{Av};\quad B=\langle[\sin 2\phi/r^3]\rangle_{Av};\quad C=\langle[1/r^3]\rangle_{Av}.$$

A, B, C will be evaluated later in this Appendix for particular types of motion.

For powdered samples, it is now necessary to form $\bar{y}^2$ (which we will call z) and average (i) for ϕ_0 over a circle and (ii) for θ' over a sphere.

(i) gives $\bar{z}^{\phi_0}=(9/8)\sin^4\theta'(A^2+B^2+2C^2)+C^2(1-3\sin^2\theta')$
(ii) gives $\bar{z}=\tfrac{3}{5}(A^2+B^2)+\tfrac{1}{5}C^2$.

For a rigid pair of nuclei separated by distance r_0, $\bar{z}=\tfrac{4}{5}r_0^6$. The ratio ρ of the second moments for moving and rigid cases is therefore

$$\rho=\tfrac{1}{4}r_0^6(3A^2+3B^2+C^2). \quad (5)$$

In principle the problem is now determined and it only remains to find A, B, and C for the type of motion encountered. Several simple cases will now be considered.

Case (i). One nucleus fixed and the other executing uniform motion round a circle. This is a case encountered when one molecule is fixed and the neighbor molecule is uniformly rotating. In Fig. 11, P is the fixed nucleus, Q is the nucleus moving uniformly round a circle of radius p and center O. Let OP, PQ be q, r respectively. OPQ is ϕ and POQ will be called β.

$$r^2=q^2+p^2-2qp\cos\beta=(q+p)^2(1-k^2\cos^2\beta/2)$$

where

$$k^2=\frac{4qp}{(q+p)^2}.$$

Since β takes all values equally from 0 to 2π,

$$C=\langle[1/r^3]\rangle_{Av}=\frac{1}{\pi(q+p)^3}\int_0^{\pi}\frac{d\beta}{(1-k^2\cos^2\beta/2)^{\frac{3}{2}}}$$

$$=\frac{2}{\pi}\frac{E(k)}{(q+p)(q-p)^2}.$$

$$A=\langle[\cos 2\phi/r^3]\rangle_{Av}=C-2D,$$

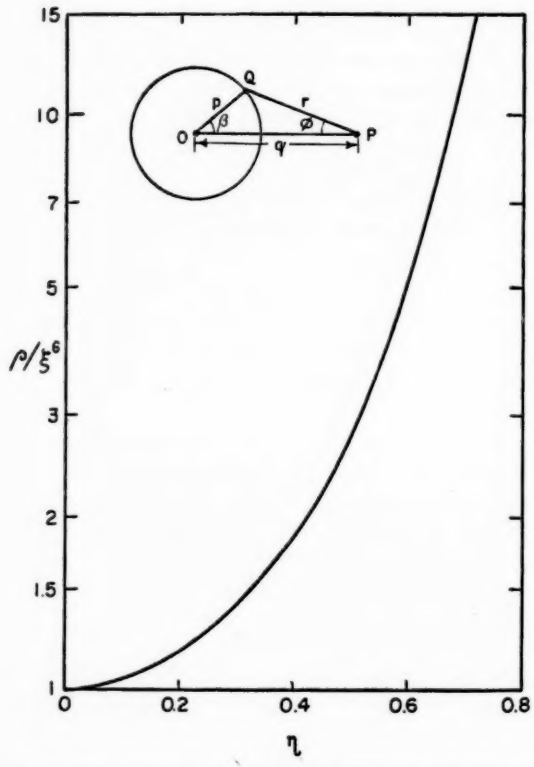

FIG. 11. The variation of the second moment reduction factor ρ with $\eta(=p/q)$, when one nucleus (P in the inset diagram) is fixed, and the other, Q, moves uniformly round a circle.

where $D=\langle[\sin^2\phi/r^3]\rangle_{Av}$. Since $r\sin\phi=p\sin\beta$

$$D=\frac{1}{\pi}\cdot\frac{1}{(q+p)^5}\int_0^\pi\frac{p^2\sin^2\beta d\beta}{(1-k^2\cos^2\beta/2)^{5/2}}$$

$$=\frac{1}{3\pi}\cdot\frac{1}{(q-p)^2(q+p)q^2}[(q^2+p^2)E(k)-(q-p)^2K(k)],$$

$$B=2\langle[\sin\phi\cos\phi/r^3]\rangle_{Av}=\frac{2p}{\pi(q+p)^5}\int_0^\pi\frac{\sin\beta(q-p\cos\beta)d\beta}{(1-k^2\cos^2\beta/2)}$$

$$=\frac{2}{3\pi q}\cdot\frac{q-p}{(q+p)^3}\left[\left(\frac{q+p}{q-p}\right)^3-1\right]$$

$$+\frac{4p}{3\pi q^2(q+p)}\left[\frac{q}{(q+p)^2}-\frac{1}{(q-p)}\right].$$

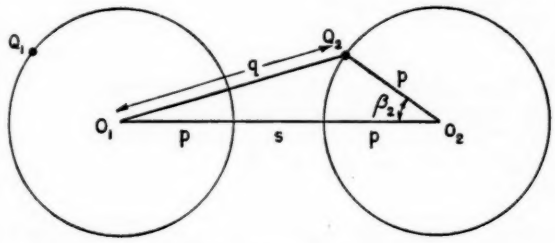

FIG. 12. Diagram illustrating the motion discussed in Appendix II, Case (ii).

Putting $\eta=p/q$ and $\xi=r_0/q$, we have

$$\rho=[c^2+\tfrac{3}{4}b^2-3cd+3d^2]\xi^6,$$

with

$$b=\frac{4\eta(\eta^3+3\eta^2-3\eta+3)}{3\pi(1+\eta)^3(1-\eta)^2}$$

$$c=\frac{2E(k)}{\pi(1+\eta)(1-\eta)^2}$$

$$d=\frac{(1+\eta^2)E(k)-(1-\eta)^2K(k)}{3\pi(1-\eta)^2(1+\eta)}.$$

Values of ρ/ξ^6 obtained from these relations are plotted in Fig. 11.

Case (ii). Both nuclei rotating. We shall consider the case in which the nuclei Q_1 and Q_2 move uniformly round circles of the same radius p, centers O_1 and O_2 (Fig. 12). It will be assumed that there is no phase correlation between the two rotations. The closest distance of approach of the two circles is called s, and the distance O_1O_2 is q. If the second nucleus had been fixed while the first rotated, then the value of the means A, B, C would be those given in Case (i) for the particular value of q concerned. In this case, however, Q_2 also takes all points equally round a second circle.

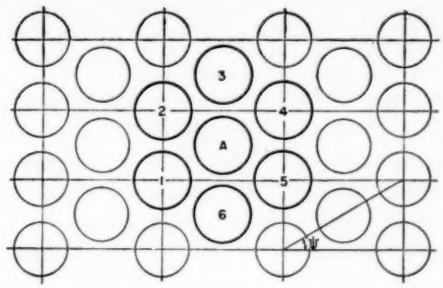

FIG. 13. Diagram illustrating the application of Appendix II, Case (ii) to long chain paraffins.

It is, therefore, necessary to average the values given in Case (i) over all q. Thus, for example,

$$C=\langle[1/r^3]\rangle_{Av}=\frac{2}{\pi^2p^3}\int_0^\pi\frac{\eta^3E(k)d\beta_2}{(1+\eta)(1-\eta)^2}.$$

For a given s/p, η can be expressed as a function of β_2, and the integral evaluated graphically. Evaluations have been made for $s/p=\frac{2}{3}$, 1 and $\frac{3}{2}$. Writing Eq. (5) in the form $\rho=(\mu r_0/p)^6$, the respective values of μ are found to be 0.503, 0.406, 0.304. Other values of μ in this range may be readily interpolated.

As an example of the application of this result, the effect on the intermolecular contribution for the normal paraffins will be considered. Figure 13 shows a section through several unit cells of the crystal lattice normal to the length of the carbon chains. There is one molecule at the corner of each rectangle, and one at each center. Except for one atom in each end group, all the hydrogen atoms are equidistant from the rotational axis of the molecule. The circles in Fig. 13 are then a projection of the loci of all the protons in these molecules (the neglected protons at each end of the chain describe a smaller circle). Consider molecule A. The only neighboring molecules we need consider are those numbered 1–6. If ψ is still somewhat greater than 30°, that is to say, if the orthorhombic axial ratio has not quite reached the hexagonal value, then molecules 3 and 6 will be slightly farther away from A than the other four. Consider one proton somewhere in the middle of molecule A. Its nearest neighbors in molecule 1 will be the two in its plane of rotation and the four bonded to the next carbon atoms above and below the plane. Since the motions of the latter four are not coplanar with the proton from A the theory is not strictly applicable to them. However, the line joining the centers of rotation is only 16° above the plane, so that the theory should be a good approximation provided the correct distances are preserved. The three approximately equidistant molecules A, 1, 2, cannot rotate as a set of meshed gear wheels so the assumption that there is no phase correlation seems reasonable. The assumption of uniformity of rotation is only seriously invalidated if the energy of a molecule is barely greater than the potential barrier

against rotation. If, however, the temperature is such that practically all the molecules are rotating, the assumption will be good enough.

Applying the foregoing theory to the six neighboring protons in each of the molecules 1–6, the contribution to the second moment is found to be 2.0 gauss^2. The other protons belonging to the neighboring molecules are elevated at much greater angles above the plane of rotation, and the results of this section are not applicable to them. Fortunately, however, they are also much farther away so that their motion is less effective, and in any case their contribution is much smaller. In the non-rotating case their contribution was 0.6 gauss^2, and little inaccuracy will be caused in the total if their contribution is assumed unchanged in the rotating case. The total intermolecular contribution is, therefore, 2.6 gauss^2 for the rotating case, compared with 7.8 gauss^2 in the rigid case.

THE JOURNAL OF CHEMICAL PHYSICS VOLUME 18, NUMBER 5 MAY, 1950

The Logical Position of the "Average Bond Energy," the "Dissociation Energy of a Bond," and the "Force Constant"

M. SZWARC AND M. G. EVANS
Department of Chemistry, University of Manchester, England

(Received July 1, 1949)

The concepts of "bond dissociation energy" and "average bond energy" are analyzed. A mathematical treatment is suggested which makes it possible in principle to distribute the energy of atomization among the various bonds of the molecule. The relationship between the "bond dissociation energy," "average bond energy," and "reorganization energy" is examined in the light of various molecular force fields.

THE idea of "bond energy" was introduced into the chemical literature by Fajans,[1] who assumed that the amount of energy necessary for breaking any particular bond was a constant magnitude, characteristic for each type of bond, and independent of the environment of the bond within the molecule. Therefore, the heat of atomization of any molecule was regarded as an additive property, being given by the sum of all bond energies corresponding to the bonds existing in that particular molecule. The assumption of constancy of the bond energy led to the conclusion that the bond energy $M-A$ was given by $1/n$ of the heat of atomization of the molecule MA_n. Similarly the bond energy $M-B$ might be computed from the heat of atomization of the molecule MA_kB_i by subtracting from it the k-fold value of the bond energy $M-A$, obtained from the heat of atomization of MA_n, and dividing the remaining quantity by i. Thus a system of bond energies was evolved which was based on the experimental material provided by heats of combustion of various compounds. The data concerned with the energies required for the direct dissociation of the molecule into two parts, formed by breaking any particular bond, were available only for a few diatomic molecules; and, of course, these dissociation energies were identified with the bond energies.

The subsequent, very fruitful development of the idea of bond energy[2] demonstrated clearly that the assumption of constancy of bond energy could not be retained. About the same time several experimental methods were invented which made it possible to determine the dissociation energy of various bonds in polyatomic molecules. It was soon realized that the bond energy and the "dissociation energy of a bond" are not identical magnitudes. Thus, the intrusion of the idea of the dissociation energy of a bond and the accepted principle of variations of bond energies have caused a great deal of confusion in the present literature on these subjects. We decided, therefore, to examine the logical position of both concepts: Of bond energy, subsequently referred to as the "average bond energy," and of the dissociation energy of the bond. We shall also try to point out the interrelations existing between the various measured magnitudes, usually correlated with the average bond energy, and to clear up, to some extent, the ambiguities accumulated in the literature.

We start by defining the dissociation energy of the bond. The dissociation energy of the bond $A-B$ in the molecule (or radical) M is the endothermicity of the reaction in which M is decomposed into two fragments R_1 and R_2 (atoms, radicals or molecules) formed by breaking the bond $A-B$ only.*

$$M=R_1+R_2-D(A-B) \text{ kcal./mole.}$$

It should be stressed that this endothermicity must be computed for the state in which both the reactant M and the products R_1 and R_2 are in gas phase at zero pressure and at 0°K. It follows from this definition that the dissociation energy of the bond is unambigu-

[1] K. Fajans, Ber. **53**, 643 (1920); **55**, 2826 (1922).
[2] L. Pauling, *The Nature of Chemical Bond* (Cornell University Press, Ithaca, 1940).

* In cyclic molecules the breaking of certain bonds may produce one fragment only.

ously determined by the description of the initial state, i.e., molecule or radical M in a specified electronic state, and the final state, i.e., the fragments R_1 and R_2 in the specified electronic states. It is obvious also that no restrictions need be imposed on the path of the reaction which leads to this dissociation, as the variation of the path does not change the endothermicity of the reaction, i.e., the dissociation energy of the bond.

Passing now to the concept of the average bond energy, denoted subsequently by the symbol $\tilde{q}_a$, we find that it is not possible to define this quantity in a simple manner. As we have already mentioned, the concept of the average bond energy is based on the notion of the heat of atomization, and in the definition of the latter we find the first difficulty, i.e., the necessity of making some assumptions about the state of reference. We realize that the dissociation of a bond is a real and, in principle, observable physical process, and thus the final state is determined by the course of physical events. On the other hand the process of atomization is a speculative one, at least as long as it is visualized as taking place in one stage only. Therefore, we are at liberty to choose the final state, i.e., the electronic state of the atoms eventually formed, in an arbitrary way. This arbitrary nature of the concept of heat of atomization might be removed by an exact statement of the reference states of the atoms.[3] By stating this reference state, one is defining in an unambiguous way, at least in principle, the magnitude of the heat of atomization; however, still more formidable difficulties are encountered when we try to distribute this heat of atomization between the various bonds existing in the molecule. This process of distribution is unambiguous only in the molecules of the type MX_n, which contain bonds exclusively of one kind, and where we might postulate an equal share for each bond and thus to derive $\tilde{q}_a=(1/n)\cdot Q_a$. ($Q_a$ denotes heat of atomization.) However, in the molecules of the type MX_mY_p, or still more complicated molecules, we lack a procedure which makes the distribution of Q_a between the various bonds an unambiguous operation. Let us illustrate this point by an example. Suppose that we know the heat of atomization of CH_2Cl_2, making some definite assumptions concerned with the atomic reference states of C, H and Cl. The determination of $\tilde{q}_a$ for C—H and $\tilde{q}_a$ for C—Cl in this molecule can be achieved in three different ways:

1. We assume the $\tilde{q}_a$ of C—H in CH_2Cl_2 to be equal to $\tilde{q}_a$ of C—H in CH_4, and then from the knowledge of Q_a we derive the value of $\tilde{q}_a$ of C—Cl in CH_2Cl_2.
2. We assume the $\tilde{q}_a$ of C—Cl in CH_2Cl_2 to be equal to $\tilde{q}_a$ of C—Cl in CCl_4, and then from the knowledge of Q_a we derive the value of $\tilde{q}_a$ of C—H in CH_2Cl_2.
3. We assume, for reasons which are of a more or less speculative nature, that $\tilde{q}_a$ of C—H in CH_2Cl_2 is slightly greater or slightly smaller than the $\tilde{q}_a$ of C—H in CH_4, and then using the Q_a we obtain the corresponding value of $\tilde{q}_a$ of C—Cl in CH_2Cl_2.

Obviously all three methods would in general lead to different results, and there is no logical reason why we should favor one way or another. This state of affairs makes the determination of $\tilde{q}_a$'s very uncertain, and the situation is particularly obscure for big organic molecules which contain a variety of bonds.

We feel, therefore, that there is need of some exact definition which will make the operation of distribution of Q_a between the various bonds an unambiguous process. We will now outline such a definition and examine further its logical position.

Let us consider a molecule composed of m atoms connected by n bonds. The relative position of these atoms in the molecule may be described in terms of any set of $3m-6$ mutually independent coordinates. We can choose for this purpose a set containing the lengths of the n bonds $r_1, r_2, \cdots r_n$ as n coordinates and supplement them with any other $3m-6-n$ coordinates, let us say $\alpha_1, \alpha_2, \cdots \alpha_{3m-6-n}$, which are independent of the r's and which are functions of angles only. Hence, the variation of any r_k coordinate corresponds to stretching of the k bond, while the variation of any α_i coordinates causes deformation of the molecule such as bending, twisting, and so on.*

We denote now by E the potential energy of the molecule measured from a zero level represented by the separate atoms, each of them being in some definite electronic state. E is, therefore, a function of all r's and α's, and

$$dE=\sum_1^n \frac{\partial E}{\partial r_k}\cdot dr_k+\sum_1^{3m-n-6} \frac{\partial E}{\partial \alpha_i}\cdot d\alpha_i.$$

The variation of E caused by mere stretching of the bonds is given as

$$\delta E=\sum_1^n \frac{\partial E}{\partial r_k}\cdot dr_k$$

and the heat of atomization Q_a is given by

$$Q_a=\sum_1^n \int_{r_{k_0}}^{\infty} \frac{\partial E}{\partial r_k}\cdot dr_k \qquad (1)$$

the integration being performed on any path lying on the surface determined by the set of $3m-n-6$ equations:

$$\alpha_i=\alpha_{i_0}$$

r_{k_0} and α_{i_0} being here the values of the coordinates r's and α's in the original molecule. We choose now from

[3] For example, see L. Pauling, Sommerfeld Festschrift, Zeits. f. Naturforsch **3a**, 438 (1948); L. Pauling, Proc. Nat. Acad. Sci. **35**, 229 (1949).

* This need not be always true in cyclic molecules. However, the further conclusions are not affected.

the set of permissible integration paths the one which is described by the additional set of n equations:

$$r_k=\gamma\cdot r_{k0}$$

γ being a variable which changes from 1 to ∞. Thus by defining the integration path we have determined the value of every individual integral

$$\int_{r_{k0},L}^{\infty}\frac{\partial E}{\partial r_k}\cdot dr_k.$$

L denotes here this particular integration path, and we suggest as a definition of the average bond energy $\tilde{q}_a$ the value of the above integral,

$$\tilde{q}_a=\int_{r_{k0},L}^{\infty}\frac{\partial E}{\partial r_k}\cdot dr_k. \tag{2}$$

The $\tilde{q}_a$'s defined in this way have the following properties:

1. $\sum\tilde{q}_{a_i}=Q_a$
2. For any two bonds, k and i which are indistinguishable in the molecule, i.e., their interchange does not change the molecule, the corresponding $\tilde{q}_{a_k}$ and $\tilde{q}_{a_i}$ are equal.

From the properties 1 and 2 we deduce the property 3.

3. For a molecule containing n indistinguishable bond only

$$\tilde{q}_a=(1/n)\cdot Q_a.$$

These are the properties which one would expect to be characteristic of any intuitively introduced concept of the average bond energy. The great advantage of our definition of $\tilde{q}_a$ lies in the fact that for a molecule containing various kinds of bonds the $\tilde{q}_a$'s are rigorously determined by the character of this molecule only. This character is described by the potential energy which is given as a function of r's and no reference to any molecules of the type MA_n is necessary. Moreover, this definition does not imply that in molecules MA_n and MA_kB_{n-k} the $\tilde{q}_a$'s corresponding to the bonds $M-A$ need be equal.

Before this subject is pursued further it is desirable to mention another interpretation of our definition of $\tilde{q}_a$ which, although less exact than the former one, affords a useful picture of the situation. One might visualize $\tilde{q}_a$ as the work done in order to stretch two bonded atoms from their original position in a molecule to an infinite distance, while at the same time the whole molecule swells infinitely without loosing its original shape.

We are now in a position to discuss the interrelation between the average bond energy, the dissociation energy of the bond, and the "reorganization energy." Let us express the dissociation energy of the bond by an integral similar to that which has been used for the definition of the average bond energy.

$$D=\int_{r_{k0},P}^{\infty}\frac{dE}{dr_k}\cdot dr_k, \tag{3}$$

where

$$\frac{dE}{dr_k}=\frac{\partial E}{\partial r_k}+\sum_{i=1}^{n}{}'\frac{\partial E}{\partial r_i}\cdot\frac{dr_i}{dr_k}+\sum_{j=1}^{3m-n-6}\frac{\partial E}{\partial\alpha_j}\cdot\frac{d\alpha_j}{dr_k} \tag{4}$$

($\sum'$ summation over all i's with the exception of $i=k$). In the integral (3) P denotes the integration path which is the reaction path of the process of dissociation of the bond k. Formally P may be defined in the following way: For every *fixed* value of r_k all the remaining parameters r_i and α_j are to be found from the set of $3m-7$ equations:

$$\partial E/\partial r_i=0 \quad \text{for } i\neq k$$
$$\partial E/\partial\alpha_j=0 \quad \text{for all } \alpha_j\text{'s.}$$

Comparing this definition of the dissociation energy of the bond with the definition of the average bond energy (2) discussed previously, we see that the essential distinction lies in the different integration path. While path P, being the reaction path, corresponds to a physical and in principle observable process, path L corresponds to a purely imaginary process which does not occur in Nature.

Substitution of dE/dr_k from (4) into Eq. (3) yields (5):

$$D=\int_{r_{k0},P}^{\infty}\frac{\partial E}{\partial r_k}\cdot dr_k+\int_{r_{k0},P}^{\infty}A\cdot dr_k, \tag{5}$$

where

$$A=\sum_{i=1}^{n}{}'\frac{\partial E}{\partial r_i}\cdot\frac{dr_i}{dr_k}+\sum_{j=1}^{3m-n-6}\frac{\partial E}{\partial\alpha_j}\cdot\frac{d\alpha_j}{dr_k}.$$

In our opinion the second term of (5) should represent the interesting entity called by Norrish[4] the reorganization energy, while the first term may perhaps represent the entity called by Walsh[5] the bond energy. As Walsh's bond energy has not been defined in a rigorous way, it may be that he understands by his term bond energy the work which should be done in order to break the bond in question in a process in which the remainder of the molecule is kept rigidly in the configuration corresponding to the initial state. In this case the reorganization energy would be given by the work performed in the transformation of the radical from the initial state to the final state in which it exists. These quantities are expressed mathematically by the integrals (6) and (7), respectively:

$$\int_{r_{k0},C}^{\infty}\frac{\partial E}{\partial r_k}\cdot dr_k \tag{6}$$

[4] L. H. Long and R. G. W. Norrish, Proc. Roy. Soc. **187A**, 337 (1946).
[5] A. D. Walsh, J. Chem. Soc. **1948**, 398 (1947).

and

$$D-\int_{r_{k_0},C}^{\infty}\frac{\partial E}{\partial r_k}\cdot dr_k, \qquad (7)$$

C being a new integration path which is defined by the equations:

$$r_i=r_{i_0}=\text{const. } i\neq k$$
$$\alpha_j=\alpha_{j_0}=\text{const. for all } j.$$

The following point, however, needs emphasis. If one accepts the integral (5) or (6) as a definition of Walsh's bond energy one finds that the sum of such bond energies is not equal to the heat of atomization. Therefore, the equation $\sum$ bond energies$=Q_a$ cannot be used for the calculation of bond energies defined in this manner.* Hence, in our opinion, the entities defined by integral (5) or (6) should not be called "bond energies."

Having defined in a general way the various quantities which should be relevant to the ideas of average bond energy and dissociation energy of the bond, we can now discuss their relationship in the case of some special molecular force fields. As yet we have not specified the character of the molecular force field. It seems that the simple valency force field is the best first approximation to the real molecular force field. In this approximation one assumes that:

$$\partial E/\partial r_k \text{ for all } r_k\text{'s and } \partial E/\partial\alpha_j \text{ for all } \alpha_j\text{'s}$$

are functions only of one r_k or α_j respectively.† Therefore, if the molecular force field is a simple valency force field then:

1. The integral

$$\int_{r_{k_0}}^{\infty}(\partial E/\partial r_k)\cdot dr_k$$

must be independent of the integration path.
2. The reaction path P must be identical with the path C.
3. The reorganization energy defined either by (5) or by (7) must be zero.

This means that in the simple valency force field the average bond energy is equal to the dissociation energy of the bond and to the entities defined either by (5) or by (6). According to this approximation, the final configuration of the radical produced by the breaking of any bond should be identical with the configuration of those atoms in the original molecule.

It thus becomes evident that the identification of the average bond energy with the dissociation energy of the bond, so generally accepted in the early days of the theory, arose from the belief that the molecular force field is represented by the simple valency force field. The system built up on this hypothesis was only in approximate agreement with experiment, but at least it was self-consistent. However, any approximation leading to a better agreement with experiment must introduce the idea of interaction between the non-bonded atoms. As a result of this interaction $\partial E/\partial r_k$ ceases to be a function of r_k only, hence the average bond energy should be different from the dissociation energy of the bond and the final configuration of the radical different from the initial configuration of those atoms in the original molecule. Studies of vibrational spectra proved beyond doubt that interaction between non-bonded atoms must be taken into account even for small deformations of the molecule.[6] The importance of these interactions is immensely magnified by the process of dissociation, where one can expect profound changes in the structure of fragments produced e.g. in the hybridization of the remaining bonds.

Numerical values for the dissociation energy of the bond or for the heat of atomization of the molecule could, in principle, be obtained by making various assumptions about the character of the molecular force field. Both these quantities are measurable and, therefore, the conclusions of the theory might be verified by experiment. On the other hand, any predicted values of the average bond energy (or bond energies as defined by (5) or by (6)) cannot be verified experimentally as the average bond energy is *in principle* not a measurable quantity.‡ To overcome this difficulty it was necessary to *assume* some relationship between the average bond energy and some other properties of the bond which are measurable, e.g., the bond length or the stretching force constant. The use of the former property may be justified, and in the hands of Pauling[2]

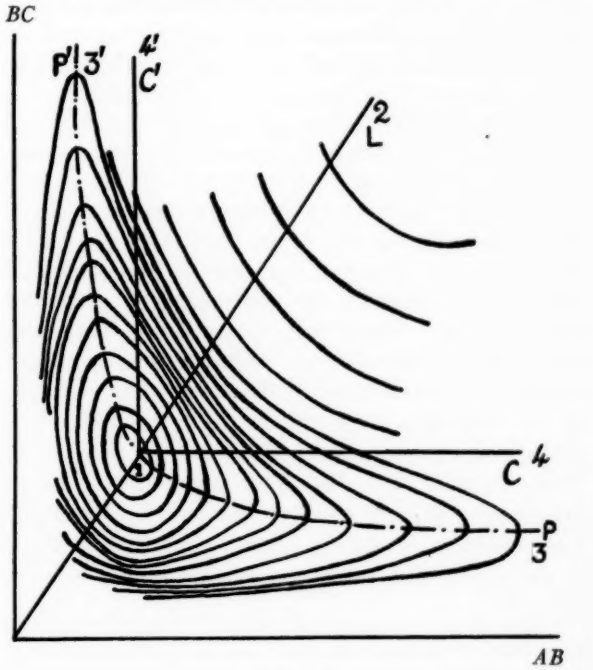

FIG. 1.

* It seems that this point was not sufficiently appreciated by Walsh.

† E.g., if terms of higher order than $(r-r_0)^3$ are neglected $\partial E/\partial r_k=k(r_k-r_{k_0})-3\beta(r_k-r_{k_0})^2$.

[6] For example, J. W. Linnett, Quarterly Reviews, **1**, 73 (1947).

‡ It may be argued that the situation is different for molecules of the type MA_n. Strictly speaking, however, it is the heat of atomization which is measured experimentally.

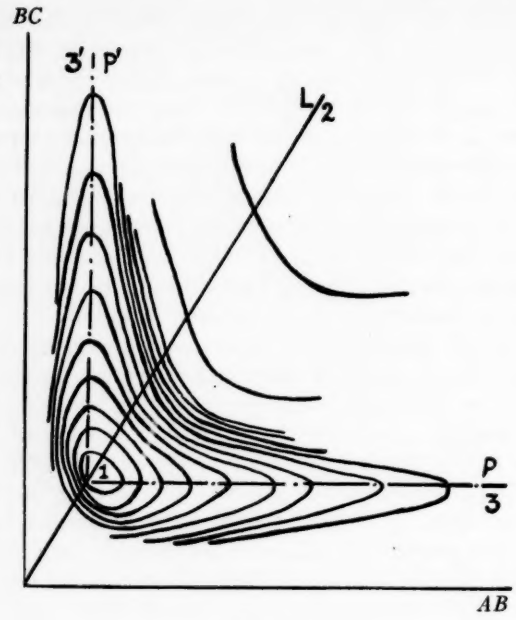

FIG. 2.

it produced most important results. The use of the latter, however, seems to be particularly questionable. The numerical value of the stretching force constant is derived from the experimental vibrational frequencies combined with some assumed structure of the molecular force field. Fortunately, there are methods which enable us to check whether the assignment of a particular force field to some particular molecule is correct.[6] If the molecular force field were a simple valency force field, then the stretching force constant could be taken as a measure of the stretching deformability of the bond in question.¶ Hence, it would be at least logical to expect some relationship between this force constant and the average bond energy. However, if the molecular force field has some more elaborate structure, then the stretching deformability of the bond is not given by the stretching force constant only, but by some expression which should contain, in addition to the stretching force constant, some other terms e.g., the cross-terms. Therefore, in this case there would be no logical justification for a relationship between the numerical value of the stretching force constant, derived from such a complicated force field, and the average bond energy. Thus it should be realized that statements of the type "bond A is slightly stronger than bond B because its force constant is slightly greater than that of B," are of very doubtful significance because the numerical values of these force constants have usually been derived from some complicated force field, and very often different force fields have been used for the two molecules which are compared.||

In conclusion we would like to stress that the real task of theory is to account for the quantities which have been measured, and to predict values for quantities which can be measured. Hence, the effort of theoreticians should be concentrated on calculating bond dissociation energies or heats of atomization which are both measurable quantities. Any discussion of average bond energies must always be very vague as soon as we abandon the principle of the constancy of average bond energies and any theoretical predictions about them cannot be verified experimentally.

APPENDIX

The ideas discussed above may be illustrated in a simple way for a linear triatomic molecule. Figure 1 represents the potential energy contour-map in coordinates r_{AB} and r_{BC} for such a molecule ABC. Point 1 represents the original molecule $A-B-C$. The straight line 1–2 represents the path L. The difference between the levels corresponding to points 2 (at infinity) and 1 gives the heat of atomization Q_a. The average bond energies $\tilde{q}_{AB}$ and $\tilde{q}_{BC}$ are obtained by integration of $\partial E/\partial r_{AB}$ and of $\partial E/\partial r_{BC}$ respectively along the line 1–2.

The lines along the potential energy valleys 1–3 and 1–3′ represent the paths P and P' corresponding to the dissociation processes $ABC \rightarrow A+BC$ and $ABC \rightarrow AB+C$ respectively. The difference between the levels of points 3 (at infinity) and 1 gives $D(A-BC)$; similarly $D(AB-C)$ is given by the difference between 3′ (at infinity) and 1. It should be noted that—

$$D(A-BC)+D(AB-C) \neq Q_a,$$

but

$$Q_a = D(A-BC)+D(B-C) \quad \text{or} \quad Q_a = D(AB-C)+D(A-B),$$

($D(B-C)$ and $D(A-B)$ are the dissociation energies of the bonds in the radicals BC and AB respectively.)

Lines 1–4 and 1–4′, which are parallel to the respective coordinate axes represent the paths C and C'. These are the integration paths used in the integrals (6) and (7).

Figure 2 represents the potential energy contour-map for the same molecule, but this time the molecular force field is a simple valency force field. Under these conditions the potential energy valleys run parallel to the axes of coordinates and the distinction between P (1–3) and C (1–4) disappears. The dissociation energy given by the difference in the levels of points 3 (at infinity) and 1 is the same as the difference between the levels corresponding to points 3′ and 2 (both at infinity). Therefore in this case:

$$D(A-BC)+D(AB-C)=Q_a,$$
$$\tilde{q}_{AB}=D(A-BC),$$

and

$$\tilde{q}_{BC}=D(AB-C).$$

¶ Even in the case of the simple valency force field the numerical value of the force constant depends on the correction for anharmonicity.

|| We must emphasize again that for very big changes in bond energies and force constants there is some qualitative relationship showing that the increase of one quantity is going parallel with the increase of the other. The reason for this parallelism is obvious. For such big changes one may expect to get the correct trend from the first approximation, i.e., from the treatment based on the simple valency force field, which requires this type of relationship.

Expansion of the Montmorillonite Lattice on Hydration

I. CORNET*
University of California, Berkeley, California
(Received October 3, 1949)

When exposed to water vapor, water, or some non-aqueous solvents, montmorillonitic clays display expansion of their lattices. Assuming that the expansion on hydration is a uni-dimensional swelling phenomenon, a thermodynamic analysis has been made which furnishes quantitative evaluation of interplanar forces. This analysis indicates that for lattice expansions of 3 or 4A from the dehydrated contracted state, the force between montmorillonite lattice layers is substantially constant; but for greater expansions the force diminishes in a complex manner. The analysis also indicates the possibility of determining quantitatively the forces exerted by molecules of solvents which expand the lattice, providing ion exchange does not occur. Problems in determining molecular forces and structure are discussed.

INTRODUCTION

THE clay mineral montmorillonite has a layer lattice which in chemical composition and crystal structure is similar to pyrophyllite; the crystal structure Pauling proposed for pyrophyllite[1] has been assigned to montmorillonite with but few modifications by Hofmann,[2,3] Marshall,[4] Hendricks[5] and others. Montmorillonite differs markedly from pyrophyllite in that it possesses high base exchange capacity† and a variable crystal spacing along the c axis. A current crystal structure[6] of montmorillonite which accounts for the differences between montmorillonite and pyrophyllite shows (Fig. 1) regular two-dimensionally crystalline sheets with some isomorphous replacement of magnesium ions for aluminum ions; the crystalline sheets are superposed without any regularity, except for a constant separation, and are held together by relatively weak forces. The crystalline sheets have a diameter of 1000 to 3000A.[7]

When montmorillonite is exposed to water, the lattice swells.[2] The variable crystal spacing along the c axis (the 001 spacing) was first determined for various vapor pressures by Hofmann and Bilke,[8] and has since been studied by other investigators.[9,10]

EXPERIMENTAL PROCEDURE AND RESULTS

Samples of montmorillonite saturated with three different cations were exposed to various vapor pressures in desiccators with sulfuric acid-water solutions. When equilibrium was attained, small quantities of the clays were placed in thin walled glass capillary tubes, and returned to the desiccators for one to two weeks to assure equilibrium again. The capillary tubes were then removed and rapidly sealed in a small flame, the seal being at least 2 cm from any clay in the tubes. The tubes were then x-rayed to obtain the c spacings, using Cu $K\alpha$-radiation. Lattice spacings were measured from photometric curves after graphical correction for scattered radiation. Data after Hofmann and Bilke[8] are given in Table I. If 001 spacing be plotted against the vapor pressure on rectangular coordinates, a sigmoid curve is obtained.

THERMODYNAMIC ANALYSIS

The crude mechanical model of the system water liquid-water vapor-montmorillonite (Fig. 2) shows how energy changes in the system must balance. For isothermal pressure changes of infinitesimal magnitude, the change in free energy of the water $=\Delta F=RT\ln(p/p_0)$ where p = the pressure of the water vapor and p_0 = saturation vapor pressure of water at temperature T. This change in free energy must equal the work done on the ideal (frictionless) hydraulic pump system. The pump work is transmitted through the jack to separate the crystalline sheets or layers of the montmorillonite an infinitesimal distance dx, the work of separation being done against an interplanar force f. Summing the energy terms

$$-\Delta F=-RT\ln(p/p_0)=-RT\ln h=\int f\,dx,$$

where h is the relative humidity. This analysis is consistent with the thermodynamic treatment of swelling presented by Katz,[11] but restricted to the case of one-dimensional swelling.

The change in free energy during hydration is shown as a function of the 001 spacing in Fig. 3.

---

* Assistant Professor of Mechanical Engineering; Consultant on Clay Research, Institute of Transportation and Traffic Engineering.

[1] L. Pauling, Proc. Nat. Acad. Sci. **16**, 123–129 (1930).

[2] Hofmann, Endell, and Wilm, Zeits. f. Krist. **86**, 340–8 (1933),

[3] Hofmann, Endell, and Wilm, Zeits. f. angew. Chemie **47**. 539–47 (1934).

[4] C. E. Marshall, Zeits. f. Krist. **91**, 433–49 (1935).

[5] S. B. Hendricks, J. Geol. **50**, 276 (1942).

† Base exchange capacity is the quantity of ammonium ions a material will retain on leaching with neutral normal ammonium acetate; it is usually expressed as milli-equivalents per hundred grams of oven dry colloid.

[6] D. M. C. MacEwan, Trans. Faraday Soc. **44**, 306, 349–367 (1948).

[7] v. Ardenne, Endell, and Hofmann, Ber. deut. keram. Ges. **21**, 209–27 (1940).

[8] U. Hofmann and W. Bilke, Kol. Zeits. **77**, 238–51 (1936).

[9] Bradley, Grim, and Clark, Zeits. f. Krist. **97**, 216–22 (1937).

[10] Hendricks, Nelson, and Alexander, J. Am. Chem. Soc. **62**, 1457–64 (1940).

[11] J. R. Katz, Trans. Faraday Soc. **29**, 279–300 (1933).

TABLE I. Variation of interplanar spacing of montmorillonite on hydration.

t °C	p_{H_2O} mm	Ca-montmorillonite 001 spacing, A	H-montmorillonite 001 spacing, A	Na-montmorillonite 001 spacing, A
21	0.0	11.25	11.4	10.1
21	0.4	12.1	12.8	11.3
21	2.4	13.4	—	12.7
21	4.9	14.6	14.5	12.9
21	8.7	15.1	15.3	14.
21	12.0	15.6	15.6	14.5
21	14.5	15.7	16.1	16.
21	16.7	17.8	18.9	17.8
21	18.65			
20	17.5	20.7*	20.45*	≫30.*

* Measured in distilled water.

DISCUSSION: RESULTS OF THE THERMODYNAMIC ANALYSIS

The slopes of the curves in Fig. 3 represent rates of change of energy with changes in displacement; the slope of a curve at any lattice spacing is therefore the force existing during an infinitesimal lattice displacement at that 001 spacing. For any one of the three curves shown a single higher order equation might possibly be obtained to fit the data. From the physical standpoint, it may be more fruitful to regard the curves as complex.

For vapor pressures of 0.4 mm to about 7.0 mm the expansion of the montmorillonites shown is characterized by a high, and substantially constant, rate of energy change during expansion. For the Na, Ca, and H saturated clays, the slopes are approximately 3.5, 2.7, and 3.3 (respectively), $\times 10^{10}$ ergs per mole per A of lattice expansion. This constancy of slope, or force, indicates that for the expansion involved, about 3 or 4A, the lattice may be analyzed substantially as a set of extended planes, and this force should depend primarily on the surface density of the electric charges.[12]

For the next 1 or 2A of lattice expansion the slopes of the curves, or the forces, diminish rapidly; the forces are inversely proportional to a power of the radius, as might be expected with dipoles. For Ca and H montmorillonite this transition appears to be quite abrupt at 14 to 15 mm pressure. This may indicate shortcomings in the experimental data, but more likely the differences between the three curves in the transition zone are due to differences in degree of hydration of the cations with which the clays are saturated.

For vapor pressures above 15 mm, the rate of change of free energy with lattice expansion of the clays is small, decreasing with increasing expansion, till the curves intersect the abscissa or approach it asymptotically. Unfortunately the data are insufficient to warrant quantitative statements, but it appears that for these broad expansions of the montmorillonite lattice, the slopes indicate a complex system of dipoles, with forces inversely proportional to higher powers of the displacement. For these high vapor pressures, there may be many layers of water molecules in the interplanar space. The lattice spacing in water is the result of equilibrium among forces (a) between water molecules, (b) between lattice layers, and (c) between water molecules and the lattice layers.

The initial expansion of the montmorillonite lattice from its dry state to a vapor pressure of 0.5 mm has not been discussed yet. Although there are no data presented for this range of vapor pressures, it seems clear that the curves of Fig. 3 must show discontinuity between the dry contracted lattice and the expanded spacings. No spacing should be found which is much too small to accommodate the water molecules. This behavior has been clearly demonstrated experimentally in a study of the sorption of anhydrous ammonia gas

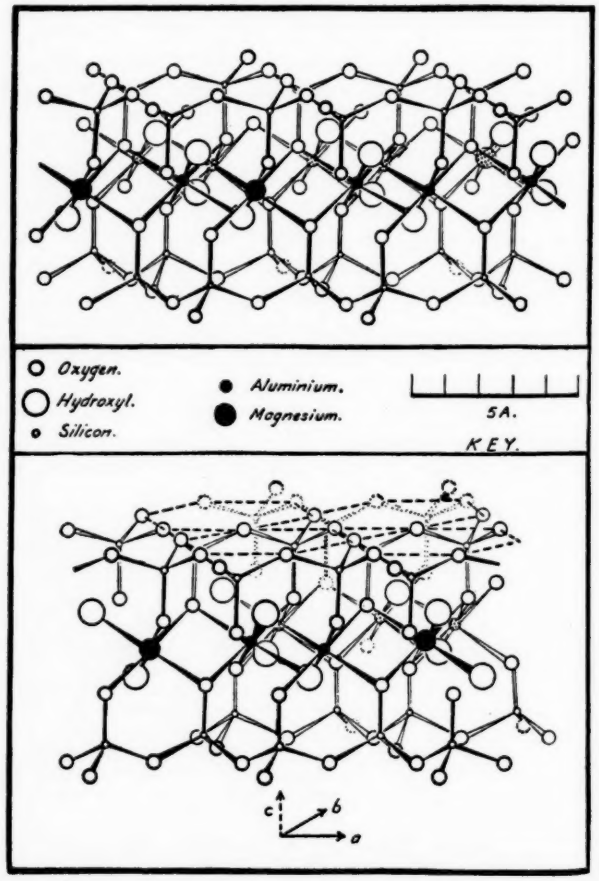

FIG. 1. The structure of montmorillonite. Background Al and Mg ions are spotted. Two structural sheets irregularly superposed are shown. The magnesium content of montmorillonite is from 1 to $\frac{2}{3}$ Mg^{++} per unit cell (containing 4 six-coordinated ions), so the replacement rate shown here (Mg^{++} in 5 octahedral positions out of 18) is rather higher than average. In the lower montmorillonite sheet, some of the rings of six oxygen ions are indicated by means of dotted lines, and one side of each hexagon has been omitted to avoid confusion. Each ring has a hole in the center, beneath which is an OH^- ion (after MacEwan, reference 6).

[12] W. D. MacMillan, *The Theory of Potential* (McGraw-Hill Book Company, Inc., New York, 1930), first edition, cf. pp. 42, 153, 209.

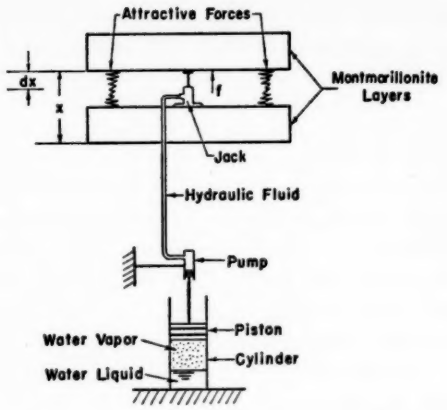

FIG. 2. Thermodynamic model of the process of expansion of montmorillonite on hydration. The work of isothermal expansion of the water vapor in the large cylinder $= \int PdV = -\Delta F = -RT \ln(P_2/P_1)$. This must equal $\int_{x_1}^{x_2} f dx$, where f is the force acting during the infinitesimal displacement, dx, in the lattice spacing x.

by dry hydrogen bentonite.[13] The x-ray patterns show distinct (001) spacings for a Wyoming-type hydrogen bentonite that has been dried at 100°C. Small quantities of ammonia, if admitted slowly, are sorbed without changing the x-ray pattern; this sorption occurs on exterior planar and on broken bond surfaces.[13] With larger quantities of ammonia, or more rapid admission of the gas, the lattice expands. The line which characterizes the (001) spacing grows broad and diffuse. In some samples at this stage there is no (001) line and the sample appears to be amorphous. At about 23 millimeters pressure of ammonia, the (001) lines indicate wider spacings, showing that the montmorillonite planes are separating. From this stage on, sharp distinct (001) spacings, showing lattice expansions of more then 2.2 A, are observed. Thereafter the lattice expands fairly regularly; as the ammonia pressure increases, the (001) spacing widens. A similar loss of x-ray pattern and subsequent re-orientation was observed by P. R. Stout in his study of the fixation of phosphate ion by kaolinite and halloysite.[14]

DISCUSSION: IMPORTANCE OF FURTHER UNDERSTANDING OF MONTMORILLONITE

Montmorillonitic clays, commonly called "bentonite," are of considerable importance in industry. They are used in making ceramics, binding foundry molding and core sands, emulsifying asphalt and other bituminous products, carrying insecticides, suspending electrolytes in dry cells.[15] In the oil and petroleum refining industry, montmorillonitic clays have been important as drilling muds,[16] as absorbents for purifying,[15] and as catalysts or catalyst carriers in the Thermofor catalytic cracking process.[17,18] Most of these applications of bentonite depend on the colloidal properties, the physical and chemical reactivity of the montmorillonite lattice.

Because of this industrial importance, and because montmorillonite appears related to soil colloids,[19,20] its structure has been investigated vigorously. However, an important theoretical consideration has arisen which intensifies the need for further and quantitative knowledge of montmorillonite. Investigators have been studying the expansion of montmorillonite by various organic compounds, and have interpreted the structure of the absorbed organic molecules from this expansion.[6,21–23] This application is not only illuminating, but it may possibly be extended to indicate quantitatively the forces acting between molecules, especially on adsorbing surfaces,[23] thus contributing to studies of permeability, immunology, catalysis and other fields.

To avoid misunderstanding, it should be noted that the force between montmorillonite lattice layers determined by this thermodynamic analysis of the swelling is the resultant force acting during an infinitesimal displacement of the lattice planes. The total free energy change between any two states of the lattice may include free energy changes due to hydration of cations, orientation of solvent molecules between the planes, and polarization of molecules between the lattice planes. The thermodynamic model shown in Fig. 2 is not intended to imply a concept of simple plates held

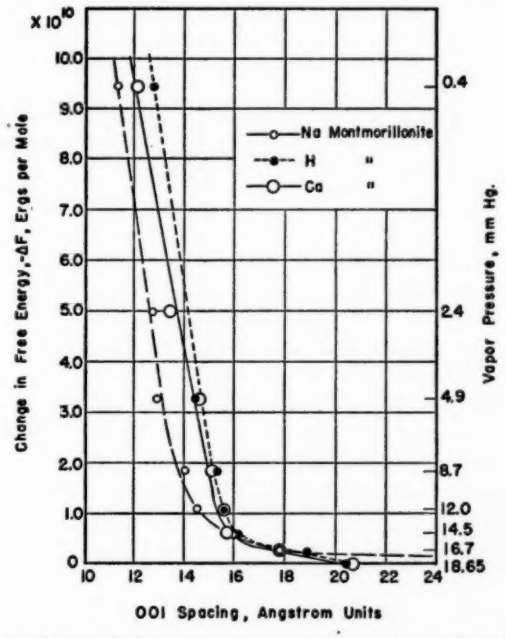

FIG. 3. Change in free energy on expansion of montmorillonite clays during hydration.

[13] I. Cornet, J. Chem. Phys. **11**, 217–226 (1943).
[14] P. R. Stout, Proc. Soil Sci. Soc. Am. **4**, 177–182 (1939).
[15] C. W. Davis and H. C. Vacher (revised by J. E. Conley), U. S. Dept. of Interior, Tech. Paper 609, 83 pp. (1940).
[16] Loomis, Ford, and Fidiam, A.I.M.E. Tech. Publ. 1201, Petrol. Tech., 12 pp. (1940).
[17] Davidson, Ewing, and Shute, Natl. Petrol. News, 5 pp. (July 7, 1943).
[18] R. C. Davidson, Petrol. Refiner, 12 pp. (Sept. 1947).
[19] S. B. Hendricks and W. H. Fry, Soil Sci. **29**, 457–479 (1930).
[20] Kelley, Dore, and Brown, Soil Sci. **31**, 25–55 (1931).
[21] S. B. Hendricks, J. Phys. Chem. **45**, 65–81 (1941).
[22] W. F. Bradley, J. Am. Chem. Soc. **67**, 975–981 (1945).
[23] D. M. C. MacEwan, Nature. **162**, 935–39 (1948).

together by simple forces; in a montmorillonite saturated with a cation like sodium or lithium, at vapor pressures approaching saturation, the forces of the original alumino-silicate layers will be greatly modified by the absorbed water which may be regarded as part of a new structure.

Studies of the swelling of montmorillonite in various solvents occasionally have been complicated by the possibility of cation exchange. For example, it may be desirable to avoid amines[24] in studying the swelling of a hydrogen montmorillonite; solvents displaying more or less prominent hydrogen bond formation[25] and small coulombic interaction with hydrogen montmorillonite would be recommended.[24]

[24] I. Cornet, "A Study of the Location and the Properties of Reactive Spots in Montmorillonitic Clay Lattices," Ph.D. Thesis, University of California, 119 pp. (October, 1942).
[25] H. L. Huggins, J. Org. Chem. 1, 407–456 (1936).

Structures determined by studies of the lattice expansion of montmorillonite should be regarded in light of the polarizing environment of the interplanar spaces. Bradley has stated that the interaction between hydrogen atoms of aliphatic chains with oxygen ions of the silicate surface involves energy comparable in magnitude with that for O—H···O bonds of a water system, and he has postulated polarization of aromatic rings as a whole.[22]

In summary, the thermodynamic analysis of Fig. 3 evaluates force at any lattice displacement, providing ion exchange has not occurred, and providing that effects of variations in hydrogen bonding and in solvation of cations are considered. The same source, preparation and particle size of montmorillonite should be used for thermodynamic calibration analysis as is used for the study of swelling in solvents.

THE JOURNAL OF CHEMICAL PHYSICS VOLUME 18, NUMBER 5 MAY, 1950

The Determination of Energy Levels from Thermodynamic Data. I. The Effect of Experimental Error

ELLIS BLADE AND GEORGE E. KIMBALL
Department of Chemistry, Columbia University, New York, New York
(Received October 6, 1949)

The problem of calculating energy levels from thermodynamic data can be reduced to that of inverting the Laplace transform, for which several procedures have been developed. Using the method of Widder, we show that the resultant calculated energy level density function consists of a series of broadened peaks, whereas in the true density the levels are represented by a series of Dirac delta-functions.

Alternatively, if the distribution of the energy levels is specifically assumed to be composed of discrete energies, the calculation reduces to the moment problem.

In either case the calculation is shown to have an inherent "resolving power," in that levels within a certain closeness cannot be distinguished as separate. By a generalization of this idea, it is shown that the computation can lead to a knowledge of the over-all density of energy levels within a given region, but cannot reveal their exact locations.

1. INTRODUCTION

STATISTICAL mechanics provides a relationship between the quantum-mechanical energy levels of a system and the thermodynamic properties. For a system of identical, weakly interacting molecules, the relationship is expressible in terms of the partition function,

$$Q(\beta)=\sum e^{-\beta E_i}, \tag{1}$$

where E_i is the i-th energy level of a molecule, and $\beta=1/kT$. The free energy of the system is related to the partition function by

$$F=-kT\ln(Q^N/N!) \tag{2}$$

if the system contains N molecules, and the other thermodynamic properties can be found from F by well-known methods.

When the energy levels are known, the calculation of the thermodynamic functions is a straightforward process, and is known to give accurate results. On the other hand, attempts to reverse this process, to find energy levels, have been less successful. It has been found that energy levels calculated in this way are subject to large errors. It is the purpose of this paper to investigate the origin of these errors and the extent to which information concerning energy levels can be derived from thermodynamic data.

2. THE PARTITION FUNCTION AS A LAPLACE TRANSFORM

It has been pointed out by Bauer[1] that the partition function is mathematically the Laplace transform of the energy level density. That is, if the energy levels can be expressed by a density function $g(E)$ such that

[1] S. H. Bauer, J. Chem. Phys. 6, 403–404 (1938); 7, 1097–1102 (1939).

$g(E)dE$ is the number of energy levels between E and $E+dE$, and the zero of energy is chosen so that all the levels have positive energies, then

$$Q(\beta)=\int_0^\infty g(E)e^{-\beta E}dE. \tag{3}$$

Because of the discrete nature of the levels, the density function is actually a sum of Dirac delta-functions,[2]

$$g(E)=\sum\delta(E-E_i), \tag{4}$$

and it is better to consider the partition function as a Laplace-Stieltjes transform[3]

$$Q(\beta)=\int_0^\infty e^{-\beta E}dG(E), \tag{5}$$

where $G(E)$ is the number of energy levels below E. The problem of determining the energy levels is then that of inverting the transform (3) or (5).

A number of methods of inversion of the Laplace transform are known. Typical is that proposed by Post and developed by Widder.[4] As applied to the Laplace transform (3), the operator $L_{n,E}(Q(\beta))$ is defined by

$$L_{n,E}(Q(\beta))=\frac{(-1)^n}{n!}\left[\frac{d^nQ(\beta)}{d\beta^n}\right]_{\beta=n/E}\left(\frac{n}{E}\right)^{n+1}. \tag{6}$$

Then

$$\lim_{n\to\infty}L_{n,E}(Q(\beta))=g(E). \tag{7}$$

To apply this method, one must know the partition function and all its derivatives at values of β which are larger and larger as the value of n is increased. That is, the thermodynamic functions must be known with greater and greater precision at lower and lower temperatures. Sooner or later the limitations of experimental technique actually force a stop to this process, and the value of $L_{n,E}(Q(\beta))$ for some finite n must be used as an approximation to $g(E)$. The question is therefore, how good is this approximation?

Applying the operator to the original expression (1) for Q, we find

$$L_{n,E}(Q(\beta))=\sum_i\frac{E_i{}^nn^{n+1}}{E^{n+1}}\exp(-nE_i/E). \tag{8}$$

It is easily seen that any term in this sum vanishes for $E=0$ and for $E\to\infty$, and it can be shown that it reaches a maximum for $E=(n/n+1)E_i$. For large n, the term approaches a Gauss error function

$$\frac{1}{(2\pi)^{\frac{1}{2}}\sigma}\exp[-(E-E_i)^2/2\sigma^2]. \tag{9}$$

with a standard deviation

$$\sigma=E_i/(n)^{\frac{1}{2}}. \tag{10}$$

The effect of terminating the inversion process at a given n is therefore to replace each delta-function in the true density of energy levels, by a broad peak whose width is inversely proportional to $(n)^{\frac{1}{2}}$.

This broadening of the peaks in the energy level density is somewhat analogous to the broadening of the lines in a spectrum, caused by using a spectroscope of low resolving power. It is therefore convenient to express the result of terminating the approximation at a given value of n, by saying that the resolving power of the method for an energy level E_i is $E_i/(n)^{\frac{1}{2}}$. If two or more levels lie closer together than this amount, the peaks in the approximate energy level density function will overlap so much that the individual levels cannot be distinguished.

Other methods lead to similar difficulties. For example, Bauer[1] suggests approximating the partition function by a polynomial in the absolute temperature, or what is the same thing, an expression of the form

$$Q=\sum_{j=1}^{n}a_j\beta^{-(j+1)}. \tag{11}$$

The inverse Laplace transform of such an expression is easy to find without further approximation, giving

$$g(E)=\sum_{j=1}^{n}\frac{a_j}{j!}E^j. \tag{12}$$

Because of the fact that this function is a polynomial of the n-th degree, it cannot have more than $n-1$ maxima and minima, and it may have fewer. Hence at most $n/2$ peaks can appear in the calculated density, and those peaks which are present will be far from the shape of delta-functions. This lack of resolution is similar to that found by the use of the Post-Widder operator.

In effect, all methods of inversion require expressing the partition function in terms of some polynomial $P(\beta)$, for example, in the form

$$Q(\beta)=f(\beta)P(\beta), \tag{13}$$

where $f(\beta)$ is some conveniently chosen function. Although $P(\beta)$ can be made to fit any function as closely as we please by taking its degree large enough, the higher derivatives of $P(\beta)$ become increasingly poor representations of the derivatives of the function, as the degree is increased. In the usual procedures for numerical approximation in which functions are replaced by polynomials, the degree n of the polynomial is chosen in such manner that the $(n+1)st$ differences of the given set of values are of the order of the experimental errors of the data. Choosing n in this way amounts to the assumption that the $(n+1)st$ derivatives of the given function are zero. If such a process

[2] P. A. M. Dirac, *The Principles of Quantum Mechanics* (Oxford University Press, New York, 1940), Edition 2.
[3] Compare, D. V. Widder, *The Laplace Transform* (Princeton University Press, Princeton, 1941).
[4] D. V. Widder, reference 3, Chapter VII.

is used to find $P(\beta)$ in (13), any subsequent procedure requiring derivatives of $Q(\beta)$ higher than the n-th, is doomed to failure because of the fact that completely arbitrary values have been introduced for these derivatives.

The inversion of the function (13) can always be imagined to be carried out by the Post-Widder process. For small values of n, the operator $L_{n,E}$ introduces only derivatives of small order, but represents the energy levels by broad peaks. As n is increased the peaks should sharpen, but because the errors in the derivatives increase with n, an unknown function is introduced which obscures the desired result. Eventually, for large n, the unknown function becomes by far the most prominent part of the result.

This effect is well illustrated in the following example. It is perfectly feasible to represent $Q(\beta)$ itself by a polynomial in positive powers of β, up to the accuracy allowed by the data. If this polynomial is inverted directly, using Laplace transform pairs, the density of energy levels is found to be zero everywhere except at the origin, $E=0$, where a superposition of the delta-function and its "derivatives" is found. This result is obviously nothing like the correct answer, but if the inversion is carried out with the operator $L_{n,E}$, with even a small value of n, we can get an approximate density function. For example, even if we choose $n=1$, some useful information results, namely,

$$g(E)=-\left(\frac{1}{E}\right)^2\left[\frac{dQ(\beta)}{d\beta}\right]_{\beta=1/E}=\frac{1}{k}\left[\frac{dQ}{dT}\right]_{T=E/k}. \quad (14)$$

In the best heat capacity work, data are obtained which might justify the use of a fourth-degree approximating polynomial, but not higher. In obtaining the partition function from such data, the heat capacity is integrated twice, so that, after expanding the logarithms which occur, Q is representable by a sixth-degree polynomial. In other words, we may know as many as six derivatives of Q, but no more. The best knowledge we can obtain of the energy levels is that corresponding to the operator $L_{6,E}$, which will give a resolving power for a level at E_i, of $E_i/(6)^{\frac{1}{2}}$. The uncertainty in the position of each level is about 40 percent. It is obvious that even a substantial increase in the degree of the polynomial would produce only a slow improvement in this situation.

3. THE MOMENT METHOD

It may be objected that the above argument, based on the inversion of the Laplace transform, makes no use of the fact that we *know* that the true density of energy levels is representable in the form (4), a sum of delta-functions. That is, there might be methods, taking advantage of the discreteness of the energy levels, which would be capable of substantially greater accuracy. We shall show next that this cannot be so.

In a method where the energy levels are considered to be discrete, we need a somewhat different definition of resolving power. We shall say that two levels are resolved if, and only if, when they are replaced by a doubly degenerate level at their mean value, the resulting change in the partition function is not less than the standard deviation of the latter, within the temperature range over which the partition function is known. If such a replacement never causes such a change, it is therefore impossible to prove that the two levels have distinct energies.

Suppose that the two levels have energies $E_0+\Delta E_0$ and $E_0-\Delta E_0$. The contribution Q_{12} of the pair to the partition function is then

$$Q_{12}=e^{-\beta(E_0-\Delta E)}+e^{-\beta(E_0+\Delta E)}. \quad (15)$$

Replacing the pair by a doubly degenerate pair at E_0 changes this contribution to

$$Q_{12}'=2e^{-\beta E_0} \quad (16)$$

and the change in the partition function is

$$\Delta Q_{12}=Q_{12}-Q_{12}'=e^{-\beta E_0}(e^{\beta\Delta E}+e^{-\beta\Delta E}-2). \quad (17)$$

If ΔE is small, this expression becomes

$$\Delta Q_{12}=e^{-\beta E_0}\beta^2(\Delta E)^2. \quad (18)$$

The maximum value of ΔQ_{12} occurs when $\beta=2/E_0$, or

$$\Delta Q_{12\,\max}=4e^{-2}(\Delta E/E_0)^2=0.54(\Delta E/E_0)^2. \quad (19)$$

If the standard deviation of the errors in Q is σ, the two levels are just resolved, according to our definition, when

$$\Delta E=1.36(\sigma)^{\frac{1}{2}}E_0. \quad (20)$$

If σ depends on temperature, it is the value at the temperature for which $\beta E_0=1$ which is to be used.

This result can be generalized in the following way. Consider a group of r levels, of energies $E_0+\epsilon_i$, with $|\epsilon_i|<\Delta E$. The contribution Q_r of the group of levels to the partition function is

$$Q_r=\sum_{i=1}^{r} e^{-\beta(E_0+\epsilon_i)}=e^{-\beta E_0}\sum_n (-1)^n\frac{\beta^n}{n!}\mu_n, \quad (21)$$

where μ_n is the n-th moment of the ϵ_i, defined by

$$\mu_n=\sum_{i=1}^{r}\epsilon_i{}^n. \quad (22)$$

Now since $|\mu_n|<r\Delta E^n$, it can be shown that the term in μ_n contributes less than

$$r\frac{n^n e^{-n}}{n!}\left(\frac{\Delta E}{E_0}\right)^n. \quad (23)$$

As n increases, this expression becomes small, and eventually will become less than the standard deviation of the errors in Q. Hence only a finite number of the moments can be determined.

Now suppose that each of the ϵ_i is changed to $\epsilon_i+\delta\epsilon_i$, where $\delta\epsilon_i$ is given by

$$\delta\epsilon_i=\lambda\frac{(\Delta E)^2}{\prod_{j\neq i}(\epsilon_i-\epsilon_j)}, \tag{24}$$

where λ is an arbitrary constant of proportionality, and $2\Delta E$ is the energy interval containing all the levels. To the first order in λ the resulting changes in the moments are

$$\delta\mu_n=n\sum_i \epsilon_i{}^{n-1}\delta\epsilon_i=n(\Delta E)^n\lambda\sum_i\frac{\epsilon_i{}^{n-1}}{\prod_{j\neq i}(\epsilon_i-\epsilon_j)}. \tag{25}$$

We now propose to show that, to the first order in λ, $\delta\mu_n$ vanishes for every $n<r$, when the array of $\delta\epsilon_i$ is chosen as in (24).

To show this, we note that the sum in (25) is a rational function of the ϵ_i, whose denominator is

$$\prod_k\prod_{j<k}(\epsilon_k-\epsilon_j).$$

The numerator of this function is

$$\nu=\sum_i(-1)^{r+1}\epsilon_i{}^{n-1}\prod_{\substack{j<k\\ j\neq i\\ k\neq i}}(\epsilon_k-\epsilon_j), \tag{26}$$

which is a homogeneous polynomial whose degree is not greater than

$$\frac{(r-1)(r-2)}{2}+n-1.$$

Now, if, for some arbitrary p and q, we put $\epsilon_p=\epsilon_q$, all the terms in this sum vanish except for those in which $i=p$ and $i=q$. Hence

$$\nu=(-1)^{r-p}\epsilon_p{}^{n-1}\prod_{\substack{j<k\\ j\neq p\\ k\neq p}}(\epsilon_k-\epsilon_j)+(-1)^{r-q}\epsilon_q{}^{n-1}\prod_{\substack{j<k\\ j\neq q\\ k\neq q}}(\epsilon_k-\epsilon_j).$$

Since $\epsilon_p=\epsilon_q$, the factors $\epsilon_p{}^{n-1}$ and $\epsilon_q{}^{n-1}$ are equal, and furthermore the same factors occur in both products, except for signs. It is easily seen that exactly $|p-q|-1$ terms will have their signs changed. If the difference between p and q is even, then $(-1)^{r-p}=(-1)^{r-q}$, but an odd number of factors in the two products have opposite signs, and ν vanishes. If the difference between p and q is odd, the signs of an even number of factors change, but $(-1)^{r-p}=-(-1)^{r-q}$ and ν vanishes again.

We have therefore shown that the numerator ν vanishes whenever any ϵ_p is equal to any ϵ_q. It follows that ν is divisible by

$$\prod_{j<k}(\epsilon_k-\epsilon_j).$$

But this product is of degree $[r(r-1)/2]$, and if $n<r$, the degree is greater than $[(r-1)(r-2)/2]+n-1$, which is possible only if ν vanishes identically. It follows that $\delta\mu_n$ vanishes for $n<r$, which is what we set out to prove.

Returning now to the expansion for Q_r, Eq. (21), we see that the replacement of the ϵ_i by $\epsilon_i+\delta\epsilon_i$ causes a change δQ, of which the leading term is

$$\delta Q=e^{-\beta E_0}(-1)^r(\beta^r/r!)\delta\mu_r.$$

By a simple extension of the preceding argument, $\delta\mu_n$ can be shown to have the absolute value $r(\Delta E)^r\lambda$. Using the fact that

$$e^{-\beta E_0}\beta^r\leqq\frac{r^re^{-r}}{E_0{}^r}$$

we find that

$$\delta Q<\frac{r^re^{-r}}{(r-1)!}\left(\frac{\Delta E}{E_0}\right)^r\lambda. \tag{27}$$

It follows that λ can be as large as

$$\frac{(r-1)!}{r^re^{-r}}\left(\frac{E_0}{\Delta E}\right)^r\sigma$$

without causing appreciable shifts in the value of Q_r. In terms of the energy levels, the shifts are of the order of

$$\delta E_i=\frac{\epsilon_0{}^r}{\prod_{j\neq i}(\epsilon_i-\epsilon_j)}\frac{(r-1)!}{r^re^{-r}}\sigma. \tag{28}$$

If there is a large number of energy levels, whose separations are small compared to the absolute value of the energy, the errors in the determination of the exact positions can be large.

Both of the foregoing analyses show that the particular method of calculation is immaterial to the conclusion about the final result of the energy level calculation. The positions of the levels can be determined from thermodynamic data only to within a certain zone of uncertainty, dependent upon the magnitude of experimental error in the data. That is, the uncertainty is inherent in the problem itself, and it is large enough to drastically limit the practical computation of energy levels. Such a computation leads to a knowledge of the overall energy level density within a given region, but cannot reveal the exact locations of the levels.

The Determination of Energy Levels from Thermodynamic Data. II. The Heights of Potential Energy Barriers Restricting Intramolecular Rotation

ELLIS BLADE AND GEORGE E. KIMBALL
Department of Chemistry, Columbia University, New York, New York

(Received October 6, 1949)

The uncertainty in the distribution of the energy levels implies a corresponding uncertainty in the shape of the associated potential energy function. The estimation of barrier heights is known to depend upon the shape of the potential, therefore implicitly upon the energy level distribution. We apply these ideas to the restricted rotation problem by introducing a shape parameter into the assumed potential function, and show that the currently accepted barrier height ranges should be widened. On the basis of our modified function, we found the following barrier heights to be consistent with published thermodynamic data: ethane 1550 to 2700 calories per mole; 1,1,1-trifluoroethane 2300 to 8300; methanol 800 to 3000.

1. INTRODUCTION

THE characteristics of internal rotational degrees of freedom of molecules have to be determined indirectly by appeal to thermodynamic data, owing to the inadequacy of the needed spectroscopic information. Because of the difficulties now made plain in Part I of this paper, it has never been found practical to work directly from the thermodynamic data toward the energy levels, but it is customary to start by assuming a plausible shape of potential function opposing the rotation, based on the known internal geometry of the molecule. This assumption is tantamount to selecting, *a priori*, the general pattern of the energy level distribution for this degree of freedom. Inasmuch as the positions of the levels and the calculated thermodynamic properties depend on the height as well as the shape of the potential barrier, it is necessary to repeat the calculation for several heights, until the calculated property reaches agreement with the measured value.[1]

The calculated thermodynamic properties are not very sensitive to changes in the distribution of energy levels, as was discussed in Part I. Therefore it should be possible to meet the given thermodynamic conditions with any one of a variety of energy level distributions, belonging to a corresponding variety of barrier shapes.

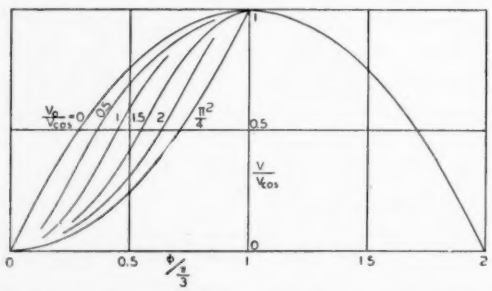

FIG. 1. The two-parabola potential function. This figure shows how the shape of the potential curve can be changed while the barrier height remains fixed.

[1] G. Glockler, Rev. Mod. Phys. **15**, 111–173 (1943); E. B. Wilson, Jr., Chem. Rev. **27**, 17–38 (1940); K. S. Pitzer, Chem. Rev. **27**, 39–57 (1940) and others.

The heights of these barriers will in general depend on their shapes, so the selection of the barrier shape ought to be one of the principal considerations in the study of the restricted rotation problem.

As a matter of fact, on account of the lack of any really complete information about the secondary forces acting within molecules,[2] the selection of barrier shapes has been dictated by mathematical convenience, and the cosine potential

$$V=(V_{\cos}/2)(1-\cos n\phi) \tag{29}$$

has been almost universally used.[3] On the other hand, there have been numerous warnings that the magnitudes of calculated barriers might come out very differently if other barrier shapes were to be employed.[4] In the succeeding sections of this paper, one such possibility is explored.

2. THE TWO-PARABOLA POTENTIAL

It is desirable in this study to have separate parameters for the height and the shape of the potential function. In order to be able to establish a connection with the usually assumed cosine function, we shall start with a parabola whose curvature at its lowest point is the same as that of the cosine. Since this curvature governs the spacing of the lowest levels, the distribution of energy levels will start out in the familiar way, like that belonging to the cosine potential.

For such a potential with three minima, and of double amplitude $V_{\cos}$,

$$V=(V_{\cos}/2)(1-\cos 3\phi) \tag{30}$$

[2] Compare K. S. Pitzer, J. Am. Chem. Soc. **70**, 2140–2145 (1948); Aston, Isserow, Szasz, and Kennedy, J. Chem. Phys. **12**, 336–344 (1944); Gorin, Walter, and Eyring, J. Am. Chem. Soc. **61**, 1876–1886 (1939), and others.

[3] Tabulations of thermodynamic functions for this form of potential have been provided by the following authors: J. O. Halford, J. Chem. Phys. **15**, 364–367 (1947); K. S. Pitzer and W. D. Gwinn, J. Chem. Phys. **10**, 428–440 (1942); K. S. Pitzer, J. Chem. Phys. **5**, 469–472 (1937).

[4] A. Charlesby, Proc. Phys. Soc. London **54**, 471–487 (1942); G. B. Kistiakowsky, J. R. Lacher, F. Stitt, J. Chem. Phys. **7**, 289–296 (1939); E. B. Wilson, Jr., J. Chem. Phys. **6**, 740–745 (1938); K. S. Pitzer and J. D. Kemp, J. Am. Chem. Soc. **60**, 1515–1516 (1938); K. S. Pitzer, J. Chem. Phys. **5**, 469–472 (1937).

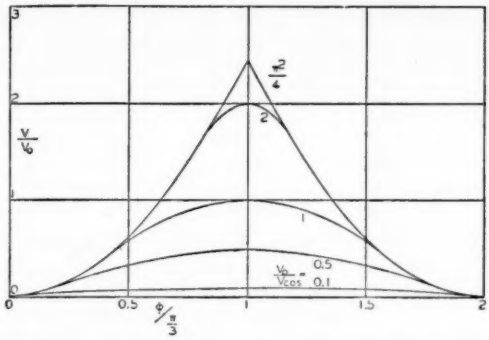

FIG. 2. The two-parabola potential function. This figure shows how the shape of the potential curve can be changed while retaining a fixed curvature at the minima. The *nominal* barrier height $V_{\cos}$ is kept constant.

the curvature at each of these minima is

$$\left[\frac{d^2V}{d\phi^2}\right]_{\phi=0}=\frac{9}{2}V_{\cos}. \tag{31}$$

Hence the parabolas for the three lower parts of the potential function must be of the form

$$V_1=\frac{9}{4}V_{\cos}\phi^2, \qquad \left(-\frac{4}{3\pi}\frac{V_0}{V_{\cos}}\leqq\phi\leqq\frac{4}{3\pi}\frac{V_0}{V_{\cos}}\right). \tag{32a}$$

For the upper three parts we shall take other parabolas, concave downward, of the form

$$V_2=V_{\cos}\frac{V_0}{V_{\cos}}\left[1-\frac{9}{\pi^2-4(V_0/V_{\cos})}\left(\phi-\frac{\pi}{3}\right)^2\right], \qquad \left(\frac{4}{3\pi}\frac{V_0}{V_{\cos}}\leqq\phi\leqq\frac{2\pi}{3}-\frac{4}{3\pi}\frac{V_0}{V_{\cos}}\right). \tag{32b}$$

These parabolas join smoothly at the end points of their respective intervals, and the whole potential is represented by a smooth composite curve of parabolas opening alternately upward and downward.

This potential has the same curvature at its bottoms as the cosine potential of height $V_{\cos}$, from which it was derived, and we take this height as the first or height parameter. The second or shape parameter is the ratio $V_0/V_{\cos}$, of the actual barrier height V_0, to the nominal or cosine barrier height $V_{\cos}$. The characteristics of these curves are shown in Figs. 1 and 2.

It is not possible, for an arbitrary potential such as (32), to integrate Schroedinger's equation in closed form, therefore we used approximate quantum conditions derived by the phase integral method (WKB method),[5] namely,

$$\cos\theta_C\cosh(\theta_N+\ln 2)=s^6 \tag{33}$$

$s=1$ for S_{6n} and A_{6n} levels.

$=-\frac{1}{2}$ for S_{6n+2} and A_{6n+4} levels.

where

$$\theta_C=\int_C\left[\frac{8\pi^2I}{h^2}(E-V)\right]^{\frac{1}{2}}d\phi$$

and

$$\theta_N=\int_N\left[\frac{8\pi^2I}{h^2}(V-E)\right]^{\frac{1}{2}}d\phi$$

are the phase integrals, with C denoting the classical region of motion, and N the non-classical. S and A designate wave functions symmetrical and antisymmetrical respectively, with respect to one of the planes of symmetry. Above the barrier the S_{6n} and A_{6n} levels approach each other and finally coalesce to form the C_{6n} (common) rotational levels. The subscripts on these symbols express the total number of nodes of the wave function per revolution, which is double the rotational quantum number. Figure 3 shows the inter-relations of these quantities. In group-theoretical language, the S_{6n} levels belong to the representation A_1 of the group C_{3v}; the A_{6n} levels to A_2; and the S_{6n+2} and the A_{6n+4} to E.

This diagram, for a hypothetical case, shows how the energy levels are distributed for various potentials. The harmonic oscillator levels are found along the straight line, at places where the phase integral θ_C reaches the

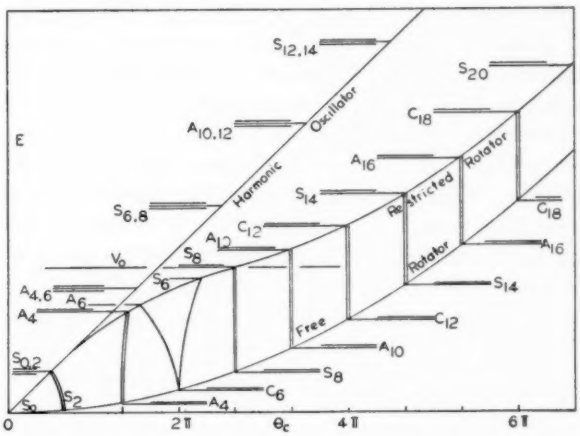

FIG. 3. Relation of the levels of the restricted rotator to those of the limiting oscillator and the limiting free rotator.

[5] W. H. Furry, Phys. Rev. **71**, 361–371 (1947); A. K. Saha, Proc. Nat. Inst. Sci. India **10**, 373–385 (1944); E. Persico, I, Nuovo Cimento **15**, 133–138 (1938); R. E. Langer, Phys. Rev. **51**l 669–676 (1937); E. C. Kemble, Phys. Rev. **48**, 549–561 (1935), and others.

[6] We derived this condition from the two given by H. D. Koenig, Phys. Rev. **44**, 657–665 (1933) in the forms

$$\theta_C=(n+\tfrac{1}{2})\pi-(-1)^n\cdot 2\arctan\tfrac{1}{2}e^{-\theta_N},$$

$$\theta_C=(n+\tfrac{1}{2})\pi+(-1)^n\cdot 2\arctan\frac{2e^{\theta_N}}{1+4e^{2\theta_N}+(1+4e^{2\theta_N}+16e^{4\theta_N})^{\frac{1}{2}}}.$$

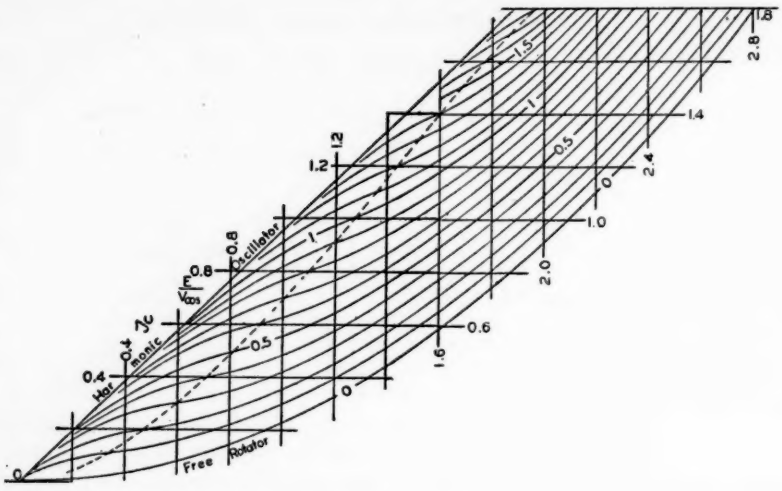

FIG. 4. Energy level diagram.

values $(2n+1)\pi/2$. These levels, alternately symmetric (S) and antisymmetric (A), would ordinarily be single, but the presence of three equal potential minima results in a treble degeneracy. The numerical subscripts express the number of nodes per revolution, in the wave function to which the respective levels belong.

At the other extreme, the levels of the plane rotator, without any restricting potential, are distributed along the parabola wherever the phase integral θ_C reaches the values $2n\pi/3$. The initial rotational level S_0 (not marked) is single; the rest are doubly degenerate. The members of each pair belong to a symmetric and an antisymmetric wave function, respectively. The symbols S, A, and C (common) designate the fate of these levels in the presence of a parabolic potential, corresponding to a harmonic oscillator. The rotational quantum numbers are half the number of nodes of the wave functions, expressed by the subscripts.

The vertical joining-lines and curves between the free-rotator-line and the restricted-rotator-line connect the positions of the levels under these two potential conditions. The S and A rotational levels remain doubly degenerate as the potential increases from zero, but the C-levels below the barrier V_0 split into two parts. In the transition zone, just below the barrier top, these levels remain separate single levels in the restricted rotator. In the lowest or vibrational region of the restricted rotator, the splitting C-levels join with their doubly degenerate neighbors on both sides, and go over into the trebly degenerate levels of the harmonic oscillator.

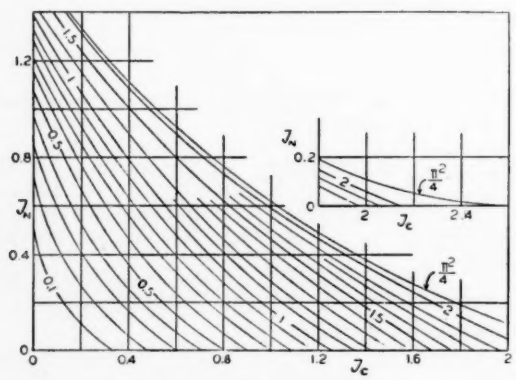

FIG. 5. Phase integral diagram.

The energy levels can be found by the following method: If we introduce the parameter α defined by

$$\alpha=[(8\pi^2 I/h^2)V_{\cos}]^{\frac{1}{2}} \tag{34}$$

then $\theta_C=\alpha J_C$ and $\theta_N=\alpha J_N$, where

$$J_C=\int_C\left(\frac{E-V}{V_{\cos}}\right)^{\frac{1}{2}}d\phi,$$
$$J_N=\int_N\left(\frac{V-E}{V_{\cos}}\right)^{\frac{1}{2}}d\phi. \tag{35}$$

For a given ratio $V_0/V_{\cos}$, we can plot $E/V_{\cos}$ as a function of J_C, the energy level diagram, and J_N as a function of J_C, the phase integral diagram. These plots, for a number of values of $V_0/V_{\cos}$, are shown in Figs. 4 and 5 respectively.

Now if θ_N is large, Eq. (33) takes the approximate form

$$\cos\theta_C=0 \tag{36}$$

or

$$J_C=\frac{(n+\frac{1}{2})\pi}{\alpha} \tag{37}$$

where n is an integer. For any given n we can find an approximate value of J_C from (37). Then, from the phase integral diagram, Fig. 5, we can find an approximate value of J_N. This value of J_N gives a value of θ_N which can be used in Eq. (33) to obtain an improved value of θ_C and hence J_C. This process can be iterated, to find values of J_C and J_N which simultaneously satisfy Eq. (33) and the relationship portrayed in Fig. 5. The iteration converges rapidly, especially for the levels which are not very close to the top of the barrier. For

TABLE I. Restricted rotational heat capacity in ethane.

T °K	92.4	93.1	93.5	94.3	97.4	98.4	99.6	100.5	134.1
C_v	6.57	6.51	6.55	6.55	6.59	6.60	6.64	6.64	7.22
C_v/R	3.307	3.277	3.297	3.297	3.317	3.322	3.342	3.342	3.634
Less 3	0.307	0.277	0.297	0.297	0.317	0.322	0.342	0.342	0.634
C_{vib}/R	0.001	0.001	0.001	0.001	0.002	0.002	0.002	0.002	0.027
C_{rr}/R	0.306	0.276	0.296	0.296	0.315	0.320	0.340	0.340	0.607

these levels, the first approximation, given by (37), is sufficiently close for many purposes.

In practice it is convenient to modify Eq. (33) to the form

$$\sin\Delta\theta_C=(-1)^{n+1}s\ \mathrm{sech}(\theta_N+\ln 2) \tag{38}$$

in which $\Delta\theta_C=\theta_C-(n+\frac{1}{2})\pi$ is the correction to the original $\theta_C=(n+\frac{1}{2})\pi$. This procedure gives the values of θ_C for levels below the top of the barrier. Above the barrier the levels occur in pairs, the approximate quantization being like that of the free rotator,

$$J_C=\frac{2\pi n}{\nu\alpha} \tag{39}$$

where ν, the symmetry number for restricted rotation, is 3 for the ethane-like systems under discussion here.

Figure 3 shows the results for a typical case. This plot is similar to Fig. 4, and shows a comparison of restricted rotator levels for $V_0/V_{\cos}$ equal to 0.5, with the corresponding levels of the related harmonic oscillator and of the completely free rotator. The abscissae and ordinates are θ_C and E, respectively.

The statistical calculations of entropy for the various modes of motion, referred to in the following section, are based on the formulas:

$$\frac{S_{\text{trans}}}{R}=\ln\left(\frac{2\pi mkT}{h^2}\right)^{\frac{3}{2}}\frac{kT}{p}e^{5/2}, \tag{40}$$

$$\frac{S_{\text{rot}}}{R}=\ln\frac{[2^9\pi^7(kT)^3ABCe^3]^{\frac{1}{2}}}{\sigma h^3}, \tag{41}$$

$$\frac{S_{\text{vib}}}{R}=\frac{x}{e^x-1}-\ln(1-e^{-x}), \tag{42}$$

where $x=h\nu_0/kT$.

The entropy for the remaining degree of freedom, that of restricted rotation, has to be obtained directly from the individual energy levels. It lies somewhere between that for pure oscillation, Eq. (42), and that for pure rotation, given by

$$\frac{S_{\text{free rot}}}{R}=\ln\frac{2\pi}{\sigma}\left(\frac{2\pi I_{\text{red}}kTe}{h^2}\right)^{\frac{1}{2}}. \tag{43}$$

3. APPLICATIONS

Ethane

The low temperature heat capacity data on gaseous ethane, published by Kistiakowsky, Lacher, and Stitt,[4] and the vibrational frequency assignment of Karweil and Schaefer or of Stitt,[7] was used to obtain the residual heat capacity data in Table I, corresponding to the internal oscillation-rotation. We fitted the experimental heat capacity from the last line of this table, with four curves as follows, assuming a 1 percent spread in the original data, as given by the authors: 1. through the upper limits of the data, 2. through the lower limits of the data, 3. through the lower limit at the lowest temperature and the upper limit at the highest temperature, and 4. through the upper limit at the lowest temperature and the lower limit at the highest temperature.

TABLE II. Ethane barrier heights based on two-parabola potential.

Curve	$V_{\cos}$ nominal barrier cm^{-1}	$V_0/V_{\cos}$	V_0 cm^{-1}	V_0 cal./mole ±150
1.	791	0.88	700	2000
2.	936	0.80	745	2150
3.	1250	0.48	595	1700
4.	692	1.24	858	2450
5.	813	1.10	892	2550

The ground state was taken as the zero of energy. It was found necessary to use three excited levels to make these curves pass through the given data, but no more than three were determinable because of the absence of heat capacity data for the immediately higher temperatures. The fitting was done by assuming a set of energy levels, computing the corresponding heat capacity over the given temperature range, and plotting these results on the same diagram with the experimental data. The

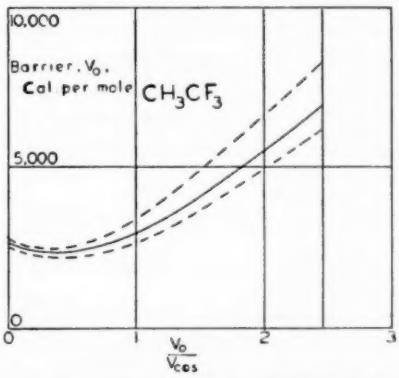

FIG. 6. Barrier-height ranges for $MeCF_3$.

[7] J. Karweil and K. Schaefer, Zeits. f. physik. Chemie **40B**, 357–375 (1938); F. Stitt, J. Chem. Phys. **7**, 297–307 (1939).

TABLE III. Entropy and barrier heights for methanol.

	Crawford 1940*	French, Rasmussen 1946**			Rowlinson 1948†	Eucken, Franck 1948††	This paper
S(MeOH, liquid, 298.16K)	30.26‡	30.26‡	30.26	30.26			30.26‡
S(vaporization, 298.16K)		30.015[a]	30.447[b]	30.688[c]			30.006
S(MeOH, vapor, 298.16K)		60.28	60.71	60.95			60.27
S(sat. vapor to ideal gas, 1 atmos.)		−3.566	−3.566	−3.566			−3.458
S(calorimetric, 298.16K, 1 atmos.)	56.63[d]‡‡	56.71	57.14	57.38	56.63‡‡	—[e]	56.81
S(translational)							36.324
S(rotational)							19.020
S(translational plus rotational)	55.331	55.291	55.291	55.291			55.344
S(vibrational)	0.257	0.220	0.220	0.220			0.220
S(restricted rotation)—by difference	1.05	1.20	1.63	1.87			1.25
S(statistical)	56.64	56.71	57.14	57.38	57.62[f]	—[e]	56.81
Estimated barrier, calories per mole	3400[g]	2360	1340¶, ¶¶	—	1300¶, ¶¶	1800	800 to 3000

* See reference 11d.
** See reference 11c.
† See reference 11b.
†† See reference 11a.
‡ See reference 12.
‡‡ See reference 11h.
¶ See reference 11e.
¶¶ See reference 11f.
[a] Latent heat 8949.4, reference 13.
[b] Latent heat 9078, from S. Young (1911).
[c] Latent heat 9150, from E. Bartoszewicz, Roczniki Chem. 11, 90–94 (1931).
[d] Based on reference 12, 13 and ICT vapor-pressure data, as reported by L. S. Kassel (reference 11h).
[e] Eucken and Franck did not base their estimate on entropy values.
[f] Rowlinson reported that a barrier of 1300 is consistent with his own supersonic heat capacity measurements, 64 to 176°C, but there still remain 0.99 entropy units unaccounted for, which he ascribes to possible partial disorder in the MeOH crystal at low temperatures, due to H-bonding (max. $=R\ln 2$), as previously suggested by Kassel (reference 11h).
[g] The alternative to the high barrier was thought to be the existence of partial disorder in the crystal (max. $=R\ln 3$).

first four of the partition functions below represent the fitted curves. Number five corresponds to the energies proposed by Kistiakowsky, Lacher, and Stitt, namely 275, 520, and 725 cm^{-1}.

1. $Q_1=1+e^{-390/T}+e^{-640/T}+e^{-900/T}$,
2. $Q_2=1+e^{-425/T}+e^{-685/T}+e^{-900/T}$,
3. $Q_3=1+e^{-490/T}+e^{-565/T}+e^{-775/T}$,
4. $Q_4=1+e^{-365/T}+e^{-720/T}+e^{-960/T}$,
5. $Q_5=1+e^{-395/T}+e^{-748/T}+e^{-1041/T}$.

In fitting the two-parabola potential function to the energies of these five systems, we made the assumption (validated later) that the first levels were sufficiently far below the barrier top to justify the harmonic oscillator approximation. The nominal barrier height V_{cos} and the quantized abscissae J_{HO} were therefore determined by the relations

$$\frac{E_0}{V_{cos}}=\frac{3}{\pi}(J_{HO})_0=\frac{3}{\pi}\frac{\pi/2}{\alpha}=\frac{1.5}{(8\pi^2 I/h^2)^{\frac{1}{2}}(V_{cos})^{\frac{1}{2}}}.$$

With the abscissae J_{HO}, established from the first energy level, taken with the ordinates E/V_{cos} corresponding to the higher levels, we plotted points on the energy level diagram to determine preliminary values of the ratio V_0/V_{cos}. In general, each such point fell on a different curve of the family, so a compromise value of the ratio had to be used. Then, with the established value of V_{cos}, and several trial values of V_0/V_{cos}, we recomputed the energy levels, including the splitting, for comparison with the initially given set of levels. The results of this study are presented in Table II. Because of the difficulty of making the given empirically found energies exactly fit an energy level curve of the family, particularly in the presence of the splitting, the precision of the barrier heights in the last column may be taken to be about 150 calories per mole.

The wide variety of energy level distributions which can be used to fit the observed heat capacity data illustrates the indeterminacy of this type of calculation, discussed in Part I. This indeterminacy results in a spread of possible barrier heights, ranging from 1700 to 2550 calories per mole, all capable of agreement with the thermodynamic data, under the assumption of the two-parabola potential. In view of the uncertainty of 150 calories per mole, in selecting the ratio V_0/V_{cos}, the range may be taken as 1550 to 2700. It is interesting to note that most of the possible fits give barriers lower than those commonly assumed.

1,1,1-trifluoroethane

Russell, Golding, and Yost[8] measured the heat capacity of $MeCF_3$ from 15 to 225K, and on the basis of

[8] Russell, Golding, and Yost, J. Am. Chem. Soc. 66, 16–20 (1944).

the vibrational frequency assignment of Hatcher and Yost[9] they estimated the cosine barrier hindering internal rotation of this molecule to lie between 3040 and 3950 calories per mole. Their results are based on a calculated entropy for internal rotation, of 1.47±0.14 cal./deg./mole. With their mean entropy value we were able to choose parameters for the two-parabola potential in such a way as to find barrier heights ranging from 2400 to 6800 calories per mole (Fig. 6), the lower value being for the broad-topped barrier, and the higher one for the barrier with the cusp-top (see Figs. 1 and 2). When we used the extreme entropy values, which included the uncertainties of measurement, we found values ranging from 2300 to 8300 calories per mole.

In the series of energy levels on which these results are based, the elevation of the first excited state above the ground state ranged from 200 to 300 cm^{-1}. The lowest of these values is not much higher than the infrared determination of 180 cm^{-1} recently reported by J. R. Nielsen,[10] but is in somewhat greater disagreement with the 165 cm^{-1} estimated by B. P. Dailey,[10] on the basis of microwave spectra.

In spite of the fact that the discrepancy between 200 cm^{-1} and 180 cm^{-1} seems small, the shift occurs in a region where its effect on the entropy is large. If Nielsen's figure of 180 cm^{-1} is accepted, the entropy of internal rotation based on a two-parabola potential calculates to be a minimum of 1.82 cal./deg. mole, and with most such barriers considerably higher. The discrepancy is so large that either the shape of the barrier is very different from the two-parabola type, or there is some difficulty in the calculation of the entropy of internal rotation.

Methanol

The rotational energy barrier in methanol has been estimated at various values from about 1300 to 3400 calories per mole.[11] At least a part of this spread may be ascribed to the sensitivity of the barrier calculation toward the variations in reported entropy values (Table III) (see Part I of this paper).

In our calculation we used Kelley's calorimetric entropy of the liquid, 30.26±0.2,[12] and Fiock, Ginnings, and Holton's latent heat, 1168.4 international joules per gram,[13] or 8946.6 calories per mole. The ideal-gas entropy change for compression to 1 atmos. from the vapor pressure, 0.1632 atmos.,[13] is $R\ln P = -3.602$, but the saturated vapor is not quite ideal. If we attribute the departure from ideality to the presence of a small amount of dimeric methanol, following the suggestion of DeVries and Collins,[14] the entropy correction is found to be

$$R\ln P - \theta\Delta S^0 + R\ln[\theta^\theta(1-2\theta)^{(1-2\theta)}(1-\theta)^{(-1+\theta)}P^{-\theta}] = -3.602+0.299-0.155 = -3.458$$

where θ is the mole-fraction of methanol in the dimeric form, and $\Delta S^0 = -10.302$* is the standard entropy change for the reaction

$$2\mathrm{MeOH} \rightleftarrows (\mathrm{MeOH})_2.$$

In our statistical calculations we used the molecular constants of Koehler and Dennison, based on the work of Borden and Barker,[11] and we used the vibrational assignment of Noether.[15]

Our entropy value, 1.25, admits barrier heights of the two-parabola potential function, between about 1400 and 2000 calories per mole, not taking into consideration the uncertainties in the calorimetric data. If the aggregate of these uncertainties is taken to be ±0.3, the range of admissible barrier heights increases to 800 and 3000 calories per mole (Fig. 7).

The shape of the barrier-height curve for methanol differs fundamentally from that for trifluoroethane, pointing to a probable difference in the nature of the forces responsible for the barrier.

4. CONCLUSIONS

An important application of the calculation of energy levels from thermodynamic data is the prediction of barrier heights, for example, those restricting internal rotation of molecules. Thermal data, by themselves, are insufficient for this purpose, because of the inherent indeterminacy of the energy level distribution. By choosing various shapes of potential curves, which is the same thing as rearranging the relative positions of the energy levels, one arrives at an excessively wide range of barrier heights, all consistent with published thermodynamic data. That is, the best modern thermodynamic

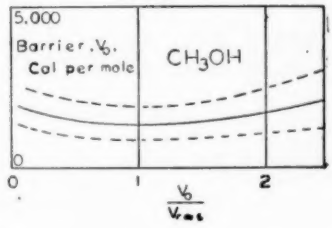

FIG. 7. Barrier-height ranges for methanol.

[9] J. B. Hatcher and D. M. Yost, J. Chem. Phys. **5**, 992–993 (1937).
[10] Indirect private communication.
[11] a. A. Eucken and E. U. Franck, Zeits. f. Elektrochemie **52**, 195–204 (1948); b. J. S. Rowlinson, Nature **162**, 820–821 (1948); c. F. A. French and R. S. Rasmussen, J. Chem. Phys. **14**, 389–394 (1946); d. B. L. Crawford, Jr., J. Chem. Phys. **8**, 744 only (1940); e. J. S. Koehler and D. M. Dennison, Phys. Rev. **57**, 1006–1021 (1940); f. A. Borden and E. F. Barker, J. Chem. Phys. **6**, 553–563 (1938); g. J. O. Halford and B. Pecherer, J. Chem. Phys. **6**, 571–575 (1938); h. L. S. Kassel, J. Chem. Phys. **4**, 493–496 (1936); i. J. O. Halford, J. Chem. Phys. **2**, 694–696 (1934).
[12] K. K. Kelley, J. Am. Chem. Soc. **51**, 180–187 (1929).
[13] Fiock, Ginnings, and Holton, Nat. Bur. Stand. Research Paper 312 (1931).
[14] T. DeVries and B. T. Collins, J. Am. Chem. Soc. **63**, 1343–1346 (1941).
* Calculated from the orthobaric data of Fiock, Ginnings, and Holton.
[15] H. D. Noether, J. Chem. Phys. **10**, 693–699 (1942).

technique is inadequate for the determination of barrier heights.

The barrier height range can be narrowed down when thermodynamic properties of the gas can be obtained for low temperature ranges, as with ethane. The uncertainty is greatest when the barrier height has to be estimated from data at a single temperature only, especially if this temperature is relatively high, as with the methanol calculation.

We cannot look for a complete answer to the restricted rotation problem until we have a better understanding of intramolecular forces, upon which to rest better assumptions about the shape of the potential function. Nevertheless, the gathering of improved barrier information, on a considerable variety of molecule types, will certainly lead to new ideas about the forces, so the barrier problem and the force problem are two aspects of the same unknown. More complete thermal data at very low temperatures would be a great help, because through their use we could decrease the range of uncertainty. The expected improvement would be much greater for some compounds than for others.

THE JOURNAL OF CHEMICAL PHYSICS VOLUME 18, NUMBER 5 MAY, 1950

On the Fluctuation of Energy of Gases in the Bose-Fermi Quantum Statistics

KOLOMAN SZÉLL
University of Szeged, Szeged, Hungary
(Received October 14, 1949)

The energy fluctuation of monatomic gases is calculated in the Bose-Fermi quantum statistics computing the mean values by the Bose and Fermi distribution functions and on the base of the entropy equation. The obtained results are compared with Fürth's calculations.

IN the Bose-Fermi quantum statistics fluctuations deviating from classical statistics occur. Fürth[1] dealt with phenomena of fluctuation of monatomic gases obeying the Bose-Fermi quantum statistics. Fürth calculated the energy fluctuation on the base of the fundamental assumptions of the Bose-Fermi statistics without the distribution function. These fundamental assumptions are as follows: According to Bose in the phase space of an atom of the gas system any number of atoms can be present in one cell of the size of h^3 (h is Planck's constant). In the Fermi quantum statistics, which are based on Pauli's principle, one cell can at the most contain one atom. In the classical statistics where there are no interactions among the particles there should be the probability of the ith cell containing only one particle: p_i and the counter probability: $q_i=1-p_i$. The probability that n_i atoms are in the ith cell is

$$w(n_i)=(n_i{}^N)p_i{}^{n_i}q_i{}^{N-n_i},$$

where N is the number of the atoms of the gas system.

In the Bose quantum statistics

$$w(n_i)=\text{constant } p_i{}^{n_i}q_i{}^{N-n_i},$$

where A can be determined from the equation

$$\sum_{n_i=0} w(n_i)=1.$$

In the Fermi quantum statistics

$$w(0)\neq 0, \quad w(1)\neq 0, \quad w(2)=w(3)=\cdots=w(N)=0.$$

[1] R. Fürth, Zeits. f. Physik **48**, 323 (1928).

Fürth investigated on the base of these equations the energy fluctuations of the monatomic gases. It follows from the Bose-Fermi's quantum assumptions that there are interactions among the particles of the system which are not classical interactions.

In the following, the energy fluctuation of the Bose, respectively Fermi gases is calculated in a small partial volume at weak degeneration. The author computes in two ways: by calculation of the mean values employing the Bose, respectively Fermi distribution function and on the base of the entropy equation. In contrast with Fürth's calculations, in the first approximation the energy fluctuation of the molecules are considered as independent of one another in the small partial volume at slight degeneration.

The energy fluctuation of gas in a partial volume consists of two parts. The first part is the consequence of the change of velocity of molecules in the partial volume, the average velocity will be greater or smaller. The second part ensues through the variation of the number of molecules of the partial volume. Sometimes it is greater, sometimes it is smaller than an average value. The two parts of the energy fluctuation are: the *heat fluctuation* and *density fluctuation*, respectively.

1. HEAT FLUCTUATION

Let us consider a system of monatomic gases having uniform temperature T. The walls of the vessel containing the gas should be heat isolators. Let us investigate a small partial volume V_1 of the volume of the vessel $V=V_1+V_2$.

Let us denote the values of gas energy in the case of uniform distribution in the partial volume V_1, V_2, respectively, E_1, E_2.

The mean square deviation of the energy of a molecule from its mean value is

$$\langle(\epsilon-\bar{\epsilon})^2\rangle_{Av}=\langle\epsilon^2\rangle_{Av}-\bar{\epsilon}^2. \tag{1}$$

The average energy of a molecule in the partial volume in the Bose-Fermi statistics is

$$\bar{\epsilon}=\frac{\dfrac{2\pi V_1(2m)^{\frac{3}{2}}}{h^3}\displaystyle\int_0^\infty \frac{\epsilon^{\frac{1}{2}}d\epsilon}{(e^{\epsilon/kT}/A)\mp 1}}{n_1}, \tag{2}$$

in which the upper sign refers to the Bose statistics, the lower to the Fermi, n_1 is the mean number of molecules in the volume V_1. The parameter $A=c^{-a}$ can be determined from the equation

$$n_1=\sum n_i'=\frac{2\pi V_1(2m)^{\frac{3}{2}}}{h^3}\int_0^\infty \frac{\epsilon^{\frac{1}{2}}d\epsilon}{(e^{\epsilon/kT}/A)\mp 1}. \tag{3}$$

By expanding into series of the integrand at small degeneration ($A<1$) only retaining the terms necessary for a first approximation we obtain

$$n_1=\frac{An_1}{2^{\frac{1}{2}}y}\pm\frac{A^2n_1}{8y}, \tag{4}$$

where

$$y=\frac{h^3}{(4\pi mkT)^{\frac{3}{2}}}\frac{n_1}{V_1}, \tag{5}$$

so that

$$A=2^{\frac{1}{2}}y(1\mp y). \tag{6}$$

By expanding into series of the integrand in Eq. (2) we find at small degeneration

$$\bar{\epsilon}=\tfrac{3}{2}kT(1\mp y). \tag{7}$$

The mean value of the square of energy is

$$\langle\epsilon^2\rangle_{Av}=\frac{\dfrac{2\pi V_1(2m)^{\frac{3}{2}}}{h^3}\displaystyle\int_0^\infty \frac{\epsilon^{5/2}d\epsilon}{(e^{\epsilon/kT}/A)\mp 1}}{n_1}$$

$$=15/4(kT)^2(1\mp y). \tag{8}$$

Therefore (1) becomes

$$\langle\epsilon^2\rangle_{Av}-\bar{\epsilon}^2=\tfrac{3}{2}(kT)^2(1\pm y/2). \tag{9}$$

If in the small partial volume V_1 the energy changes of the molecules are independent at slight degeneration, the relative mean square of heat fluctuation is[2]

$$\frac{\langle(E_1-\bar{E}_1)^2\rangle_{Av}}{\bar{E}_1^2}=\frac{\langle E_1^2\rangle_{Av}-\bar{E}_1^2}{\bar{E}_1^2}=\tfrac{2}{3}n_1(1\pm 5/2y), \tag{10}$$

where $1\pm 5/2$ is the factor of degeneration which is in the classical statistics one.

According to Fermi's calculations[3] in which the interactions of the molecules considered the mean relative square of fluctuation is

$$\frac{\langle E_1^2\rangle_{Av}-\bar{E}_1^2}{\bar{E}_1^2}=\tfrac{2}{3}n_1(1\pm 5/4y). \tag{11}$$

Consequently the Bose, respectively Fermi forces give at weak degeneration according to Eqs. (10), (11) a twice smaller correction term, even also in the extremely small partial volume, than the value neglecting the interactions among the molecules.

For calculating on the base of the entropy equation $W=e^{T/k}$ we take the extremely small changes of the energies of the partial volumes V_1 and V_2, respectively at constant molecule number. Thus

$$E_1'=\bar{E}_1+\epsilon', \quad E_2'=\bar{E}_2-\epsilon'. \tag{12}$$

By expanding into series of the entropy of the two partial volumes with respect to ϵ', neglecting the terms of higher order in ϵ', we obtain the well known equation

$$\langle E_1^2\rangle_{Av}-\bar{E}_1^2=kT^2\partial\bar{E}_1/\partial T. \tag{13}$$

Substituting in (13)

$$\bar{E}_1=\tfrac{3}{2}n_1kT(1\mp y), \tag{14}$$

we again obtain Eq. (10). The additive law of entropy, which is generally not valid in the case of systems depending upon each other, was applied here.

2. FLUCTUATION OF DENSITY

Let the volume V_1, V_2, respectively, of the molecules n_1 and n_2, respectively of the gas which is in thermodynamic equilibrium vary with v. Thus

$$V_1'=V_1+v, \quad V_2'=V_2-v. \tag{15}$$

The total entropy of gas is

$$S=\bar{S}_1+\left(\frac{\partial\bar{S}_1}{\partial V_1}\right)_{E_1}v+\left(\frac{\partial^2\bar{S}_1}{\partial V_1^2}\right)_{E_1}\frac{v^2}{2}$$

$$+\bar{S}_2-\left(\frac{\partial\bar{S}_2}{\partial V_2}\right)_{E_2}v+\left(\frac{\partial^2\bar{S}_2}{\partial V_2^2}\right)_{E_2}\frac{v^2}{2}. \tag{16}$$

The terms of higher than quadratic order in v are negligibly small. $\bar{S}_1$ and $\bar{S}_2$, respectively, denote the entropy of the molecules n_1 and n_2, respectively, in the case of the uniform partition of the molecules. The index of the brackets indicates that the energy of n_1 and n_2, respectively, is assumed to be constant.

$$\left(\frac{\partial\bar{S}_1}{\partial V_1}\right)_{E_1}=\left(\frac{\partial\bar{S}_2}{\partial V_2}\right)_{E_2}=\frac{p}{T}$$

[2] Considering the following law of the probability theory: x_1, x_2, $\cdots x_n$ should be independent variables of each other. The mean value of square of their sum, if $\bar{x}_i=0(i=1, 2\cdots n)$ is given by the equation

$$\langle(x_1+x_2+\cdots+x_n^2)\rangle_{Av}=\langle x_1^2\rangle_{Av}+\langle x_2^2\rangle_{Av}+\cdots+\langle x_n^2\rangle_{Av}.$$

[3] R. Fürth, Zeits. f. Physik 48, 334 (1928), Eqs. (38) and (39).

in which p is the pressure, therefore

$$\left\{\left(\frac{\partial \bar{S}_1}{\partial V_1}\right)_{E_1}-\left(\frac{\partial \bar{S}_2}{\partial V_2}\right)_{E_2}\right\}v=0. \tag{17}$$

Since in the Bose-Fermi statistics the equation $p=\frac{2}{3}(E_1/V_1)$ is also valid, considering (7) it becomes

$$p=\frac{n_1kT}{V_1}(1\mp y). \tag{18}$$

$(\partial^2\bar{S}_2/\partial V_2^2)_{E_2}v^2/2$ is in the equation of the state probability negligibly small. Furthermore

$$\left(\frac{\partial^2\bar{S}_1}{\partial V_1^2}\right)_{E_1}=-\frac{kn_1}{V_1^2}(1\mp 2y). \tag{19}$$

The equation of the state probability: $W=c^{S/k}$ is with the aid of Eqs. (16), (17), (18), (19)

$$Wdv=\text{constant}\exp\left(\frac{-n_1(1\mp 2y)v^2}{2V_1^2}\right)dv. \tag{20}$$

Hence the mean, respectively relative mean square of the volume fluctuation of n_1 molecules is given by

$$\langle(V-V_1)^2\rangle_{Av}=\int_{-\infty}^{+\infty}v^2Wdv=\frac{V_1^2}{n_1(1\mp 2y)}, \text{ respectively} \tag{21}$$

$$\frac{\langle(V-V_1)^2\rangle_{Av}}{V_1^2}=\frac{1}{n_1(1\mp 2y)}=\frac{1\pm 2y}{n_1}, \tag{22}$$

$$\frac{\langle(V-V_1)^2\rangle_{Av}}{V_1^2}=\frac{\langle(d_1-d)^2\rangle_{Av}}{d_1^2}=\frac{\langle(n_1-n)^2\rangle_{Av}}{n_1^2} \tag{23}$$

where d,d_1 and n,n_1 are the suitable density and molecule numbers in the volume V_1. The relative mean square of the fluctuation of the molecule number is in volume V_1

$$\frac{\langle(n_1-n)^2\rangle_{Av}}{n_1^2}=\frac{1\pm 2y}{n_1}. \tag{24}$$

According to Fürth[4] this value is

$$\frac{1\pm y}{n_1}. \tag{25}$$

In consequence of the interaction of molecules the correction term is again twice smaller than the value on neglecting the actions among the molecules at small degeneration.

[4] R. Fürth, Zeits. f. Physik **48**, 328–330 (1928), Eqs. (16), (17), (18), (23), and (24).

THE JOURNAL OF CHEMICAL PHYSICS VOLUME 18, NUMBER 5 MAY, 1950

The Contribution of the Surface of the Specific Heat of Disperse Systems

H. KOPPE
University of British Columbia, Vancouver, Canada
(Received October 18, 1949)

A theory of Brager and Schuchowitzky concerning the contribution of the surface of the specific heat is extended to the interfaces of binary systems.

THE determination of the total surface of a highly dispersed substance is of importance for many problems. Usually, only rough estimates could be made from a determination of the size and number of the particles and some assumptions of their geometrical form (e.g., spherical). But lately, Brager and Schuchowitzky[1] have pointed out that there is a measurable property of such systems which is directly proportional to the total area of the surface, namely a certain contribution to the specific heat at very low temperatures. Only, the formulas given by Brager and Schuchowitzky apply to a free surface, whereas in the case of colloidal solutions, which are of main interest, it is rather the interface between two solids (e.g., the colloidal substance and ice), which has to be determined. It is the aim of this paper to generalize the theory for this case. In doing this, we do not start from the method of Brager and Schuchowitzky, but use the very lucid representation of the problem which has been given by Frenkel.[2]

The contribution of surface to the specific heat is generally given by the derivative of surface energy with respect to temperature. Customarily, one connects surface energy with the differences of the forces acting on an atom within the bulk of the material and on its surface respectively. This difference may depend on temperature, but it can be easily shown that this contribution to surface energy is proportional to the thermal energy of the substance in bulk and in particular varies with T^4 for low temperatures. But there is

[1] A. Brager and A. Schuchowitzky, Acta Physicochimica (URSS) **21**,•1001 (1946).

[2] J. Frenkel, *Kinetic Theory of Liquids* (Oxford University Press, London, 1946), p. 314.

another somewhat more intricate contribution to surface energy. If the thermal energy of a solid is derived according to Debye's theory, use is made of the eigenfrequencies of a cube with fixed boundaries, with an asymptotical law for the distribution of eigenfrequencies,

$$Z(\nu)=\frac{4\pi}{3}V\left\{\frac{1}{v_L{}^3}+\frac{2}{v_T{}^3}\right\}\nu^3. \tag{1}$$

Here $Z(\nu)$ is the number of eigenfrequencies $\leq\nu$, V the volume of the cube and v_L and v_T the longitudinal and transverse velocities of sound. However, in a cube, whose surface is not fixed, but can move freely, there are no purely longitudinal or transverse waves, but always a mixture of both. This leads to a slight shift of the eigenfrequencies and instead of (1) we have now

$$Z'(\nu)=Z(\nu)+ZA(\nu)=\frac{4\pi}{3}V\left[\frac{1}{v_L{}^3}+\frac{2}{v_T{}^3}\right]\nu^3+\pi A\frac{\nu^2}{v_R{}^2}, \tag{2}$$

where A is the area of the surface, and v_R is the velocity of the surface waves of Rayleigh.[3] These surface waves are a special form of motion of a solid, in which only a thin layer is in motion. For solids satisfying Cauchy's relations, $v_R=0.92v_T$.

It can be seen at once from (2) that there should be a contribution to the specific heat which is proportional to the surface area and to T^2 for low temperatures.

Now we have to generalize (2) for the case in which there is no free surface, but an interface between two solids. Frenkel obtained (2) by a calculation of the eigenfrequencies of a free sphere.[4] The appropriate procedure therefore, would be to make the same calculations for a sphere surrounded by a spherical shell of the second material. But these calculations would be very complicated and therefore an attempt is made to get the result by means of a suitable generalization of (1).

The appearance of v_R in (2) indicates that the effect of the surface on the distribution of eigenfrequencies is due to the existence of a peculiar state of motion as described by Rayleigh's theory. It can be supposed that a possible contribution of an interface to the specific heat should depend on the possibility of an analog of Rayleigh surface waves for the interface between two solids. This problem has been investigated in a former paper[5] and the results will be shortly summarized here. The essential point is, that these interfacial waves can exist only subject to certain conditions, which can be seen in details from Fig. 1. (Roughly, the torsional modulus μ_1 of the solid of the higher acoustical density has to be at least 2.5 times

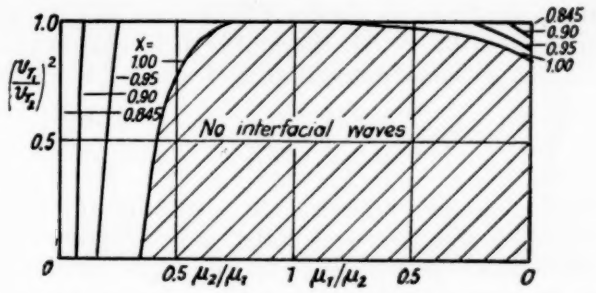

FIG. 1. Diagram for the determination of the velocity v_G of the interfacial waves on the interface of two substances satisfying Cauchy's relations. v_{T_1} and v_{T_2} are the velocities of transversal waves of sound, μ_1 and μ_2 the respective torsional moduli. (The labeling of the two substances has to be done such that $v_{T_1}<v_{T_2}$.) The diagram shows the lines $x=$const. where x is the ratio $v_G{}^2/v_{T_1}{}^2$. Within the shaded area there are no interfacial waves possible. If Cauchy's relations are not satisfied in both substances, then v_G has to be calculated by the methods indicated in reference 5.

larger than the corresponding μ_2 of the other solid). This means that in a disperse system consisting of two solids a contribution of the area of the interfaces to the specific heat exists only if the two solids differ enough in their constants of elasticity.

There is at the most one interface wave for a given wave vector. The velocity v_G is subject to the condition

$$v_R{}^{(1)}\leq v_G\leq v_T{}^{(1)}.$$

$v_T{}^{(1)}$ is the velocity of transverse waves in the solid of the higher acoustical density (this always being labeled with the suffix 1). It seems therefore that the interface waves correspond to the Rayleigh waves of the solid of higher density, the waves of the other solid being suppressed.

The additional term in (2) which is of importance here is, apart from a numerical factor, fixed by dimensional reasons. That this numerical factor has the value π, is a result of the calculations of Frenkel and Gubanow. It is unlikely that it will change by passing from a free surface to the interface between two solids. On the other hand, it should be expected that v_R has to be replaced by the velocity v_G of the interfacial waves.

The determination of the limiting frequency ν^* remains somewhat problematical. According to Frenkel, ν^* has to be determined so that $Z(\nu^*)$ equals the number of degrees of freedom, i.e., three times the number of atoms. With respect to the behavior of the interfacial waves, these should be treated as surface waves of the acoustically denser solid. For the following calculations, however, this point is of no importance, for they refer to a range of temperatures for which ν^* has no influence on the thermal properties.

We are now prepared to pass on to the calculation of the surface contributions $e_\nu{}^A$ and U^A. The latter quantity is, neglecting the zero-point energy, given by

$$U^0=\int_0^{\nu^*}\frac{h\nu}{e^{h\nu/kT}-1}dZA(\nu)=2\pi A\frac{k^3T^3}{h^2v_G{}^2}\int_0^{h\nu/kT}\frac{x^2}{e^x-1}dx. \tag{4}$$

[3] Lord Rayleigh, London Math. Soc. **17** (1887), A. E. H. Love, *Elasticity* (Cambridge University Press, London, 1906), second edition, p. 295.

[4] J. Frenkel and Gubanow, J. Exper. Theor. Phys. **16**, 435 (1946).

[5] H. Koppe, Zeits. f. angew. Math. Mech. **28**, 355 (1948).

If T is small enough, the upper limit of the integral can be replaced by ∞. The integral is then equal to $\zeta(3)=1.202$. Differentiation with regard to T yields

$$e_\gamma{}^0=6\pi\zeta(3)\frac{k^3}{h^2}\frac{T^2A}{v_G{}^2}=3.243\cdot10^{-2}\frac{\text{cal.}}{\text{sec.}^2}\cdot\frac{T^2A}{v_G{}^2}.$$

Since ν^* has been neglected, the range of temperatures for which this formula is valid, has an upper limit which may be somewhere about 30°K, but which is not of importance, since experiments must be done at considerably lower temperatures, in order that $e_\nu{}^A$ is sufficiently large compared to the rest of the specific heat. But there is also a lower bound for the validity of (5) which we shall presently establish. It has been mentioned already that interfacial waves, and with them the surface component of the specific heat, exist only if the two substances are different enough. Since both the differences in the elastical constants as well as in the densities, which determine whether interfacial waves are possible or not, vary with temperature, it could be possible that for certain combinations of solids interfacial waves cease to be possible, if the temperature rises above (or drops below) a critical value. This would result in a discontinuity of the specific heat, resembling a phase-transition of second order. Actually, this cannot happen for the following reason: It has been mentioned already that interfacial waves take place only in a thin layer which should be small compared with the diameter of the colloidal particles. But the theory of these waves[5] shows that the penetration depth approaches infinity at least within the acoustically denser substance if the representative point of the binary system approaches the shaded area in Fig. 1. If, therefore, the penetration depth is not small compared with the size of the particles, the present theory is no longer valid, and the specific heat depends not only on the area of the surface of the particles, but also on their geometrical form.

This is essential in another respect: even for fixed elastical constants and densities the penetration depth of the interfacial waves depends on the frequency:

$$\delta=\frac{v_T}{2\pi\nu}\left(\frac{x}{1-x}\right)^{\frac{1}{2}}. \tag{6}$$

The parameter x can be taken from Fig. 1. In any case, δ becomes infinite if ν approaches zero. In order that (5) is valid, it must be postulated that δ is small compared with the mean diameter D of the particles at least for these frequencies ν_M which contribute most to $e_\nu{}^A$. ν_M can be found from the derivative of the integrand of (4),

$$\nu_M=1.6(kT/h)$$

and therefore we get as a necessary condition for the validity of (5)

$$\frac{1.6k}{h}\frac{TD}{v_T}\left(\frac{1-x}{x}\right)^{\frac{1}{2}}>1 \tag{7}$$

or, if we disregard extremely small values of the square root

$$(T\cdot D)/v_T\geq10^{-11}\text{ sec.} \tag{8}$$

To give a numerical example, we may assume that $v_T\sim10^5$ cm sec.$^{-1}$. $D\sim10^{-6}$ cm, then T must be >1°K. The question then arises whether the whole effect is large enough to make an application feasible. This splits at once into two subquestions: whether it is possible to obtain reasonably good experimental values of $e_\nu{}^A$, and whether it is possible to calculate A from these values. We answer the second question first. In order to obtain A, v_G must be known, and it has to be calculated from the constants of elasticity. It is advisable then, first to calculate or to obtain experimentally the value of v_T, then $v_G{}^2=xv_T{}^2$ where x can be obtained from the diagram of Fig. 1. It is really not very critical, for x can only vary within rather narrow limits: $0.845\leq x\leq1$. $e_\nu{}^A$ itself according to definition, is the difference between the specific heat of the sample and that of the same amount of bulk material. It is necessary to consider, for which temperatures this difference would be sufficiently large. Now the specific heat of the sample consists of two (or three) parts: the specific heat of the lattice vibrations, the contribution of the surface, and the specific heat of the electrons if metallic phases are present. But these three contributions vary as T^3, T^2, and T, respectively. Therefore T should not be too high, for then the large specific heat of the lattice vibrations would screen the whole effect. On the other hand, the temperature should not be too low, for then the specific heat of the electrons would become predominant. (This refers of course, only to cases where metals are present, which are therefore less favorable.) A short calculation shows then that in most cases a compromise is possible, and for particles of a size of about 10^{-6} cm, $e_\nu{}^A$ can amount to about 10 percent of the specific heat at temperatures of about 1°K. If one assumes an accuracy of about 1 percent for the total specific heat, then the surface could be calculated with an accuracy of about 10 percent at most.

Summarizing the results, we can state that the contribution of the interface between two solids is, if one excludes some limiting cases, very nearly the same as the contribution which would arise from an equal free surface of the acoustically denser substance. The calculations have been based on the simple Debye-model, and it is known that this model is not too accurate. However, it might be assumed that the qualitative result stated above is independent of the special model.

In conclusion, it should be stated that surface effects of this kind could be expected also in eutectical alloys and even in polycrystalline samples of substances with a high elastical anistropy.

Compressibility of Gases at High Temperatures. III. The Second Virial Coefficient of Helium in the Temperature Range 600°C to 1200°C*

J. L. YNTEMA† AND W. G. SCHNEIDER
Division of Chemistry, National Research Laboratories, Ottawa, Canada
(Received November 16, 1949)

An apparatus is described for measuring the second virial coefficient of gases up to 1200°C. The method of measurement is based on a modification of an expansion method described previously. Results of measurements of the second virial coefficient of helium at 600°, 800°, 1000°, and 1200° are given.

INTRODUCTION

IN a recent paper[1] measurements of the second virial coefficient of helium over the temperature range 0°C to 600°C were reported. An expansion method was employed in these measurements. By a slight modification of the apparatus and technique it has been possible to extend the measurements to higher temperatures. In the present paper second virial coefficient measurements from 600°C to 1200°C are described. These measurements have been undertaken, in part, in an attempt to obtain information about the intermolecular potential field of helium. A comparison of the experimental information obtained in this way with several theoretically derived potential fields reported in the literature, is given in the following paper.

METHOD

The isotherms of helium, at temperatures above 100°C and pressures below 75 atmospheres, can be represented accurately by a linear equation of the form:

$$PV=A+BP, \tag{1}$$

where A and B are the first and second virial coefficients, respectively. It is convenient for our present purpose to express the virials in terms of Amagat units. To measure A and B we have made use of an expansion method[2,3] which eliminates the necessity of a direct volume measurement and thus makes possible compressibility measurements at high temperatures, where volume measurements could not ordinarily be carried out with the required degree of precision. In the modification of the expansion method employed in the present work, one gas pipet is maintained at a high temperature T, while the second pipet is maintained at 0°C. The obvious advantage of this is that only one pipet is heated to the high temperature, resulting in a considerable simplification in carrying out the measurements. Thus the first pipet constructed of platinum alloy is heated in a furnace, while the second pipet, constructed of stainless steel, is simply immersed in an ice bath. If P_m is the measured pressure when all the gas is originally contained in the first pipet at temperature T, and P_{m+1} the pressure measured after the gas has been expanded as well into the pipet at 0°C, it can easily be shown that:[3]

$$P_m/P_{m+1}+(B_0/A_0)(P_m-P_{m+1}) -(M-1)(B_T/A_T)^2P_mP_{m+1} =M+(M-1)(B_T/A_T)(P_m+P_{m+1}), \tag{2}$$

where A_0 and B_0 are the virial coefficients at 0°C, which are presumed known, and

$$M=1+TV_0/T_0V_T. \tag{3}$$

Here V_T and V_0 are, respectively, the volume of the first pipet at temperature T and the volume of the second pipet at 0°C. The third term on the left is very small and can easily be evaluated by successive approximations. Accordingly, if a series of expansions are carried out over a range of pressures, then by plotting the left-hand side of (2) *vs.* P_m+P_{m+1}, a straight line is obtained whose intercept on the zero pressure axis is related to the volume ratio of the pipets. From the value of the intercept and the slope of the plot, B_T/A_T, the ratio of the virials at temperature T, is obtained. But

$$A_T=A_0(T/T_0). \tag{4}$$

Hence, if A_0 is known the second virial can be obtained at any temperature T (the temperature of the first pipet). While, in principle, B_T can be obtained analytically from any two sets of pressure measurements, a better "smoothing" of the data is obtained by carrying out a series of expansions over a fairly wide pressure range and fitting the best straight line through the points.

The above method has been thoroughly tested and found to give under our experimental conditions, a precision of about 2 percent in B at 600°C. The most serious limitation in the method is due to the fact that the expansion valve, and its associated capillaries cannot be heated to the temperature of the first pipet, resulting in a small "dead space" which must be corrected for. This correction, which is discussed in detail below, increases with increasing temperature, and hence must be evaluated with considerable precision.

* Contribution No. 2123 from the National Research Council, Ottawa, Canada.
† National Research Council (Canada) Postdoctoral Fellow.
[1] W. G. Schneider and J. A. H. Duffie, J. Chem. Phys. **17**, 751 (1949).
[2] E. S. Burnett, J. App. Mech. **3**, A137 (1936).
[3] W. G. Schneider, Can. J. Research **27B**, 339 (1949).

EXPERIMENTAL

To carry out the measurements, the following conditions, which are very similar to those encountered in high temperature gas thermometry,[4] are required:

(i) The volume of the pipet must not change with pressure. To meet this requirement the pipet (together with its heater) is housed in a pressure vessel so that the pressure inside and outside the gas pipet wall could be balanced at all times.

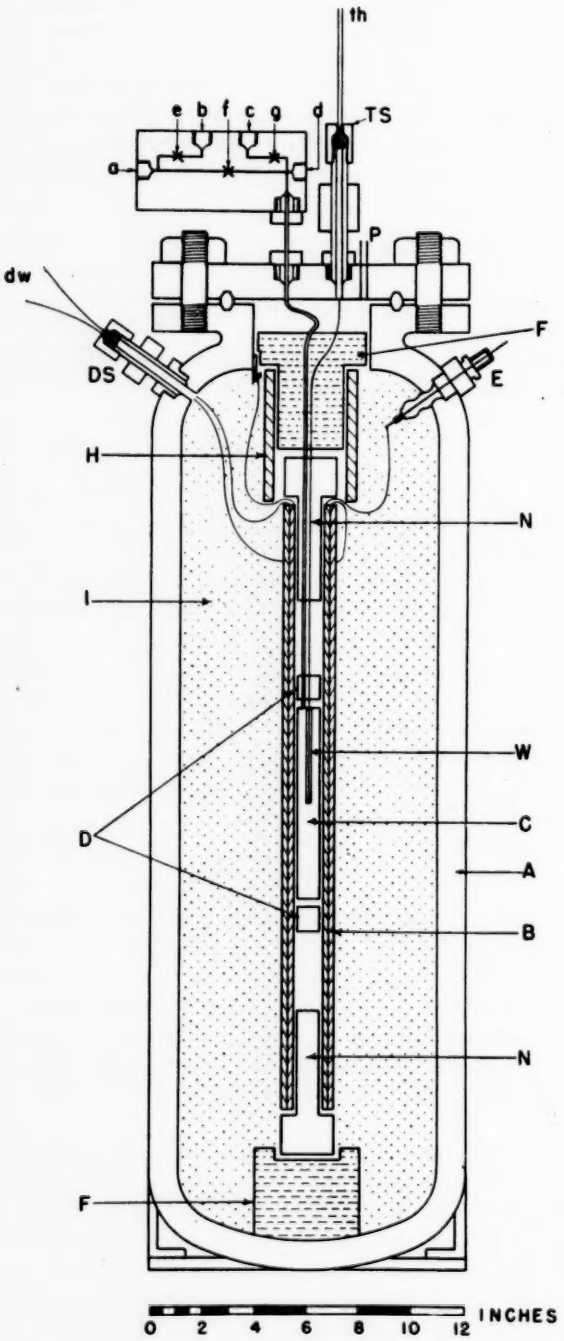

FIG. 1. Furnace and pipet assembly.

[4] A. L. Day and R. B. Sosman, Carnegie Institute Publication, No. 157 (1911).

(ii) Within the temperature range under consideration the pipet must remain impervious to helium. This consideration dictated the use of platinum or a platinum alloy for the pipet material.[5]

(iii) The temperature of the pipet must be maintained uniform within narrow limits and the mean temperature of the pipet accurately measurable.

(iv) The dead space (unheated volume) should be reduced to a very small value.

The Furnace and Pipet Assembly

Figure 1 shows a schematic drawing of the furnace and pipet assembly. The gas pipet, *C*, is suspended at the center of the cylindrical furnace tube, *B* which is housed in the pressure vessel, *A*. The insulating material *I* consists of pure calcined aluminum oxide powder.

The pressure vessel was constructed** from a length of seamless pressure tubing having an inside diameter of 10 inches and a wall thickness of 1 inch. Domed ends were machined and butt-welded to the tube, the top end opening in a flange, to which a cover $1\frac{1}{4}$ inches thick was bolted. The pressure seal was affected by means of an annealed copper ring. The over-all length of the furnace was 38 inches.

The assembly of the furnace core, *B*, has been previously described.[6] It consists of two fitted concentric alundum tubes 24 inches long, the inner tube having a bore of $1\frac{1}{8}$ inches, the outer tube a bore of $1\frac{1}{2}$ inches. The outside surface of the inner tube was grooved in a lathe in such a manner that a heavy heating wire and a light resistance wire could each be wound bifilarly, and the light wire could be wound between turns of the heavy heating wire. The heating wire consisted of No. 16 B & S platinum −10 percent rhodium wire, which was iridium free, in order to avoid contamination of the thermocouple. One side of the heater was grounded to the pressure vessel, the other lead was brought out by means of a "spark-plug" type electrode, *E*. The furnace was heated from a stabilized 110-volt a.c. source. The resistance detector wire consisted of No. 32 B & S platinum, to which No. 24 platinum leads were joined. The leads were brought out through a single insulator, *DS*. The latter consisted of a steel fitting, which was bored to take a two-hole porcelain insulator through which the resistance wire leads, *dw*, were led. The pressure seal was made as follows: The outer end of *DS* terminated in an inverted conical seat, at the apex of which the porcelain insulator terminated. The end was further threaded to take a gland nut. Before the gland nut was put in place, the end of the insulator was built up and packed with a partially softened Apiezon wax (or DeKhotinsky cement with a low softening point). The gland nut was then slowly tightened while the joint was carefully heated with a torch to allow the wax to flow. In order

[5] W. H. Keesom, *Helium* (Elsevier Publishing Company, Amsterdam, 1942), p. 132.

** Constructed by the National Research Council Central Workshop.

[6] W. G. Schneider and N. R. S. Hollies, Rev. Sci. Inst. 21, 94 (1950).

to prevent the wax softening while the furnace was being heated, the insulator was equipped with a small water cooling jacket immediately below the wax seal.

The gas pipet was fabricated by the Johnson Matthey and Mallory Company. Iridium free platinum −10 percent rhodium alloy was used for the pipet material. This alloy was preferred to pure platinum because of its greater hardness and tensile strength at elevated temperatures. The pipet had an over-all length of 19.0 cm, outside diameter of 2.7 cm, a wall thickness of 2.5 mm, and a volume of 66.7 cc. Through the exact center of the upper end, a small thermocouple well, *W*, was welded which extended down to the center of the pipet. A capillary of the same alloy with a 0.6 mm bore was also sealed through the top of the pipet, and was of sufficient length to extend to a point just below the furnace cover. At this point it was hard-soldered to a 3-inch length of 0.4 mm-bore steel capillary. The latter was brought through the furnace cover to a multiple needle valve block immediately above the furnace cover. The needle valve block which is shown schematically in Fig. 1 consists of the expansion valve, *f*, and two further valves, *e* and *g*, which provide for evacuation and filling of the gas pipets. The second pipet, made of stainless steel with a $\frac{3}{8}$ inch-wall thickness, was joined at *a*; its volume was 11.0 c.c. and could be reduced as desired by adding brass plugs in order to obtain a convenient pressure reduction on expansion of the gas. The free piston pressure gauge was joined at *d* through a mercury U-tube previously described.[3]

The pipet was positioned in the center of the furnace core. The latter was closed at both ends with fitted alundum bricks,† *N*, which projected a distance of 4 inches into either end of the furnace core. The pipet was suspended from the upper brick by means of two No. 20 B & S platinum-10 percent rhodium wires. Two additional bricks, *F*, were used, one at the bottom and one at the top. A short length of a larger diameter alundum tube, *H*, served to hold the powdered insulation in place and permit easy access to the furnace core.

Temperature Measurement and Control

The temperature was measured with a platinum-platinum-10 percent rhodium thermocouple made from No. 30 B & S wire.†† This thermocouple was calibrated against a standard thermocouple which had been calibrated at the gold, silver and antimony points by the Heat and Thermometry Section of the National Research Council of Canada. The thermocouple was insulated with high temperature alundum insulators¶ having a double bore through which the wires were threaded. The insulator fitted snugly into the thermocouple well of the pipet. Above the pipet the thermocouple was wrapped with platinum foil to shield it from stray emfs arising from a possible rectifying action of the heating current at high temperatures.[7] The thermocouple leads were brought through a wax pressure seal on the cover, exactly similar to the seal used for the resistance detector wire, and terminated in a mercury pool in an ice bath. Copper wire leads were led from the ice junction to the potentiometer. A Leeds and Northrop Wenner potentiometer calibrated by the Bureau of Standards was used for the e.m.f. measurements.

Control of the furnace temperature was effected by the change in resistance of the platinum detector resistance wire wound on the inner furnace core. An automatic temperature controller, which has been previously described,[6] provided temperature regulation to within ±0.03°C, as measured by the thermocouple at the center of the furnace. The heating current of the furnace could be accurately adjusted to obtain any desired temperature up to 1200°C.

The temperature gradients existing in the furnace along the length of the pipet were examined in advance of the measurements. This is an important problem since the thermocouple measures only the mean temperature at the center of the pipet. Moreover, temperature gradients along the length of the pipet may be expected to be greater below 1000°C, where heat transfer takes place largely by conduction and convection, while above 1000°C radiational transfer becomes more important and will ensure a fairly uniform temperature distribution, particularly when radiation shields are introduced. To study the magnitude of the temperature gradient below 1000°, a stainless steel pipet was constructed with the same dimensions as the platinum pipet and with three thermocouple wells in the top of the pipet, one of which terminated $\frac{1}{2}$ inch above the bottom of the pipet, one at the center of the pipet, and the third one inch below the top. By using three thermocouples, which had been intercompared, and with the same length of each thermocouple immersed in the hot zone, the temperature of the ends of the pipet relative to the center could be examined. It was found that with only a free gas space above and below the pipet, the temperature at the ends of the pipet were as much as two or three degrees below that at the center. By inserting a fitted alundum brick above and below the pipet, (shown at *D* in Fig. 1) the temperature at the ends differed by less than 0.5° from that at the center. The bricks which were $1\frac{1}{2}$ inch long, and whose surface nearest the pipet had been covered with platinum foil, served the double purpose of reducing convective heat losses at the ends of the pipet, and acting as radiation shields.

† Supplied by Norton Company, Worcester, Massachusetts.

†† Supplied by Johnson Matthey and Mallory Company and estimated to be within one degree of the international temperature scale up to 1100°C.

¶ Supplied by Norton Company.

[7] W. P. White, *Temperature* (Reinhold Publishing Company, New York, 1941), p. 282.

TABLE I. Summary of coefficients in the series equation, $PV=A_T+B_TP$, for helium.

	Volume expressed in terms of: Amagat units		cm³/mole*		No. of expansions
Temp. °C	A_T	$B_T\times10^3$	A_T	B_T	
0	0.999475	0.525	22415.2	11.77	
100	1.365369	0.509	30621.1	11.42	
200	1.731262	0.494	38827.0	11.08	
300	2.097156	0.480	47032.9	10.76	
400	2.463050	0.466	55238.8	10.45	
500	2.828943	0.452	63444.7	10.14	
600	3.194837	0.438	71650.6	9.82	
600	3.194837	0.437	71650.6	9.80	27
800	3.926624	0.409	88062.4	9.17	34
1000	4.658411	0.386	104474.2	8.66	35
1200	5.390198	0.365	120886.0	8.19	30

* The value of the normal volume used to convert to units of cm³/mole was 22427.0 cm³, where the molecular weight of helium was taken as 4.00248 g and the normal density as 0.178467×10^3 g/cm³ (see reference 5, p. 28).

Pressure Measurements

The pressures were measured with a free piston gauge described previously.[3] As before, the gauge was calibrated against the vapor pressure of carbon dioxide at 0°C.

Procedure

The purification of the helium was described in reference 1. With the furnace adjusted to the desired temperature, the gas was slowly compressed over mercury into the gas pipet, while at the same time compressed nitrogen was allowed to flow into the furnace pressure vessel so that the pressure inside and outside the gas pipet increased at the same rate. After the filling the two pressures were adjusted to within one atmosphere. After recording the equilibrium pressure the gas was expanded into the second pipet which had been previously evacuated. The expansion was carried out slowly, and the pressure on the outside of the pipet reduced simultaneously to avoid excessive pressure differences between the inside and outside of the pipet wall. With the temporary small pressure differences involved in these operations (at most 5 atmospheres), and with the wall thickness of the pipet used, it is extremely unlikely that any distortion of the pipet walls occurred. This was confirmed by measuring the pipet volume by a low pressure gas expansion method before and after a series of runs; the two measurements were in good agreement.

A large number of expansions at each of the temperatures 600°, 800°, 1000°, and 1200° were carried out, covering a pressure range from 6 to 60 atmospheres. During these measurements the temperature of the dead space outside the furnace was recorded, the temperature being maintained uniform over most of the dead space by water cooling. The volume of the dead space was determined separately by a gas expansion from a small calibrated volume as reported by Kaminsky and Blaisdell.[8]

TREATMENT OF DATA

Before the pressure-ratio plot can be constructed, the recorded pressures must be corrected for baromatric pressure, dead-space volumes, air buoyancy of the steel weights, etc., as described in reference 1. Of these the dead space correction is the most troublesome, and warrants some explanation here. The problem reduces to finding a correction factor F, such that

$$P_f=FP_e, \tag{5}$$

in which P_e is the pressure actually measured, and P_f is the true pressure which would have been observed if all the gas in the dead space (capillaries, etc.) had been at the same temperature as that of the gas pipet. In our present case, there will be a correction factor, which we denote by F_1, associated with the first pipet and its dead space up to the expansion valve (see Fig. 1); and a factor F_2, associated with the total dead space of both pipets (gas expanded). Assuming first the perfect gas law to be adequate for correction purposes, the factors are given by:

$$F_1{}^\circ=(T/V)\sum(v/t)_i, \tag{6}$$

$$F_2{}^\circ=[TT_0/(VT_0+V_0T)]\sum(v/t)_i. \tag{7}$$

Here T and T_0 are the temperatures of the first and second pipets respectively, V is the total gas volume (including dead-space) before the gas is expanded, and $V+V_0$ the total volume after the gas is expanded. It is assumed that the volume available to the gas can be divided into separate parts with volume v, each with its own discrete temperature t, and the quotient v/t is summed for all such parts. These conditions were approached by most of the dead-space regions but not for the capillary from the high temperature pipet to the valve block. The temperature distribution along the capillary was measured in a separate experiment with a second thermocouple, while the pipet was maintained in turn at each of the four temperatures used.

If instead of the perfect gas law, Eq. (1) is used for computing the corrections one obtains

$$F_1=\frac{ST}{V-STB_T'P_e} \tag{8}$$

$$F_2=\frac{1}{2P_e}\cdot\frac{(B_0'+B_T')P_eS-[(V_T/T)+(V_0/T_0)]+(\{(B_0'-B_T')P_eS+[(V_T/T)-(V_0/T_0)]\}^2+(4V_TV_0/TT_0))^{\frac{1}{2}}}{(V_TB_0'/T)+(V_0/T_0)B_T'-B_T'B_0'P_eS} \tag{9}$$

[8] J. Kaminsky and B. E. Blaisdell, Rev. Sci. Inst. **10**, 57 (1939).

Here B_T' and B_0' are, respectively, B_T/A_T and B_0/A_0 and

$$S=\sum_i\left(\frac{v}{t(1+B_t'P_e)}\right)_i.$$

This requires that the virials B_t' at each of the temperatures t, the temperature of the separate parts which make up the total volume, be known. This is ordinarily the case except for the virial B_T corresponding to the temperature T of the gas pipet, which is the quantity being measured. The problem was resolved by using an iteration process: an approximate value of B_T was used in computing S, and F_1 and F_2. These correction factors were then used to obtain the true pressures and construct a pressure-ratio plot, from which B_T was obtained to the first approximation.

A second approximation, which was found to be sufficient in the present case, was then carried through.

The expressions (8) and (9) are too cumbersome for routine computation. It was found possible to approximate these to a sufficient degree of accuracy by the expressions:

$$F_1=F_1^\circ(1-\alpha P_e), \tag{10}$$

$$F_2=F_2^\circ(1-\beta P_e), \tag{11}$$

where F_1° and F_2° are the factors given by Eqs. (6) and (7) and α and β are empirical constants which were obtained by working out (8) and (9), respectively, at a single pressure (in our case a pressure of 40 atmos. was chosen). Then by means of (10) and (11) the correction factors can be computed for any measured pressure P_e.

At first sight it would appear that, if the dead space is sufficiently small (in the present case amounting to less than 0.8 percent of the total volume), the correction factors given by Eqs. (6) and (7) should be sufficiently accurate. Yet surprisingly enough, at say 1000°, the use of the perfect gas law correction factors can lead to an error in B_{1000} of nearly 10 percent. The explanation of this is as follows: B is evaluated from the slope of a straight line which is determined almost wholly by the pressure ratio, P_m/P_{m+1}, the first term of Eq. (2). Remembering that $P_m=F_1P_e$ and a similar relation for P_{m+1}, and assuming for the present the error in P_e to be negligible, then it is obvious that any error in the ratio F_1/F_2 will cause an error in the slope and hence in B. Errors in evaluating the volumes and temperatures of the dead space, for example will not cause an appreciable error in B (of the order of 0.3 percent in our measurements), because these will appear in both F_1 and F_2 and hence will largely cancel in the ratio. On the other hand, when the correction factors given by (10) and (11) are used instead of the perfect gas law correction factors, F_1 and F_2 are now pressure dependent, and since the pressure at which F_1 is computed (pressure before expansion) is always greater than that at which F_2 is computed (pressure after expansion), and moreover since α is greater than β the change in F_1 will be greater, and the ratio F_1/F_2 is decreased. That is to say, if the perfect gas law correction factors are used, the value of B so obtained will be too high, by an amount estimated to be 10 percent at 1000°.

The fitting of the data was carried out in the following way. Using first the pressures corrected by Eqs. (6) and (7) the *LHS* of Eq. (2) with the third term omitted was plotted against P_m+P_{m+1}. The value of B thus obtained was used to calculate F_1 and F_2 according to Eqs. (8) and (9) and (10) and (11). After correcting the pressures with these factors, a new fit was made. This process was repeated until the difference in the values of B used to calculate F_1 and F_2 and that obtained from the plot by least squares was negligible. Then the third term on the *LHS* of Eq. (2) was included. Since this term affected the value of B by less than 0.3 percent, it was not necessary to carry the iteration process further.

The points on the final plot showed some scatter, and as mentioned above these points were fitted by least squares without weighting. The probable error in the slope from which B was calculated, was computed to be about 1.8 percent below 1000° and somewhat higher at 1200°. Taking into account all other sources of error (e.g. errors in calibrations, temperature measurements, etc.), the probable error in B is estimated at about 2 percent at 600, $2\frac{1}{2}$ percent at 800 and 1000°, and somewhat less than 3.5 percent at 1200°.

RESULTS

The results of the present measurements of the second virial of helium at 600°, 800°, 1000°, and 1200° are summarized in Table I. The number of expansions carried out at each temperature are shown in the last column. Included also are the previous measurements from 0° to 600° as reported in reference 1. The values

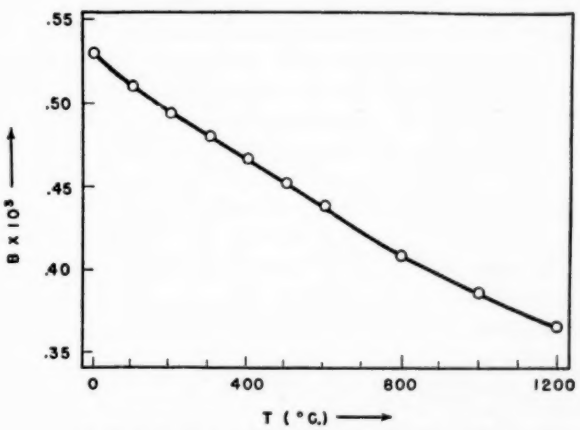

FIG. 2. Plot of the second virial coefficient of helium *vs.* temperature.

of A_0 and B_0 required in obtaining the new values were taken from the latter set of data. The combined results from 0° to 1200° are shown graphically in Fig. 2. In this temperature range, the second virial is decreasing almost linearly with temperature. A slight leveling-off is, however, apparent at the higher temperatures, which is perhaps to be expected, since it is unlikely that the second virial can become zero at high temperatures.

ACKNOWLEDGMENT

We wish to thank Mr. Y. Lupien for assistance in the measurements, and Mr. D. Haun for assistance in the computations.

THE JOURNAL OF CHEMICAL PHYSICS VOLUME 18, NUMBER 5 MAY, 1950

On the Intermolecular Potential of Helium*

J. L. YNTEMA† AND W. G. SCHNEIDER
National Research Council, Ottawa, Canada

(Received November 16, 1949)

Experimental values of the second virial coefficient from 0°C to 1200°C (see preceding paper) were used to test various intermolecular potential functions for helium. A Lennard Jones potential,

$$E(r)=\lambda r^{-n}-\mu r^{-m},$$

with $m=6$ and with n either 9 or 12 could not be made to fit the experimental data over the entire temperature range. The coefficients λ and μ derived from the data showed a marked temperature dependence. The theoretically calculated potentials of Slater and Kirkwood and of Margenau were found to give values of the second virial which were approximately 8.5 percent and 27 percent lower, respectively, than the experimental values. A potential function with exponential repulsion, which gives a more satisfactory fit with the experimental data, was derived empirically. A semi-empirical expression given by Keyes (reference 17) for B as a function of temperature was also compared.

THE second virial coefficient of a gas can be used to obtain information about the intermolecular potential field of the molecules composing the gas by means of the relation

$$B(T)=2\pi N\int_0^\infty\left\{1-\exp\frac{-E(r)}{k(T)}\right\}r^2dr, \qquad (1)$$

where $B(T)$ is the second virial coefficient, N is the Avogadro number, k the Boltzmann constant, and $E(r)$ expresses the intermolecular potential energy of a pair of molecules as a function of their mutual separation r. Since Eq. (1) expresses B as a function of temperature, it is desirable to have accurate experimental values of the second virial over a wide temperature range. Various plausible forms for the potential $E(r)$ can be substituted in Eq. (1) and the values of B so calculated can be compared with the experimental values. Previous attempts to arrive at a potential function for helium, (for a summary of which the work of Keesom[1] should be consulted), or to test certain functions arrived at by *a priori* calculations, have been hampered by inadequate experimental data. For the most part two sets of experimental data have been used: (i) the measurements of Holborn and Otto[2] which extend from −258°C to +400°C and (ii) the measurements of Keesom and co-workers at Leiden[3] which extend from −258°C to +100°C. These two sets of data differ at 100° by about 6 percent and at −258° by about 14 percent. A more serious limitation perhaps is the fact that most of the measurements were made over a temperature range below 0°, where quantum corrections to the second virial derived from Eq. (1) become large. Equation (1) was derived on the basis of classical statistics, and since at present the quantum correction is somewhat uncertain, it is desirable to make use only of the virial data at the higher temperatures, where classical behavior can be assumed. Accordingly it appeared worth while to use the new virial data of the preceding paper, which extend from 0°C to 1200°C, for testing various potential functions for helium.

The desirability of including all the virial data at present available in the literature and analyzing the data to arrive at a "best" value at each temperature was considered. Besides the two sets of data mentioned above, several other measurements[4,5] are available, but these do not extend over a wide temperature range. The large discrepancy between the Berlin and Leiden data

* Contribution No. 2122 from the National Research Council, Ottawa, Canada.

† National Research Council (Canada) Postdoctoral Fellow.

[1] W. H. Keesom, *Helium* (Elsevier Publishing Company, Amsterdam, 1942), p. 47.

[2] L. Holborn and J. Otto, Zeits. f. Physik **33**, 1–11 (1925); see also J. Otto, Zeits. f. Instrumentenk. **48**, 257–8 (1928).

[3] See reference 1, page 34.

[4] R. Wiebe, V. L. Gaddy, and C. Heins, J. Am. Chem. Soc. **53**, 1721–5 (1931).

[5] A. Michels and H. Wouters, Physica **8**, 923 (1941).

is difficult to explain and is well beyond the limits of experimental error. The new measurements are in excellent agreement with the data of Holborn and Otto at 0°, 100°, and 200° (see Table I) but are about 3 percent higher at 300° and 400°. Included in Table I (column 3) are values of the second virial deduced from the Joule-Thompson coefficient measurements of Roebuck and Osterberg[6] by means of the relation:[7]

$$B_T = B_0 + \int_{T_0}^{T} \frac{C_p^{\circ}\mu_0}{RT^2} dT, \tag{2}$$

where μ_0 is the Joule-Thompson coefficient (at temperature T) extrapolated to zero pressure and C_p° is the zero pressure heat capacity. For the integration constant B_0, the value of B at 0°C obtained from compressibility measurements was used, and is shown in parenthesis in the table. The agreement with the new virial data is excellent over the whole temperature range above 0° for which the Joule-Thompson coefficients were available. The estimated error in the latter is about one percent, that of the virial data listed in column 2 over the same temperature range is likewise about one percent. Thus the two sets of data are internally consistent within the experimental error. In view of these considerations it was deemed sufficient for the present purpose to use only the new virial data as listed in column 2 of Table I.

TABLE I. Comparison of experimental second virial coefficient data for helium.

Temp. 0°C	$B_T \times 10^3$ (Amagat units) New measurements	From J.T. coeff., Eq. (2)	Holborn and Otto	Keesom *et al.*
0	0.525	(0.525)	0.524	0.501
100	0.509	0.513	0.508	0.480
200	0.494	0.495	0.494	
300	0.480	0.482	0.468	
400	0.466		0.452	
500	0.452			
600	0.438			
800	0.409			
1000	0.386			
1200	0.365			

COMPARISON WITH A LENNARD JONES POTENTIAL

The Lennard Jones potential, given by

$$E(r) = \lambda r^{-n} - \mu r^{-m}, \tag{3}$$

where λ, μ, n and m are constants, is now frequently applied in physical problems with n and m assigned the values 12 and 6, respectively. While admittedly an approximate potential, it is mathematically more convenient than the potential functions with exponential repulsion. It is of interest therefore to see how well it satisfies the experiment virial data for helium.

To make the comparison we have used the original method of Lennard Jones,[8] as well as a later modification by Buckingham.[9] Substitution of (3) in Eq. (1) and integration leads to:

$$B = \tfrac{2}{3}\pi N(\lambda/\mu)^{3/n-m} F(y), \tag{4}$$

where

$$F(y) = y^{3/n-m}\left\{\Gamma\left(\frac{n-3}{n}\right) - \sum_{s=1}^{\infty} C_s y^s\right\} \tag{5}$$

and y is a temperature function given by

$$y = \mu/kT(kT/\lambda)^{m/n}. \tag{6}$$

The coefficients C_s are given by:

$$C_s = 3\Gamma\left(\frac{cm-3}{n}\right) \Big/ c!n.$$

On taking logarithms of Eqs. (4) and (6) there results:

$$\log B = \log F(y) + \log \tfrac{2}{3}\pi N(\lambda/\mu)^{3/n-m}, \tag{7}$$

$$\log T = -\frac{n}{n-m}\log y - \frac{1}{n-m}\log \lambda^m/\mu^n - \log k. \tag{8}$$

Hence by plotting log B *vs.* log$T$ on a sheet of transparent graph paper and log$F(y)$ *vs.* $-n/n-m$ log$y$ on another sheet, the two curves should be superposable, if the correct values of n and m are chosen, simply by moving one curve with respect to the other parallel along each of the two axes. From the amount of shifting necessary along each of the two axes to obtain superposition, the values of λ and μ can be calculated, as indicated by Eqs. (7) and (8). In Fig. 1 and Fig. 2 are shown the resulting superposition of the experimental data on the theoretical curve using respectively a 9th and a 12th power repulsion with a 6th power attraction. The estimated uncertainty in the experimental points is indicated by the vertical arrows. Neither curve gives a good fit to the experimental data over the whole temperature range although the 9th power repulsion is slightly better; the superposition shown in the figures is considered to be the best fit obtainable and yielded the following potentials:

For

$$n = 12, \quad E(r) = (329r^{-12} - 0.95r^{-6}) \times 10^{-12} \text{ erg.} \tag{9}$$

$$n = 9, \quad E(r) = (53.1r^{-9} - 2.46r^{-6}) \times 10^{-12} \text{ erg.} \tag{10}$$

where r is in angstrom units.

Considerable uncertainty is involved in fitting the curves in the above manner since the experimental data in the neighborhood of the Boyle point (approx. −240°C), which are very useful for obtaining the correct shifting along both axes, were not used. This, however, will not invalidate the above conclusions regard-

[6] J. R. Roebuch and H. Osterberg, Phys. Rev. **43**, 60 (1933); *ibid.* 45, 322 (1934).
[7] See N. G. Whitelaw, Physica **1**, 749 (1934).
[8] J. E. Lennard Jones, Proc. Roy. Soc. **A107**, 636 (1925).
[9] R. A. Buckingham, Proc. Roy. Soc. **A168**, 264 (1938).

TABLE II. Values of the constants λ and μ in $E(r)=\lambda r^{-n}-\mu r^{-6}$ for helium at different temperatures.

	Temperatures used	λ	μ
$n=9$	0°/100°	57.7×10^{-12} erg-(A)^9	2.73×10^{-12} erg-(A)^6
	400°/500°	39.3	1.37
Buckingham*		51.0	2.37
$n=12$	0°/100°	362×10^{-12} erg-(A)^{12}	1.10×10^{-12} erg-(A)^6
	400°/500°	258	0.45
Buckingham*		356	1.09

* Values calculated by Buckingham, Proc. Roy. Soc. **A168**, 264 (1938).

TABLE III. Comparison of calculated virial coefficients for helium.

Temp. 0°C	B_T in cm³/mole Measured values	Eq. (19)	Slater and Kirkwood	Margenau	Keyes
0	11.77	11.87	10.77	8.45	11.73
100	11.42	11.44			11.46
200	11.08	11.03			11.18
300	10.76	10.66			
400	10.45	10.34			10.68
500	10.14	10.04			
600	9.82	9.78	8.98	7.34	10.27
800	9.17	9.33			9.93
1000	8.66	8.95		6.70	9.64
1200	8.19	8.62	7.34		9.39

ing the correct value of n, but it may cause quite a large uncertainty in the values of λ and μ. Accordingly λ and μ were also evaluated by an alternative method due to Buckingham.[9] Let new quantities X and Y be defined by:

$$X=(\lambda/\mu)^{3/n-m}; \tag{11}$$

$$Y=(\mu^n/\lambda^m)^{1/n-m}; \tag{12}$$

then Eqs. (4) and (6) can be written as follows:

$$\log X=\log\frac{3}{2\pi N}B-\log F(y), \tag{13}$$

$$\log Y=\frac{n}{n-m}\log y+\log kT. \tag{14}$$

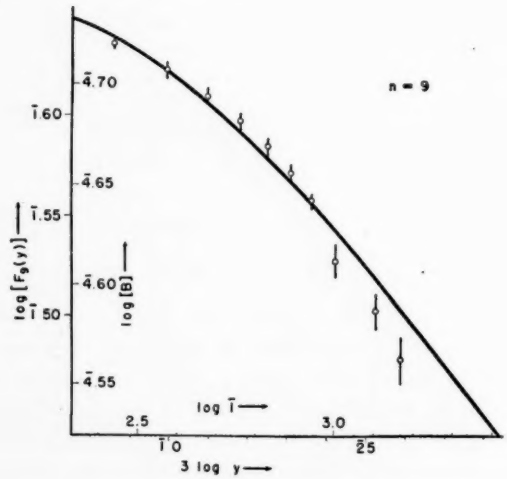

FIG. 1.

Moreover, $\log\lambda$ and $\log\mu$ are related to X and Y by

$$\log\lambda=\tfrac{1}{3}n\log X+\log Y, \tag{15}$$

$$\log\mu=\tfrac{1}{3}m\log X+\log Y, \tag{16}$$

which follow from (11) and (12). For a given temperature, B can be taken from the observations and its value inserted in (13). Equations (13) and (14) then determine a relation between $\log X$ and $\log Y$ in parametric form. This relation can be shown as a curve in the ($\log X$, $\log Y$) plane, the intersection of two such curves for observed values of B at two temperatures determines $\log X$ and $\log Y$, and hence also λ and μ. Employing this method Buckingham found that most of the intersections lie within a fairly well-defined area, and by taking the median values of the ordinates and abscissas, suitable average values for λ and μ were found. With the present data, it was found that above 300°C, the intersection points were not localized in the ($\log X$, $\log Y$) plane, but varied so as to cause λ and μ to decrease with temperature. Furthermore, the points of intersection at the higher temperatures are not well defined because the two curves intersect at a very small angle. The results for several temperatures are shown in Table II. For comparison the values obtained by Buckingham are also given. Since λ and μ are not constant it is obviously impossible to determine uniquely the value of n, the repulsion exponent, from the experimental data over the whole temperature range. For the same reasons also the above methods are not capable of yielding accurate information about the position of the minimum of the potential energy curve (see Fig. 5).

INTERMOLECULAR POTENTIALS WITH EXPONENTIAL REPULSION

It has been shown theoretically[10] that to a first approximation the repulsion energy (overlap energy) can be represented by $be^{-r/\rho}$ where b and ρ are constants.

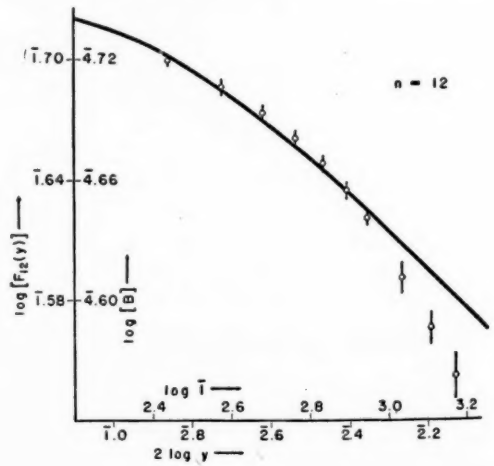

FIG. 2.

[10] J. C. Slater, Phys. Rev. **32**, 349 (1928).

The *a priori* calculations of Slater and Kirkwood[11] yielded for the complete potential for helium the expression:

$$E(r)=\left(770^{-r/.217}-\frac{1.49}{r^6}\right)\times10^{-12}\text{ erg.} \quad (17)$$

Several values of B calculated with this potential by a numerical integration of Eq. (1) are shown in Table III, together with the experimental values. The calculated values are lower by about 8.5 percent. The present calculated values are about 4 percent lower than the calculations of Kirkwood and Keyes[12] using the same potential.

The expression (17) neglects the dipole-quadrupole interaction, which, as pointed out by Margenau[13] will constitute a sizeable fraction of the total dispersion energy. The final potential arrived at by Margenau[14]

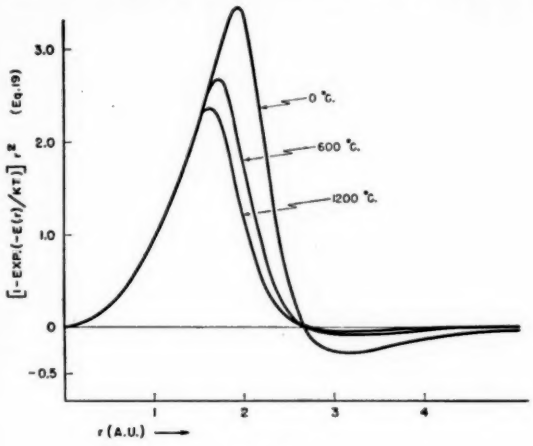

FIG. 3.

is as follows:

$$E(r)=\left(770e^{-r/.217}-560e^{-r/.187}-\frac{1.39}{r^6}-\frac{3.0}{r^8}\right)\times10^{-12}\text{ erg,} \quad (18)$$

where r is expressed in angstrom units. The calculated values of B at 0°, 600° and 1000° using this potential are given in column 5 of Table III, and are approximately 27 percent lower than the experimental values.

Finally an attempt was made to develop empirically a potential function of the form

$$E(r)=be^{-r/\rho}-(c_1/r^6)-(c_2/r^8),$$

which would give a good fit with the experimental virial data over the whole temperature range from 0° to 1200°. For the constant c_1, the value 1.24×10^{-12} erg-(A)^6, derived by London[15] was used. For c_2 the value

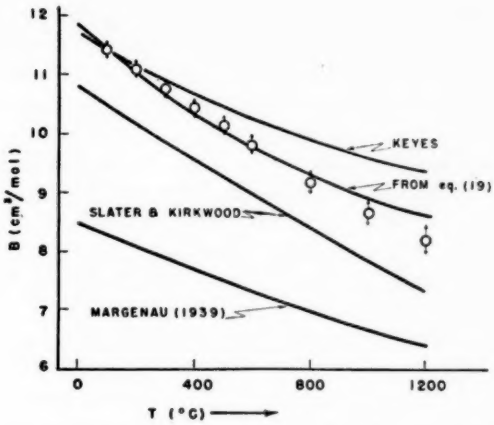

FIG. 4. Comparison of the calculated and measured second virial coefficients for helium. The vertical arrows represent the experimental uncertainty in the measured points.

1.89×10^{-12} erg-(A)^8 was selected, which was calculated by Margenau[16] to correspond with the above value of c_1. Then the constants b and ρ were fitted by a trial and error process to obtain a satisfactory fit with the experimental data. It was not found possible to obtain a fit using $c_1=1.49\times10^{-12}$ erg-(A)^6 and $c_2=3.29\times10^{-12}$ erg(A)^8 which were likewise given by Margenau.[13] The final expression for the potential is given by

$$E(r)=\left(1200e^{-r/.212}-\frac{1.24}{r^6}-\frac{1.89}{r^8}\right)\times10^{-12}\text{ erg.} \quad (19)$$

Using this potential, values of B, shown in Table III, were calculated by numerical integration of Eq. (1). To show the relative contribution at various temperatures of the terms in the integrand, the latter is plotted as a function of r in Fig. 3. Since for values of r below

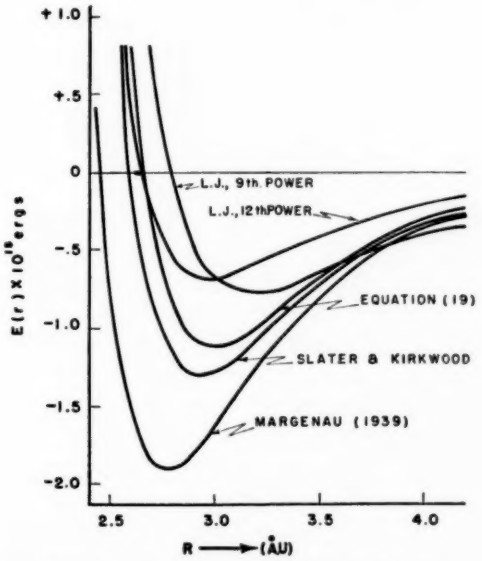

FIG. 5. Potential energy curves for helium.

[11] J. C. Slater and J. Kirkwood, Phys. Rev. **37**, 682 (1931).
[12] J. Kirkwood and F. G. Keyes, Phys. Rev. **37**, 832 (1931).
[13] H. Margenau, Phys. Rev. **38**, 747 (1931).
[14] H. Margenau, Phys. Rev. **56**, 1000 (1939).
[15] F. London, Zeits. f. Physik **63**, 245 (1930).
[16] H. Margenau, Rev. Mod. Phys. **11**, 1 (1939).

1.0A, the dispersion energy tends to large negative values, the potential given by (19), and of course also the potentials (17) and (18), become negative in the neighborhood of 0.7A. In all computations the contribution of the dispersion energy to the integrand was neglected for values of r below 1.0A. At this separation, which is less than half of the low velocity collision diameter for helium (see Fig. 5), dispersion forces as such can have no meaning. The overlap energy also, as calculated theoretically (10), becomes unreliable below 1.0A, and since in this region the exponential term in Eq. (1) is negligibly small, the integrand was replaced by r^2 in the region from 0 to 1.0A. The total contribution from this region to the second virial amounted to approximately 1.26 cm³/mole. Contributions to the integrand for $r>15.0$A were, within the accuracy of the present computations, negligible.

Figure 4 shows a graphic comparison of the values of B calculated using the potentials (17), (18), and (19) with the experimental curve. Included for comparison also is a curve calculated from a formula due to Keyes,[17]

$$B=4.00248T^{-\frac{1}{2}}(16.4873-74.09T^{-\frac{1}{2}}-24.6T^{-1}) \quad (20)$$

which was derived semi-empirically assuming a Lennard-Jones potential.

In Fig. 5, the potentials given by (9, 10, 17–19) are shown in the region of the minimum. The minima of the two Lennard-Jones potentials (9, 10) are both smaller than that of the potentials with exponential repulsion. As pointed out earlier the former involve considerable uncertainty; of the latter it is apparent that the Slater and Kirkwood potential, and more particularly the modified potential of Margenau either underestimate the overlap energy, or overestimate the dispersion energy, or possibly both. To make a more accurate comparison it would be highly desirable to have accurate crystal data for helium in order to establish the position of the minimum.

[17] F. G. Keyes, *Temperature* (Reinhold Publishing Corporation, 1941), p. 45.

THE JOURNAL OF CHEMICAL PHYSICS VOLUME 18, NUMBER 5 MAY, 1950

Light Scattering in the Critical Region. I. Ethylene

H. A. CATALDI AND H. G. DRICKAMER
Department of Chemistry, University of Illinois, Urbana, Illinois

(Received November 18, 1949)

1. In the neighborhood of the critical point, light scattering reveals the presence of four regions: a. A region where the light scattering depends on the inverse fourth power of the wave-length. b. A region of increasing scattering and decreasing dependence on wave-length, beginning about a degree above the critical temperature, and extending about a degree. The maximum scattering in this region is of the order of 100 times the initial value. c. An abrupt decrease in scattering, accompanied by absorption which sets in at a higher temperature for the shorter wave-length. d. A large and erratic increase in scattering, apparently resulting from condensation.

2. The scattering observed upon cooling and heating are identical, provided the temperature does not drop below the temperature for zero scattering or condensation.

3. The wave-length dependence of light scattering is not completely described by any existing theory.

4. Applying the Ornstein-Zernike equation where it is possible, one calculates clusters of about 20 molecular diameters more than a degree above the critical temperature. These clusters increase rapidly with decreasing temperature.

NOMENCLATURE

k = Boltzmann's constant
N_0 = Avagadro's number
p = pressure
r = distance of observer from scattering source
R = ratio of scattered to initial intensity
T = temperature
V = molar volume
β = isothermal compressibility
λ = wave-length of light
μ = refractive index
σ = distance of molecular interaction, interpreted as cluster diameter.

ALTHOUGH there has been much discussion concerning light scattering in the critical region, there is a great scarcity of data, particularly using monochromatic light. The best known investigations of this nature are those of Keesom,[1] Bhattacharya,[2] and Andant.[3] None of these is conclusive, so a series of investigations have been undertaken in this laboratory. The first of these are reported in this and the following paper. These initial investigations involved the measurement of ninety degree scattering as a function of temperature for various fixed densities. The wave-length's used were the 405μ, 436μ, and 546μ lines of the mercury spectrum, referred to as "violet," "blue" and "green" hereafter. The substance covered in this paper

[1] W. H. Keesom, Ann. d. Physik **35**, 591 (1911).
[2] D. K. Bhattacharya, Proc. Ind. Assoc. Cult. Sei. **8**, 277 (1923).
[3] M. A. Andant, Comptes Rendus **176**, 430 (1923); J. de phys. et rad. **5**, 193 (1924).

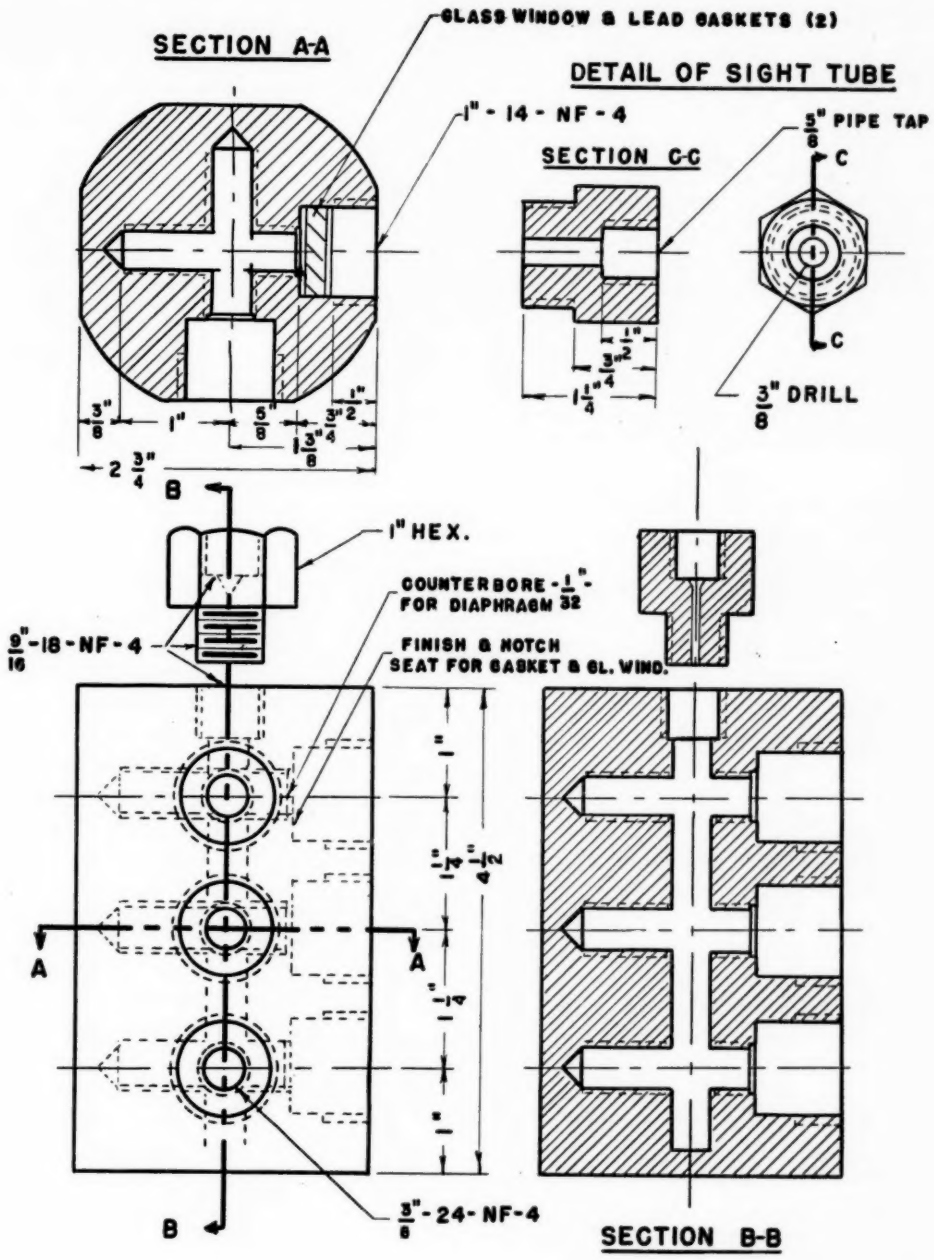

FIG. 1. Detail of bomb.

was spectroscopically pure ethylene obtained from Phillips Petroleum Company. Similar data for ethane are reported in the following paper.

THEORY

The theory of light scattering by individual molecules was developed by Lord Rayleigh[4] and is discussed in most texts on electromagnetic optics. Smoluchowski[5] and Einstein[6] modified this approach for application to the critical region. Basically they assumed scattering units consisting of volumes large enough so that density fluctuations in neighboring volumes would be independent, yet small compared with a wave-length of light. By considering that the fluctuation in dielectric constant resulting from density fluctuations results in the scattering of light, they obtained the following relation for the 90° scattered light.

$$R=\frac{\pi^2 kT\beta(\mu^2-1)^2(\mu^2+2)^2}{18\lambda^4 V^2}. \qquad (1)$$

This expression becomes infinite at the critical point. Smoluchowski attempted to circumvent this difficulty in the following manner: in the above derivation the fluctuation in the volume (or density) is obtained by

[4] Lord Rayleigh, Phil. Mag. **41**, 447 (1871).
[5] M. Smoluchowski, Ann. d. Physik **25**, 225 (1908).
[6] A. Einstein, Ann. d. Physik **33**, 1275 (1910).

using the work function A expanded in a Taylor's series in the volume and keeping only the first (non-zero) term. By keeping further terms in the expansion Smoluchowski obtained a finite scattering formula, which, however, gave a scattering at the critical point no longer proportional to the volume of the scattering medium. The scattering always remains proportional to λ^{-4}.

Ornstein and Zernike[7] pointed out that the conditions imposed by Smoluchowski and Einstein, i.e., independent volumes small compared with the wave-length of light, would scarcely apply in a region of large fluctuations such as the critical region. By assuming a correlation coefficient for fluctuations in neighboring volumes, they obtained the equation:

$$R=\frac{\pi^2kTV(\mu^2-1)^2(\mu^2+2)^2}{18V^2[-(\partial p/\partial V)\lambda^4+(4\pi^2/3)(N_0kT/V)\sigma^2\mu^2\lambda^2]}. \quad (2)$$

The correlation coefficient is contained in σ. Where this is negligible the formula reduces to that of Einstein and Smoluchowski. σ^2 has the dimensions of area, and can be considered as a measure of the scattering cross section. If we assume that the scattering is caused by nuclei or clusters this gives a measure of cluster diameter.

This formula indicates that the dependence of scattering on wave-length changes from λ^{-4} (Rayleigh scattering) to λ^{-2} at the critical point.

If one has measurements at two wave-lengths it is possible to calculate σ from the measurements of scattered light only, as long as $\partial p/\partial V$ is not zero, and if we neglect the dependence of refractive index on wave-length. Then

$$R=\frac{A}{B\lambda^4+C\lambda^2} \quad (2a)$$

$$\frac{R_1}{R_2}=\frac{\beta\lambda_2^4+C\lambda_2^2}{\beta\lambda_1^4+C\lambda_1^2} \quad (3)$$

$$\frac{B}{C}=\frac{(\lambda_1^4/\lambda_2^4)(R_1/R_2)-1}{1-(\lambda_1^2/\lambda_2^2)(R_1/R_2)}\lambda_2^2=\rho. \quad (4)$$

ρ can be obtained from measurements of scattered light at two wave-lengths. Thus

$$\sigma^2=\frac{3\rho(-(\partial p/\partial V))V^2}{4\pi^2\mu^2RT}. \quad (5)$$

A somewhat different result has been obtained by Rocard[8] using a different approach. Since his results do not seem to be applicable they will not be considered.

Mie[9] has developed a theory of light scattering by particles large compared to the wave-length of light. This may well apply quite near the critical point, but since it requires measurements at two or more angles it cannot be tested by the data obtained to date in this investigation.

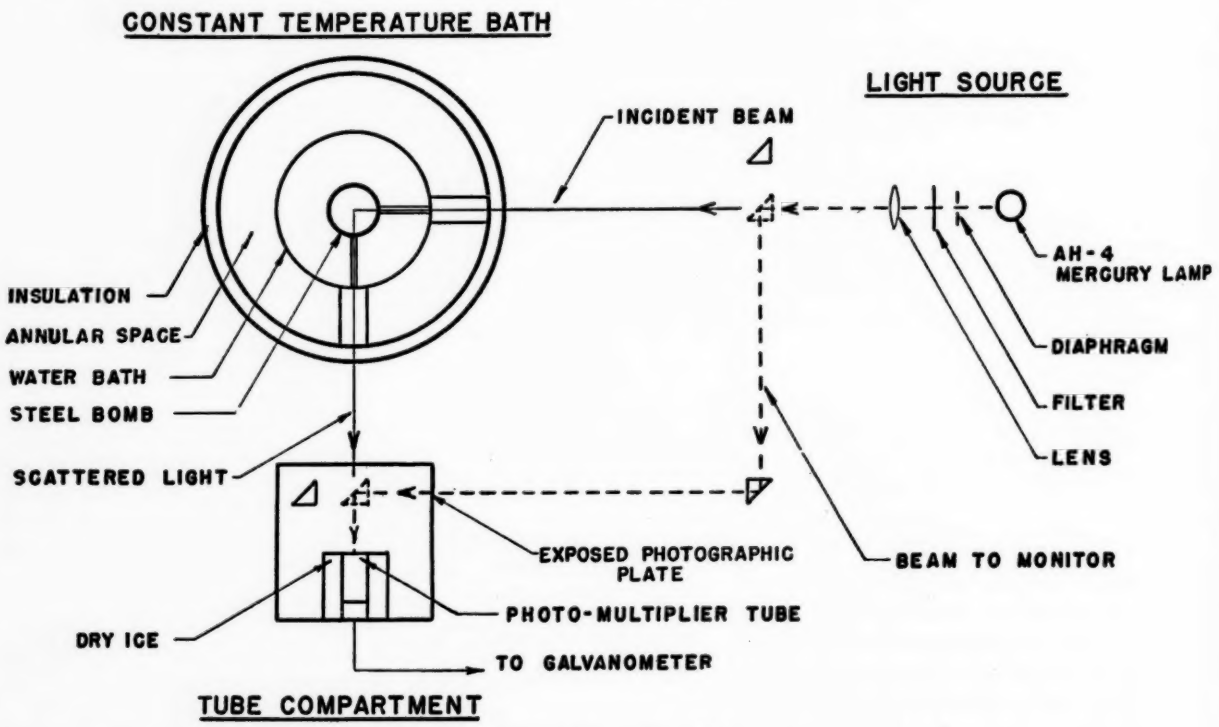

FIG. 2. Schematic layout of optical system.

[7] L. S. Ornstein and F. Zernike, Proc. Acad. Sci. Amst. **17**, 793 (1914); Phys. Zeits. **27**, 761 (1926).
[8] Y. Rocard, J. de phys. et rad. **4**, 165 (1933).
[9] G. Mie, Ann. d. Physik (1911).

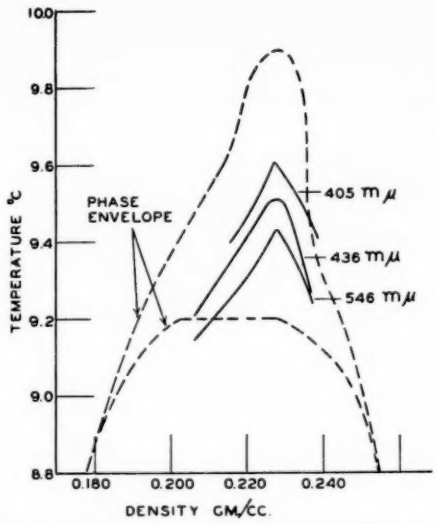

FIG. 3. Temperature of maximum scattering.

EQUIPMENT AND PROCEDURE

The equipment is shown in Figs. 1–2. The light source was an AH-4 mercury lamp. The lines were isolated by use of Corning glass filters. The bomb was built with windows at three levels and a prism system was developed as shown for introducing light and measuring scattered light at each level. The purpose of this was to follow the time dependence of events in the bomb. The holes in the bomb were chased with a fine thread to reduce reflected light. No measurable reflections were obtained when the bomb was properly positioned. The monitor system was used to measure changes in the light source and in the tube sensitivity. The scattered light was measured with a IP21 photo-multiplier tube, using 90 volts per stage. The power source was a pack of B-batteries. The signal was measured by means of a type R galvanometer of sensitivity 7×10^{-5} microamperes per mm. The results were corrected for nonlinearity of the scale. The photo-tube was cooled with dry ice to reduce noise level. The receiving prisms and photo-tube were enclosed in an airtight compartment containing silica gel to maintain low humidity. This was necessary to prevent condensation on the prisms and tube face. It was possible to replenish the dry ice packing without opening the low humidity box.

The exposed photographic plate used on the monitor beam was necessary to reduce the intensity of the light entering the photo-tube. Since the plate was not neutral the monitor could not be used directly in relative intensity calculations. The relative intensities of the light leaving the filters were measured using the monitor system without the photographic plate and a rotating disk with a 3° sector cut out. The measurements gave relative values of the lines (green:blue:violet) 1.60:1.00:0.150, the accuracy of the violet reading is somewhat less than the others because of the smaller intensity. Scattering measurements out in the region where the λ^{-4}-law should apply indicated that the ratio should be 1.62:1.00:0.136, and this latter ratio was used in all calculations.

The temperatures were measured on a calibrated Beckmann thermometer. The bath was controlled roughly by a mercury regulator, but ultimate precise control was obtained by hand. The temperature could be held to ±0.001°C.

The pressure was measured with a 500–800 Bourdon type gauge calibrated against a dead weight gauge. It could be read to one p.s.i. It was found that this introduced considerable uncertainty in the density determination, and in future work a much more accurate pressure-measuring device is planned.

The runs were made in the following manner. Gas was introduced while the temperature was held well above the critical to facilitate density measurements. The pressure was read and density determined. The bomb was then cooled gradually taking scattering and monitor readings. The bomb was then reheated, sometimes taking additional readings. When the original temperature was restored gas was added or removed depending on whether a higher or lower density was desired.

RESULTS

In all, twenty-two runs were made at densities varying from 0.174 to 0.266.[10] For densities near the critical four distinct regions were found:

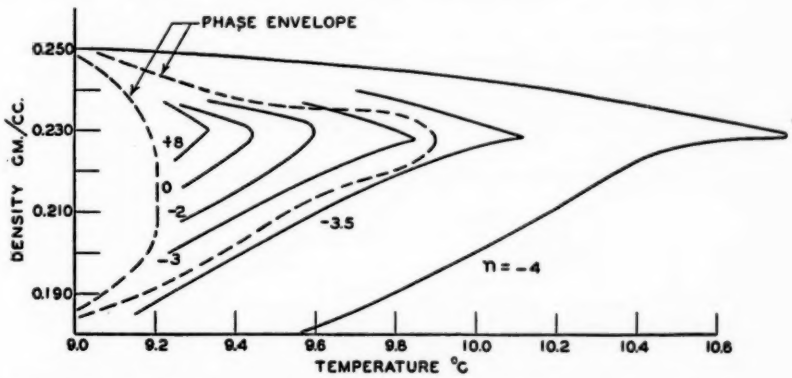

FIG. 4. Dependence of scattering on wave-length.

$$\frac{\text{Corrected blue intensity}}{\text{Corrected green intensity}}=\left(\frac{\lambda_B}{\lambda_G}\right)^n.$$

[10] The original data can be found in the Ph.D. thesis by H. A. Cataldi, "Light Scattering in the Critical Region," University of Illinois Library, 1949.

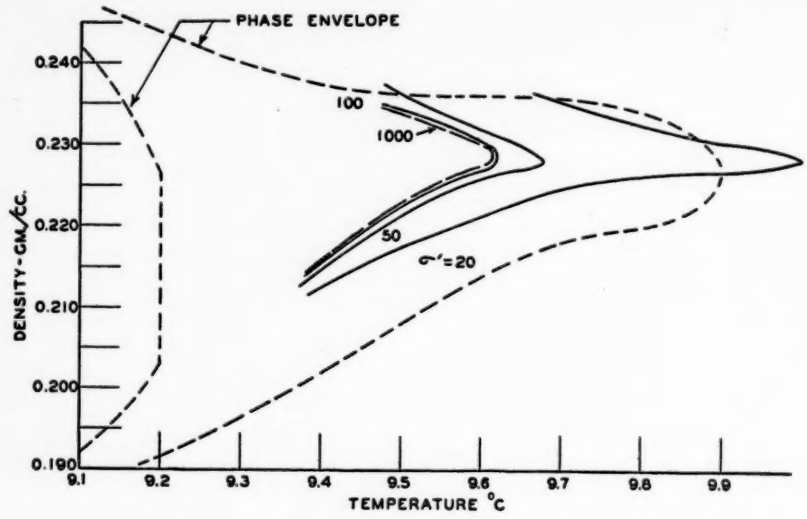

FIG. 5. Distance of molecular interaction or cluster diameter (expressed in molecular diameters) calculated from Ornstein and Zernike equation (based on the scattering of the blue and green lines).

1. The region well above the critical where the λ^{-4}-law holds.
2. A region of rapidly increasing scattering magnitude combined with a decreasing dependence on wave-length. This region began about 11°C and extended down to approximately 9.5°C.
3. A region of rapidly decreasing scattering with the violet decreasing first and then the blue, followed by the green. The scattered light essentially disappeared at the minimum. This is undoubtedly due to multiple scattering or absorption of the original beam.
4. A region of rapid and erratic increase of scattering. As will be explained later, this apparently resulted from condensation in the form of mist.

There were two distinct types of runs designated as "reversible" and "irreversible." If a run was carried only to the end of region three, but not into region four, it was possible to reheat and repeat the results obtained on the cooling cycle. If region four was entered it was found that on reheating, the points did not fall on the cooling curve until well past the point of maximum scattering.

For any given density the temperature of maximum scattering depended on the wave-length. This is shown in Fig. 3. The dotted curves indicate the phase envelope obtained by Maass *et al.*[11] by two methods. The upper curve represents standard *p-v-t* measurements, the lower curve *p-v-t* measurements in a shaken bomb.

From the scattering values at any two wave-lengths corrected for relative intensity of the initial beam, it is possible to calculate the dependence of scattering on wave-legnth at any point. Figure 4 illustrates the results calculated from the blue-green lines. It appears evident that none of the existing theories except Mie's holds for temperatures below the point of maximum scattering. The rapid decrease in scattering apparently corresponds to absorption or multiple scattering of light of short wave-length preferentially in the original beam.

For the runs made at densities considerably away from the critical, the maximum was considerably less pronounced, but the region of erratic scattering is present at the phase envelope. This indicates again that the erratic "irreversible" scattering is the result of condensation.

For the increasing portion of the curve before the maximum it is possible to calculate cluster diameters using Eq. (5). The results calculated for the blue-green lines are shown in Fig. 5. The values of σ are in molecular diameters. Since the theory is not generally applicable the exact significance of these results is not evident, but they are shown as a matter of interest.

The use of the three levels at any density and temperature did not yield any startling results. After sufficient time the relative readings at the three levels were always the same. It was noted that any change in temperature or density always effected the scattering in the lower level first and the change proceeded up the bomb like a slowly traveling wave.

On further work the transmitted light will be measured as well as the scattered light so as to eliminate the effect of absorption of multiple scattering.

H. A. Cataldi would like to acknowledge the assistance of the Shell Fellowship Committee during part of this work.

[11] O. Maass and S. N. Naldrett, Can. J. Research **B18**, 118, (1940).

Light Scattering in the Critical Region. II. Ethane

A. L. Babb and H. G. Drickamer
Department of Chemistry, University of Illinois, Urbana, Illinois
(Received November 18, 1949)

Light scattering experiments have been performed on ethane in the critical region, using apparatus and procedure previously applied to ethylene. The results are qualitatively quite similar to those obtained for ethylene, indicating that no theory so far developed completely describes the phenomenon.

USING the equipment and methods described in the previous paper, light scattering measurements were made on spectroscopically pure ethane obtained from the Phillips Petroleum Company.

Thirty-two runs were made covering densities from 0.170 to 0.234 gram per cc.[1] The results were qualitatively very similar to those obtained for ethylene. Again there appear to be four regions:

(1) A region where the λ^{-4}-law holds.
(2) A region of increasing scattering and decreasing wave-length dependence.
(3) A region of rapid decrease in scattering.
(4) A region of large and erratic scattering.

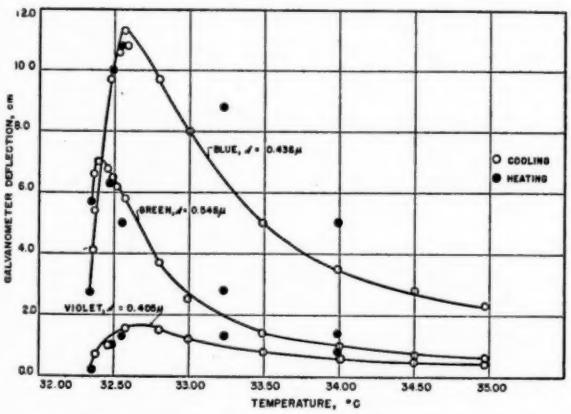

FIG. 1. Scattering as a function of temperature, reversible cycle.

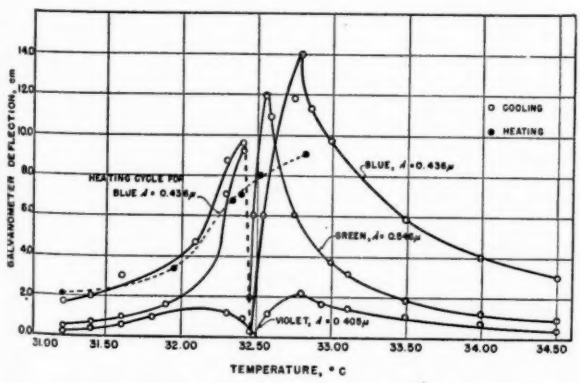

FIG. 2. Scattering as a function of temperature, irreversible cycle.

[1] The original data can be obtained from the M.S. thesis of A. L. Babb "Light Scattering in the Critical Phase," University of Illinois Library, 1949.

The runs were reversible unless region four was entered. Typical reversible and irreversible runs are shown in Figs. 1 and 2.

The temperature of maximum scattering for the violet, blue, and green lines are shown in Fig. 3. All these maxima occur distinctly above the critical point, normally taken to be 32.28°C.

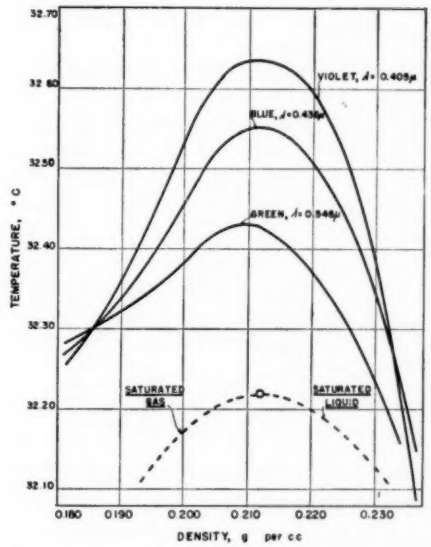

FIG. 3. Temperature of maximum scattering.

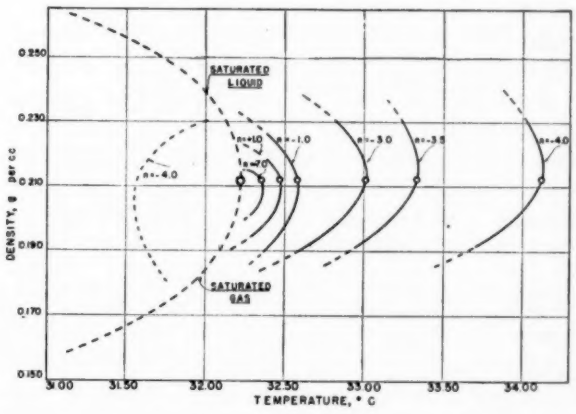

FIG. 4. Dependence of scattering on wave-length.

$$\frac{\text{Corrected blue intensity}}{\text{Corrected green intensity}} = \left(\frac{\lambda_B}{\lambda_G}\right)^n$$

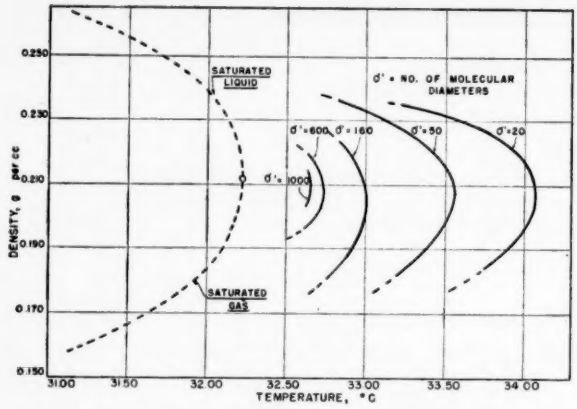

FIG. 5. Distance of molecular interaction or cluster diameter (expressed in molecular diameters) calculated from Ornstein and Zernike's equation. (Based on the scattering of the green and blue lines.)

The dependence of scattering on wave-length is shown in Fig. 4. In this case, runs were made far enough down into the mixed liquid-vapor phase to indicate that the λ^{-4}-law applies less than a degree below the critical point.

Cluster diameters calculated from Eq. (5) of the previous article are shown in terms of molecular diameters in Fig. 5.

From the results of those introductory works it can be seen that no theory so far developed completely describes the phenomena in the critical region. For a complete test, it will be necessary to obtain more accurate densities (in this work they were limited by the accuracy of one p.s.i. in the pressure reading) and to measure transmitted as well as scattered light. Both these refinements are being undertaken in this laboratory.

THE JOURNAL OF CHEMICAL PHYSICS VOLUME 18, NUMBER 5 MAY, 1950

The Approximate Rate of Exchange between Iodine Atoms and Molecules

RICHARD M. NOYES AND JOSEPH ZIMMERMAN*
Department of Chemistry, Columbia University, New York, New York
(Received December 27, 1949)

The rate constant for the exchange reaction of iodine atoms with iodine molecules in hexane at 25° has been estimated by an indirect method. The rate constant is approximately 1.3×10^{-13} (atom/ml)$^{-1}$ sec.$^{-1}$ or 8×10^{10} (mole/ml)$^{-1}$ sec.$^{-1}$. The energy of activation for the exchange is probably between 2 and 3 kilocalories.

INTRODUCTION

THE exchange reactions between halide ions and halogen molecules are known to proceed rapidly. Dodson and Fowler[1] showed that bromide and iodide ions exchange completely with the corresponding halogens in less than 1 minute, and Halford[2] from a comparison of competing reactions showed that the rate constant for the formation of trichloride ion from chlorine and aqueous chloride ion lies between 6.7×10^{6} and 1.7×10^{13} (mole/ml)$^{-1}$ sec.$^{-1}$. There do not appear to be any corresponding data on the isotopic exchange between halogen atoms and molecules. In fact, to our knowledge the ortho-para conversion of hydrogen[3] is the only study of the rate of exchange of a neutral atom with a diatomic molecule of the same element.

In connection with a study[4] of the exchange of iodine atoms with *trans*-diiodoethylene in hexane solution at 25°, it became apparent that the data provided an approximate rate constant for the exchange reaction between iodine atoms and molecules. If a solution of iodine and *trans*-diiodoethylene is illuminated with visible light, the following processes take place:

$$I_2+h\nu\rightarrow 2I \tag{1}$$

$$2I\xrightarrow{k_1}I_2 \tag{2}$$

$$I+C_2H_2I_2\xrightarrow{k_2}C_2H_2I_2+I \tag{3}$$

$$I+I_2\xrightarrow{k_4}I_2+I, \tag{4}$$

where reactions (3) and (4) represent exchanges which can be followed with the use of isotopic tracers, and the k's are rate constants (in (atom/ml)$^{-1}$ sec.$^{-1}$) for the indicated reactions. Let us adopt the following conventions:

q_a = number of quanta absorbed per ml per second,

ϕ = primary quantum yield of process (1) so defined that $\phi=1$ corresponds to the formation of two iodine atoms for each quantum absorbed,

I = concentration of iodine atoms per ml,

* Based on a Dissertation submitted by Joseph Zimmerman to the Faculty of Pure Science of Columbia University in partial fulfillment of the requirements for the Ph.D. degree in Chemistry.

[1] R. W. Dodson and R. D. Fowler, J. Am. Chem. Soc. **61**, 1215 (1939).

[2] R. S. Halford, J. Am. Chem. Soc. **62**, 3233 (1940).

[3] K. H. Geib and P. Harteck, Zeits. f. physik. Chemie (Bodenstein Festband), 849 (1931); A. Farkas and L. Farkas, Proc. Roy. Soc. **152A**, 124 (1935).

[4] J. Zimmerman and R. M. Noyes, J. Chem. Phys. **18**, 658 (1950).

a = concentration of iodine molecules in any convenient units,

b = concentration of *trans*-diiodoethylene in the same units as a, and

x = fraction of iodine-131, initially all present as I_2, which is present in I_2 at time t.

If it is assumed[4,5] that the distribution of iodine-131 in the atoms and molecules is the same, the rate of exchange with the diiodoethylene is given by

$$-d(2ax)/dt = k_2 I[(a+b)x - a]. \quad (5)$$

However, process (3) will, on the average, result in a change in the distribution of radioactivity only if the entering iodine atom last reacted by process (1) or (4); if the iodine atom last reacted by process (3), an additional exchange with diiodoethylene will not be detected. At any instant the fraction of iodine atoms which last reacted by process (1) or (4) rather than by process (3) is

$$\frac{2\phi q_a + k_4 aI}{2\phi q_a + k_4 aI + k_2 bI}. \quad (6)$$

Then the corrected expression for the rate of transfer of radioactivity to the diiodoethylene is

$$-\frac{d(2ax)}{dt} = k_2 I[(a+b)x - a]\frac{2\phi q_a + k_4 aI}{2\phi q_a + k_4 aI + k_2 bI}. \quad (7)$$

This equation reduces to Eq. (5) if $(2\phi q_a + k_4 aI) \gg k_2 bI$, which will be the case except in weak light and a very high value of b/a. In our experiments $b \gg a$, and the runs were stopped when $bx \gg a$. Then integration of Eq. (7) leads to

$$-\ln x = \frac{k_2 bIt(2\phi q_a + k_4 aI)}{2a(2\phi q_a + k_4 aI + k_2 bI)} \quad (8)$$

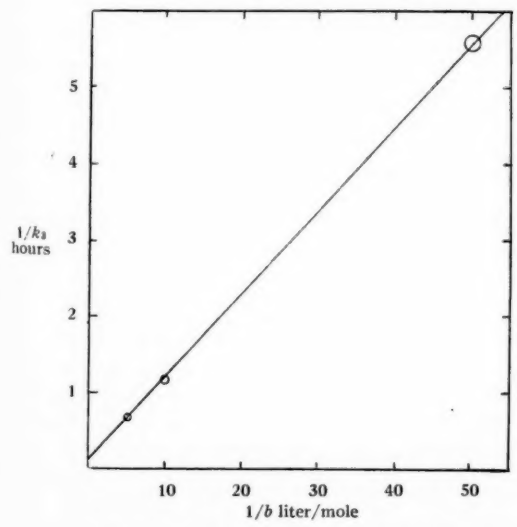

FIG. 1. Relation between rate of exchange and concentration of diiodoethylene.

[5] Noyes, Dickinson, and Schomaker, J. Am. Chem. Soc. **67**, 1319 (1945).

TABLE I. Effect of diiodoethylene concentration on rate of exchange.*

b = Conc. $C_2H_2I_2$ (moles/liter)	k_3 hours^{-1}	Average k_3	k_3/b (moles/liter)$^{-1}$ hr.$^{-1}$
2.00×10^{-2}	0.179	0.179	8.95
	0.179		
1.00×10^{-1}	0.856	0.861	8.61
	0.866		
2.00×10^{-1}	1.504	1.494	7.47
	1.484		

* Conditions: a = Conc. $I_2 = 3.46\times10^{-5}$ moles/liter. $q_a = 2.7\times10^{11}$ quanta/ml sec. Temp. = 25.0°. $\lambda = 436$ mμ.

TABLE II. Rate constants for reactions of iodine atoms in hexane.

Rate constant $k = CT^{\frac{1}{2}}e^{-E/RT}$	Value at 25° (atom/ml)$^{-1}$ sec.$^{-1}$	$CT^{\frac{1}{2}}$ at 25° (atom/ml)$^{-1}$ sec.$^{-1}$	E cal./mole
k_1	1.8×10^{-11}		
k_2	4.3×10^{-18}	7.5×10^{-12}	8500[5]
k_4	1.3×10^{-13}		

and $-\log x = k_3 t$ where

$$1/k_3 = \frac{4.605a}{k_2 Ib} + \frac{4.605a}{2\phi q_a + k_4 aI} = A/b + B. \quad (9)$$

For a series of runs in which a and ϕq_a are constant, if $1/k_3$ is plotted against $1/b$, a straight line should be obtained from whose slope and intercept it is possible to calculate k_2 and k_4.

EXPERIMENTAL RESULTS

The procedure for carrying out the exchange experiments has been described elsewhere.[4] In Table I are presented the results of a series of experiments performed in a degassed system with the same solution of radioactive iodine and different concentrations of diiodoethylene. The data demonstrate that the apparent first-order rate constant falls off as b is increased, and the plot in Fig. 1 shows that Eq. (9) is obeyed to the precision of the experiments.

DISCUSSION

The best values of A and B from Eq. (9) are $A = 0.109$ (mole-liter) hour and $B = 0.106$ hour. Then $A/B = 1.02$ mole/liter. If we use the modified value of Rabinowitch and Wood[4,6] that $I/q_a^{\frac{1}{2}} = 1.8\times10^5$, then $k_2 = 4.34\times10^{-18}$ (atom/ml)$^{-1}$ sec.$^{-1}$ $= 2.61\times10^6$ (mole/ml)$^{-1}$ sec.$^{-1}$. Also, $A/B = (2\phi q_a + k_4 aI)/k_2 I = (1/\tau_s + k_4 a)/k_2$, where τ_s is the mean lifetime of an atom chain and is of the order of 0.31 sec.[4] Then $k_4 = 1.3\times10^{-13}$ (atom/ml)$^{-1}$ sec.$^{-1}$ $= 8\times10^{10}$ (mole/ml)$^{-1}$ sec.$^{-1}$. The precision of duplicate runs in Table I indicates that A is prob-

[6] E. Rabinowitch and W. C. Wood, Trans. Faraday Soc. **32**, 547 (1936).

ably known to at least ±2 percent; the uncertainty in the absolute value of k_2 is considerably greater because the calculation involves the photo-stationary concentration of iodine atoms. The data do not permit an accurate evaluation of k_4, but it does not appear that this quantity can be less than 0.6×10^{-13} nor more than 2×10^{-13}.

Since the experiments were only carried out at one temperature, we do not know the energy of activation for process (4). However, certain limits can be set with some confidence by comparison with the rates of other iodine atom reactions in the same solvent. The pertinent data on these reactions are presented in Table II.

A decision as to activation energy depends upon whether the exchange of iodine atoms with molecules is activation controlled or diffusion controlled.

If process (4) is activation controlled, it can presumably be fitted by an equation of the form $k=CT^{\frac{1}{2}}e^{-E/RT}$ where E is the energy of activation for the exchange. The configurational requirements for the exchange of an atom with an iodine molecule can hardly be more severe than those for exchange with a diiodoethylene molecule. Then 7.5×10^{-12} is a lower limit to $CT^{\frac{1}{2}}$ at 25°, and 2.4 kcal. is a lower limit for the activation energy. On the other hand, $CT^{\frac{1}{2}}$ can hardly be greater than 9.2×10^{-11}, the calculated[4] rate constant for the collision of iodine atoms in the gas phase. Hence the maximum activation energy is 3.9 kcal.

The activation energies in the preceding paragraph are of the order of magnitude to be expected for diffusion processes. It therefore seems profitable to compare the rate of process (4) with the rate of recombination of iodine atoms, which is presumably a diffusion-controlled reaction which proceeds without activation energy. If the difference between k_1 and k_4 is entirely an energy effect, the energy of activation for the exchange of atoms and molecules is 2.9 kcal. Actually, the energy of activation can be expected to be somewhat less because of steric requirements for the $I+I_2$ reaction which are lacking in the recombination of atoms.

If the energies of activation for the diffusion and exchange reactions are almost equal, the interpretation of the data is more complicated, but the range of permissible activation energies should not be much affected. It therefore appears that the energy of activation of the process almost certainly lies between 2 and 3 kilocalories, but it cannot be determined with precision. This result is in agreement with the 2.0 kcal. calculated with the assumption[7] that the activation energy is 5.5 percent of the energy of the bond that is broken.

ACKNOWLEDGMENT

We are indebted to the U. S. Atomic Energy Commission for the allocation of the iodine-131 used in these experiments.

One of us (JZ) is indebted to the Allied Chemical and Dye Corporation for a fellowship.

[7] J. O. Hirschfelder, J. Chem. Phys. **9**, 645 (1941).

THE JOURNAL OF CHEMICAL PHYSICS VOLUME 18, NUMBER 5 MAY, 1950

The Primary Quantum Yield of Dissociation of Iodine in Hexane Solution

JOSEPH ZIMMERMAN* AND RICHARD M. NOYES
Department of Chemistry, Columbia University, New York, New York

(Received December 27, 1949)

The primary quantum yield for the photo-dissociation of iodine in degassed hexane at 25° has been calculated from measurements of the mean lifetime of the chains involved in the exchange of iodine atoms with *trans*-diiodoethylene. The primary quantum yield to an accuracy of ±15 percent is 0.59 at 436 mμ and 0.37 at 578 mμ. The deviation of this quantity from unity is affected both by the "primary recombination" of atoms which fail to escape from the original "cage" of solvent molecules, and by the "secondary recombination" of the original atoms by diffusion during a time which is very short compared to that in which either is apt to encounter an atom from another molecule.

The specific rate constant for the recombination of iodine atoms in hexane solutions has been determined and has been shown to be about one fifth of the rate constant for collision in the gas phase.

The presence of air decreases the rate constant for the photochemical exchange of iodine with diiodoethylene by a factor of four and increases the apparent mean lifetime of iodine atoms by a factor of one hundred.

INTRODUCTION

WHEN a solution of iodine in a non-polar solvent such as hexane is illuminated with visible light of suitable wave-length, dissociation of the iodine to atoms occurs according to the following equations:

Process	*Rate of process*	
$I_2\rightarrow 2I$	$dI/dt=2\phi q_a,$	(1)
$I+I\rightarrow I_2$	$-dI/dt=2k_1I^2,$	(2)

where q_a is the number of quanta absorbed per ml per second, ϕ is the primary quantum yield of dissociation so defined that $\phi=1$ corresponds to two iodine atoms

* Based on a Dissertation submitted by Joseph Zimmerman to the Faculty of Pure Science of Columbia University in partial fulfillment of the requirements for the Ph.D. degree in Chemistry. Persons desiring to consult the more complete report or obtain a microfilm thereof may address the Library, Columbia University, New York, New York.

formed for each quantum absorbed, and k_1 is the specific rate constant (in $(\text{atom/ml})^{-1}$ sec.^{-1}) for the recombination of iodine atoms (I).

If the solution is illuminated continuously, a stationary concentration of iodine atoms is attained when the rate of formation of atoms is equal to the rate of recombination. Under these conditions, the stationary concentration,

$$I_s=(\phi q_a/k_1)^{\frac{1}{2}}. \tag{3}$$

In the continuum in the dilute gas phase, $\phi=1$.[1] However, in the liquid phase there is the possibility that ϕ will be less than unity because of the return of the excited molecule to the ground state after collision with the solvent molecules or because of "primary recombination." According to Franck and Rabinowitch[1] an atom formed in the dissociation process may lose kinetic energy to the solvent while still in the neighborhood of its former partner, thus increasing the probability of collision with that partner. Rabinowitch and Wood[2] later expanded upon this theory, considering the atoms as being trapped by a "cage" of solvent molecules from which they can escape only by a process of diffusion during which they have an opportunity of colliding several times. However, they concluded that since the same diffusion consideration would also slow down normal recombination (k_1), the stationary concentration of atoms would be approximately independent of the amount of primary recombination.

Previous investigators have made a few attempts to evaluate ϕ in some liquid phase reactions, but the methods were indirect and the conclusions were not very definite.

Atwood and Rollefson,[3] in studying the photolysis of oxalyl bromide and the photo-oxidation of nitrosyl chloride in carbon tetrachloride solution found that the quantum yield is less in the liquid than in the gas at all the wave-lengths studied for the latter reaction, but that in the former reaction the quantum yield for the liquid approaches that for the gas at short wave-lengths. They concluded that their results were more easily explained by a deactivating effect of the solvent on the excited molecule than by primary recombination.

Dickinson[4] reported that for the iodine sensitized decomposition of ethylene iodide in carbon tetrachloride solution at 76.6°C if B is the fraction of absorbed quanta which results in dissociation of iodine molecules, then $B_{4358\text{A}}:B_{5461\text{A}}:B_{5780\text{A}}=1:0.87:0.75$.

Tamblyn and Forbes[5] in studying the photo-iodination of diiodoacetylene in hexane at 0° found that the ratios of quantum yields at 4358A, 5461A, and 5780A were 1:0.29:0.27.

Miller and Willard,[6] in studying the exchange reaction between bromine and bromotrichloromethane, compared their data for the photochemical and thermal exchange reactions and deduced that only one out of every 400 bromine molecules which absorb a photon in solution produce bromine atoms which escape without primary recombination. They came to this conclusion by assuming that the equilibrium constant for the thermal dissociation of bromine into bromine atoms is the same in the liquid as in the gas, and that the specific rate constant for recombination is that calculated for the gas phase from the kinetic theory. If this constant is less in the liquid than in the gas, the primary quantum yield of dissociation is even less than one in 400.

Wachholtz[7] in 1927 studied the bromine atom catalyzed isomerization of maleic to fumaric acid. By comparing quantum yields in the light induced reaction with the yields where the bromine atoms were produced by the action of ferrous ions, he found that at a wave-length of 436 mμ only one out of every 50 quanta absorbed produced bromine atoms which separated. However, he did not make comparisons at comparable concentrations of bromine atoms, and his conclusions are not necessarily valid.

Rabinowitch and Wood[8] determined the concentration of iodine atoms produced upon illumination of an iodine solution by measuring the decrease in absorption by the solution as a result of the illumination. They observed that the iodine atom concentration varied as the square root of the absorbed intensity but noted no wave-length dependence. We have averaged the results of all of their reported measurements on solutions of iodine in hexane at 25° and find that $I_s/q_a^{\frac{1}{2}}=1.62\times10^5\pm0.15\times10^5$ $(\text{sec. atom/ml})^{\frac{1}{2}}$.

The mean lifetime, τ_s, of the iodine atoms is given by the expressions

$$\tau_s=\frac{I_s}{2k_1I_s^2}=\frac{1}{2k_1I_s}=\frac{I_s}{2\phi q_a}. \tag{4}$$

Hence

$$\phi\tau_s=I_s/2q_a. \tag{5}$$

From their data Rabinowitch and Wood calculated $\phi\tau_s$ for a given concentration. They then calculated the mean lifetime of the same concentration of iodine atoms in gas phase provided that recombination took place with every collision and that the collision diameter was 5A. They found that in hexane solution $\phi\tau_s$ for the liquid was approximately equal to τ_s which they calculated for the gas. They concluded that either (1) $\phi=1$ in the liquid and τ_s is the same in the liquid as in

[1] J. Franck and E. Rabinowitch, Trans. Faraday Soc. **30**, 120 (1934).
[2] E. Rabinowitch and W. C. Wood, Trans. Faraday Soc. **32**, 1381 (1936).
[3] K. Atwood and G. K. Rollefson, J. Chem. Phys. **9**, 506 (1941).
[4] R. G. Dickinson, Chem. Rev. **17**, 413 (1935). R. G. Dickinson and N. P. Nies, J. Am. Chem. Soc. **57**, 2382 (1935).
[5] J. W. Tamblyn and G. S. Forbes, J. Am. Chem. Soc. **62**, 99 (1940).
[6] A. A. Miller and J. E. Willard, J. Chem. Phys. **17**, 168 (1949).
[7] F. Wachholtz, Zeits. f. Elektrochemie **33**, 545 (1927).
[8] E. Rabinowitch and W. C. Wood, Trans. Faraday Soc. **32**, 547 (1936).

the gas, or (2) $\phi<1$ in the liquid as a result of primary recombination and τ_s is greater than for the gas. To choose between the two possibilities, it is necessary to determine the mean lifetime of the iodine atoms in solution.

Dickinson[9] was apparently the first to point out that τ_s could be measured in this system by the use of intermittent light, and that ϕ could therefore be determined. The rotating sector method of measuring mean lifetimes was used by Berthoud and Bellenot[10] in studying the photochemical reaction of iodine with potassium oxalate. Its use was developed by Briers, Chapman, and Walters[11] and by Dickinson.[12] The latter treatment will be used in our work.

In addition to the symbols ϕ, q_a, k_1, I_s, and τ_s which have already been defined, let us adopt the following conventions:

t_1 = duration of a light period,

pt_1 = duration of a dark period. (In all our experiments $p=3$),

I_1 = concentration of iodine atoms at the beginning of a dark period,

I_2 = concentration of iodine atoms at the end of a dark period,

$b=t_1/\tau_s$,

$\bar{I}_L$ = average value of iodine atom concentration during a light period,

$\bar{I}_D$ = average value of iodine atom concentration during a dark period, and

$\bar{I}$ = average value of iodine atom concentration over a complete cycle.

Upon integrating a combination of Eqs. (1) and (2) over a light period, we obtain

$$\tanh^{-1}\frac{I_1}{I_s}-\tanh^{-1}\frac{I_2}{I_s}=2k_1I_st_1=\frac{t_1}{\tau_s}=b. \tag{6}$$

Similarly, on integrating Eq. (2) over a dark period, we obtain

$$\frac{1}{I_2}-\frac{1}{I_1}=2k_1pt_1=\frac{pb}{I_s}. \tag{7}$$

The average value of I during a light period is

$$\bar{I}_L=\frac{1}{t_1}\int_0^{t_1} I_s\tanh[2k_1I_st+\tanh^{-1}(I_2/I_s)]dt$$
$$=\frac{1}{4k_1t_1}\ln\frac{1-(I_2/I_s)^2}{1-(I_1/I_s)^2}. \tag{8}$$

The average value of I during a dark period is

$$\bar{I}_D=\frac{1}{pt_1}\int_0^{pt_1}\frac{dt}{2k_1t+1/I_1}=\frac{1}{4k_1pt_1}\ln(I_1^2/I_2^2). \tag{9}$$

Then

$$\bar{I}=\frac{\bar{I}_L+p\bar{I}_D}{p+1}. \tag{10}$$

By appropriate manipulation[12] we finally obtain

$$\frac{\bar{I}}{I_s}=\frac{1}{p+1}\left[1+\frac{1}{b}\ln\left(1+\frac{pb}{1+I_s/I_1}\right)\right] \tag{11}$$

where

$$I_1/I_s=\frac{pb\tanh b}{2(pb+\tanh b)}\left[1+\left(1+\frac{4}{pb\tanh b}+\frac{4}{p^2b^2}\right)^{\frac{1}{2}}\right]. \tag{12}$$

From these equations it is possible to obtain a set of values of $\bar{I}/I_s$ for all values of b.

Experimentally, $\bar{I}/I_s$ may be determined for different sector speeds (varying t_1) and the points plotted on a graph with $\log t_1$ as the abscissa. Then, by shifting the theoretical and experimental curves horizontally until the best fit is obtained, the corresponding values of t_1 and b and hence the value of τ_s may be found. Alternatively, the equations may be used to calculate b from a single observed value of $\bar{I}/I_s$.

In order to measure $\bar{I}/I_s$ under different conditions of intermittent illumination we have used the exchange reaction between radioactive iodine and *trans*-diiodoethylene. Noyes, Dickinson, and Schomaker[13] studied the kinetics of this reaction and found that the rate was first order in iodine atoms. Their data can be fitted by an equation of the form

$$-d(2ax)/dt=k_2I[(a+c)x-a] \tag{13}$$

where a = concentration of molecular iodine, c = concentration of *trans*-diiodoethylene, x = fraction of radioactivity present in iodine at time t, (at $t=0$, $x=1$), and k_2 = specific reaction rate constant for the reaction

$$C_2H_2I_2+I^*\rightarrow C_2H_2II^*+I. \tag{14}$$

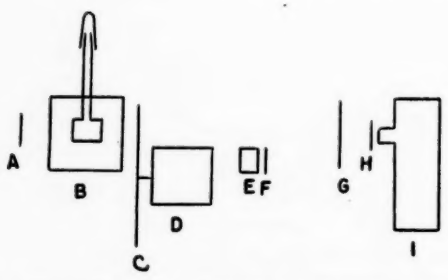

FIG. 1. Apparatus for photochemical exchange experiments.

A Thermopile
B Reaction cell in thermostatted chamber
C Sector
D Motor and gear box
E Photo-tube compartment
F Shutter
G Lens
H Filter
I Mercury arc and housing

[9] R. G. Dickinson, J. Phys. Chem. **42**, 740 (1938).
[10] A. Berthoud and H. Bellenot, Helv. Chim. Acta **7**, 307 (1923).
[11] Briers, Chapman, and Walters, J. Chem. Soc. 562 (1926).
[12] W. A. Noyes, Jr. and P. A. Leighton, *The Photochemistry of Gases* (Reinhold Publishing Corporation, New York, 1941), p. 202.
[13] Noyes, Dickinson, and Schomaker, J. Am. Chem. Soc. **67**, 1319 (1945).

In our experiments $c \gg a$, and the runs were stopped while $cx \gg a$. Hence

$$\ln x = -k_2 c I t/2a \quad \text{and} \quad -(1/t)\log x = k_3, \qquad (15)$$

where k_3 in any solution is directly proportional to the iodine atom concentration. Hence, if we determine k_3 for continuous illumination (k_{3s}) and for various sector speeds, $k_3/k_{3s} = \bar{I}/I_s$.

This treatment assumes that the distribution of radioactivity in the free iodine atoms is the same as that in the iodine molecules. Although this assumption is usually valid, it breaks down for very large ratios of diiodoethylene to iodine concentration.[14] However, even under these conditions $k_3/k_{3s} = \bar{I}/I_s$.

EXPERIMENTAL METHOD

Materials

The hexane used in these experiments was of commercial grade. It was purified by stirring for four hours with concentrated sulfuric acid, after which it received four similar treatments with 30 percent fuming sulfuric acid. It was then washed with sodium carbonate solution and water, stirred for four hours with acid potassium permanganate solution, and washed with sodium carbonate solution. After two additional washes with water, it was dried over calcium chloride and then distilled. The hexane collected came over between 78° and 79.5°. To test for purity according to our needs, a solution of radioactive iodine in hexane was prepared and exposed to strong illumination from a tungsten lamp for one hour. At the end of that time the activity which was not extractable with aqueous sulfite was measured to determine what fraction of the iodine had reacted with the solvent. The amount was less than 0.1 percent.

The *trans*-diiodoethylene was prepared by passing tank acetylene (purified by passage through water and sulfuric acid[15]) into a solution of iodine in 95 percent ethyl alcohol.[16] The resulting material was purified by repeated recrystallization from 95 percent ethyl alcohol.

Resublimed iodine was used without further purification.

Solutions of radioactive iodine in hexane were prepared by shaking inactive solutions with a small amount of an aqueous solution of carrier-free iodine-131 obtained from the Oak Ridge National Laboratory on allocation from the United States Atomic Energy Commission.

Apparatus and Procedure

The arrangement of the equipment used in the rate experiments is illustrated in Fig. 1.

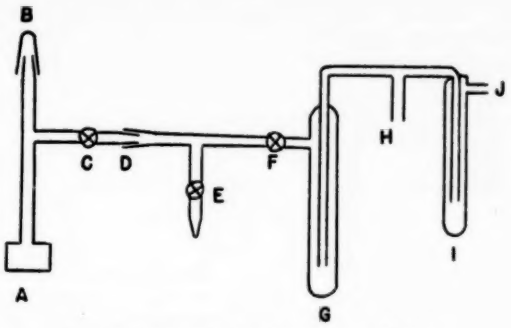

FIG. 2. Apparatus for degassing solutions.

A Cell
B Ground glass cover
C, E, F Stopcocks
D Ground glass joint
G, I Traps
H Lead to manometer
J Lead to vacuum pump.

Illumination was provided by an AH_4 mercury arc operating from the 115v a.c. output of a Sola Constant Voltage transformer. The jacket around the lamp was cooled by passing through it the thermostatted water at 25° issuing from the reaction chamber. The light was monochromatized by using Corning filters Nos. 3389 and 5113 for isolating the 436 mμ line, and Nos. 3480 and 4303 for the 578 mμ line. Since the light source was operated on a 60-cycle alternating current, the intensity varied with a frequency of 120 cycles per second. This variation is so fast compared to the mean lifetime of the rate controlling intermediate that the lamp should produce the same reaction rate as a direct current lamp emitting the same average intensity of illumination.

The intensity of the lamp was controlled manually by means of a Powerstat which varied the voltage input to the lamp transformer. The relative intensity was measured by a 929 photo-tube directly coupled to a 6J5 amplifier. The anode voltages for both the photo-tube and amplifier were supplied by dry cell batteries and variable potentiometers and were always kept at 15.0 volts. The bias voltage for the grid of the 6J5 was adjusted so that, with a shutter in front of the photo-tube, a current of 2 microamperes was read on the amplifier 0–100 microampere plate microammeter.

The absolute intensity of the light reaching the reaction mixture was measured by means of an Eppley Line Thermopile with bismuth and silver elements and a 2284b Leeds and Northrup galvanometer which were calibrated against a Bureau of Standards lamp. A constant check was kept on the sensitivity of the galvanometer using a fixed voltage supplied by a 2 volt storage battery and a fixed resistance. In calculating the absolute intensity incident on the reaction mixture, the intensity measured on the thermopile was corrected for reflections at the various interfaces.[17] Although the lamp emitted a significant amount of infra-red radiation, some of which was passed by the filters, all of this radiation was filtered out by the 8 cm of water in the reaction chamber.

[14] R. M. Noyes and J. Zimmerman, J. Chem. Phys. **18**, 656 (1950).

[15] J. S. Reichert and J. A. Nieuwland, *Organic Syntheses, Collective Volume I* (John Wiley and Sons, Inc., New York, 1932), p. 224.

[16] H. P. Kaufman, Ber. **55B**, 249 (1922).

[17] Reference 12, p. 85.

TABLE I. Effect of oxygen on mean lifetime.*

Light period (minutes)	k_3 (hours^{-1})	$2k_3/k_{3a}$
continuous	0.292	
continuous	0.279	
continuous	0.301	
continuous	0.301	
1	0.133	0.91
1	0.132	0.90
15	0.086	0.59

* Conditions: Solutions in contact with air. Conc. $I_2 = 3.41 \times 10^{-5}$ mole/liter. Conc. $C_2H_2I_2 = 1.01 \times 10^{-1}$ mole/liter. $q_a \approx 9 \times 10^{11}$ quanta/ml sec. $\lambda = 436$ mμ.

TABLE II. Effect of diiodoethylene concentration on mean lifetime in air.*

Conc. $C_2H_2I_2$ (mole/liter)	Light period (seconds)	k_3 (hours^{-1})	Average $2k_3/k_{3a}$
4.0×10^{-2}	continuous	0.0465	
	continuous	0.0460	
	31	0.0210	0.90
	31	0.0208	
2.0×10^{-1}	continuous	0.268	
	continuous	0.265	
	26	0.188	0.70
	23	0.180	0.67

* Conditions: Solutions in contact with air. Conc. $I_2 = 3.46 \times 10^{-5}$ mole/liter. $q_a = 2.7 \times 10^{11}$ quanta/ml sec. $\lambda = 436$ mμ.

TABLE III. Measurements of mean lifetime and primary quantum yield in degassed solutions.

Series	Conc. I_2 mole/liter	Conc. $C_2H_2I_2$ mole/liter	λ mμ	q_a quanta/ml sec.	τ_a sec.	ϕ
I	3.46×10^{-5}	1.00×10^{-1}	436	2.7×10^{11}	0.27±0.02	0.65
II	3.46×10^{-5}	1.00×10^{-1}	436	2.7×10^{11}	0.36±0.06	0.48
III	1.04×10^{-4}	1.00×10^{-1}	436	1.35×10^{12}	0.12±0.01	0.64
IV	3.46×10^{-5}	2.00×10^{-1}	436	2.7×10^{11}	0.31±0.04	0.56
V	3.46×10^{-5}	1.00×10^{-1}	578	2.7×10^{11}	0.41±0.07	0.33

A quartz lens of 10 cm diameter and 13 cm focal length was used to render the light parallel. At a particular spot in the beam and at the same voltage the intensity of the light emitted by the thermostatted lamp was constant and reproducible to one percent. The maximum variation in intensity incident on various parts of the cell was 15 percent, and the intensity at the center agreed within 2 percent with the average obtained by an integration process.

The two sectors which were used were made of black Bakelite and were cut with one 90° and two 45° openings, respectively. The former had a thickness of $\frac{1}{2}$ inch at the boundaries, and the latter a thickness of $\frac{1}{4}$ inch. The sector was driven by a universal gear-reduced motor operating from the a.c. output of a Sola Constant Voltage transformer at approximately 22 r.p.m. normal speed. The speed could be varied by means of a Powerstat. A gear box provided 8:1, 1:1, and 1:8 ratios between sector and motor speeds. These features allowed considerable variation in sector speed. Over a period of one hour the variation in the speed of the sector was found to be ±1 percent. A mathematical analysis[18] was made of the diffusion of iodine atoms during the time that the shadow of the sector was moving across the face of the cell. Under the conditions prevailing in all experiments, diffusion was found to have a negligible effect on rates of formation and destruction of iodine atoms on the light and dark sides of the moving boundary.

TABLE IV. Measurement of mean lifetime in series III.*

t_1 sec.	k_3 hours^{-1}	$2k_3/k_{3a}$	b	τ_a sec.	Weight
0.0535	0.214	0.980	0.46	0.116	0.2
0.104	0.202	0.924	1.08	0.096	0.5
0.110	0.200	0.916	1.15	0.096	0.5
0.319	0.179	0.820	2.30	0.139	1.0
0.715	0.156	0.714	5.00	0.143	0.8
5.00	0.118	0.540	53	0.094	0.3
				Av=0.12	

* Conditions: Conc. $I_2 = 1.04 \times 10^{-4}$ mole/liter. Conc. $C_2H_2I_2 = 1.00 \times 10^{-1}$ mole/liter. $q_a = 1.35 \times 10^{12}$ quanta/ml sec. $\lambda = 436$ mμ. $k_{3a} = 0.437$ hour^{-1}.

TABLE V. Measurement of mean lifetime in series V.*

t_1 sec.	k_3 hours^{-1}	$2k_3/k_{3a}$	b	τ_a sec.	Weight
0.417	0.186	0.780	3.00	0.14	0.8
0.417	0.210	0.880	1.55	0.27	0.8
0.812	0.188	0.788	2.80	0.29	1.0
0.833	0.196	0.822	2.25	0.37	1.0
1.15	0.185	0.775	3.10	0.37	1.0
1.25	0.186	0.780	3.00	0.42	1.0
5.72	0.164	0.709	5.10	1.12	0.7
9.05	0.139	0.582	21.0	0.43	0.5
				Av=0.41	

* Conditions: Conc. $I_2 = 3.46 \times 10^{-5}$ mole/liter. Conc. $C_2H_2I_2 = 1.00 \times 10^{-1}$ mole/liter. $q_a = 2.7 \times 10^{11}$ quanta/ml sec. $\lambda = 578$ mμ. $k_{3a} = 0.477$ hour^{-1}.

The reactions were carried out in a cylindrical Pyrex cell with optically flat sides. The length of the cell was 3.00 cm and the diameter was about 3.2 cm.

During a reaction the cell was placed in a chamber, two sides of which had optically flat windows the same size as those of the cell. Thermostatted water was pumped into the chamber so that the temperature was 25.0°. A clip within the chamber ensured reproducible placing of the cell.

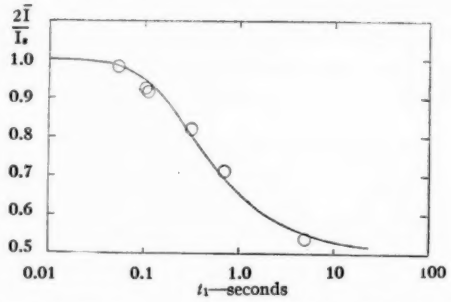

FIG. 3. Measurement of mean lifetime in series III.

[18] See asterisk reference to by-line.

The light absorbed by the dilute iodine solutions was never more than a few percent of the incident radiation and could not be measured with sufficient accuracy by differences in thermopile readings. Therefore the increase in optical density due to the iodine was measured in 10-cm cells in a Beckmann Spectrophotometer, and the absorption in the 3-cm light path of the reaction cell was calculated with the use of Lambert's Law. It was found that at 436 mμ a $3.46\times10^{-5}M$ solution of iodine absorbed only 1.17 percent of the incident radiation in a 3-cm light path.

To prepare an experiment, 10.00 ml of radioactive iodine solution and 12.77 ml of *trans*-diiodoethylene solution were pipetted into the cell. In experiments carried out in the absence of air the contents of the cell were degassed with the apparatus illustrated in Fig. 2. All of the joints were greased with Apiezon *N* stopcock grease, and the evacuation was carried out with a Cenco Hyvac pump. The contents of the cell were frozen with liquid nitrogen during the time that they were being pumped on. Between pumpings, the stopcock *C* was closed, and the contents of the cell were warmed to room temperature. The cell was pumped five times during the preparation of a run.

In some experiments in which the cell had been immersed deeply in liquid nitrogen, a blue discharge was noticed in the neck of the cell during the warming of the contents. Although the phenomenon was not understood, it was postulated that the small crystals which condensed on the lower part of the neck of the cell developed a static charge which discharged when the pressure inside the system was beginning to build up. The discharge could be prevented if the cell was lowered gradually into liquid nitrogen so that the entire contents were frozen well below the neck and in one mass. It was not shown with certainty whether or not this discharge was responsible for some erratic results.

After the degassing was complete, the cell was placed in the reaction chamber and brought to 25°. After illumination with continuous or intermittent light for a measured period, air was let into the cell and the contents were extracted with a dilute aqueous solution of sodium sulfite to reduce the iodine. The aqueous layer was diluted to a known volume and was drawn into the glass jacket surrounding a Geiger counter tube filled with argon-alcohol. The counter was designed by Professor Richard W. Dodson and was made in these laboratories.

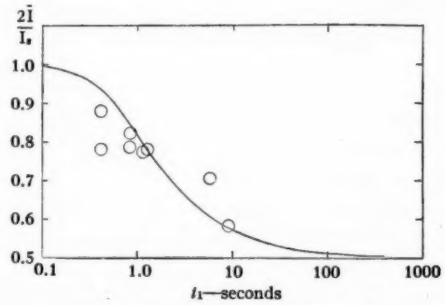

FIG. 4. Measurement of mean lifetime in series V.

TABLE VI. Dependence of rate constant on wave-length.*

λ mμ	q_a quanta/ml sec.	k_3 hours^{-1}	$\bar{k}_3$
578	2.7×10^{11}	0.692	0.702
578	2.7×10^{11}	0.712	
436	2.7×10^{11}	0.876	0.888
436	2.7×10^{11}	0.900	

* Conditions: Conc. $I_2=3.46\times10^{-5}$ mole/liter. Conc. $C_2H_2I_2=1.00\times10^{-1}$ mole/liter.

Thermal experiments were prepared in the same way as the photochemical experiments but were not illuminated.

RESULTS AND DISCUSSION

Thermal Reaction

The rate of the exchange reaction in unilluminated solutions was studied briefly in order to determine whether it would be necessary to correct the results for exchange caused by atoms initiated during the dark periods. The rate constant, k_3, for the thermal reaction was 0.0024 hour^{-1} under conditions where the rate constant in the illuminated solution was of the order of 0.8 hour^{-1}. Therefore the rate constant for thermal exchange is only about 0.3 percent of that for photochemical exchange, and it is unnecessary to apply the corrections for dark reaction developed by Matheson *et al.*[19]

The rate of the thermal reaction was very subject to catalytic effects. Drying the solution reduced the rate by a factor of five, but even in dried solutions the rate at 25° was twice that calculated by extrapolating the data obtained formerly[13] with more concentrated iodine solutions at 75 to 100°. When the concentration of iodine was increased from 3.5×10^{-5} to 3.3×10^{-4} mole/liter, k_3 was reduced by a factor of 7 instead of by the factor of 3.1 which would be expected from the kinetics observed at greater concentrations of iodine atoms. If the exchange in these thermal runs with very dilute iodine proceeds by the same mechanism as the photochemical exchange, the kinetic chain length is at least 10^4 and the mean lifetime of a chain is of the order of a few minutes. Therefore, the large catalytic effects are not surprising.

Effect of Water

Noyes, Dickinson, and Schomaker[13] worked with iodine concentrations of at least 2×10^{-3} mole/liter and either illuminated the solutions intensely or heated them to at least 75°. They did not observe any effects

[19] Matheson, Auer, Bevilacqua, and Hart, J. Am. Chem. Soc. 71, 497 (1949).

due to either oxygen or water. As noted above, we have observed a considerable effect of water in thermal experiments at 25°. However, there was no corresponding effect on photochemical experiments. Solutions which had been dried with magnesium perchlorate gave erratic results, but the addition of water to the dried solutions did not affect the rate. Therefore, either water exerts an effect only on the equilibrium between iodine atoms and molecules, or the effect on the exchange process is not important unless the concentration of iodine atoms is less than the 8×10^{10} atoms/ml which we calculate to have been present in our experiments. Because of the possibility of introducing impurities with the drying agent, the solutions used in the studies with intermittent light were not dried.

Effect of Oxygen

Under the conditions of our experiments, oxygen had a pronounced effect on the rate of the exchange reaction and a spectacular effect on the mean lifetime of the rate controlling intermediate. In a series of runs where k_3 for the reaction with oxygen removed was 0.639 hour^{-1}, k_3 in air was 0.152 hour^{-1}. The rate in air was slower by a factor of 4.2.

The results of some experiments in air with intermittent light are presented in Tables I and II. The data in Table I suggest that the mean lifetime is of the order of 45 seconds. If this were the true mean lifetime of iodine atoms, the primary quantum yield of dissociation would be less than 0.01, and primary recombination of iodine atoms would play an important part in the photochemical dissociation of iodine at 436 mμ. However, the experiments in degassed systems described later indicate that the true mean lifetime is less by a factor of about 100.

The data presented in Table II show that increasing the concentration of diiodoethylene causes a decrease in the mean lifetime in the presence of air. The data also indicate that the rate of exchange in air increases by an amount which is somewhat more than proportional to the increase in concentration of diiodoethylene.

It is possible to account qualitatively for the behavior in the presence of oxygen on the basis of either of two intermediates. One is a $C_2H_2I_3O_2$ radical which decomposes slowly during a dark period and which removes iodine atoms by combining with them to form I_2. The other is a long-lived IO_2 radical whose decomposition is speeded by reaction with I atoms or with diiodoethylene. We do not have sufficient information to come to any definite decision on this matter.

Photochemical Exchange in Degassed Solutions

With the technique finally adopted it was possible to get reproducible results from any one set of solutions, but there was some variation in rate when different sets of solutions were used. Since these variations were greater than any conceivable uncertainties in the concentrations of the reactants, they were apparently due to the presence of reaction-affecting impurities which probably came from the original aqueous solution of radioactive iodide. However, the experiments with intermittent illumination fitted the theoretical curve, and variations in stationary rate constant were not accompanied by systematic variations in calculated primary quantum yield. Therefore, it appears that the impurities did not affect the formation or recombination of iodine atoms but exerted their influence on the rate constants for the exchange of iodine atoms with diiodoethylene or with iodine molecules.

Measurements of Mean Lifetime in Degassed Solutions

As was pointed out in the Introduction, the value of $\bar{I}/I_s$ from a single experiment with intermittent light can be used to calculate b and hence τ_s. However, the probable error in this procedure depends upon the value of b in the particular experiment. Thus in the vicinity of $b=2$ a one percent error in the measured value of $\bar{I}/I_s$ results in a 5 percent error in the calculated value of b, while in the vicinity of $b=0.5$ or 100, the same error causes a 25 percent error in the calculated value of b. Hence results calculated from values of l_1 corresponding to values of b in the more sensitive region should be weighted more heavily.

In each series of experiments made with intermittent light values of k_3/k_{3s} were plotted against $\log l_1$, and an approximate value of τ_s was estimated from the plot. On the basis of this estimate, a rough value of b was calculated for each value of l_1, and a weighting factor was calculated. Then for each experiment the exact value of b and hence of τ_s was calculated from Eqs. (11) and (12). The best value of τ_s for the series was calculated by averaging the results of the individual experiments with the use of the weighting factors. In principle the new value of τ_s could then be used to reassign weighting factors, but this was never necessary.

The results of five series of determinations of mean lifetime under various conditions are presented in Table III. In order to indicate the precision of the data, the results of individual experiments in the best and worst series are presented in Tables IV and V and are plotted in Figs. 3 and 4. The precision measure assigned to each mean lifetime was obtained by dividing the weighted average deviation by the square root of the sum of the weights.

Effect of Wave-Length

From Eqs. (4) and (5) it follows that $\phi=1/4q_ak_1\tau_s^2$, and the primary quantum efficiency at different wavelengths is inversely proportional to $q_a\tau_s^2$. The results of mean lifetime measurements at 436 and 578 mμ presented in Table III indicate that $\phi_{578}/\phi_{436}=0.56$. However, the ratio depends upon the square of τ_s and is therefore not known very precisely.

A more precise value of relative quantum yields can probably be obtained by measuring stationary rate

constants with the same solutions at different wavelengths. Since $I_s=(\phi q_a/k_1)^{\frac{1}{2}}$ and since k_{3s} is proportional to I_s, it follows that

$$\phi_{578}/\phi_{436}=(q_{a436}(k_{3s578})^2)/(q_{a578}(k_{3s436})^2).$$

The data presented in Table VI indicate that $\phi_{578}/\phi_{436}=0.62$ in very satisfactory agreement with the less precise result from mean lifetime measurements.

This latter treatment is not necessarily valid, since at 436 mμ the products of dissociation are one normal $^2P_{\frac{3}{2}}$ atom and one excited $^2P_{\frac{1}{2}}$ atom, while at 578 mμ the products of dissociation are two normal atoms. It is possible that the reactivity of the excited atom is greater than that of the normal atom. However, it is not very probable, in the liquid phase, that an excited atom could maintain its excitation for much longer than one or two exchanges. Since, as we shall show later, one atom produces approximately 76 exchanges during its lifetime, it is unlikely that the initial state of excitation could appreciably influence the reaction rate.

Calculation of Primary Quantum Yield

The absolute value of ϕ cannot be calculated from our data alone but can be calculated with the use of data by Rabinowitch and Wood.[8] These authors observed that $I_s/q_a^{\frac{1}{2}}$ at 25° was independent of wavelength between 470 and 550 mμ. As the best approximation we can make, we shall assume that their value is midway between the values of this quantity at 436 and 578 mμ. Then $(I_s/q_a^{\frac{1}{2}})_{436}=1.8\times10^5$ and $(I_s/q_a^{\frac{1}{2}})_{578}=1.4\times10^5$. The values of ϕ calculated from our experiments with the use of these values are included in Table III. When the values of ϕ_{436} are weighted for percentage uncertainties in different values of τ_s, we obtain that $\phi_{436}=0.59$. Then $\phi_{578}=0.59\times0.62=0.37$.

The value of ϕ_{436} is calculated with the use of three measured quantities. The absorbed light, q_a, is probably known at least within 5 percent. The consistency of the data of Rabinowitch and Wood indicates that they measured $I_s/q_a^{\frac{1}{2}}$ to ±9 percent. The individual values of τ_s from each series appear to be reliable to ±15–20 percent. Therefore, the value of ϕ_{436} obtained by averaging would seem to be valid to ±15 percent or better. However, the limiting factor in the reliability of this quantity is how well the Rabinowitch and Wood data apply to our system.

Average Kinetic Chain Length

The average kinetic chain length can be calculated as the rate of appearance of radioactivity in the diiodoethylene divided by the rate of production of iodine atoms. Average kinetic chain length $=-(d(2ax)/dt)/2\phi q_a$. At a diiodoethylene concentration of 1.00×10^{-1} moles/liter and an absorption of 2.7×10^{11} quanta/ml sec., the average kinetic chain length is 76. Since the average time of a chain is 0.31 sec., the average exchange frequency is 240 sec.$^{-1}$.

Rate of Recombination of Iodine Atoms

The rate constant for the recombination of iodine atoms, $k_1=\phi q_a/I_s^2$. From our data $k_1=1.8\times10^{-11}$ (atoms/ml)$^{-1}$ sec.$^{-1}$. In the gas phase the rate constant for collision between iodine atoms having a diameter of 4.3A, the van der Waals diameter, is 9.2×10^{-11}.

DISCUSSION

The value of the absolute quantum yield calculated above depends upon the applicability of the data of Rabinowitch and Wood to our system. However, an entirely independent calculation substantiates the validity of our treatment. Noyes, Dickinson, and Schomaker[13] studied the thermal exchange reaction at 75 to 100°. If their rate constants are extrapolated to 25° and compared with the rate constant observed for the photochemical exchange when $q_a=2.7\times10^{11}$ quanta/ml sec., we conclude that $I_s/I_{\text{thermal}}=4.4\times10^3$. Here I_{thermal} is the concentration of iodine atoms in thermal equilibrium with molecular iodine at concentration of 3.46×10^{-5} mole/liter. The equilibrium constant for iodine in the gas phase can be calculated from spectroscopic data.[20] If it is assumed that the same constant is applicable in hexane solution, $I_{\text{thermal}}=2.0\times10^7$ atoms/ml and $I_s/q_a^{\frac{1}{2}}=1.7\times10^5$ in astonishingly good agreement with the value from Rabinowitch and Wood.

The amount by which ϕ is less than unity does not necessarily provide a measure of the primary recombination of atoms which fail to escape from the "cage" in which they are formed. Atoms which are located in neighboring cages may recombine by diffusion in a period of time which is short compared to the period between exchanges with diiodoethylene. Since the recombination of the two atoms from the same molecule proceeds at a rate which is very nearly proportional to q_a instead of to $q_a^{\frac{1}{2}}$, the mean lifetime data as determined by intermittency studies are not concerned with these events. We shall attempt to treat this "secondary recombination" in a subsequent paper.

However, there is abundant evidence that primary recombination is involved in some systems. The average value which Rabinowitch and Wood obtained for $I_s/q_a^{\frac{1}{2}}$ for iodine in hexane was 1.6×10^5, while for iodine in carbon tetrachloride the average value for this quantity was 1.0×10^5. This indicates that carbon tetrachloride is more successful in reducing the primary quantum yield of dissociation than is hexane. The fact that carbon tetrachloride molecules are heavier than hexane molecules makes it seem plausible that they would form a more effective "cage" to prevent the separation of two newly formed iodine atoms. Also, the value of $\phi_{578}/\phi_{436}=0.62$ which we obtain seems to require that primary recombination is effective in at least 38 percent of the cases in which iodine absorbs

[20] J. E. Mayer and M. G. Mayer, *Statistical Mechanics* (John Wiley and Sons, Inc., New York, 1946), p. 469. F. R. Bichowsky and F. D. Rossini, *The Thermochemistry of Chemical Substances* (Reinhold Publishing Corporation, New York, 1936), p. 25.

light of 578 mμ. We may compare our value of 0.62 for this ratio with 0.75 which Dickinson[4] reported for iodine in carbon tetrachloride solution at 76.6° and with 0.27 for hexane solution at 0° which comes from the data of Tamblyn and Forbes.[5] If we accept the Tamblyn and Forbes ratio at its face value, it implies a pronounced temperature dependence of the relative quantum yield. However, there is an alternative possibility. They found almost the same quantum yield at 546 as at 578 mμ, thus implying some sort of rapid change in ϕ in the neighborhood of the gas phase convergence wave-length of 499 mμ. An analysis of their data shows that their chains were quite short. Therefore, it is possible that the greater reactivity of the excited atoms produced at 436 mμ was responsible for some of the difference in rate.

In all of the foregoing discussion we have used the term "primary recombination" to refer to the situation in which the two iodine atoms of a molecule recombine without ever escaping from the solvent cage in which the molecule was originally located. Some authors prefer to use the term "deactivation."[3] The iodine molecule in the ground state ($^1\Sigma_{og}^+$) absorbs a quantum and is raised to the $^3\Pi_{ou}^+$ state which has a minimum in its potential energy-distance curve. In the presence of a strong magnetic field, predissociation to the unstable $^3\Pi_{ou}^-$ state occurs, and the molecule dissociates into two normal atoms. Van Vleck[21] showed that inhomogeneous electric fields should also cause quenching of fluorescence and predissociation and Turner[22] found that iodine fluorescence is greatly diminished by introducing argon as a foreign gas. Van Vleck points out that the first excited state of argon is so high that there can be no possibility of energy transfers in which argon atoms are excited, and the results can only mean that predissociation results from the intense and highly inhomogeneous fields from argon atoms at the time of collision with excited iodine molecules.

Rabinowitch and Wood[8] explained the fact that they observed no falling off in iodine atom concentration in solution at wave-lengths greater than 499 mμ by using Van Vleck's mechanism, where the inhomogeneous electric fields of the solvent molecules permit predissociation to the unstable $^3\Pi_{ou}^-$ state.

If we consider that an iodine molecule is "dissociated" if it is in the $^3\Pi_{ou}^-$ state or in the $^3\Pi_{ou}^+$ state with an energy exceeding 57 kcal./mole (2.5 ev), even though its internuclear distance is the normal bonding distance, then a value of ϕ less than one means that "primary recombination" has occurred. If we consider that the iodine molecule is still a molecule because of its internuclear distance, then a value of ϕ less than one means that the excited iodine molecule has been "deactivated" by the solvent. The distinction between deactivation and primary recombination appears to be meaningless in terms of measurements at present available to us.

ACKNOWLEDGMENT

This investigation was conceived by the late Professor Roscoe G. Dickinson of the California Institute of Technology, and the authors regret that he never lived to see it undertaken.

We are indebted to Professors George E. Kimball and Jacob J. Beaver for many helpful discussions during the progress of the work. We are also grateful to the United States Atomic Energy Commission for the allocation of the iodine-131 used in these experiments.

One of us (JZ) is indebted to the Allied Chemical and Dye Corporation for a fellowship.

[21] J. H. Van Vleck, Phys. Rev. **40**, 544 (1932).
[22] L. A. Turner, Zeits. f. Physik **65**, 464 (1930).

Absorption by H_2S Vapor in the Region 3.6μ to 4.5μ

R. H. NOBLE
Michigan State College, East Lansing, Michigan

AND

H. H. NIELSEN
Ohio State University, Columbus, Ohio

(Received October 20, 1949)

The region near the absorption band of hydrogen sulfide vapor at 3.7μ has been measured with high resolution. The data obtained corroborate some of the previously published work on this molecule. Results were obtained, however, which are difficult to reconcile with a predicted band based on a model of the probable size and shape of H_2S.

INTRODUCTION

CONSIDERABLE ambiguity exists concerning the infra-red spectrum of hydrogen sulfide vapor. This is particularly true concerning the region near 3.7μ which has been measured with high resolution by Nielsen and Barker[1] and later by Sprague and Nielsen.[2] This band lies in the region where one might expect the vibration ν_3 to be located.

H_2S is a non-linear triatomic molecule with three normal vibrations of the same type as H_2O. The frequencies of the "stretching" modes, ν_1 and ν_3, are approximately the same while the frequency of the "bending" mode, ν_2, has a value of about one-half that of the other two. If H_2S and H_2O have in general similar shapes and normal vibrations, they might be expected to show similarities in their infra-red spectra. Many comparisons may be made, but we shall be concerned with the regions associated with their respective ν_1 and ν_3 vibrations.

While ν_1 of H_2O vapor absorbs only weakly in the infra-red, the one strong Raman line at 3652 cm^{-1} arises from ν_1. For H_2S vapor one strong Raman line has been found at 2611 cm^{-1} and is therefore assumed to be ν_1.

The fundamental ν_3 of H_2O vapor absorbs strongly in the infra-red. This band is about 200 cm^{-1} wide and has its center at 3756 cm^{-1}, which is about 100 cm^{-1} removed from ν_1. One might postulate a ν_3 band for H_2S, therefore, which is about 200 cm^{-1} wide and has its center at 2700 cm^{-1}. The band of Nielsen and Barker[1] in this region has its center near the expected place but is only 100 cm^{-1} wide. It has been pointed out by Hainer and King,[3] who have attempted an analysis of this band using punch card methods, that the band does not extend over a sufficiently great frequency range. They have, therefore, suggested that the region reported is in reality only the *R* branch and that the *P* and *Q* branches have simply escaped detection.

In order to investigate this point this region has been carefully explored to considerable distances on both sides of the region reported by Nielsen and Barker[1] with a self-recording, vacuum, prism-grating spectrometer.[4] The preliminary data were shown and discussed by us[5] at the New York meeting of the American Physical Society in January 1947. This region has been remeasured by Wilson and Cross[6] using a prism spectrometer with a fluorite prism. They report considerable absorption between 2620 cm^{-1} and 2450 cm^{-1} which they suggest is in the region where the *P* branch predicted by Hainer and King[3] must lie. We wish to present our measurements over this region for the sake of comparing them with those obtained by Nielsen and Barker[1] and Wilson and Cross.[6] No attempt will be made to analyze what has been found.

EXPERIMENTS AND RESULTS

The grating used for this investigation was of the echelette reflection type with approximately 7500 lines per inch. It was made by R. W. Wood. The grating constant was determined by using several of the emission lines of mercury as calibration standards. Comparison of the H_2S lines obtained here with those of Nielsen and Barker[1] measured with another grating on another spectrometer attests to the accuracy of this phase of the work, since the mean deviation for the fifteen strongest lines is 0.4 cm^{-1}.

The H_2S gas was contained in a cylindrical glass absorption cell 5 cm in diameter and 30 cm long fitted with windows of sodium chloride. The pressure of the gas in the cell was approximately 70 cm of mercury. An attempt was made to purify the gas by vacuum distillation. This was successful for all contaminants except a very small amount of CO_2 whose ν_3-band appeared in the vicinity of 2350 cm^{-1} in our records. The housing surrounding the spectrometer and the absorption cell was evacuated to a pressure of less than 1 mm of mercury to eliminate falsification by atmospheric bands.

A survey was first made with relatively wide slits over a long interval on each side of the 3.7μ band. The central portion of the ink recording produced by the spectrograph is reproduced in Fig. 1. In making this

[1] H. H. Nielsen and E. F. Barker, Phys. Rev. **37**, 727 (1931).
[2] A. D. Sprague and H. H. Nielsen, J. Chem. Phys. **5**, 85 (1937).
[3] R. M. Hainer and G. W. King, J. Chem. Phys. **15**, 89 (1947).
[4] Bell, Noble, and Nielsen, Rev. Sci. Inst. **18**, 48 (1947).
[5] R. H. Noble and H. H. Nielsen, Phys. Rev. **71**, 484 (1947).
[6] E. A. Wilson and P. C. Cross, J. Chem. Phys. **15**, 687 (1947).

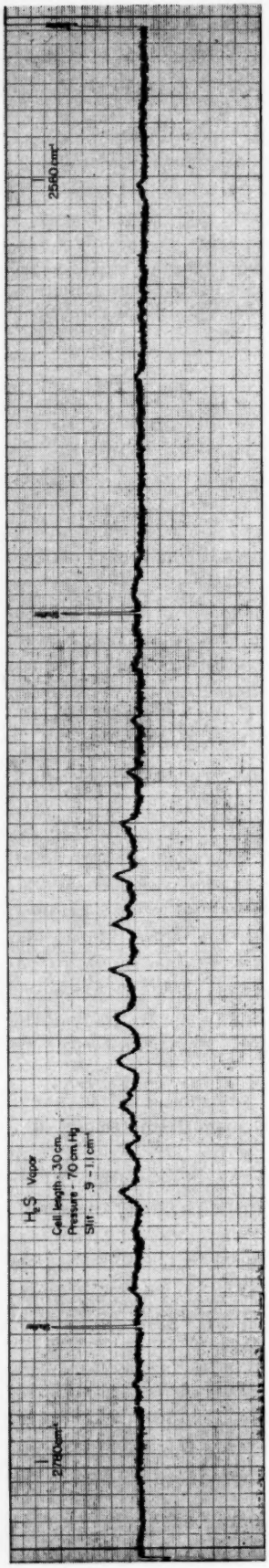

FIG. 1. Part of a survey recording of the spectrum of H_2S vapor near 3.7μ.

record, the gain of the amplifier circuit was reduced so that the zero drift of the instrument over the two hour period required was minimized. The total deflection is indicated at several points by closing an opaque shutter for a short time. The record extends over a long distance on either side of the region reported by Nielsen and Barker.[1] The band reported by them may be observed, but no more absorption lines of comparable intensity appear.

The same region was remeasured with narrower slits and greatly increased gain on the amplifier. A percent absorption plot compiled from three such records is shown in Fig. 2. Here it may be seen that some absorption lines exist on the low frequency side of the region reported by Nielsen and Barker, However, this absorption seems to be of a different order of magnitude from that predicted here by Hainer and King.[3] The intensity of absorption rises again in the region near 2440 cm^{-1}

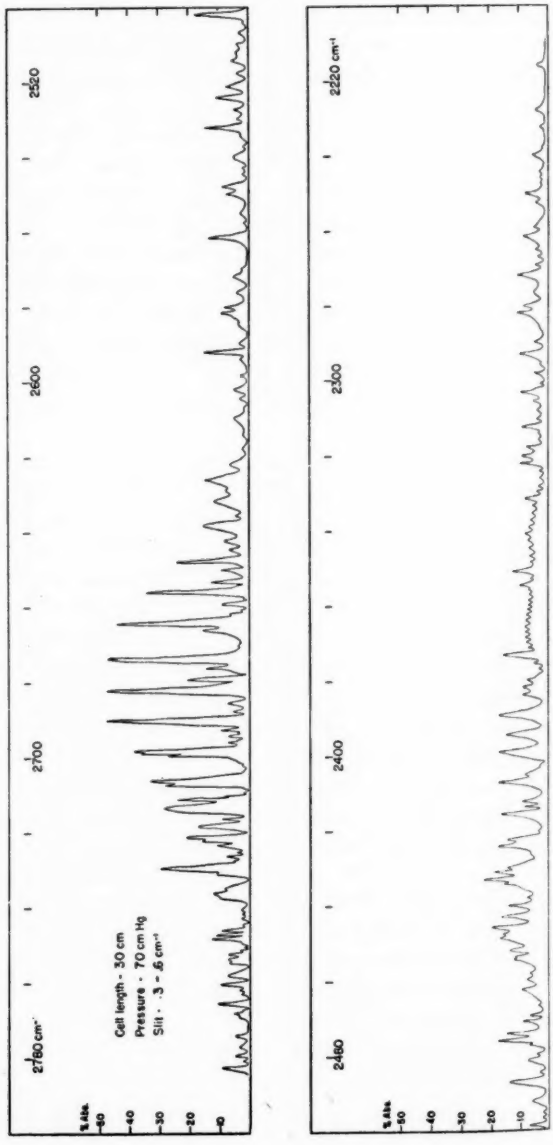

FIG. 2. Absorption of H_2S vapor in the region 3.6μ to 4.5μ.

as was first noted by Bailey, Thompson, and Hale[7] who gave it the assignment $2\nu_2$.

In a very general way the curve given by us in Fig. 2 resembles that given by Wilson and Cross.[6] In their data, the region from 2620 cm^{-1} to 2500 cm^{-1}, even though it absorbs less strongly than that near 2700 cm^{-1}, might be interpreted as part of an absorption band extending from 2740 cm^{-1} to 2500 cm^{-1}.

Our results differ from theirs in that the relative intensities of absorption are different. In particular the region from 2620 cm^{-1} to 2500 cm^{-1} has weaker absorption. Our data show no evidence that this region constitutes one-half of an absorption band whose other half extends from 2740 cm^{-1} to 2620 cm^{-1}.

[7] Bailey, Thompson, and Hale, J. Chem. Phys. **4**, 625 (1936).

THE JOURNAL OF CHEMICAL PHYSICS VOLUME 18, NUMBER 5 MAY, 1950

Proton Nuclear Magnetic Resonance Studies in KH_2PO_4, KH_2AsO_4, $NH_4H_2PO_4$, and $NH_4H_2AsO_4$

ROGER NEWMAN*
Lyman Laboratories, Harvard University, Cambridge, Massachusetts
(Received January 9, 1950)

Studies have been made of the proton magnetic resonance absorption at 30 Mc/sec. in KH_2PO_4, KH_2AsO_4, $NH_4H_2PO_4$, and $NH_4H_2AsO_4$. Both line shapes and relaxation times have been measured from 87°K to 293°K.

The potassium salts show closely similar magnetic resonance properties. Their relaxation times show relatively small variation in the temperature interval studied. The characteristic times derived therefrom do not obey any simple exponential law in the reciprocal temperature. Single crystals of KH_2PO_4 do not seem to show anisotropy in the relaxation time. A formula is given which relates the anisotropy of the motion of magnetic dipoles to the anisotropy of transverse local field variation.

The ammonium salts show two minima in their relaxation time *vs.* temperature curves. One minimum corresponds to a temperature at which the acid hydrogens are the most effective relaxation agent and the other to a temperature where the ammonium ion hydrogens are most effective. The line shapes are also of a composite character. This is most clearly shown below 100°K where the absorption lines appear to be superpositions of the broad NH_4 line for which that of NH_4Cl is typical and the narrow line found in KH_2PO_4 or KH_2AsO_4.

Possible interpretations of the experimental results are discussed with reference to the motions of the protons in these crystals.

INTRODUCTION

PREVIOUS work[1–3] has shown the utility of the nuclear resonance technique in the study of crystals containing protons whose motions are other than the thermal vibrations of a rigid lattice. With this in mind it was thought worth while to make a study of the isomorphic salts, KH_2PO_4 (KDP), KH_2AsO_4 (KDA), $NH_4H_2PO_4$ (ADP) and $NH_4H_2AsO_4$ (ADA). It will be recalled that these salts undergo phase transitions of the second order at the temperatures shown in Table I.[4–7] The transitions are accompanied, in the case of the potassium salts, by abnormally large increases in the dielectric constant in the direction of the **c** axis of these tetragonal crystals as one passes through the transition region toward lower temperatures.[8] A smaller decrease in the dielectric constant obtains in the **a** direction. This is an example of the so-called ferroelectric transition. The ammonium salts likewise show increases in the dielectric constant in the direction of the **c** axis, but shattering of the crystals makes a complete study impossible. The most complete theoretical treatment of the problem is that due to Slater, which we shall briefly describe for future reference.

THEORY OF THE TRANSITION[9]

According to the theory, the acidic hydrogens form hydrogen bonds between the oxygens of two adjacent XO_4^{3-} groups. The cations do not enter into consideration. The O—H—O bonds lie approximately parallel to either the **a** or the **b** direction.[10] They may

* DuPont Postdoctoral Fellow in Chemistry (1949–50).
[1] H. S. Gutowsky and G. E. Pake, J. Chem. Phys. **16**, 1164 (1948).
[2] F. Bitter *et al.*, Phys. Rev. **71**, 738 (1947).
[3] A. M. Sachs, Ph.D. Thesis, Harvard University (1949).
[4] C. C. Stephenson and J. G. Hooley, J. Am. Chem. Soc. **66**, 1397 (1944).
[5] C. C. Stephenson and A. C. Zettlemoyer, J. Am. Chem. Soc. **66**, 1402 (1944).
[6] C. C. Stephenson and A. C. Zettlemoyer, J. Am. Chem. Soc. **66**, 1403 (1944).
[7] C. C. Stephenson and H. E. Adams, J. Am. Chem. Soc. **66**, 1409 (1944).
[8] G. Busch, Helv. Phys. Acta **11**, 269 (1938).
[9] J. C. Slater, J. Chem. Phys. **9**, 16 (1941).
[10] J. West, Zeits. f. Krist. **74**, 306 (1930); L. Helmholtz and R. Levine, J. Am. Chem. Soc. **64**, 354 (1942).

FIG. 2. Absorption of H_2S vapor in the region 3.6μ to 4.5μ.

TABLE I. Temperatures and entropies of transition.

Salt	Temperature, °K	Entropy* (cal./mole/°K)
KH_2PO_4	122	0.74
KH_2AsO_4	96	0.90
$NH_4H_2PO_4$	148	1.05
$NH_4H_2AsO_4$	216	1.02

* The entropy of the hydrogen bond transition is 0.81 as calculated from Slater's theory.

be considered to form the links of a chain that runs either parallel to **a** or to **b**. It is assumed, as it is for ice where a somewhat similar situation prevails, that there are two equilibrium positions for the hydrogens along the O−H−O bond; one closer to one of the XO_4^{3-} groups involved and vice versa. The assumption is made, again as for ice, that there will only be two hydrogens close to any XO_4^{3-} group. With this assumption it turns out that the electric dipole moment associated with each of the $H_2XO_4^-$ groups will be directed either parallel to the positive **c** axis, anti-parallel, or perpendicular to it depending on which of the sites nearest the XO_4^{3-} group are occupied with hydrogens. It is further assumed that the dipoles parallel or anti-parallel to the **c** axis have zero energy in the absence of an external electric field, while those perpendicular to it have some energy ϵ. By an evaluation of the statistics Slater is able to show that a transition should occur (the theory predicts one of the first order), the transition being essentially a change from a disordered system of hydrogen bonds above the transition point to an ordered arrangement below it. The ordered system is characterized by the fact that all the $H_2XO_4^-$ dipoles are identically aligned parallel or anti-parallel to the **c** axis. In order to account for the fact that a macrocrystal is not polarized in the absence of a field, the concept of micro-domains is introduced. The different domains are considered to be randomly polarized with respect to the **c** axis and thus produce no net polarization.

The entropy change in the transition, as calculated from Slater's theory, is in good agreement with the experimentally obtained values for the potassium salts. For the ammonium salts the experimental values seem too high.

THEORY OF NUCLEAR SPIN RELAXATION[11]

We shall not repeat the detailed development of the relaxation theory here, but merely outline the various concepts and indicate how they will be applied in what follows.

When a proton, which possesses a spin of $\frac{1}{2}$ and a magnetic moment of maximum eigenvalue μ, is placed in a homogeneous magnetostatic field H_0 the double degenerate state is split. The separation between the $m=+\frac{1}{2}$ and $m=-\frac{1}{2}$ states being equal to

$$2\mu H_0 = h\nu_{\text{Larmor}}. \tag{1}$$

We assume for the moment that there is a mechanism whereby a collection of such proton spins, each individually quantized, (i.e., little interaction between them) can achieve thermal equilibrium. That is,

$$N_+/N_- = \exp(2\mu H_0/kT), \tag{2}$$

where N_+ and N_- are the number of spins which are plus and minus respectively. If now an oscillating magnetic field of the Larmor frequency, ν_L, is introduced perpendicular to H_0, it can induce transitions $+\rightarrow-$ and the reverse. The two transition probabilities are the same, but since N_+ is greater than N_-, a small net absorption of energy, proportional to N_+-N_-, takes place and can be measured.

Obviously if there is no mechanism whereby the energy absorbed from the magnetic radiation by the spin system can be dissipated, the latter will soon saturate. That is N_+ will equal N_- and no further energy can be absorbed. However, there are mechanisms through which the Zeeman energy of the nuclei can be dissipated to the various degrees of freedom available to the whole crystal. These we shall discuss below; it suffices here to know that they exist. With such a mechanism in action, an equilibrium will be set up such that the energy absorbed by the spin system from the radiation field will equal that given by the spins to the crystal as a whole. Thus the equilibrium ratio N_+/N_- and hence the strength of absorption at a given intensity of magnetic radiation will indicate the effectiveness of the mechanism of Zeeman energy dissipation, i.e., the relaxation mechanism. It may be shown, in fact, that the integrated absorption coefficient at any radiation field strength H_1 is proportional to $(1+\gamma^2H_1^2T_1T_2)^{-1}$. Here T_1 is the relaxation time defined below and $1/T_2$ is essentially the line width of the absorption. In current practice the latter is measured as the distance between the points of maximum slope of the absorption curve. γ is the gyromagnetic ratio, which equals $2\mu/\hbar$ for protons.

The quantity T_1 has its definition in the experimental fact, theoretically confirmed, that the recovery of a spin system from saturation, as observed with an extremely small H_1, follows a first-order rate law for which $1/T_1$ is the rate constant. In some cases T_1 is too short to measure directly. One can then measure the strength of the absorption as a function of H_1. Since T_2 is always measurable, T_1 can be found from the relation mentioned above. Actually the saturation curve method used experimentally causes some modification in this formulation, but it still remains true that a given degree of saturation corresponds to the same value of $H_1^2T_1T_2$ for most of the cases that arise.

It is now necessary to consider the form of the magnetic interaction of protons with each other. The interaction Hamiltonian may be written as the sum of the

[11] N. Bloembergen *et al.*, Phys. Rev. **73**, 679 (1948); The material of this section is a condensation of the theoretical development given in this reference.

interactions by pairs of protons. Each term in the sum may be written as

$$V_{ij}=\gamma^2\hbar^2 r_{ij}^{-3}(A+B+C+D+E+F)$$

where

$$A=I_{zi}I_{zj}(1-3\cos^2\theta_{ij}),\quad(\Delta m=0)$$

$$B=-\tfrac{1}{4}[(I_{xi}-iI_{yi})(I_{xj}+iI_{yj})+(I_{xi}+iI_{yi})(I_{xj}-iI_{yj})]\times(1-3\cos^2\theta_{ij}),\quad(\Delta m=0),$$

$$C=-\tfrac{3}{2}[(I_{xi}+iI_{yi})I_{zj}+(I_{xj}+iI_{yj})I_{zi}]\times\sin\theta_{ij}\cos\theta_{ij}\exp[-i(\phi_{ij}-\gamma H_0 t)],\quad(\Delta m=1)$$

$$D=-\tfrac{3}{2}[(I_{xi}-iI_{yi})I_{zj}+(I_{xj}-iI_{yj})I_{zi}]\times\sin\theta_{ij}\cos\theta_{ij}\exp[i(\phi_{ij}-\gamma H_0 t)],\quad(\Delta m=-1)$$

$$E=-\tfrac{3}{4}(I_{xi}+iI_{yi})(I_{xj}+iI_{yj})\times\sin^2\theta_{ij}\exp[-2i(\phi_{ij}-\gamma H_0 t)],\quad(\Delta m=2)$$

$$F=-\tfrac{3}{4}(I_{xi}-iI_{yi})(I_{xj}-iI_{yj})\times\sin^2\theta_{ij}\exp[2i(\phi_{ij}-\gamma H_0 t)],\quad(\Delta m=-2).$$

Here θ_{ij} and ϕ_{ij} are the polar and azimuthal angles of the internuclear vector r_{ij}, in a system of polar coordinates in which H_0 is the pole. I_x, etc., are the components of the nuclear spin. Δm is the change in m_i+m_j which each term can produce. The time factors arise out of the precession of the spins around H_0 with the Larmor frequency. We now note that if the space factors of the time dependent terms C through F are themselves time dependent and can be expanded in Fourier integrals in ν, and if the appropriate Fourier coefficients $J(\nu_L)$ and $J(2\nu_L)$ are not zero, these terms become secular perturbations. They provide a mechanism whereby magnetic energy may be emitted or absorbed, the requisite energy going to or coming from the crystal lattice. Thus a mechanism is provided, through which a spin system can exchange energy with an essentially infinite heat source and thus attain thermal equilibrium with it.

We define

$$\langle\textstyle\sum_j|\sin\theta_{ij}(t)\cos\theta_{ij}(t)\exp[i\phi_{ij}(t)]r_{ij}^{-3}(t)|^2\rangle_{Av}=\int_{-\infty}^{\infty}J_1(\nu)d\nu$$

and

$$\langle\textstyle\sum_j|\sin^2\theta_{ij}\exp[2i\phi_{ij}(t)]r_{ij}^{-3}(t)|^2\rangle_{Av}=\int_{-\infty}^{\infty}J_2(\nu)d\nu.$$

It can now be shown that when the transition probabilities are developed in terms of the elements $J_1(\nu_L)$ and $J_2(2\nu_L)$, a first-order differential equation in the number of surplus spins $n=N_+-N_-$ results. It is of the form

$$dn/dt=1/T_1(n_0-n)\qquad(4)$$

where n_0 is the spin surplus at thermal equilibrium and $1/T_1$, the reciprocal of the previously introduced relaxation time equals

$$9/8\gamma^4\hbar^2[J_1(\nu_L)+\tfrac{1}{2}J_2(2\nu_L)]=1/T_1.\qquad(5)$$

In crystals of the type we are considering there are two different types of motion. The first are those of a rigid lattice which turn out to be unimportant for the present purpose. The second are the essentially random motions which, strictly speaking, a true crystal would not have. Examples of these derived from the present study might be the jumping of an acidic hydrogen from one position of equilibrium to another, or the rotation of an ammonium ion from one orientation of equilibrium to another. The motions of the various individuals are almost unrelated to one another and their analysis is best handled by the statistical method that is employed in the theory of fluctuations. The latter shows that if $F(t)$ is some function of the space variables of a proton, which is expandable in a Fourier integral of the form

$$\langle|F(t)|^2\rangle_{Av}=\int_{-\infty}^{\infty}J(\nu)d\nu$$

then,

$$J(\nu)=\langle|F(t)|^2\rangle_{Av}2\tau_c(1+4\pi^2\nu^2\tau_c^2)^{-1}.\qquad(6)$$

Here $J(\nu)$ is the component of the Fourier spectrum of frequency ν. The correlation time, τ_c, is a time which is characteristic of the motion and is in many respects similar to the relaxation time which occurs in the Debye theory of dielectric dispersion. It may be regarded as something like the reciprocal of the mean frequency of the motion.

Substituting Eq. (6) into Eq. (5) we find that if the indicated time averages can be replaced by an average over a sphere, then

$$1/T_1=3/10\gamma^4\hbar^2/r^6\left[\frac{\tau_c}{1+4\pi^2\nu_L^2\tau_c^2}+\frac{2\tau_c}{1+16\pi^2\nu_L^2\tau_c^2}\right].\qquad(7)$$

It may aid the reader if some of the features of the above formulation are pointed out. If T_1 is plotted against increasing τ_c for a given ν_L, we would observe a decrease in T_1 to a minimum when τ_c equaled $(2^{\frac{1}{2}}\pi\nu_L)^{-1}$. As τ_c becomes larger, T_1 increases without limit. This simply means that since $1/\tau_c$ is in the nature of the mean frequency of the random motion, we get the most effective relaxation when it is of the order of the Larmor frequency of the nuclei involved. For mean frequencies very much higher or very much lower than the Larmor frequency little relaxation takes place.

A previous investigation[3] of the relaxation times of some ammonium salts has shown that τ_c was representable as const.$\times\exp(E/kT)$. This is readily conceived if the motions concerned, involve passage over some potential barrier of height E. However, as will be seen later on, τ_c as measured does not always admit of such a simple formulation.

EXPERIMENTAL

The apparatus used has already been described.[11] It consisted of a watercooled electromagnet operated from heavy storage batteries. A fine control of the magnetic

field was operated from an auxiliary power supply and field coils. The calibration of the fine field control was checked periodically and showed no change. The electronics system is that of reference 11 whose only modification was the inclusion of a square wave magnetic field modulator and a source of high voltage d.c.

The thermal equipment was that developed previously in this laboratory.[3,12] It consisted of a stainless steel Dewar flask of a design suitable for holding a sample in the magnetic field; a probe designed to conduct heat away from the sample, and a heating coil wound on the probe. The heating coil was used to obtain temperatures higher than those normally achieved with a given refrigerant. Temperatures were measured with a copper-constantan thermocouple imbedded in the wall of the probe. Experiment showed that, with the exception of a small time lag, a thermocouple placed in the center of the sample reached the same temperature as the one in the wall to within 0.5°C. Measurements were always taken after a static condition had been reached for times longer than the observed time lag.

The materials used were all commercial reagent grade chemicals with the exception of the ADA. The latter was prepared by mixing stoichiometric amounts of solutions of reagent grade ammonium bicarbonate and arsenic acid. The product was recrystallized three times and dried in a desiccator for 48 hours. The salt analyzed as 10.44 percent NH_3 as compared with the 10.71 percent that the pure salt would show. For the present purposes this was deemed satisfactory.

Samples of the commercial reagents, KDP and ADP, were allowed to dry in a desiccator for periods up to a week. They showed no change in resonance properties from the undesiccated material. The results reported here are for undesiccated material, except in the case of ADA. A sample of KDP, prepared from the commercial material by slow recrystallization from distilled water, also showed no change in its resonance properties.

The powdered samples used were compressed into cylinders of such a size as to fit snugly into the probe coil. It was thought that since the materials used were piezoelectric, compression might produce some effect. However, the various results for the compressed powders agreed with those for the uncompressed powders at several check points. The former has the virtue of producing a better signal to noise ratio, because of the increased filling of the probe coil.

The single crystals of KDP used were supplied by the Brush Development Company.† They were slabs 0.5 $\times 0.5 \times 3$ cm in dimensions. The **c** axis was perpendicular to the crystal and perpendicular to one of its faces.

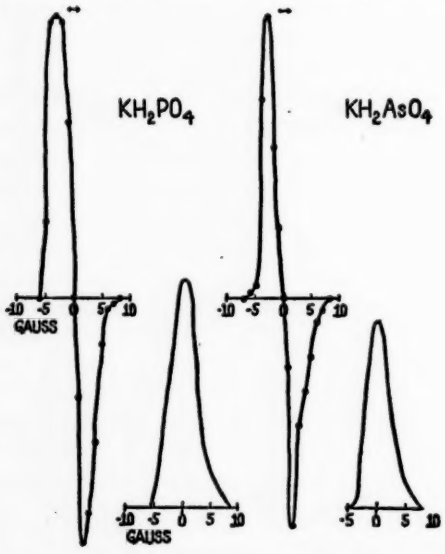

FIG. 1. Line shapes for KH_2PO_4 and KH_2AsO_4 at 87°K. The measured derivative of the absorption curve is given on the left, the absorption curve to the right.

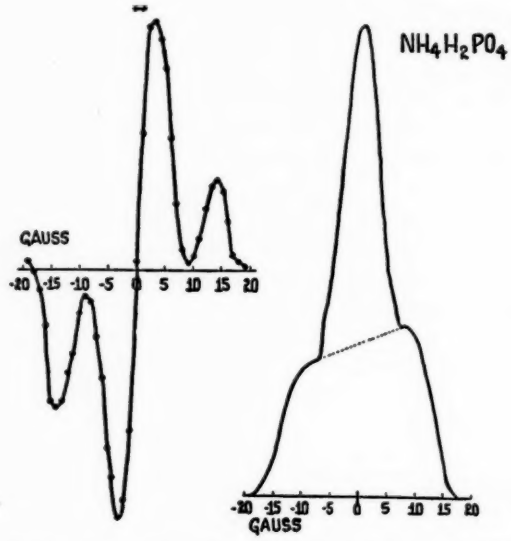

FIG. 2. Line shape of $NH_4H_2AsO_4$ at 87°K. See caption of Fig. 1.

All the results herein reported were made at 30 Mc/sec. Measurement of relaxation times were made for the most part by the saturation curve method.[11] We have omitted reporting these saturation curves as the results that they show are more clearly given in the T_1 *vs.* temperature curves.

The relative values of T_1 as obtained from the saturation curves are good to about 10 percent. The absolute values of the relaxation times were obtained by calibrating the saturation curves with the directly measured relaxation time of KDP at 87°K. This latter quantity is not very accurately measurable. However, as we are more interested in relative values of the relaxation times than in their absolute values, the failure to fix the latter very precisely was not important.

[12] E. H. Turner Ph.D. Thesis, Harvard University (1949).

† The author is indebted to the Brush Development Company for supplying suitably cut single crystals of KDP and ADP.

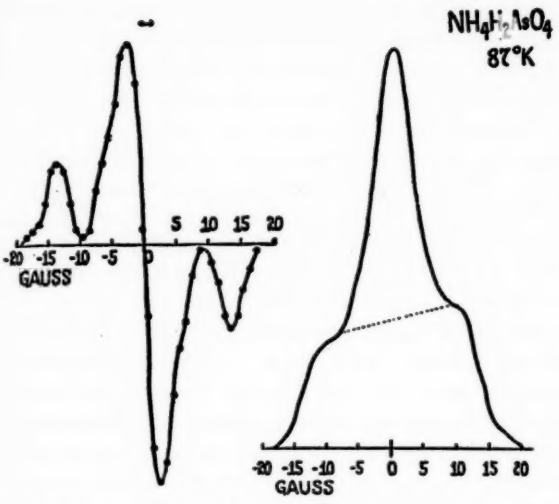

FIG. 3. Line shape of $NH_4H_2PO_4$ at 87°K. See caption of Fig. 1.

The line shapes were taken in the usual way using a modulation amplitude, small compared with the breadth of the line.[11] The modulation amplitude used is indicated by arrows on the appropriate figures. This method gives the derivative of the absorption curve as the experimentally measured quantity. The absorption curve is obtained by graphical integration. The slight asymmetry of some of the line shapes is caused by a shift in the balance of the r-f bridge during the course of a run. It is almost impossible to avoid at low temperatures.

RESULTS AND DISCUSSION OF LINE SHAPE AND LINE WIDTH MEASUREMENTS

A. KDP and KDA

The line width *vs.* temperature curves for KDP and KDA are shown in Fig. 5a. A rather small change in line width occurs from about 253°K to 243°K for the KDP and from 213°K to 203°K for the KDA. The broadened lines undergo no further change as the temperature is lowered. The second moments of the absorption bands have been calculated according to Van Vleck's formula,[13] with the assumption that the hydrogens lay fixed midway along the O—H—O bond. The values 3.4 and 3.5 gauss^2 were found for KDP and KDA respectively. These compare well with the values 3.2±0.7 for KDP and 3.5±0.7 for KDA obtained experimentally at 87°K from curves whose prototypes are shown in Fig. 1. The rather large experimental uncertainty in the determination of the second moment makes a more refined assumption as to the position of the hydrogens unwarrantable. In view of the crystal structure it was doubtful whether it would produce much change in any event.

B. ADP and ADA

The line width *vs.* temperature curves for ADP and ADA are shown in Figs. 7a and 8a respectively. They show a slight, steady increase in the line width as the temperature is lowered. If one's interest is confined to the separation of the points of maximum slope of the absorption nothing very spectacular occurs. However, if instead one looks at the line shape as the temperature is lowered, an interesting effect is observed. Namely, at about 113°K for ADP and 103°K for ADA, structure, in the form of symmetrically placed shoulders, begins to appear on the sides of the band. The structure becomes more pronounced as the temperature is lowered. In Figs. 2 and 3 the absorption bands for the two substances and their experimentally measured derivatives are shown for the lowest temperature obtainable, 87°K. As a measure of the effect, a quantity p is defined as the ratio of the crest to trough height of the side branches to the crest to trough height of the central branch of the derivative curve. In Fig. 4, p is shown plotted against temperature.

There are three possible interpretations of the fine structure patterns, but of these only one is entirely consistent with all known facts. The first is that the structure arises from the magnetic interaction of two protons placed close to one another and far away from all others, while other protons not as unsymmetrically located give rise to the central branch of the absorption. On this basis one can calculate, after the method of Pake,[14] that the unique interproton distance is 1.1 A.U. The best possibility in this case is that the two acid hydrogens no longer lie on the usually assumed O—H—O bonds; but, rather that the two O—H bonds of a given XO_4^{3-} are directed toward one another, more or less in the plane defined by the oxygens to which they are attached and the central X atom. The central branch might then be thought to arise from the protons of the ammonium ion. We must reject this hypothesis on the grounds that one would expect the potassium salts to show the same behavior and it would, of course, invalidate the hydrogen bond theory.

The second interpretation is that the band resembles that which arises from a system of three protons symmetrically placed close together.[15] This seems entirely out of the question in the present case.

The last interpretation and the one which we believe to be correct is that the band arises from the superposition of a broad flat band and a more narrow peaked band. The broad flat band may be thought to arise from the ammonium ion protons and the narrow peaked band arising from the resonance of the acid hydrogens. Indeed, when one superposes a typical broadened ammonium resonance band[15] with the band obtained from KDP or KDA, the observed band is qualitatively reproduced. As a more quantitative test of our assumption, the observed absorption bands were divided in two by the dotted lines indicated in the appropriate figures. The areas above and below the lines were then

[13] J. H. Van Vleck, Phys. Rev. **74**, 1168 (1948).

[14] G. E. Pake, J. Chem. Phys. **16**, 327 (1948).

[15] H. S. Gutowsky *et al.*, J. Chem. Phys. **17**, 972 (1949).

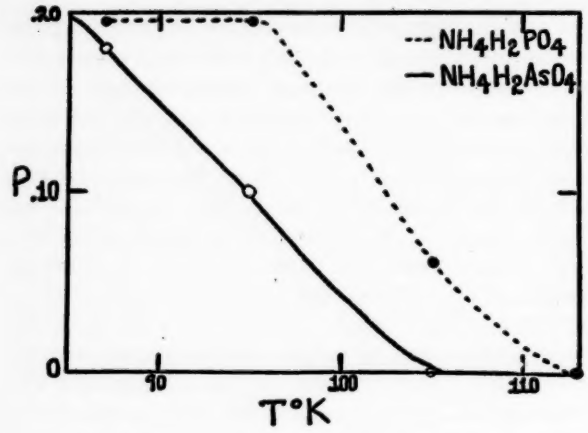

FIG. 4. Line shape parameter p *vs.* temperature for $NH_4H_2PO_4$ and $NH_4H_2AsO_4$.

computed. The results for the curves shown are that the ratios of the areas above the lines to those below are 0.55 and 0.57 for ADP and ADA respectively. Since the acid protons are half as numerous as the protons of the ammonium ion, these ratios are to be compared with the theoretical value 0.50. We regard the agreement as entirely satisfactory in view of the somewhat arbitrary way of choosing a dividing line.

Superposition of the resonance properties of the two types of hydrogens will be encountered again when the relaxation time measurements are discussed. Superpositions will undoubtedly be found when more complex materials are studied in the future. This bespeaks a word of caution in the interpretation of the ambiguities that may arise.

RESULTS AND DISCUSSION OF RELAXATION TIME MEASUREMENTS

A. KDP and KDA Powders

In Fig. 5b the results of the relaxation time measurements for KDP and KDA are shown. The two curves are quite similar in their temperature dependence, although the relaxation times differ at corresponding temperatures by about a factor of five. The curves are quite remarkable in that they show very little change in relaxation time with temperature. The total variation over the range covered is only about a factor of ten. In view of the previous experience of this laboratory, such a small variation was regarded as highly anomalous and it was thought that paramagnetic impurities might be responsible. The work of Bloembergen[16] demonstrated that under certain conditions, para-magnetic impurities could entirely determine the nuclear relaxation of a crystal. They accomplish this first by a direct interaction mechanism and second by acting as a sink for nuclear spin excitons, which diffuse toward the para-magnetic particles.

In order to test whether para-magnetic material was indeed responsible for the results, the commercial KDP was recrystallized and its relaxation time measured at room temperature and at 87°K. No change was noted, but this might simply have meant that an equilibrium was reached in the impurity concentration in the salt. Impurities present in concentrations greater than one part in 10^6 are effective. A rough analysis of the reagent KDP showed that its iron content was no greater than one part in 10^6 and was perhaps less.

The second observation to be considered on the possible influence of para-magnetic impurities is the result obtained with single crystals of KDP. Here it was found that the values of the relaxation time agreed with those for the commercial micro-crystalline material at several temperatures. In as much as these crystals were prepared under different and presumably more ideal circumstances than the commercial material it would be indeed surprising if the effective impurity content in the two cases was the same.

It is, therefore, concluded that although such impurities are present and to some extent effective, they are probably not the principal agent in the production of the observed relaxation phenomena. This role then falls to the protons themselves. It will be on the basis of this assumption that the data will be analyzed.

In Fig. 6 plots of the $\log\tau_c$ *vs.* reciprocal temperature are shown for KDP and KDA. The values of τ_c were obtained from the relaxation time data for the powders by fitting the observed data to the theoretical T_1 *vs.* τ_c curve.‡ The two curves are quite similar, as were the relaxation curves from which they stem. It was originally hoped, before these experiments were initiated, that the τ_c would be expressible as const.$\times\exp(\epsilon'/kT)$.

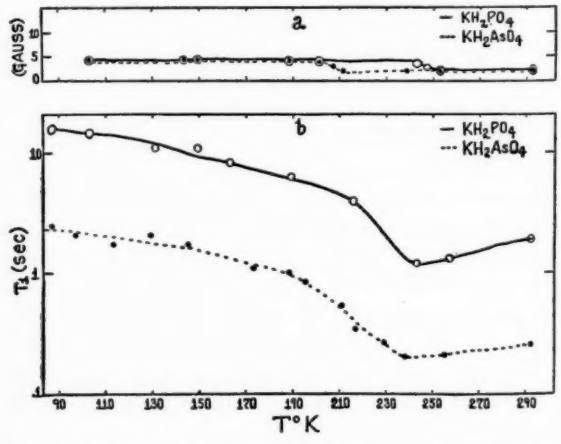

FIG. 5. (a) Line width and (b) relaxation time *vs.* temperature for KH_2PO_4 and KH_2AsO_4.

[16] N. Bloembergen, Physica **15**, 386 (1949).

‡ Since Eq. (7) considers only the interaction of like nuclei, it is not appropriate to the present case where the effect of the phosphorus and arsenic atoms on the protons must be considered. Further, in deriving it the assumption was made that time averages could be replaced by averages over a sphere. This is again not true in these crystals. However, as the required modifications will not appreciably alter the dependence of T_1 on τ_c, we shall forego rigor for simplicity and use Eq. (7) as it stands. This will not affect the validity of the qualitative remarks that are made.

Perhaps then ϵ' could have been identified, in some way, with the energy ϵ which appears in Slater's theory. Obviously τ_c cannot be expressed in this simple form. If the motion, whose effect was producing the relaxation, was activation controlled these curves would be straight lines. Their strong departure from linearity makes one strongly suspect that this is not the case.

If one makes the logical assumption that the relaxation effective motion of the proton consists of a jump from one position of equilibrium along the O—H—O bond to the other, there are cogent reasons to believe that quantum mechanical tunneling of the hydrogen through the separating potential barrier would be important. There is first the fact that the single hydrogen atom is very light and second the fact that the barrier width is very narrow. The O—H—O bond length is 2.54A in both KDP and KDA.[10] If the equilibrium O—H distance is, as in ice,[17] 0.99A then the whole barrier width is only 0.56A. Bell[18] has considered the problem of the passage of a hydrogen atom from one side of a symmetric Eckert potential barrier to the other. The barrier considered was roughly four times the width of this one and 10^{-12} ergs (13,000 cal./mole) in height. He found that tunneling made an appreciable contribution to the motion. When the log of the effective rate constant was plotted against reciprocal temperature, there was a very pronounced departure from linearity at lower temperatures. Bell's formulas have been applied to the present case using a value of the barrier height (2.7×10^{-12} ergs) which seemed appropriate under the combined considerations of geometry and the form of the parabola expressing the potential energy of stretching of a single O—H bond. In this way, the contributions to the effective rate constant of motion, from the zeroth and first excited levels of the vibrator, have been calculated. The result showed that at room temperature and below, the zero level made a more effective contribution by a factor of 10^6, thus making the rate virtually independent of temperature. The method of calculation was such that its results cannot be entertained very seriously. However, it suggests that under somewhat less drastic conditions than those imposed here, the observed insensitivity of τ_c to temperature could indeed be explained.

As an incidental investigation the effect on the relaxation time produced by the imposition of an electrostatic field on the sample was measured. A field of 16,000 volts/cm produced no observable effect either below, at, or above the transition temperatures of these salts. However, as relaxation times measure changes in local conditions rather than long range effects, it is perhaps not surprising that a field of this magnitude produces no measurable effect.

[17] L. Pauling, *The Nature of the Chemical Bond* (Cornell University Press, Ithaca, 1940), p. 302.
[18] R. P. Bell, Proc. Roy. Soc. **139**, 466 (1933).

B. Single Crystals of KDP

The relaxation time of a single crystal of KDP was measured at 87, 100, 114, and 200°K as a function of crystal orientation. Measurements were made with the crystalline **c** axis parallel or perpendicular to the d.c. magnetic field. To within the precision of the measurement the relaxation time appeared isotropic at these temperatures. Unfortunately due to the small size of the crystals in our possession this precision was lower that the figure ±10 percent quoted previously. An early series of measurements made at the lowest temperature indicated an anisotropy in the relaxation time, but a subsequent series failed to confirm it. It seems fairly probable that the anisotropic effect was not real.

We shall try to explain the observed isotropy in terms of the model of the proton's motion that was suggested above; namely, jumps from one equilibrium point on the O—H—O bond to the other. Since this motion is anisotropic with respect to the crystal axes we might expect that it would produce a corresponding anisotropy in the relaxation time.

Before proceeding, it is first necessary to obtain a formula which relates the square of the change in the transverse component of the local field due to one nucleus at the position of another, to the displacement of either nucleus. That is, we wish essentially to calculate the radiation field H_1^2 which results at a given nucleus and is effective in inducing transitions in it, when either the nucleus in question or one of its magnetic neighbors moves. This formula is given in Eq. (8) and its derivation is given in the Appendix to this paper.

$$F(\psi,\alpha,\beta)=r^6h_i^2/3\mu^2\lambda^2=1+\cos^2\alpha+\sin^2\psi(\sin^2\alpha\,\sin^2\beta \\ .+3\cos^2\alpha)+2\sin\psi\,\cos\psi\,\cos\alpha\,\sin\alpha\,\cos\beta, \quad (8)$$

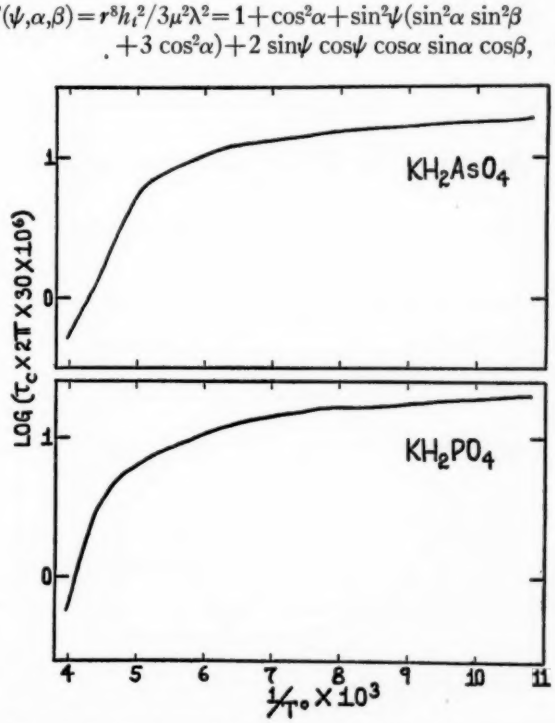

FIG. 6. Log_{10} of correlation time *vs.* reciprocal temperature for KH_2PO_4 and KH_2AsO_4.

where the symbols have the following significance: h_i^2 = the square of the change in the component of the local field perpendicular to $\mathbf{H}_0$, the axis of quantization, $\mathbf{r}$ = the internuclear distance, μ = the magnetic moment of the neighbor, $\boldsymbol{\lambda}$ = the displacement distance (a differential), α = the angle between the internuclear vector $\mathbf{r}$ and the displacement vector $\boldsymbol{\lambda}$, ψ = the angle between the internuclear vector $\mathbf{r}$ and $\mathbf{H}_0$, and β = the azimuth angle of the displacement vector $\boldsymbol{\lambda}$ in a system of the spherical polar coordinates in which $\mathbf{r}$ is the z axis and the plane defined by $\mathbf{r}$ and $\mathbf{H}_0$ is the zero of azimuth.

The quantity on the right side of Eq. (8) has been computed from the known crystal structure of KDP for the different possible types of interaction. It is assumed that the protons jump individually in the manner hypothesized above. The results of the computation are shown in Table II.

The A process arises from the interaction of two hydrogens which lie along the same chain in the plane perpendicular to **c** and share the same PO_4 group. The B process arises from the interaction of two hydrogens which are attached to the same PO_4 group, but which lie in different chains, one running perpendicular to the other, both of course running perpendicular to **c**. The C process arises from the interaction of a proton with a phosphorous atom belonging to the PO_4 group to which it is attached.

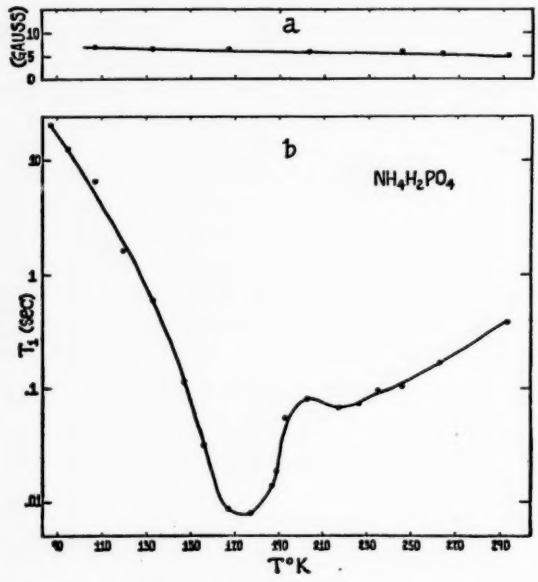

FIG. 7. (a) Line width and (b) relaxation time *vs.* temperature for $NH_4H_2PO_4$.

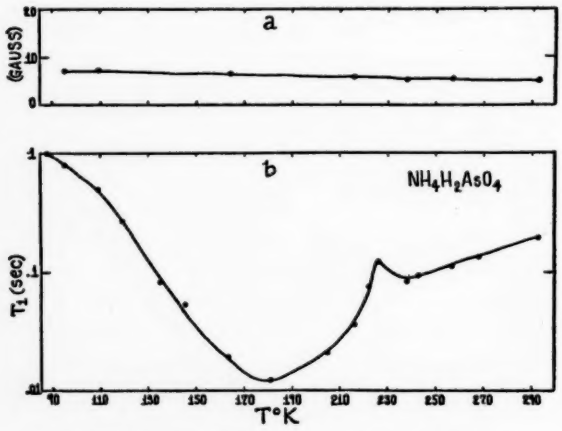

FIG. 8. (a) Line width and (b) relaxation time *vs.* temperature for $NH_4H_2AsO_4$.

Let anisotropy be defined as the ratio of the relaxation times for the two orientations of the crystal. Since $1/T_1$ is proportional to h_i^2 we note from Table II that the largest anisotropy would develop if process A were dominant. Actually process C alone might be expected to be greater than either of the other two by a factor of 25. This arises out of the fact that although the moment of the phosphorus atom is about a third that of the proton, the shorter hydrogen-phosphorus distance more than compensates for it.

In this light the greatest anisotropy that would develop in KDP would be 1.3. Regrettably the present measurements are too imprecise to test this conclusion. However, in the reverse sense it indicates why, to the allowed error, the relaxation time of these crystals was isotropic.

C. ADP and ADA Powders

In Figs. 7b and 8b the results of the relaxation time measurements are shown for ADP and ADA respectively. The curves are qualitatively similar. Both show two minima, deep ones at about 173° and 180°K and shallow ones at 217° and 240°K.

Although a quantitative interpretation is out of the question, these curves can be satisfactorily explained on a qualitative basis. At the high temperature side of a curve we may assume, out of analogy with the ammonium halides, that the ammonium ion is jumping around too rapidly to provide a good mechanism for the relaxation of its own protons. However, the acid hydrogens, as may be seen from the relaxation curves of the potassium salts, are moving near the optimum jumping rate and are able to provide a mechanism for both their own relaxation and for that of the ammonium ion protons. As the temperature is lowered the ammonium ion is somewhat more effective in its self-relaxation, while the acid hydrogens remain nearly constant in effectiveness. This accounts for the gradual decrease in T_1 down to the shallow minimum. By this temperature, the acid hydrogens are beginning to jump at less than the optimum rate, as seen from the sharp rise in the KDP and KDA curves at this point. Therefore, the ADP and ADA curves come out of the minimum. As the temperature is lowered still further, the ammonium ion begins to jump near the optimum rate for relaxation and thus provides the most effective relaxation mechanism for the majority of the protons in the crystal. This accounts for the deepness of the second minimum. Now, as the jumping rate of the ammonium ion de-

creases below the optimum value, this relaxation mechanism becomes less effective and the curve begins to rise. However, it does not rise as sharply as do the ammonium halide curves and in fact is convex upward below a certain temperature. This is because the acid hydrogens still provide a relaxation mechanism by virtue of their movement, which is almost independent of the temperature at that point.

In Figs. 9 and 10, we have plotted $\log\tau_c$ against reciprocal temperature. The values of τ_c were obtained from Eq. (7) using the deep minima as basing points for the calculation.

It may be seen from these figures that in the region of the deep minima of the relaxation curves, where the motion of the ammonium ion provides the best mechanism for its own relaxation, the $\log\tau_c$ *vs.* $1/T°$ curves are reasonably good straight lines. The slopes in terms of $\ln\tau_c$ are 3200°K (6400 cal./mole) and 1540°K (3080 cal./mole) for ADP and ADA respectively. In the studies of the ammonium halides and iodate the corresponding slopes ranged from 2370°K to 1450°K.

One may interpret the slopes thus obtained as barrier heights to the rotational motion of the ammonium ion. Doubtless this is not very far from the truth. If one possesses a potential function's height and knows something about its shape, from spectroscopic sources, it is theoretically possible to determine its angular periodicity. Unfortunately, the calculation of this period in the case of the ammonium halides was not too definitive and was not repeated with the present data.

Obviously, since the majority of the resonance signal in the case of the ammonium salts is due to protons which have no essential connection with the hydrogen bond transition, it could not be expected that the various results found for these salts would shed much light on that transition. However, the similarity between the relaxation time and line shape data obtained here and those obtained for the ammonium halides (with the exception of the hydrogen bonded fluoride) suggest that there should be other similarities as well. For example, the halides display large specific heat anomalies due to what is now thought to be an order disorder transition. In this light, it is rather surprising that ADP and ADA do not show two specific heat anomalies; one for the hydrogen bond transition, and a second due to the ammonium ion. Perhaps the fact that the entropy of the single observed transition is somewhat too large[6,7] is indicative of some sort of coalescence of the two types of transitions. This might also explain why ADP and ADA crystals shatter at their transition points, while KDP and KDA go through theirs without effect.

Mason[19] has suggested that some of the peculiarities of ADP and ADA might be explained if hydrogen bonds were formed between the nitrogen of an ammonium ion and oxygens of the surrounding XO_4^{3-} groups. The present results cannot give support to this hypothesis. They show that the mean lifetime of an ammonium ion against some sort of rotatory jump is of the order of 10^{-7} sec. for ADP and 10^{-8} sec. for ADA at their respective transition temperatures. Only if one proton were bonded and the others free to turn about the ion's C_3 axis, could the results be made compatible with a bonding hypothesis. There seems to be no *a priori* reason for such an assumption.

TABLE II. $F(\psi,\alpha,\beta)$ for different interaction processes for two orientations of a KH_2PO_4 crystal.

	A	B	C
$c \parallel H_0$	9.4	4.2	4
$c \perp H_0$	6.4	4.1	3

APPENDIX

In ths section Eq. (8) is derived. The derivation is due to Professor E. M. Purcell.[20]

Let a nucleus undergoing resonance be placed at the origin of a set of cartesian axes. Let a magnetic dipole of components $(\mu_x\mu_y\mu_z)$ be placed on the z axis at a distance r from the origin. We wish now to calculate the change in magnetic field at the origin when the dipole at $(00r)$ is displaced arbitrarily by a distance $\boldsymbol{\lambda}=(\Delta x\Delta y\Delta z)$ small compared with r.

The field at the origin due to the z component of the dipole, μ_z, is

$$H_x=3\mu_z xz/r^5, \quad H_y=3\mu_z yz/r^5, \quad H_z=\mu_z(3z^2/r^5-1/r^3).$$

Hence for a dipole at $(00r)$

$$\partial H_x/\partial x=3\mu_z/r^4, \quad \partial H_y/\partial y=3\mu_z/r^4, \quad \partial H_z/\partial z=-6\mu_z/r^4$$

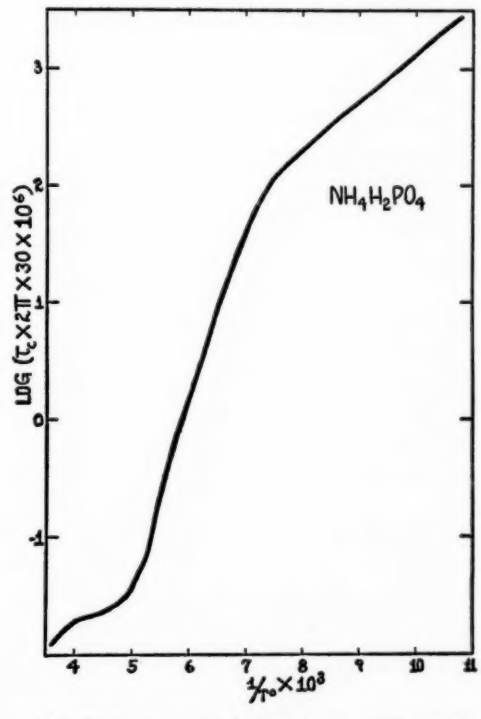

FIG. 9. Log_{10} of correlation time *vs.* reciprocal temperature for $NH_4H_2PO_4$.

[19] W. P. Mason, Phys. Rev. **69**, 173 (1946).

[20] E. M. Purcell (private communication).

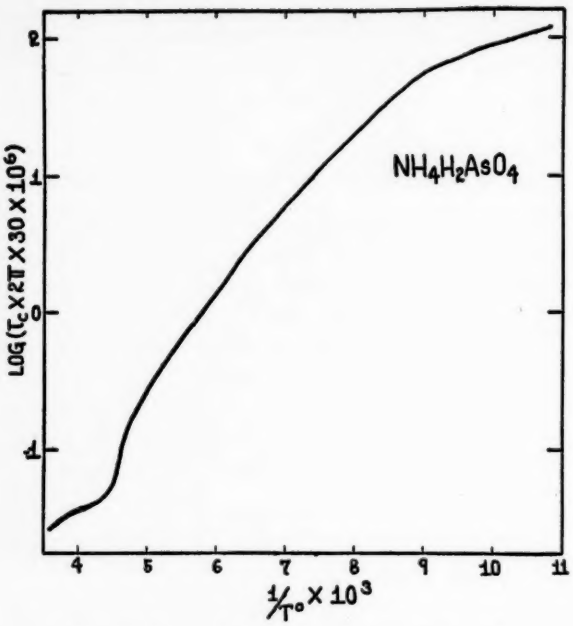

FIG. 10. Log_{10} of correlation time *vs.* reciprocal temperature for $NH_4H_2AsO_4$.

and all other derivatives are zero. In a similar manner using the contributions to the field from the x and y components of the dipole it is found that

$$\partial H_x/\partial z=3\mu_x/r^4, \quad \partial H_z/\partial x=3\mu_x/r^4$$

and

$$\partial H_y/\partial z=3\mu_y/r^4, \quad \partial H_z/\partial y=3\mu_y/r^4.$$

If $\mathbf{h}=(h_xh_yh_z)$ defines the change in field at the origin due to the displacement of the dipole $\boldsymbol{\lambda}$, then by substituting in the above it is found that

$$\begin{aligned}\tfrac{1}{3}h_xr^4&=\mu_z\Delta x+\mu_x\Delta z,\\ \tfrac{1}{3}h_yr^4&=\mu_z\Delta y+\mu_y\Delta z,\\ \tfrac{1}{3}h_zr^4&=\mu_y\Delta y+\mu_z\Delta x-2\mu_z\Delta z.\end{aligned}$$

Now let the dipole be specified in spherical polar coordinates by the polar angle θ and the azimuthal angle ϕ measured from the yz plane, such that

$$\begin{aligned}\mu_z&=\mu\cos\theta,\\ \mu_x&=\mu\sin\theta\sin\phi,\\ \mu_y&=\mu\sin\theta\cos\phi.\end{aligned}$$

Similarly let the jumping direction of the dipole be characterized by the polar angle α and the aximuthal angle β, such that

$$\begin{aligned}\Delta x&=\lambda\sin\alpha\sin\beta,\\ \Delta y&=\lambda\sin\alpha\cos\beta,\\ \Delta z&=\lambda\cos\alpha.\end{aligned}$$

Now let there be an external magnetic field $\mathbf{H}_0$, whose direction is specified in this system of polar coordinates by the polar angle ψ and zero azimuthal angle. We want to calculate the mean square component of $\mathbf{h}$ which is perpendicular to this direction. That is, if $x'y'$ is the plane perpendicular to $\mathbf{H}_0$, then

$$h_{x'}=h_x$$

and

$$h_{y'}=h_y\cos\psi-h_z\sin\psi.$$

From this it follows, after appropriate substituting, squaring, and averaging over all orientations θ and ϕ of the dipole, that

$$r^6h_{x'}{}^2/9\mu^2\lambda^2=\tfrac{1}{3}(\sin^2\alpha\sin^2\beta+\cos^2\alpha)$$

and

$$\begin{aligned}r^6h_{y'}{}^2/9\mu^2\lambda^2=&\cos^2\psi(\tfrac{1}{3}\sin^2\alpha\cos^2\beta+\tfrac{1}{3}\cos^2\alpha)+\sin^2\psi(\tfrac{1}{3}\sin^2\alpha\sin^2\beta\\ &+\tfrac{1}{3}\sin^2\alpha\cos^2\beta+4/3\cos^2\alpha)+\sin\psi\cos\psi(\tfrac{2}{3}\cos\alpha\sin\alpha\cos\beta).\end{aligned}$$

Since the square of the desired transverse component $h_t^2=h_{x'}{}^2+h_{y'}{}^2$ we find after adding and simplifying that

$$\begin{aligned}F(\psi,\alpha,\beta)=r^6h_t{}^2/3\mu^2\lambda^2=&1+\cos^2\alpha+\sin^2\psi[\sin^2\alpha\sin^2\beta+3\cos^2\alpha]\\ &+2\sin\psi\cos\psi\cos\alpha\sin\alpha\cos\beta. \quad (8)\end{aligned}$$

In this derivation two assumptions have been made. The first is that by using the individual components of the dipole it is implied that the time during which the dipole moves is short compared the period of its Larmor precession. The second is that averaging the orientation of the dipole over-all θ and ϕ is valid.

ACKNOWLEDGMENT

I should like to express my appreciation to the E. I. DuPont de Nemours Company whose fellowship grant made this work possible. My very warmest thanks go to Professor E. M. Purcell for his very instructive advice and criticism.

The Mercury Photo-Sensitized Decomposition of Decane in the Liquid State*

M. K. PHIBBS AND B. deB. DARWENT
Division of Chemistry, National Research Council, Ottawa, Canada
(Received December 12, 1949)

The decomposition of liquid decane photo-sensitized by dissolved mercury to λ2537 has been investigated between 0° and 134°C. The only important products are hydrogen and eicosanes. The initial act is probably the breaking of a C—H bond with the production of a hydrogen atom and a decyl radical. The decyl radicals recombine to form eicosanes without undergoing any detectable disproportionation to form decene and decane. The quantum yield of the production of hydrogen is about 0.10 at 0°C and increases to 0.45 at 134°C. The low quantum yield and its temperature dependence may be due to either an inefficient primary act or to recombination of hydrogen atoms and decyl radicals in liquid "cages."

INTRODUCTION

THE mercury photo-sensitized reactions of several paraffin hydrocarbons have been investigated in the gas phase but no such reactions in the liquid phase have been reported. Reichardt and Bonhoeffer[1] have shown that liquid hexane is capable of dissolving a significant concentration of mercury and that the saturated solutions so obtained absorbed a considerable fraction of light in the region 2530–2650A. Hence, with a suitable source of incident light Hg ($^3P_1$) atoms should be formed at a reasonable rate in the body of the liquid. Reichardt and Bonhoeffer also found that the absorption line of a saturated solution of mercury in hexane showed all the characteristics of extreme pressure broadening with Stark effect splitting of the maximum into twin peaks. It was of interest to find out whether excited mercury atoms formed under such conditions were capable of causing the decomposition of paraffins, as is the case in the gas phase, or whether the energy would be frittered away through collision of the excited mercury atoms with groups of paraffin molecules. Decane was chosen because of its relatively low vapor pressure and ready availability. The results given below were obtained in a preliminary investigation which, however, has established the occurrence of a photo-sensitized reaction and provided information about the behavior of decyl radicals in solution in decane.

EXPERIMENTAL

The hexane and decane were reagent grade products of Brickmann and Company. Since these liquids were found to absorb completely below 2800A (1 cm cell, Beckmann quartz spectrophotometer) they were passed through dry silica gel, which removed all of the light absorbing impurities.[2] The product obtained was completely transparent, in 1 cm depths, to light of 2400A and longer and absorbed only 2 to 3 percent at 2300A.

The absorption spectra of saturated solutions of mercury in hexane and decane at 25°C was obtained using a pair of matched 10-cm cylindrical quartz cells for pure solvent and saturated solution in a Beckmann quartz spectrophotometer.

The apparatus used for investigating the mercury photosensitized decomposition of decane is illustrated in Fig. 1. The reaction vessel *A* was a cylindrical quartz cell (12-cm long, 5-cm diameter) with plane quartz faces. It was wrapped, except for the windows, with asbestos paper and a heating coil of Nichrome ribbon which allowed the temperature of the cell to be varied at will. For experiments above room temperature it was found necessary to heat the connecting tubing between the cell and the mercury cut-off *I* to a temperature slightly higher than that of the cell. This was accomplished by a second coil of Nichrome ribbon and prevented bumping or boiling of the decane in the cell which, when occurring, caused the results to be erratic. The temperature was measured by a thermocouple in the well *S* which extended to the axis of the cell. Temperatures below 25°C were obtained by placing pieces of dry ice on the surface of the cell. Rapid agitation of the contents of the cell was obtained by means of a glass rotary magnetic stirrer *C*. This was held in place by two tungsten needles, one at either end, and was driven by a horseshoe magnet *D*. The latter was rotated by an air driven motor and was coupled magnetically to the stirrer by an Alnico rod *E*. It was found that rapid agitation greatly facilitated the degassing of the liquid and maintained saturation with mercury: it also ensured a constant temperature throughout the cell. A combined McLeod gauge, gas burette and Toepler pump connected to the reaction vessel provided a means for measuring the gaseous products of the reaction.

The light source (*G*) was a conventional low pressure discharge in mercury and neon. This was found to be almost as efficient and much steadier in operation than a medium pressure mercury lamp and about 40 times as effective as a hydrogen discharge.

In a typical experiment the cell was filled with decane and a drop of mercury via the side tube *B* which was then sealed off. Air was removed from the decane and the "dead space" by evacuation at *F*, dry ice being placed in a paper cone around the neck of the reaction

* Contribution No. 2120 from the National Research Council, Ottawa, Canada.
[1] H. Reichardt and K. F. Bonhoeffer, Zeits. f. Physik **67**, 780 (1930).
[2] Graff, O'Connor, and Sloan, Ind. Eng. Chem. (Anal. Ed.) **16**, 556 (1944).

vessel to reduce loss of decane by evaporation. The pressure was measured by raising the level of the mercury to *M*, stopcock *R* being kept shut, freezing out decane vapor in the side tube *N* with liquid air and using the volume above the side tube as a conventional McLeod gauge. In this manner the decane could be degassed sufficiently to produce a "sticking" vacuum. Fifteen minutes after switching on the mercury-rare gas lamp (*G*), the shutter *H* was opened and irradiation carried out for a definite period. After the run, with the stirrer still operating, the mercury in the burette was lowered to *K* and the burette filled with gas. The decane was frozen out as previously in *N* after the burette had been isolated from the reaction vessel by letting the mercury up to *M*. The volume of non-

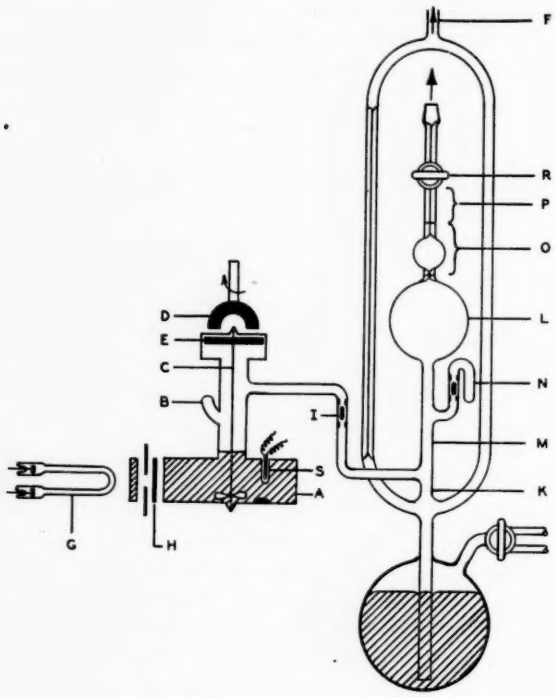

FIG. 1. Apparatus.

condensable gas was measured in the calibrated volume *O* and/or *P* and collected in a detachable reservoir by opening *R*. Stopcock *R* was lubricated with a glycerol-silica gel grease[3] which is not attacked by decane. The operation was repeated several times until all the non-condensable gas had been measured and collected. The same 250 cc charge of decane was used for subsequent experiments since the accumulation of liquid products was negligible. The gas phase reaction was investigated in the same apparatus by using only a small amount of decane (about 2 cc) and heating the cell to 120°C. At this temperature the vapor pressure of decane is 150 mm.

The high molecular weight products of the reaction were isolated in sufficient quantity for analysis by doing extended experiments (190 hours) in a similar apparatus with a much smaller reaction vessel (1 cm thick and 5 cm diameter) provided with a heated palladium tube through which the hydrogen produced could escape.

The quantum input to the cell was measured by the use of 0.5 *N* monochloroacetic acid as an actinometer as recommended by Smith, Leighton, and Leighton.[4]

The gaseous products were analyzed by conventional methods (passage through a hot palladium tube and oxidation by hot copper oxide) and were found to consist entirely of hydrogen.

The liquid remaining from the 190 hour experiment was fractionally distilled. The residue, after removal of the decane, was fractionated under reduced pressure and the physical properties of the fractions determined.* Both the "decane" and the heavier fractions were examined for unsaturates by the Baeyer test; no unsaturated compound was found in any fraction.

RESULTS

The absorption curve of a saturated solution of mercury in decane at 25°C is shown in Fig. 2. The general shape is similar to the curve for hexane obtained by Bonhoeffer and Reichardt.[1] The curve shows all the features such as increased width, shift of the peak and asymmetry associated with an absorption line pressure broadened in the extreme. The Stark effect splitting of the maximum into twin peaks is clearly evident. The only difference between the curves obtained by us for decane and hexane is that the twin peaks of the decane curve are shifted about 6A to the red compared with those for the hexane curve.

The results given in Table I show that the rate of production of hydrogen at 25°C is independent of time and that there is no induction period associated with the reaction; this is in good agreement with the results obtained for the similar reactions of the lower alkanes in the gas phase. A control experiment in which mercury was excluded showed that no reaction occurred and therefore one can be confident that none of the reaction observed when mercury was added was due to the direct photolysis.

The effect of temperature on the rate is shown in Table II. One effect of increasing temperature is to cause an increase in the solubility of mercury. This leads to increased absorption which would of itself lead to an increased rate. To allow for this effect, the percentage of λ2537 absorbed at each temperature was determined photometrically† relative to that at 25°C, and the results were used in estimating quantum yields.

[3] I. E. Puddington, Anal. Chem. **21**, 316 (1949).

[4] Smith, Leighton, and Leighton, J. Am. Chem. Soc. **61**, 2299 (1939).

* The molecular weights of the fractions were measured by Dr. I. E. Puddington of these laboratories, by the use of a sensitive differential manometer—see I. E. Puddington, Can. J. Res. **B27**, 151 (1949).

† The photometer measurements were made by Dr. H. J. Bernstein of this laboratory.

The fraction of incident light absorbed, given in column 3 of Table II, is taken from the photometer results and may be compared with the figures of column 4 which are values calculated from the solubility data[1] of mercury in hexane on the assumption that Beer's law is obeyed; these are given to provide a rough comparison since no data for the solubility of mercury in decane are available. The results indicate a steady increase of the quantum yield of hydrogen production with increasing temperature. An experiment at the highest temperature used, in the absence of light, showed that no reaction had occurred, so that it is quite safe to ascribe the production of hydrogen found to the reaction between $Hg(^3P_1)$ atoms and decane and indicates that thermal cracking of the liquid decane was negligible.

The physical properties of the fractions of the heavy product isolated from the long run are given in Table III. In that experiment 17.6 cc of decane were irradiated and 6.6 cc of heavy products obtained. This is about the amount expected from the conditions of the experiment. It seems very likely, from the physical properties, that the liquid consisted largely of a mixture of isomeric eicosanes ($C_{20}H_{42}$) with possibly small amounts of heavier paraffins (C_{30}) in the last fraction.

The Baeyer test showed that unsaturates were absent, within the sensitivity of the test, from all fractions. This indicates that disproportionation of decyl radicals did not occur to any marked extent.

DISCUSSION

The nature of the products, hydrogen and eicosanes, show that the reaction between $Hg(^3P_1)$ atoms and liquid decane is of the same general type as the similar reactions of $Hg(^3P_1)$ atoms with the lower paraffin hydrocarbons which have been investigated in the gas phase. Hence, it is fairly certain that the initial reaction consists of the breaking of a C—H bond:

$$Hg(^3P_1)+C_{10}H_{22}\rightarrow C_{10}H_{21}+H+Hg(^1S_0) \qquad (1)$$

leading to the formation of a hydrogen atom and a decyl radical. The final products are formed by the recombination of decyl radicals:

$$2C_{10}H_{21}\rightarrow C_{20}H_{42} \qquad (2)$$

and by the reaction of H atoms and the substrate:

$$H+C_{10}H_{22}\rightarrow C_{10}H_{21}+H_2 \qquad (3)$$

to form molecular hydrogen and a decyl radical. It may easily be shown that reaction (3) is so much faster than the recombination of two H atoms that the latter possibility may be ignored as a fate of H atoms.

The quantum yield is much less than that demanded by the above three reactions and has been shown to increase with temperature. This inefficiency may be due either to an inefficiency in the primary act or to the recombination of H atoms and decyl radicals. If the recombination is responsible for the inefficiency it will be necessary to postulate some sort of "cage effect" as suggested by Franck and Rabinowitsch[5] since, in liquid decane, the concentration of decane is so large that essentially all H atoms disappear by reaction (3) unless an efficient "cage" promoted recombination. Further investigations of this type of reaction are being made in this laboratory and it is hoped that they will provide a means of distinguishing between these two possibilities.

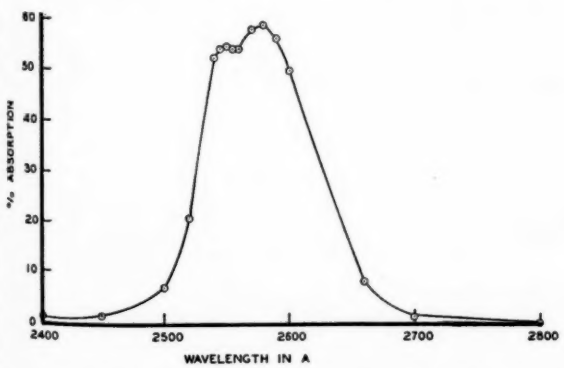

FIG. 2. Absorption curve of saturated solution of Hg in decane.

TABLE I. Temperature: 25°C; Quantum input = 1.77×10^{-4} einsteins/hr.

Duration of run in minutes	30	30	60	90
H_2 produced cc at N.T.P.	0.195	0.198	0.385	0.625

TABLE II. Quantum input = 1.48×10^{-4} einsteins/hr. All experiments of 30 minutes duration.

	Temperature °C	H_2 produced cc at N.T.P.	% quantum input absorbed photometer data	% quantum input absorbed Beer's law hexane	ϕ_{H_2}
Liquid phase	0	0.046	28.0	13.0	0.099
	9	0.069	38.5	23.3	0.107
	9	0.076	38.5	23.3	0.118
	25	0.166	50.0	50.0	0.200
	60	0.508	100.0	100.0	0.306
	100	0.641	100.0	100.0	0.386
	134	0.749	100.0	100.0	0.451
Gas phase	120	0.867	100.0		0.522
	120	0.840	100.0		0.506
				Av.	0.514

TABLE III.

Fraction no.	Volume cc liquid	B.P.	r.i. $\frac{20°C}{D}$	Molecular weight
1	4.3	303	1.4418	279±7
2	1.9	329	1.4500	373
3	0.4	329	1.4706	
n-eicosane		309.7	1.4425 (extrapolated)	282

[5] J. Franck and E. Rabinowitsch, Trans. Farady Soc. **30**, 120 (1934).

One interesting result obtained is that no decenes were found in the products. It has often been claimed that alkyl radicals have a great tendency to disproportionate when produced in solution. Bamford and Norrish,[6] who photolyzed a variety of aldehydes and ketones in paraffinic solvents, claimed that the large (octyl) radicals which were produced by the reaction of the solvent with the smaller alkly radicals formed by the photolysis, disproportionated, and produced unsaturated compounds which could be detected. The results obtained in the present study are in disagreement with the conclusions of Bamford and Norrish on this point. Our results show clearly that decyl radicals are produced in the mercury photo-sensitized reactions of decane, that the decyl radicals do recombine to form eicosanes and that they do not disproportionate. Bamford and Norrish found significant amounts of lower olefins in their products and it is quite possible that the unsaturation that they ascribed to octene may have been produced by polymerization of the lower olefins rather than by disproportionation of large alkyl radicals.

[6] C. H. Bamford and R. G. W. Norrish, J. Chem. Soc. 1544 (1938).

THE JOURNAL OF CHEMICAL PHYSICS VOLUME 18, NUMBER 5 MAY, 1950

Note on Mayers' Theory of Cluster Integrals

KODI HUSIMI
Osaka University, Osaka, Japan
(Received January 4, 1950)

The cluster integrals, b_l, in the condensation theory are expressible as a sum of products of irreducible integrals K_R. The coefficient of each member of the sum is derived in a simple manner.

IN their excellent text book, *Statistical Mechanics*, J. E. Mayer and M. G. Mayer[1] present a certain connection between the "cluster integrals" b_l and the "irreducible integrals" β_K. Their reasoning in establishing this connection is rather elementary and very complicated. Before I enter into an alternative analytical discussion of the subject, I want to generalize the notion of irreducible integrals which may be applied to any statistics, whereas Mayer's seem to be inseparably connected with the classical statistics and with the restricting assumption of binary interaction between the gas molecules. It concerns certain integrals of the form

$$N!I_N=\int^{(N)}\cdots\int W(1,2,\cdots,N)d1d2\cdots dN$$

with

$$W(1,2,\cdots,N)=\exp(-\beta V(1,2,\cdots,N)).$$

Here $V(1,2,\cdots,N)$ is the energy of the configuration of the molecules $1,2,\cdots,N$ (numerals also represent the coordinates of the molecules), and $\beta=1/KT$. W is symmetrical in its N arguments. In treating this multiple integral Ursell[2] devised a method of expansion which may be described according to Kahn and Uhlenbeck[3] as follows: We introduce successively new functions U by the scheme:

$$W(1)=U(1)$$
$$W(1,2)=U(1,2)+U(1)U(2)$$
$$W(1,2,3)=U(1,2,3)+U(1,2)U(3)+U(23)U(1)+U(31)U(2)+U(1)U(2)U(3).$$

[1] J. E. Mayer and M. G. Mayer, *Statistical Mechanics* (John Wiley and Sons, Inc., New York, 1940).
[2] H. D. Ursell, Proc. Cambridge Phil. Soc. **23**, 685 (1927).
[3] B. Kahn and G. E. Uhlenbeck, Physica **5**, 399 (1938).

Then the symmetrical functions U have the property that they vanish everywhere except at the points where the arguments are close to each other. This is a consequence of the assumed short range of interaction forces. In general, $W(1,2,\cdots,N)$ is of the form

$$W(1,\cdots,N)=\sum_{\Sigma lml=N} S\left\{\prod^{m_1}U(i)\prod^{m_2}U(ik)\cdots\prod^{m_l}U(i_1\cdots i_l)\cdots\right\}.$$

The first summation S is the symmetrization of the U-products and the second summation $\sum$ extends over all partitions of the number N. The number of terms in S, each of which gives on integration the same values

$$\prod_{l=1}^{N}(l!J_l)^{m_l}$$

where

$$l!J_l\equiv\int^{(l)}\cdots\int U(1,2,\cdots,l)d1d2\cdots dl\equiv V\cdot l!b_l,$$

is easily computed and is given by

$$\frac{N!}{\prod_l (l!)^{m_l}m_l!}$$

so that

$$I_N=\sum_{\Sigma lml=N}\prod_l\frac{(J_l)^{m_l}}{m_l!}.$$

This is Ursell's development. In order to attain Mayer's development, we introduce another infinite set of func-

tions V defined by

$$U(1,2)=V_1(1,2)$$

$$U(1,2,3)=V_2(1,2,3)+V_1(12)V_1(23)+V_1(23)V_1(31)+V_1(31)V_1(12)$$

$$U(1,2,3,4)=V_3(1,2,3,4)+\sum_{12\text{ terms}}V_2(123)V_1(34)+\sum_{12\text{ terms}}V_1(12)V_1(23)V_1(34)+\sum_{3\text{ terms}}V_1(12)V_1(13)V_1(14)$$

$$U(1,2,3,4,5)=V_4(12345)+\sum_{60\text{ terms}}V_3(1234)V_1(45)+\sum_{15\text{ terms}}V_2(123)V_2(345)+\sum_{60\text{ terms}}V_1(12)V_1(23)V_1(34)V_1(45)+\sum_{60\text{ terms}}V_1(12)V_1(23)V_1(24)V_1(45)+\sum_{5\text{ terms}}V_1(12)V_1(13)V_1(14)V_1(15).$$

The method of construction is the following. U with l arguments is a sum of isobaric products ΠV_R with $\sum R=l-1$. In each product the variables are never separated in groups, so that the product is not factorized into factors with mutually foreign variables. But the two and more V's within a product contain one and only one common variable. Further the products are of such nature that, if a common variable is omitted, the product is factorized into several factors with mutually different variables. The V's are totally symmetric functions. The introduction of V's are based on the assumption that the mutual potential energy of the molecules is dependent only on their relative coordinates, not on their absolute position in space, so long as the influence of the gas enclosure is neglected.

Then the integral of the product of the V's are reducible to the product of integrals of the individual V's. For we have, e.g.,

$$\int V_2(123)V(3\cdots)\cdots d1d2d3\cdots=\int V_2(123)d1d2\cdot\int V(3\cdots)\cdots d3\cdots$$

since the first integral becomes independent on the common variable 3. The individual integrals

$$K_R=\int V_R(12\cdots R,R+1)d1d2\cdots dR$$

are just Mayer's irreducible integrals. Every product of the form,

$$\prod^{n_1}V_1\prod^{n_2}V_2\cdots\prod^{n_R}V_R\cdots\quad\left(\sum_R Rn_R=l-1\right),$$

with given numbers of factors $n_1,n_2,\cdots n_R,\cdots$ all give rise to one and the same integral, i.e.,

$$K_1{}^{n_1}K_2{}^{n_2}\cdots K_R{}^{nR}\cdots\quad\cdot v,$$

where v is the volume of the gas enclosure. And the problem under our discussion is to determine the number $T(n_1n_2,\cdots n_R\cdots)$ of different products with the above form in the representation of a given $U(12\cdots l)$. The numbers $T(n_1,0,0,0,\cdots)$ have been subjects of many mathematicians since the time of Cayley, as the number of "trees" with given number l of the molecules. A modern method of obtaining $T(n_1,0,0,\cdots)$ has been given by G. Bol.[4] We want to generalize his method to our problem of $T(n_1n_2\cdots n_R\cdots)$.

The starting point is the establishment of a recursion formula. This is obtained if, in a given generalized tree

$$\prod^{n_1}V_1\prod^{n_2}V_2\cdots\prod^{n_{R+1}}V_R\cdots,$$

a factor V_R is omitted. Then the tree is separated in general into $(R+1)$ trees. These may have $n_{h,m}V_h$'s $(m=1,2,\cdots,R,R+1)$.

We have of course $\sum_m n_{h,m}=n_h$. An elementary consideration will lead to the recursion formula

$$(n_R+1)\cdot(R+1)!\cdot T(n_1,n_2,\cdots,n_R+1,\cdots)=\sum_{(n_h,m)}l!\prod_{m=1}^{R+1}\frac{l_m T(\cdots n_{hm}\cdots)}{l_m!}$$

$l_m=1+\sum_h hn_{h,m}$ is the number of molecules contained in the tree $\{\cdots,n_{h,m}\cdots\}$ and the above summation extends over all partitions $n_h=\sum n_{hm}$ of $n_h(h=1,2,\cdots,h=R$ inclusive).

In order to solve the recursion formula we introduce a generating function

$$F(x,y_1,y_2\cdots)=\sum_{\substack{(n_R=0,1,\cdots,\infty)\\ l=1+\sum Rn_R}}\frac{T(n_1n_2\cdots)x^l y_1{}^{n_1}y_2{}^{n_2}\cdots}{l!}.$$

It has a redundant variable $F(x,y_1,y_2,\cdots)=\lambda F(\lambda^{-1}x,\lambda y_1,\lambda^2 y_2,\cdots)$ and satisfies Euler's equation

$$x\frac{\partial F}{\partial x}=F+y_1\frac{\partial F}{\partial y_1}+2y_2\frac{\partial F}{\partial y_2}+\cdots.$$

The recursion equation becomes now

$$(R+1)!\frac{\partial F}{\partial y_R}=\left(x\frac{\partial F}{\partial x}\right)^{R+1}$$

[4] G. Bol, Abhandl. Math. Seminar Hansischen Univ. **12**, 242 (1938). (I thank Mr. Kasuga for bringing my notice to the paper.)

which leads, combined with Euler's equation, to

$$x\frac{\partial F}{\partial x}=F+\sum_{R=1}\frac{Ry_R}{(R+1)!}\left(x\frac{\partial F}{\partial x}\right)^{R+1}.$$

This equation may be considered as an ordinary differential equation with fixed parameters y_R.

Let

$$G\equiv x\frac{\partial F}{\partial x}.$$

Then the equation becomes

$$G=F+\sum\frac{Ry_R}{(R+1)!}G^{R+1}.$$

or, after differentiatiation by G, considered as independent variable,

$$1=\frac{dF}{dG}+\sum\frac{y_R}{(R-1)!}G^R.$$

Since

$$\frac{dx}{x}=\frac{dF}{dG}\frac{dG}{G}$$

it gets the form

$$\frac{dx}{x}=\left\{1-\sum_R\frac{y_R}{(R-1)!}G^R\right\}\frac{dG}{G},$$

which integrates immediately to

$$x=G\exp\left\{-\sum_{R=1}\frac{y_R}{R!}G^R\right\}.$$

$T(n_1\cdots)$ will now be obtained as the coefficient of x^l in the power series of G times l. Cauchy's theorem now gives

$$\frac{1}{2\pi i}\oint\frac{Gdx}{x^{l+1}}$$

$$=\frac{1}{2\pi i}\oint\frac{\exp(l\sum y_RG^R/R!)}{G^{l-1}}\left(1-\sum\frac{y_R}{(R-1)!}G^R\right)\frac{dG}{G}$$

$$=\frac{1}{2\pi i}\oint\frac{1}{l}\frac{\exp(l\sum y_RG^R/R!)}{G^l}dG$$

$$=\frac{1}{l}\sum_{\Sigma hn_h=l-1}\prod_h\frac{1}{n_h!}\left(\frac{ly_h}{n!}\right)^{n_h},$$

and the final formula is obtained:

$$T(n_1n_2\cdots n_R\cdots)=\frac{l!}{\prod_R(R!)^{n_R}n_R!}l^{\Sigma n_R-2}.$$

As one sees the generating function F or G here introduced plays an important role in the further discussions of Mayer's condensation theory. In fact, if we put $y_R=K_R\equiv R!\beta_R$ in $F(x,y_1\cdots)$, we have

$$F(x,K_1,K_2,\cdots)=\sum b_lx^l\equiv X(x)$$

and $G=x(\partial F/\partial x)$, $x=G\exp(-\sum y_RG^R/R!)$ are equivalent to

$$y=xX'(x),\quad x=ye^{-\phi(y)},\quad \phi(y)\equiv\sum_{K=1}^{\infty}\beta_Ky^K$$

(for notation, see Kahn-Uhlenbeck[3]).

The theory of this report was formulated several years ago and printed in our book on quantum statistical mechanics in Japanese.[5] Mr. Y. Muto has successfully applied it to the theory of multi-component systems and the idea may be useful in a wider circle of statistical problems.

[5] K. Husimi, Ed., *Quantum Statistical Mechanics* (Kyoritu Syuppan K.K., 1948).

The Vibrational Spectra and Structure of Inorganic Molecules. I. The Infra-Red Spectrum of F_2O from 2.5 to 25μ

H. J. BERNSTEIN AND J. POWLING*
National Research Council, Ottawa, Canada

(Received November 4, 1949)

The infra-red spectrum of gaseous F_2O has been obtained from 2.5 to 25μ at pressures of 10 mm to 600 mm Hg in a 10-cm cell and at 600 mm Hg in a meter cell.

All three fundamentals have been observed and identified.

The fine structure of a $\perp$ band was resolved and gave an estimate of the bond distance and apex angle as 1.38±0.03A and 101.5±1.5°, respectively.

The upper and lower limits of the constants of a quadratic potential function with all possible interaction constants have been obtained.

THE infra-red spectrum of gaseous F_2O has been obtained with fair resolution by Hettner, Pohlman, and Schumacher[1] at pressures of 3 and 215 mm Hg. These authors believed their sample contained CF_4 as impurity and attributed some of the many bands observed to CF_4. The remaining bands, however, lent themselves to interpretation on the basis of two frequency assignments (see Table I).

Sutherland and Penney[2] have reinterpreted the spectrum obtained by Hettner *et al.* assuming all the bands observed by these authors to be due to F_2O. Their assignment is given in Table I for comparison.

Having a pure sample[3] of F_2O at our disposal, it was considered of interest to reinvestigate the infra-red spectrum.

The spectra were obtained at various pressures in a 10-cm cell and a one-meter cell with a Perkin-Elmer infra-red spectrometer (Model 12C) used in conjunction with a Brown recorder. At a pressure of 600 mm Hg in a 10-cm cell no bands were observed in the KBr region of the spectrum. Since a low lying fundamental may occur in this region the region was also investigated with a meter gas cell and at a pressure of 600 mm Hg. The complete spectrum is shown in Fig. 1. The fine structure resolved in the band at 10.8μ is shown in Fig. 2. The frequencies and numbering for the band are given in Table II.

DISCUSSION

F_2O has the symmetry of the C_{2v} point group and three fundamental modes of vibration. The fundamentals ν_1 and ν_2 are of type A_1 (totally symmetric vibrations) and the fundamental ν_3 is of type B_1 (antisymmetric in plane vibration). All modes are allowed in the infra-red.

The OF bond distance and apex angle of F_2O found by electron diffraction[4] are 1.41±0.05A and 100±3°, respectively. The moments of inertia are then

$$I_A = 15.3\times10^{-40} \text{ c.g.s. unit}$$
$$I_B = 73.9\times10^{-40} \text{ c.g.s. unit}$$
$$I_C = 89.2\times10^{-40} \text{ c.g.s. unit}$$

and the molecule is an approximate symmetric top with the axis of least moment of inertia as the figure axis.

Since the induced moment during the type A_1 vibration is $\perp$ to the axis of least moment of inertia which is the figure axis of an approximate symmetric top,[4] and the induced moment in the type B_1 vibration is $\parallel$ to this axis, the type A_1 bands are $\perp$ bands with a doublet contour, and the type B_1 band is a $\parallel$ band with *PQR* branches.

The band at 828 cm^{-1} is immediately identified as $\nu_3(\parallel)$ because of its *PQR* contour and further because its observed *PR* separation (28 cm^{-1}) is very nearly the same as the expected theoretical value[5] for a $\parallel$ band calculated from

$$\Delta\nu_{PR} = [S(\beta)/\pi](KT/I)^{\frac{1}{2}} = 27.5 \text{ cm}^{-1}.$$

Since the value for the least moment of inertia is about 15.3×10^{-40} c.g.s. unit, the $\perp$ band should have a doublet contour with fine structure spacing approximately equal to 3.7 cm^{-1}. The band at 929 cm^{-1} is then without question a type A_1 band ($\perp$). The band at 461 cm^{-1} is also a type A_1 band because of its doublet contour, although the slits were too wide to resolve its fine structure. It is extremely unlikely that the strong band at 929 cm^{-1} is the overtone of the weak 461-cm^{-1} band, so these bands must be the fundamentals ν_1 and ν_2 respectively.[6]

The observed spectrum is interpreted satisfactorily on the basis of these fundamentals and a complete assignment is given in Table III.

By comparing the spectrum of F_2O obtained in this work with that of Hettner *et al.* and the spectrum of

* National Research Laboratories Postdoctorate Fellow (1949).

[1] Hettner, Pohlman, and Schumacher, Zeits. f. Physik **96**, 203 (1935).

[2] G. B. B. M. Sutherland and W. G. Penney, Proc. Roy. Soc. London **A156**, 678 (1936).

[3] The purity of the sample estimated from the quantitative reaction $F_2O+4HI=2I_2+2HF+H_2O$ was 99.1 percent F_2O.

[4] L. R. Maxwell, J. Opt. Soc. Am. **30**, 374 (1940).

[5] S. L. Gerhard and D. M. Dennison, Phys. Rev. **43**, 197 (1933). In this formula, I is the mean of the middle and greatest moments of inertia.

[6] There is another way by which $2\nu_2$ can gain intensity, namely, by Fermi resonance between ν_1 and $2\nu_2$. No evidence of Fermi resonance, however, is apparent in the 10.8μ region. This may be due to a very small interaction energy between the ν_1 and $2\nu_2$ levels.

TABLE I.

Infra-red spectrum of F_2O Hettner *et al.*	Interpretation I. Hettner		Interpretation II. Hettner	Interpretation Sutherland and Penney
2544				$2\nu_1+2\nu_2$
2190				$2\nu_3$
1740			fundamental	$\nu_1+2\nu_2$
1280	fundamental		fundamental	$\nu_1+\nu_2$
1110				ν_3 fundamental
926	fundamental	870	fundamental	$2\nu_2$
833	fundamental			ν_1 fundamental
625				$\nu_3-\nu_2$
492				ν_2 fundamental

TABLE II. F_2O 170 mm Hg.

K	Obs. cm^{-1}
10	963.0
9	959.5
8	956.4
7	952.8
6	949.0
5	945.4
4	942.6
3	(939.5)
2	(935.0)
1	(931.2)
0	
−1	(927.7)
−2	(923.6)
−3	(921.0)
−4	917.0
−5	913.6
−6	910.5
−7	907.5
−8	904.5
−9	902.5
−10	899.0
−11	895.5
−12	893.2
−13	891.0

CF_4 it is apparent that the complexity of Hettner's spectrum was due to CF_4 as impurity (see Table IV).

FINE STRUCTURE OF THE BAND AT 10.8μ AND A REFINEMENT OF THE MOLECULAR DIMENSIONS OBTAINED BY ELECTRON DIFFRACTION

Since the F_2O molecule is an approximate symmetric top the frequency of the Q branches is given by[7]

$$\nu=\nu_0+(A'-B')\pm 2K(A'-B') +[(A'-B')-(A''-B'')]K^2. \quad (1)$$

The differences between the rotational constants of the upper and lower states are obtained from

$$^RQ_K-{}^PQ_K=4K(A'-B') \quad (2)$$

and

$$^RQ_{K-1}-{}^PQ_{K+1}=4K(A''-B'') \quad (3)$$

respectively. The band center may be obtained from

$$^RQ_K+{}^PQ_{K+1}=2\nu_0+[(A'-B')-(A''-B'')] \times[K^2+(K+1)^2]. \quad (4)$$

One might expect relations (2) and (3) to be valid for higher K values for an approximate symmetric top since the effects of K-type doubling are minimized. Also, the spectrum near the band origin may be complicated by weak overlapping with $2\nu_2=922\ cm^{-1}$. Since ν_2 is so very much weaker than ν_1 it is extremely unlikely that $2\nu_2$ will contribute much to the band ν_1, especially at higher K values. Table V gives values of $A''-B''$ and $A'-B'$ obtained from relations (2) and (3) for higher K values. The mean values obtained are

$$A''-B''=1.60\pm 0.02\ cm^{-1},$$
$$A'-B'=1.60\pm 0.02\ cm^{-1}.$$

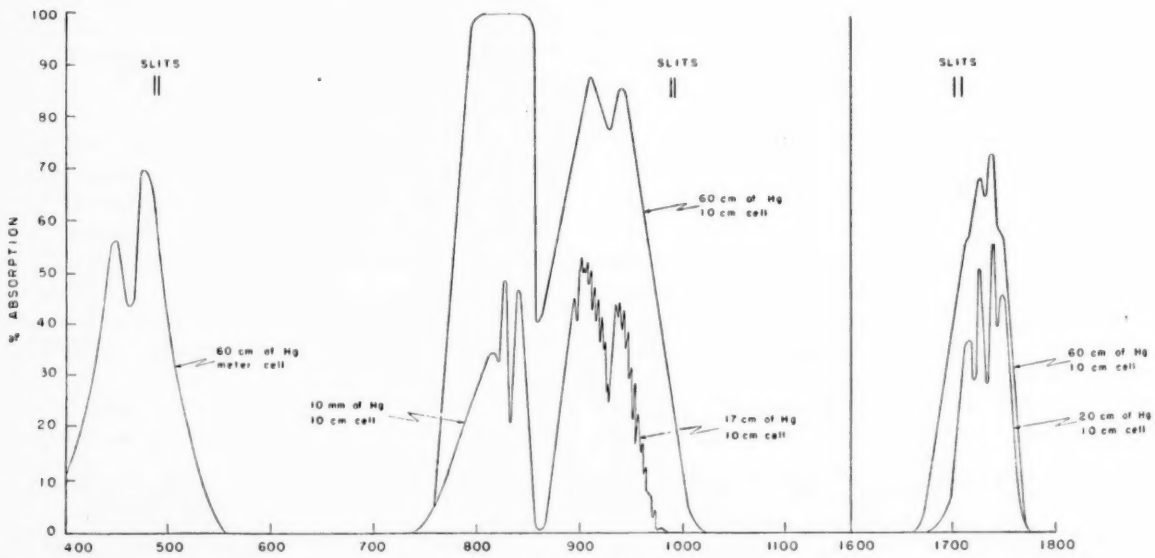

FIG. 1. Frequency in cm^{-1}.

[7] G. Herzberg, *Infrared and Raman Spectra of Polyatomic Molecules* (D. Van Nostrand Company, Inc., New York, 1945), p. 483.

TABLE III.

Infra-red band cm^{-1}	Structure	Separation cm^{-1}	Assignment
1700–1764 (m)	*PQR* and doublet		$\nu_1+\nu_3(B_1)$ and $2\nu_1(A_1)$ [a]
929 (s)	Doublet	30	$\nu_1(A_1)$
826 (v.s.)	*PQR*	28	$\nu_3(B_1)$
461 (w)	Doublet	27	$\nu_2(A_1)$

[a] The band at ~1740 cm^{-1} is primarily due to the combination tone $\nu_1+\nu_3$ with $2\nu_1$ probably contributing some intensity. $2\nu_3$ would have to have a very large anharmonicity with opposite sign to appear in this region.

TABLE IV.

F_2O this work	F_2O Hettner *et al.*[a]	CF_4[b]
	2544	2541
	2190	2180
1740	1740	
	1280	1265
	1110	1112
929	926	
826	833	
	625	630
	492	
461		

[a] See reference 1.
[b] Bailey, Hale, and Thompson, Proc. Roy. Soc. London **A167**, 555 (1938). These authors did not investigate the spectrum as far down as 492 cm^{-1}.

Since $(A'-B')-(A''-B'')=0\pm0.04$ cm^{-1} it is not possible to obtain an accurate value of ν_0 from Eq. (4). In the above formula B'' is actually $(B''+C'')/2$ so that

$$A''-B''=1.60\pm0.02\ cm^{-1}$$

$$=28.00\left[\frac{1}{I_A}-\frac{1}{2}\left(\frac{1}{I_B}+\frac{1}{I_C}\right)\right]cm^{-1}$$

where the I's are in units of 10^{-40}. Letting r be the O–F distance in A, and 2θ the apex angle, substitution for I_A, I_B, and I_C in terms of r and 2θ gives the relation

$$r^2=17.5\pm0.20\left[\frac{1}{18.7\cos^2\theta}-\frac{1}{2}\left(\frac{1}{18.7\cos^2\theta+63.05\sin^2\theta}+\frac{1}{63.05\sin^2\theta}\right)\right].$$

In Table VI the OF bond distances have been calculated from this equation for one degree changes in 2θ from $2\theta=97°$ to $2\theta=103°$.

These limiting values for 2θ are indicated by the error of the electron diffraction measurement,[4] namely, $2\theta=100\pm3°$. Since the electron diffraction result for the OF bond distance is 1.41±0.05A, the first three values of r_{OF} in Table VI are excluded, leaving the only possible range of values for 2θ and r consistent with the moment of inertia obtained from the spacing of the fine structure. In this way the electron diffraction results may be refined to

$$r_{OF}=1.38\pm0.03A,$$
$$2\theta=101.5\pm1.5°.$$

POTENTIAL FUNCTION OF F_2O

A suitable quadratic potential function for F_2O is given by

$$2V=K[(\delta r_1)^2+(\delta r_2)^2]+K_{2\theta}(r\delta_{2\theta})^2+2K_1\delta r_1\delta r_2+2K_2(\delta r_1+\delta r_2)r\delta_{2\theta}$$

where δr_1, δr_2, $\delta_{2\theta}$ are the displacements of bond 1, bond 2, and the apex angle, respectively, from the equilibrium configuration. K, $K_{2\theta}$, K_1, and K_2 are the bond stretch-

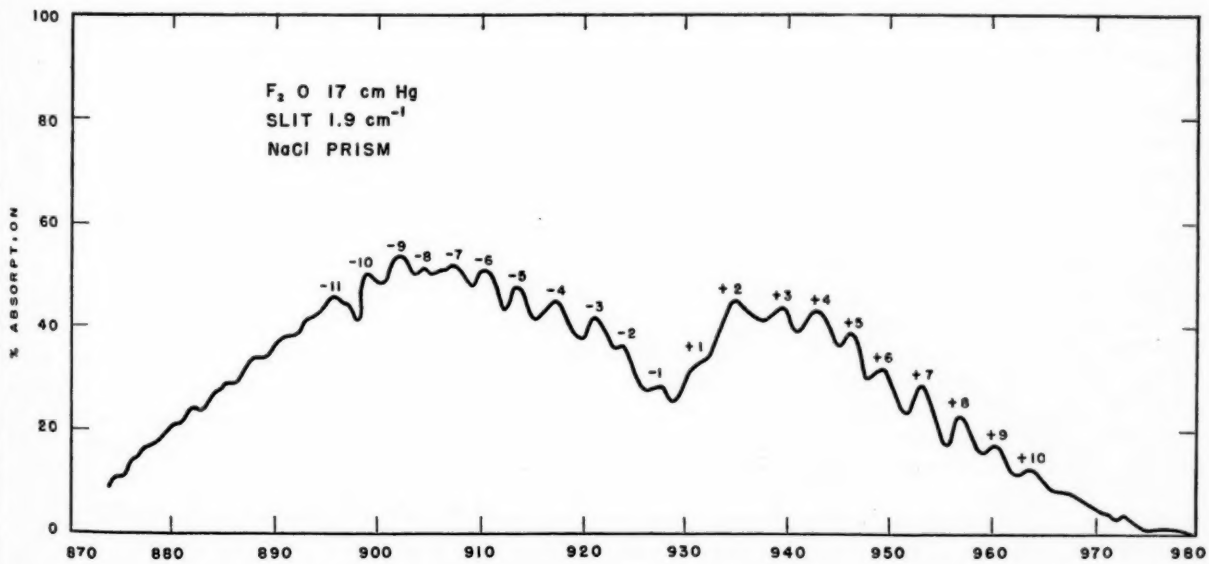

FIG. 2. FREQUENCY IN cm^{-1} (BAND AT 10.8 μ).

TABLE V. F_2O 170 mm Hg.

K	${}^RQ_{K-1}$	${}^PQ_{K+1}$	$4K(A''-B'')$	$A''-B''$
11	963.0	893.2	69.8	1.585
10	959.5	895.5	64.0	1.600
9	956.4	899.0	57.4	1.603
8	952.8	902.5	50.3	1.575
7	949.0	904.5	44.5	1.590
6	945.4	907.5	37.9	1.580
5	942.6	910.5	32.1	1.605
4	(939.5)	913.6	25.9	(1.622)
			Mean	1.60±0.02 cm^{-1}
K	${}^RQ_K$	${}^PQ_K$	$4K(A'-B')$	$A'-B'$
10	963.0	899.0	64.0	1.600
9	959.5	902.5	57.0	1.585
8	956.4	904.5	51.9	1.621
7	952.8	907.5	45.3	1.619
6	949.0	910.5	38.5	1.605
5	945.4	913.6	31.8	1.590
4	942.6	917.0	25.6	1.600
			Mean	1.60±0.02 cm^{-1}

TABLE VI.

2θ	r_{OFA}
97	1.298±0.007
98	1.317±0.008
99	1.336±0.007
100	1.355±0.008
101	1.373±0.008
102	1.396±0.008
103	1.415±0.008

TABLE VII. Force constants of the F_2O molecule in units of 10^5 dynes per cm for various potential functions.

	Four-constant potential function	Potential function with $K_2=0$	Potential function with $K_1=0$	K from Badger's rule[a]
K	3.21 to 5.23	3.63, 2.62	3.17	5.4±0.8
$K_{2\theta}$	0.05 to 1.67	0.84, 1.66	0.46, 3.43	
K_1	0.04 to 2.06	0.46, −0.56	0.0	
K_2	0.00 to 0.98	0.0 0.0	−0.78, 2.31	

[a] Substituting for the OF bond distance (1.38±0.03A) into Badger's relation $K(r-0.68)^3=1.86\times10^5$ dynes per cm gives $K=5.4\pm0.8\times10^5$ dynes per cm [J. Chem. Phys. 2, 128 (1934).]

ing, bond deformation, and interaction constants, respectively.

If M is the mass of the oxygen atom and m the mass of the fluorine atom in atomic units, the determinantal equation gives[8]

$$\lambda_1+\lambda_2=(K+K_1)\left(\frac{1}{\mu}+\frac{\cos2\theta}{M}\right)+2K_{2\theta}\left(\frac{1}{\mu}-\frac{\cos2\theta}{M}\right)-\frac{4K_2}{M}\sin2\theta, \quad (5)$$

$$\lambda_1\lambda_2=\frac{M+2m}{Mm^2}[2K_{2\theta}(K+K_1)-4K_2{}^2], \quad (6)$$

$$\lambda_3=(K-K_1)\left(\frac{1}{\mu}-\frac{\cos2\theta}{M}\right), \quad (7)$$

where $\mu=Mm/(M+m)$ and $\lambda_i=0.590\times10^{-6}\nu_i{}^2$ for ν_i in cm^{-1}.

It has been shown that a four-constant potential function is necessary to describe the dynamics of symmetrical non-linear triatomic molecules and that the interaction constants K_1 and K_2 are equally important.[9]

The three frequencies are not sufficient to evaluate the four force constants of these equations but considerable information may be obtained as to the upper and lower limits that these constants may have.

With the values $\nu_1=929$ cm^{-1}, $\nu_2=461$ cm^{-1}, $\nu_3=828$ cm^{-1}, and $2\theta=101.5°$ elimination of K_1 and K_2 from Eqs. (5)–(7) gives a quadratic relation between K and $K_{2\theta}$. For K to have real roots it is found that 0.05×10^5 dynes per cm $\leqslant K_{2\theta}\leqslant 1.67\times10^5$ dynes per cm. The maximum and minimum values that K can take are given by the condition $\partial K/\partial K_{2\theta}=0$. Numerically, this condition is satisfied for $K_{2\theta}=0.514$ and 1.20×10^5 dynes per cm. Substituting these values for $K_{2\theta}$ in the quadratic expression for K as a function of $K_{2\theta}$ gives the upper limit of K as 5.23×10^5 dynes per cm and the lower limit of K as 3.21×10^5 dynes per cm.

From Eq. (7) the upper limit and lower limit of K_1 is found to be 2.06 and 0.04×10^5 dynes per cm, respectively.

From Eq. (5) the upper and lower limits of K_2 are found to be 0.98 and 0.0×10^5 dynes per cm, respectively.

In Table VII the force constants are given for the complete four-constant potential function; when $K_2=0$; and for $K_1=0$.

When $K_2=0$, two sets of force constants are obtained whereas when $K_1=0$, K is obtained directly from Eq. (7) and substitution in (5) and (6) gives two sets of values for $K_{2\theta}$ and K_2. The columns give corresponding sets of the constants.

An approximation to the ratio $(\nu_1/\nu_3)^2$ is given by

$$(\nu_1/\nu_3)^2=[(K+K_1)/(K-K_1)]\times[(M+\mu\cos2\theta)/(M-\mu\cos2\theta)].$$

In a linear molecule such as CO_2 or CS_2 the value of $\mu\cos2\theta$ is of the same order of magnitude as M so that the ratio $(M+\mu\cos2\theta)/(M-\mu\cos2\theta)$ is small (since $\cos2\theta=-1$). This ratio is so small that the R.H.S. of the above equation remains <1 even after multiplied by the force constant ratio. For F_2O, however, since 2θ is closer to 90° than to 180° the $\mu\cos2\theta$ term is very much less than the M so that $(M+\mu\cos2\theta)/(M-\mu\cos2\theta)$ is only slightly less than one. As a result the force constant ratio is responsible for making the R.H.S. greater than one and thus $\nu_3<\nu_1$.

[8] Ta-You Wu, *Vibrational Spectra and Structure of Polyatomic Molecules* (J. W. Edwards, Ann Arbor, Michigan, 1946), p. 163.
[9] Coulson, Duchesne, and Manneback, Vol. comm. Victor Henri, Maison Desoer, Liège (1947–48), p. 33.

It is apparent then why ν_3 is less than ν_1 for F_2O whereas in other symmetric triatomic molecules ν_3 is usually greater than ν_1.

ACKNOWLEDGMENT

Thanks are due Miss E. Miller for reduction of the spectra.

THE JOURNAL OF CHEMICAL PHYSICS VOLUME 18, NUMBER 5 MAY, 1950

Magnetic Evidence for d^3s Bond Hybridization in Chromium (II) Acetate. The Oxidation State of Chromium in a Reported Tris(8-Hydroxyquinoline) Chromium (II)

WILLIAM R. KING, JR. AND CLIFFORD S. GARNER
Department of Chemistry, University of California, Los Angeles, California
(Received December 27, 1949)

Magnetic susceptibilities of solid $Cr(OOCCH_3)_2$ and its monohydrate were measured, and these compounds were shown to contain no unpaired electrons. This fact indicates that the four unpaired $3d$ electrons of the normal Cr^{++} ion are paired in these compounds, the three $3d$ orbitals thus made available being utilized in the formation of covalent bonds. The fourth covalent bond probably involves use of the $4s$ orbital of chromium. This evidence may constitute the first example of d^3s bond hybridization postulated by Pauling. Susceptibility measurements were also carried out on tris(8-hydroxyquinoline) chromium (III) and a reported tris(8-hydroxyquinoline) chromium (II). The evidence indicates both to be the same compound, with the chromium having a tripositive oxidation state.

INTRODUCTION

IN the course of other work on chromium compounds we have investigated the magnetic susceptibilities of chromium (II) acetate and its monohydrate. The orange-tan and red colors, respectively, of these compounds and their moderately low (<1 percent) solubility in water suggest a different type of bonding of the chromium from that in the typical blue and very soluble salts of dipositive chromium, such as the perchlorate and chloride. The magnetic results presented in this paper bear out this idea and indicate d^3s (or possibly d^3p) bond hybridization for chromium in the acetate. Pauling[1] has pointed out that three d eigenfunctions may be used together with some s and p character to give equivalent tetrahedrally directed bond eigenfunctions of "strength" 2.950, nearly equal to the maximum "strength" of 3, and he has concluded that examples of such bonds should be provided by $CrO_4^=$, $MoO_4^=$, and related oxy-ions. Although the magnetic criterion[1,2] for bond type cannot be applied to these latter ions, it may be applied to divalent chromium compounds.

Hume and Stone[3] prepared by the action of an excess of 5 percent 8-hydroxyquinoline in 2f. CH_3COOH on chromium (II) chloride solution an orange-yellow compound which they assumed to be an 8-hydroxyquinoline chromium (II), i.e., "chromous 8-hydroxyquinolate." On the basis of his analyses of the purified compound, indicating three 8-hydroxyquinolate addenda per chromium atom, Hume[4] suggested the possibility of d^2sp^3 bonding of the chromium in this compound. In order to investigate this point we prepared this compound by the method of Hume and Stone,[3] and also prepared tris(8-hydroxyquinoline) chromium (III), and measured the magnetic susceptibility of each. The results indicate that these two compounds are identical, with the chromium in the tripositive oxidation state. In the case of the presumed chromium (II) compound, the Cr (II) is apparently oxidized to Cr (III) by the 8-hydroxyquinoline during the preparation.

PREPARATION AND ANALYSIS OF COMPOUNDS

Chromium (II) Acetate Monohydrate

Freshly prepared solutions of dichlorotetraquo chromium (III) chloride (c.p. green $CrCl_3 \cdot 2H_2O$) were reduced with amalgamated zinc in an upflow-type Jones reductor.[3] The resulting chromium (II) solution was run directly into an excess of saturated $NaOOCCH_3$ solution covered by a layer of petroleum ether in order to exclude air. The precipitated $Cr(OOCCH_3)_2 \cdot H_2O$ was washed free of excess $NaOOCCH_3$ and Zn^{++} with O_2-free water. The resultant water slurry was used for magnetic measurements. For analyses the precipitate was washed with C_2H_5OH and then with $(C_2H_5)_2O$ and dried in a stream of O_2-free N_2. The analyses (27.6 percent Cr, C/Cr=3.94) indicate the formula $Cr(OOCCH_3)_2 \cdot H_2O$ (27.6 percent Cr, C/Cr=4.00). The compound had a red color.

[1] L. Pauling, J. Am. Chem. Soc. **53**, 1367 (1931).
[2] L. Pauling, *The Nature of the Chemical Bond* (Cornell University Press, Ithaca, New York, 1945), second edition, p. 112.
[3] D. N. Hume and H. W. Stone, J. Am. Chem. Soc. **63**, 1200 (1941).
[4] D. N. Hume, Master's Thesis, U.C.L.A. (1941).

Chromium (II) Acetate

$Cr(OOCCH_3)_2 \cdot H_2O$ was converted to the anhydrous compound by heating for six hours at 100°C in vacuum over P_2O_5. The anhydrous acetate had an orange-tan color and was extremely pyrophoric. Analyses gave 30.3 percent Cr and 68.5 percent CH_3COO^-, corresponding to the formula $Cr(OOCCH_3)_2$ (30.6 percent Cr, 69.4 percent CH_3COO^-).

"Tris(8-hydroxyquinoline) Chromium (II)"

The method of Hume and Stone,[3] as outlined below, was used for the preparation of this reported compound. $Cr(OOCCH_3)_2 \cdot H_2O$ was treated with a minimum amount of cold O_2-free 6f. HCl to give a solution of chromium (II) chloride which was added to an excess of 5 percent 8-hydroxyquinoline in 2f. CH_3COOH, using a layer of petroleum ether to exclude air. The orange-yellow precipitate formed was washed with boiled distilled water and filtered off in a stream of O_2-free N_2. The product was dried in a vacuum desiccator over $CaCl_2$. To minimize chance of oxidation, further purification was not attempted. The analyses (9.33 percent Cr) correspond to the formula $Cr(C_9H_6ON)_{3.5}$, indicating contamination with excess 8-hydroxyquinoline in agreement with the findings of Hume[4] when final purification was omitted.

Tris(8-hydroxyquinoline) Chromium (III)

This compound was prepared from c.p. $CrCl_3 \cdot 2H_2O$ by the method of Austin.[5] Analyses gave 10.7 percent Cr; calculated for $Cr(C_9H_6ON)_3$ is 10.73 percent Cr.

MAGNETIC MEASUREMENTS

Magnetic susceptibilities were determined at room temperature by the Gouy method.[6] The electromagnet used was water cooled and had a thermostated air chamber around the pole pieces between which the glass susceptibility tubes were suspended. The field between the pole pieces could be held constant by manual regulation of the current to within 0.2 percent. In general, weighings were made at three field strengths generated at 10, 12, and 15 amperes. The weight changes at 12 and 15 amperes were reduced by experimentally determined factors to changes at 10 amperes and the resulting changes averaged with the closely agreeing change at 10 amperes to give the reported values Δw (in milligrams). All measurements were made relative to air in the lower half of the susceptibility tubes.

Susceptibility values were calculated by comparison of the Δw values found for the various substances with the Δw value for water saturated with N_2 measured under the same conditions. The specific susceptibility of water was taken as -0.722×10^{-6} from the results of Auer.[7] Values so determined were corrected for the diamagnetic contribution by the use of Pascal constants and susceptibility values for closely related diamagnetic substances.[8] The values have been calculated only for comparison purposes in order to give the number of unpaired electrons, and because of the probable presence of small amounts of paramagnetic impurities or partial oxidation to paramagnetic Cr (III) the values have little significance in an absolute sense. The magnetic moments μ (in molal Bohr magnetons) were then computed from the molal paramagnetic susceptibilities, χ_{molal}, by the use of the equation[9] $\mu = 2.84 \times (\chi_{molal} T)^{\frac{1}{2}}$, T being the absolute temperature, 297°K, and Curie's law behavior being assumed.

RESULTS

Chromium (II) acetate monohydrate.—Water: $\Delta w = -9.4$. Slurry of 4.07 g $Cr(OOCCH_3)_2 \cdot H_2O$ and 8.20 g H_2O in a volume of 11.98 ml (covered by thin layer of petroleum ether to exclude air): $\Delta w = -6.2$, $\chi_{molal} = 94\times10^{-6}$; calculated for no unpaired electrons, $\Delta w = -8.4$, $\chi_{molal} = -85\times10^{-6}$; calculated for 2 unpaired electrons, $\Delta w = +70.6$, $\chi_{molal} = 2700\times10^{-6}$. Conclusion: no unpaired electrons.

Chromium (II) acetate.—Water: $\Delta w = -8.9$. 3.28 g solid $Cr(OOCCH_3)_2$ under N_2, apparent density 0.55 g/ml: $\Delta w = +15.5$, $\chi_{molal} = 430\times10^{-6}$; calculated for no unpaired electrons, $\Delta w = -2.9$, $\chi_{molal} = -80\times10^{-6}$; calculated for 2 unpaired electrons, $\Delta w = +130$, $\chi_{molal} = 3600\times10^{-6}$. The slight paramagnetism indicated here was believed to be due to partial oxidation to Cr (III). To check this assumption the $Cr(OOCCH_3)_2$ was reconverted to the monohydrate by opening the N_2-filled susceptibility tube under fresh-boiled, N_2-saturated distilled H_2O and allowing 9.22 g H_2O to enter the tube. The resulting red slurry was then measured, giving the following results. Water: $\Delta w = -9.4$. Slurry: $\Delta w = +5.8$, $\chi_{molal} = 570\times10^{-6}$. Inasmuch as the red monohydrate was shown to be diamagnetic the slight paramagnetism remaining must be due to oxidation to Cr (III). The presence of 3 percent Cr (III) in the sample would account for the results, if one assumes the Cr (III) to be present as Cr_2O_3. Conclusion: no unpaired electrons.

Tris(8-hydroxyquinoline) chromium (III).—Water: $\Delta w = -9.1$. 5.61 g $Cr(C_9H_6ON)_3$, apparent density 0.42 g/ml: $\Delta w = +73.4$, $\mu = 4.18$; spin moment calculated for 2 unpaired electrons is 2.83; for three, 3.88; for four, 4.90. Conclusion: three unpaired electrons.

"Tris(8-hydroxyquinoline) chromium (II)".—Water: $\Delta w = -9.1$. 7.76 g compound, apparent density 0.58 g/ml: $\Delta w = +82.7$, $\mu = 4.08$. Conclusion: compound contains three unpaired electrons.

DISCUSSION

The observation that $Cr(OOCCH_3)_2$ contains no unpaired electrons eliminates ionic bonding with the

[5] E. T. Austin, Analyst **63**, 710 (1938).
[6] L. G. Gouy, Comptes Rendus **109**, 935 (1889).
[7] H. Auer, Ann. d. Physik **18**, 593 (1933).
[8] P. W. Selwood, *Magnetochemistry* (Interscience Publishers, Inc., New York, 1943), p. 51.
[9] J. H. Van Vleck, *Electric and Magnetic Susceptibilities* (Oxford University Press, London, 1932), p. 228.

chromium as Cr^{++} (4 unpaired electrons) and shows that three $3d$ oribitals of the chromium atom are involved in the formation of covalent bonds. The chromium atom is presumably attached by essentially covalent bonds to four acetate oxygen atoms. Kimball[10] has given two stable configurations for a tetracovalent atom making use of three d orbitals, namely, d^3s and d^3p. The former is tetrahedral and the latter is an irregular tetrahedron. Although the magnetic evidence does not distinguish between these two possible configurations, it seems likely that the former may be favored. All other chromium (II) compounds which have been studied[3] magnetically previously appear to contain either 2 or 4 unpaired electrons per Cr, corresponding to octahedral covalent bonding or ionic bonding, respectively.

[10] G. E. Kimball, J. Chem. Phys. **8**, 188 (1940).

The experimental result that the "tris(8-hydroxyquinoline) chromium (II)" reported by Hume and Stone[3] and tris(8-hydroxyquinoline) chromium (III) gave, within the estimated experimental uncertainty of 3 percent, the same magnetic moment for Cr in addition to the same color and empirical formula indicates that these compounds are actually the same, and that the Cr is in the tripositive oxidation state. It seems likely that the 8-hydroxyquinoline oxidizes the Cr (II) during the course of the preparation, although attempts to find the tetrahydro-8-hydroxyquinoline which might be anticipated as a reduction product in our preparation of the reported compound failed, apparently due to difficulties of separation arising from complexing of the reduction product with the Cr (III).

THE JOURNAL OF CHEMICAL PHYSICS VOLUME 18, NUMBER 5 MAY, 1950

The Asymmetric Rotor. VIII. The Hydrogen Sulfide Band at 6300 Cm^{-1}*

HARRY C. ALLEN, JR.** AND PAUL C. CROSS**
Metcalf Research Laboratory, Brown University, Providence, Rhode Island
AND
M. K. WILSON***
California Institute of Technology, Pasadena, California
(Received January 23, 1950)

The absorption spectrum of hydrogen sulfide in the region 6140 to 6420 cm^{-1} has been measured and the rotational fine structure analyzed through the use of published energy tables for the rigid rotor and a classical correction for centrifugal distortion. The excited state constants giving the best fit are $A^*=10.39$, $B^*=8.90$, and $C^*=4.55$ cm^{-1}. The band center is located at 6289.5 cm^{-1}.

The value of $I_C-I_A-I_B$ and the strong Q branch, indicating the non-vanishing electric moment derivative to be along the least inertial axis, show the upper vibrational level to be the (111) state.

INTRODUCTION

At the present time the detailed rotational analysis of only one highly resolved absorption band of hydrogen sulfide has been published. This is the $(n_s,n_\pi,n_\delta)=(130)$ band at 9911 cm^{-1}.[1,2] Hainer and King[3] have analyzed by punched card methods the band envelope at 3.7μ as one-half of the ν_σ-fundamental. Recently Grady, Cross, and King[4] have reported the analysis of two overlapping bands believed to be the (310) at 10194 cm^{-1} and the (400) at 10188 cm^{-1}. Up to this time no rotational analysis has been made of a band involving the δ-mode of vibration. This paper will present a rotational analysis of a band envelope at 1.6μ believed to be the (111) band.

EXPERIMENTAL

Tank hydrogen sulfide (Ohio Chemical and Manufacturing Company) was twice distilled over phosphorous pentoxide and was immediately used for the spectroscopic investigation. Adequate absorption was obtained with a path-length of 106 cm and a pressure of one atmosphere.

This region was investigated with an automatic recording, one meter vacuum spectrograph which was recently described by Badger, Zumwalt, and Giguère.[5]

The spectrum was taken in the first order of a replica grating with 7500 lines per inch, using a lead sulfide cell as the photosensitive element and a slit width of 0.05 mm, corresponding to 0.85 cm^{-1} at 2μ.

The band shows well-defined P and R branches.

* Based on a thesis submitted by Harry C. Allen, Jr. in partial fulfillment of the requirements for the Master of Science degree at Brown University. The work reported herein was supported in part by the Office of Naval Research under Contract N6ori-88, T. O. 1.
** Now at the University of Washington, Seattle, Washington.
*** Now at Harvard University, Cambridge, Massachusetts.
[1] P. C. Cross, Phys. Rev. **47**, 7 (1935).
[2] B. L. Crawford, Jr. and P. C. Cross, J. Chem. Phys. **5**, 371 (1937).
[3] R. M. Hainer and G. W. King, J. Chem. Phys. **15**, 89 (1947).
[4] Grady, Cross, and King, Phys. Rev. **75**, 1450 (1949).
[5] Badger, Zumwalt, and Giguère, Rev. Sci. Inst. **19**, 861 (1948).

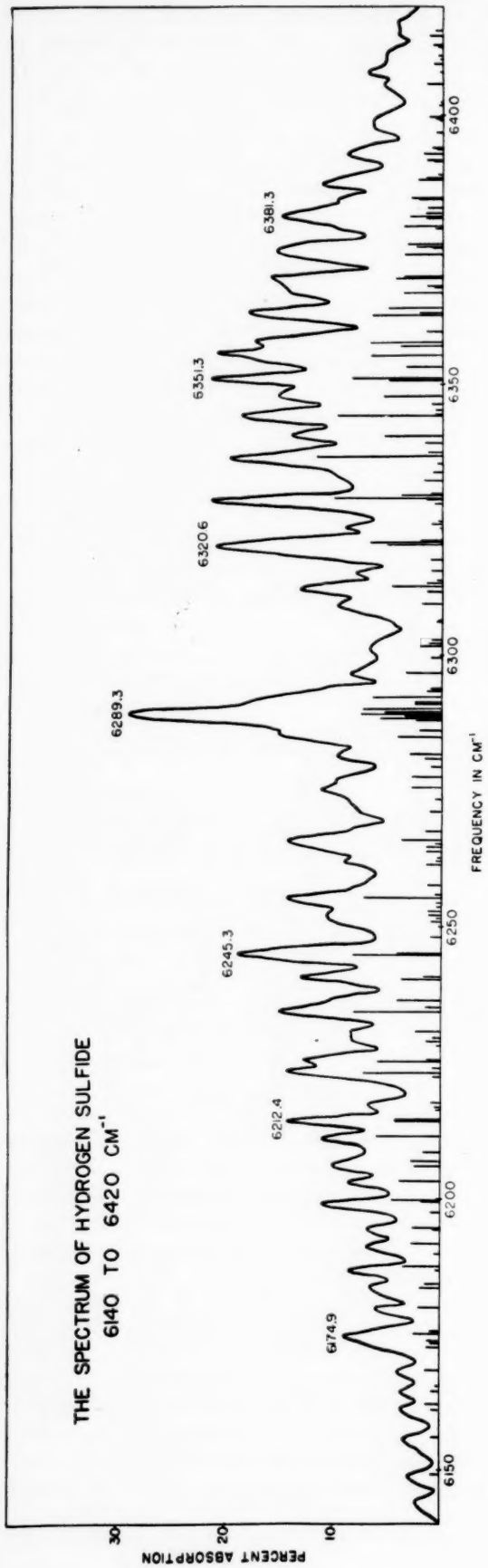

FIG. 1. Calculated and observed band at 6289.5 cm^{-1}.

There is an extremely strong absorption located near the center of the band which suggests a collected Q branch. The experimental resolution seems to be of the order of 2 cm^{-1}.

VIBRATIONAL ASSIGNMENT

The absorption band at 1.6μ corresponds to an energy range for which there are six possible vibrational assignments. Dennison[6] has shown that as $\rho=B/A$ becomes smaller, the Q branch of type A bands tends to collect at the center. On the other hand, there is a gap at the center of a type B band regardless of the value of ρ. It was thus concluded that this band was an A type band, i.e., the electric moment oscillates along the least inertial axis. Hence this axis is perpendicular to the symmetry axis, n_σ must be odd and this leaves only two possibilities for the vibrational assignment, (111) and (103). Arguments relating to the relative intensities, to the dependence of the moments of inertia on n_δ, and especially to the value of $\Delta=I_C-I_A-I_B$ indicate a strong preference for the former. The rotational analysis, however, is independent of the vibrational assignment except for the effect of the symmetry of the excited vibrational state on the selection rules.

ANALYSIS

The resolution was not adequate to enable an assignment of specific transitions through the use of the known ground state energies as published with the analysis of the 9911 cm^{-1} band.[1] Hence the stochastic procedure of analysis was used.

The energy levels corresponding to an assumed set of inertial parameters for the excited state were readily derived from published tables.[7]

To obtain the relative intensities of the individual lines in the band, it was necessary to combine the published line strengths[8] with appropriate Boltzmann factors determined from the known ground state. These excited state energies, the known ground state energies, and the relative line intensities were then used to synthesize a computed spectrum for comparison with the experimental spectrum.

An initial estimate of the excited state inertial constants was required. The strong transitions in the P and R branches are strongly dependent on C^*, while they are practically independent of A^* and B^*. Since the slight convergence of the R branch indicates that C^* is slightly less than $C=4.732$ cm^{-1}, the value $C^*=4.60$ cm^{-1} was used for the first approximation.

The strong transitions of the Q region are very sensitive to A^*, being practically independent of B^* and C^*, hence the very sharp collected Q branch requires that A^* be nearly equal to A (10.37 cm^{-1}).

[6] D. M. Dennison, Rev. Mod. Phys. **3**, 280 (1931).
[7] King, Hainer, and Cross, J. Chem. Phys. **11**, 27 (1943).
[8] Cross, Hainer, and King, J. Chem. Phys. **12**, 210 (1944).

The transitions involving levels of intermediate energy or τ-values are primarily dependent on B^* although they are more sensitive to the other inertial parameters, A^* and C^*, than was true in the previous cases. This dependence can be seen by consulting the table of derivatives previously published.[1] The initial estimates of B^* were selected such that κ assumed the values of 0.5, 0.4$\cdots$etc.

The derivative of the transition energies with respect to the inertial constants furnished the means by which these constants could be ascertained accurately with a minimum of calculation. The various inertial constants were readjusted by fitting the transitions most sensitive to each constant until a satisfactory calculated representation of the experimental data was obtained.

To maintain consistency with the original ground state energies, a classical centrifugal stretching correction was applied to the term values of the energy levels.[1,9]

The above procedure allows C^* to be fixed very closely. A^* was fixed by integrating the Q region over a finite slit width as described by Hainer and King.[3] It was possible to vary B^* over a considerable range without materially affecting the picture; hence, it is the least accurate of the constants.

Approximately 300 transitions were calculated. These are plotted along with the observed spectrum in Fig. 1. Transitions of less than 1.0 in arbitrary intensity units were omitted in the plot unless they contributed materially to the picture. In these units the maximum line intensity is 7.5 and the number of lines with intensity greater than 1.0 is 150. In evaluating the calculated spectrum the effect of an integration of the intensities over a finite slit width must be borne in mind. Figure 1 shows the detail to which the calculated spectrum reproduces the observed absorption.

The excited state constants giving the best fit for the observed spectrum are

$$A^*=10.39\pm0.02 \quad B^*=8.90\pm0.04 \quad C^*=4.55\pm0.01$$
$$\nu_0=6289.5\pm0.5 \text{ cm}^{-1}.$$

DISCUSSION

Mecke[10] first showed that for water vapor the effective moments of inertia did not satisfy the condition $I_A+I_B=I_C$ which applies to rigid planar bodies. Darling and Dennison[11] have introduced the parameter $\Delta=I_C-I_A-I_B$ in their treatment of the water vapor band system. They have given an expression for Δ of the following form:

$$\Delta=k_\delta(n_\delta+\tfrac{1}{2})+k_\sigma(n_\sigma+\tfrac{1}{2})$$

which makes use of its near-zero dependence on n_τ. Hainer and King[3] point out that this should still be true in the case of hydrogen sulfide, and that $k_\delta \gg k_\sigma$. The form of this expression shows that the Δ for the (111) state should be three times the value of the (000) state. The results

$$(000) \quad k_\delta/2+k_\sigma/2=0.103\times10^{-40} \text{ g cm}^2$$
$$(111) \quad 3k_\delta/2+3k_\sigma/2=0.32$$

confirm this prediction. If n_δ were greater than one in the excited state, one would reasonably expect an even larger Δ. This evidence leaves little doubt that this is the (111) state.

The authors wish to express their appreciation to Professor R. M. Badger for the use of his spectrograph and to Mr. Thomas Hutton for his aid in carrying out the numerous calculations.

[9] This correction is readily evaluated for individual energy levels and hence has some advantage over methods which involve Nedius calculations.

[10] R. Mecke *et al.*, Zeits. f. Physik **81**, 313, 445, 465 (1933).
[11] B. T. Darling and D. M. Dennison, Phys. Rev. **57**, 128 (1940).

The Infra-Red Spectrum of $N^{15}N^{14}O$ and the Force Constants of Nitrous Oxide*

W. S. Richardson and E. Bright Wilson, Jr.
Mallinckrodt Chemical Laboratory, Harvard University, Cambridge, Massachusetts
(Received December 27, 1949)

The infra-red spectrum of $N^{15}N^{14}O$ has been studied. The observed bands together with those already known for $N^{14}N^{14}O$ provide sufficient data to calculate a reasonable set of force constants for the nitrous oxide molecule. The zeroth-order stretching frequencies for $N^{15}N^{14}O$ and the force constants derived from them are also calculated. In the observed frequency approximation the N—N, N—O and interaction constants have been assigned the values 17.9, 11.4, and 1.4×10^5 dynes/cm, respectively. These values are consistent with the picture that N_2O is a resonance hybrid of the two (principal) structures $\bar{N}=\overset{+}{N}=O$ and $N\equiv\overset{+}{N}-\bar{O}$.

I. INTRODUCTION

THE infra-red spectrum of nitrous oxide has been studied in considerable detail by Plyler and Barker.[1] Using a grating instrument they established the origins of the stretching vibrations ν_1 and ν_3 to be at 1285.4 cm^{-1} and 2224.1 cm^{-1} respectively. These two values should be sufficient to establish the values of the principle stretching force constants if the cross term in the most general quadratic potential function is neglected. However, this calculation leads to imaginary force constants. If slight adjustments in the frequencies are made so that the force constants become real, the values obtained are unsatisfactory.

The investigation of the spectrum of an isotopic modification of the molecule provides a means of obtaining an additional datum from which the interaction constant, f_{12}, in the potential function

$$2V=f_1\Delta r_1^2+f_2\Delta r_2^2+2f_{12}\Delta r_1\Delta r_2 \qquad (1)$$

may be determined. With this end in view the spectrum of $N^{15}N^{14}O$ has been obtained.

II. EXPERIMENTAL

Ammonium nitrate[2] containing 63 atom percent of N^{15} in the ammonium ion and normal abundance of N^{15} in the nitrate ion was subjected to pyrolysis and the evolved N_2O trapped with liquid air. An investigation of the microwave spectrum of the product showed it to be a mixture of $N^{15}N^{14}O$ and $N^{14}N^{14}O$. The species $N^{15}N^{15}O$ and $N^{14}N^{15}O$ were present only to the extent expected from normal abundance of N^{15} at the central nitrogen position.

The isotope effect on the 2224 cm^{-1} band (ν_3) was observed with a Perkin-Elmer spectrograph (slightly modified) at Brown University. A CaF_2 prism was used. The sample, at a total pressure of the isotopic mixture of 6 cm of Hg, was contained in a 5 cm cell equipped with NaCl windows. The bands for the two isotopic species showed some overlap, but this was readily corrected by subtracting out the absorption of a sample of normal N_2O at a pressure equivalent to its partial pressure in the mixture. The 1285 cm^{-1} band was observed with a Baird Associates, Inc., Model B (NaCl prism) infra-red recording spectrophotometer. Again the bands of the two species overlapped quite seriously, but this was overcome by running a sample of normal N_2O in the comparison beam of the spectrograph. The pressure of N_2O in the comparison beam was adjusted to be equivalent to its partial pressure in the mixture, the resultant spectrum being only that of $N^{15}N^{14}O$. By working at relatively low total absorption of the mixture, the sensitivity of the spectrograph was not seriously impaired by the absorption of $N^{14}N^{14}O$. The spectra were taken by a point by point technique, rather than by continuous recording, resulting in a slight enhancement of the sensitivity and resolution.

The isotope effect on the bending mode (ν_2) was not investigated.

III. RESULTS

The observed infra-red bands, together with the isotopic shifts and the frequencies recalculated from the force constants obtained below, are collected in Table I. The values given for $N^{14}N^{14}O$ are those of Plyler and Barker[1] which were also used as wave-length calibration points for the $N^{15}N^{14}O$ bands.

The Teller-Redlich product rule[3] provides a check on the observed isotopic shifts. For these two modes it takes the form:

$$\frac{\omega_1\omega_3}{\omega_1^i\omega_3^i}=\left(\frac{M}{M^i}\cdot\frac{m^i}{m}\right)^{\frac{1}{2}}=1.0235 \qquad (2)$$

$$(\nu_1\nu_3)/(\nu_1^i\nu_3^i)=1.024. \qquad (3)$$

The agreement is seen to be very good with the observed frequencies (ν), although the product rule applies rigorously only to the zeroth-order frequencies

* The research reported in the following paper was made possible by funds extended Harvard University by the ONR under ONR Contract N5ori-76, Task Order V.

[1] E. K. Plyler and E. F. Barker, Phys. Rev. **38**, 1827 (1931).

[2] Eastman Kodak Company, Rochester, New York.

[3] See for instance G. Herzberg, *Infra-Red and Raman Spectra of Polyatomic Molecules* (D. Van Nostrand Company, Inc., New York, 1945), p. 231.

TABLE I. Observed and calculated frequencies for $N^{14}N^{14}O$ and $N^{15}N^{14}O$.

Designation	$N^{14}N^{14}O$ obs.[a]	Freq. (cm^{-1}, vac) calc.[b]	$N^{15}N^{14}O$ obs.	Freq. (cm^{-1}, vac) calc.[b]	$\Delta\nu$ (cm^{-1}) obs.
ν_1	1285.0	1284.3	1267.5	1267.9	17.5
ν_3	2223.5	2224.0	2201.0	2200.7	22.5

[a] See reference 1.
[b] Calculated from force constants in Eq. (6).

(ω). The ratio for the zeroth-order frequencies obtained below is 1.025.

IV. FORCE CONSTANTS FROM THE OBSERVED FREQUENCIES

Solution of the vibrational secular equation for a linear XYZ molecule using the potential energy as given by Eq. (1) gives the following pair of equations for the stretching force constants in terms of the zeroth-order normal frequencies.

$$\lambda_1+\lambda_3=(\mu_x+\mu_y)f_1+(\mu_y+\mu_z)f_2-2\mu_y f_{12}, \quad (4)$$

$$\lambda_1\lambda_3=(\mu_x\mu_y+\mu_x\mu_z+\mu_y\mu_z)(f_1f_2-f_{12}^2), \quad (5)$$

where μ is the reciprocal of the mass of the atom in question and $\lambda=4\pi^2\omega^2$. Substitution of the observed frequencies (ν) for the two isotopic species gives three equations from which f_1, f_2, and f_{12} may be determined (the two forms of Eq. (5) are redundant in the product rule). The resulting values are, in units of 10^5 dynes/cm

$$\begin{aligned} &\text{N}-\text{N bond} \quad f_1=17.88,\\ &\text{N}-\text{O bond} \quad f_2=11.39,\\ &\qquad\qquad f_{12}=1.36. \end{aligned} \quad (6)$$

V. ZEROTH-ORDER FREQUENCIES

By observation of a sufficient number of combination and overtone bands for $N^{14}N^{14}O$, the zeroth-order frequencies have been calculated. They are $\omega_1=1299.8$ cm^{-1} and $\omega_3=2276.5$ cm^{-1} (reduced to vacuum).[4] Following Dennison[5] we may write

$$\omega_j=\nu_j(1+\alpha_j), \quad (7)$$

$$\omega_j{}^i\cong\nu_j{}^i[1+\alpha_j(\nu_j{}^i/\nu_j)], \quad (8)$$

in order to estimate the jth zeroth-order frequency for $N^{15}N^{14}O$. The resulting frequencies are given in Table II.

If these zeroth-order frequencies are used in Eqs. (4) and (5) to compute the force constants, we find, in units of 10^5 dynes/cm:

$$\begin{aligned} &\text{N}-\text{N bond} \quad f_1=18.98,\\ &\text{N}-\text{O bond} \quad f_2=11.50,\\ &\qquad\qquad f_{12}=1.43. \end{aligned} \quad (9)$$

VI. ERRORS

Because of the high resolving power of the grating spectrograph used by Plyler and Barker[1] on $N^{14}N^{14}O$ the band origins for this molecule are probably accurate to 0.1 cm^{-1} as given in Table I. However, the relatively lower resolving power of the prism instruments used to measure the isotopic shifts makes it necessary to consider the effect of possible errors in the location of band origins of $N^{15}N^{14}O$ on the values of the force constants. For the purposes of calculations the frequencies were rounded off at the nearest cm^{-1}, but errors of the order of 2 to 3 cm^{-1} are possible. To examine the effect of errors of this type on the force constants, let us consider that each of the shifts is in error by 2 cm^{-1}. If both shifts were too large or too small by this amount, serious deviation from the product rule would result. However, if one were too large and the other too small, the product rule would still show a good fit. If this latter condition prevails, the interaction force constant may be in error by as much as $\pm0.3\times10^5$ dynes/cm and the principle force constants, f_1 and f_2, by as much as ±0.7 and $\pm0.3\times10^5$ dynes/cm, respectively.

TABLE II. Zeroth-order frequencies for $N^{14}N^{14}O$ and $N^{15}N^{14}O$.

Designation	$N^{14}N^{14}O$ obs.[a]	Freq. (cm^{-1}, vac) calc.[b]	$N^{15}N^{14}O$ obs.[c]	Freq. (cm^{-1}, vac) calc.[b]
ω_1	1299.8	1298.8	1281.9	1283.0
ω_3	2276.5	2277.1	2252.9	2252.3

[a] See reference 3, page 278.
[b] Calculated from force constants in Eq. (9).
[c] Calculated from Eqs. (7) and (8).

VII. DISCUSSION

If the most important resonating structures which describe the state of the N_2O molecule are

$$\text{N}\equiv\overset{+}{\text{N}}-\bar{\text{O}} \quad (a)$$

and

$$\bar{\text{N}}=\overset{+}{\text{N}}=\text{O}, \quad (b)$$

we may expect the principle force constants to reflect the (roughly) $2\frac{1}{2}$-fold order of the N—N bond and the $1\frac{1}{2}$-fold order of the N—O bond. It is clear that the new values obtained above indicate this property, while the older values[6] for $N^{14}N^{14}O$ neglecting the interaction constant ($f_1=14.6$ and $f_2=13.7\times10^5$ dynes/cm) do not. These two structures also point to a positive interaction constant, since the force required to stretch the N—N bond by Δr_1 is $f_1\Delta r_1+f_{12}\Delta r_2$ so that a positive interaction constant implies a stiffening of N—N as N—O is stretched, in accord with the resonance picture.

In using the isotopic shifts to obtain f_{12} for a linear triatomic molecule, considerable care must be exercised. It may be that quite small errors ($\sim$1 to 2 cm^{-1}) in measurement of the shifts will lead to large variations in the value of f_{12} and in the values of the principle force constants. While this condition is not too serious in N_2O as noted above, it becomes prohibitive in the pair $ClC^{12}N-ClC^{13}N$ where an error of 2 cm^{-1} in the

[4] See reference 3, page 278.
[5] D. M. Dennison, Rev. Mod. Phys. 12, 175 (1940).
[6] Reference 3, p. 174.

shifts (still consistent with the product rule) leads to an error of $\pm 1\times 10^5$ dynes/cm in f_{12}.[7]

In general the above calculations tend to emphasize two important points.

1. The numerical value of the bond stretching force constants of a molecule may be very sensitive to the value of cross terms in the potential energy function which are normally considered small and often neglected. Therefore, in comparing the value of a given bond force constant in a series of analogous molecules, care must be taken either to evaluate the cross terms or to investigate the effect of reasonable values for them on the force constant in question. These latter effects must be considered in the light of possible errors in the value of the force constant in question.

2. Small, but significant, changes in the force constants occur when the observed frequencies are corrected to the zeroth-order frequencies. Thus small changes in the value of a given force constant through a series of compounds may not be significant if the anharmonicities involved are not comparable (for instance in comparing the force constants of a molecule containing hydrogen with those of one that does not).

[7] W. S. Richardson and E. Bright Wilson, Jr., J. Chem. Phys. **18**, 155 (1950).

VIII. ACKNOWLEDGMENT

The authors wish to express their gratitude to Dr. D. F. Hornig of Brown University for permission to use the Perkin-Elmer spectrograph and to Dr. E. Nixon and Mr. J. Thomas for assistance in obtaining the spectra. We also wish to thank Mr. K. McAfee who ran the microwave analysis of the enriched N_2O sample.

THE JOURNAL OF CHEMICAL PHYSICS VOLUME 18, NUMBER 5 MAY, 1950

A Theoretical Basis for the Antoine Vapor Pressure Equation

F. GUTMANN AND L. M. SIMMONS
The New South Wales University of Technology, Sydney, Australia
(Received December 27, 1949)

The Antoine vapor pressure equation $\log p = A - B/(t+C)$ is theoretically derived from van der Waals equation and the energy of an assembly of Einstein oscillators. The values of the Antoine parameter C are shown to be related to the characteristic frequency of the liquid. The values of this parameter obtained from vapor pressure data are shown to agree with those calculated from viscosity and from the velocity of propagation of sound.

FOR want of an accurate vapor pressure equation with a satisfactory theoretical background, many frankly empirical vapor pressure equations have been proposed. Among these, that of C. Antoine[1] is outstanding in simplicity and in the precision with which it represents the experimental data. It is generally written thus:

$$\log p = A - B/(t+C)\cdots, \qquad (1)$$

where p is the vapor pressure of a liquid at t°C, and A, B, and C are empirically determined constants for the liquid.

In 1946 G. W. Thomson[2] reviewed the applicability of this equation and concluded that it is entirely adequate for data of all but the very highest precision, from the triple point up to a reduced temperature of 0.75, and that two Antoine equations, one up to a reduced temperature of 0.75, the other from that temperature to the critical temperature, are much more convenient to use and fully as accurate as the best empirical equations which have been designed to fit the entire liquid range. The simplicity and precision of the Antoine equation has led to its increasing use to express vapor pressure data in recent years, particularly in view of the fact that it can be used to calculate the heat of vaporization quite precisely.[3]

The Antoine equation has hitherto completely lacked theoretical significance, and it is the purpose of the present communication to provide such a theoretical basis.

In 1912, by regarding a solid as an assembly of Einstein resonators, P. Debye[4] expressed the thermal energy of a solid as a function of the absolute temperature, $\phi(T)$. In the following year this treatment was extended to van der Waals gases and liquids by H. Tetrode,[5] who wrote van der Waals equation in the following form:

$$(p+a/v^2)(v-b) = \frac{3N}{\gamma_M{}^3}\int_0^{\gamma_M} \frac{h\gamma}{e^{h\gamma/kT}-1}\gamma^2 d\gamma\cdots, \qquad (2)$$

where γ is the frequency of a possible mode of vibration and γ_M the highest value thereof. Equation (2) differs

[1] C. Antoine, Comptes Rendus **107**, 681, 836, 1143 (1888).
[2] G. W. Thomson, Chem. Rev. **38**, 1 (1946).
[3] G. W. Thomson, Chem. Rev. **38**, 33 (1946).
[4] P. Debye, Ann. d. Physik **IV-39**, 789 (1912).
[5] H. Tetrode, Physik. Zeits. **14**, 212 (1913).

from the original van der Waals equation of state in that it expresses the thermal energy of a liquid in terms of the vibrational energy possessed by an assembly of Einstein oscillators.

In 1913 there seemed to be little justification for this application to liquids of the reasoning used by Debye for a crystalline solid. The quasi-crystalline structure of liquids has since been thoroughly established by G. W. Stewart[6] and others, and still more recently C. E. Waring and P. Becher[7] have calculated reaction constants by regarding a liquid as a quasi-crystalline lattice of Einstein oscillators. It therefore seems opportune to develop Tetrode's modification of van der Waals equation.

While the integral in Eq. (2) cannot be solved in a closed form, Debye[4] has used a solution for it in the form of a series (Eq. (3)). This he does by developing $(e^{h\gamma/kT}-1)^{-1}$ into a series involving Bernoulli numbers B_n which converges when the variable of integration is $<2\pi$. Writing ξ for $h\gamma/kT$:

$$(e^{\xi}-1)^{-1}=\frac{1}{\xi}-[\tfrac{1}{2}]+\xi\sum_{1}^{\infty}(-1)^{n-1}\frac{B_n}{(2n)!}\xi^{2n-1}. \quad (3)$$

Equating the energy $h\gamma_M$ of the highest possible vibrational frequency to an equivalent characteristic temperature $k\theta_0$, the integrated form of Eq. (2) is:

$$(p+a/v^2)(v-b)=RT-\tfrac{3}{8}R\theta_0+\frac{RT\theta_0^2}{20T^2}-\frac{RT\theta_0^4}{1680T^4}+\cdots. \quad (4)$$

In 1948 F. T. Wall[8] showed that the van der Waals equation leads to the well-known "$1/T$" form of vapor pressure equation

$$\ln p=A'-B'/T, \quad (5)$$

where p is the vapor pressure of a liquid at T°K, and A' and B' are constants for the liquid and are related to its van der Waals constants. However, it is known that this $1/T$ form of vapor pressure equation is inadequate for expressing experimental data except over very limited temperature ranges, this being evidenced by the bowing of the plots of $\ln p$ *versus* $1/T$.

Applying to the integrated form of Tetrode's equation of state (4) reasoning which is analogous to that used by Wall, the latter's approximation for the volume of a van der Waals liquid then becomes:

$$v=b+[b^2\phi(T)/a]+[2b^3\phi^2(T)/a^2]-[b^4\phi(T)p/a^2]+\cdots, \quad (6)$$

where $\phi(T)$ stands for the right-hand side of Eq. (4). Since $\phi(T)$ is not larger than RT, the series in Eq. (6) will converge at least as rapidly as Wall's original series.

Furthermore, Wall's Eq. (2) for the fugacity of a van der Waals liquid now becomes:

$$\ln f=\frac{b}{v-b}-\frac{2a}{v\phi(T)}+\ln\frac{\phi(T)}{v-b}\cdots \quad (7)$$

Continuing with Wall's treatment by assuming that the fugacity f equals the vapor pressure, p, his Eq. (7) then becomes:

$$\ln p=A-B/\phi(T)\cdots. \quad (8)$$

If only the first term of the series for $\phi(T)$ is retained, then Eq. (8) reduces to the $1/T$ form of vapor pressure equation. A better approximation is obtained by retaining also the second term, whereupon Eq. (8) becomes identical in form with the Antoine vapor pressure equation. Little advantage can be expected by retaining still more terms because for all practical values of T the series rapidly converges.

In Eq. (1) the Antoine constant C can thus be identified with $273.16-\frac{3}{8}\theta_0$ and should therefore be calculable from the maximum vibrational frequency γ_M. This quantity has been computed for a number of liquids by Waring and Becher[7] from viscosity data and also from the velocity of propagation of sound. When thus calculated for those organic liquids tabulated by Waring and Becher, C is found to lie between 234 and 254.5. Thomson[9] states that for data of moderate precision, $C=230$ appears to be a suitable average value for most organic compounds boiling between 0 and 150°C, in agreement with the values obtained with the aid of the present theory.

[6] G. W. Stewart, Phys. Rev. **35**, 296, 726 (1930) and later publications.
[7] C. E. Waring and P. Becher, J. Chem. Phys. **15**, 488 (1947).
[8] F. T. Wall, J. Chem. Phys. **16**, 508 (1948).
[9] See reference 3, p. 30.

The Infra-Red Absorption Spectrum of Diborane

W. E. ANDERSON* AND E. F. BARKER
Randall Laboratory of Physics, University of Michigan, Ann Arbor, Michigan
(Received January 3, 1950)

The infra-red absorption spectrum of diborane has been examined under high resolution from 3.7μ to 30μ with automatic recording grating spectrometers. The rotational fine structure in two bands of each of the three types characteristic of asymmetric top molecules has been measured. All results and observations are consistent with the conclusion that diborane has the bridge structure, and belongs to the same symmetry point group, V_h, as ethylene. The observation and structure of the band with center at 368.7 cm^{-1} provides spectroscopic evidence that the molecule is non-planar, and makes more definite the assignment of fundamental frequencies. Data on all bands fit quite well the symmetric top approximation, since accidentally two principal moments of inertia are approximately the same, and calculations yield accurate values for certain rotational constants.

INTRODUCTION

DIBORANE is a so-called "electron deficient" molecule for which the structure has been under discussion for a long time. Stitt[1] made a study of the infra-red spectrum from 1.7μ to 25μ with a prism spectrometer, and attempted to explain the results on the basis of an ethane-type structure. Bell and Longuet-Higgins[2] gave a normal coordinate treatment for the bridge model, and made an identification of the absorption bands observed by Stitt with the normal vibrations. Price[3] re-examined the infra-red absorption spectrum using a prism spectrometer capable of resolving some of the rotational fine structure of two bands. His results indicate decisively that the bridge model, symmetry point group V_h, is favored over the ethane-type structure, symmetry point group D_{3d} or D_{3h}.

Examination of the infra-red absorption spectrum has now been made from 3.7μ to 30μ with high resolution grating spectrometers. The rotational fine structures of six bands have been resolved; fundamental frequencies can now be assigned more definitely, and certain rotational constants determined.

EXPERIMENTAL

The sample of diborane was prepared in the Chemistry Department of the University of Chicago. During the course of the investigation it was purified several times by fractionation and distillation. The appreciable quantity of ethane detected in the sample was not removed because of the difficulty of the separation and the fact that the strong bands of ethane and diborane do not overlap.

The principal instrument used was the grating spectrometer with potassium bromide foreprism originally described by Hardy,[4] but modified in this study for automatic recording. The radiation beam from a Nernst glower was chopped with a period of about eight seconds, and received on a single-junction thermocouple of the usual Michigan design. The Firestone-type amplifier[5] was followed by several stages of electronic amplification, diode rectifiers, and *RC* filters so that only the envelope of the individual rotational lines was traced by the Speedomax recorder. With the exception of Fig. 5, photographs of band records shown were taken directly from charts made by the recorder pen on tracing paper. The design of the Firestone amplifier and the electronic amplifying system involved circuits with long time constants, and accordingly required slow rotation of gratings, but precluded drifts from temperature changes and other common causes.

The grating-instrument constants for the fine gratings were determined from records made in several orders of 1.014μ line of mercury or the 1.083μ line of helium. For the coarse gratings, secondary standard lines in the absorption spectra of atmospheric CO_2 near 14.7μ and H_2O vapor near 6.0μ were used, the positions of these lines having been very accurately measured in this laboratory.[6]

To observe the diborane absorption band in the region from 22.5μ to 30μ, it was necessary to use the long wave-length vacuum spectrograph of large aperture developed by Randall and Firestone.[7] In this instrument which uses photographic recording, overlapping of higher orders of short wave-lengths was prevented by using a NaCl shutter, paraffin wax filter and one reflection from a CaF_2 plate. The energy available in the region from 27μ to 30μ is greatly reduced by the poor transmission of materials mechanically strong enough to serve as cell windows, which must withstand atmospheric pressure in the arrangement employed. The cell used in this instrument was of silverplated brass, 10 cm long, with silver chloride windows 1 mm thick, one of which had to be about 15 by 10 centimeters to prevent serious limitation of the radiation beam behind the exit slit where it was mounted. The instability of diborane requires that it be kept in a vessel which

* Present address: The Citadel, Charleston, South Carolina.
[1] F. Stitt, J. Chem. Phys. **9**, 780 (1941).
[2] R. P. Bell and H. C. Longuet-Higgins, Proc. Roy. Soc. **183A**, 357 (1945).
[3] W. C. Price, J. Chem. Phys. **16**, 894 (1948).
[4] J. D. Hardy, Phys. Rev. **38**, 2162 (1931).
[5] F. A. Firestone, Rev. Sci. Inst. **3**, 163 (1932).
[6] R. H. Gillete and E. H. Eyster, Phys. Rev. **56**, 1113 (1939).
[7] H. M. Randall and F. A. Firestone, Rev. Sci. Inst. **9**, 40 (1938).

TABLE I. Experimental conditions.

Region microns	Grating or prism	Cell length cm	Slit width cm^{-1}	Gas pressure mm Hg
2.71	Quartz	10	(a)	120
3.83	7200	12	0.58	6
3.83	7200	12	0.72	24
3.97	7200	12	0.67	15
4.26	LiF	10	(a)	196
5.02	7200	12	0.48	456
5.02	4800	12	0.75	560
5.38	7200	12	0.46	74
5.38	LiF	10	(a)	35
6.26	NaCl	10	(a)	6
8.52	2400	12	0.46	20
10.28	2400	12	0.46	75
27.16	1200	12	0.92	46
27.16	900	10	2.22	100

[a] Slit widths continuously varied.

TABLE II. Fundamental frequencies of diborane.*

Species	Band type	Designation Revised	Designation Price**	Frequency cm^{-1}
a_g	R	ν_1		2523
	R	ν_2		2102
	R	ν_3		1180
	R	ν_4		793
a_u	R	ν_5		1013[a]
b_{1g}	R	ν_6	b_{2g} ν_{11}	2591[a]
	R	ν_7	b_{2g} ν_{12}	606[a]
b_{1u}	IR C	ν_8	b_{2u} ν_{13}	1988.0
	IR C	ν_9	b_{2u} ν_{14}	972.7
b_{2g}	R	ν_{10}	b_{1g} ν_6	1321[a]
	R	ν_{11}	b_{1g} ν_7	764[a]
b_{2u}	IR B	ν_{12}	b_{1u} ν_8	2608.6
	IR B	ν_{13}	b_{1u} ν_{10}	1857
	IR B	ν_{14}	b_{1u} ν_9	368.7
b_{3g}	R	ν_{15}		1745[a]
b_{3u}	IR A	ν_{16}		2519.5
	IR A	ν_{17}		1604[b]
	IR A	ν_{18}		1173.8

* R: Raman active; IR: Infra-red active. Raman frequencies from data on liquid diborane (references 12 and 13).
** See reference 3.
[a] From data of Pitzer (reference 13).
[b] From data of Price (reference 3).

can be evacuated to the order of 10^{-4} mm of Hg pressure. Beyond 30μ there was insufficient energy transmitted by the silver chloride to permit consistent measurements even with relatively wide slits and maximum gain of the amplifier used.

The vacuum prism spectrograph described most recently by Oetjen[8] was used to examine the envelope of several bands which are overlapped by strong atmospheric absorptions.

A summary of experimental conditions is given in Table I.

ASSIGNMENT OF FREQUENCIES

The normal vibrations on the bridge model according to Bell and Longuet-Higgins[2] are given in Fig. 1, where the frequency designations shown are those based on the discussion which follows. These designations differ in certain aspects from those given in references 2 and 3. Because of the extensive tables and other material on symmetry point group V_h, and especially on ethylene, given by Herzberg,[9] it has seemed desirable to designate the axes of reference in the molecule in conformity with those adopted for ethylene. This designation of axes requires interchanging subscripts 1 and 2 in the symbols for symmetry species of the normal vibrations as given by Price,[3] and requires renumbering of nine of the eighteen fundamentals to conform to this convention.[10] Either designation is consistent, but because of the almost complete similarity of the spectra, confusion is liable to result if different schemes are used for diborane and ethylene. In consequence of these variations from Price's notation and other changes in assignments, the designations by Price[3] are included in Table II, which summarizes the fundamental frequency assignments. The vacuum correction has been applied to all wave number values.

When observed under high resolution the diborane spectrum reveals three distinct types of bands. These are designated as type A, type B, and type C, depending on the direction of variation of the electric moment along the axis of least, intermediate, or greatest moment of inertia, respectively. Since the well-resolved bands include two of each of these three types characteristic of an asymmetric top molecule, and since an exact counterpart of these bands can be found among the similarly resolved bands of ethylene for those vibrations not essentially involving the bridge hydrogens, the validity of the bridge structure seems definitely estab-

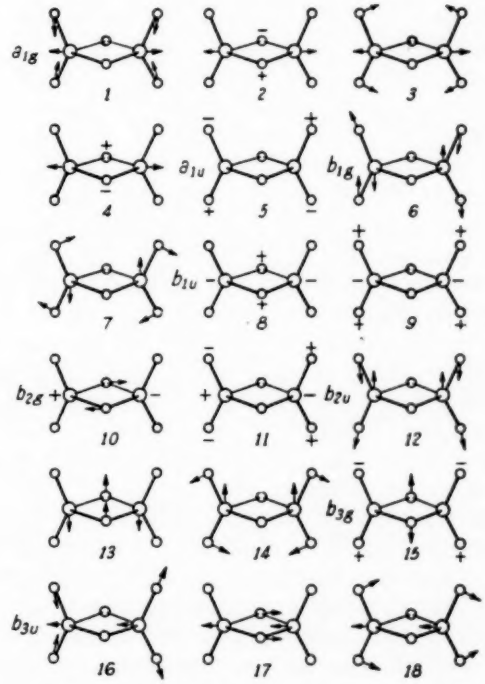

FIG. 1. Normal vibrations of diborane, B_2H_6. (Bell and Longuet-Higgins, reference 2.)

[8] Oetjen, Kao, and Randall, Rev. Sci. Inst. **13**, 515 (1942).
[9] G. Herzberg, *Infrared and Raman Spectra* (D. Van Nostrand Company, Inc., New York, 1945).
[10] Reference 9, pp. 107, 272.

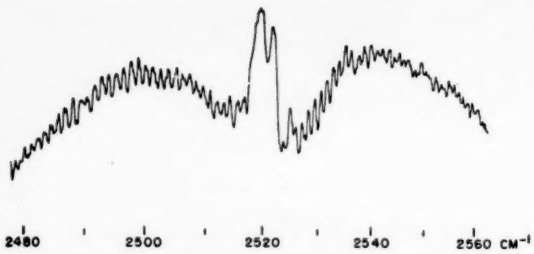

FIG. 2. Type A band at 2519.5 cm^{-1}. Echlette grating, 7200 lines per inch. Slit width, 0.67 cm^{-1}. Gas pressure, 15 mm of Hg.

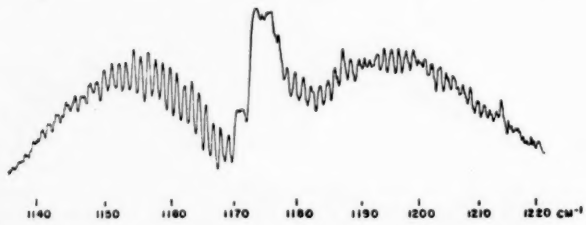

FIG. 3. Type A band at 1173.8 cm^{-1}. Echlette grating, 2400 lines per inch. Slit width, 0.46 cm^{-1}. Pressure 20 mm of Hg.

lished. Whether the infra-red data can be used to decide between planar and non-planar possibilities is discussed below. The clues for the identification of normal vibrations with observed absorption bands are found in the envelopes of the resolved bands and in the analogy with the assignments for ethylene.

The type A bands at 2519.5 cm^{-1} and 1173.8 cm^{-1} are shown in Fig. 2 and Fig. 3, and are identified as such by Price[3] with ν_{16} and ν_{18} respectively. The other fundamental band corresponding to species b_{3u} is obscured by the 6.2μ water band, but records obtained with the prism spectrograph confirm the assignment made by Price of the band in this region as ν_{17}.

Three prominent and strong type B bands which correspond to vibrations of symmetry species b_{2u} have been observed at 2608.6 cm^{-1}, 1857 cm^{-1}, and 368.7 cm^{-1}, and can reasonably be assigned respectively as ν_{12}, ν_{13}, and ν_{14}. Reproductions of the band at 2608.6 cm^{-1} are given in Fig. 4. The representation of the band at 368.7 cm^{-1} is shown in Fig. 5. Ordinates for this curve were obtained by dividing recorded galvanometer swings obtained with diborane in the absorption cell by the swings when the cell was evacuated. While the effects of water vapor were completely removed in each case, the large variation in transmission of the silver chloride windows over the spectral region covered made this procedure necessary in order to obtain the true shape of this band.

Observation of the band at 1857 cm^{-1} with automatic recording is made most difficult because of intense water vapor absorption in this region. The technique used with the grating spectrometer was to make one curve with the absorption cell filled to a suitable pressure with diborane, and one curve with the evacuated cell in the radiation beam. Frequent calibration marks were placed on each curve, and at intervals of 20 or 30 seconds of arc, deflections from the zero were measured, percent transmission calculated and plotted. The steep slopes of the water vapor lines, even when the complete record of the band was stretched out to a length of about 12 feet, made the resulting curve somewhat uncertain; consequently the rotational fine structure is too ragged to permit analysis comparable with that of the well-resolved bands. This band has also been studied with a lithium fluoride prism in the vacuum spectrograph. While it exhibits some unusual features, the shape, intensity, spectral extent, and line separation, where observable, are all consistent with its interpretation as a fundamental of species b_{2u}. Also, no allowed combination seems to fit the absorption at 1857 cm^{-1}.

Bell and Longuet-Higgins[2] and Price[3] assigned 412 cm^{-1} or 430 cm^{-1} respectively to the vibration shown as ν_{13}. Both Price and Stitt,[1] whose data Bell and Longuet-Higgins used, observed only a small part of the high frequency branch of the band centered at 368.7 cm^{-1}, and accordingly the true character of this band has not previously been known. Observations covering the spectral region from 332 cm^{-1} to 480 cm^{-1} revealed no other bands.

The identification of the frequency 368.7 cm^{-1} with the motion indicated for ν_{14} instead of with that for ν_{13} is made principally by comparison with the analogous motion in C_2H_4 for which the frequency is 810 cm^{-1} as recently reported.[11] Assignment of 1857 cm^{-1} or any other comparable frequency to this vibration appears unjustified, since the restoring forces are exexpected to be less in diborane than in ethylene.

Type C bands correspond to the vibrations of symmetry species b_{1u} in which variation of the electric moment is along the axis of maximum moment of inertia. The most prominent band of this type is the absorption at 972.7 cm^{-1} shown in Fig. 6, which is identified with ν_9. The other fundamental of this sym-

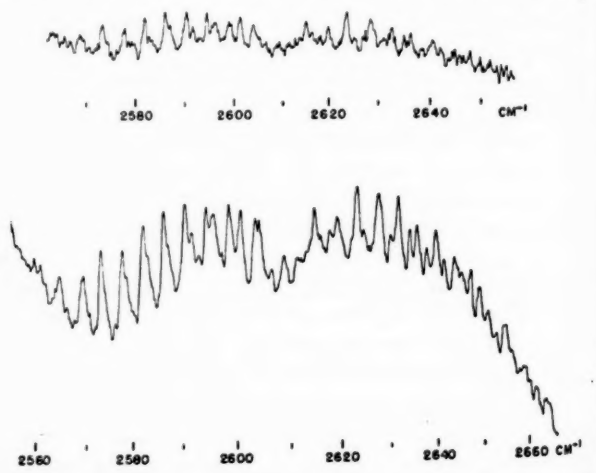

FIG. 4. Type B band at 2608.6 cm^{-1}. Echlette grating, 2400 lines per inch. Top curve: Slit width, 0.58 cm^{-1}. Gas pressure, 6 mm of Hg. Bottom curve: Slit width, 1.3 cm^{-1}. Gas pressure, 24 mm of Hg.

[11] B. L. Crawford, Jr., Phys. Rev. **76**, 161(T) (1950).

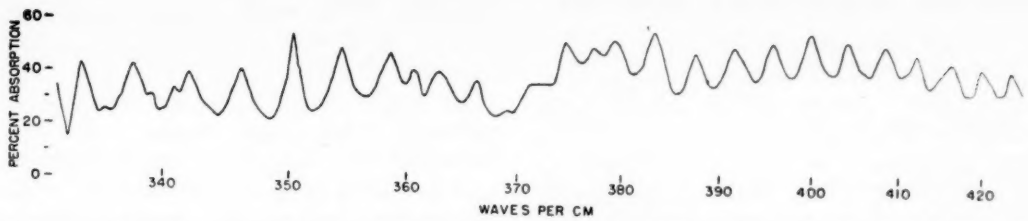

FIG. 5. Percent absorption curve of band at 368.7 cm^{-1}. Echlette grating, 900 lines per inch. Slit width, 2.22 cm^{-1}. Gas pressure, 100 mm of Hg.

metry species appears to be the absorption of medium intensity at 1988.0 cm^{-1}, since neither of the remaining unassigned strong absorptions has the proper characteristics. From the records made with the LiF prism in vacuum, the strong absorption at 2353 cm^{-1} is a typical band of type A, which can readily be accounted for as a combination band. The absorption at about 3670 cm^{-1} is quite strong, but observations in air fail to reveal its structure because of water vapor absorption. Moreover, both the quartz and the lithium fluoride prisms used in the vacuum spectrograph have troublesome absorptions in this region. Indications are, however, that the band is also type A, and several allowed combination bands of this type can be predicted for the region. The frequency 3670 cm^{-1} is probably too high for the fundamental vibration ν_8 involving motion of the bridge hydrogen atoms along the axis of maximum moment of inertia.

The band at 1988.0 cm^{-1} is unquestionably type C, although here also the observations are hampered by water vapor absorptions, and plotting of percent absorption curves is necessary in order to work through some of the water lines. The rotational fine structure, however, stands out prominently enough to yield data in good agreement with measurements of the strong type C band at 972.7 cm^{-1}.

Measurements of the Raman-active frequencies for liquid diborane originally made by Anderson and Burg[12] have been repeated recently by Pitzer and his associates.[13] The values obtained by the latter are included in Table II for those cases where the two observations disagree. Assignments of these frequencies have been made by comparison with the frequencies in ethylene[14] as modified by the recent work of Crawford,[11] it being considered in general that the frequencies in diborane will be less than those in C_2H_4. The value 606 cm^{-1} is taken as ν_7, since the comparable infra-red active vibration is taken as the low frequency ν_{14}. (These vibrations are "in phase" and "out of phase" combinations of the BH_2 rocking motion.) The frequency 1745 cm^{-1} was assigned as ν_{15}, symmetry species b_{3g}, in order to obtain possible combinations to account for certain weak bands.

The infra-red active combination bands can be calculated by using the rules set forth by Herzberg,[15] which may be summarized by stating that only combinations of levels of different symmetry species and opposite symmetry with respect to inversion at the center of symmetry will be allowed. Price[3] has given assignments for many of the combination bands, but differences in assignments of fundamental frequencies used here make possible certain plausible predictions which Price was not able to make. Assignment of combination bands is given in Table III. An attempt has been made to account for the higher frequency bands which appear to involve only binary combinations of the fundamentals. The predicted band types agree generally in those cases experimentally observed by Price[3] except possibly in the region 1267–1405 cm^{-1} where the observations seem rather indefinite.

The selection rules and activities of vibrations which were used above apply to $B_2{}^{11}H_6$ and $B_2{}^{10}H_6$ of symmetry species V_h. However the molecule $B^{11}B^{10}H_6$ which is half as numerous as $B_2{}^{11}H_6$ and eight times as numerous as the other possible molecule in natural diborane belongs to symmetry point group C_{2v} which has different selection rules and activities from V_h. In $B^{11}B^{10}H_6$ vibrations corresponding to species A_g, B_{1g}, B_{2g}, and B_{3g} become infra-red active with frequencies slightly increased from the values in the $B_2{}^{11}H_6$ Raman spectrum because of the isotope effect. However, most of these vibrations cannot be observed since they fall within regions covered by other strong infra-red active fundamentals.

The isotope effect is apparent in all the diborane bands so far resolved except possibly the band at 27μ. The central maxima (or central minima for the type B bands) exhibit major and minor components with the weaker component at higher frequency as expected since $B^{11}B^{10}H_6$ has smaller mass and is only one-half as numerous as $B_2{}^{11}H_6$. For the strong type B and type C bands which are well resolved, definite series of lines due to the two more numerous molecules may be identified.

Near the central maxima of the type A bands at 2519.5 and 1173.8 cm^{-1}, Figs. 2 and 3, there are prominent absorption maxima which appear to be due neither to the isotope effect nor to changes in rotational energy. It seems reasonable to identify these absorption maxima with the Q-branches of upper stage bands.[16]

[12] T. F. Anderson and A. B. Burg, J. Chem. Phys. **6**, 586 (1938).
[13] Private communication.
[14] Reference 9, p. 326.
[15] Reference 9, p. 126.
[16] Reference 9, p. 267.

DETERMINATION OF ROTATIONAL CONSTANTS

The electron diffraction data for diborane when interpreted on the non-planar bridge model[17] indicate a difference of less than 7 percent between the two larger moments of inertia. While extreme accuracy in locating the positions of hydrogen atoms is not obtained by this method it is evident that diborane is accidentally (not because of its symmetry) almost a symmetric top. Accordingly, the analysis of the rotational fine structure observed in the infra-red absorption bands can be discussed on the symmetric top approximation. The notations and relations given by Herzberg[9] will be used in giving the results of this analysis.

For a slightly asymmetric prolate top such as diborane, use of the combination relations yields, in addition to the values of the band centers, the rotational constants $A=h/(8\pi^2cI_A)$, and $\bar{B}=(B+C)/2$, where $B=h/(8\pi^2cI_B)$ and $C=h/(8\pi^2cI_C)$, h being Planck's constant and c the velocity of light in vacuum. I_A, I_B, and I_C are the principal moments of inertia listed in the order of increasing magnitude. They are the so-called effective moments, which are in first approximation, linear functions of the vibrational quantum numbers due to the vibration-rotation interaction. In the analysis for the slightly asymmetric case, use of small K values is avoided since lines with small K are most sensitive to the deviation from a symmetric top.

Table IV shows the positions of the lines and the assigned J values in the type A bands (parallel bands) at 2519.6 and 1173.8 cm^{-1}. The values of

$$\frac{R(J-1)+P(J)}{2}$$

for each band show so little systematic change with increasing J that simple averages were used to determine the band centers. The vacuum correction has been applied in all tables.

For the band at 2519.6 cm^{-1} the values of $\Delta_2F''(J)$ and $\Delta_2F'(J)$ fell almost exactly on straight lines; for the 1173.8 cm^{-1} band the curves leveled off somewhat with increasing value of J. In each case a least-squares method was used to find the best representation of straight lines to fit the plotted points. The slopes of these lines, $4\bar{B}''$ and $4\bar{B}'$, were compared directly with the computed values of $\Delta_2F''(J)/(J+\frac{1}{2})$ and $\Delta_2F'(J)/(J+\frac{1}{2})$ to obtain the mean absolute deviations indicated in Table X, which summarizes the rotational constants and band centers for all bands analyzed. Computations of this type form a check on the correctness of assignment of J values.

For the type A bands nearly every line appearing under the resolution obtained is accounted for, except those in or near the central maxima. In these type A bands, in first approximation, only the subsidiary maxima adjacent to the central maxima reveal the isotope effect indicating the presence of $B^{11}B^{10}H_6$.

The analysis of the type B and type C bands (perpendicular bands) on the symmetric top approximation is less satisfactory, as expected. Tables V through IX show the line positions and the K values assigned for the resolved type B and type C bands.

In the regions of 972.7 cm^{-1} and 2608.6 cm^{-1} the series of especially strong ${}^RQ_K$ and ${}^PQ_K$ lines were naturally identified with the molecules $B_2{}^{11}H_6$. However, another very prominent series of lines in each of these bands may be identified as associated with the next most numerous isotopic molecule $B^{11}B^{10}H_6$. The combination relations have been applied to each of

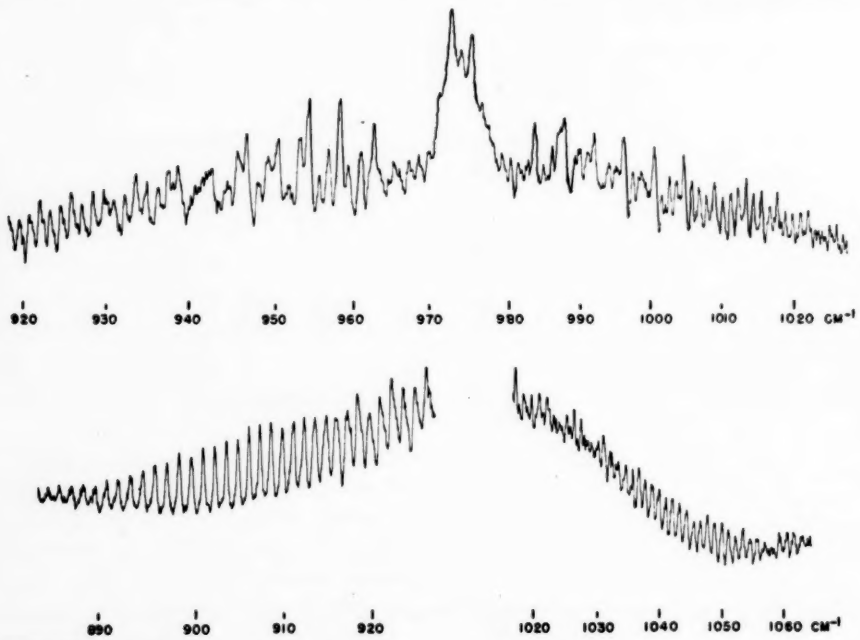

FIG. 6. Type C band at 972.7 cm^{-1}. Echlette grating, 2400 lines per inch. Top curve: Slit width, 0.46 cm^{-1}. Gas pressure, 75 mm of Hg. Bottom curves: Gas pressure, 150 mm of Hg. Negative branch: slit width, 0.38 cm^{-1}. Positive branch: slit width, 0.53 cm^{-1}.

[17] S. H. Bauer, Chem. Rev. 31, 43 (1942).

TABLE III. Infra-red combination bands of diborane.

Observed frequency Stitt	Price	Intensity	Assignment	Calculated frequency	Band type predicted
673					
685			Doubtful		
	811				
831	831	very weak	$\nu_3 - \nu_{14}$	811	*B*
	849		ν_4 (a_1)*	806	*A*
1274	1267	med. weak			
1311	1302	med. weak			
1377	1377	med. weak	$\nu_{15} - \nu_{14}$	1376	*C*
1405	1405	med. weak			
1722		weak	$\nu_9 + \nu_{11}$	1737	*A*
	2088		$\nu_{15} + \nu_{14}$	2114	*C*
2134	2124	very weak	ν_2 (a_1)*	2102	*A*
	2143				
	2200				
2217	2215	very weak	$\nu_7 + \nu_{17}$	2210	*B*
	2230				
2353	2345	strong	$\nu_3 + \nu_{18}$	2354	*A*
3135	3135	very weak	$\nu_3 + \nu_8$	3168	*C*
3670	3600–		$\nu_1 + \nu_{18}$	3697	*A*
	3700	strong	$\nu_3 + \nu_{16}$	3700	*A*
			$\nu_2 + \nu_{17}$	3706	*A*
4040	4035	very weak	$\nu_2 + \nu_8$	4090	*B*
4250	4155	weak	$\nu_1 + \nu_{17}$	4127	*A*
			$\nu_6 + \nu_{17}$	4195	*B*
	4350	weak	$\nu_1 + \nu_{13}$	4380	*B*
	4473	very weak	$\nu_6 + \nu_{13}$	4448	*A*
4550		very weak	$\nu_1 + \nu_8$	4511	*C*
	4815	very weak	$\nu_2 + \nu_{12}$	4711	*B*
	5022	very weak	$\nu_1 + \nu_{16}$	5043	*C*
5150	5140	weak	$\nu_1 + \nu_{12}$	5132	*B*
	5210	very weak	$\nu_6 + \nu_{12}$	5200	*A*

* Isotopic molecule $B^{11}B^{10}H_6$.

TABLE IV. Line positions in the type *A* bands of diborane.

	Band at 2519.5 cm^{-1}			Band at 1173.3 cm^{-1}	
J	*P* branch	*R* branch	*J*	*P* branch	*R* branch
0		2521.17	0		1175.44
1			1		1176.53
2	2517.29	2523.26	2	1171.17	1177.35
3	2516.10	2524.47	3	1170.21	1178.18
4	2514.97	2525.48	4	1168.86	1179.46
5	2513.76	2526.62	5	1167.69	1180.72
6	2512.66	2527.70	6	1166.57	1181.97
7	2511.43	2528.90	7	1165.40	1183.27
8	2510.08	2530.14	8	1164.25	1184.56
9	2508.97	2531.20	9	1163.13	1185.80
10	2507.83	2532.36	10	1161.99	1187.06
11	2506.78	2533.64	11	1160.71	1188.21
12	2505.57	2534.76	12	1159.60	1189.49
13	2504.44	2535.89	13	1158.44	1190.47
14	2503.36	2537.00	14	1157.36	(1192.29)
15	2502.08	2538.27	15	1156.21	
16	2500.86	2539.36	16	1155.11	1193.47
17	2499.67	2540.45	17	1154.04	1194.54
18	2498.54	2541.47	18	1152.86	1195.68
19	2497.27	2542.75	19	1151.84	1196.88
20	2496.01	2543.83	20	1150.64	1198.07
21	2494.84		21	1149.65	1199.20
22	2493.70		22	1148.46	
23	2492.38		23	1147.55	1201.14
24	2491.19		24	1146.44	1202.15
25	2490.04		25	1145.40	1203.19
26	2488.99	2550.58	26	1144.22	1204.56
27	2487.59	2551.72	27	1142.95	1205.90
28	2486.33	2552.74	28		1207.14
29	2485.24	2553.94	29	1140.76	1208.35
30	2484.08		30	1139.64	1209.49
31	2482.95	2556.52	31	1138.37	1210.54
32	2481.56				
33	2480.41			Maxima in *Q* branch at 1173.16 and 1174.33	
34	2479.16				
	Maxima in *Q* branch at 2518.94 and 2520.23				

these series of lines. The deviations listed in the tables give the mean values of the absolute deviations of the several frequencies calculated using the observed line positions, from the values computed with the equations fitted by a least-squares method to the plotted points. The method of selected points was used to deduce equations for the curves from which the positions of the band centers were determined.

For the type *C* band at 972.7 cm^{-1}, the band center corresponding to the heavier molecule lies at the lower frequency as expected, and the values for the rotational constant $(A-\bar{B})$ are larger. For the type *B* band at 2608.6 cm^{-1} the results of the analysis are not as satisfactory in the case of the isotopic molecule $B^{11}B^{10}H_6$. The band center for the lighter molecule lies at higher frequency, but the values of the rotational constants come out to be somewhat larger, due perhaps to overlapping of the lines in the negative branch of the band.

The several combination relations for *K* numbers from 3 to 8 or 9 in the band at 368.7 cm^{-1} all yield nearly constant values. Consequently simple averages were used for the values of these quantities from which the band center and the rotational constant $(A-\bar{B})$ in the upper and lower vibrational states were calculated. Data on this band fit the symmetric top approximation exceedingly well. The fact that the values of the rotational constants for the upper and lower states coincide within the probable errors indicates very little interaction between rotation and vibration.

Analysis over the same range of *K* values is not so satisfactory for the type *C* band at 1988.0 cm^{-1}. While the resolved lines extend to much higher and lower values of frequency than those represented by *K* numbers of 8 or 9, beyond these numbers the stronger lines no longer have the appropriate nearly uniform spacing observed in the high frequency branch. Possible causes for this effect include: (1) the presence of lines due to water vapor which are more intense and numerous than in the high frequency branch, and (2) the overlapping of the much stronger band with center at 1857 cm^{-1}.

CONCLUSION

Measurements in the infra-red absorption spectrum of diborane of the rotational fine structure in two bands of each type characteristic of asymmetric top molecules have lead to reliable values for the centers of these bands and values for rotational constants $(A-\bar{B})$ and $\bar{B}$. All observations and results are consistent with the conclusion that diborane has the bridge structure and belongs to the same symmetry point group, V_h, as ethylene. Nearly all observed absorption bands seem

TABLE V. Line positions in the 2608.6 cm^{-1} band of diborane.*

K	Negative branch	K	Positive branch	K	Negative branch	K	Positive branch
	2608.72		2611.42	10	2568.10s	10	2650.22s
	2607.95		2612.27		2566.19		2651.86
1	2606.39s	1	2614.46s		2565.86		2653.16
	2604.60		2617.18s		2565.37	11	2654.12s
2	2603.68s	2	2619.06s		2564.68		2655.22
	2602.15		2619.92	11	2563.56s		2657.19
	2600.64s		2620.55		2562.39	12	2658.48
3	2598.48s		2621.74		2560.22		2659.64
	2597.30	3	2622.78s	12	2559.44s		2660.77
	2596.59		2623.91		2558.33		2662.77
	2595.62s		2625.50		2557.22		2663.41
	2595.09	4	2626.97s		2555.70		2663.99
4	2593.91s		2627.55		2554.97		2665.49
	2592.44		2628.40		2548.88		2666.31
	2591.17		2629.75		2547.70		2668.09
5	2589.72s		2630.27		2546.61		2669.27
	2588.40	5	2631.08s		2545.36		2670.41
	2586.93		2632.38		2544.45		2671.61
	2586.27		2633.27s				2672.64
6	2585.39s	6	2634.86s				2673.44
	2582.86		2635.71				2674.69
	2581.93		2636.58				2675.84
7	2581.18s		2638.16				2676.93
	2578.91	7	2638.88s				2677.86
	2577.73s		2640.42				2679.19
8	2576.68s		2641.77				2680.04
	2575.23	8	2642.79s				2680.93
	2573.42		2643.27				2682.39
	2572.68		2644.22				2683.24
9	2572.28s		2645.14				2686.71
	2570.95	9	2646.39s				2687.65
	2569.89		2647.77				2688.73
	2569.14		2648.37				2689.67
	2568.54						

* The more intense lines are marked s.

TABLE VI. Line positions in the 368.7 cm^{-1} band.

K	$^{P}Q_K$	$^{R}Q_K$
0		370.94
1	366.10	374.96
		376.92
2	362.96	379.18
	360.47	
3	358.28	383.04
4	354.36	387.30
5	350.21	391.38
6	346.22	395.34
7	341.95	399.50
8	337.73	403.55
9	333.62	407.85
10		411.84
		416.12
		419.63
		423.47
		425.33
		427.81
		430.52

reasonably accounted for on the basis of the assignments of fundamental frequencies and combinations thereof. However, observation under high resolution in vacuum is needed to clear up uncertainties in the regions 1250–1900 cm^{-1} and 3600–3750 cm^{-1}.

From the analysis of the rotational fine structure on the symmetric top approximation, average values of the rotational constants in the ground states have been

TABLE VII. Line positions in the 1988.0 cm^{-1} band.*

Negative branch	Positive branch	Negative branch	Positive branch
1987.41	1994.05	1946.46	2048.98
1986.84	1994.90	1944.71	2050.10s
1986.34	1995.92	1942.58	2051.52
1985.82s	1997.47s	1941.42	2052.84s
1985.22	1998.32	1940.17	2053.82
1984.71		1939.91s	2054.97
1984.22	2001.24s	1939.20	2056.29s
1983.02	2002.22	1938.00s	2057.23
1982.53	2003.53	1937.06s	2058.57
1981.63	2004.52	1935.89	2059.76
1981.33s	2005.06	1935.18	2062.16s
1980.85	2006.11s	1934.66	2063.20
1979.56		1933.94	2066.95
1978.25		1931.80	2067.72
1977.37s	2010.06s	1930.79	2069.15
1976.88	2012.05	1929.98s	2070.26
1975.16	2013.07	1928.75	2071.32
1974.17	2013.94s	1927.72	2072.54
1973.08s	2015.53	1926.56	2076.06
1971.72	2016.86	1925.65	2078.33
1970.76	2017.66		2080.56
1970.27	2019.18		2082.32
1969.20	2020.45		
1968.69	2021.31s		
1967.64	2023.15		
1966.34	2024.39		
1964.94	2025.15s		
1964.29	2026.86		
1963.28s	2028.09		
1962.11	2028.97s		
1960.36	2030.28		
1959.41s	2031.03		
1958.18	2031.73		
1957.02	2032.53s		
1955.96	2034.51		
	2036.25s		
1953.84s	2037.77		
1952.35	2039.77s		
1951.40	2042.90		
1950.30	2045.59		
1949.15s	2046.69s		
1947.80	2047.74		

* The more intense lines are marked s. Strong lines in central maximum at 1990.59, 1991.28, and 1991.97 cm^{-1}.

deduced as follows: $\tilde{B}''=0.582\pm0.002$ cm^{-1}, and $(A''-\tilde{B}'')=2.080\pm0.005$ cm^{-1}. From the value for $\tilde{B}''$ the product of the two larger moments of inertia divided by their sum is 48.1×10^{-40} g cm^2. The value of A'' yields for the minimum moment of inertia a magnitude of 10.5×10^{-40} g cm^2. Electron diffraction data interpreted on the non-planar bridge model predict the values of 49.2×10^{-40} g cm^2 and 10.7×10^{-40} g cm^2, respectively, for $B_2{}^{11}H_6$.

The appearance of the type B band at 368.7 cm^{-1} with a gap or trough at the band center is interpreted as spectroscopic evidence that the diborane molecule is not planar. If the bridge hydrogens were in the same plane as the four terminal hydrogens, the out-of-the-plane bending vibration involving the bridge hydrogens would cause variation of the electric moment along the axis of greatest moment of inertia. A type C band would then be expected for the lowest frequency band.

The comparative regularity observed in the so-called perpendicular bands, type B and type C, also is evi-

TABLE VIII. Line positions in the 972.7 cm^{-1} band of diborane.*

Negative branch cm^{-1}	Positive branch cm^{-1}	Negative branch cm^{-1}	Positive branch cm^{-1}
971.22	976.34	930.66	1016.14
969.84	977.14	930.10	1016.73
968.47	977.94	929.42	1017.23
967.06	978.86	928.66	1017.76
965.75	979.53	928.14	1018.33
965.18	979.97	927.53	1018.88
964.43	981.05	926.82	1019.43
964.07	982.31	925.55	1020.58
963.70	983.31s	924.66	1021.16
962.45s	984.58	924.29	1021.69
960.77	985.13	923.02	1022.12
959.17	985.80	921.80	1022.75
958.13s	986.49	920.46	1023.21
956.74	987.05	919.34	1023.74
955.50	987.45s	917.93	1024.15
954.12s	988.95	916.67	1024.88
952.92	989.72	915.44	1025.42
951.63	990.82	914.34	1025.98
951.22	991.64s	913.02	1027.08
950.09s	992.90		
949.84	993.69	911.78	1027.61
949.11	994.79s	910.46	1028.13
948.70	995.82	909.21	1028.73
947.85	997.09		
947.48	998.31	907.81	1029.77
946.13s	998.72	906.62	1030.60
945.03	999.47	905.31	1031.62
943.98	1000.09s	904.07	1032.91
943.57	1001.12	902.79	1034.13
942.94	1001.67	901.50	1035.16
942.07s	1002.21	900.22	1036.09
940.99	1003.23	899.58	1037.17
939.41	1004.28s	898.95	1038.46
938.86	1005.43	897.69	1039.56
938.26s	1006.50	897.17	1040.69
937.70	1007.58	896.47	1041.64
937.08	1008.58s	895.14	1042.73
935.80	1009.83	893.87	1043.87
935.31	1010.86	893.05	1044.96
934.58s	1011.91	892.68	1045.97
933.73	1012.94s	891.36	1047.10
933.25	1013.99	890.16	1048.27
932.00	1015.13	888.91	1049.41
		887.74	1050.54
			1051.61
			1052.64
			1053.74
			1055.01

* The more intense lines are marked s. Strong lines in central maximum at 972.66, 973.79, and 975.13 cm^{-1}.

TABLE IX. Line positions in the type *C* bands.

	Band at 1988.0 cm^{-1}			Band at 972.7 cm^{-1}	
K	^PQ_K	^RQ_K	K	^PQ_K	^RQ_K
0		1990.59			
1	1985.82	1994.90	1	971.22	978.86
2	1981.63	1998.32	2	967.06	983.31
3	1977.37	2002.22	3	962.45	987.45
4	1973.08	2006.11	4	958.23	991.64
5	1968.69	2010.06	5	954.12	995.82
6	1964.29	2013.94	6	950.09	1000.09
7	1960.36	2017.66	7	946.13	1004.28
8	1955.96	2021.31	8	942.07	1008.58
9	1951.40	2025.15	9	938.26	1012.94
10		2028.97	10	934.58	1017.23
11		2032.53	11	930.66	1021.69
12		2036.25	12	926.82	1025.98
13		2039.77	13	923.02	1030.63

TABLE X. Summary of results on symmetric top approximation.

Type *A* bands

Region μ	Band center cm^{-1}	Average deviation	Absorption maximum cm^{-1}	$4\bar{B}''$ cm^{-1}	Average deviation	$4\bar{B}'$ cm^{-1}	Average deviation
3.97	2519.54	0.082	2518.94	2.332	0.005	2.336	0.008
8.52	1173.78	0.083	1173.16	2.316	0.025	2.265	0.025

Type *B* bands

Region μ	Band center cm^{-1}	Average deviation	Absorption minimum cm^{-1}	$A''-\bar{B}''$ cm^{-1}	Average deviation	$A'-\bar{B}'$ cm^{-1}	Average deviation
3.83	2608.61	0.078	2607.53	2.081	0.004	2.065	0.003
(a)	2609.92	0.175	2610.11	2.138	0.013	2.108	0.009
27.12	368.68	0.059	368.23	2.058	0.003	2.056	0.004

Type *C* bands

Region μ	Band center cm^{-1}	Average deviation	Absorption maximum cm^{-1}	$A''-\bar{B}''$ cm^{-1}	Average deviation	$A'-\bar{B}'$ cm^{-1}	Average deviation
5.02	1988.00	0.054	1990.63	2.116	0.009	2.071	0.006
10.28	972.66	0.045	972.66	2.079	0.005	2.087	0.008
(a)	975.29	0.097	975.13	2.054	0.006	2.065	0.009

[a] Assigned to the molecule $B^{11}B^{10}H_6$.

dence that the molecule is non-planar, since this configuration would be expected to be more symmetric, that is the two larger moments of inertia would be more nearly equal, than for the planar model.

Before the molecular dimensions can be uniquely determined, it will be necessary to resolve and analyze absorption bands of B_2D_6 as well as $B_2{}^{10}H_6$, both of which compounds can be produced and undoubtedly can be handled with no more difficulty than experienced with ordinary diborane. The values of rotational constants deduced for $B^{11}B^{10}H_6$ are probably not satisfactory for calculations of dimensions.

Lack of agreement between the experimental observations and the results of the normal coordinate treatment of Bell and Longuet-Higgins[2] indicates the need for a more rigorous theoretical study of the vibrations of the bridge model for the type molecule X_2Y_6. The experimental results already obtained can then be used to deduce reliable values for the force constants of diborane.

ACKNOWLEDGMENT

It is a pleasure to acknowledge our indebtedness to the Chemistry Department of the University of Chicago for the sample of diborane. Special thanks are due Mr. A. C. Bond, then of the Chemistry Department, University of Michigan, for procuring the diborane sample, and for much assistance in purifying and handling the gas. To Dr. L. G. Smith, formerly of this laboratory, appreciation is due for his contributions to the design of an amplifier for automatic recording of infra-red absorption bands.

Vibrational Spectra of the Four Lowest Nitroparaffins

DON C. SMITH,* CHI-YUAN PAN, AND J. RUD NIELSEN
Department of Physics, University of Oklahoma, Norman, Oklahoma
(Received January 26, 1950)

The infra-red spectra from 2 to 22μ of nitromethane, nitroethane, 1-nitropropane and 2-nitropropane have been obtained for both vapor and liquid phases. The Raman shifts have been measured for the liquids, and for nitromethane the polarizations of the bands have been determined.

A satisfactory interpretation of the spectra has been obtained for nitromethane on the basis of assigned fundamental frequencies that agree with those proposed previously by Wells and Wilson, except for the B_1 methyl rocking mode. The fundamental frequencies have not been determined for the other compounds, but the positions of the nitro group absorptions have been determined empirically.

INTRODUCTION

WELLS and Wilson[1] have measured the infra-red spectrum of nitromethane vapor and, using additional Raman data for the liquid, have made assignments of all but one of the fundamental vibrational frequencies. Further evidence of the validity of these assignments has been given by T. P. Wilson's[2] work on deuterated nitromethane and by Wittek's[3] investigation of the Raman spectra of nitroparaffins.

Nielsen and Smith,[4] in dealing with problems of quantitative analysis, have presented the only published infra-red spectra of nitroparaffins in the liquid state. However, their spectra did not extend beyond 15μ and, as in the case of Wells' and Wilson's spectrum of nitromethane vapor, the resolution employed was not as great as that now available. No spectral data for gaseous nitroparaffins other than nitromethane have been reported.

In the present work new infra-red spectra of nitromethane, nitroethane, 1-nitropropane, and 2-nitropropane have been obtained over the range from 2 to 22μ for both the liquid and the gaseous phase. New measurements of the Raman shifts for these compounds in the liquid state are given, and for nitromethane new depolarization values for the strongest Raman bands are included. On the basis of the new data, one change is proposed in the fundamental frequencies of nitromethane assigned by Wells and Wilson,[1] and a tentative identification of the nitro group frequencies in the four lowest nitroparaffins is presented.

EXPERIMENTAL

The samples of nitromethane, nitroethane, 1-nitropropane, and 2-nitropropane, all highly purified, were the same as those used previously.[4] The infra-red spectra were determined with a large research-type spectrometer described elsewhere.[5] Interchangeable 60° rocksalt and potassium bromide prisms with 150×100 millimeter faces were used for the ranges from 2 to 14 and from 14 to 22μ, respectively. The spectra of the vapors are shown in Fig. 1 and those of the liquids in Fig. 2. The vapor pressures in millimeters of Hg and cell thicknesses in millimeters are shown on the curves. The strongest absorptions for the liquids were measured with a 0.009-mm cell filled with a 10 percent solution of nitroparaffin in CCl_4. The observed wave numbers of the infra-red absorption maxima (or "shoulders") of gaseous and liquid nitroparaffins are given in Tables I to IV. Rough estimates of the intensities and in some cases of the shapes of the bands are given under the heading "Description," the abbreviations *vs* very strong, *s* strong, *m* medium, *w* weak, *vw* very weak, etc., *b* broad, *d* diffuse and *sh* sharp being used.

The Raman spectra of the liquid nitroparaffins were photographed with a three-prism Lane-Wells spectrograph. The speed of the camera (somewhat similar to the Schmidt type) is f/3.5, and the linear dispersion is 14.5A/mm at 4400A. The wave numbers of the observed Raman frequencies and descriptive data for the bands are given in Tables I to IV. The depolarization ratios for the stronger bands of nitromethane are also listed in the last column of Table I. For sharp bands the Raman frequencies are accurate to within ± 0.5 cm^{-1}, and the infra-red absorption frequencies below 2000 cm^{-1} are accurate to within ± 1.0 cm^{-1}.

The infra-red data for nitromethane vapor are in good agreement with those of Wells and Wilson, except that many of the bands have been resolved into two or more components. The Raman frequencies for nitromethane are within one or two wave numbers of those given by Wittek, except for her value 1210 cm^{-1}, which was not observed, and her bands at 3038 and 3062 cm^{-1}, which were observed here as a single broad band at 3055 cm^{-1}. Six new very weak bands not observed by Wittek have been found. The depolarization values are also in good agreement with those of Wittek, except for the band at 1104 cm^{-1} which here is definitely depolarized. In place of the Raman frequency 2904 cm^{-1} for nitroethane found by Wittek, two frequencies at 2890 and 2912 cm^{-1} are definitely observed, and a new band at 2749 cm^{-1} has been found. For 1-nitropropane seven

* Present Address: Naval Research Laboratory, Washington, D. C.

[1] A. J. Wells and E. B. Wilson, Jr., J. Chem. Phys. **9**, 314 (1941).
[2] T. P. Wilson, J. Chem. Phys. **11**, 361 (1943).
[3] H. Wittek, Zeits. f. physik. Chemie **B51**, 187 (1942).
[4] J. Rud Nielsen and D. C. Smith, Anal. Chem. **15**, 609 (1943).
[5] Nielsen, Crawford, and Smith, J. Opt. Soc. Am. **37**, 296 (1947).

new bands have been observed, and for 2-nitropropane four new bands.

NITROMETHANE

The fifteen fundamental frequencies of nitromethane fall into four vibrational classes as shown in the first column of Table V. The approximate vibrational motion associated with these fundamentals is indicated in the second column. All fundamentals, except the totally inactive A_2 twisting frequency, are allowed in both infra-red and Raman spectra. Identification of the fundamental frequencies in the observed spectra therefore depends mainly upon the polarization of the Raman lines and the contours of the infra-red bands in the gaseous state. Raman frequencies belonging to A_1 are polarized, while those belonging to B_1 and B_2 are depolarized.

It has been assumed that the symmetry of the nitromethane molecule is approximately determined by the $C-NO_2$ group, and that this has the symmetry C_{2v}. Using this configuration and the molecular dimensions C–N = 1.46A, N–O = 1.21A, C–H = 1.08A, ONO = 127°, and HCH = 109°, three moments of inertia 67.4×10^{-40} g cm², 73.8×10^{-40} g cm² and 135.5×10^{-40} g cm² are obtained, the smallest value being that about an axis coinciding with the C–N bond. According to the theory of Badger and Zumwalt[6] infra-red bands belonging to A_1 (type A bands) should have a sharp central branch with single asymmetrically-shaped branches on either side having maxima about 14 cm^{-1} from the central branch. Bands belonging to class B_1 will be of type B and should have no central branch, but on either side of the band center there should appear a doublet which, at best, will hardly be resolved. The maxima should be from 3.5 to about 14 cm^{-1} from the band center, depending upon the resolution and accuracy achieved in mapping the band contour. Bands belonging to B_2 will be of type C and should consist of a relatively strong central branch with weak broad branches about 19 cm^{-1} on either side.

Most of the infra-red bands observed for the vapor have well-defined contours corresponding to the three types of bands expected. The observed positions of the fundamentals are listed in the third column of Table V, and the contour data are listed in columns four and five. For the liquid state, the observed infra-red and Raman frequencies are in very close agreement (Table I), and only the Raman values for the fundamentals, together with the observed depolarization ratios of the bands, are listed in Table V.

The A_1 fundamentals are easily identified by the polarization data, and the corresponding infra-red bands have the appropriate contour. The infra-red bands at 477, 1443, and 1586 cm^{-1} have the contour of type B bands and are accordingly assigned to B_1 fundamentals. There is only one band, at 605 cm^{-1}, that is definitely a type C band, and this must be assigned to the NO_2 rocking fundamental of class B_2. Another B_2 fundamental may be expected near 1475 cm^{-1}, and although there are no well-defined bands in this region the weak, but rather sharp maximum at 1482 cm^{-1} is assigned to this fundamental. In the region of 3000 cm^{-1} the bands obtained with rocksalt prism (Fig. 1) did not exhibit well-defined contours. However, with a lithium fluoride prism some additional detail was observed. Weak

[6] R. M. Badger and L. R. Zumwalt, J. Chem. Phys. **6**, 711 (1938).

TABLE I. Infra-red and Raman frequencies of nitromethane.

Infra-red				Raman		
Vapor		Liquid		Liquid		
cm^{-1}	Description	cm^{-1}	Description	cm^{-1}	tion	Depolarization
ca. 467	*vw, vb*	482	*m*	480.8	*m*	0.9
487	*vw, b*					
ca. 585	*vw, b*					
605	*w, sh*	608	*m, sh*	608	*w*	
ca. 607	shoulder					
645	*s*					
658	*s, sh*	656	*s*	656.5	*s, sh*	0.39
671	*s*					
904	*m*					
914	*m, sh*					
918	*m, sh*	917	*m, sh*	918.8	*vs, sh*	0.05
931	*m*					
		960	*w*			
ca. 1087	*m, b*					
1100	*m, sh*	1100	*s*	1104	*w, d*	0.9
ca. 1111	shoulder					
—						
ca. 1154	*vw, b*					
—						
1208	*vw, sh*	1209	*w, sh*			
ca. 1220	shoulder					
ca. 1284	shoulder					
1311	*vw, sh*	1312	*vw*	1313	*w*	
—						
ca. 1362	shoulder					
1377	*s, sh*	1379	*s, sh*	1377.3	*s, sh*	0.2
ca. 1390	shoulder					
1397	*s, sh*	1404	*s, sh*	1401.4	*vs, sh*	0.28
1412	*m*					
1437	*w*	*ca.* 1429	*s*	1427	*w, vd*	
1449	*w*					
1482	*w*					
1522	*w*					
1580	*vs*					
1592	*vs*	1570	*vs, sh*	1562	*m, d*	0.83
		1754	*vw*	1730	*vvw, d*	
		1828	*w, sh*	1830	*vvw*	
		ca. 1852	*vw*			
		ca. 1980	*vw*			
ca. 2040	*vw*	2033	*w*			
		ca. 2212	*vw*			
		2283	*w*	2290	*vvw*	
		ca. 2315	*vw*	2315	*vw*	
ca. 2475	*w*	2475	*m*			
		ca. 2540	*vw*			
				2744	*vw*	
ca. 2770	*w*			2771	*vw*	
ca. 2872	shoulder	2810	*w*	2840	*vw, d*	
ca. 2955	shoulder					
2972	*m, sh*	2950	*m*	2967.8	*s, sh*	0.05
ca. 2990	shoulder					
ca. 3065	shoulder	3060	*m*	3055	*w, vd*	0.9
		3600	*vw*			
		3660	*w*			
		3830	*vw*			
		4150	*w*			
		4460	*w*			

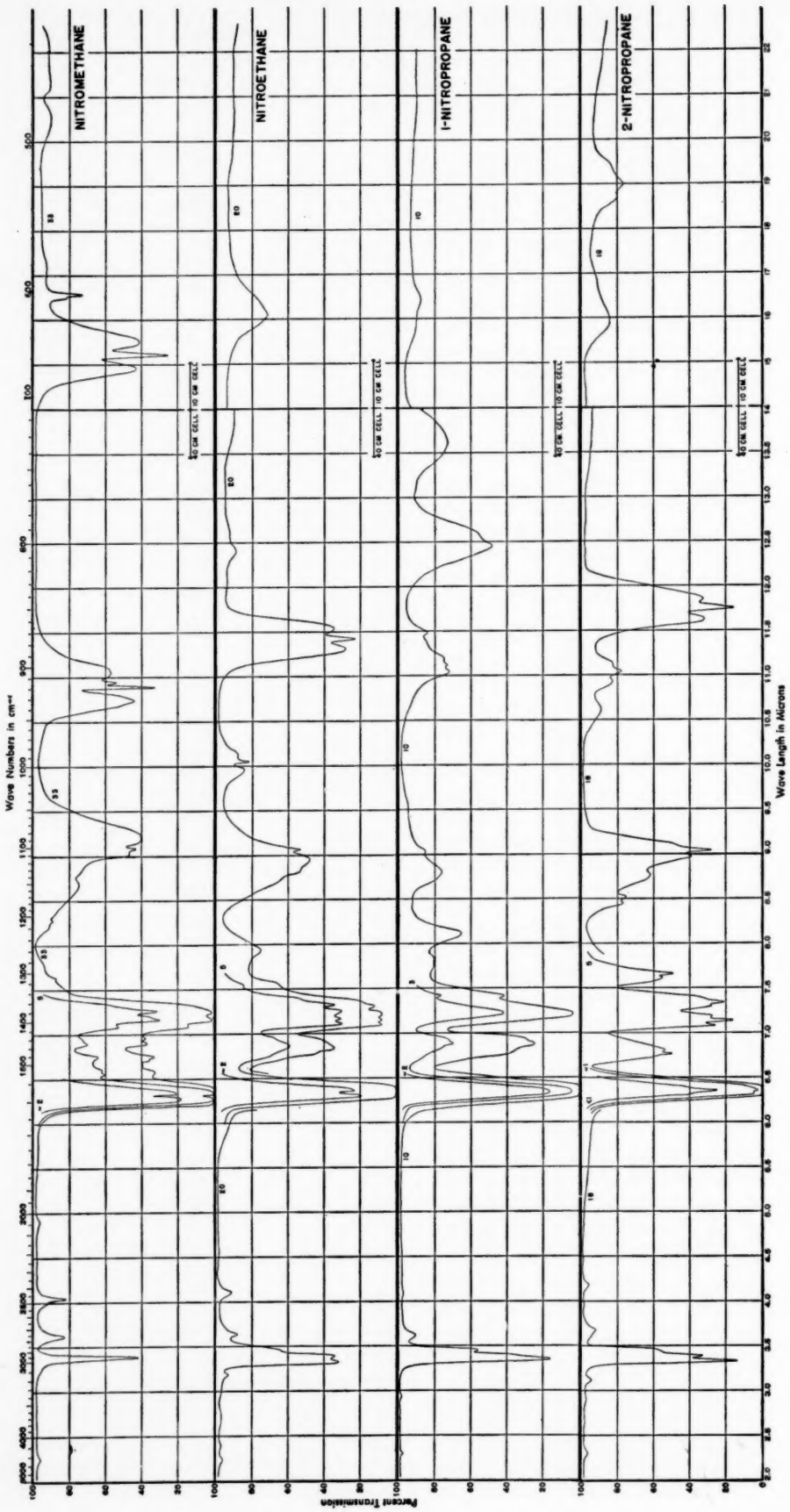

FIG. 1. Infra-red absorption spectra of the four lowest nitroparaffins in the gaseous state.

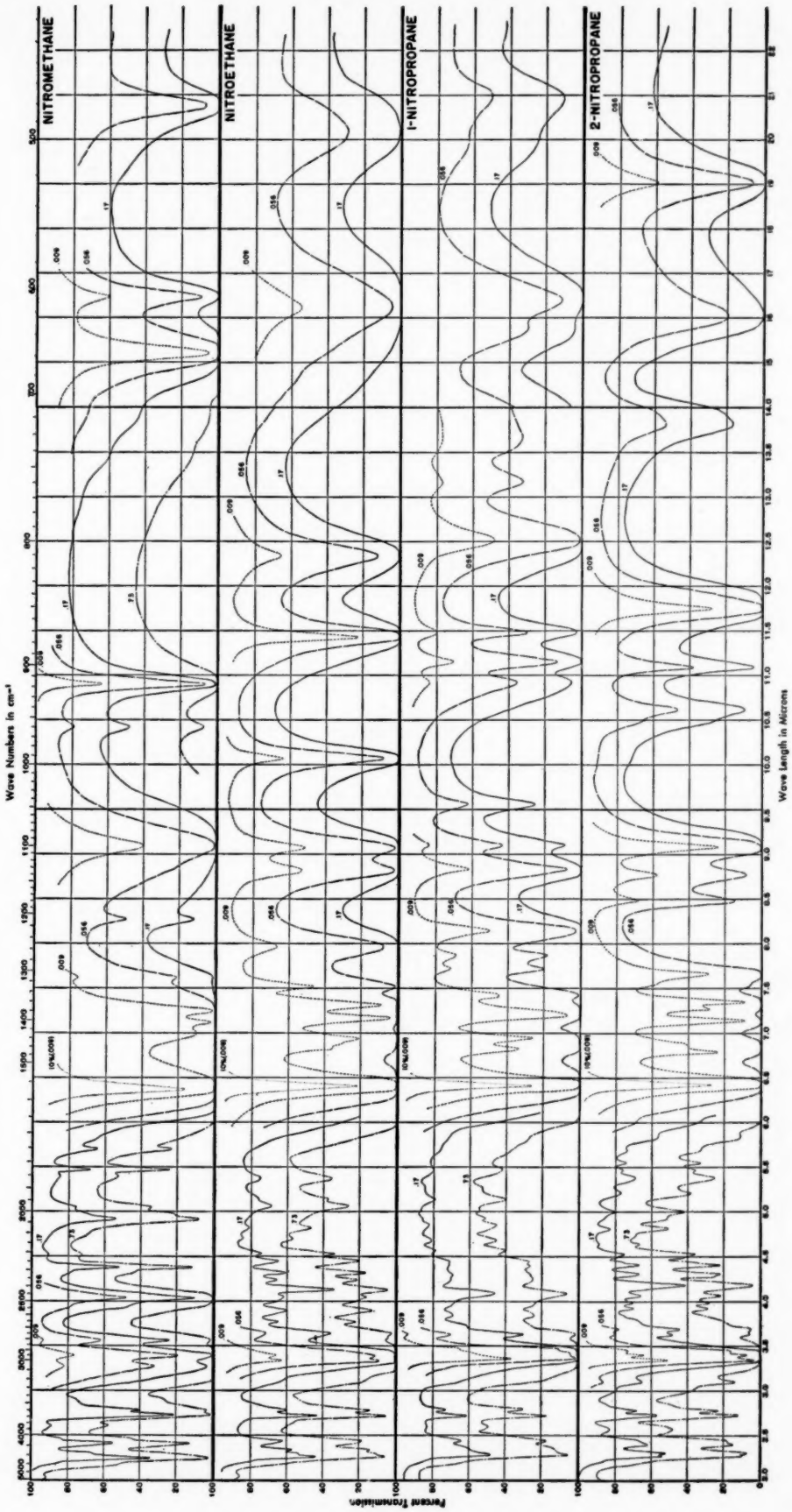

FIG. 2. Infra-red absorption spectra of the four lowest nitroparaffins in the liquid state.

TABLE II. Infra-red and Raman frequencies of nitroethane.

Infra-red Vapor cm⁻¹	Description	Infra-red Liquid cm⁻¹	Description	Raman Liquid cm⁻¹	Description
				295	*w, d*
		ca. 495	*m, b*	491	*m, d*
ca. 621	*m, b*	616	*m*	614	*m, d*
807	*vw*	810	*m*		
866	*m*				
876	*m, sh*	875	*s, sh*	874.7	*vs, sh*
884	*m*				
985	shoulder				
996	*w, sh*	993	*m, sh*	993	*w*
1005	*w, b*				
1103	*w, sh*	1103	*s, sh*	1101.6	*m, sh*
1118	*m*				
ca. 1124	shoulder	1134	*s*		
ca. 1150	shoulder				
ca. 1260	*w, b*	1255	*m*	1267	*vw, d*
ca. 1326	shoulder	1330	*s, sh*	1331	*w,*
ca. 1352	shoulder				
1366	*s, sh*	1365	*s, sh*	1366.5	*s*
1379	*s*				
1397	*s, sh*	1395	*s, sh*	1395.0	*s*
1406	*s*				
ca. 1440	shoulder	1441	*s, sh*	1440	*m, d*
1458	*m*	*ca.* 1452	shoulder	1456	*vw, d*
ca. 1480	shoulder	*ca.* 1465	shoulder		
1573	*vs*	1560	*vs, sh*	1554	*m, d*
1588	*vs*				
		1862	*w*		
		1946	*vw*		
		1976	*w*		
		2075	*vw*		
		2128	*vw*		
		2208	*vw*		
		2247	*w*		
		2315	*w*		
		2358	*w*		
ca. 2435	*w*	2420	*w*		
		ca. 2470	*vw*		
		2560	*w*		
		2650	*vw*		
ca. 2750	*w*	2750	*w*	2749	*vw*
				2890	*vw*
				2912	*w*
2950	*m*	2950	*m*	2951	*s*
				2971	*m*
3010	*m*	3000	*m*	3001	*m, d*
		ca. 3225	shoulder		
		3600	*w*		
		3680	*w*		
		4100	*w*		
		4270	*vw*		
		4430	*w*		

TABLE III. Infra-red and Raman frequencies of 1-nitropropane

Infra-red Vapor cm⁻¹	Description	Infra-red Liquid cm⁻¹	Description	Raman Liquid cm⁻¹	Description
				214	*vw, vd*
				281	*vvw, vd*
				347.6	*w*
				381	*vvw, d*
		ca. 477	*w*	476	*w*
		ca. 502	shoulder	504	*vw, d*
ca. 610	*w, b*	611	*m*	609	*w, d*
		ca. 635	shoulder	633	*vw, d*
ca. 735	*m, b*	*ca.* 737	*m, b*	736	*vvw*
		759	*m*		
ca. 794	shoulder	799	*s*	800	*vw*
804	*m*				
872	*w*	871	*m*	871.8	*s, sh*
ca. 894	shoulder				
900	*m, sh*	897	*m, sh*	898.3	*s, sh*
906	*m*				
		916	*m*	915	*vw, d*
				985	*vvw, vd*
				1035.7	*w*
		1046	*w*	1047	*w*
ca. 1106	*w*	1099	*w*	1098	*vw, d*
ca. 1136	*m, b*	1133	*m, sh*	1131	*w*
1231	*m*	1229	*s*	1229	*w, d*
ca. 1271	*vw*	1287	*m*	1271	*w*
ca. 1289	*vw*	1295	*m*	1298	*w*
1238	*m, sh*	*ca.* 1348	*s*	1346	*m, d*
1385	*s*	1389	*s*	1383	*vs, d*
ca. 1440	shoulder	1439	*s, sh*	1438	*s*
1451	*m, sh*			1459	*m, d*
ca. 1465	shoulder	1464	*s, sh*		
1578	*vs, b*	1560	*vs, sh*	1552	*m*
		ca. 1828	*vw*		
		ca. 1900	shoulder		
		1946	*vw*		
		1996	*vvw*		
		2028	*vvw*		
		ca. 2062	*vw*		
		ca. 2137	*vw*		
		2188	*vw*		
		2247	*vvw*		
		2273	*vvw*		
		ca. 2353	*vw, b*		
		2445	*w*		
		ca. 2600	*vw, b*		
ca. 2765	*w*	2760	*w, sh*	2751	*vw*
		ca. 2800	shoulder	2884.9	*s, sh*
2900	*m*	*ca.* 2930	shoulder	2943	*vs, d*
2985	*s, sh*	2980	*s, sh*	2975	*s, d*
		3580	*vw*		
		3680	*w*		
		ca. 3850	*vvw*		
		4100	*vw*		
		4390	*w*		

shoulders appeared about 17 cm^{-1} on either side of the strong 2972 cm^{-1} fundamental, and another weak poorly-defined band appeared at 2065 cm^{-1}. The former has been assigned to the A_1 symmetrical C—H stretching mode of the methyl group, and it is assumed that the corresponding unsymmetrical methyl vibrations of class B_1 and B_2 are represented by the latter. Thus, except for two methyl rocking modes (B_1 and B_2), all of the active fundamentals are rather easily identified; and, with this exception, and with slight differences resulting from higher experimental accuracy, the assignments given in Table V are identical with those proposed previously.[1,2]

Wells and Wilson[1] have assigned 1097 cm^{-1} to the CH_3 rocking B_1 vibration and 1153 cm^{-1} to the CH_3 rocking B_2 vibration. The latter assignment is objectionable, since the band near 1150 cm^{-1} is (a) exceptionally weak for a fundamental, (b) absent in the spectrum of the liquid, and (c) seems to have no central branch, as it should if it belonged to B_2. Moreover, as seen in Fig. 1, the absorption near 1100 cm^{-1} does not have the contour of other type B bands, but appears to be caused by overlapping bands. We have assumed, therefore, that the strong absorption around 1100 cm^{-1} is caused by both the B_1 and the B_2 CH_3 rocking fundamentals. The sharp maximum at 1100 cm^{-1} is interpreted as the central branch of the B_2 band, and the center of the B_1 band is assumed to be close to the

broad maximum at 1090 cm^{-1}. Because of the proximity of these two bands it is not possible to check their contours with any degree of certainty. It may be mentioned that the isotope shifts observed by T. P. Wilson[2] for deuterated nitromethane have little bearing upon this revision of Wells and Wilson's assignment of the CH_3 rocking fundamentals, since the corresponding fundamentals for the deuterated compound have not been definitely established.

Except for the unknown A_2 torsional frequency and the somewhat uncertain B_2 frequencies at 1482 and 1100 cm^{-1}, the assignment given in Table V is now established beyond doubt. Practically all of the remaining infra-red and Raman bands observed are readily interpreted as combinations and overtones, as given in Table VI. Two of the fundamentals at 918 and 605 cm^{-1} have what appear to be additional central branches located at 914 and 607 cm^{-1}, respectively. These are possibly "upper stage" bands caused by a transition from an excited vibrational level to an upper level in which this vibration remains excited.

NITRO GROUP FREQUENCIES

For nitroethane, 1-nitropropane, and 2-nitropropane, no vibrational analysis has been attempted because of the lower symmetry of these molecules and the resulting meaningless band contours and greater complexity of the spectra. However, as pointed out by Wilson,[2] it seems reasonable that the vibrations involving mainly the nitro group should be governed by essentially the same potential in each of the four lowest nitroparaffins. It should therefore be possible to identify some of the bands in the spectra of the higher nitroparaffins by comparison with the known spectrum of nitromethane and arrive at a useful set of frequencies characteristic of the nitro group. This has been done by empirical correlation of the spectra shown in Figs. 1 and 2 and the data in Tables I to IV. The results are given in Table VII which lists the infra-red vapor phase frequencies of the nitro group vibrations for the four lowest nitroparaffins together with similar data for deuterated nitromethane as taken from the paper by Wilson.[2]

The unsymmetrical stretching frequency around 1580 cm^{-1} is by far the most characteristic nitro group vibration. For each of the five compounds in the gaseous state it appears in a spectral interval of only 15 cm^{-1}, although the band contour varies considerably from vapor to vapor. The identification of the symmetrical stretching frequency is less certain because of its proximity to a methyl frequency. For each compound the lower frequency absorption maximum in the region from 1350 to 1400 cm^{-1} has somewhat arbitrarily been ascribed to the nitro vibration. It appears between 1363 and 1385 cm^{-1}. The C—N stretching frequency, having the value 918 cm^{-1} in nitromethane, is depressed as the alkyl group becomes larger, appearing at 804 cm^{-1} in 1-nitropropane. However, because of the appearance of other skeletal vibrations in this region when the paraffin chain becomes longer, identification of a C—N stretching frequency in 1-nitropropane is uncertain.

TABLE IV. Infra-red and Raman frequencies of 2-nitropropane.

Infra-red Vapor		Infra-red Liquid		Raman Liquid	
cm^{-1}	Description	cm^{-1}	Description	cm^{-1}	Description
				278	*w, d*
				320	*w, d*
				356	*w, d*
ca. 516	shoulder				
526	*w*	525	*m, sh*	525.4	*s, sh*
ca. 534	shoulder				
ca. 590	shoulder				
ca. 630	*w, b*	623	*m*	620	*m, d*
		ca. 724	*m*	719	*vvw, d*
844	*m*				
851	*m, sh*	851	*s, sh*	851	*vs, sh*
860	*m*				
ca. 898	shoulder				
906	*w, sh*	902	*m, sh*	903	*w*
914	*w*				
ca. 943	*w, b*	943	*m*		
		ca. 955	shoulder	955	*vw, d*
ca. 1097	shoulder				
1107	*m, sh*	1101	*s, sh*	1101.5	*m, sh*
1115	*m*				
ca. 1140	*w, b*	1140	*m*	1140	*w*
1174	*w*	1179	*m, sh*		
1184	*w*				
1305	*m, sh*	1305	*s, sh*	1305	*m, d*
1313	*m*	*ca.* 1325	shoulder	1332	*vvw*
ca. 1356	shoulder				
1363	*s, sh*	1361	*s, sh*	1359.3	*vs, sh*
1370	*s*	1376	*m, sh*		
1391	*s*				
1401	*s, sh*	1401	*s, sh*	1399.7	*s, sh*
1412	*s, sh*				
1468	*m*	*ca.* 1455	shoulder	1446	*s,*
1477	*m, sh*	1473	*s, sh*	1465	*w, d*
ca. 1485	shoulder				
ca. 1562	shoulder				
1575	*vs, sh*	1558	*vs, sh*	1551	*m*
ca. 1585	shoulder				
		1802	*vw*		
		1828	*vvw*		
		1859	*w*		
		1919	*vw*		
		2000	*vw*		
		2079	*vw*		
		2155	*vvw*		
		2208	*w*		
		2268	*w, sh*	2256	*vvw*
		2320	*w*		
ca. 2390	*vw*	2392	*w, sh*	2396	*vvw*
		2457	*vw*		
		2510	*vw*		
		2545	*vw*		
ca. 2725	*vw, b*	2710	*w*	2734	*vw*
		2760	*w*		
		ca. 2900	shoulder	2926	*s, d*
2950	*s, sh*	2940	*s, sh*	2949.1	*vs, sh*
3005	*s, sh*	2990	*s, sh*	2997	*s, d*
		3230	*vw*	3224	*vvw, vd*
		3600	*vw, sh*		
		3660	*w, sh*		
		ca. 3890	*vw, b*		
		4170	*w*		
		4350	*w*		
		4410	*w*		

TABLE V. Fundamental frequencies for nitromethane.

Vibrational class	Vibrational motion	Infra-red (vapor) frequency	Band type	$\nu - \nu_0$ (obs.)	Raman (liquid) frequency	Depolarization
				14 cm^{-1} (calc.)		
A_1	CH_3 sym. stretching	2972 cm^{-1}	A	~17	2967.8	0.05
(Totally symmetrical)	CH_3 sym. bending	1397		15	1401.4	0.28
	NO_2 sym. stretching	1377		15	1377.3	0.2
	NO_2 sym. bending	658		13	656.5	0.39
	C−N stretching	918		13.5	918.8	0.05
A_2	CH_3 twisting	Inactive			Inactive	
				3.5 to 14 cm^{-1} (calc.)		
B_1	CH_3 unsym. stretching	~3065	B	—	3055	0.9
(Parallel to NO_2 plane)	CH_3 unsym. bending	1443		6	1427	—
	CH_3 rocking	1087		—	1104	0.9
	NO_2 unsym. stretching	1586		6	1562	0.83
	NO_2 rocking	477		10	481	0.9
				19 cm^{-1} (calc.)		
B_2	CH_3 unsym. stretching	~3065	C	—	3055	0.9
(Perpendicular to plane)	CH_3 unsym. bending	1482		—	—	—
	CH_3 rocking	1100		—	1104	0.9
	NO_2 rocking	605		20	608	—

TABLE VI. Assignment of infra-red and Raman bands of nitromethane not interpreted as fundamentals.

Observed* I.R.	Ra.	Assignment**
960 (*l*)		2×477=954
1208 (*g*)		2×605=1210
1140 (*g*)		477+658=1135
1311 (*g*)	1313 (*l*)	2×658=1316
1522 (*g*)		918+605=1523
	1730 (*l*)	658+1087=1745
1754 (*l*)		658+1100=1758
1828 (*l*)	1830 (*l*)	2×918=1836
1852 (*l*)		476+1377=1853
1980 (*l*)		605+1377=1982
2033 (*l*)		658+1377=2035
2212 (*l*)		2×1100=2200
2283 (*l*)	2290 (*l*)	918+1377=2295
2315 (*l*)	2315 (*l*)	918+1397=2315
2475 (*g*)		1100+1377=2477 or 1087+1397=2484
2540 (*l*)		1100+1443=2543?
	2744 (*l*)	2×1377=2754
2770 (*g*)	2771 (*l*)	1377+1397=2774
2810 (*l*)		1377+1443=2820 or 2×1397=2794
	2840 (*l*)	1397+1443=2840
2872 (*g*)		1397+1482=2879 or 2×1443=2886
3600 (*l*)		658+2972=3630
3660 (*l*)		605+3065=3670
3830 (*l*)		918+2972=3890
4150 (*l*)		1087+3065=4152
4460 (*l*)		1397+3065=4462 or 1482+2972=4454

* *l*=liquid; *g*=gas.
** Using vapor phase fundamental frequencies.

TABLE VII. Empirical correlation of the nitro group frequencies* in nitroparaffins.

	CH_3NO_2	CD_3NO_2**	$C_2H_5NO_2$	$(CH_3)_2CHNO_2$	$C_2H_5CH_2NO_2$
NO_2 sym. stretch	1377	1384 cm^{-1}	1366 cm^{-1}	1363 cm^{-1}	1385 cm^{-1}
C−N stretch	918	879	876	851	804
NO_2 sym. bend	658	632	621	630	610
NO_2 unsym. stretch	1586	1571	1580	1575	1578
NO_2 rock	477	424	—	—	—
NO_2 rock	605	560	495†	526	477†

* Infra-red measurements in the vapor state.
** Values taken from the paper by Wilson (see reference 2).
† Measured for the liquid state.

The symmetrical bending frequency of the nitro group is easily identified and appears in the spectral interval 610 cm^{-1} to 658 cm^{-1}. The two rocking frequencies vary considerably in this group of compounds and are therefore the least useful of the nitro group frequencies. The higher of these rocking frequencies is probably assigned correctly in Table VII, except perhaps for 1-nitropropane where the frequency given may correspond to a carbon skeletal vibration. The other rocking frequency is apparently beyond the range of the infra-red measurements, except in the case of nitromethane.

The Vapor Pressure of Plutonium Halides*

T. E. PHIPPS,† G. W. SEARS,‡ R. L. SEIFERT,¶ AND O. C. SIMPSON
Argonne National Laboratory, Chicago, Illinois

(Received June 13, 1949)

Vapor pressure measurements have been made with three halides of plutonium by a modification of the Knudsen effusion method. Measurements with solid plutonium trifluoride from 1200°K to 1440°K give the vapor pressure-temperature relation $\log_{10}p_{mm}=12.468-21{,}120/T$. Measurements with liquid plutonium trifluoride from 1440°K to 1770°K give $\log_{10}p_{mm}=11.273-19{,}400/T$. Measurements with solid plutonium trichloride from 850°K to 1007°K give $\log_{10}p_{mm}=12.726-15{,}910/T$; with liquid trichloride from 1007°K to 1250°K give $\log_{10}p_{mm}=9.509-12{,}590/T$. Measurements with solid plutonium tribromide from 800°K to 929°K give $\log_{10}p_{mm}=13.386-15{,}280/T$; with liquid tribromide from 929°K to 1100°K give $\log_{10}p_{mm}=10.321-12{,}360/T$.

I. INTRODUCTION

ACCURATE quantitative determinations can be made for very small amounts of plutonium compounds by the methods of radiochemical assay. This fact made it possible to determine the vapor pressure of plutonium compounds by a modification of the Knudsen effusion method.[1] In this modification a small, but known, fraction of the vapor effusing from the circular orifice of an oven is collected on a target and measured by radiochemical assay. According to the kinetic theory of gases, Q, the total number of moles of gas striking an area of a cm² of surface per second, is given by the relation,

$$Q=pa(2\pi MRT)^{-\frac{1}{2}}, \qquad (1)$$

where p is the pressure of the gas (in c.g.s. units), M is the molecular weight of the gas molecule, R is the gas constant per mole, and T is the absolute temperature of the gas. If a substance is heated at constant temperature in vacuum in an oven, in which the only opening is a small circular thin-edged orifice having an area of a cm², Q moles of vapor will effuse from the orifice as given by Eq. (1), where p is the vapor pressure of the substance at the oven temperature T. If the effective evaporation area of the substance is very large compared to the total area of the orifice plus the effective area of any leaks in the oven, p will be the saturation vapor pressure of the substance at the oven temperature.

The intensity distribution of the vapor effusing from a thin-edged orifice is given by the cosine distribution law.[2] If the orifice is not a thin-edged hole but rather a short cylindrical opening, the angular distribution is not given by the cosine distribution law.[3] At large angles to the axis of such an orifice the intensity of effusing vapor will be less than for a thin-edged orifice of equal size. However, along the axis of such an orifice the intensity of effusing vapor is the same as in the case of a thin-edged orifice. The intensity of vapor effusing within a small solid angle about the axis of a cylindrical orifice is given as a close approximation by the cosine distribution law. The total amount of vapor effusing within such a small solid angle will therefore correspond to a calculable fraction of the total amount of vapor which would effuse from a thin-edged orifice of equal area. At any oven temperature this latter quantity is given by Eq. (1) as a function of the pressure of the vapor in the oven and the cross-section area of the orifice. Therefore, if only that portion of vapor is collected which effuses within a small solid angle about the orifice axis, it becomes possible to determine accurately the vapor pressure of the oven charge even though the oven orifice is not a perfect thin-edged hole.

In this investigation a circular collimator was placed at a distance from the orifice. The plane of the collimator was parallel to the plane of the orifice, and the line joining the centers of collimator and orifice was normal to their planes. The distance from orifice to collimator, r, was large compared to the diameter of the collimator, D. From the cosine distribution law the fraction of effusing vapor which passes through such a collimator is equal to $D^2/(D^2+4r^2)$. Therefore N, the number of moles of vapor passing through the collimator per second, is given by

$$N=paD^2/(D^2+4r^2)(2\pi MRT)^{\frac{1}{2}}. \qquad (2)$$

The plutonium halide vapor which passed through the collimator in a measured period of time was condensed on a target, which was cooled by liquid air in order to insure condensation of all vapor molecules striking the target. The amount of halide in the resulting deposit on the target was determined by radiochemical assay. The number of alpha-disintegrations per minute was determined in a high geometry parallel-plate alpha-chamber. Under these counting conditions the activity per microgram of Pu^{239} was 7.10×10^4 registered disintegrations per minute. If it is assumed

* This paper is based on work performed under Contract No. W-7401-eng-37 for the Manhattan Project at the Metallurgical Laboratory, Chicago, Illinois.

† Present address: Department of Chemistry, University of Illinois, Urbana, Illinois.

‡ Present address: General Electric Company, Schenectady, New York.

¶ Present address: Department of Chemistry, Indiana University, Bloomington, Indiana.

[1] M. Knudsen, Ann. d. Physik **29**, 179 (1909).

[2] M. Knudsen, Ann. d. Physik **28**, 75 (1909).

[3] P. Clausing, Zeits. f. Physik **66**, 471 (1930).

that the molecules of plutonium halide vapor contain only one plutonium atom per molecule, then N is also given by

$$N=10^{-6}c/7.10\times10^{4}(239)60\tau=9.82\times10^{-16}c/\tau, \quad (3)$$

where c is the number of registered alpha-disintegrations per minute for the deposit on the target and τ is the time in minutes during which vapor was allowed to condense on the target. By equating Eqs. (2) and (3), substituting proper values for constants, solving for p, and converting the units of p to mm Hg, one obtains

$$p_{\text{mm}}=1.684\times10^{-14}c(D^2+4r^2)(MT)^{\frac{1}{2}}/a\tau D^2. \quad (4)$$

The values of a and r vary with oven temperature and are calculated for each oven temperature from the values at 25°C and the linear coefficients of thermal expansion for the materials involved.

II. APPARATUS

Since the plutonium halides react readily with water and oxygen it was essential that each sample of halide be placed in the oven and into the experimental apparatus with minimum contact with oxygen or water vapor. After the sample was placed in the apparatus and the apparatus was evacuated it was desirable to make as many measurements as possible before any gas was admitted to the system. In order to accomplish this the apparatus shown in Fig. 1 was used. This apparatus permitted at least fifty measurements of vapor pressure to be made at different oven temperatures while a high vacuum was constantly maintained.

The charge of halide was placed in a tantalum oven

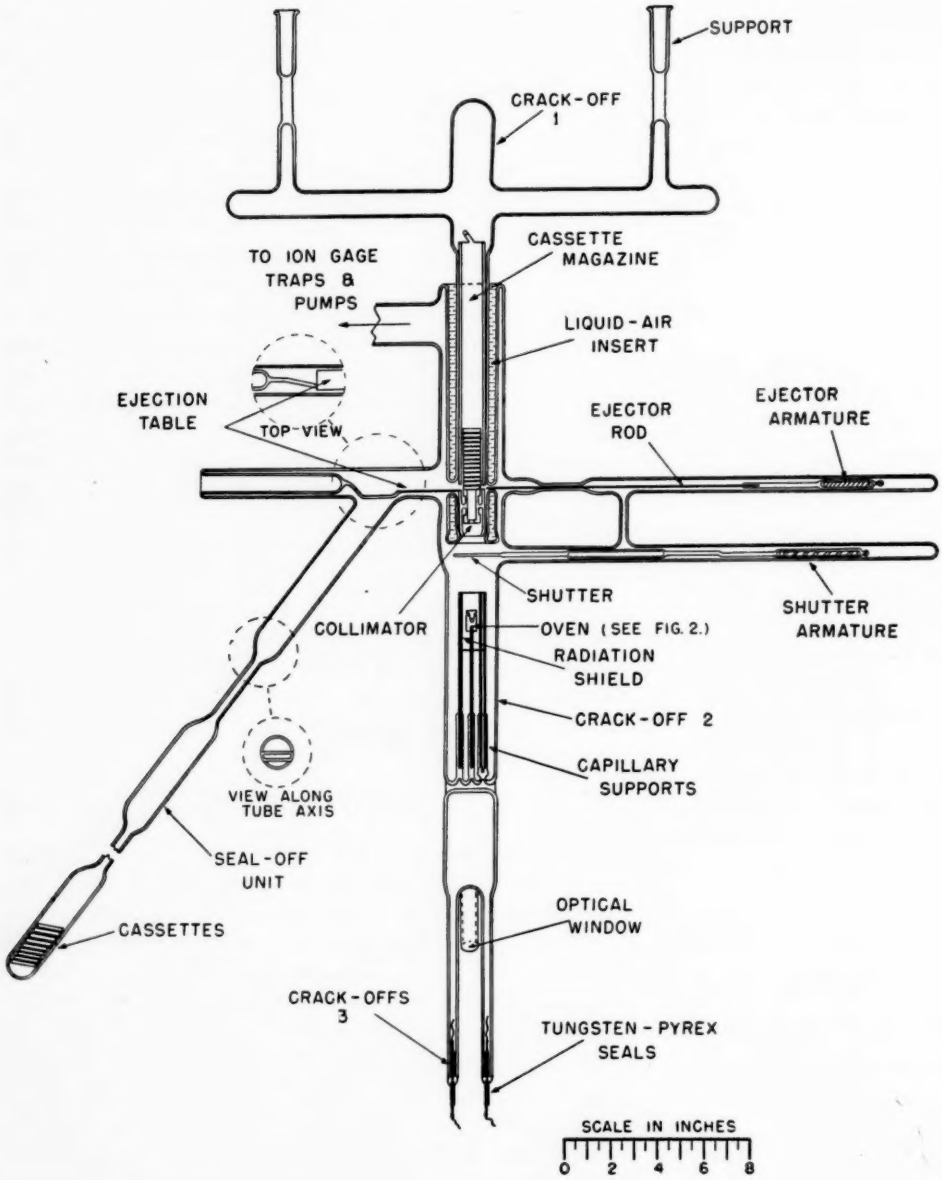

FIG. 1. Apparatus for the measurement of the vapor pressure of plutonium halides.

equipped with a chromel *P*-alumel thermocouple and a "black-body" hole for temperature determination by optical pyrometry. The construction of the oven is shown in Fig. 2. The orifice was formed in a disk of 5-mil tantalum foil by polishing off a tiny pimple which had been formed at the center of the disk with a steel point. The resulting hole was reamed and the disk surface was polished further. The orifice formed by this procedure was almost perfectly circular.[4] The thickness of the tantalum at the edge of the orifice was 1 to 3 mil. The orifice disk was spotwelded to the top of the oven. The oven was supported by a 100-mil tungsten rod, which was in turn held in a Pyrex capillary tube support. A tantalum radiation shield encircled the oven. The shield, constructed from 5-mil tantalum foil, was supported by three tungsten rods in such a way that the foil was bent into a spiral which, without closing upon itself, still enclosed the effusion vessel. The radiation shield was not used during the measurements with plutonium tribromide since the oven temperatures required could be easily obtained without the shield.

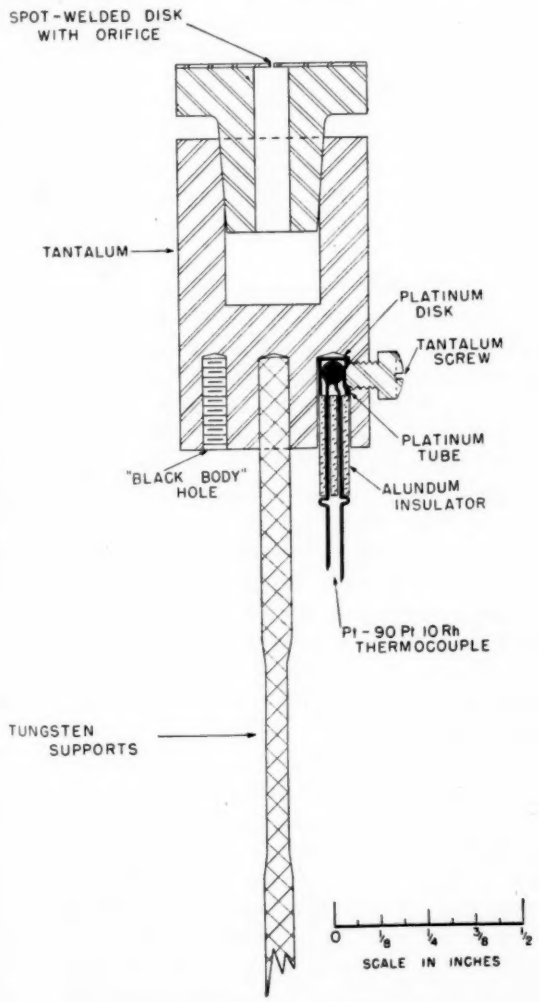

FIG. 2. Effusion oven detail.

[4] See also Phipps *et al.*, J. Chem. Phys. **18**, 724 (1950).

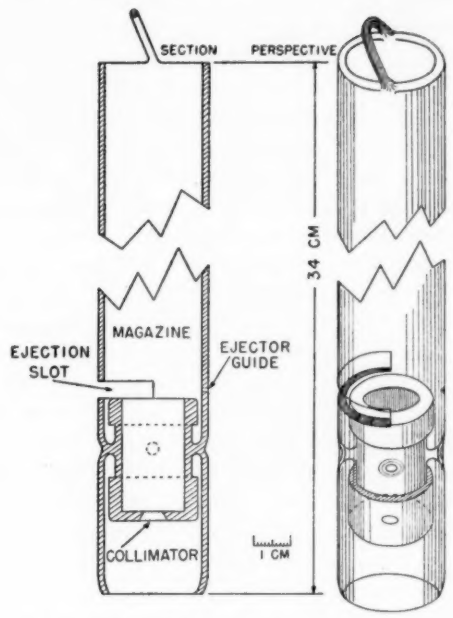

FIG. 3. Cassette magazine and collimator.

The thermocouple wires were hard-soldered to 40-mil tungsten leads sealed into the ends of 12-mm Pyrex tubes. These tubes were made nine inches long to permit cooling the junctions in an ice-water bath without interfering with the observation of the oven through the optical window at the bottom of the apparatus.

A Pyrex collimator was constructed and sealed into the end of the Pyrex cassette magazine as shown in Fig. 3. The collimator was beveled at a 45 degree angle on the lower side. The cassette magazine was constricted slightly at the bottom with a curvature to fit the curvature of the inside of the liquid-air insert. The cassette magazine was placed in the liquid-air insert as shown in Fig. 1. The distance from orifice to collimator was measured by means of a pointed tungsten rod equipped with a sliding brass collar. A small clip spring held the collar in place, but permitted it to be moved with slight pressure. A setscrew permitted the collar to be fastened in place. With the cassette magazine in place the tungsten rod was carefully lowered through the collimator until the brass collar rested on the top of the collimator plate and the tungsten point touched the oven top near the orifice. The distance from tungsten tip to brass collar was measured with a 12-inch vernier caliper. The oven and cassette magazine could be removed and replaced through the top of the apparatus at "crack-off 1". The positions of oven and collimator were definite as shown by the reproducibility of the orifice-to-collimator distance.

Openings were provided through the liquid-air insert to correspond to the shape and position of the ejection slot and ejector guide in the cassette magazine. An ejector rod of 50-mil tungsten was sealed to a Pyrex-enclosed iron armature and placed in the side arm as shown in Fig. 1. The side arm contained a capillary

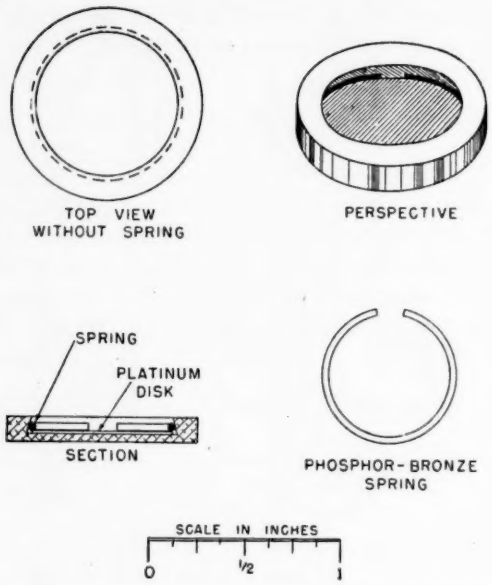

FIG. 4. Aluminum cassette for holding platinum disk target.

constriction to direct the ejector rod through the liquid-air insert and the ejector guide in the cassette magazine.

A Pyrex shutter was provided as shown in Fig. 1. The shutter and ejector rod were moved in the vacuum by the action of solenoids on the iron armatures. The solenoids rested on suitable tracks.

A piece of optical Pyrex plate served as the ejection table and was sealed in position as shown. The various parts were aligned so that when the ejector rod was moved forward it pushed the lowest target in the cassette magazine out of the ejection slot onto the ejection table. Further motion of the rod pushed the target off the end of the ejection table and permitted it to fall down into the "seal-off unit" (Fig. 1). When the ejector rod was pulled back to its original position the next target would fall into position above the collimator. The constrictions in the "seal-off unit" were so shaped that the targets could slide through.

For use in this apparatus the targets had to be designed to protect the vapor deposit from contact with any part of the apparatus during the removal of the target from its position above the collimator. Two types of targets were used. The targets which were used for the first measurements of the vapor pressure of plutonium trifluoride were glass disks cut from double spherical hanging-drop microscope slides, having spherical segments 18 mm in diameter and 1.75 mm deep. The slides had a thickness of 3 mm. The target disks were 25 mm in diameter and were cut from the microscope slides concentric with the depressions. A thin deposit of nickel was evaporated onto the depression side of the targets. Each target was numbered and the numbered targets were placed in consecutive order in the cassette magazine (Fig. 1) with the nickelized sides toward the collimator.

In order to conform to the standard method of radiochemical assay for plutonium as used in this laboratory the nickelized glass targets were replaced by platinum targets for later measurements with plutonium trifluoride and for all the measurements with the other halides. The platinum targets were 0.75-in. disks of 0.005-in. platinum foil. In order that the targets might be used in the apparatus shown in Fig. 1 they were mounted in aluminum cassettes as shown in Fig. 4. The platinum disk rested on the bottom of the aluminum cassette and was held in place by a phosphor-bronze spring. Both the platinum targets and cassettes were numbered. With each design of target the deposit of plutonium halide was protected by a raised edge so that it could not come in contact with any part of the apparatus at any time.

III. EXPERIMENTAL PROCEDURE

The tantalum oven was initially outgassed by induction heating in an auxiliary vacuum apparatus. To prevent the oven top from sintering to the oven during this operation the two parts of the oven were separated by a loose fitting cap of tungsten foil which was placed on the lower section of the oven. The oven top was placed on the tungsten cap and held in place by a 0.060-in. diameter tungsten rod which passed through the cap into the oven and part way into the oven top. The oven parts were then heated in a vacuum to about 2000°C for about three hours. After the oven was outgassed the chromel *P*-alumel thermocouple was attached.

The samples of plutonium halides were obtained from N. R. Davidson of the Metallurgical Laboratory as small crystals sealed in small quartz ampoules. The charge of plutonium halide was placed in the oven in a dry-box and the oven top was firmly put in place. The following operations were performed as rapidly as possible: the oven was lowered into position (Fig. 1), the loaded cassette magazine was introduced, the thermocouple wires were hard-soldered to the tungsten lead-ins, crack-offs 1 and 3 were sealed, and the apparatus was evacuated. During the introduction of the oven and cassette magazine a stream of dry nitrogen was passed through the apparatus. After the oven was in place the pressure in the apparatus was constantly maintained at 10^{-6}-mm Hg or less until all the measurements were completed.

After liquid air was placed in the liquid-air insert the oven was heated by induction to the temperature desired for the vapor pressure measurement. The Pyrex tube surrounding the oven was cooled by an air blast. When a constant oven temperature was obtained the shutter was moved from beneath the collimator for a measured period of time. When the shutter was again in place below the collimator, the lowest target, which contained the deposit of plutonium halide, was ejected by forcing in the ejector rod until the target was pushed off the end of the ejection table and fell down to the

lowest compartment of the seal-off unit. The ejector rod was retracted and the next target fell into position above the collimator. The oven temperature was changed to a different value and the next target was exposed and ejected in a similar manner.

The exposed targets which had collected in the end compartment of the seal-off unit were removed from the apparatus by sealing off the end compartment. This was done by careful heating of the lowest constriction with a hand torch. After the flat constriction had collapsed and sealed off the end compartment, the lower part of the collapsed section was heated to the softening point and the end compartment was pulled off. The compartment was then cracked open and the targets were removed. Each target was placed on the lower plate of a high geometry parallel-plate alpha-chamber and the amount of halide which had been deposited on the target during its exposure was determined by the measurement of the number of alpha-disintegrations per minute.

Since two different types of targets were used in measurements with plutonium trifluoride, it was necessary to determine whether there was any difference in the measured activity of a deposit of plutonium halide on a curved nickel surface and on a flat platinum surface. The cassette magazine was loaded with fourteen targets, alternating nickelized glass and platinum targets. The oven, containing plutonium tribromide, was maintained at constant temperature while five-minute exposures were made on the first seven targets and ten-minute exposures were made on the remaining seven targets. In each group of seven targets the average count of the alpha-disintegrations on the platinum targets was divided by the average count for the nickelized glass targets. The resulting ratio was used to correct all data obtained with the curved nickelized targets to corresponding values for deposits on flat platinum targets. Within the accuracy of the measurements the resulting correction factor was the same, 1.105, for both groups of seven targets. The factor was therefore considered to be independent of the activity of the deposit on the target.

At each oven temperature the vapor pressure of the halide was calculated by Eq. (4).

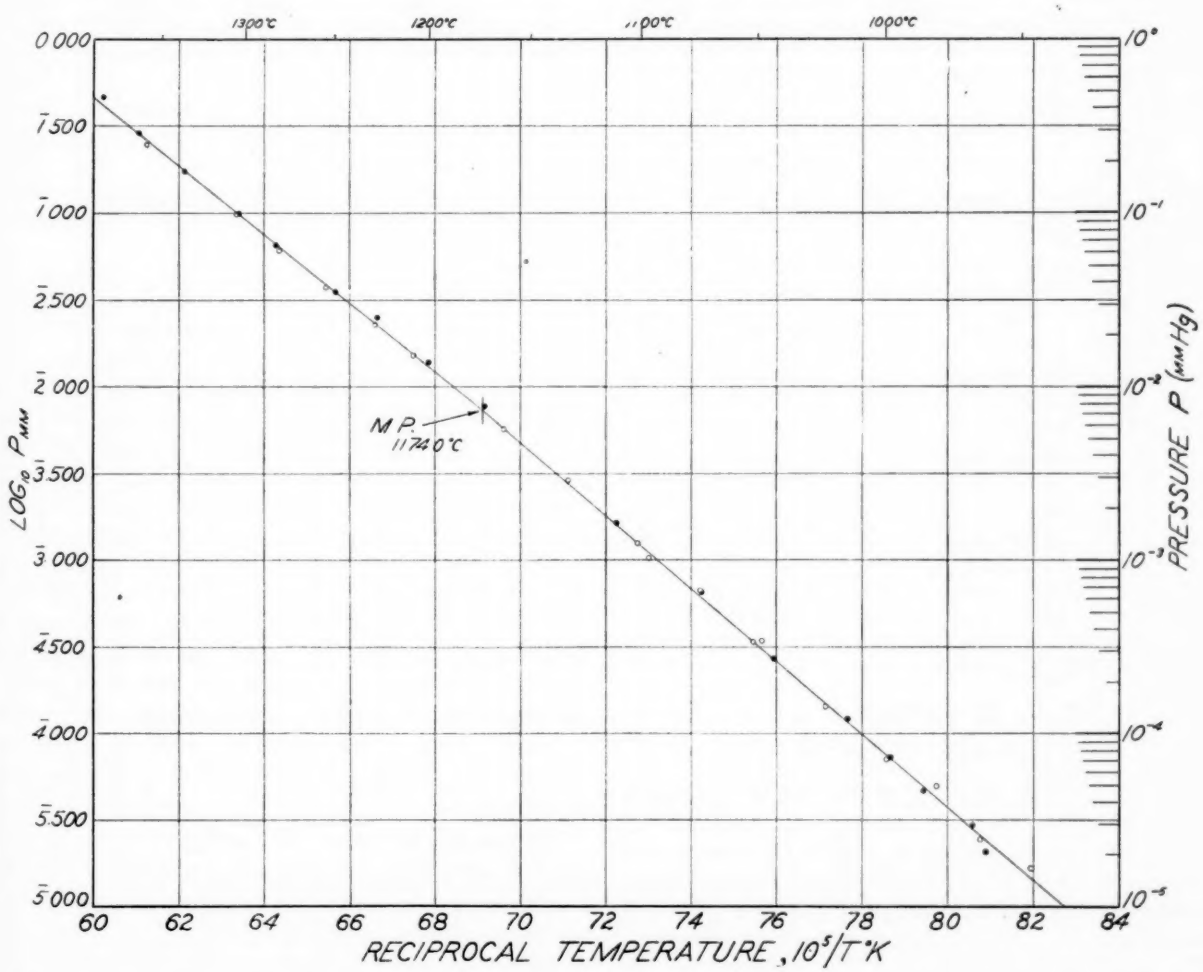

FIG. 5. The vapor pressure of plutonium trifluoride. The circles correspond to the data in Table I. The dots correspond to the data in Table II. The lines are least squares lines for the combined data.

TABLE I. Vapor pressure of plutonium trifluoride. Series I (nickelized glass targets).

Target no.	Exposure time τ (min.)	Counts per minute c	Temp. °K	Logarithm of the vapor pressure $\log_{10} p_{mm}$	Recip. temp. $1/T \times 10^3$
1–12	10.00	1.40± 0.43	1220.7	$\bar{5}.15$ ±0.13	81.92
1–13	10.00	7.20± 0.91	1273.2	$\bar{5}.870$ ±0.055	78.54
1–14	10.00	31.9± 1.2	1321.8	$\bar{4}.525$ ±0.016	75.65
1–15	10.00	94.7 ± 3.0	1369.6	$\bar{3}.004$ ±0.014	73.01
1–16	100.00	16.27± 0.35	1220.0	$\bar{5}.216$ ±0.010	81.97
1–17	13.02	6.12± 0.25	1254.0	$\bar{5}.682$ ±0.018	79.75
1–18	30.00	20.23± 0.41	1272.6	$\bar{5}.8419$±0.0097	78.58
1–19	20.00	26.85± 0.47	1296.2	$\bar{4}.1447$±0.0085	77.15
1–20	10.00	31.39± 0.51	1325.2	$\bar{4}.5181$±0.0080	75.46
1–21	10.00	58.26± 0.95	1347.5	$\bar{4}.7901$±0.0080	74.21
1–22	10.00	114.4 ± 1.3	1374.7	$\bar{3}.0872$±0.0060	72.74
1–23	10.00	265.1 ± 2.0	1406.2	$\bar{3}.4568$±0.0046	71.11
1–24	5.00	253.6 ± 2.4	1436.7	$\bar{3}.7430$±0.0054	69.60
1–25	5.00	416.4 ± 3.2	1457.6	$\bar{3}.9612$±0.0044	68.61
1–26	5.00	663.9 ± 4.3	1481.6	$\bar{2}.1672$±0.0040	67.50
1–27	2.00	400.3 ± 3.1	1501.6	$\bar{2}.3481$±0.0051	66.60
1–28	2.00	650.2 ± 4.1	1528.2	$\bar{2}.5623$±0.0047	65.44
1–29	2.00	1040.4 ± 5.7	1554.1	$\bar{2}.7699$±0.0044	64.35
1–30	2.00	1676. ±11.	1578.8	$\bar{2}.9801$±0.0047	63.34
1–31	2.00	4117. ±27.	1633.2	$\bar{1}.3771$±0.0046	61.23

TABLE II. Vapor pressure of plutonium trifluoride. Series II (platinum targets).

Target no.	Exposure time τ (min.)	Counts per minute c	Temp. °K	Logarithm of the vapor pressure $\log_{10} p_{mm}$	Recip. temp. $1/T \times 10^3$
2– 3	17.20	5.50± 0.33	1241	$\bar{5}.469$±0.038	80.59
2– 4	100.01	22.20± 0.60	1236	$\bar{5}.310$±0 030	80.90
2– 5	40 13	31.51± 0.71	1271	$\bar{5}.864$±0.028	78.68
2– 6	41.10	51.86± 0.91	1288	$\bar{4}.073$±0.026	77.67
2– 7	20.00	56.00± 0.94	1317	$\bar{4}.424$±0.025	75.93
2– 8	10.00	67.33± 1.0	1347	$\bar{4}.810$±0.025	74.24
2– 9	10.43	174.7 ± 2.0	1384	$\bar{3}.211$±0.023	72.25
2–11	10.00	757.4 ± 4.6	1446	$\bar{3}.876$±0.020	69.15
2–12	5.00	675.4 ± 4.1	1474	$\bar{2}.130$±0.018	67.84
2–13	5.00	1135.4 ± 8.2	1501	$\bar{2}.359$±0.017	66.63
2–14	5.00	1709. ±11.	1523	$\bar{2}.540$±0.017	65.67
2–15	2.00	1247.8 ± 8.7	1556	$\bar{2}.806$±0.017	64.28
2–16	2.00	1900. ±16.	1577	$\bar{2}.991$±0.016	63.40
2–17	2.00	3301. ±25.	1610	$\bar{1}.235$±0.015	62.13
2–18	2.00	5418. ±37.	1638	$\bar{1}.454$±0.015	61.06
2–19	2.00	8721. ±89.	1661	$\bar{1}.663$±0.015	60.22

IV. RESULTS

Plutonium Trifluoride

The oven charge consisted of 25.5 mg of plutonium trifluoride which had been prepared by A. Florin by heating plutonium dioxide at 600°C in a stream of hydrogen and hydrogen fluoride. The root-mean-square diameter of the oven orifice at 25°C was 0.01475± 0.00006 cm. The distance from orifice to collimator at 25°C was 10.366 ±0.008 cm. The diameter of the collimator which was used for all measurements was 0.5235±0.0015 cm.

TABLE III. Vapor pressure of plutonium trichloride.

Target no.	Exposure time τ (min.)	Counts per minute c	Temp. °K	Logarithm of the vapor pressure $\log_{10} p_{mm}$	Recip. temp. $1/T \times 10^3$
2–18	3.00	818.1 ±9.1	1135.9	$\bar{2}.3383$±0.0059	88.04
2–19	3.00	878.9 ±9.6	1137.7	$\bar{2}.3698$±0.0059	87.90
2–20	3.00	883.4 ±9.6	1136.7	$\bar{2}.3718$±0.0059	87.97
2–21	3.00	871.8 ±9.5	1136.0	$\bar{2}.3660$±0.0059	88.03
2–23	30.00	7.72±0.25	908.9	$\bar{5}.267$ ±0.015	110.02
2–24	15.00	14.10±0.36	940.8	$\bar{5}.837$ ±0.012	106.29
2–25	10.00	53.83±0.90	985.9	$\bar{4}.6043$±0.0088	101.43
2–26	10.00	94.7 ±1.2	1003.0	$\bar{4}.8532$±0.0073	99.70
2–27	10.00	191.9 ±1.3	1023.4	$\bar{3}.1641$±0.0048	97.71
2–29	5.00	561.5 ±3.8	1092.9	$\bar{3}.9450$±0.0045	91.50
2–30	2.00	360.3 ±4.1	1118.8	$\bar{2}.1551$±0.0065	89.38
2–31	2.00	561.4 ±5.2	1139.0	$\bar{2}.3515$±0.0058	87.80
2–32	2.00	350.1 ±3.4	1118.1	$\bar{2}.1425$±0.0060	89.44
2–33	5.00	434.9 ±4.6	1087.2	$\bar{3}.8330$±0.0058	91.98
2–34	5.00	175.9 ±2.8	1050.8	$\bar{3}.4328$±0.0078	95.17
2–35	11.00	250.4 ±3.4	1034.3	$\bar{3}.2405$±0.0069	96.68
2–36	10.00	112.2 ±1.3	1009.5	$\bar{4}.9282$±0.0062	99.06
2–38	15.00	9.75±0.24	933.3	$\bar{5}.675$ ±0.012	107.15
2–39	31.00	8.25±0.21	912.9	$\bar{5}.282$ ±0.012	109.54
2–40	60.00	3.12±0.24	879.0	$\bar{6}.565$ ±0.034	113.77
2–41	22.00	13.85±0.35	933.3	$\bar{5}.661$ ±0.012	107.15
2–42	10.00	57.5 ±1.1	988.0	$\bar{4}.633$ ±0.011	101.22
2–44	5.00	361.6 ±2.2	1076.5	$\bar{3}.7508$±0.0044	92.89
2–45	2.00	488.3 ±3.5	1129.0	$\bar{2}.2891$±0.0052	88.57
2–46	1.10	679.8 ±6.0	1173.3	$\bar{2}.7003$±0.0073	85.23
2–47	1.20	1942.9 ±9.6	1222.8	$\bar{1}.1271$±0.0060	81.78
2–48	2.00	378.1 ±3.9	1119.6	$\bar{2}.1762$±0.0062	89.32
2–49	10.00	212.7 ±2.2	1032.6	$\bar{3}.2107$±0.0057	96.84

Two series of measurements were made with the same oven and charge. In series I nickelized glass targets were used and the oven temperature was determined by the thermocouple. The temperature of the oven during the last exposure was above the maximum temperature for a chromel *P*-alumel thermocouple. During series II the thermocouple was no longer reliable and measurement of oven temperature was made with a Leeds and Northrup optical pyrometer. The surface temperature of the oven bottom was measured, since the optical path was too long to give a sufficiently large image of the "black-body" hole to permit accurate adjustment of the pyrometer. The measured apparent temperature of the bottom of the oven was corrected for the emissivity of the tantalum surface, the transmissivity of the optical window and the reflectivity of the mirror which was used to change the optical path. Flat platinum targets (Fig. 4) were used in series II.

The results for these two series of measurements are given in Tables I and II and are shown graphically in Fig. 5. The calculated vapor pressures are based on the assumption that the molecular form of the vapor is PuF_3. The equations of the two lines given in Fig. 5 were calculated by the method of least squares. Equal weight was given each series of measurements. The

resulting equations are as follows:

Solid, $T=1200°K$ to $1440°K$,

$$\log_{10}p_{mm}=(12.468\pm0.074)-(21{,}120\pm100)/T; \quad (5)$$

Liquid, $T=1440°K$ to $1770°K$,

$$\log_{10}p_{mm}=(11.273\pm0.034)-(19{,}399\pm53)/T. \quad (6)$$

The probable errors assigned to the constants in the above equations are the calculated probable errors based only on the residuals of the experimental points from the most probable line and indicate the reproducibility of the data. The inherent and systematic errors were approximately the same for the measurements with the different halides and will be discussed later.

Plutonium Trichloride

The oven charge consisted of 35.5 mg of plutonium trichloride which had been prepared by N. R. Davidson and I. Karle by treating oven dried plutonium hydroxide with carbon tetrachloride at 750–800°C. The root mean square diameter of the oven orifice at 25°C was 0.0159 ± 0.0001 cm. The distance from orifice to collimator at 25°C was 10.229 ± 0.006 cm. All temperature measurements were made with the thermocouple.

The resulting data are given in Table III and are shown graphically in Fig. 6. The calculated vapor pressures are based on the assumption that the molecular form of the vapor is $PuCl_3$.

The equations of the two lines shown in Fig. 6, as

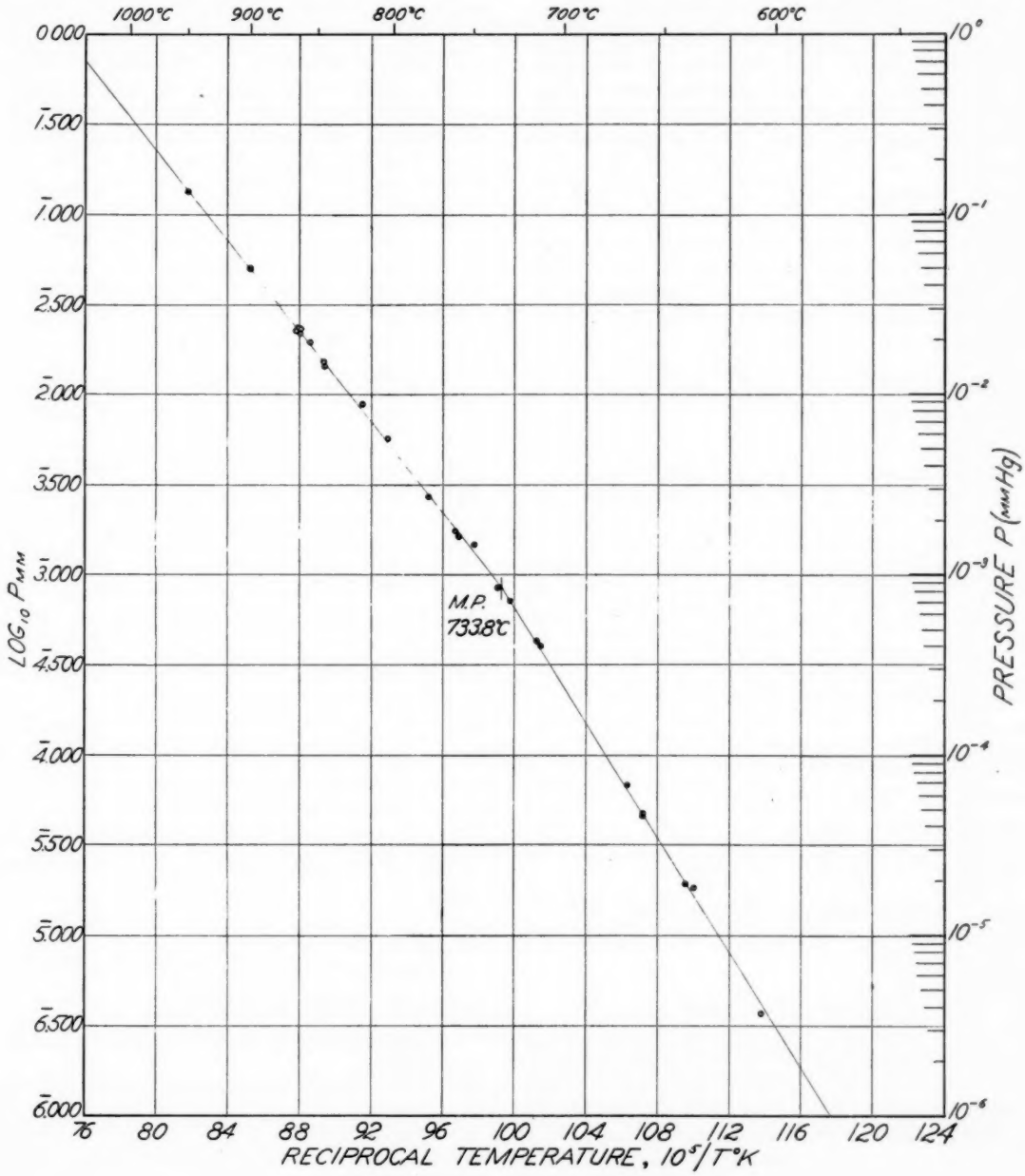

FIG. 6. The vapor pressure of plutonium trichloride.

TABLE IV. Vapor pressure of plutonium tribromide.

Target no.	Exposure time τ (min.)	Counts per minute c	Temp. °K	Logarithm of the vapor pressure $\log_{10}p_{mm}$	Recip. temp. $1/T\times10^5$
1–16	20.00	159.7 ±1.6	925.1	$\bar{4}.8647\pm0.0061$	108.10
1–26	20.00	194.6 ±1.7	931.6	$\bar{4}.9520\pm0.0057$	107.34
1–27	15.00	340.1 ±2.9	957.8	$\bar{3}.3252\pm0.0055$	104.41
1–28	10.00	394.5 ±3.1	974.2	$\bar{3}.5692\pm0.0053$	102.65
1–29	11.00	690.0 ±4.4	990.7	$\bar{3}.7741\pm0.0048$	100.94
1–30	10.00	1014.5 ±5.6	1007.4	$\bar{3}.9864\pm0.0045$	99.27
1–31	10.00	553.1 ±3.8	986.5	$\bar{3}.7186\pm0.0049$	101.37
1–32	15.00	386.2 ±3.1	962.5	$\bar{3}.3814\pm0.0053$	103.90
1–33	20.00	244.6 ±2.0	938.6	$\bar{3}.0528\pm0.0055$	106.54
1–40	15.00	224.2 ±2.1	943.8	$\bar{3}.1411\pm0.0058$	105.95
1–41	20.00	176.3 ±1.1	928.0	$\bar{4}.9083\pm0.0051$	107.76
1–42	10.00	273.8 ±2.3	962.5	$\bar{3}.4081\pm0.0054$	103.90
1–43	10.00	420.5 ±2.9	977.8	$\bar{3}.5977\pm0.0049$	102.27
1–44	10.00	318.4 ±3.3	967.9	$\bar{3}.4748\pm0.0060$	103.32
1–45	16.00	314.1 ±3.2	952.7	$\bar{3}.2615\pm0.0060$	104.96
1–46	20.00	218.9 ±2.0	934.5	$\bar{3}.0037\pm0.0058$	107.01
1–47	20.00	64.84±0.73	903.5	$\bar{4}.4682\pm0.0074$	110.68
1–48	25.00	45.65±0.63	889.8	$\bar{4}.2157\pm0.0084$	112.38
1–49	30.00	27.23±0.47	872.4	$\bar{5}.9080\pm0.0096$	114.63
1–50	60.00	10.69±0.31	839.5	$\bar{5}.193\pm0.014$	119.12
2– 1	20.00	100.5 ±0.9	915.5	$\bar{4}.6613\pm0.0067$	109.23
2– 2	300.00	5.14±0.22	795.3	$\bar{6}.165\pm0.020$	125.74
2– 3	30.00	21.54±0.43	868.5	$\bar{5}.805\pm0.011$	115.14
2– 4	25.00	36.83±0.54	883.9	$\bar{4}.1211\pm0.0086$	113.14
2– 5	20.00	52.84±0.62	898.8	$\bar{4}.3783\pm0.0076$	111.26
2– 6	20.00	240.7 ±1.3	937.4	$\bar{3}.0456\pm0.0048$	106.68
2– 7	10.00	337.2 ±2.9	970.1	$\bar{3}.5002\pm0.0055$	103.08
2– 8	10.00	707.8 ±4.4	996.0	$\bar{3}.8277\pm0.0046$	100.40
2– 9	5.00	872.2 ±3.2	1029.3	$\bar{2}.2263\pm0.0040$	97.15
2–10	3.00	792.8 ±3.9	1045.3	$\bar{2}.4099\pm0.0044$	95.67
2–11	2.00	1028.1 ±7.6	1072.5	$\bar{2}.7042\pm0.0054$	93.23
2–12	2.10	1395.7 ±9.5	1082.6	$\bar{2}.8177\pm0.0053$	92.37
2–13	2.00	756.1 ±3.9	1059.0	$\bar{2}.5681\pm0.0050$	94.43
2–14	5.00	1103.5 ±5.1	1037.2	$\bar{2}.3300\pm0.0042$	96.41
2–15	10.00	1082.4 ±3.1	1009.6	$\bar{2}.0150\pm0.0038$	99.05
2–16	10.00	554.5 ±0.7	985.3	$\bar{3}.7194\pm0.0039$	101.49
2–17	15.00	390.2 ±1.8	960.8	$\bar{3}.3855\pm0.0045$	104.08
2–18	20.00	182.4 ±1.1	928.4	$\bar{4}.9231\pm0.0050$	107.71
2–19	25.00	26.06±0.39	877.4	$\bar{5}.9693\pm0.0088$	113.97
2–20	30.00	16.83±0.31	865.4	$\bar{5}.697\pm0.010$	115.55
2–21	60.00	17.82±0.39	850.0	$\bar{5}.417\pm0.012$	117.65
2–22	50.00	22.18±0.43	859.2	$\bar{5}.594\pm0.010$	116.39
2–23	40.00	32.59±0.52	871.7	$\bar{5}.8610\pm0.0091$	114.72
2–24	30.00	34.77±0.49	878.8	$\bar{4}.0157\pm0.0085$	113.79
2–25	30.00	49.30±0.64	887.7	$\bar{4}.1695\pm0.0081$	112.65
2–26	32.00	97.13±0.96	901.6	$\bar{4}.4392\pm0.0071$	110.92
2–27	25.00	102.97±0.99	907.7	$\bar{4}.5732\pm0.0070$	110.17
2–28	25.00	146.7 ±1.5	916.5	$\bar{4}.7288\pm0.0070$	109.11
2–29	20.00	164.9 ±1.3	926.0	$\bar{4}.8786\pm0.0055$	107.99
2–30	20.00	278.0 ±1.4	939.7	$\bar{3}.1087\pm0.0047$	106.42
2–31	20.00	222.6 ±1.1	933.0	$\bar{3}.0107\pm0.0048$	107.18
2–32	20.00	148.9 ±1.3	923.5	$\bar{4}.8339\pm0.0065$	108.28
2–33	25.00	125.5 ±1.4	913.5	$\bar{4}.6604\pm0.0073$	109.47
2–34	30.00	96.20±0.96	902.1	$\bar{4}.4632\pm0.0071$	110.85
2–35	30.00	65.20±0.59	893.8	$\bar{4}.2923\pm0.0070$	111.88
2–36	30.00	43.19±0.59	884.4	$\bar{4}.1112\pm0.0083$	113.07
2–37	40.00	35.21±0.50	873.9	$\bar{5}.8951\pm0.0085$	114.43
2–38	40.00	20.55±0.39	863.0	$\bar{5}.659\pm0.010$	115.88
2–39	50.00	16.85±0.37	854.0	$\bar{5}.473\pm0.011$	117.10
2–40	60.00	13.99±0.34	845.7	$\bar{5}.311\pm0.013$	118.25
2–41	25.00	113.4 ±1.3	911.4	$\bar{4}.6158\pm0.0074$	109.72
2–42	20.00	171.2 ±1.6	928.1	$\bar{4}.8956\pm0.0059$	107.75
2–43	20.00	303.3 ±2.2	942.4	$\bar{3}.1471\pm0.0053$	106.11
2–44	21.00	396.3 ±2.5	950.1	$\bar{3}.2437\pm0.0049$	105.25
2–45	15.00	486.9 ±2.5	967.9	$\bar{3}.4832\pm0.0046$	103.32
2–46	10.00	569.2 ±3.2	987.1	$\bar{3}.7312\pm0.0045$	101.31
2–47	10.00	811.1 ±4.0	999.2	$\bar{3}.8875\pm0.0043$	100.08
2–48	5.00	792.5 ±4.0	1025.2	$\bar{2}.1838\pm0.0044$	97.54
2–49	5.00	998.9 ±4.7	1035.3	$\bar{2}.2864\pm0.0042$	96.59
2–50	10.00	2029.3 ±8.1	1036.1	$\bar{2}.2933\pm0.0039$	96.52
2–51	10.00	942.1 ±4.5	1007.0	$\bar{3}.9542\pm0.0043$	99.30
2–52	10.00	333.2 ±2.4	969.3	$\bar{3}.4948\pm0.0051$	103.17
2–53	20.00	337.6 ±2.1	948.0	$\bar{3}.1949\pm0.0049$	105.48

TABLE IV.—*Continued*

calculated by the method of least squares, are as follows:

Solid, $T=850°\text{K}$ to $1007°\text{K}$,

$$\log_{10}p_{mm}=(12.726\pm0.126)-(15{,}910\pm120)/T; \quad (7)$$

Liquid, $T=1007°\text{K}$ to $1250°\text{K}$,

$$\log_{10}p_{mm}=(9.428\pm0.075)-(12{,}587\pm82)/T. \quad (8)$$

The probable errors assigned to the constants are based only on the residuals of the experimental points from the most probable line.

Plutonium Tribromide

The oven charge consisted of 15 mg of plutonium tribromide which had been prepared by E. K. Hyde by treating plutonium hydroxide with hydrogen bromide at 800°C. The root-mean-square diameter of the oven orifice at 25°C was 0.01590 ± 0.00006 cm. The distance from orifice to collimator at 25°C was 10.589 ±0.008 cm. All temperature measurements were made with the thermocouple.

The resulting data are given in Table IV and are shown graphically in Fig. 7. The calculated vapor pressures are based on the assumption that the molecular form of the vapor is $PuBr_3$.

The equations of the two lines shown in Fig. 7, as calculated by the method of least squares, are as follows:

Solid, $T=800°\text{K}$ to $929°\text{K}$,

$$\log_{10}p_{mm}=(13.386\pm0.077)-(15{,}280\pm69)/T; \quad (9)$$

Liquid, $T=929°\text{K}$ to $1100°\text{K}$,

$$\log_{10}p_{mm}=(10.237\pm0.033)-(12{,}356\pm32)/T. \quad (10)$$

V. DISCUSSION OF ERRORS

The quantities in Eq. (4) which are subject to random experimental errors are c, τ, and T. The uncertainty in c arises from the statistical fluctuation in the total

number of counts observed for the target, the uncertainty in the time of counting, and the uncertainty in the resolution loss correction. The probable errors calculated for the experimental values of c are given in Tables I to IV. A probable error of ± 0.01 min. was estimated for the measurement of the time of beginning and ending each exposure. This gives a total probable error in τ of ± 0.014 min. The probable random experimental error in T as measured by the chromel P-alumel thermocouple was estimated to be ± 0.3 deg. This included errors in measuring the thermoelectric potential, errors due to fluctuations in the temperature of the cold junction, and errors due to fluctuations in the oven temperature. For each experimental point the probable random error in T was converted to a corresponding error in $\log p$ by multiplying the probable error in $1/T$ by the slope of the $\log p$ *vs.* $1/T$ curve. The probable error in each value of $\log p$ as given in Tables I to IV is the total error obtained by combining the probable errors in c, τ, and T (in accordance with Eq. (4)) with the error in $\log p$ which corresponded to the probable error in $1/T$. In the calculation of the most probable $\log p$ *vs.* $1/T$ line the values of $1/T$ were then considered to be exact, with all random experimental errors attributed to $\log p$. The weighting factors used in the calculation of the constants of the most probable lines were proportional to the reciprocal of the square of the tabulated probable errors of $\log p$.

In addition to the random errors in T there existed possible systematic errors which were constant for each given value of T. These included the deviation of the thermoelectric potential of the thermocouple from the manufacturer's calibration and also the difference between the oven temperature at the thermocouple and the lowest temperature within the oven. The latter error was the greater and was estimated on the basis of measured thermal gradients in a dummy oven. It was estimated that the total probable systematic error in T from these sources was probably no greater than ± 2.0 deg.

There are a number of other possible systematic errors which affect all the calculated values of p in a given series of measurements by the same percentage. These errors, therefore, affect only the intercept of the

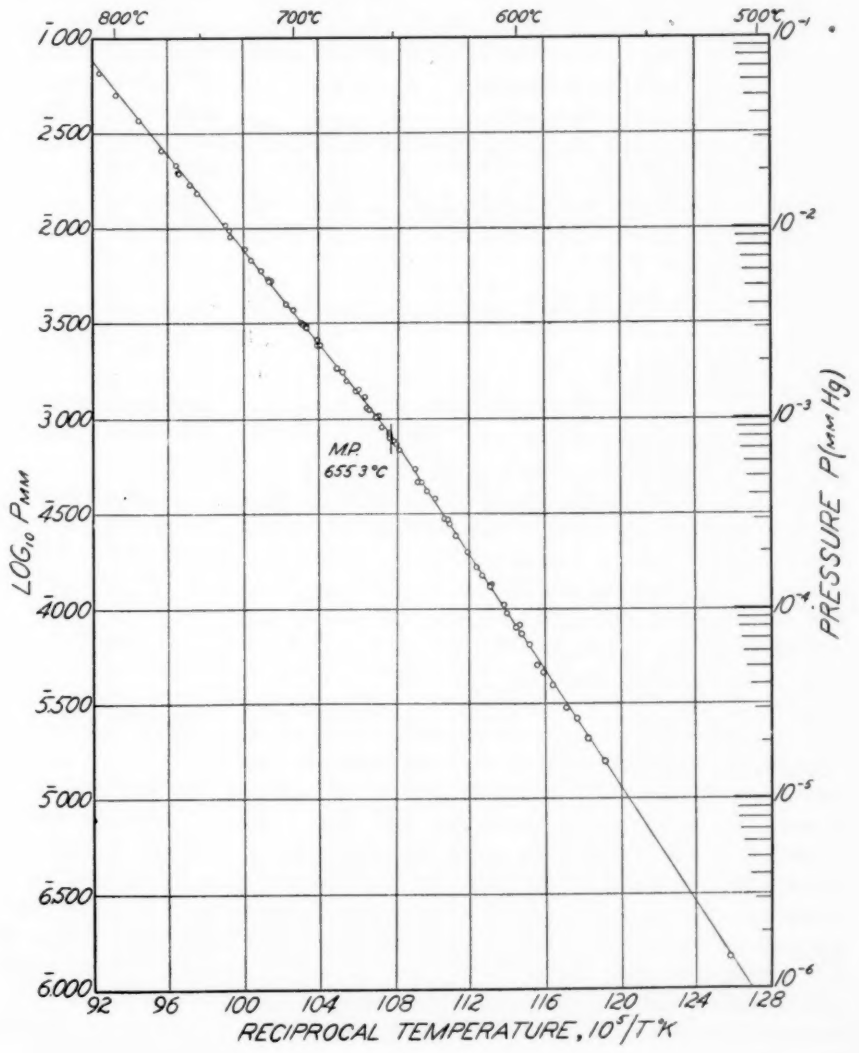

FIG. 7. The vapor pressure of plutonium tribromide.

TABLE V. Tabulation of values of constants to be used in Eqs. (12) and (13).

Halide	Melting point °K	State	A	B	$\bar{\pi}\cdot10^4$	$C\cdot10^{-4}$	$D\cdot10^4$
Plutonium trifluoride	1442±9	Solid	12.468	21,120	7.43	1.44	1.49
		Liquid	11.273	19,400	6.48	0.62	1.49
Plutonium trichloride	1033±5	Solid	12.726	15,910	10.4	1.60	1.21
		Liquid	9.509	12,590	9.11	0.77	10.2
Plutonium tribromide	954±5	Solid	13.386	15,280	11.2	0.62	1.12
		Liquid	10.321	12,360	10.2	0.20	5.53

$\log p$ *vs.* $1/T$ line. Among these systematic errors are those involved in the determination of D, r, and a (Eq. (4)). The probable errors in the determination of these quantities were calculated from the residuals of individual measurements from the average of several measurements, and from the probable inaccuracy of the measuring device. The probable errors of D and r and of the orifice diameter, from which a is calculated, are given with the data.

Additional small uncertainties exist in regard to the value of the specific activity of Pu^{239} under the counting conditions which were used to determine c and also in regard to the actual mass of Pu^{239}. It was estimated that error from this source did not exceed ±2 percent. Uncertainty arising from failure to place the collimator at the point of maximum intensity of vapor was estimated to be less than 1.0 percent.

The errors discussed above are relatively small compared to the error which will be present if the wrong assumption has been made concerning the molecular nature of the volatilizing species. However, the values of vapor pressure as here reported can be readily corrected if future measurements indicate that the molecular forms of the vapors are not PuF_3, $PuCl_3$, and $PuBr_3$.

A possible error for which correction cannot be made with certainty is the error arising from the possible presence of impurities in the oven charge. The only impurity which may have been present in each halide in significant amount was the corresponding oxyhalide. If not present in the original sample, some oxyhalide may have been formed during transfer of the material to the oven or after the charge was placed in the oven. The amount of oxygen present in the oven during the evacuation of the system and the initial heating of the oven is an unknown quantity. The maintenance of a pressure of less than 10^{-6} mm Hg in the system during the entire series of measurements prevented any significant conversion of halide to oxyhalide after the initial measurements. The reproducibility of the vapor pressure measurements substantiates this fact. Conversion of halide to oxyhalide would not affect the reproducibility of the measurements if two phases were present at all oven temperatures, or if the vapor pressures of halide and oxyhalide were the same. These two possibilities were eliminated in the case of plutonium tribromide and plutonium oxybromide at oven temperatures above 980°K by the following experiment.

TABLE VI. Molar heats of sublimation, vaporization, and fusion and entropy of fusion of the plutonium halides.

	PuF_3	$PuCl_3$	$PuBr_3$
ΔH of sublimation, kcal. mole^{-1}	96.6±0.5	72.8±0.6	69.9±0.3
ΔH of vaporization, kcal. mole^{-1}	88.7±0.2	57.6±0.4	56.5±0.2
ΔH of fusion, kcal. mole^{-1}	7.9±0.5	15.2±0.7	13.4±0.3
ΔS of fusion, cal. mole^{-1} deg.$^{-1}$	5.5±0.4	14.7±0.7	14.0±0.4

After the vapor pressure measurements were completed with the tribromide an attempt was made to convert the remaining tribromide to oxybromide by admitting oxygen to the oven. Since it was not possible to determine when complete conversion of the tribromide had occurred with no further oxidation to oxide, it was not possible to make vapor pressure measurements with pure oxybromide; and unfortunately all measurements in this experiment were made at oven temperatures above 980°K. However, the data showed that above 980°K the vapor pressure of the material in the oven decreased with additional oxidation. Therefore the reproducibility of the vapor pressure data for plutonium tribromide indicates a constant composition of the material in the oven during the measurements.

The mechanical difficulties and health hazard involved made it inadvisable to attempt to open the oven after the measurements to remove a sample of material for analysis. The oven top usually became sintered to the oven during the experiment. Removal of a sample under oxygen-free conditions would have been more difficult than the original charging of the oven.

An indication of the purity of the material in the oven during the course of the experimental measurements can be obtained from a comparison of the melting points as obtained from the vapor pressure curves with the melting points of the pure halides. This can be done for the plutonium trichloride and tribromide. H. P. Robinson[5] made a direct measurement of the melting point of a sample of plutonium trichloride which was prepared at the same time as the sample used for the vapor pressure measurements. It was found that the sample did not have a sharp melting point, but had a melting range from 740°C to 790°C. Plutonium trichloride which was sublimed in vacuum had a sharp melting point at 760 ±5°C. Similar measurements[5] were made with a sample of plutonium tribromide which had been prepared by a different procedure than that used in the preparation of the sample for vapor pressure measurements. The original sample had a melting point range from 650°C to 690°C. A portion of the plutonium tribromide which was sublimed in vacuum melted sharply at 681±5°C. A direct measurement of the melting point of plutonium trifluoride was not made.

The amount of oxyhalide present can be calculated and the experimental vapor pressure curves can be corrected if the following assumptions are made: (1) that the vapor pressure of the oxyhalide is very small

[5] H. P. Robinson (unpublished work).

compared to that of the halide; (2) that the oxyhalide and trihalide do not form a solid solution but instead form two separate solid phases; (3) that the oxyhalide and trihalide are miscible in the liquid phase; and (4) that the liquid phase approximates ideal solution behavior. The first assumption is supported by the decrease in volatility of plutonium tribromide when it was intentionally oxidized and also by the fact that the trichloride and tribromide could be purified for the melting point determination by sublimation in vacuum. The second assumption is consistent with the crystal structures of the solids.[6] Plutonium trichloride and plutonium tribromide crystallize in the hexagonal and orthorhombic systems respectively. The corresponding oxyhalides crystallize in the tetragonal system. If the above assumptions are correct, the experimental vapor pressure curves for the solid halides are correct and the experimental $\log p$ *vs.* $1/T$ curves for the liquid halides should be raised sufficiently to give a melting point corresponding to the value obtained by direct measurement.

Calculations based on these assumptions indicate that the value of the intercept of Eq. (8) is low by 0.081 ± 0.030 and the value of the intercept of Eq. (10) is low by 0.084 ± 0.021. These values correspond to 17 ± 6 mole percent of PuOCl in the plutonium trichloride sample and 18 ± 4 mole percent of PuOBr in the plutonium tribromide sample. The production of this amount of oxyhalide in the samples used required only 8.73 micromoles of oxygen in the case of the trichloride and 2.82 micromoles in the case of the tribromide. It is possible that these small amounts of oxygen might have been present in spite of the precautions taken during the preparation and transfer of the samples and in spite of the initial outgassing of the oven. The melting point determinations were made by Robinson[4] without removing the trihalide samples from the quartz tubes in which they were prepared and sealed. His measurements indicated the presence of some oxyhalide in such samples.

The accumulative effect of the various errors may be expressed by a relation of the following form:

$$\epsilon_{\log p}=\pm\{[(1/T)-\bar{x}]^2[\epsilon_s^2+(f_T S)^2] +(\epsilon_K/2.303K)^2+\epsilon_c^2\}^{\frac{1}{2}}, \quad (11)$$

where $\epsilon_{\log p}$ is the probable error of the value of $\log_{10} p_{\text{mm}}$ as calculated by the corrected experimental equations; T is the absolute temperature at which p is calculated; $\bar{x}$ is the root mean square of the experimental values of $1/T$ (considering the weighting factors); S is the slope of the $\log p$ *vs.* $1/T$ curve; ϵ_s is the probable error in S as calculated from the residuals of the experimental points from the "most probable line"; f_T is the probable fractional systematic error in T; K is the constant in Eq. (4) multiplied by the geometry factor $(D^2+4r^2)/aD^2$; ϵ_K is the probable error in K; and ϵ_c is the probable error in the correction on the experimental curve for the presence of oxyhalide.

VI. SUMMARY

For the purpose of summarizing all the results, the constants of the corrected vapor pressure equations are defined by the equation,

$$\log_{10} p_{\text{mm}}=A-B/T; \quad (12)$$

and the terms in Eq. (11) which are constant for a given series of measurements are combined to give the following equation for the probable error in a value of $\log_{10} p$ (as calculated by the corresponding Eq. (12)):

$$\epsilon_{\log p}=\pm\{[(1/T)-\bar{x}]^2C+D\}^{\frac{1}{2}}. \quad (13)$$

Values of the constants A, B, $\bar{x}$, C, and D are given in Table V.

The thermodynamic quantities which can be calculated from the corrected vapor pressure equations are given in Table VI.

The authors wish to express their appreciation to Mr. N. D. Erway and Mr. L. O. Gilpatrick for technical assistance during the course of this investigation.

[6] W. H. Zachariasen, Plutonium Project Record, Vol. 14B, No. 20.6 (to be published).

The Volatility of Plutonium Dioxide*

T. E. PHIPPS,† G. W. SEARS,‡ AND O. C. SIMPSON
Argonne National Laboratory, Chicago, Illinois

(Received June 13, 1949)

The volatility of plutonium dioxide has been measured in the temperature range 1320°C to 1790°C by a modification of the Knudsen effusion method. The plutonium dioxide was heated in vacuum in a tantalum oven. Under these conditions the dioxide was reduced to a lower oxide, or oxides, which maintained a constant reproducible vapor pressure throughout further heating. Either an oxide was formed which was stable under the conditions of the experiment or thermal reduction continued with the formation of a second solid or liquid phase. The thermal reduction of the oxide was reversed by heating the reduced oxide in a low pressure atmosphere of oxygen.

I. INTRODUCTION

THE Knudsen effusion method[1] can be used for the determination of vapor pressures which are less than 0.1 mm of Hg. By this method the vapor pressure of a substance is calculated from the rate at which vapor effuses through a small orifice into an evacuated space. The total amount of vapor thus effusing through an orifice at a given pressure is a function of the nature of the orifice edge. A perfect "knife-edge" orifice is required to obtain the most accurate results if the measurement is based on the total amount of vapor which effuses. Accurate results can be obtained even with a dull-edged orifice if measurement is restricted to that part of the vapor which effuses within a small solid angle about the normal to the plane of the orifice. This modification of the original Knudsen method has been discussed in another paper.[2]

A sample of the material to be investigated is placed in an oven, the only opening in which is a small circular orifice. The area of the orifice must be very small compared to the evaporation surface of the material in the oven, and the thickness of the orifice edge should be as small as possible relative to the orifice diameter. A circular collimator is placed at a distance from the orifice so that the planes of orifice and collimator are parallel and so that the line joining the centers of collimator and orifice is perpendicular to their planes. If the diameter of the collimator is small compared to the distance from orifice to collimator, the amount of vapor effusing from the orifice and passing through the collimator approximates very closely the amount of vapor which would pass through the collimator from a perfect "knife-edge" orifice of the same diameter. The number of moles, N, of vapor passing through the collimator per second under these conditions is given by the equation

$$N = paD^2/(D^2+4r^2)(2\pi MRT)^{\frac{1}{2}}, \quad (1)$$

where p is the equilibrium vapor pressure of the material in the oven at the absolute oven temperature T; a is the area of the orifice; D is the diameter of the collimator; r is the distance from orifice to collimator; M is the molecular weight of the vapor molecule; and R is the molar gas constant.

In this investigation the vapor passing through the circular collimator was condensed on liquid-air cooled targets and the amount of material on each target was determined by measuring its alpha-activity. N is also given by the equation

$$N = c10^{-6}/gs239n60\tau, \quad (2)$$

where c is the number of registered disintegrations per minute for a given target (corrected for background and counter resolution loss); g is the geometrical efficiency of the alpha-chamber used in measuring c (i.e., the fraction of the disintegrations which are registered); s is the number of disintegrations per minute per microgram for Pu^{239}; n is the number of plutonium atoms per vaporizing molecule; and τ is the time in minutes the target was exposed to the vapor beam. Equating Eqs. (1) and (2) and solving for the vapor pressure of the material in the oven at temperature T, one obtains

$$p = [cT^{\frac{1}{2}}/\tau][(D^2+4r^2)/aD^2] \times [M^{\frac{1}{2}}/n239gs][10^{-6}(2\pi R)^{\frac{1}{2}}/60]. \quad (3)$$

The value of the first factor on the right of Eq. (3) may be different for each target which is exposed to vapor. The value of the second factor on the right is dependent on the dimensions of the experimental apparatus and varies slightly with furnace temperature. The value of the third factor is determined by the composition of the vaporizing molecules, the specific activity of the radioactive atom present, and the geometrical efficiency of the counting chamber. If s and c are determined by the same counting procedure, any error in the value used for g will be cancelled.

The value of the effective specific activity, gs, for deposits of Pu^{239} on platinum plates counted in a high geometry parallel-plate alpha-chamber ($g \cong 0.52$) was

* This paper is based on work performed under Contract No. W-7401-eng-37 for the Manhattan Project at the Metallurgical Laboratory, Chicago, Illinois.

† Present address: Department of Chemistry, University of Illinois, Urbana, Illinois.

‡ Present address: General Electric Company, Schenectady, New York.

[1] M. Knudsen, Ann. d. Physik **29**, 179 (1909).

[2] Phipps, Sears, Seifert, and Simpson, J. Chem. Phys. **18**, 713 (1950).

taken to be 7.10×10^4 disintegrations per minute per microgram. Since the formula of the evaporating molecule in equilibrium with plutonium dioxide was not known, the values 239 and 1 were arbitrarily taken for M and n, respectively, for the calculations of the vapor pressure of the oxide. If these values are substituted in Eq. (3) and the units of pressure changed to mm of Hg, then

$$p=[cT^{\frac{1}{2}}/\tau][(D^2+4r^2)/aD^2]2.603\times10^{-13}\text{ mm of Hg.} \quad (4)$$

II. APPARATUS

Two different designs of apparatus were used in the measurements of the volatility of plutonium dioxide. The two pieces of apparatus differed primarily in the type of target used, in the number of experimental measurements that could be made without breaking the vacuum in the apparatus, and in the method for determining the temperature of the oven. The same oven and sample of plutonium dioxide were used in each apparatus.

The construction of the tantalum effusion oven is shown in Fig. 1. The oven orifice was formed at the center of a disk of 0.005-inch tantalum sheet which had the same diameter as the top of the effusion oven. The orifice was prepared by the following process. With the tantalum disk supported upon a block of lead, a fine-honed steel point was brought to bear against the center of the disk. A very light blow of a small hammer produced a tiny dimple in the disk. The resulting knob on the bottom of the disk was ground off with 3/0 emery polishing paper until light showed through at the position of the extrusion. The disk was polished with 4/0 polishing paper. The hole was then reamed to the desired size with an extra fine jeweler's pivot broach of baguette size. The edges of the hole were burnished by means of a tungsten taper prepared as follows: a fine tungsten wire, while being rotated, was heated near its end in a hot flame; and the tapered section thus formed was then polished with 3/0 and 4/0 emery polishing paper. Holes produced by this method showed a very good approximation to roundness even under high magnification (within 0.8 percent). Six or eight different diameters of the orifice were measured with a microscope equipped with a screw micrometer eyepiece which had been calibrated against a standard 2-mm micrometer scale having 0.01-mm divisions. The tantalum disk having an orifice of proper size was selected and spotwelded to the top of the effusion oven. The orifice used in this investigation had a root mean square diameter of 0.03792 cm.

The completed oven was outgassed in an auxiliary vacuum apparatus before it was used. To prevent cohesion of the oven top to the oven base during outgassing the oven base was provided with a loose fitting cap made of tungsten sheet which was drilled centrally to allow a short tungsten rod of 0.060-in. diam. to pass through it. This short rod, resting upon the inner bottom of the oven base, passed through the tungsten cap and into the hole of the oven top, stopping short of the orifice plate. The oven parts were heated in vacuum by induction to about 2000°C. Heating was continued for two or three hours or until a vacuum of 1×10^{-5} mm of Hg pressure could be maintained with the oven at 2000°C.

Initial measurements of the volatility of plutonium dioxide were made with apparatus I, shown in Fig. 2. In order to introduce the charged oven and the tantalum radiation shield the lower section of apparatus I was removed by cracking the outer tube at "crack-off 2" (Fig. 2). The two standard taper "locator" ground joints insured reproducibility of oven and collimator alignment when the outer tube was again sealed.

A nickel collimator piece was held in place in the liquid-air insert by two tungsten loop springs as shown in Fig. 2. The target consisted of a strip of nickelized mica which was bolted to a Pyrex plate target holder. A Pyrex-enclosed iron armature was sealed to the Pyrex target holder and rested on a track made of a section of Pyrex tubing which had been cut lengthwise. The target strip was marked into ten sections and a

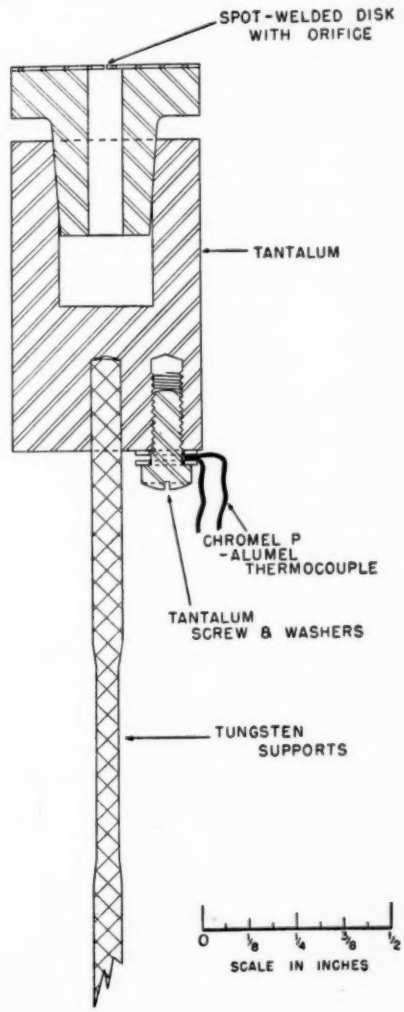

FIG. 1. Design of effusion oven.

corresponding reference scale was attached to the outside of the tube containing the armature track. The target strip was moved from outside the vacuum by a permanent magnet acting on the slide armature. It was possible to locate the center of each section of the target strip directly above the collimator. The target was cooled by radiation to the liquid air insert.

After a series of measurements in apparatus I the oven was transferred to apparatus II, which is shown in Fig. 3 with an alternate oven support. The oven support which was actually used resembled that shown in Fig. 3 with respect to omission of thermocouple leads and provision of a window for observation by optical pyrometer of the bottom of the oven; but it resembled that shown in Fig. 2 with respect to method of support of oven and radiation shield. Apparatus II also differed from apparatus I in the type of target used and in the provision for making many more measurements without having to break the vacuum in the apparatus to remove and replace targets.

Platinum disk targets (0.75-in. diam.×0.005 in.) were used in Apparatus II. Each platinum target rested on a disk of 0.020-in. nickel plate on the bottom of an aluminum cassette, as shown in Fig. 4. The two metal disks were held in place by a phosphor bronze spring. The nickel disks served to make the target holder ferromagnetic. Fifty or more cassettes, each containing a numbered platinum target, were stacked in the cassette magazine (Fig. 3) in order of the target numbers.

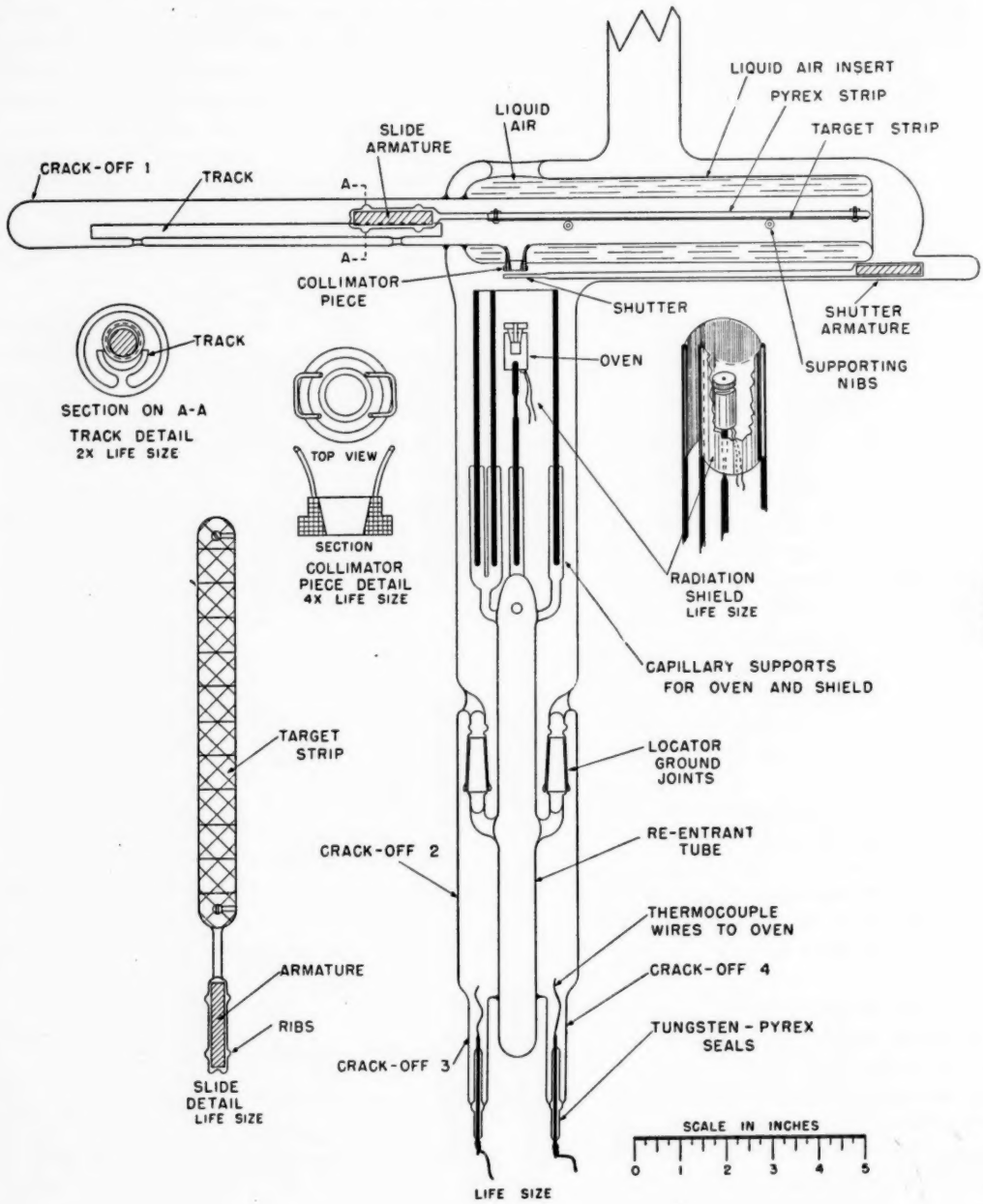

FIG. 2. Apparatus I for the measurement of the volatility of plutonium dioxide.

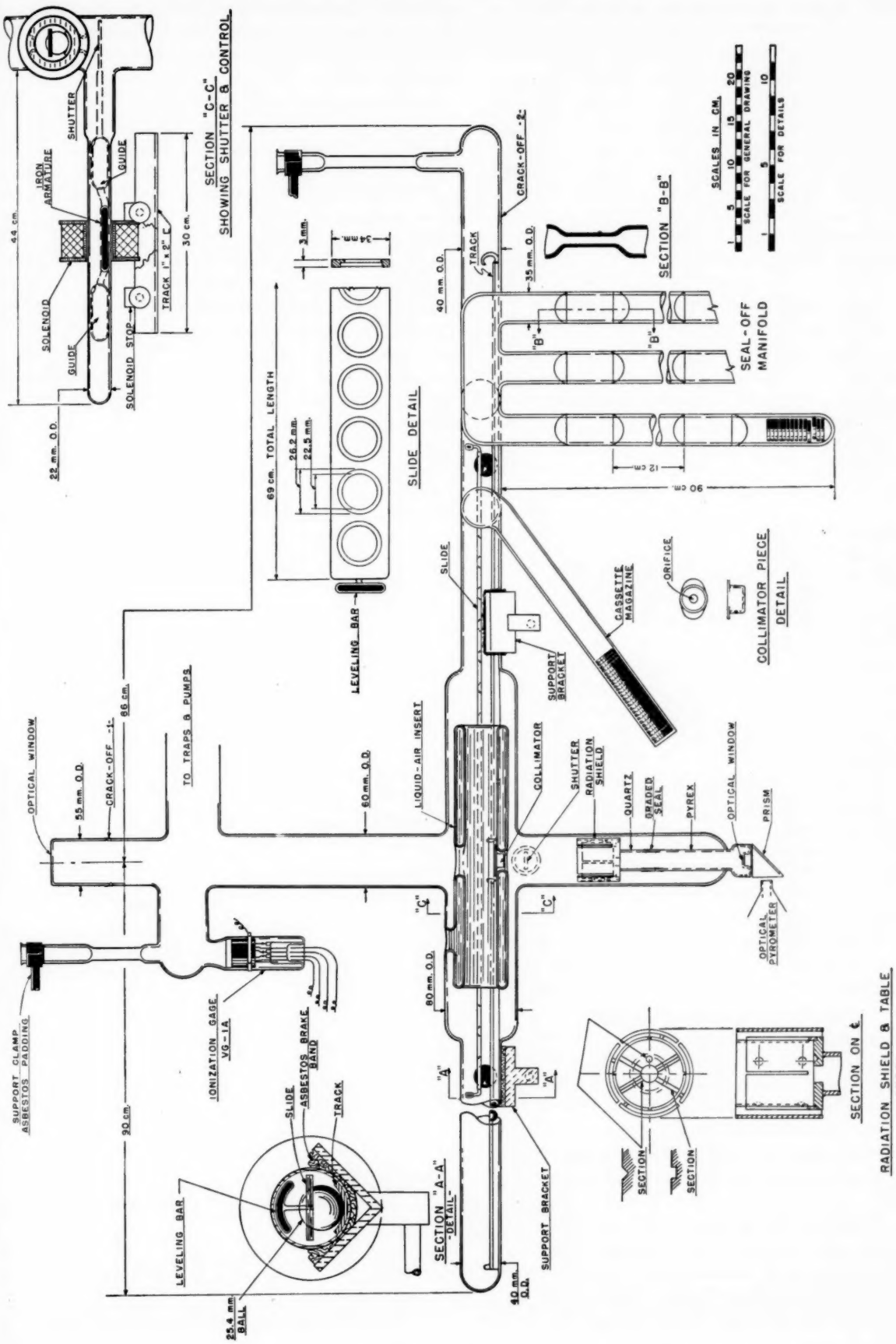

FIG. 3. Apparatus II for the measurement of the volatility of plutonium dioxide.

TABLE I. Apparent vapor pressure of plutonium dioxide as measured with apparatus I.

Target number	Exposure time τ (min.)	Counts per minute c	Temp. °K	Logarithm of vapor pressure $\log_{10} p_{mm}$	Reciprocal temperature $(1/T)\times 10^5$
1	11.22	10.4	1779.9	$\bar{6}.757$	56.18
2	10.21	5.2	1743.2	$\bar{6}.487$	57.37
3	20.25	2.6	1674.4	$\bar{7}.879$	59.72
4	42.25	0.8	1589.9	$\bar{7}.063$	62.90
5	40.71	1.0	1595.5	$\bar{7}.138$	62.68
6	20.24	3.6	1675.4	$\bar{6}.022$	59.69
7	10.40	9.8	1746.2	$\bar{6}.759$	57.27
8	10.15	22.5	1787.2	$\bar{5}.135$	55.95
9	20.05	49.1	1793.6	$\bar{5}.179$	55.75
10	30.00	52.7	1761.9	$\bar{5}.031$	56.76
11	51.61	25.2	1704.8	$\bar{6}.469$	58.66
12	49.75	4.1	1632.5	$\bar{7}.681$	61.26
13	50.01	4.9	1633.5	$\bar{7}.761$	61.22
14	40.02	23.8	1703.5	$\bar{6}.555$	58.70
15	29.97	75.2	1765.5	$\bar{5}.187$	56.64
16	19.78	106.0	1803.9	$\bar{5}.520$	55.44
17	10.16	55.6	1806.6	$\bar{5}.530$	55.35

In apparatus II the slide consisted of a strip of optical Pyrex glass sheet 33 mm wide, 690 mm long, and 3 mm thick, through which were drilled 21 equally spaced holes, 22.5 mm in diameter. Each hole, except the central one and the end ones, was counter-drilled to a diameter of about 26.3 mm and to a depth of about 2 mm. Thus an annular ledge was formed for the support of the aluminum target holders. The central hole was made oversize to permit passage of the collimator piece through it. The slide was supported by two one-inch stainless steel balls which engaged the slide in the first and last holes. Eighteen holes remained for the reception of targets. To bridge the gap between the liquid-air insert and the horizontal side arms, and thus have a continuous smooth surface for the steel balls to roll upon, glass tracks were provided, made from a 35-mm Pyrex tube cut lengthwise into three equal strips. To permit leveling of the slide after translation, a small glass-encased curved bar of iron was sealed to each end of the slide. The slide was moved back and forth and leveled by action on these iron bars of two external Alnico permanent magnets.

A "seal-off manifold" was attached to one end of the tube which contained the track for the slide. The purpose of this manifold was to permit removal of exposed targets from the evacuated apparatus. The constrictions in the tubes of this manifold had a slot-shaped cross section, which allowed the ferromagnetic cassettes to be carried through by manipulation of an outside magnet.

The collimator in apparatus II was made from Pyrex. The oven was introduced through "crack-off 1" (Fig. 3) and lowered in succession through the top opening of the liquid-air insert, through the large central hole in the slide and finally through the bottom opening of the liquid-air insert, to its final resting place above its capillary support. The collimator piece was then lowered into its seat in the bottom opening of the liquid-air insert.

Each apparatus was provided with a magnetically controlled shutter. The shutter design shown in Fig. 3 operated more smoothly than that shown in Fig. 2. In each apparatus the oven was heated by induction and the glass walls surrounding the oven were cooled by an air blast.

The vacuum line, for apparatus II as well as for apparatus I, consisted of two liquid-nitrogen cooled traps and a single-stage high velocity mercury vapor diffusion pump, supported by a double-stage mercury diffusion pump and a mechanical pump. The system could maintain a vacuum of 10^{-6} to 10^{-7} mm of Hg pressure while the oven was at operating temperature. The vacuum line of apparatus II was provided with an "oxygen-leak" to maintain a low partial pressure of oxygen in the system. A Western Electric D-79512 ionization gauge was attached for the measurement of the oxygen pressure and a McLeod gauge and liquid-nitrogen cooled mercury trap were attached for the calibration of the ionization gauge.

III. PROCEDURE

The volatility of plutonium dioxide was measured in vacuum and also at low partial pressures of oxygen. The outgassed oven was charged with a 10-mg sample of plutonium dioxide, prepared by drying the hydroxide. The oven was first placed in apparatus I.

Volatilization in Vacuum

After evacuation of the apparatus, with the first section of the target strip in place above the collimator, and with the shutter in place below the collimator, the

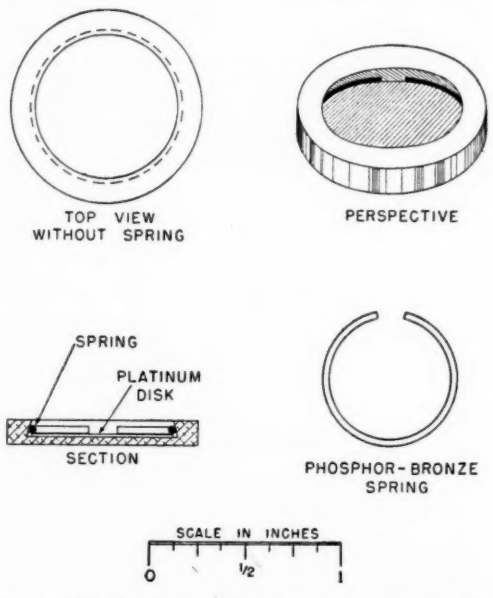

FIG. 4. Aluminum target holder used in apparatus II.

oven was heated to constant temperature by induction. With the oven at constant temperature the shutter was moved from beneath the collimator for a measured period of time and again moved into position below the collimator. The oven temperature was changed while the target strip was being moved into position for deposition on the second section. The procedure described above was repeated at the new oven temperature. Thus ten exposures of the target were made at different oven temperatures. The oven was cooled, dry air was admitted to the system and the target strip was removed through "crack-off 1" (Fig. 2). The target strip was cut into the ten marked sections and the amount of plutonium oxide deposited on each section was determined by counting the alpha-disintegrations per minute for each deposit. The vapor pressure was calculated by Eq. (4). Although the value of g, Eq. (3), may be different for deposits on a nickelized mica surface than for deposits on a platinum surface, the difference is small and may be neglected in view of the other errors present in the data for apparatus I.

Initial measurements indicated that the volatility of plutonium dioxide was too low in the temperature range of the chromel-alumel thermocouple to give a sufficiently large deposit on the target. Measurements were therefore made at higher temperatures. Each oven temperature was calculated from the surface brightness temperature of the top of the oven as measured with an optical pyrometer sighting through the side wall of the apparatus. This calculation involved correction for the emissivity of the tantalum surface and for the transmissivity of the Pyrex tube.

In order to obtain measurements at higher oven temperatures than could be reached in apparatus I the oven was transferred to apparatus II. Measurements were made at different oven temperatures by the same procedure described above. The oven temperature was calculated from the observed brightness temperature of the bottom of the oven.

In apparatus II the ferromagnetic target holders were loaded on the target slide by manipulation of a permanent magnet outside the apparatus. After exposure of all the targets on the slide, the slide was moved over to the "seal-off manifold" and the exposed targets were removed from the slide and carried into the lowest compartment of one of the tubes of the manifold by manipulation of a permanent magnet outside the apparatus. New targets were magnetically loaded onto the slide from the cassette magazine. To remove the exposed targets from the apparatus the constriction above the compartment containing the targets was carefully heated with a hand torch. The

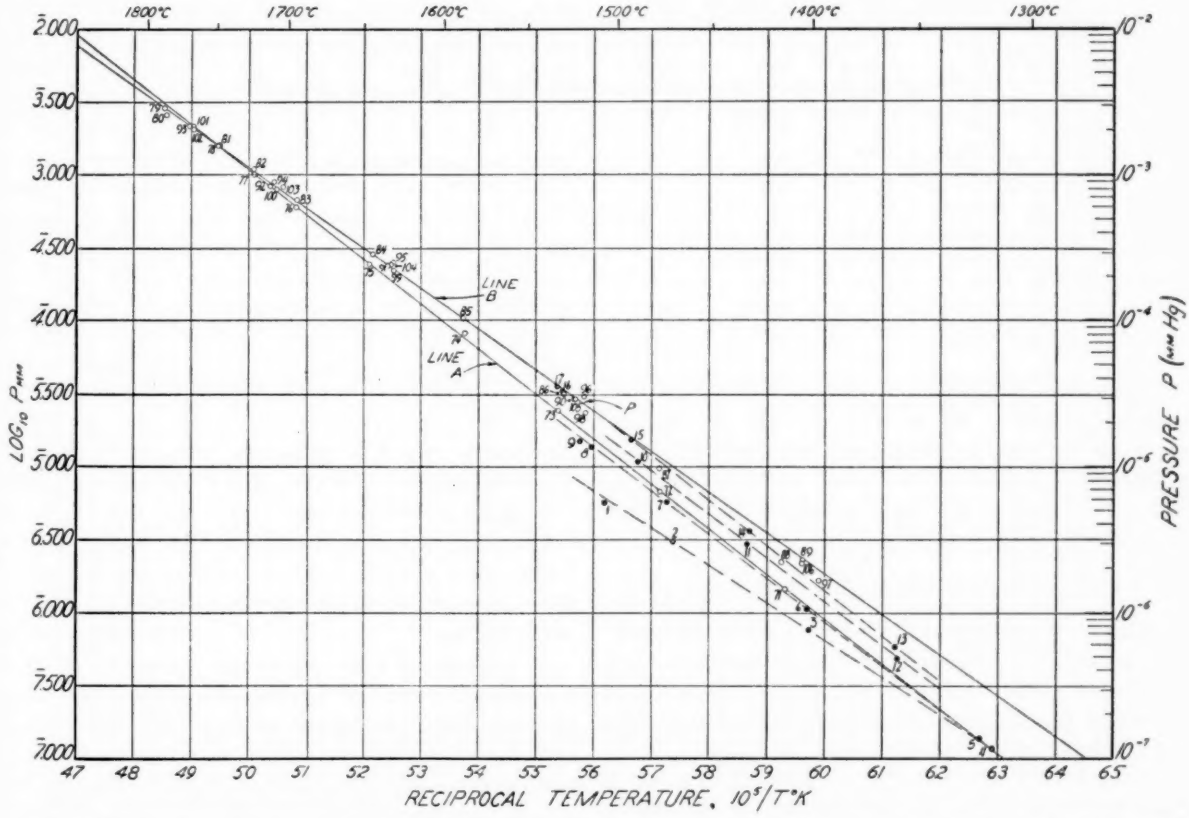

FIG. 5. Apparent vapor pressure of plutonium dioxide as measured in high vacuum from a tantalum effusion vessel. The dark circles indicate measurements made with apparatus I. The light circles indicate measurements made with apparatus II. Line *B* is the "least squares line" for the partial pressure of the plutonium oxide vapor in equilibrium with the final steady state obtained by the decomposition of the dioxide.

TABLE II. Apparent vapor pressure of plutonium dioxide as measured with apparatus II.

Target number	Exposure time τ (min.)	Counts per minute c	Temp. °K	Logarithm of vapor pressure $\log_{10} p_{mm}$	Reciprocal temperature $(1/T)\times 10^5$
71	100.00	57.5	1686.0	$\bar{6}.1495$	59.31
72	52.00	140.0	1750.1	$\bar{6}.8281$	57.14
73	30.00	288.8	1805.9	$\bar{5}.3882$	55.37
74	20.00	637.3	1860.6	$\bar{5}.9145$	53.75
75	10.00	935.5	1919.9	$\bar{4}.3890$	52.09
76	10.00	2290.7	1967.6	$\bar{4}.7833$	50.82
77	6.00	2287.3	1996.5	$\bar{3}.0076$	50.09
78	4.00	2370.3	2021.3	$\bar{3}.2019$	49.47
79	4.50	4781.	2060.4	$\bar{3}.4597$	48.53
80	4.00	4235.	2059.4	$\bar{3}.4127$	48.56
81	4.00	2397.	2020.7	$\bar{3}.2066$	49.49
82	6.00	2478.	1996.8	$\bar{3}.0425$	50.08
83	10.00	2580.	1967.3	$\bar{4}.8348$	50.83
84	10.00	1099.2	1918.0	$\bar{4}.4589$	52.14
85	20.00	813.3	1861.6	$\bar{4}.0205$	53.72
86	30.00	375.0	1802.7	$\bar{5}.5012$	55.47
87	50.00	193.8	1750.3	$\bar{6}.9862$	57.13
88	101.00	91.6	1687.7	$\bar{6}.3474$	59.25
89	100.00	93.6	1677.4	$\bar{6}.3597$	59.62
90	30.00	347.6	1797.2	$\bar{5}.4676$	55.64
91	10.00	916.7	1908.1	$\bar{4}.3788$	52.41
92	3.00	949.	1985.6	$\bar{4}.9255$	50.36
93	2.25	1820.	2042.1	$\bar{3}.3392$	48.97
94	3.00	1016.8	1983.1	$\bar{4}.9551$	50.43
95	10.00	969.4	1904.8	$\bar{4}.4028$	52.50
96	30.00	360.2	1791.6	$\bar{5}.4824$	55.82
97	100.00	67.5	1669.6	$\bar{6}.2166$	59.90
98	30.00	278.0	1790.4	$\bar{5}.3698$	55.85
99	10.00	848.	1904.3	$\bar{4}.3449$	52.51
100	3.00	912.2	1981.0	$\bar{4}.9077$	50.48
101	2.00	1631.7	2039.6	$\bar{3}.3427$	49.03
102	2.40	1838.	2039.6	$\bar{3}.3154$	49.03
103	3.00	942.2	1976.6	$\bar{4}.9213$	50.59
104	10.00	932.5	1905.8	$\bar{4}.3861$	52.47
105	30.00	345.9	1796.2	$\bar{5}.4654$	55.67
106	100.00	88.7	1677.7	$\bar{6}.3367$	59.61

constriction was collapsed and the compartment sealed off without allowing air to enter the apparatus. The targets were removed from the compartment and analyzed by radiochemical assay. In no case was there evidence that any of the deposit had been lost from a target during these operations.

Volatilization in Oxygen Atmosphere

Measurements of volatility of the oxide were also made at very low partial pressures of oxygen. The needle valve of the "oxygen-leak" was adjusted to give the desired partial pressure of oxygen in the system while the vacuum pumps were kept in operation. The oven was heated at each desired temperature for a period of time before the target was exposed to vapor. It was desired that equilibrium be established with respect to oxidation in the oven before each measurement was made. Deposition of vapor on the targets was made

TABLE III. Apparent vapor pressure of plutonium dioxide as measured in a low pressure atmosphere of oxygen.

Target number	Exposure time τ (min.)	Counts per minute c	Oxygen pressure P_0 (mm)	Logarithm of vapor pressure $\log_{10} p_{mm}$	Reciprocal temperature $(1/T)\times 10^5$
107	2.00	1003.	1.3×10^{-3}	$\bar{3}.2025$	49.51
108	2.00	752.	1.3×10^{-3}	$\bar{3}.0748$	50.09
109	2.00	591.	1.3×10^{-3}	$\bar{4}.9685$	50.51
110	3.00	452.	1.3×10^{-3}	$\bar{4}.6717$	51.51
111	5.00	341.	1.3×10^{-3}	$\bar{4}.3223$	52.71
112	10.00	227.	1.3×10^{-3}	$\bar{5}.8384$	54.14
113	20.00	143.	1.3×10^{-3}	$\bar{5}.3298$	55.72
114	30.00	57.	1.3×10^{-3}	$\bar{6}.7498$	57.32
115	50.00	29.9	6.9×10^{-5}	$\bar{6}.1683$	59.09
116	100.00	12.9	6.9×10^{-5}	$\bar{7}.4931$	61.31
117	30.00	55.5	6.9×10^{-5}	$\bar{6}.6668$	56.98
118	20.00	127.	6.9×10^{-5}	$\bar{5}.2093$	55.31
119	10.00	176.	6.9×10^{-5}	$\bar{5}.6576$	53.76
120	5.00	227.	6.9×10^{-5}	$\bar{4}.0750$	52.38
121	5.00	221.	6.0×10^{-4}	$\bar{4}.0750$	52.44
122	5.00	192.	1.3×10^{-3}	$\bar{4}.0750$	52.41
123	3.45	318.	6.9×10^{-5}	$\bar{4}.3867$	51.31
124	2.50	392.	6.9×10^{-5}	$\bar{4}.6221$	50.43

by the same procedure as outlined for the measurements in vacuum.

Surface brightness temperatures of the oven were measured and corrections applied for the transmissivity of the optical window, for the reflectivity of the mirror used to change the optical path, and for the emissivity of the tantalum surface. The correction for the emissivity of the tantalum surface was more difficult and uncertain in the presence of oxygen than in vacuum since the emissivity of tantalum in oxygen is not the same as that of a clean tantalum surface. In general, oxides have high emissivities compared to those of metals.[3] When the tantalum oven was heated in a small pressure of oxygen it was found that the brightness temperature of the surface was somewhat lower than for the clean tantalum oven heated in vacuum with the same power input. The lower oven temperature resulted from the higher total emissivity of the oxidized surface plus the slight loss of heat by conduction at the low pressures involved. The higher spectral emissivity of the oxidized surface resulted in a brightness temperature which was nearer the true oven temperature than was the case with the clean tantalum oven. Therefore for a given power input the actual temperature of the oven in oxygen was considerably lower than in the high vacuum experiment.

If it is assumed that the actual power input into the oven was the same in vacuum and in the oxygen atmosphere for the same power setting of the oscillator, and that the energy lost from the oven by conduction at the low pressures of oxygen was negligible compared to the energy lost by radiation, then the Stefan-Boltzmann

[3] R. L. Weber, *Temperature Measurement and Control* (The Blakiston Company, Philadelphia, 1941), p. 417.

law gives the following relation

$$E=\epsilon_t AT^4=(\epsilon_t)_0 AT_0^4, \quad (5)$$

where E is the power input, A is the product of the Stefan-Boltzmann constant and the area of oven surface, ϵ_t and $(\epsilon_t)_0$ are the total emissivities of the tantalum surface in a high vacuum and under oxygen respectively, and T and T_0 are the corresponding absolute oven temperatures. Equation (5) neglects the temperature of the surroundings compared to the oven temperature. The actual oven temperatures T, and T_0 are related to the corresponding brightness temperatures T_b and $(T_b)_0$ (corrected for transmissivity of window and reflectivity of mirror) by the Wien equations,

$$(1/T)-(1/T_b)=K\log_{10}\epsilon_\lambda \quad (6)$$

and

$$(1/T_0)-[1/(T_b)_0]=K\log_{10}(\epsilon_\lambda)_0, \quad (7)$$

where K is a constant involving the characteristic wave-length λ of the pyrometer filter, and ϵ_λ and $(\epsilon_\lambda)_0$ are the spectral emissivities of the tantalum surface in vacuum and in the oxygen atmosphere. The oven temperatures may be calculated if it is assumed that the percent change in the spectral emissivity due to the oxygen atmosphere is the same as the percent change in the total emissivity; namely, that

$$\epsilon_t/(\epsilon_t)_0=\epsilon_\lambda/(\epsilon_\lambda)_0. \quad (8)$$

From Eqs. (5), (7), and (8) it follows that

$$K(\log_{10}\epsilon_\lambda+4\log_{10}T)=(1/T_0)-[1/(T_b)_0]+4K\log_{10}T_0. \quad (9)$$

Since T_b and $(T_b)_0$ were measured and ϵ_λ and K are known constants, T may be calculated by Eq. (6) and the true temperature of the oven in the oxygen atmosphere, T_0, may be calculated by Eq. (9).

IV. RESULTS

Measurements in Vacuum

The experimental data for each target used in apparatus I and the corresponding vapor pressures calculated by Eq. (4) are given in Table I and shown in Fig. 5 by the dark circles. The order in which the measurements were made is indicated in the figure by the numbers appearing beside the experimental points. It can be seen that the results did not follow the expected linear relation of log p and $1/T$, but instead indicated a progressive change toward higher rates of vaporization. Since initial vapor unsaturation in the effusion oven seemed unlikely on account of the finely divided state of the PuO_2 sample, it was assumed that thermal reduction of the PuO_2 was taking place.

That thermal reduction may occur under these conditions was confirmed by later independent experiments[4] on the heating in vacuum of a sample of PuO_2 resting on a tantalum strip. X-ray analysis of such a

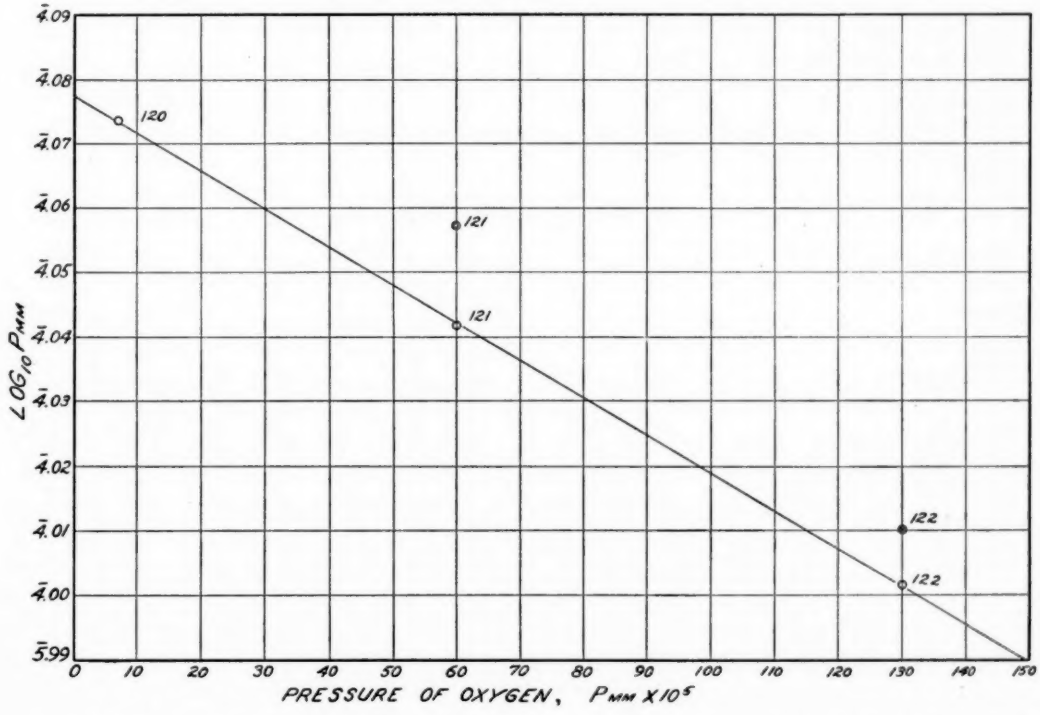

FIG. 6. Effect on the measured vapor pressures due to scattering of the vapor beam by small pressures of oxygen. The open circles are based on the assumption of constant oven temperature. The dark circles are based on the assumption that the oven temperature measurements were exact.

[4] E. F. Westrum (unpublished work).

sample after heating showed the presence of a phase of composition between PuO_2 and Pu_2O_3, roughly Pu_4O_7. Since the partial pressure of oxygen in the effusion oven may have been greater than the partial pressure of oxygen above the tantalum strip, the same reduction product may not have been obtained in both cases. This thermal reduction is analogous to that of praseodymium dioxide, which decomposes in vacuum at 400°C to give Pr_6O_{11} and at higher temperatures to give lower oxides.[5]

In order to continue measurements at higher temperatures where thermal decomposition would be more rapid and also in order to obtain more accurate temperature measurements (an optical window had not been provided in apparatus I) the measurements were continued in apparatus II. The resulting experimental data are given in Table II and shown in Fig. 5 by the open circles. The order in which measurements were made is given by the order of the target numbers. Target number 71 was used for the first measurement in apparatus II.

Line *A* (Fig. 5), obtained by inspection, represents the data obtained with increasing oven temperature. After the measurement at 1748°C further measurements gave results corresponding to line *B* in Fig. 5. Repeated traversals up and down the whole temperature range failed to show any further significant change in the vapor pressure at temperatures above about 1520°C (point *P*, Fig. 5). Apparently a steady state or quite slowly varying state was reached by the initial heating to the high temperatures. The partial pressure of plutonium oxide vapor in equilibrium with this steady state is given by line *B*. The equation for line *B*, as calculated by least squares treatment of the data above 1520°C, is

$$\log_{10} p_{mm} = 11.010 - 27{,}910/T. \qquad (10)$$

Below 1520°C the experimental points scatter somewhat owing partly to statistical errors involved in analyzing the very weak deposits and partly perhaps to some reoxidation which may have taken place at the lower temperatures. Conceivably at the lower temperatures the oxygen decomposition pressure above the higher oxide might have been less than the residual oxygen pressure around the oven. In such case, oxygen would have entered the oven and caused some reoxidation.

Measurements in Oxygen Atmosphere

If a small constant pressure of oxygen is present which is insufficient at a high temperature to cause reoxidation of the material in the steady state indicated by line *B* of Fig. 5, it may be sufficient to cause oxidation at some lower temperature. Such oxidation would

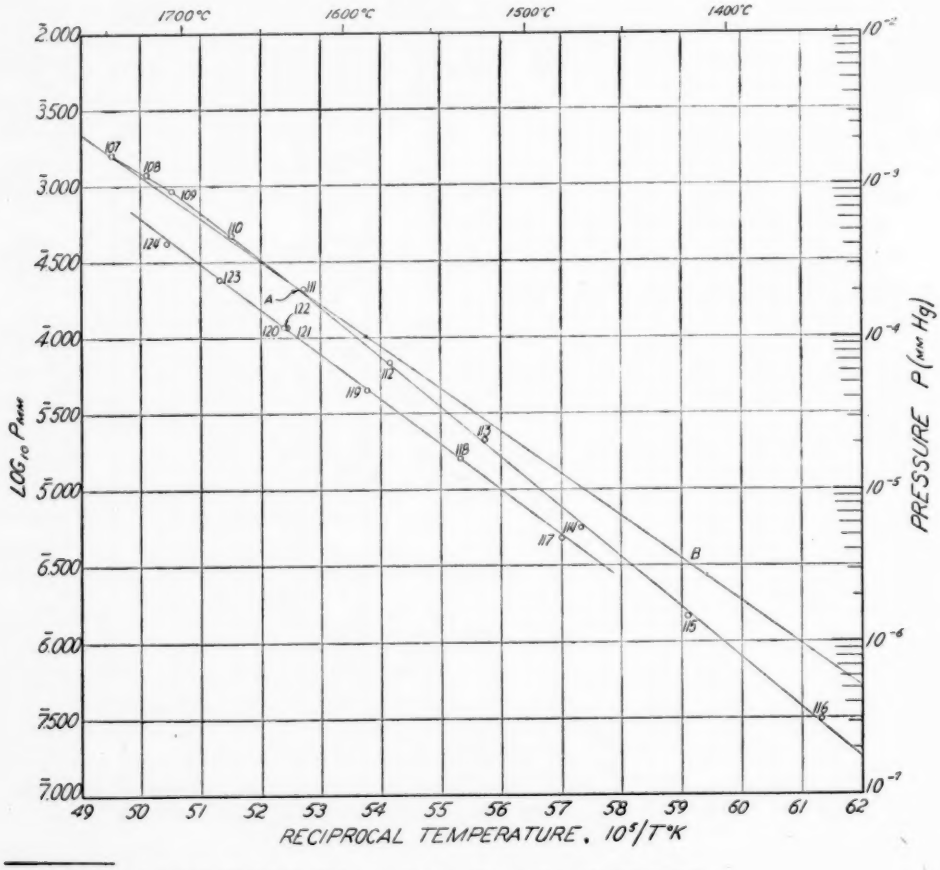

FIG. 7. Volatility of plutonium oxide in its "steady state" under small pressures of oxygen. Line *B* of Fig. 5 is included for comparison.

[5] H. A. Pagel and P. H. M. P. Brinton, J. Am. Chem. Soc. 51, 42 (1929).

decrease the vapor pressure below the values for the "steady state." To determine whether this would occur the volatility of the plutonium oxide was measured in oxygen atmospheres at low pressure. These measurements were made with the oxide which remained in the oven after the measurements in vacuum. The resulting experimental data are given in Table III. The partial pressures of oxygen given in the table are the pressures on the outside of the oven. The oxygen pressure inside the oven is indeterminate, depending as it does upon the rate of effusion of oxygen through the orifice and the rate at which the oxygen reacts with the plutonium oxide and with the tantalum surface of the oven.

The atmosphere of oxygen in the apparatus scattered the beam of effusing vapor. Correction must be made for this scattering. An estimate of the magnitude of this correction was obtained by inter-comparison of targets 120, 121, and 122, which were exposed at the same oven temperature but at different oxygen pressures. Theoretically a plot of $\log_{10}p$ against the pressure of oxygen for these three points should show a linear relationship provided that the differences between the activities of the three targets arose from the scattering effect only. However, a temperature variation of a very few degrees during the exposure of the three targets would have caused an error in the calculated vapor pressure of the same magnitude as the scattering correction. Constancy of oven temperature was dependent on three factors: (1) the power input to the oven; (2) the nature of the outer surface of the oven; and (3) the heat loss from the oven by conduction through the gas. The power setting of the oscillator was maintained the same during these three relatively short exposures and therefore the power input to the oven was constant. Whether the oven surface changed during the exposures depended on the stability of the oxide layer formed during the earlier lengthy heating in oxygen at 1.3×10^{-3} mm of Hg. If the tantalum surface reached equilibrium with this atmosphere and underwent no change during the intervening measurements at lower oxygen pressures then the oven surface would not have oxidized further during these three exposures and radiation loss would have been constant. The oxygen pressure was different for each of these exposures, which would result in a variation of the loss by conduction and the production of a slight variation in the oven temperature. However, the total variation from this source was doubtless less than the probable experimental error in the measurement of the oven temperature.

Figure 6 shows the plot of $\log_{10}p$ *vs.* P_o, the pressure of oxygen, for these three targets. The open circles are plotted under the assumption that the oven temperature was the same for each measurement. If the measured oven temperatures are assumed to be exact and the measurements for targets 121 and 122 are corrected to the temperature of target 120 by use of an approximate slope of the vapor pressure line, corrected values are obtained which are represented by the dark circles in Fig. 6. The linear relationship of the open circles may be entirely fortuitous. In any case it is clear that the scattering correction for targets 107–114 and 122 will be about 0.08 in $\log_{10}p$ while it will be about 0.02 for target number 121 and about 0.005 for targets 115–120, 123, and 124. The logarithms of the corrected vapor pressures are given in Table III and are shown graphically in Fig. 7. Line *B* of Fig. 5 is included in Fig. 7 for comparison.

The small discrepancies at the high temperatures between the data of this experiment (targets 107–111) and the data obtained in the high vacuum experiment are not thought to be significant in view of the uncertainties in the temperature and scattering corrections. Therefore it is concluded that above a temperature of about 1900°K (point *A*, Fig. 7) the phase or phases present were the same as those present in the vacuum experiments, whereas below 1900°K oxidation took place. When the oxygen pressure was decreased (targets 115–120) the volatility did not increase during the time of the measurements. Approximately equal times were allowed between corresponding points on the way down and on the way up the temperature scale. The rate of oxidation on the way down was determined for the most part by the rate of effusion of oxygen into the oven at the relatively high pressure of 1.3×10^{-3} mm of Hg, whereas the rate of thermal decomposition on the way up was determined by the rate of effusion of oxygen out of the oven under a very much lower oxygen pressure differential. Therefore the amount of material which might have been reduced between exposures from target 117 to 120 would have been less than that oxidized in equal periods of time between exposures from target 111 to 116.

Since tantalum reacts with oxygen at high temperatures the partial pressure of oxygen in the oven may at all times have been considerably different from the measured pressure outside the oven. Therefore no quantitative deductions can be made from these data. However, the following qualitative conclusions can be made from the experimental observations.

(1) Reduction of PuO_2 occurs when it is heated in vacuum in a tantalum oven.

(2) At least up to 1750°C the reduction occurs without immediate formation of a second solid or liquid phase.

(3) The equilibrium partial pressure of the oxide present in the vapor phase gradually increases with increasing reduction of the solid oxide.

(4) When the partial pressure of the volatile oxide increases to a value which is approximately four to five times that characteristic of the original dioxide a "steady state" is reached. In this "steady state" the vapor pressures, measured as a function of tempera-

ture, are reproducible after further heating of the oven in vacuum. This may be due either to continued reduction with the formation of a second solid or liquid phase or to the formation of a stable oxide which does not undergo further reduction at the partial pressure of oxygen maintained in the oven under the conditions of the experiment.

(5) The "steady state" may again be oxidized if it is heated in an atmosphere of oxygen exceeding a critical pressure, which no doubt is a function of temperature.

THE JOURNAL OF CHEMICAL PHYSICS VOLUME 18, NUMBER 5 MAY, 1950

Markoff Chains and Excluded Volume Effect in Polymer Chains

ELLIOTT W. MONTROLL*
University of Pittsburgh, Pittsburgh, Pennsylvania
(Received January 23, 1950)

In most of the theoretical work on statistical properties of polymer chains one includes (for mathematical simplicity) configurations which correspond to several monomers located at the same point. Here a mathematical method based on the theory of Markoff chains is used to eliminate short-range excluded volume effects in polymer chains formed on space lattices. Those aspects of the theory of Markoff chains which are important in this problem are briefly reviewed.

If $a_s(s=j-k)$ is the correlation coefficient between the x component of the position of the jth monomer and that of the kth, then the root-mean-square distance between ends of a chain of degree of polymerization N is proportional to $N^{\frac{1}{2}}$ (as $N\to\infty$) provided that $a_s\to 0$ more rapidly than $A/s^{1+\epsilon}$ (as $s\to\infty$). Here A is a constant and ϵ is an arbitrarily small positive constant. This condition is satisfied in a chain in which any group of n_0 successive monomers do not overlap each other or any monomers in neighboring groups of n_0 provided $n_0 \ll N$.

A detailed analysis of a polymer chain on a square lattice is given.

I. INTRODUCTION

A KNOWLEDGE of the geometrical configuration of polymer chains and the distribution of monomer elements in such chains is necessary for theoretical investigations of polymer solutions and of the elastic behavior of polymers. In most of the current polymer literature configuration and distribution problems are solved with the assumption that polymers are formed by the successive addition of C—C bonds in a random manner with the restriction that bond angles have specified values (and perhaps that attractive or repulsive forces act between monomer elements twice removed). This mode of conceptual construction of a chain does not prohibit the formation of configurations in which several atoms exist in the same place. Hence the standard polymer models have particle densities larger and root-mean-square lengths shorter than those of real polymers.

In this paper we shall discuss a mathematical scheme for the investigation of statistical properties of polymer chains whose carbon atoms lie on points of a periodic space lattice. By application of the theory of Markoff chains, we can treat models in which the short-range overlapping of atoms is eliminated. Our detailed calculations will be restricted to chains whose carbon atoms lie on a square lattice. They are now being extended to chains on simple cubic and diamond type lattices. It seems that an analogous mathematical method using integral equations can be employed in the analysis of chains which are not restricted to lattices.

We shall introduce those formulas from the theory of Markoff chains[1] that will be needed for our application. For completeness a brief discussion of long-range order in Markoff chains will be included in the Appendix.

Let us consider polymer chains which can be formed on a square lattice; that is, two-dimensional polymers with bond angles of 90° and with a constant bond distance between monomers. Several of the configurations drawn in Fig. 1 (b, c) cannot exist because they contain lattice points which are occupied by two monomers.

Those overlaps which occur when a monomer four removed from a given monomer returns to the position of the given monomer will be called first-order overlaps (see b in Fig. 1). Overlaps of monomers 12 removed (see c) will be called second-order overlaps, etc. Inasmuch as first-order overlaps are so much more probable than those of higher order one can expect them to be the primary source of the deviations from random models.

It is known that the mean square distance between two distant points in a random model of a polymer chain is proportional to the number of monomers be-

* Present address: Physics Branch, Office of Naval Research, Washington, D. C.

[1] For a more detailed discussion of the general theory see, for example, M. B. Hostinsky, *Methodes Générales du Calcul des Probabilités* (Gauthier-Villars, Paris, 1931); M. Frechet, *Reserches Théoriques Modernes sur le Calcul des Probabilités* (Gauthier-Villars, Paris, 1938); or E. Montroll, Ann. Math. Stat. 18, 18 (1947).

tween the two points. We shall now, in a heuristic way, find the conditions under which the same result is obtained in a chain with correlations between configurations of bonds in the chain. Physically these correlations may result from an attraction or repulsion (which leads to excluded volume effects) between monomers or indirectly through the interaction of the chain with its solvent or neighboring chains.

If x_j represents the x component of the vector connecting the jth and $j+1$st monomers, then the x component of the length of the chain is given by

$$X_n=x_1+x_2+\cdots+x_n.$$

The possible values of x_j for a chain on a quadratic lattice are $-a$, 0, a (where a is the bond length). The mean value $E(x_j)$ of x_j is zero. We represent the mathematical expectation or average value of X_n^2 by $E(X_n^2)$. Then

$$E(X_n^2)=\sum_{j=1}^{n}E(x_j^2)+2\sum_{j=1}^{n-1}\sum_{k=j+1}^{n}E(x_jx_k),$$

where $E(x_jx_k)$ is the correlation coefficient between the jth and kth components. In very long chains end effects are of secondary importance; hence as $n\to\infty$ we can assume that $E(x_jx_k)$ is a function of $(k-j)$ when j and k are not too close to the ends of the chain. Then if $(k-j)=s$, we have as $n\to\infty$

$$E(X_n^2)\sim na_0+2\sum_{s=0}^{n-1}(n-s)a_s;\quad a_s=E(x_jx_k).$$

In a random chain all correlation coefficients a_s $(s>0)$ are zero and the classical result $E(X_n^2)\sim na_0$ follows. By using several examples, we can show that $E(X_n^2)$ is proportional to n in chains whose long-range correlations decrease faster than $a_s=A/s^{1+\epsilon}$, where ϵ is an arbitrarily small positive number. Let $a_s\sim A\exp(-Bs)$ as $s\to\infty$ $(B>0)$. Then

$$\sum_{s=1}^{n-1}(n-s)A\exp(-Bs)\sim nAe^{-B}/(1-e^{-B}).$$

Hence

$$E(X_n^2)\sim n\{a_0+2Ae^{-B}(1-e^{-B})^{-1}\}.$$

When $a_s\sim A/s^B$ $(B>0)$, we have

$$\sum_{s=1}^{n-1}(n-s)A/s^B\simeq\begin{cases}An/(B-1)\text{ if }B>1\\ An\log n\text{ if }B=1\\ An^{2-B}/(2-B)(1-B)\text{ if }0<B<1.\end{cases}$$

Therefore $E(X_n^2)\sim n[a_0+2A(B-1)^{-1}]$ if $B>1$, $2An\times\log n$ if $B=1$ and $2An^{2-B}/(2-B)(1-B)$ if $B<1$.

A correlation coefficient A/s is somewhat analogous to long-range Coulomb forces and one of the form As^{-B} $(B<1)$ involves long-range order of the type observed in a crystal lattice. One of the fundamental questions in the theory of excluded volume effects is: Are the long-range effects large enough to make $E(X_n^2)$ of order greater than n? After making several approximations, Flory[2] has obtained an expression for $E(X_n^2)$ of the form An^{2-B} where $1>B>0.8$. It is important that more research be done on some polymer model to completely settle this point one way or the other. We shall show at the end of this paper that if one constructs a chain by joining smaller chains of n_0 monomers each, in such a way that each monomer in a given subchain is influenced only by other monomers in its own and neighboring subchains, then the root-mean-square distance between the ends of the chain is proportional to $n^{\frac{1}{2}}$(as $n\to\infty$) no matter how large n_0 is chosen to be. The punch card investigations of configurations of polymer chains now being pursued by Dr. Gilbert King[3] should be helpful in deciding a form for the long-range correlation functions.

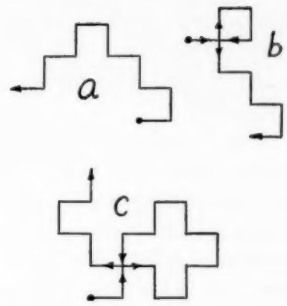

FIG. 1. Sample configurations of chains on a square lattice.

In the remaining analysis we shall limit ourselves to models which exclude first-order overlaps but which permit the much less probable overlaps of higher order. Our analysis can, in principle, be generalized to include any desired order of overlap, but this generalization leads to the determination of characteristic values and vectors of matrices of very high order.

Our main calculation will be equivalent to an investigation of a random walk on a square lattice in which the walker (a) must turn to the left or right after each step (retreating is prohibited!), (b) is not allowed to reoccupy any lattice point in four steps, (c) has a two-step memory such that his nth step is influenced by his $(n-2)$nd.

This model corresponds to the wanderings of an ill-mannered random walker who is not allowed to return to any lattice point he has passed until a time longer than that required for him to take 11 steps. After that time he is forgiven and is again allowed to revisit old points.

First we shall compare the number of possible paths under these limitations with the number of paths which are possible when (b) is relaxed. We can restrict our calculation to paths which start with a step in the positive x direction (or in polymer language with chains whose first bond lies in the x direction and whose second bond is connected to the right end of the first). By symmetry the ratio of the number of restricted paths to

[2] P. J. Flory, J. Chem. Phys. 17, 303 (1949).
[3] G. King, ONR progress reports.

that of the number of random paths in this case is exactly the same as it is when the first step is in the negative direction or in the positive or negative y directions.

Those paths which are consistent with (a) and (b) can be represented by a sequence of right (R) and left (L) turns such as LLRLRLLRLR (see a in Fig. 1) which do not contain three successive R's or L's (three successive turns in a given direction yield a first-order overlap). A polymer of degree of polymerization $(n+2)$ has $(n+1)$ bonds and can be represented by a sequence of n R's and L's. Below we enumerate the possible sequences for $n=1$, 2, and 3.

$n=1$		L			R	
$n=2$	LL		LR	RL		RR
$n=3$	LLR	LRL	LRR	RLL	RLR	RRL.

Every possible sequence ends in either class (i) LR or RL, or (ii) LRR or RLL. If $n=4$ all sequences of class (i) can be constructed by attaching an L(R) to those of $n=3$ which end in R(L). Those of class (ii) can be formed by adding RR (LL) to those sequences of $n=2$ which end in L (R). Hence if y_n is the number of possible $(n+2)$-mers, we have $y_4=y_3+y_2$. In general it is clear that similar reasoning leads to the difference equation $y_n=y_{n-1}+y_{n-2}$ subject to $y_1=2$ and $y_2=4$.

The solution of this equation is

$$y_n=[1+3\cdot 5^{-\frac{1}{2}}]x_1^{n-1}+[1-3\cdot 5^{-\frac{1}{2}}]x_2^{n-1};$$
$$x_j=\tfrac{1}{2}[1-(-1)^j 5^{\frac{1}{2}}].$$

Since the number of unrestricted $(n+2)$-mers is 2^n, the fraction of these without first-order overlap is (as $n\to\infty$) $f_n\sim 1.171(0.809)^{n-1}$.

Even when n is as small as 10, $f_n\sim 178/1024=0.18$. Hence we see that *most* of the configurations counted in a random model are forbidden when only first-order overlaps are taken into account.

II. THEORY OF MARKOFF CHAINS

1. Characterization of a Simple Markoff Chain

Let the infinite set of dependent variables z_0, z_1, z_2, $\cdots$ be related so that the probability distribution of z_j is uniquely defined by that of z_{j-1} and the law of dependence is independent of j. Chains of variables with these properties are called simple Markoff chains after the Russian mathematician who first studied them systematically.

Let the possible values of z_j $(j=0, 1, 2, \cdots)$ be a_1, a_2, $\cdots a_n$. Then the probability distribution of z_j is defined by

$$p_m(j)=pr(z_j=a_m) \quad m=1, 2, \cdots N \text{ and } j=0, 1, 2, \cdots. \quad (1)$$

(We follow the common notation of the theory of probability and read the symbol $pr(z_j=a_m)$ as the probability that z_j equals a_m.)

These numbers can be represented as components of an N-vector

$$\mathbf{P(j)}=\{p_1(j), p_2(j), \cdots, p_N(j)\}. \quad (2)$$

Inasmuch as z_j is postulated certainly to have one of the values of the set $a_1, a_2, \cdots, a_N$ we have

$$\sum_{m=1}^{N} p_m(j)=1 \text{ for all } j. \quad (3)$$

A simple Markoff chain is completely characterized by $P(0)$, the probability distribution of z_0, and the N^2 *transition probabilities*

$$p(n\to m)=p_{mn}=pr(z_{j+1}=a_m \text{ if } z_j=a_n) \quad (4)$$
$$p_{mn}\geq 0 \quad \text{if} \quad 1\leq n, m\leq N.$$

Since $z_j=a_n$ implies with certainty that z_{j+1} has one of the values $a_1, a_2, \cdots, a_N$, we have

$$\sum_{m=1}^{N} p_{mn}=1 \text{ for } n=1, 2, \cdots, N. \quad (4a)$$

The probability of the simultaneous occurrence of two compatible events is the product of the unconditional probability of the occurrence of one of the events by the conditional probability of the other assuming that the first has occurred. Hence

$$pr(z_{j+1}=a_m \text{ and } z_j=a_n)=p_{mn}p_n(j). \quad (5)$$

Inasmuch as the probability of the occurrence of a given event is the sum of the probabilities of the mutually exclusive ways in which the event can happen, we have

$$p_m(j+1)=\sum_{n=1}^{N} p_{mn}p_n(j) \text{ for } m=1, \cdots, N \text{ and } j=0, 1, \cdots. \quad (6)$$

The distribution of z_{j+2} follows immediately from that of z_j by iteration of (6). Then

$$p_m(j+2)=\sum_{n=1}^{N} p_{mn}p_n(j+1)$$
$$=\sum_{n_2=1}^{N}\left(\sum_{n_1=1}^{N} p_{mn_1}p_{n_1n_2}\right)p_{n_2}(j). \quad (7a)$$

In general,

$$p_m(j+k)$$
$$=\sum_{n_1=1}^{N}\sum_{n_2=2}^{N}\cdots\sum_{n_k=1}^{N} p_{mn_1}p_{n_1n_2}\cdots p_{n_{k-1}n_k}p_{n_k}(j). \quad (7b)$$

Hence $p_m(k)$ can be obtained from the initial distribution $p_m(0)$ by application of (7) when $j=0$. The multiple summation process is unwieldy for direct computation. To avoid it we express these relations in matrix form.

The transition probabilities p_{mn} which characterize a simple chain are completely exhibited in the Markoff

or stochastic matrix

$$\mathbf{P}=(p_{mn}). \tag{8}$$

By a direct computation it is clear that the components of $\mathbf{P}\cdot\mathbf{P(j)}$ are $p_m(j+1)$ $(m=1, 2, \cdots, N)$. Hence $\mathbf{P}\cdot\mathbf{P(j)}=\mathbf{P(j+1)}$ and

$$\mathbf{P(j+k)}=\mathbf{P}\cdot\mathbf{P(j+k-1)}=\mathbf{P}^2\cdot\mathbf{P(j+k-2)}=\cdots=\mathbf{P}^k\cdot\mathbf{P(j)}. \tag{9}$$

Now let $\mathbf{r}_1, \cdots, \mathbf{r}_N$ be the set of right-hand characteristic vectors (r.c.v.) of $\mathbf{P}$; $\mathbf{s}_1, \cdots, \mathbf{s}_N$ the set of left characteristic vectors (l.c.v.); and $\lambda_1, \cdots, \lambda_N$ the corresponding characteristic values (c.n.). These quantities satisfy the equations

$$\mathbf{P}\mathbf{r}_k=\lambda_k\mathbf{r}_k \quad \text{and} \quad \mathbf{s}_k\mathbf{P}=\lambda_k\mathbf{s}_k. \tag{10}$$

It is well known that $\mathbf{s}_j\cdot\mathbf{r}_k=0$ if $\lambda_j\neq\lambda_k$ and that the sets $\{\mathbf{s}_j\}$ and $\{\mathbf{r}_j\}$ can be normalized so that $\mathbf{s}_j\cdot\mathbf{r}_j=1$.

The characteristic vector $\mathbf{s}_1=(1, 1, \cdots, 1)$ is a l.c.v. of every Markoff matrix, for by (8) and (4a) we have

$$\mathbf{s}_1\cdot\mathbf{P}=\left(\sum_m p_{m1}, \sum_m p_{m2}, \cdots, \sum_m p_{mN}\right)=(1, 1, \cdots, 1)=\mathbf{s}_1.$$

The c.n. of $\mathbf{s}_1=\mathbf{1}$ is $\lambda_1=1$. The modulus of every c.n. of a Markoff matrix is ≤ 1. Let the components of a r.c.v., $\mathbf{r}$, be $x_1, x_2, \cdots, x_N$. Then $\sum_n p_{mn}x_n=\lambda x_m$, and $|\lambda||x_m|=|\sum_n p_{mn}x_n|\leq\sum_n|p_{mn}||x_n|$ for every m. Hence

$$|\lambda|\sum_m|x_m|=\sum_{m,n}p_{mn}|x_n|\leq\sum_n|x_n|\sum_m p_{mn}=\sum_n|x_n|$$

so that $|\lambda|\leq 1$. It is convenient to order the c.n.'s of $\mathbf{P}$ so that $1=\lambda_1\geq|\lambda_2|\geq|\lambda_3|\geq\cdots\geq|\lambda_N|$.

The probability distribution vector $\mathbf{P(0)}=\{p_1(0), \cdots, p_N(0)\}$ can be expanded in a Fourier series in the r.c.v. $\{\mathbf{r}_j\}$:

$$\mathbf{P(0)}=\sum_{j=1}^N c_j\mathbf{r}_j, \quad \text{where} \quad c_j=\mathbf{s}_j\cdot\mathbf{P(0)}. \tag{11a}$$

Clearly the normalization condition (3) implies that

$$c_1=\mathbf{s}_1\cdot\mathbf{P(0)}=(1, 1, \cdots, 1)\cdot\{p_1(0), \cdots, p_N(0)\}=1. \tag{11b}$$

Hence $\mathbf{P(0)}=\mathbf{r}_1+\sum_2{}^N c_j\mathbf{r}_j$. Since $\mathbf{P}^k\mathbf{r}_j=\lambda_j\mathbf{r}_j$, the probability distribution vector $\mathbf{P(k)}$ has a simple Fourier series:

$$\mathbf{P(k)}=\mathbf{P}^k\mathbf{P(0)}=\mathbf{P}^k\mathbf{r}_1+\sum_2^N c_j\mathbf{P}^k\mathbf{r}_j=\mathbf{r}_1+\sum_{j=2}^N \mathbf{c}_j\lambda_j{}^k\mathbf{r}_j. \tag{12a}$$

If the components of $\mathbf{r}_j$ are $\{r_{j1}, r_{j2}, \cdots, r_{jN}\}$, then

$$pr(z_k=a_m)=r_{1m}+\sum_{j=2}^N c_j\lambda_j{}^k r_{jm}. \tag{12b}$$

When several c.n. of a Markoff matrix are equal, the matrix has the same number of linearly independent c.v. corresponding to c.n. as the degree of its degeneracy. By taking the appropriate linear combinations of these c.v.'s the validity of (12) is preserved.

2. Averages over Markoff Chains

The average value of a function $f_k=f_k(z_k)$ is given by

$$E(f_k)=\sum_{m=1}^N f_k(a_m)pr(z_k=a_m)=\mathbf{f}_k\cdot\mathbf{r}_1+\sum_{j=2}^N c_j\lambda_j{}^k(\mathbf{f}_k\cdot\mathbf{r}_j), \tag{13}$$

where $\mathbf{f}_k$ is the vector whose components are $f_k(a_m)$. The average value of a function $f_{ks}(z_k, z_s)$ where $s>k$ is given by

$$E(f_{ks})=\sum_{m,t=1}^N f_{ks}(a_m, a_t)pr(z_k=a_m)pr(z_s=a_t \text{ if } z_k=a_m)=\sum_{m,t=1}^N\left[r_{1m}+\sum_{u=2}^N c_u r_{um}\lambda_u{}^k\right]f_{ks}(a_m, a_s)\times\left[r_{1t}+\sum_{j=2}^N s_{jm}r_{jt}\lambda_j{}^{s-k}\right]. \tag{14}$$

Similar expressions exist for averages of functions of more than two variables.

A special case of (14) that will be needed later is obtained by letting (a) $f_{ks}(z_k, z_s)=x(z_k)x(z_s)$, (b) $E(x(z_k))=0$ for every k, and (c) $|\lambda_j|<1$ if $j>1$. Under these conditions (13) implies that

$$-\mathbf{x}\cdot\mathbf{r}_1=\sum_2^N c_j\lambda_j{}^k(\mathbf{x}\cdot\mathbf{r}_j).$$

Since this is true for every k, $\mathbf{x}\cdot\mathbf{r}_1=0$. Therefore (14) reduces to

$$E(x_kx_s)=\sum_{m=1}^N\left(r_{1m}+\sum_{u=2}^N c_u r_{um}\lambda_u{}^k\right)x(a_m)\sum_{j=2}^N s_{jm}(\mathbf{x}\cdot\mathbf{r}_j)\lambda_j{}^{s-k}=O[\exp-a(s-k)]; a>0. \tag{14a}$$

The distribution function of the sum

$$\sum_n=U(z_0, z_1)+U(z_1, z_2)+--+U(z_{n-1}, z_n) \tag{15}$$

can be expressed in terms of

$$f_n(w)=\sum_{a_0=1}^N\cdots\sum_{a_n=1}^N pr(x_j=a_0)\prod_{j=0}^{n-1}\{pr(z_j=a_j \text{ if } z_{j-1}=a_{j-1})\exp[iwU(a_j, a_{j+1})]\}. \tag{16a}$$

By repeating the type of analysis used at the beginning of this section one has:

$$f_n(w)=\sum_{k=1}^N\{\mathbf{s}_k(w)\cdot\mathbf{P(0)}\}\{\mathbf{1}\cdot\mathbf{r}_k(w)\}\Lambda_k{}^n(w), \tag{16b}$$

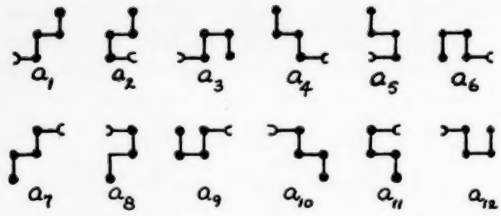

FIG. 2. The possible configurations of four successive bonds (with the first bond horizontal). The bond that is to be attached to the preceding part of the chain is the one connected to the open semicircle.

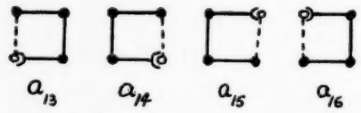

FIG. 3. The impossible configurations of four successive bonds.

where $\mathbf{s}_k(w)$ and $\mathbf{r}_k(w)$ are respectively the l.c.v. and r.c.v. of the matrix whose elements are $[pr(z_j=a \text{ if } z_{j-1}=b)]\exp[iwU(a,b)]$ and $\Lambda_k(w)$ is the corresponding characteristic value. Indeed, when s and t are points of continuity of the distribution function of $\sum_n$

$$pr(s<\sum_n \leqslant t)=\lim_{T\to\infty}\frac{1}{2\pi i}\int_{-T}^{T}(e^{-iws}-e^{-iwt})f(w)dw/w. \quad (17)$$

It can be shown that in the limit as $n\to\infty$, $pr(\sum_n \leq t)$ becomes Gaussian provided that the transition probability matrix $\mathbf{P}$ has a single c.n. of modulus unity.

This summary of the properties of Markoff chains is based on the three papers of reference 1. Hostinsky's little monograph was the first to give a detailed analysis of the characteristic value theory of Markoff chains.

III. STATISTICAL PROPERTIES OF POLYMER CHAINS ON SQUARE LATTICES

Now let us find the root-mean-square distance between ends of chains which do not contain first-order overlaps. All those chains whose first bond lies in the x direction can be constructed by the successive addition of the following links

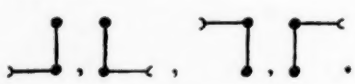

Of the 16 possible four-bond chains that can be formed from pairs of these only the 12 in Fig. 2 do not contain first-order overlaps. The four in Fig. 3 are forbidden. If the construction of these forbidden configurations is started the fourth bond in a_{13} must be placed so that a_5 results; a_{14} becomes a_2, a_{15} becomes a_{11}, and a_{16} becomes a_8.

For the purpose of describing a polymer chain as a Markoff chain, it is convenient to imagine long chains as a sequence of 4-mers. Indeed they can be represented by the sequence $z_0z_1z_2\cdots z_n$ where each z_j is a 4-mer of the set $a_1, a_2, \cdots, a_{12}$.

To find the $pr(z_0=a_k)$ let us construct 4-mers in such a manner that the probability of the sth particle being as far away from the $(s-3)$rd as possible is β while that of it being as near as possible (without overlap) is $\alpha=1-\beta$. The configuration a_1 can be constructed by first placing a bond to the right of the starting point. The probability of this placement is one-half. The probability of the second bond going to the left of the direction of the first is also one-half. The probability of the third going to the right is β, as is also that of the fourth going to the left. Hence $pr(z_0=a_1)=(\frac{1}{4})\beta^2$. In a similar manner we obtain

$$p_k(0)=pr(z_0=a_k)=\begin{cases}(\frac{1}{4})\beta^2 & \text{if } k=1,4,7,10\\ (\frac{1}{4})\alpha & \text{if } k=2,5,8,11\\ (\frac{1}{4})\alpha\beta & \text{if } k=3,6,9,12.\end{cases}$$

$$\mathbf{P}(0)=(\tfrac{1}{4})\{\beta^2,\alpha,\alpha\beta,\beta^2,\alpha,\alpha\beta,\beta^2,\alpha,\alpha\beta,\beta^2,\alpha,\alpha\beta\}. \quad (18)$$

The transition probabilities (p_{jk}) can be computed in a straightforward manner. Let us find $p_{13}=pr(z_{j+1}=a_1 \text{ if } z_j=a_3)$. The first new bond added to a_3 is forced to the left of path direction to prevent overlap (see b in Fig. 4). The probability of the second new bond going to the left is α. The third is forced to the left and the fourth goes to the left with a probability β. Hence $p_{13}=\alpha\beta$. Some transition probabilities are zero; for example, an a_1 followed by an a_6 yields a first-order overlap. The complete transition probability matrix is

$$\mathbf{P}=\begin{pmatrix}A_1 & A_2 & A_3 & A_4\\ A_2 & A_1 & A_4 & A_3\\ A_3 & A_4 & A_1 & A_2\\ A_4 & A_3 & A_2 & A_1\end{pmatrix}, \quad (19a)$$

where

$$\mathbf{A}_1=\begin{pmatrix}\beta^4 & \beta^4 & \alpha\beta\\ \alpha^2 & \alpha^2 & 0\\ \alpha\beta^3 & \alpha\beta^3 & \alpha^2\end{pmatrix} \quad \mathbf{A}_2=\begin{pmatrix}\alpha\beta^2 & \alpha\beta^2 & 0\\ \alpha\beta^2 & \alpha\beta^2 & 0\\ \alpha^2\beta & \alpha^2\beta & 0\end{pmatrix}$$

$$\mathbf{A}_3=\begin{pmatrix}0 & 0 & 0\\ 0 & 0 & \alpha\beta\\ 0 & 0 & 0\end{pmatrix} \quad \mathbf{A}_4=\begin{pmatrix}\alpha\beta^2 & \alpha\beta^2 & \beta^3\\ 0 & 0 & 0\\ \alpha^2\beta & \alpha^2\beta & \alpha\beta^2\end{pmatrix}. \quad (19b)$$

It is easy to verify that the sum of the elements of each column is equal to unity. Of course the fact that $\alpha+\beta=1$ must be used.

The characteristic values of $\mathbf{P}$ are the same as those of $\mathbf{Q}=\mathbf{R}^{-1}\mathbf{P}\mathbf{R}$ where

$$\mathbf{R}=\frac{1}{2}\begin{pmatrix}(1) & (1) & (1) & (1)\\ (1) & (-1) & (1) & (-1)\\ (1) & (1) & (-1) & (-1)\\ (1) & (-1) & (-1) & (1)\end{pmatrix}=\mathbf{R}^{-1}; \quad (1)=\begin{pmatrix}1 & 0 & 0\\ 0 & 1 & 0\\ 0 & 0 & 1\end{pmatrix}. \quad (20)$$

If $\mathbf{r}$ and $\mathbf{s}$ are the r.c.v. and l.c.v. of $\mathbf{P}$, then those of $\mathbf{Q}$ are $\mathbf{R}^{-1}\mathbf{r}$ and $\mathbf{sR}$. The matrix $\mathbf{Q}$ is of the form

$$\mathbf{Q}=\begin{bmatrix}\mathbf{Q}_1 & 0 & 0 & 0\\ 0 & \mathbf{Q}_2 & 0 & 0\\ 0 & 0 & \mathbf{Q}_3 & 0\\ 0 & 0 & 0 & \mathbf{Q}_4\end{bmatrix} \tag{21}$$

where

$$\left.\begin{aligned}\mathbf{Q}_1&=\begin{bmatrix}\beta^4+2\alpha\beta^2 & \beta^4+2\alpha\beta^2 & \alpha\beta+\beta^3\\ \alpha^2+\alpha\beta^2 & \alpha^2+\alpha\beta^2 & \alpha\beta\\ \alpha\beta^3+2\beta\alpha^2 & \alpha\beta^3+2\beta\alpha^2 & \alpha^2+\alpha\beta^2\end{bmatrix}\\ \mathbf{Q}_2&=\begin{bmatrix}\beta^4-2\alpha\beta^2 & \beta^4-2\alpha\beta^2 & \alpha\beta-\beta^3\\ \alpha^2-\alpha\beta^2 & \alpha^2-\alpha\beta^2 & \alpha\beta\\ \alpha\beta^3-2\beta\alpha^2 & \alpha\beta^3-2\beta\alpha^2 & \alpha^2-\alpha\beta^2\end{bmatrix}\end{aligned}\right\} \tag{21a}$$

$$\left.\begin{aligned}\mathbf{Q}_3&=\begin{bmatrix}\beta^4 & \beta^4 & \alpha\beta-\beta^3\\ \alpha^2+\alpha\beta^2 & \alpha^2+\alpha\beta^2 & -\alpha\beta\\ \alpha\beta^3 & \alpha\beta^3 & \alpha^2-\alpha\beta^2\end{bmatrix}\\ \mathbf{Q}_4&=\begin{bmatrix}\beta^4 & \beta^4 & \alpha\beta+\beta^3\\ \alpha^2-\alpha\beta^2 & \alpha^2-\alpha\beta^2 & -\alpha\beta\\ \alpha\beta^3 & \alpha\beta^3 & \alpha^2+\alpha\beta^2\end{bmatrix}.\end{aligned}\right\} \tag{21b}$$

Now the characteristic vectors of $\mathbf{Q}$ can be divided into four classes such that those in a given class correspond to the c.n. of a single $\mathbf{Q}_j$. Then

$$\mathbf{r}_j=\mathbf{R}\cdot\{\xi_j^{(1)},\xi_j^{(2)},\xi_j^{(3)},0,0,0,\cdots,0\}\quad j=1,2,3 \tag{22a}$$

$$\mathbf{r}_j=\mathbf{R}\cdot\{0,0,0,\xi_j^{(1)},\xi_j^{(2)},\xi_j^{(3)},0,0,\cdots,0\}\quad j=4,5,6 \tag{22b}$$

$$\mathbf{r}_j=\mathbf{R}\cdot\{0,0,0,0,0,0,\xi_j^{(1)},\xi_j^{(2)},\xi_j^{(3)},0,0,0\}\quad j=7,8,9 \tag{22c}$$

$$\mathbf{r}_j=\mathbf{R}\cdot\{0,0,\cdots,0,\xi_j^{(1)},\xi_j^{(2)},\xi_j^{(3)}\}\quad j=10,11,12, \tag{22d}$$

where the ξ_j's are the r.c.v. of the $\mathbf{Q}_k$'s. The same distribution of zeroes exists in the corresponding s_j's.

In order to find the root-mean-square distance between pairs of monomer elements in our chains we need the Fourier coefficients $\{c_j\}$ of the expansion

$$\text{prob}(z_0=a_m)=\sum_{j=1}^{N} c_j r_{jm}\quad\text{where}\quad c_j=\mathbf{s}_j\cdot\mathbf{P}(\mathbf{0}), \tag{22a}$$

and $\mathbf{P}(\mathbf{0})$ is given by (18). Since $c_j=(\mathbf{s}_j\cdot\mathbf{R})\mathbf{R}^{-1}\mathbf{P}(\mathbf{0})$, and $\mathbf{R}^{-1}\cdot\mathbf{P}(\mathbf{0})=\frac{1}{2}\{\beta^2,\alpha,\alpha\beta,0,0,\cdots,0\}$ we see that $(\mathbf{s}_j\cdot\mathbf{R})$ is orthogonal to $\mathbf{R}^{-1}\cdot\mathbf{P}(\mathbf{0})$ when $j>3$. Hence $c_4=c_5=\cdots=c_{12}=0$. From the expressions for $\mathbf{s}_1$, $\mathbf{s}_2$, $\mathbf{s}_3$, $\mathbf{r}_1$, $\mathbf{r}_2$, and $\mathbf{r}_3$ that we shall obtain later it follows that $c_1=1$, $c_2=\alpha^3$, and $c_3=0$; therefore

$$\mathbf{P}(\mathbf{k})=\mathbf{r}_1+\alpha^{4k+3}\mathbf{r}_2. \tag{23b}$$

The x component, $x(a_1)$, of the distance between the two ends of a 4-mer in configuration a_1 is $2a$; and that of the y component is also $2a$. The corresponding components for all configurations are given by the vectors $\mathbf{x}$ and $\mathbf{y}$ whose elements are $x(a_k)$ and $y(a_k)$

$$\mathbf{x}=2a(1,0,1,-1,0,-1,-1,0,-1,1,0,1) \tag{24a}$$

$$\mathbf{y}=2a(1,1,0,1,1,0,-1,-1,0,-1,-1,0). \tag{24b}$$

On some occasions $\mathbf{x}$ and $\mathbf{y}$ will be represented by column vectors with the same elements as (24). Equation (22) implies that

$$\mathbf{x}\cdot\mathbf{r}_j=\mathbf{s}_j\cdot\mathbf{x}=0\quad\text{unless}\quad j=10,11,12 \tag{25a}$$

$$\mathbf{y}\cdot\mathbf{r}_j=\mathbf{s}_j\cdot\mathbf{y}=0\quad\text{unless}\quad j=7,8,9. \tag{25b}$$

If we let $\mathbf{R}_n$ be the vector which connects the two ends of a chain of n 4-mers, we have $\mathbf{R}_n=\mathbf{i}X_n+\mathbf{j}Y_n$ where $\mathbf{i}$ and $\mathbf{j}$ are unit vectors in the x and y direction and

$$X_n=\sum_{k=0}^{n-1} x(z_k)\quad\text{and}\quad Y_n=\sum_{k=0}^{n-1} y(z_k). \tag{26}$$

The average value of the vector $\mathbf{R}_n$, $E\{\mathbf{R}_n\}=\mathbf{i}\sum_k E\{x(z_k)\}+\mathbf{j}\sum_k E\{y(z_k)\}$ vanishes from symmetry considerations. This result can easily be verified by combining (13), (23), and (25).

The mean square distance between ends of our polymer chain is given by

$$E\{R_n^2\}=E\{X_n^2+Y_n^2\}=\sum_{j=0}^{n-1} E\{x^2(z_j)+y^2(z_j)\}$$

$$+2\sum_{k=0}^{n-2}\sum_{j=k+1}^{n-1} E\{x(z_j)x(z_k)+y(z_j)y(z_k)\}. \tag{27}$$

The $x^2(z)+y^2(z)$ vector is $\mathbf{U}=4a^2(2,1,1,2,1,1,2,1,1,2,1,1)$. Hence (13) and (23) imply

$$E\{x^2(z_j)+y^2(z_j)\}=\mathbf{U}\cdot\mathbf{r}_1+\alpha^{4j+3}\mathbf{U}\cdot\mathbf{r}_2 \tag{28}$$

when $j>k$, we find by application of (13), (23), and (25) that

$$\begin{aligned}&E\{x(z_j)x(z_k)+y(z_j)y(z_k)\}\\ &=\sum_{t,\,m=1}^{12}[r_{1m}+\alpha^{4k+3}r_{2m}][x(a_m)x(a_t)\\ &\qquad+y(a_m)y(a_t)]\left[r_{1t}+\sum_{u=2}^{12} s_{um}r_{ut}\lambda_u{}^{j-k}\right]\\ &=\sum_{m=1}^{12}[r_{1m}+\alpha^{4k+3}r_{2m}]\\ &\qquad\times\left\{\sum_{u=2}^{12} s_{um}\lambda_u{}^{j-k}[x(a_m)\mathbf{x}\cdot\mathbf{r}_u+y(a_m)\mathbf{y}\cdot\mathbf{r}_u]\right\}.\end{aligned} \tag{29}$$

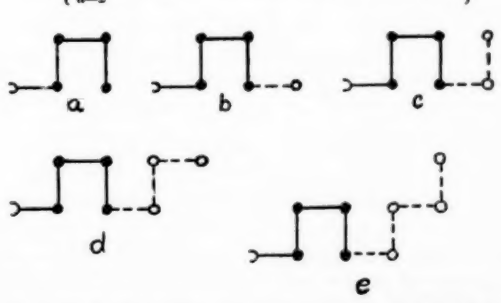

FIG. 4. Steps in the construction of an a_1 which follows an a_3.

In order to complete our calculation, we must find the c.v. and c.n. of $\mathbf{Q}$. Since $\mathbf{x}\cdot\mathbf{r}_j=\mathbf{y}\cdot\mathbf{r}_j=0$ if $j=4, 5, 6$, we do not need the c.v. which correspond to the c.n. of $\mathbf{Q}_2$. Furthermore each of the matrices $\mathbf{Q}_j$ have a c.n. $\lambda=0$. We shall represent these by $\lambda_3=\lambda_6=\lambda_9=\lambda_{12}=0$. Equations (28) and (29) indicate that the corresponding c.v. do not enter into our problem.

We can determine the c.n. and c.v. of $\mathbf{P}$ in the usual manner. Those which correspond to the c.n. of $\mathbf{Q}_1$ are

$$\lambda_1=1, \quad \mathbf{r}_1=[1/4(1+\alpha)]\{\beta,\alpha,\alpha,\beta,\alpha,\alpha,\beta,\alpha,\alpha,\beta,\alpha,\alpha\} \tag{30a}$$

$$\mathbf{s}=(1,1,1,1,1,1,1,1,1,1,1,1) \tag{30b}$$

$$\lambda_2=\alpha^4, \quad \mathbf{r}_2=-[1/4\alpha(1+\alpha)] \times\{\beta,-1,\alpha,\beta,-1,\alpha,\beta,-1,\alpha,\beta,-1,\alpha\} \tag{31a}$$

$$\mathbf{s}_2=(\alpha,\alpha,-1,\alpha,\alpha,-1,\alpha,\alpha,-1,\alpha,\alpha,-1) \tag{31b}$$

$$\lambda_3=0, \quad \mathbf{s}_3=(\alpha,0,-\beta,\alpha,0,-\beta,\alpha,0,-\beta,\alpha,0,-\beta). \tag{32}$$

The c.n. of $\mathbf{P}$ which are c.n. of $\mathbf{Q}$ are $\lambda_7=\alpha^2\exp-\varphi$ and $\lambda_8=\alpha^2\exp\varphi$ and $\lambda_9=0$, where $\varphi=\cosh^{-1}\{1+\frac{1}{2}\beta^4\alpha^{-2}\}$ and λ_7 and λ_8 satisfy

$$\lambda^2-\lambda(\beta^4+2\alpha^2)+\alpha^4=0, \quad \lambda_9=0. \tag{33}$$

These characteristic values are plotted in Fig. 5 as a function of α. The corresponding c.v. of $\mathbf{P}$ are ($k=7, 8$)

$$\mathbf{r}_k=\frac{1}{4(\alpha\beta^6-q_k^2)}\{\beta^4, w_k, \alpha\beta^3, \beta^4, w_k, \alpha\beta^3, -\beta^4, -w_k, -\alpha\beta^3, -\beta^4, -w_k, -\alpha\beta^3\} \tag{34a}$$

$$\mathbf{s}_k=(q_k, q_k, \beta^3, q_k, q_k, \beta^3, -q_k, -q_k, -\beta^3, -q_k, -q_k, -\beta^3), \tag{34b}$$

where $q_k=\alpha^2-\alpha\beta^2-\lambda_k$ and $w_k=-(q_k+\beta^4)$. The c.n. of $\mathbf{Q}$ also satisfy (33). We choose $\lambda_{10}=\lambda_7$ and $\lambda_{11}=\lambda_8$.

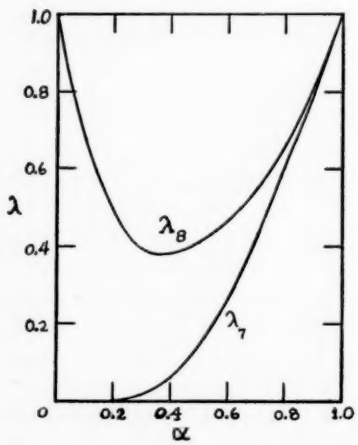

FIG. 5. The variation of the characteristic values λ_7 and λ_8 as a function of the interaction constant α. As $\alpha\to0$ monomers show increasingly strong attraction, as $\alpha\to1$ strong repulsion. The random case corresponds to $\alpha=\frac{1}{2}$.

Then, for $k=10, 11$, we have

$$\mathbf{r}_k=-\frac{1}{4(n_k^2+\alpha\beta^6)}\{\beta^4, m_k, \alpha\beta^3, -\beta^4, -m_k, -\alpha\beta^3, -\beta^4, -m_k, -\alpha\beta^3, \beta^4, m_k, \alpha\beta^3\} \tag{35a}$$

$$\mathbf{s}_k=(n_k, n_k, -\beta^3, -n_k, -n_k, \beta^3, -n_k, -n_k, \beta^3, n_k, n_k, -\beta^3) \tag{35b}$$

where $n_k=\alpha^2+\alpha\beta^2-\lambda_k$ and $m_k=-(\beta^4+n_k)$.

Equation (23b) can now be verified by application of Eqs. (30–32) to (23a). We also find that

$$\mathbf{x}\cdot\mathbf{r}_u=-2a\beta^3/(n_u^2+\alpha\beta^6) \quad \text{if} \quad u=10, 11$$

$$\mathbf{y}\cdot\mathbf{r}_u=2aq_u/(q_u^2-\alpha\beta^6) \quad \text{if} \quad u=7, 8.$$

$$\sum_{m=1}^{12} r_{jm}x(a_m)s_{um}=\frac{2a\beta(-\alpha)^{1-j}}{(1+\alpha)}(n_u-\alpha\beta^2) \quad \text{if } u=10, 11; j=1, 2.$$

$$\sum_{m=1}^{12} r_{jm}y(a_m)s_{um}=\frac{2aq_u}{1+\alpha} \text{ if } u=7, 8 \text{ and } j=1, 2.$$

Since $\lambda_7=\lambda_{10}$, $\lambda_8=\lambda_{11}$, $n_{10}=q_7+2\alpha\beta^2$ and $n_{11}=q_8+2\alpha\beta^2$.

The definition of q_u and the characteristic equation (33) imply that

$$2E\{x(z_j)x(z_k)+y(z_j)y(z_k)\}=\frac{8a^2}{(1+\alpha)(\beta^4+4\alpha^2)}\cdot\sum_{u=7}^{8}\lambda_u{}^{j-k}[2-\beta\alpha^{2+4k}]W_u \tag{36a}$$

where

$$W_u=[\alpha^3(\beta^2-2\alpha)+\lambda_u(2\alpha^2+\beta^4+\alpha\beta^2)]/(\lambda_u-\alpha^2). \tag{36b}$$

Hence Eqs. (27), (28), (30), (31), and (36) imply that

$$E\{R_n^2\}=\frac{8a^2}{(1+\alpha)}\left\{n-\frac{\beta\alpha^2}{2(1-\alpha^4)}(1-\alpha^{4n}) +\frac{1}{\beta^4+4\alpha^2}\sum_{u=7}^{8}\sum_{k=0}^{n-2}\sum_{j=k+1}^{n-1}\lambda_u{}^{j-k}[2-\beta\alpha^{4k+2}]W_u\right\}. \tag{37}$$

We need the sums

$$\sum_{k=0}^{n-2}\sum_{j=k+1}^{n-1}\lambda^{j-k}=\frac{n\lambda}{1-\lambda}-\frac{\lambda}{1-\lambda^2}+\frac{\lambda^{n+1}}{(1-\lambda)^2} \tag{38}$$

$$\sum_{k=0}^{n-2}\sum_{j=k+1}^{n-1}\alpha^{4k}\lambda^{j-k}=\frac{\lambda}{(1-\alpha^4)(1-\lambda)}-\frac{\lambda^{n+1}}{(1-\lambda)(\lambda-\alpha^4)} +\frac{\lambda\alpha^{4n}}{(1-\alpha^4)(\lambda-\alpha^4)}. \tag{38a}$$

When these expressions are substituted into (37) and the relations $\lambda_7\lambda_8=\alpha^4$ and $\lambda_7+\lambda_8=\beta^4+2\alpha^2$ are employed

one obtains (see Appendix II)

$$E\{R_n^2\}=\frac{8a^2}{(1+\alpha)}\left\{\frac{n(1+\alpha^2)}{2\alpha\beta}+\frac{\alpha^6-\alpha^4-6\alpha^3-\alpha^2-1}{8\beta^2\alpha^2(1+\alpha)}\right.$$

$$-\frac{\alpha^{4n+2}}{4\beta(1+\alpha)}+\frac{a_{n+1}}{8\alpha^2\beta^2}(1-\alpha+2\alpha^2+4\alpha^3-\alpha^4-\alpha^5)$$

$$\left.-\frac{b_{n+1}}{8\alpha^2\beta^2}(1-11\alpha+2\alpha^2+8\alpha^3-5\alpha^4+\alpha^5)\right\}, \quad (39)$$

where $a_n=(\lambda_7^n-\lambda_8^n)/(\lambda_7-\lambda_8)$ and $b_n=-\alpha^4(\lambda_7^{n-1}-\lambda_8^{n-1})/(\lambda_7-\lambda_8)$. If N is the degree of polymerization of our polymer, then $N=4n$. Since $\lambda_7=\alpha^2\exp-\varphi$ and $\lambda_8=\alpha^2\exp\varphi$ where $\varphi=\cosh^{-1}(1+\frac{1}{2}\beta^4\alpha^{-2})$, we can also write a_n and b_n as $a_n=\alpha^{2(n-1)}(\sinh n\varphi)/\sinh\varphi$ and $b_n=\alpha^{2n}[\sinh(n-1)\varphi]/\sinh\varphi$.

In the limit as $n\to\infty$ (39) reduces to (provided that $\alpha\neq 0, 1$)

$$\frac{1}{N}E\{R_n^2\}\sim\frac{a^2(1+\alpha^2)}{\alpha(1-\alpha^2)}. \quad (39a)$$

In a chain in which first-order overlaps are allowed the corresponding result can easily be shown to be

$$(1/N)E\{R_n^2\}\sim a^2\beta/\alpha. \quad (40)$$

Qualitatively this equation has the correct form because (a) when $\alpha=\beta=\frac{1}{2}$ there is no correlation between successive bonds. Hence

$$E\{R_n^2\}=E\{x_0^2+\cdots+x_{n-1}^2+y_0^2+\cdots+y_{n-1}^2\}=Na^2$$

(here the x's and y's represent x and y components of bonds and not 4-mers); (b) as $\alpha\to 0$ the probability of a first-order overlap approaches zero. Hence (40) must approach (39a) in the limit; as it does; (c) as $\beta\to 0$ the chain becomes a square with sides of length a so that $N^{-1}E\{R_n^2\}\to 0$.

The root-mean-square distance between ends of very long chains with and without first-order overlaps on a square lattice are compared in Fig. 6. It is to be noted that even in the random case, $\alpha=\frac{1}{2}$, the average chain length is increased by a factor 1.8 by excluding first order overlaps. This type of result was first suggested by Kuhn.[4]

An important feature of (39) is that $E\{R_n^2\}$ is proportional to N for all $0<\alpha<1$. In the limit as $\alpha\to 0$ or 1 the asymptotic expression (39) is not correct, for other λ's beside λ_1 have the value unity. Indeed, when $\alpha=1$, $E\{R_n^2\}=\frac{1}{4}N^2a^2$ and when $\alpha=0$, $E\{R_n^2\}=\frac{1}{2}N^2a^2$.

Now it is interesting to determine how large the degree of polymerization, N, must be in order for the asymptotic Eq. (39a) to give a good estimate to $E\{R_n^2\}$. The smallest value of N that allows one to use (39a) to estimate (39) with a relative error of less than 10 percent has been obtained by comparing (39a) with

[4] W. Kuhn, Kolloid Zeits. 87, 3 (1939).

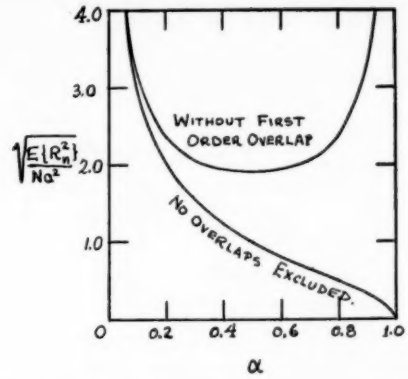

FIG. 6. Root-mean-square distance between ends of very long chains, $[E(R_n^2)]^{\frac{1}{2}}$, as a function of α. a=bond length and N =degree of polymerization.

(39). This value of N is plotted in Fig. 7 as a function of α. Even in the almost random range of $\alpha\simeq\frac{1}{2}$, N must be $\simeq 50$. This result is also valid for intermediate monomers in a long chain. Hence, on a square lattice the asymptotic formula (39a) cannot be applied to intermediate monomers unless they are separated by more than 50 bonds.

It can be shown that the mean square distance between the ends of any chain formed on a space lattice with the restriction that overlaps up to some finite order are excluded has the form of (39):

$$E\{R_n^2\}=An+B+\sum c_j e^{-nd_j}$$

where the real part of d_j is positive. The considerations which lead to the An term are given below. Equation (39) is valid only for degrees of polymerization of the form $4n=N$; it can be generalized to all values of N by adding one, two, or three bonds to all possible configurations of a $4n$-mer and computing the proper averages. On this basis one actually obtains different values of B and c_j for each set of the form $N=4n+j$ $(j=1-3)$.

Let us consider a Markoff chain with a single characteristic value of modulus 1. This chain has the property (14a):

$$E(x_k x_s)=O[\exp-a(s-k)]. \quad a>0.$$

Now suppose one constructs a polymer chain on a space lattice by piecing together subchains of degree of polymerization n_0, where n_0 is as large as one desires. If (a) these individual subchains are restricted to have configurations with no overlap and (b) the transition probability of a given configuration of a subchain being followed by another configuration of a subchain is set equal to zero when these two configurations would lead to an overlap, then one would have a Markoff chain of the type considered in our earlier discussion. The case of interest has been $n_0=4$. The configurations of a subchain in the general case could be represented by $a_1, a_2, \cdots, a_m$ and the analysis of the problem would proceed in the manner outlined in Section II. The

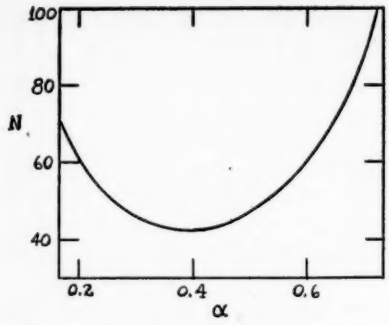

FIG. 7. Minimum degree of polymerization, N, necessary for asymptotic expression (39a), the mean square distance between chain ends, to have a relative error of less than 10 percent. This is plotted as a function of α.

matrices involved would be of considerably larger order than those obtained when $n_0=4$ and indeed when $n_0>10$ it might be hopelessly complicated to find the c.n. and c.v. of the (p_{ij}) matrix. However no matter how large n_0 might be, the correlation coefficient $E(x_k, x_s)$ decays exponentially with $(k-s)$ and the introductory discussion of this paper implies that as $n\to\infty$, $E(X_n^2)\to nA=N(A/n_0)=N\times$(constant) where $N=nn_0=$degree of polymerization of our model.

In the above model rather long-range effects can be taken into account. On the basis of the model the author doubts that one can change the relation $E(X_n^2)/N\to$ constant as $N\to\infty$. It would seem that by increasing the complication of the model one would merely increase the accuracy of the constant of interest.

We shall now describe a model experiment that could be set up to give a clearer indication of whether $E(X_n^2)/N\to$constant or, as is stated by Flory, $E(X_n^2)/N^c\to$constant where $c\neq 1$. Let strings of identical beads be constructed with the number of beads varying from about 100 to 1000. If a particular string of beads were placed in a viscous fluid and the fluid agitated, the string would go through a large number of configurations, but the individual monomers, the beads, could never penetrate one another. By painting the end beads with luminous paint, one could photograph the strings at regular intervals and observe projections of the distance between the ends. After a large number of photographs are taken, the mean square distance between a projection of the ends could be computed. This could be done for strings of various lengths and the variations of $E(X_n^2)$ with n could be determined. The experiment could also be performed with the luminescent beads at various points on the string.

In principle the exact distribution function of R_n^2 can be derived from a direct application of Eqs. (16) and (17). However, it has not yet been obtained by the author for chains on a square lattice because of the analytical complexity of the resulting expressions. However, the limiting distribution as $n\to\infty$ is Gaussian. This result follows from the central limit theorem for Markoff chains[1] or from the more general results of Bernstein[5] for the distribution of the x component of the distance X_n between ends of a chain of degree of polymerization $N=4n$, is given by

$$pr\left\{X_n<\left[\frac{N(1+\alpha^2)}{2\alpha(1-\alpha^2)}\right]^{\frac{1}{2}}ta\right\}\sim\frac{1}{(2\pi)^{\frac{1}{2}}}\int_{-\infty}^{t}\exp(-\tfrac{1}{2}t^2)dt.$$

By symmetry Y_n has the same distribution.

Since as will be discussed below, X_n and Y_n are independent variables, the distribution of $\mathbf{R}_n$ follows directly from that of X_n and Y_n. The correlation coefficient between X_n and Y_n is given by

$$E(X_nY_n)=\sum_{j=1}^{n-1}E(x_jy_j)+\sum_{i\neq j}E(x_jy_i).$$

By direct calculation one finds that

$$E(x_jy_j)=\sum_k x_j(a_k)y(x_k)pr(z_j=a_k)=0.$$

It can also be shown that $E(x_iy_j)=0$ when $i\neq j$. Qualitatively this is to be expected because the vector x has the same symmetry as the characteristic vectors of λ_{10}, λ_{11}, and λ_{12} while y has that of the vectors of $\lambda_1-\lambda_9$. Since the r.c.v. of $\lambda_{10}-\lambda_{12}$ are orthogonal to the l.c.v. of $\lambda_7-\lambda_9$, we have $E(x_jy_k)=0$.

One can obtain corrections to the Gaussian distribution by computing higher moments of the distribution by the methods used here for the calculation of $E\{R_n^2\}$ and substituting these moments into the Gram-Charlier series (the expansion of a distribution function as a linear combination of Hermite polynomials).

The application of the theory of Markoff chains to the excluded volume problem in polymers is being investigated independently by King[3] who is using punch card techniques. The author is grateful to Dr. Gilbert King for several interesting discussions of his work.

APPENDIX I. LONG-RANGE ORDER IN MARKOFF CHAINS

The distribution $\mathbf{P}(\mathbf{k})=\mathbf{r}_1$ is stationary; that is, if prob$(x_0=a_m)=r_{1m}$, then prob$(x_k=a_m)=r_{1m}$ for every integer k. This observation is a direct consequence of the fact that $\mathbf{r}_1=\mathbf{P}\mathbf{r}_1=\mathbf{P}^2\mathbf{r}_1=\cdots=\mathbf{P}^k\mathbf{r}_1$. A uniform distribution $p_m(j)=1/N$ is stationary when

$$\sum_{n=1}^{N}p_{mn}=1$$

for all m.

We shall now show how the distribution of x_k is related to that of x_0 for various classes of distributions of the c.n.'s of P of modulus 1.

(a) $\lambda_1=1$ *is the only c.n. of modulus 1.*—Since $|\lambda_j|<1$ for $j\neq 1$, we see that as $k\to\infty$ each term in the summand of (12b) tends exponentially to zero. Hence as $k\to\infty$

$$pr(x_k=a_m)\sim r_{1m}.$$

This result is independent of the initial distribution of x_0. $\mathbf{P}(\mathbf{k})=\mathbf{r}_1$

[5] S. Bernstein, Math. Ann. **97**, 1 (1926). See also P. A. P. Moran, Quart. J. Math. (Oxford) **19**, 140 (1948); Proc. Cam. Phil. Soc. **44**, 342 (1947).

is the only stationary distribution in this case. Every Markoff chain of this type approaches its stationary state as $k\to\infty$.

(b) $\lambda_1=\lambda_2=\cdots=\lambda_f=1 (f>1)$ *are the only c.n. of modulus 1.*—Since $|\lambda_j|<1$ for $j>f$, as $k\to\infty$ we have

$$pr(x_k=a_m)\sim r_{1m}+\sum_{j=2}^{f} c_j(0)r_{jm}.$$

The appearance of the $c_j(0)$'s, which depend on the distribution of x_0, implies that as $k\to\infty$ the distribution of x_k approaches a stationary value. However, this *stationary distribution depends on the distribution* of x_0 so that there is a correlation between the distributions of x_k and x_0 for all k no matter how large. In the phraseology of the theory of cooperative phenomenon *long-range order* exists in a Markoff chain which has several c.n. equal to unity. This class of chains also differs from those discussed in (a) in that several stationary distributions are possible. Indeed, every distribution of the form

$$p_m(k)=r_{1m}+\sum_{j=2}^{f} c_j r_{jm}$$

such that $\Sigma_m p_m(k)=1$ and $p_m(k)\geqslant 0$ is stationary.

(c) *The numbers* $\lambda_j=\exp(2\pi ij/q)$ *with* $q\leqslant N$, *and* $j=0, 1, \cdots, q-1$ *are the only c.n. of unit modulus.*—As $k\to\infty$, Eq. (12b) becomes

$$pr(x_k=a_m)\sim r_{1m}+\sum_{j=2}^{q-1} c_j(0)r_{jm}\exp(2\pi ij/q).$$

Hence the asymptotic distribution of x_k is periodic with period $q\leqslant N$. This periodic distribution depends on the distribution of x_0 so that long-range order exists in this case. The only stationary distribution is $p_m(k)=r_{1m}$.

It can be proven** that the only c.n. of modulus unity of a Markoff matrix of order n are roots of unity, $\exp 2\pi ij/q$, with $q\leqslant N$. Several cycles of c.n. can exist, but even in this general case the asymptotic distribution is either stationary or periodic depending on the initial distribution of x_0. For a detailed discussion of this case the reader is referred to Frechet.[1]

In general a dependence of the distribution of x_k on that of x_0 as $k\to\infty$ (that is, long-range order) exists if and only if more than one of the c.n. of the Markoff matrix are of modulus unity.

Several theorems on the roots of Markoff matrices are of interest for the discussion of long-range order. The first of these is a theorem of Frobenius: Let $p_{mn}>0$ for all m and n. Then the c.n. $\lambda_1=1$ is simple and is the only c.n. of modulus 1. Its r.c.v. is the only r.c.v. of (p_{mn}) whose components are all non-negative. A second is due to Frechet.[1] Let $p_{mn}>0$ for all m, and let λ be a c.n. of (p_{mn}). Then either $\lambda=1$ or $|\lambda|<1$.

Frobenius' theorem leads immediately to the result that long-range order cannot exist in a chain whose Markoff matrix has only positive elements.

** V. Romanovsky, Acta Math. **66**, 147 (1936) and N. Dmitriev and E. Dynkin, Comptes Rendus U.S.S.R. **49**, 159 (1945).

APPENDIX II. REMARKS ON DERIVATION OF EQ. (39)

Equation (39) was derived by combining (36)–(38). A number of symmetric functions of λ_7 and λ_8 had to be calculated. For example, the contribution of the term $n\lambda/(1-\lambda)$ of (38) to (37) required the evaluation of

$$A_1=\sum_{u=7}^{8}\frac{\lambda_u W_u}{1-\lambda_u}=\sum_u\left[\alpha^3(\beta^2-2\alpha)+\lambda_u(2\alpha^2+\beta^4+\alpha\beta^2)\right]\frac{\lambda_u}{(1-\lambda_u)(\lambda_u-\alpha^2)}$$
$$=\alpha^3(\beta^2-2\alpha)f_1+(2\alpha^2+\beta^4+\alpha\beta^2)(f_1-1),$$

where

$$f_1=\frac{\lambda_7}{(\lambda_7-\alpha^2)(1-\lambda_7)}+\frac{\lambda_8}{(\lambda_8-\alpha^2)(1-\lambda_8)};$$

but $\lambda_7\lambda_8=\alpha^4$ and $\lambda_7+\lambda_8=\beta^4+2\alpha^2$. Hence

$$(\lambda_7-\alpha^2)(\lambda_8-\alpha^2)=-\alpha^2\beta^4$$
$$(1-\lambda_7)(1-\lambda_8)=4\alpha\beta^2,$$

and

$$f_1=-\frac{1}{4\alpha^3\beta^6}\{[\alpha^4-\alpha^2\lambda_7][1-\lambda_8]+[\alpha^4-\alpha^2\lambda_8][1-\lambda_7]\}$$
$$=-\frac{1}{4\alpha\beta^6}\{2\alpha^2+2\alpha^4-(\lambda_7+\lambda_8)(1+\alpha^2)\}=(1+\alpha^2)/4\alpha\beta^2.$$

This expression for f_1 implies that

$$A_1=f_1(2\alpha^2+\beta^4+\alpha\beta^2+\alpha^3\beta^2-2\alpha^4)-(2\alpha^2+\beta^4+\alpha\beta^2)$$
$$=(\beta^4+4\alpha^2)(f_1-1)+(\alpha\beta^2-2\alpha^2)[-1+(1+\alpha^2)f_1]$$
$$=(\beta^4+4\alpha^2)(\beta^2+2\alpha^2)/4\alpha\beta.$$

The quantity A_1 also appears in the contribution of the first term of (38a) to (37).

The contribution of the remaining terms of (38a) and (38b) can be obtained in a similar manner. It is convenient for this purpose to write ($u=7, 8$)

$$\lambda_u{}^n=a_n\lambda_n+b_n,$$

where a_n and b_n are defined under Eq. (39). The validity of this equation follows from the expressions for $\lambda_7\lambda_8$ and $\lambda_7+\lambda_8$. In terms of a_n and b_n one can establish the following relations for each term in the double sum of (37):

$$\sum_{u=7}^{8}\frac{\lambda_u W_u}{(1-\lambda_u)^2}=\frac{(\beta^4+4\alpha^2)}{16\alpha^2\beta^4}\{\beta(1+\alpha^2)(\beta^2+2\alpha^2)$$
$$-\alpha^2(2\alpha^2+\beta^4+\alpha\beta^2+\alpha^3\beta^2-2\alpha^4)\}$$

$$\sum_{u=7}^{8}\frac{\lambda_u{}^{n+1}W_u}{(1-\lambda_u)^2}=\frac{(\beta^4+4\alpha^2)}{16\alpha^2\beta^3}\{a_{n+1}(1-2\alpha+7\alpha^2-4\alpha^3+11\alpha^4+2\alpha^5+\alpha^6)$$
$$+\beta b_{n+1}(1+3\alpha+6\alpha^2-10\alpha^3+5\alpha^4-\alpha^5)\}$$

$$\sum_{u=7}^{8}\frac{\lambda_u{}^{n+1}W_u}{(1-\lambda_u)(\lambda_u-\alpha^4)}=\frac{(\beta^4+4\alpha^2)}{4\alpha^4\beta^2}\{\alpha^2 a_{n+1}+(\alpha-\beta^2)b_{n+1}\}$$

$$\sum_{u=7}^{8}\frac{\lambda_u W_u}{(\lambda_u-\alpha^4)}=\frac{(\beta^4+4\alpha^2)}{4\beta^2}(3\beta^2+\alpha-\alpha^3).$$

The Effects of Saturation with Microwaves on Thermal Properties

VIRGINIA GRIFFING
Department of Chemistry, The Catholic University of America, Washington, D. C.
(Received February 20, 1950)

It is assumed that saturation with microwave is observed because the two states, J and $J+1$, are statistically filled. Under these conditions the change in the rotational partition function is temperature dependent so that thermal properties of the system could be changed. The changes in the rotational specific heat are calculated for a linear molecule. This effect would produce a change in the specific heat of HCN of about 2 parts in 10,000 if the $J=0\rightarrow1$ transition is saturated.

IN recent studies[1,2] of the absorption of microwaves by molecules, "saturation effects" have been observed which cause a decrease in the absorption coefficient and a broadening of the absorption line. Townes[1] has observed that "saturation effects" just become noticeable when radiation of 1.8 millivolts is transmitted through an absorption tube of 10.7 mm×4.3 mm cross section at a pressure of 4×10^{-2} mm. This indicates that saturation effects only become significant when the rate of absorption of the microwave is comparable with the rate of collision between the molecules.

As was first suggested by Townes,[1] Karplus and Schwinger[3] have theoretically explained both the decrease in the absorption coefficient and the broadening of the absorption line in terms of the disturbance of the thermal distribution of the molecules between the ground and excited states. The disturbance of thermal equilibrium will also result in a change in the partition function of a system saturated with microwaves. This is particularly significant for the rotational partition function, since the energy differences between states belonging to successive rotational quantum numbers are different; thus a characteristic frequency will excite only the molecules in one particular state J to the state $J+1$. If one assumes that at saturation the states J and $J+1$ are statistically filled, these two states would not be able to partake in the distribution of additional thermal energy. Thus the change in the rotational partition function is temperature dependent and would consequently result in a modification of the thermodynamic properties of the gas. It is the purpose of this paper to calculate the effects of saturation on some of the properties of a gas whose molecules can be considered as rigid rotators.

For a gas consisting of linear dipole molecules in thermal equilibrium, the rotation partition function is usually written thus

$$Q=\sum_{J=0}^{\infty}(2J+1)\exp\left[-\frac{J(J+1)\sigma}{kT}\right], \tag{1}$$

where J is the rotational quantum number, k is Boltzman's constant, T, the absolute temperature and $\sigma=h^2/(8\pi^2I)$ where I is the moment of inertia of the molecule and h is Planck's constant. Now consider the gas saturated with microwaves having the frequency of the $J=0\rightarrow1$ transition; this means that the number of particles in the $J=0$ level are not in thermal equilibrium with those in the $J=1$ and do not determine the relative number of particles in states $J\geqq1$. However, we assume that there is thermal equilibrium between successive J-states higher than 1. The "saturated" partition function thus becomes

$$Q'=1+3+\sum_{J\geq2}^{\infty}(2J+1)\exp-[J(J+1)-2]\frac{\sigma}{kT}, \tag{2}$$

$$Q'=q(Q+\delta) \tag{3}$$

where $q=e^{2\sigma/kT}$ and $\delta=(e^{-2\sigma/kT}-1)$.

Equation (3) is valid when thermal transitions are allowed between neighboring states only, i.e., $\Delta J=\pm1$. This is true in the following cases: (a) if the transitions are mainly due to blackbody radiation in dipole molecules, i.e., if the pressure is very small; (b) if collisions are involved but the interaction energy between colliding particles is such that it contains only the first power of θ, where θ is the angle of rotation. In that case the matrix element for the collision is similar to the one for dipole radiation.

In the general collision case, however, when ΔJ may be anything, the relative number of particles in any state is influenced by the number of particles in both states $J=0$ and $J=1$ and, therefore, is affected by the fact that these two states are not in thermal equilibrium. The principle of detailed balancing is then violated and one must write the following infinite set of linear equations. $N_0=N_1$

$$\sum_{i=0}^{\infty}K_{i\rightarrow J}N_i=(\sum K_{J\rightarrow i})N_J, \quad J=2,3,\cdots, \tag{4}$$

$$K_{J\rightarrow i}=K_{i\rightarrow J}\frac{g_i}{g_j}\exp\left(-\frac{\epsilon_i-\epsilon_J}{kT}\right), \tag{5}$$

then except for $K_{0\rightarrow1}$ and $K_{1\rightarrow0}$

$$Q'=\sum_{J=0}^{\infty}\frac{N_J}{N_0} \tag{6}$$

[1] C. H. Townes, Phys. Rev. **70**, 665 (1946).
[2] B. Bleaney and R. P. Penrose, Proc. Phys. Soc. **60**, 83 (1948).
[3] R. Karplus and J. Schwinger, Phys. Rev. **73**, 1020 (1948).

where N_i=number of molecules in state $J=i$, $K_{i\to J}$ =transition probability from $J=i$ to $J=J$, and Q'=non-equilibrium partition function for the general case.

However, in practice the only interesting case is the one where $\Delta J=\pm 1$, since "saturation" is only observed at low pressures. Thus for the special case discussed above, Eq. (6) becomes Eq. (3).

The deviation of the "saturated partition function," Q' (Eq. (3)) from the thermal equilibrium partition function Q (Eq. (1)) is temperature dependent and consequently this deviation will also be evident in the energy $\bar{E}'$, as well as the specific heat and other thermodynamic quantities. The average energy per mole, E', of the saturated system must be calculated explicitly* as follows:

$$\bar{E}'=\frac{N\sum_J \epsilon_J Q_J'}{Q'} \tag{7}$$

where N=Avogadro's number, $\epsilon_J=J(J+1)\sigma$,

$$Q_J'=(2J+1)\exp-\left[\frac{J(J+1)-2}{kT}\right]\sigma \quad \text{for} \quad J\geqq 1$$

$$Q_J'=e^{(2\sigma/kT)}Q_J=qQ_J$$

for

$$J=0, \quad Q_J'=Q_J=1.$$

Expressing Q' in terms of Q (the thermal equilibrium partition function) and since $\epsilon_{J=0}=0$, Eq. (8) becomes

$$\bar{E}'=\frac{Nq\sum_{J=1}^{\infty}\epsilon_J Q_J}{q(Q+\delta)}, \tag{8}$$

$$\bar{E}'=\frac{\bar{E}}{[1+(\delta/Q)]} \tag{9}$$

expanding $1+(\delta/Q)$ and neglecting second-order terms in δ^2

$$\bar{E}'=\bar{E}[1-(\delta/Q)] \tag{10}$$

expanding $e^{-2\sigma/kT}$ into a power series neglecting terms of second order and higher, and substituting the asymptotic value for the thermal equilibrium partition function,

$$Q=\frac{8\pi^2 IkT}{h^2}=\frac{kT}{\sigma}. \tag{11}$$

Then

$$Q'=Q\left(1+\frac{2}{Q}-\frac{2}{Q^2}-\frac{4}{Q^3}\right)$$

or

$$\Delta Q=2\left(1-\frac{1}{Q}-\frac{2}{Q^2}\right).$$

$$\bar{E}'=E\left[1+\frac{2}{Q^2}\right]. \tag{12}$$

Calculating the specific heat

$$C_v'=\left(\frac{dE'}{dT}\right)_v=C_v\left[1-\frac{2}{Q^2}\right]$$

or

$$C_v'=R\left[1-\frac{2}{Q^2}\right]. \tag{13}$$

There is one additional approximation of interest, even though the correction is too small to be appreciable. As the temperature is raised, maintaining saturation will mean that additional energy of the order of $(\epsilon_1\delta/Q^2)$ has been supplied by the radiation and consequently should be subtracted from Eq. (10) before C_v is calculated. Consider the specific case of HCN which has the smallest moment of inertia and consequently the smallest partition function Q, of any dipole linear molecule. At 100°K the change in C_v would be two parts in 10,000. Although it is possible to measure the specific heat of such a gas quite accurately by measuring the velocity of sound through it, it is improbable that one can measure the velocity of sound to two parts in 10,000 under these extreme conditions of 100°K and very low pressures. However, it is possible that the change in the velocity of sound in the gas when saturated with microwaves might be observable with a very good acoustic interferometer.

* Under conditions of thermal equilibrium

$$C_v=\frac{dE}{dT}=\frac{d}{dT}\left[RT^2\frac{d\ln Q}{dT}\right].$$

However, if one replaces Q by Q' in this expression one gets a quantity that differs from the modified specific heat, i.e.,

$$\frac{d}{dT}\left[RT^2\frac{d\ln Q'}{dT}\right]=R\left[1-\frac{4}{Q^2}\right].$$

Compare with Eq. (12).

Tetragonal Antiprism Bond Orbitals

GEORGE H. DUFFEY
Chemistry Department, South Dakota State College, Brookings, South Dakota

(Received January 30, 1950)

A set of eight equivalent bond orbitals of tetragonal antiprism symmetry is considered. The orbitals are of type $s^n p^3 d^{5-n}$. The acute angle between the fourfold axis and the maximum in a bond function varies from 66° 49′ to 44° 33′ as the parameter α is varied. The strongest orbitals (with a strength equal to 2.988) arise when n equals 0.9047. These are only slightly stronger than those with n equal to one.

COVALENT molecules or ions of type AB_8 may be formed when the electronic configuration of A is suitable and the radius of A is large enough so that the repulsion between the attached groups is low. The eight groups may be arranged about the central atom in several ways.[1-2] Hoard and Nordsieck[3] observed the dodecahedral arrangement in $[Mo(CN)_8]^{-4}$. Hoard[2] found that TaF_8^{-3} possessed the tetragonal antiprism structure. As a step toward understanding these structures, *spd* bond orbitals of tetragonal antiprism symmetry are considered in this note.

The angular parts of the s, p, and d wave functions, normalized to 4π, are given by the equations

$$s=1, \tag{1}$$

$$p_x=\sqrt{3}\sin\theta\cos\varphi, \tag{2}$$

$$p_y=\sqrt{3}\sin\theta\sin\varphi, \tag{3}$$

$$p_z=\sqrt{3}\cos\theta, \tag{4}$$

$$d_z=[(5)^{\frac{1}{2}}/2](3\cos^2\theta-1), \tag{5}$$

$$d_{xy}=[(15)^{\frac{1}{2}}/2]\sin^2\theta\cos 2\varphi, \tag{6}$$

$$d_{x+y}=[(15)^{\frac{1}{2}}/2]\sin^2\theta\sin 2\varphi, \tag{7}$$

$$d_{x+z}=(15)^{\frac{1}{2}}\sin\theta\cos\theta\cos\varphi, \tag{8}$$

and

$$d_{y+z}=(15)^{\frac{1}{2}}\sin\theta\cos\theta\sin\varphi, \tag{9}$$

where θ and φ are the angles used in polar coordinates. Differences in the radial parts of the wave functions are neglected and these angular parts are hybridized[4-6] to give the desired structure.

Thus set up the following functions:

$$\psi_1=\{[1/(8)^{\frac{1}{2}}]\cos\alpha\}s+[1/(8)^{\frac{1}{2}}]p_z+(1/2)p_x -\{[1/(8)^{\frac{1}{2}}]\sin\alpha\}d_z+(1/2)d_{xy}+(1/2)d_{x+z}, \tag{10}$$

$$\psi_2=\{[1/(8)^{\frac{1}{2}}]\cos\alpha\}s+[1/(8)^{\frac{1}{2}}]p_z+(1/2)p_y -\{[1/(8)^{\frac{1}{2}}]\sin\alpha\}d_z-(1/2)d_{xy}+(1/2)d_{y+z}, \tag{11}$$

$$\psi_3=\{[1/(8)^{\frac{1}{2}}]\cos\alpha\}s+[1/(8)^{\frac{1}{2}}]p_z-(1/2)p_x -\{[1/(8)^{\frac{1}{2}}]\sin\alpha\}d_z+(1/2)d_{xy}-(1/2)d_{x+z}, \tag{12}$$

$$\psi_4=\{[1/(8)^{\frac{1}{2}}]\cos\alpha\}s+[1/(8)^{\frac{1}{2}}]p_z-(1/2)p_y -\{[1/(8)^{\frac{1}{2}}]\sin\alpha\}d_z-(1/2)d_{xy}-(1/2)d_{y+z}, \tag{13}$$

$$\psi_5=\{[1/(8)^{\frac{1}{2}}]\cos\alpha\}s-[1/(8)^{\frac{1}{2}}]p_z+[1/(8)^{\frac{1}{2}}]p_x +[1/(8)^{\frac{1}{2}}]p_y-\{[1/(8)^{\frac{1}{2}}]\sin\alpha\}d_z+(1/2)d_{x+y} -[1/(8)^{\frac{1}{2}}]d_{x+z}-[1/(8)^{\frac{1}{2}}]d_{y+z}, \tag{14}$$

$$\psi_6=\{[1/(8)^{\frac{1}{2}}]\cos\alpha\}s-[1/(8)^{\frac{1}{2}}]p_z-[1/(8)^{\frac{1}{2}}]p_x +[1/(8)^{\frac{1}{2}}]p_y-\{[1/(8)^{\frac{1}{2}}]\sin\alpha\}d_z-(1/2)d_{x+y} +[1/(8)^{\frac{1}{2}}]d_{x+z}-[1/(8)^{\frac{1}{2}}]d_{y+z}, \tag{15}$$

$$\psi_7=\{[1/(8)^{\frac{1}{2}}]\cos\alpha\}s-[1/(8)^{\frac{1}{2}}]p_z-[1/(8)^{\frac{1}{2}}]p_x -[1/(8)^{\frac{1}{2}}]p_y-\{[1/(8)^{\frac{1}{2}}]\sin\alpha\}d_z+(1/2)d_{x+y} +[1/(8)^{\frac{1}{2}}]d_{x+z}+[1/(8)^{\frac{1}{2}}]d_{y+z}, \tag{16}$$

$$\psi_8=\{[1/(8)^{\frac{1}{2}}]\cos\alpha\}s-[1/(8)^{\frac{1}{2}}]p_z+[1/(8)^{\frac{1}{2}}]p_x -[1/(8)^{\frac{1}{2}}]p_y-\{[1/(8)^{\frac{1}{2}}]\sin\alpha\}d_z-(1/2)d_{x+y} -[1/(8)^{\frac{1}{2}}]d_{x+z}+[1/(8)^{\frac{1}{2}}]d_{y+z}. \tag{17}$$

These functions represent eight equivalent orthogonal bond orbitals of type $s^n p^3 d^{5-n}$ where

$$n=\cos^2\alpha. \tag{18}$$

TABLE I. Results of calculations on tetragonal antiprism orbitals with[a] $0\leq\alpha\leq\pi/2$.

n[a]	S, Strength of an orbital	θ_1, Angle between axis and maximum in ψ_1
1.0000	2.979	57° 35′
0.9047	2.988	60° 54′
0.7000	2.980	63° 10′
0.5000	2.961	64° 33′
0.3000	2.928	65° 36′
0.1000	2.869	66° 27′
0.0000	2.768	66° 49′

[a] The orbitals are of type $s^n p^3 d^{5-n}$. Note that $n=\cos^2\alpha$.

TABLE II. Results of calculations on tetragonal antiprism orbitals with $0\geq\alpha\geq-\pi/2$.

n	S, Strength of an orbital	θ_1, Angle between axis and maximum in ψ_1
1.0000	2.979	57° 35′
0.9000	2.955	53° 46′
0.7000	2.927	50° 45′
0.5000	2.897	48° 36′
0.3000	2.859	46° 49′
0.1000	2.797	45° 16′
0.0000	2.696	44° 33′

[1] G. Kimball, J. Chem. Phys. **8**, 188 (1940).
[2] Marchi, Fernelius, and McReynolds, J. Am. Chem. Soc. **65**, 329 (1943).
[3] J. L. Hoard and H. H. Nordsieck, J. Am. Chem. Soc. **61**, 2853 (1939).
[4] See L. Pauling, J. Am. Chem. Soc. **53**, 1367 (1931).
[5] L. Pauling, *The Nature of the Chemical Bond* (Cornell University Press, Ithaca, New York, 1940).
[6] R. Hultgren, Phys. Rev. **40**, 891 (1932).

These orbitals are of tetragonal antiprism symmetry D_{4d}. The Z axis coincides with the fourfold axis.

A function orthogonal to $\psi_1, \cdots \psi_8$ is given by

$$\psi_9 = (\sin\alpha)s + (\cos\alpha)d_z. \quad (19)$$

The functions were used in constructing Tables I and II. In Table I, S and θ_1 were obtained with $0 \leq \alpha \leq \pi/2$. In Table II, S and θ_1 were obtained with $0 \geqslant \alpha \geqslant -\pi/2$. Here S is the maximum value of ψ_1 and is called the strength of an orbital; θ_1 is the angle between the axis and the maximum in ψ_1 and is approximately the angle between the axis and bond one.

It is evident that the orbitals described in Table I will be preferred since they are stronger than the corresponding ones in Table II. The strongest tetragonal antiprism orbitals may be formed when n equals 0.9047. The maximum strength, 2.988, is only slightly less than the maximum strength[6] of an *spd* orbital. When the *s* and *d* orbitals are of almost equal stability, n will tend to equal 0.9047 if the tetragonal antiprism structure is assumed.

Kimball[1] reasoned that the stable bond arrangement when n equaled one was the dodecahedral arrangement since $[Mo(CN)_8]^{-4}$ has this structure. However, one would conclude from the present calculations that the tetragonal antiprism structure is one of the stable structures when n equals one.

Because of the repulsion between the attached groups in the tetragonal antiprism structure, the acute angle between the axis and a bond will tend to be different from θ_1 for all but one value of n and the effective strength of the orbitals will be reduced somewhat. If the repulsion tends to stabilize the regular tetragonal antiprism structure, this acute angle would tend to be between θ_1 and 59° 16′. (Here a regular tetragonal antiprism is defined as the square antiprism with sixteen equal edges.)

THE JOURNAL OF CHEMICAL PHYSICS VOLUME 18, NUMBER 5 MAY, 1950

Compressibilities, Force Constants, and Interatomic Distances of the Elements in the Solid State

J. Waser* and Linus Pauling
Gates and Crellin Laboratories of Chemistry, California Institute of Technology, Pasadena, California†

(Received January 23, 1950)

Available data for the compressibilities of crystalline elements are used to calculate the force constants for the assumed Hooke's law interactions between adjacent atoms. On comparison of these constants and the equilibrium interatomic distances it is found that for many substances there holds the relation discovered by Badger for diatomic gas molecules: a linear relation between the reciprocal of the cube root of the force constant and the interatomic distance, for elements of a given row in the periodic table. Deviations from this relation are in the direction of increased compressibility. They are explained as resulting from changes in bond type (that is, in electronic structure) that permit the crystal to adjust itself to the increased pressure.

INTRODUCTION

THE compressibilities of elements and compounds in the solid state[1] represent a considerable body of information which may be interpreted in terms of molecular constants. An attempt is made here to do this for substances which have simple structures, mainly those with cubic symmetry. Our considerations have been based on the concept of the existence of covalent bonds between nearest neighbors in the lattice (resonating covalent bonds in the metals). The compressibility is then used to evaluate the force constant for a Hooke's law force acting along the bonds. A relationship similar to Badger's rule[2] for molecules in the gaseous state has been found to obtain between these force constants and the interatomic distances.

There exists one difficulty with the attempt to use central forces to explain the elastic properties of crystalline matter, especially in the case of metals. Central forces imply certain relations among the various elastic constants of a crystal, the Cauchy relations, which are poorly satisfied for metals.[3] Non-central forces should, therefore, be introduced in addition to the central forces assumed above. In the usual electron theory of metals the interactions between the free electrons and the lattice of residual ion cores are of the non-central type, and the breaking down of the Cauchy relations may be thus accounted for. If all elastic constants are known for a given crystal the contributions to the energy of the crystal from the free electrons may be separated

* Present address: Department of Chemistry, Rice Institute, Houston, Texas.

† Contribution No. 1380.

[1] See P. W. Bridgman, Rev. Mod. Phys. **18**, 1 (1946).

[2] R. M. Badger, J. Chem. Phys. **2**, 128 (1934); **3**, 710 (1935).

[3] It was recently pointed out by P. S. Epstein (Phys. Rev. **70**, 915 (1946)) that the Cauchy relations are not expected to hold for the general case of central forces involving non-nearest neighbors also. However, they should be satisfied for central forces between nearest neighbors only. Cf. also C. Zener, Phys. Rev. **71**, 323 (1947).

TABLE I. Compressibilities and derived properties of the elements and some compounds.

Substance	Crystal structure[a]	D_0, A[b]	$A \times 10^7$ cm²/kg	$B \times 10^{12}$ cm⁴/kg²	$k \times 10^{3}$ [c]	$k^{-\frac{1}{2}}$	$-k' \times 10^{-5}$ [d]	Ref.[m]
Ag	*A*1	2.883	9.87	5.06	30.4	3.20	133	B 7
Al	*A*1	2.858	13.43	6.2	22.14	3.561	57	B 7
Au	*A*1	2.878	5.77	3.4	51.9	2.68	500	B 7
B			5.51	2.2				B 3
Ba	*A*2	4.343	101.9	129	7.241	5.168	1.20	B 1
Be	*A*3	2.224[g]	2.20[h]	0.70[h]	33.6[e]	3.10[e]	233[j]	B 6
		2.268[f]	2.82[i]	1.67[i]	26.5[f]	3.36[f]		
C(diam)	*A*4	1.542	1.73		609	1.18		W
Ca	*A*1	3.932	56.97	63.9	7.179	5.184	5.30	B 7
Cb	*A*2	2.853	5.700	2.22	85.0	2.27	523	B 6
Cd	*A*3	3.287[e]	18.3[h]		6.43[e]	5.38[e]		B 1
		2.973	2.1[i]		61.4[f]	2.54[f]		
Ce	*A*3	3.64	45.63	−161.4	8.29	4.94	−59.8	B 1
Co	*A*3	2.503	5.39	2.3	48.4	2.74	400	B 7
Cr	*A*2	2.493	5.19	2.19	81.6	2.31	701	B 1
Cs	*A*2	5.24	700	10,000[k]	1.27	9.22	0.7	L
Cu	*A*1	2.551	7.19	3.0	36.9	3.00	210	B 7
Fe	*A*2	2.478	5.826	0.80	72.26	2.401	118	B 9
Ga	*A*11		20					B 1
Ge	*A*4	2.445	14.11	6.09	117.7	2.040	297	B 7
Hf	*A*3	3.170	9.01	2.37	36.6	3.01	66.5	B 1
In	*A*6	3.242	25					B 1
		3.370						
Ir	*A*1	2.709	2.68	1.3	105	2.12	200	B 1
K	*A*2	4.618	356.5	285	2.201	7.686	1.78	L
La	*A*3	3.741	35.13	14.7	11.10	4.482	1.73	B 1
Li	*A*2	3.04	86.92	97.5	5.94	5.52	1.70	B 1
Mg	*A*3	3.189[e]	9.84[h]	6.51[h]	11.4[e]	4.45[e]	23.1[d]	B 1
		3.202[f]	9.84[i]	9.19[i]	11.2[f]	4.47[f]		
Mn	*A*6, *A*12, *A*13		7.91[l]	5.3				B 3
Mo	*A*2	2.720	3.60	1.19	128	1.98	1150	B 7
Na	*A*2	3.72	156.2	300	4.05	6.27	0.75	L
Nd	*A*3	3.639	32.6		11.6	4.42		B 10
Ni	*A*1	2.487	5.29	2.4	48.9	2.73	450	B 7
Pb	*A*1	3.492	23.72	20.3	15.31	4.027	34.4	B 7
Pd	*A*1	2.745	5.28	2.4	54.1	2.64	450	B 7
Pr	*A*3	3.648	33.8	13	11.2	4.47	1.3	B 1
Pt	*A*1	2.769	3.60	1.8	80.0	2.32	1100	B 7
Rb	*A*2	4.87	520	5600[k]	1.59	8.57	1.1	L
Rh	*A*1	2.684	3.606	2.73	77.43	2.345	1730	B 6
Ru	*A*3	2.672	3.42	2.13	81.3	2.31	1570	B 6
Si	*A*4	2.346	11.2		142	1.91		B 10
Sn, white	*A*5	3.17[g]	6.719[h]	4.07[h]	33.13[g]	3.113[g]		B 1
		3.016[e]	6.022[i]	4.20[i]	51.30[e]	2.691[e]		
Sn, grey	*A*4	2.80	19		100	2.16		T
Sr	*A*1	4.296	81.22	100.6	5.502	5.662	2.02	B 7
Ta	*A*2	2.854	4.79	0.4	101	2.15	79	B 7
Ti	*A*3	2.934	7.97	−0.12	38.3	2.97	46	B 1
Tl	*A*3	3.427	27.8		12.8	4.27		RW, B 1
U	*A*2, *A*15		9.66[l]	3.26				B 7
V	*A*2	2.627	6.09	2.58	73.3	2.39	498	B 1
W	*A*2	2.735	3.18	1.4	146	1.90	2060	B 1
Zn	*A*3	2.907[e]	13.50[h]	7.68[h]	7.975[e]	5.005[e]		B 8
		2.659[f]	1.59[i]	0.78[i]	71.78[f]	2.406[f]		
Zr	*A*3	3.195	10.97	7.44	30.30	3.207	148	B 1
AgBr	*B*1	2.77	27		30	3.2		RB
AgCd	*B*2	2.88	11.54	4.6	42.4	2.87		B 7
AgCl	*B*1	2.46	24		30	3.2		RJ
AgI	*B*3	2.80	40		48	2.8		RJ
AgZn	*B*2	2.74	10.30	1.9	45.0	2.81		B 7
AlSb	*B*3	2.685	18.02	19.0	99.6	2.16		B 4
AuZn	*B*2	2.73	7.54	2.4	61.4	2.54		B 7
BaS	*B*1	3.19	28.93	52.1	32.4	3.14		B 5
CaS	*B*1	2.84	22.80	38.8	36.7	3.01		B 5
CdTe	*B*3	2.80	23.3	12.2	81.6	2.31		B 4
CsI	*B*2	3.95	84.03	201.9	7.98	5.01		B 5
CuBr	*B*3	2.46	28.7	25.1	58.2	2.58		B 5
CuCl	*B*3	2.34	24.63	14.1	64.7	2.49		B 5
CuI	*B*3	2.62	27.52		64.6	2.49		B 5
CuZn	*B*2	2.55	8.95	2.5	48.4	2.74		B 7
HgTe	*B*3	2.79	19.8	25	95.7	2.19		B 4
KI	*B*1	3.53	83.7	150.7	12.4	4.32		B 1

TABLE I.—*Continued.*

Substance	Crystal structure[a]	D_0, A[b]	$A\times10^7$ cm²/kg	$B\times10^{12}$ cm⁴/kg²	$k\times10^{3}$ [e]	$k^{-\frac{1}{3}}$	$-k'\times10^{-5}$ [d]	Ref.[m]
LiI	*B*1	3.00	58.89	107.4	15.0	4.06		B 5
Mg_2Pb	*C*1	2.96	26.13	21.2	38.5	2.96		B 7
NaI	*B*1	3.23	69.36		13.7	4.18		B 5
PbS	*B*1	2.97	18.4	6.33	47.5	2.76		B 2
PbSe	*B*1	3.07	20.67	12.8	43.7	2.84		B 7
PbTe	*B*1	3.22	25.55	24.3	37.1	3.00		B 7
RbI	*B*1	3.66	93.8	197.7	11.5	4.43		B 1
SrS	*B*1	3.01	23.83	38.6	37.1	3.00		B 5
TiC	*B*1	2.16	4.72	2.2	135	1.95		B 1
TiN	*B*1	2.20	3.32	2.13	195	1.72		B 1
TlBr	*B*2	3.44	52		11.2	4.5		RJ
TlCl	*B*2	3.33	48		11.8	4.4		RJ
TlI	*B*2	3.62	68		9.0	4.8		RJ
ZnS (sphalerite)	*B*3	2.35	12.81		124.5	2.00		B 2
ZnS (wurtzite)	*B*4	2.36	13.1		122	2.01		M
ZnO	*B*4	2.01	7.5		182	1.8		M

[a] M. C. Neuburger, Zeits. f. Krist. **93**, 1 (1936), or "Strukturbericht."
[b] In case of alternate structures the one most commonly occurring indicated in table was used for calculations.
[e] k in megadynes/cm.
[d] k' in megadynes/cm².
[e] For bonds inclined to axis of highest symmetry.
[f] For bonds perpendicular to axis of highest symmetry.
[g] For bonds parallel to axis of highest symmetry.
[h] Linear compression parallel to axis of highest symmetry.
[i] Linear compression perpendicular to axis of highest symmetry.
[j] Average value calculated from volume compressibility.
[k] Estimated value.
[l] Crystalline modification investigated not reported.
[m] References to Table I:
B 1 to B 10, P. W. Bridgman:
B 1, *The Physics of High Pressure* (London, 1931).
B 2, Am. J. Sci. **10**, 483 (1925).
B 3, Proc. Am. Acad. **64**, 51 (1929).
B 4, *Ibid.* **66**, 255 (1931).
B 5, *Ibid.* **67**, 345 (1932).
B 6, *Ibid.* **68**, 27 (1933).
B 7, *Ibid.* **70**, 285 (1935).
B 8, Phys. Rev. **47**, 393 (1935).
B 9, Rev. Modern Phys. **18**, 1 (1946).
B 10, Extrapolated from compressibilities to 100,000 kg/cm², (private communication); see Proc. Am. Acad. **76**, 55 (1948).
L, Landolt and Börnstein.
M, F. Madelung and R. Fuchs, Ann. d. Physik **65**, 289 (1921).
RB, T. W. Richards and E. P. Bartlett, J. Am. Chem. Soc. **37**, 470 (1915).
RJ, T. W. Richards and G. Jones, *ibid.* **31**, 158 (1909).
RW, T. W. Richards and J. D. White, *ibid.* **50**, 3290 (1928).
T, G. Tammann and R. Kohlhass, Zeits. f. anorg. u. allgem. Chemie **199**, 209 (1931); estimated from graph on p. 223.
W, E. D. Williamson, J. Franklin Inst. **193**, 491 (1922); S. Bhagavantam and J. Bhimasenachar, Proc. Roy. Soc. (London) **A187**, 381 (1946).

from the interactions between the ion cores, and force constants for the latter may be evaluated,[4] which, however, do not contain the large part of the contribution of the free electrons which can be approximated by central forces. From our viewpoint of nearest-neighbor bonds, where the bulk of the interatomic interactions is described by a central force field, the breakdown of the Cauchy relations may be understood by assuming the operation of forces which oppose deformations of bond angles; these forces are non-central in character. For some crystals with cubic face-centered and cubic body-centered structures these angular force constants were calculated by us from the elastic constants available, and were found to be small compared to the bond stretching constants. They were negative in sign, indicating decrease of the angular potential energy upon angular deformation, and thus implying the existence of a small angular strain for the cases investigated. Unfortunately not enough data on elastic constants are available to permit the systematization of these angular force constants.

METHOD AND RESULTS

If there are n equivalent nearest-neighbor bonds of length D_0 in the unit cell of volume V_0 of a cubic crystal, then the force constant k in the equation $U(D)=(k/2)(D-D_0)^2$ for the potential energy of a bond under compression is given by the expression

$$k=\frac{9V_0}{nD_0^2A}, \tag{1}$$

where A is defined by the equation

$$(V_0-V)/V_0=Ap-Bp^2 \tag{2}$$

relating the volume at pressure p to the volume at zero pressure. Equation (1) applies also to the case of hexagonal closest packing, and was assumed to hold in addition for approximate hexagonal closest packing, as exemplified by a number of metals crystallizing with the $A3$ structure.[5] If A is measured in 10^{-7} cm²/kg, D_0 in A, and k in megadynes/cm Eq. (1) reduces to

$$k=C(D_0/A),$$

where C equals 0.1040 for the lattices $A1$ and $A3$, 0.1699 for the lattice $A2$, and 0.6794 for the lattice $A4$.

From the constant B in Eq. (2) the variation of the force constant k with distance can be calculated. If the expansion

$$k(D)=k+(D-D_0)k' \tag{3}$$

is used we obtain

$$k'=\frac{3(A^2-B)}{A^2D_0}k. \tag{4}$$

[4] K. Fuchs, Proc. Roy. Soc. (London) **153A**, 622 (1936); **157A**, 444 (1936); P. C. Fine, Phys. Rev. **56**, 355 (1939); R. B. Leighton, Thesis, California Institute of Technology, 1947; etc.

[5] The symbols $A3$, etc., are those used in the Strukturbericht.

It was assumed that this equation remains valid for approximate hexagonal closest packing.

For the metals beryllium, magnesium, zinc, and cadmium, with the $A3$ structure, and for the tetragonal modification of tin, the linear compressibilities under hydrostatic pressure parallel and perpendicular to the axis of highest symmetry are known. From these data force constants for the two types of nearest-neighbor bonds in the crystals considered were calculated from simple elastostatic considerations neglecting bond-angle restoring forces. For the $A3$ structure the following results were obtained:

$$k_1=\frac{3c^2-2a^2}{6\sqrt{3}cA_1} \tag{5}$$

$$k_2=\frac{a^2}{\sqrt{3}c}\frac{4a^2+3c^2}{4a^2A_1+3c^2A_2}, \tag{6}$$

where A_1 and A_2 are defined by the equation

$$(l_{oi}-l_i)/l_{oi}=A_ip-B_ip^2; \quad i=1,2$$

for the linear compressions perpendicular and parallel to the hexagonal axis. The force constants k_1 and k_2 apply respectively to bonds perpendicular and inclined to the hexagonal axis and a and c are the edges of the hexagonal unit cell. The corresponding equations for the white tin structure, $A5$, are

$$k_1=\frac{(4a^2+c^2)c}{4a^2A_1+c^2A_2} \tag{7}$$

$$k_2=(2a^2-c^2)/8cA_2. \tag{8}$$

The linear compressions perpendicular and parallel to the tetragonal axis are described by A_1 and A_2; a and c are the edges of the tetragonal unit cell, and k_1 and k_2 are the force constants for bonds inclined and parallel to the tetragonal axis.

It is found that the force constants (Table I) obtained in this way are linked with the interatomic distances by the relationship proposed by Badger[2] for force constants determined spectroscopically,

$$k^{-\frac{1}{3}}=a_{ij}(D_0-b_{ij}), \tag{9}$$

where a_{ij} and b_{ij} are constants and i, j indicate the rows in the periodic system in which the two partners are located. Only the case $i=j$ is treated here, since very few data for the general case are available (cf. below). The quantities a_{ii} and b_{ii} for the compressibility force constants differs somewhat from the corresponding terms for spectroscopic force constants, and the further restriction must be made that the long rows of the periodic system are to be subdivided into two parts. Table I contains the calculated force constants and the compressibilities and average interatomic distances used in the calculations. Figures 1 to 4 are graphical representations of the data. The straight lines correspond to the constants a_{ii} and b_{ii} given in Table II, together with the constants a'_{ii} and b'_{ii} used by Badger for spectroscopic force constants.

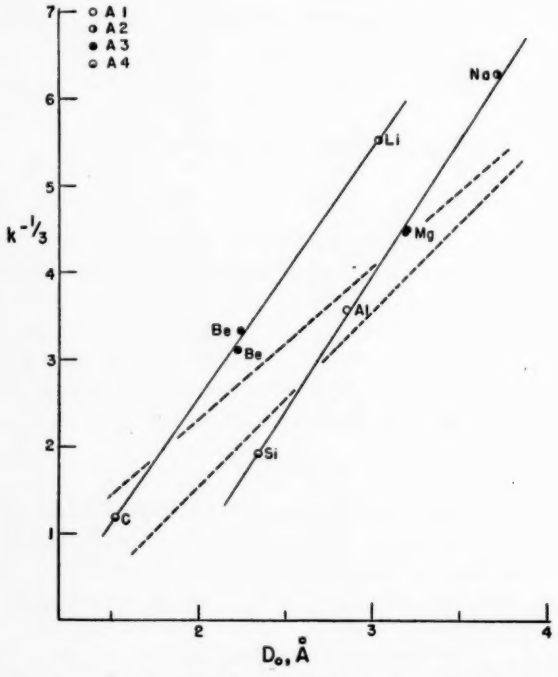

FIG. 1. Plot of the reciprocal of the cube root of the force constant of bonds *vs.* the interatomic distance for crystalline elements of the first and second short periods of the periodic system. The solid lines are curves of the Badger type drawn to represent the compressibility data, and the dashed lines are Badger's curves for the first-row and second-row elements, obtained from spectroscopic data for diatomic molecules.

TABLE II. Constants in relation 2
D_0 in A, k in megadynes/cm.

Elements	a_{ij}	b_{ij}	a'_{ij}[a]	b'_{ij}[a]
C, Be, Li	2.89	1.13	1.75	0.68
Na, Mg, Al, Si	3.10	1.73	2.04	1.25
(K), Ca, Ti, V, Ge	2.06	1.46	1.98	1.48
Cr, Fe, Co, Ni, Cu	13.3	2.31		
(Rb), Sr, Zr, Cb, Mo, Sn	2.32	1.86	2.04	1.76
Ru, Rh, Pd, Ag	4.12	2.10		
Ba, Ta, W	2.03	1.80		
Ce, Ir, Pt, Au, Tl	2.96	1.99		

[a] Corresponding constants used by Badger (see reference 2) for spectroscopic force constants.

DISCUSSION

It is interesting that for several elements in each period a relation of the Badger form holds quite well, and, moreover, that the Badger equations themselves (dashed lines in Figs. 1 to 3), which were derived completely from spectroscopic data for diatomic molecules, fit the compressibilities moderately well for some elements of the two long periods.

We might expect in general that the simple Badger relation would hold for crystals (or molecules) in which

the bond type (electronic structure) remains constant during compression. If, however, the electronic structure were to undergo a readjustment on compression, decreasing the energy of the system, the potential energy curve would be flattened, so that the force constant would be smaller and the compressibility greater than for the normal case in which this change in electronic structure does not occur. This phenomenon would cause the points in the plots of $k^{-\frac{1}{3}}$ against D_0 to lie above the normal Badger-rule lines for those substances showing such readjustment in electronic structure. We think that most of the features shown in Figs. 1 to 4 can be explained in this way.

It is reasonable to assign to the elements diamond, silicon, germanium, and grey tin, with the diamond

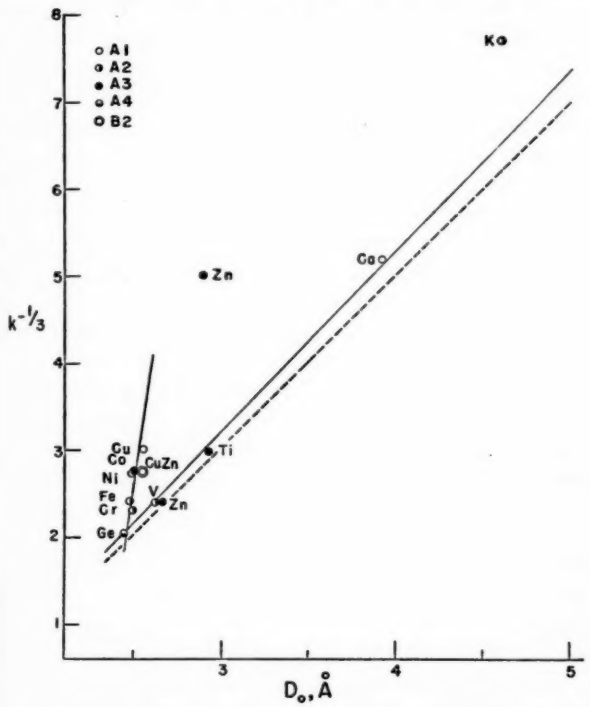

FIG. 2. Diagram showing the reciprocal of the cube root of the force constant for bonds of elements of the first long period, as a function of interatomic distance. The dashed line is Badger's spectroscopic curve.

arrangement, an electronic structure in which each atom is attached to each of its four ligates by an sp^3 single bond, and to expect this electronic structure to remain unchanged in nature on compression. The compressibilities of these elements should, then, correspond to their respective normal Badger-rule lines. Good agreement with the spectroscopic lines is indeed shown by germanium and grey tin, but the points for carbon and silicon are below their lines. Possibly the spectroscopic Badger lines for the first and second periods lie above the "normal" lines (corresponding to constant electronic structure) because of a change of electronic structure with changing interatomic distance for the diatomic molecules that provide the spectro-

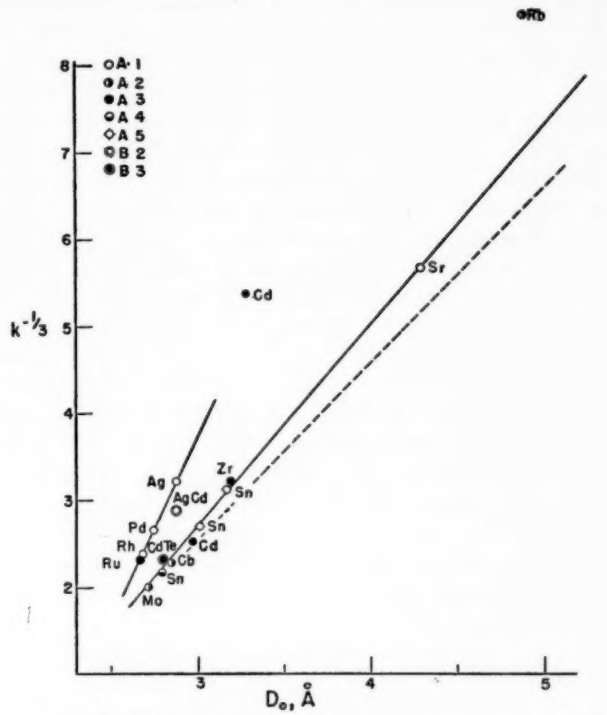

FIG. 3. Diagram showing the reciprocal of the cube root of the force constant for bonds of elements of the second long period, as a function of interatomic distance. The dashed line is Badger's spectroscopic curve.

scopic data. For most of these molecules the bond orbitals are not those corresponding to sp^3 hybridization, but are hybrids of a different nature (with more s character if the atoms have no σ unshared electron pairs, as in Li_2, and more p character if they have these unshared pairs, as in N_2), and on decrease of the interatomic distance the hybridization would be expected to change (toward sp^3 bond orbitals), leading to smaller force constants than normal.

The normal Badger lines for the two short periods may from this argument be expected to lie just below the spectroscopic lines of Fig. 1, being parallel to them and passing through the points for diamond and silicon. The high values of the other elements are presumably due to a similar change in hybridization of the bond orbitals. For one, two, and three valence electrons, the bond orbitals would have an amount of p character lying between the values minimizing the atomic energy, 0, 50 percent, and $66\frac{2}{3}$ percent, respectively (resulting from utilization of all of the s orbital), and the value giving the strongest bonds, presumably 75 percent, for sp^3 bond orbitals. At zero pressure the amount of p character seems to lie about midway between these extremes: the values 41 percent for lithium and 27 percent for sodium have been estimated by a simple calculation.[6] On compression the amount of p character would increase, and this change in bond type would lead to larger compressibilities than normal. The effect

[6] L. Pauling, Proc. Roy. Soc. (London) **196A**, 343 (1949).

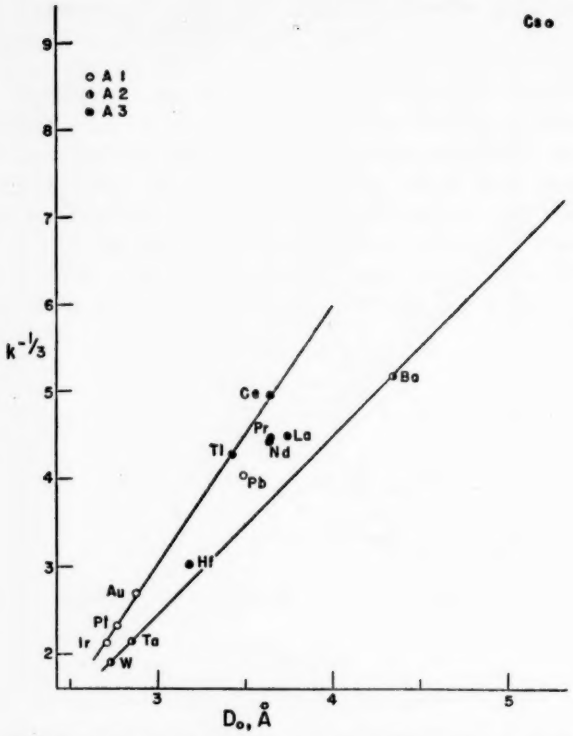

FIG. 4. Diagram showing the reciprocal of the cube root of the force constant for bonds of elements of the very long period, as a function of interatomic distance.

would be small for boron and aluminum, which have only the range of p character from $66\frac{2}{3}$ percent to 75 percent available, larger for beryllium and magnesium, and still larger for lithium and sodium; hence in a qualitative way it corresponds to a rotation of the lines around the points for diamond and silicon. Possibly a quantitative discussion of the effect would provide an explanation of the fact that the experimental points continue to approximate closely to straight lines.

For the first long period (Fig. 2) the points for calcium, titanium, vanadium, and germanium determine a straight line that lies only slightly above Badger's spectroscopic line, and the point for potassium lies considerably above the line. Similarly a straight line representing only a small rotation from Badger's line is determined for the second long period (Fig. 3) by the points for strontium, zirconium, columbium, molybdenum, and tin, the point for rubidium lying high. These facts suggest that the hybridization effect is less for these long periods than for the short periods, and that it is large only for the alkali metals.

Aside from germanium and tin, which have been discussed above, the elements fitting these lines (calcium to vanadium and strontium to molybdenum) are those that use all of their electrons outside of their noble-gas shell as metallic bonding electrons, and thus have fixed electronic structures, except for change in hybridization. (The point for chromium, which should be included in this group, lies slightly above the line.) The other metals of these long periods have more complex electronic structures, involving both metallic bonding electrons and atomic electrons outside of a noble-gas shell; and for each of these metals the electronic state is described in terms of resonance between two or more structures.[6] For iron, cobalt, and nickel the structures differ in the number of unpaired atomic electrons, and for copper and zinc (and also iron) in the number of bonding electrons. We attribute the large values of the compressibility of these elements to a change in the contributions of these resonating structures on compression; without, however, having a sufficient understanding of the phenomenon to account for the fact that the points seem to determine straight lines with slopes much greater than normal.

The points for the very long period (Fig. 4) can be enclosed by two straight lines. The lower one, which presumably lies only slightly above the normal Badger line (a spectroscopic line has not been determined), passes through the points for barium, tantalum, and wolfram. The point for cesium lies much above it, and those for lanthanum and hafnium, which would be expected to lie on it, are slightly high. The upper line is nicely determined by iridium, platinum, gold, thallium, and cerium, all of which have been assigned resonating structures (between the valences 2 and 3 for thallium, and 3 and 4 for cerium). It is interesting that the deviation for praseodymium and neodymium is just half as great as for cerium, and that the contribution of the quadrivalent structures for these elements (valence 3.1) has also been estimated[7] from their magnetic properties to be just half that for cerium (valence 3.2).

The evidence from the values of the interatomic distance and the magnetic susceptibility that ordinary metallic cerium has valence 3.2, together with the stability of quadrivalent cerium in many compounds, led us to predict that a very dense form of the metal, representing the metallic valence 4, could be made. At our suggestion Professor J. H. Sturdivant and Dr. Adam Schuch began the search for a method of preparing this form of cerium, which was finally successful.[8] The fact that the compressibility of cerium increases with increasing pressure, reaching double its initial value at 2830 kg/cm^2, whereas the compressibility of most metals decreases with increasing pressure, indicates that the valence of cerium increases rapidly under compression. Transition to the quadrivalent state has been found to have taken place at 15,000 kg/cm^2.[9]

The compressibility of lead indicates a small resonance effect for this metal, and thus supports the suggestion[6] that the structure of the metal is almost entirely determined by the bivalent state of the atom.

Zinc and cadmium crystallize in a deformed $A3$ arrangement, with axial ratio such that each atom has

[7] L. Pauling, J. Am. Chem. Soc. **69**, 542 (1947).
[8] A. Schuch and J. H. Sturdivant, J. Chem. Phys. **18**, 145 (1950).
[9] A. W. Lawson and T.-Y. Tang, Phys. Rev. **76**, 301 (1949).

six ligates at a small distance and six at a larger distance. For each element the small distance corresponds to half-bonds, and the larger distance to weaker bonds, with bond number about $\frac{1}{6}$. It has been suggested[6] that the deformation from the normal axial ratio 1.633 for the $A3$ arrangement, which would surround each atom with twelve equidistant ligates, is the result of the special stability of six half-bonds, corresponding to resonance of three bonds for each atom among six positions, and that the remaining valences of the atom are divided among the other six positions. The normal valence of zinc and cadmium is $4\frac{1}{2}$, corresponding to resonance in the ratio 3:1 between the quadrivalent state (with a metallic orbital) and the sexivalent state. The longer bond distances suggest, however, a smaller valence, about 4, at zero pressure. The observed compressibilities provide further information about the structure of these elements. For each of them the force constant for the shorter bonds is normal, whereas that for the longer bonds indicates that a change in bond type occurs on compression (Figs. 2 and 3). We may hence conclude that even when strained the shorter bonds remain half-bonds, with no change in the basal-plane electronic structure, but that the longer bonds undergo an increase in bond number when the crystal is compressed along the c axis, with increase in the valence of the metal.

White tin has a tetragonal structure somewhat resembling the hexagonal structures of zinc and cadmium; each tin atom forms four strong bonds, lying nearly in the basal plane, and two weaker ones, parallel to the c axis. The distances indicate bond numbers $\frac{1}{2}$ and $\frac{1}{4}$, respectively, corresponding to the normal metallic valence $2\frac{1}{2}$ (3:1 resonance between bivalent and quadrivalent tin). The behavior on compression is, however, different from that of zinc and cadmium; the point for the longer bonds of tin in Fig. 3, like that for the shorter bonds, lies on the lower curve, indicating that no change in bond type occurs on deformation of the crystal. We attribute the difference in behavior of tin from that of zinc and cadmium to the fact that tin has its normal metallic valence at normal pressure, and so does not tend to undergo a change in valence under compression.

Indium seems to represent a transition between cadmium and white tin. Indium has the $A6$ structure, a tetragonal variant from cubic closest packing. Only the volume compressibility has been determined. Each atom has four ligates at 3.242A and eight at 3.370A. If the $A1$ formula is used, with 3.327A as the average distance, k is calculated from the compressibility to be $1.38 \cdot 10^{-2}$, and $k^{-\frac{1}{4}}$ to be 4.17. This value is intermediate between those, 3.46 and 5.08, corresponding to the lower and upper lines of Fig. 3.

Force constants were also calculated for a number of compounds of simple structure (including alloys) involving one kind of nearest-neighbor bonds only. Table I contains these data for compounds with bonds of at least 50 percent covalent character as evidenced by the electronegativities of the constituents.[10] No general fit was obtained with Eq. (9), however, and unfortunately not enough data are available to show any general trend. Moreover since a large fraction of these compressibilities were measured with slugs of compressed powder, the reliability of part of the data is questionable. For example, the compressibility of a sample of powdered magnesium oxide was found[11] to be almost twice as great as that of the single crystal. The initial compression of finely powdered lead[12] is about 50 percent higher than that of the solid metal even after exposure to a pressure of 25,000 kg/cm^2, and only at higher pressures is the compression of the sample sensibly the same as that of the cast metal. The compressibilities of the alloys in Table I were determined from cast samples and should therefore be reliable. Bridgman made the observation that alloys showed much more irregularity and more hysteresis under compression that did the elements. Only for three alloys of simple structure with components from the same row of the periodic system (CuZn, AgCd, and CdTe) are the compressibilities available. The corresponding force constants are plotted in the appropriate figures. It is seen that Eq. (9) holds reasonably well for them.

With increasing pressure the compressibilities generally decrease, the force constants increasing with decreasing interatomic distance, as is shown by the negative values of the constants k' collected in Table I. The exception of cerium is attributed to increase in metallic valence on compression, as discussed above. The values of k' seem not to depend in any simple manner on position in the periodic table.

The work reported in this paper was carried out with the aid of a grant from the Carbide and Carbon Chemicals Corporation. We wish to thank Professor P. W. Bridgman for communicating his unpublished data to us in 1947.

[10] L. Pauling, *The Nature of the Chemical Bond* (Cornell University Press, Ithaca, 1940), second edition, Chapter 2.
[11] P. W. Bridgman, Proc. Am. Acad. **67**, 345 (1932).
[12] P. W. Bridgman, Proc. Am. Acad. **76**, 9 (1945).

Letters to the Editor

THIS section will accept reports of new work, provided these are terse and contain few figures, and especially few half-tone cuts. The Editorial Board will not hold itself responsible for opinions expressed by the correspondents. Contributions to this section should not exceed 600 words in length and must reach the office of the Managing Editor not later than the 15th of the month preceding that of the issue in which the letter is to appear. No proof will be sent to the authors. The usual publication charge ($8.00 per page) will not be made and no reprints will be furnished free.

Energy Difference of the Rotational Isomers of Liquid 1,2-Dibromoethane

YONEZO MORINO, SAN-ICHIRO MIZUSHIMA, KENJI KURATANI, AND MIKIO KATAYAMA
Chemical Laboratory, Faculty of Science, Tokyo University, Tokyo, Japan
February 28, 1950

RECENTLY Rank, Kagarise, and Axford[1] measured the energy difference ΔE between the rotational isomers in the liquid state by means of the Raman effect, and found that ΔE is 740 cal./mole for liquid 1,2-dibromoethane. We also made careful determination of ΔE of dibromoethane in the liquid state by the infra-red absorption, measuring the temperature dependence of the intensity ratio of the two absorption frequencies, one at 1192 cm^{-1} assigned to the *trans*-form and the other at 1236 cm^{-1} assigned to the gauche form. The experimental method is the same as that described in our previous paper[2] for ΔE in the gaseous state. The ratios of the optical densities $\log(I_0/I)_t/\log(I_0/I)_g$ observed at the temperatures 25°, 80°, and 160°C were, respectively, 1.260, 1.095, and 0.922. From these results we obtain 650±80 cal./mole as the value of ΔE in the liquid state,* which is in good agreement with that obtained by Rank, Kagarise, and Axford.

We have also made the intensity measurement by photographic photometry for the Raman lines at 660 cm^{-1} (*trans*-form) and at 551 cm^{-1} (gauche form) at the temperatures 34°, 88°, and 100°C, and obtained practically the same value of ΔE (760 cal./mole) as reported by Rank *et al*. The large value 2.42 kcal./mole given by Aronov, Tatevskii, and Frost,[3] or the value of Gerding and Meerman[4] cannot, therefore, be approved by our measurement as well as by that of Rank *et al*.

The measurement of dielectric constants in the liquid state gave a value 1.0 kcal./mole[5] as the energy difference between the two rotational isomers, so far as the Onsager theory for the dielectric polarization can be applied to the liquid consisting of the *trans*- and the gauche isomers. It is very interesting that this value is not much different from those obtained by the more reliable methods stated above.

The values of ΔE hitherto obtained for 1,2-dihalogenoethanes are summarized in Table I, from which we can definitely conclude that ΔE of 1,2-dibromoethane decreases on liquefaction just as in the case of 1,2-dichloroethane, although the decrement in the former is smaller than that in the latter.

TABLE I. The energy difference in kcal./mole between the rotational isomers of 1,2-dichloroethane and 1,2-dibromoethane.

	ΔE_g Gaseous state	ΔE_l Liquid state	$\Delta E_g - \Delta E_l$	E_{reac}
$C_2H_4Cl_2$	1.2[a]	0	1.2	1.0
$C_2H_4Br_2$	1.45 (infra-red)[a]	0.65 (infra-red)		
	1.4 (dipole moment)[a]	0.75 (Raman effect)	0.6	0.5
		1.0 (dielectric constant)		

[a] See reference 7.

The decrease in energy difference in the liquid state can be explained by the interaction between the molecular dipole and its induced moment in the surrounding medium.[6] According to Onsager, when a dipole of moment μ is transferred from the vacuum ($\epsilon=1$) into the medium of dielectric constant ϵ, it loses the potential energy by an amount of

$$E_{reac}=\frac{2(\epsilon-1)}{2\epsilon+1}\cdot\frac{\mu^2}{a^3}, \tag{1}$$

where a is the molecular volume. Therefore, the *trans*-isomer having no dipole is subjected to no energy change, while the gauche isomer of moment μ_g loses the energy by an amount of Eq. (1). In consequence the gauche form becomes more stable in the liquid state than in the gaseous state. Putting the following values of dipole moment and dielectric constant into the right-hand side of Eq. (1): $\mu_g=2.55D$, $\epsilon=9.87$ for dichloroethane and $\mu_g=2.2D$, and $\epsilon=4.8$ for dibromoethane, we obtain $E_{reac}=1.0$ kcal./mole for dichloroethane, and $E_{reac}=0.5$ kcal./mole for dibromoethane. These values are in good agreement with those of $\Delta E_g-\Delta E_l$ shown in Table I. We can thus explain by the induction effect of the surrounding medium why the value of ΔE becomes smaller in the liquid state than in the gaseous state and why this change of ΔE is more prominent in 1,2-dichloroethane than in 1,2-dibromoethane.

[1] Rank, Kagarise, and Axford, J. Chem. Phys. **17**, 1354 (1949).
[2] Simanouti, Tsuruta, and Mizushima, Sci. Pap. Inst. Phys. Chem. Research (Tokyo) **25**, 51 (1946).
* In calculating the energy difference between the rotational isomers of 1,2-dibromoethane we assumed the ratio of the partition functions of the two isomers to be 1, since the exact value of the torsional frequency of the *trans*-isomer is unknown.
[3] Aronov, Tatevskii, and Frost, Doklady Akad. Nauk. S. S. S. R. **60**, 387 (1948).
[4] H. Gerding and P. G. Meerman, Rec. Trav. Chim. Pays-Bas **61**, 523 (1942).
[5] Watanabe, Miyagawa, and Morino, Reports of the Radiation Chemistry Research Institute (Tokyo Univ.) **3**, 25 (1948).
[6] Watanabe, Mizushima, and Masiko, Sci. Pap. Inst. Phys. Chem. Research (Tokyo) **40**, 425 (1943); S. Mizushima and H. Okazaki, J. Am. Chem. Soc. **71**, 3411 (1949).
[7] Mizushima, Morino, Watanabe, Simanouti, and Yamaguchi, J. Chem. Phys. **17**, 591 (1949).

The Mutual Repulsive Potential between Argon Atoms

MAKOTO KUNIMUNE
Institute of Applied Science, Faculty of Engineering, Kyûsyû University, Fukuoka, Japan
February 24, 1950

THEORETICAL derivation of the thermodynamical quantities from the intermolecular potentials have been made largely for the case of rare gases, because the molecules of rare gases are monatomic and chemically saturated, and the intermolecular potential of a pair of these molecules depends only on the intermolecular distance. Out of these rare gases, argon is suitable to carry out various experiments at the moderately low temperature, and there are a number of experimental data on the properties of argon available for the comparison with theory.

Many authors[1] determined the interatomic potential of argon from the temperature dependence of the second virial coefficient. But it is unnecessary, in principle, to use such experimental data for the purpose of determining the interatomic potential of argon, since it can be determined by quantum mechanical calculation. And the author calculated the mutual repulsive interaction energy of two argon atoms according to Bleick and Mayer's method, using one-electron atomic wave functions.

According to Bleick and Mayer's[2] method the mutual repulsive energy ΔE of two argon atoms can be expressed by

$$\Delta E=W_{11}-[2/(1-S)]\sum_{ij}(s_{ji}U_{ij}'+R_{ij}^{-1}), \tag{1}$$

$$W_{11}=e^2\int U_a\rho_b d\tau=e^2\int U_b\rho_a d\tau, \tag{2}$$

TABLE I. Numerical values of mutual repulsive potential between argon atoms.

R (10^{-8} cm)	S	$\frac{-2}{1-S}\sum s_{ji}U_{ij}$	$\frac{2}{1-S}\sum\frac{1}{R_{ij}}$ (10^{-14} erg)	$-W_{11}$	ΔE
3.70	0.00232	7.63	0.447	0.98	6.20
2.64	0.0656	400	28.2	44.0	328
2.12	0.300	2750	271	410	2090

$$U_{ij}'=-e^2\int(U_{ai}'+U_{bj}')\psi_{ai}^*\psi_{bj}d\tau, \tag{3}$$

$$R_{ij}^{-1}=e^2\int\int\psi_{ai}^*\psi_{bj}(1)r_{12}^{-1}\psi_{bj}^*\psi_{ai}(2)d\tau_1d\tau_2 \tag{4}$$

$$s_{ij}=\int\psi_{ai}^*\psi_{bj}d\tau,\quad S=2\sum_{ij}|s_{ij}|^2, \tag{5}$$

where i and j are all electronic states of argon atoms which are usually denoted as $1s$, $2s$, $3s$, $2p_+$, $2p_0$, $2p_-$, $3p_+$, $3p_0$ and $3p_-$. W_{11} is the Coulomb term, U_{ij}' the mixed exchange term, and R_{ij}^{-1} the pure exchange term. ψ_{ai} and ψ_{bj} are the one-electron wave functions of argon atoms at the state i of atom a and at the state j of atom b respectively. ρ_a is the charge density (in units of e) in the neutral argon atom a, U_a is the potential due to the atom a, and U_{ai}' is the potential due to a when ith electron is missing. r_{12} is the distance between electron 1 and 2.

The solutions of Fock's equations for argon atoms have been determined numerically by Hartree and Hartree.[3] Using these functions, we calculate the integrals (2)–(4) by means of numerical integration. And the results obtained are tabulated in Table I. In the calculation of s_{ij} it is found that this approximation used here is not adequate at the short nuclear separation such as $a=2$ and 3 bohr units.

The various analytical forms of interaction potential curves are often used. Among them the one given by Lennard-Jones and Buckingham has the form

$$\Delta E(R)=-AR^{-6}+BR^{-n}, \tag{6}$$

and the other given by Buckingham has the form

$$\Delta E(R)=-aR^{-6}+b\exp(-R/\rho), \tag{7}$$

where A, B, n, a, b and ρ are all constants. The first term in Eq. (6) or (7) is the term of attraction and the second is the term of repulsion. And Buckingham determined the values of all constants from experimental data. In Table II, they are compared with the values determined from Table I, the least squares method being used to determine the constants. In Table III the values obtained from the analytical forms Eqs. (6) and (7) are compared with the calculated values in Table I. In Table III, the values obtained from the analytical forms Eq. (7) fits best and Eq. (6) with constants $B=6.60\times10^{-8}$ ergA^n and $n=10.5$ fits next best. The agreement between ρ from our calculation and the one determined from experimental values by Buckingham is surprisingly good. Details will appear in the *Progress of Theoretical Physics*.

TABLE II. The values of constants of analytical forms of potential curves.

	$\Delta E=-AR^{-6}+BR^n$			$\Delta E=-aR^{-6}+b\exp(-R/\rho)$			
	n	A (10^{-10} erg A^6)	B (10^{-10} erg A^n)		a (10^{-10} erg A^6)	ρ (Å)	b (10^{-10} erg)
(i)	9	1.70	76.8	(vii)	1.02	0.273	169
(ii)	10	1.37	205	(viii)		0.272	515
(iii)	12	1.03	1620				
(iv)	11.4	1.12	869				
(v)	10.5		660				
(vi)	12		2970				

i, ii, iii, vii: by Buckingham.
iv: by Rushbrooke.
v, vi, viii: from the values obtained in this paper.
v: varying both n and B; vi: fixing $n=12$ and varying B.

TABLE III. Comparison of numerical values of potential curves.

R (10^{-8} cm)	ΔE (10^{-14} erg) from (v)[a]	from (vi)[b]	from (viii)[c]	from Table I
3.70	7.08	4.47	6.70	6.20
2.64	242	253	298	328
2.12	2520	3690	2060	2090

[a] See Table II, v.
[b] See Table II, vi.
[c] See Table II, viii.

[1] R. A. Buckingham, Proc. Roy. Soc. **A168**, 264 (1938); O. K. Rice, J. Am. Chem. Soc. **63**, 3 (1941); G. S. Rushbrooke, Proc. Roy. Soc. Edinburgh **60**. 182 (1940).
[2] W. E. Bleick and J. E. Mayer, J. Chem. Phys. **2**, 252 (1934).
[3] D. R. Hartree and W. Hartree, Proc. Roy. Soc. **166**, 450 (1938).

A Note on the Integral Equations between Molecular Distribution Functions

SYÛ ONO
Institute of Applied Science, Faculty of Engineering, Kyûshû University, Fukuoka, Japan
February 24, 1950

MAYER[1] has derived a set of integral equations which relate variations in the potentials of average force between molecules of a system at two different fugacities. We attempt here to point out the relationship between Mayer's general variational method and the Born-Green equation[2] for pair distribution function.

Let us consider a system consisting of pure substance. Then we may define distribution functions $F_n(z,\{n\})$, that depend on the temperature T and on the fugacity z and are the functions of the coordinates, $\{n\}$, necessary to specify the positions, orientations and internal coordinates of molecules. Now we introduce the functions $G_n(z,\{n\})$ defined by

$$G_n(z,\{n\})=\exp[pV/kT](\rho/z)F_n(z,\{n\}), \tag{1}$$

where p is the pressure, V is the volume, ρ is the number density of molecules, and k is Boltzmann's constant. And we will denote the values of $G_n(z,\{n\})$ at the two different fugacities, z_α and z_β, by G_n and G_n^*, respectively. Then we assume that G_n and accordingly G_n^* depend upon a parameter y, defining the variations

$$\Psi_n=\partial\ln G_n/\partial y, \tag{2}$$

$$\Psi_n^*=\partial\ln G_n^*/\partial y. \tag{2'}$$

Mayer has obtained the set of integral equations between these variations, namely

$$\psi_k=\psi_k^*+\sum_{m\geq1}(Z^m/m!)(\Sigma\{\kappa\}_k)\int\int_V\cdots\int K_{k,\kappa,m}\psi_{\kappa+m}^*d\{m\}, \tag{3}$$

in which ψ_ν and ψ_ν^* are given by

$$\psi_\nu=(\Sigma\{n\}_\nu)(-)^{\nu-n}\Psi_n, \tag{4}$$

$$\psi_\nu^*=(\Sigma\{n\}_\nu)(-)^{\nu-n}\Psi_n^*, \tag{4'}$$

and $K_{k+n,n,m}$ by

$$K_{k+n,n,m}=(\Sigma\{\kappa\}_k)(-)^{k-\kappa}G_{\kappa+n+m}/G_{\kappa+n}. \tag{5}$$

Here the summation symbol, $(\Sigma\{\nu\}_n)$, indicates summation of functions of such sub-sets, $\{\nu\}_n$, over all sub-sets, for all values of ν, $0\leqslant\nu\leqslant n$, including a single term for which $\nu=0$. If G_n^*'s refer to $\rho=0$, they are given by

$$G_n^*=\exp[-U_n/kT], \tag{6}$$

with U_n the potential energy. We will consider the case in which the potential energy has the form

$$U_n=\sum_{i=j+1}^{n}\sum_{j=1}^{n}u(i,j), \tag{7}$$

where $u(i,j)$ is the potential energy of the pair of molecules i and j. Then ψ_n^*'s are assumed to be zero unless $n=2$. If differentiation

is performed with respect to the coordinates of one of the molecules, (1), of the set n, Eq. (3) for the cases $k=1$ and $k=2$ is reduced to

$$\psi_1=-(\rho/kT)\int_V(\partial u(1,2)/\partial x_1)[F_2(z,(1)(2))/F_1(z,(1))]d(2) \quad (8)$$

and

$$\psi_2=-(\partial u(1,2)/\partial x_1)-(\rho/kT)\int_V(\partial u(1,3)/\partial x_1)\times[\{F_3(z,(1)(2)(3))/F_2(z,(1)(2))\}-\{F_2(z,(1)(3))/F_1(z,(1))\}]d(3). \quad (9)$$

Ψ_n's are average forces so that $\Psi_1=\psi_1=0$ for the gaseous or liquid state. Hence, we obtain, from (8) and (9),

$$\{\partial F_2(z,(1)(2))/\partial x_2\}+\{F_2(z,(1)(2))/kT\}(\partial u(1,2)/\partial x_2)+(\rho/kT)\int_V F_3(z,(1)(2)(3))(\partial u(1,3)/\partial x_3)d(3)=0. \quad (10)$$

This equation was first derived by Born and Green, and used by Rodriguez[3] to study an approximate equation of state. And the Kirkwood approximation used by Kirkwood and Boggs[4] and by Rodriguez corresponds to the assumption that $\psi_n=0$ for all values of n except $n=2$. Furthermore, we can prove that the integral equation used by Kirkwood[5] to determine pair distribution function in liquid [reference 5, Eq. (33)] is also a special case of (3). The above method will be easily extended to multicomponent systems and to the case where G_n^{*}'s refer to the state at non-zero fugacity.

[1] J. E. Mayer, J. Chem. Phys. **15**, 187 (1947).
[2] M. Born and H. S. Green, Proc. Roy. Soc. **A188**, 10 (1946).
[3] A. E. Rodriguez, Proc. Roy. Soc. **A196**, 73 (1949).
[4] J. G. Kirkwood and Elizabeth Monroe Boggs, J. Chem. Phys. **10**, 394 (1942).
[5] J. G. Kirkwood, J. Chem. Phys. **3**, 300 (1935).

Ferrous-Ferric Electron Transfer Reaction in Perchloric Acid Solution

HENRY A. KIERSTEAD*
Institute for Nuclear Studies, University of Chicago, Chicago, Illinois
March 16, 1950

THE electron transfer exchange reaction between ferrous and ferric ions in 3 molar perchloric acid solution has been investigated by Van Alten and Rice[1] and Linnenbom and Wahl,[2] both using the diffusion separation technique devised by the former authors. Van Alten and Rice obtained separation factors of about 2 in favor of ferric ion and observed a half-time 18.5±2.5 days for the exchange reaction. Linnenbom and Wahl, on the other hand, obtained separation factors of 1.2 to 1.6 in favor of ferrous ion and observed complete exchange within the experimental time of 1 to 2 hours. Some preliminary experiments by the present author, using the same separation technique, provide confirmation for the long half-life observed by Van Alten and Rice and for the observation of Linnenbom and Wahl that ferrous ion diffuses more rapidly than ferric ion. Data on these experiments are collected in Table I.

Fe^{59} activity, in the form of spectroscopically pure iron powder, was supplied by the Oak Ridge National Laboratory on allocation from the Isotopes Division, U. S. AEC. The iron powder was dissolved in 3.0M perchloric acid, oxidized with excess 3 percent hydrogen peroxide, boiled to destroy the peroxide, and diluted with sufficient water and concentrated perchloric acid ("Baker's Analyzed") to make a solution 0.15M in ferric perchlorate and 3.0M in perchloric acid. Aliquots of this stock solution were mixed with solutions of ferrous perchlorate prepared in the same manner from inactive iron powder, omitting the hydrogen peroxide oxidation. The mixed solution was stored in a glass-stoppered volumetric flask for various lengths of time. The ferrous and ferric ions were then partially separated by diffusion through a sintered glass disk. Separation factors were measured by analysis for ferrous and ferric ion both before and after the diffusion separation. Ferric ion was determined by measuring the absorption by the perchlorate solution of ultraviolet light at 2400A, using a Beckmann ultraviolet spectrophotometer. 3.0M perchloric acid was used in the blank cell. A correction was made for the small absorption due to ferrous ion. Total iron was determined by the same method, after oxidizing with 3 percent hydrogen peroxide and boiling to destroy excess peroxide. Ferrous ion was obtained by difference. Samples of the solution taken before and after separation were prepared for counting by deposition as metallic iron on copper electrodes by the method of Ross and Chapin.[3]

TABLE I.

c_2 moles·l^{-1}	c_3 moles·l^{-1}	S	t days	α, %	$t_{1/2}$ days
0.952×10^{-2}	1.011×10^{-2}	3.301	0.058	1.2±0.5	—
1.071×10^{-2}	1.050×10^{-2}	2.805	6.024	10.0±0.6	39±2
1.044×10^{-2}	1.059×10^{-2}	3.983	80.14	2.8±0.5	166±12

$S=c_2'c_3/c_2c_3'$, where c_2 and c_3 are the concentrations of ferrous and ferric ions, respectively, before separation, and c_2' and c_3' are the concentrations after separation. t is the time allowed for exchange; α is the percent of exchange; and $t_{1/2}$ is the half-life for exchange, calculated from t and α.

Calculation of the percent exchange was made by the same method as that used by Van Alten and Rice.[1]

Lack of agreement between Van Alten and Rice,[1] Linnenbom and Wahl,[2] and the present author, and our failure to observe the same half-life in different experiments, may be explained by catalysis by traces of impurities in the reagents. In this connection we should like to point out that the only materials we have used in preparation of our reagents are pure metallic iron, "Baker's Analyzed" perchloric acid, hydrogen peroxide, and distilled water.

Numerous attempts by the present author to separate ferrous and ferric ions by chemical methods have all resulted in complete exchange.

We gratefully acknowledge the assistance and interest of Professor W. F. Libby, Dr. G. Zimmerman, and Dr. T. J. Neubert.

* Present address: Metcalf Research Laboratory, Brown University, Providence, Rhode Island.
[1] Van Alten and Rice, J. Am. Chem. Soc. **70**, 883 (1948).
[2] Linnenbom and Wahl, J. Am. Chem. Soc. **71**, 2589 (1949).
[3] J. F. Ross and M. A. Chapin, Rev. Sci. Inst. **13**, 77 (1942).

Carrier-Free Radioisotopes from Cyclotron Targets. VII. Preparation and Isolation of V^{48} from Titanium*

HERMAN R. HAYMOND, ROY D. MAXWELL,† WARREN M. GARRISON, AND JOSEPH G. HAMILTON
Crocker Laboratory and Divisions of Medical Physics, Experimental Medicine, and Radiology; Radiation Laboratory; University of California, Berkeley, California
March 3, 1950

V^{48} can be prepared[1] by the reactions $Ti^{47}(d,n)V^{48}$ and $Ti^{48}(d,2n)V^{48}$. The present paper reports a chemical procedure used in isolating carrier-free V^{48} from a titanium target which had been bombarded with 19-Mev deuterons in the 60-inch cyclotron at Crocker Laboratory. The carrier-free V^{48} was separated from the target element and from milligram amounts of calcium and scandium which were added as holdback carriers for the radioisotopes[2] produced concurrently by the reactions: $Ti^{48}(d,\alpha p)Ca^{45}$, $Ti^{46}(d,2p)Sc^{46}$.

The Ti target (C.P. metal powder supported on a copper target plate with 0.25 mil Ta foil) was bombarded for 200 μa-hr. at a maximum beam intensity of 20 μa. After aging for 24 hours, the Ti powder (approximately 1 g) was dissolved in a minimum volume of 36N H_2SO_4 and the solution was evaporated to dryness. 5.0 g of Na_2CO_3 and 0.1 g of $NaNO_3$ were added and the mixture was fused at 500°C for 30 minutes. The sub-micro amount of V^{48},

presumably as vanadate, was extracted from the insoluble titanium oxide by repeated washings with cold water. To remove any Ca and Sc activities which may have been extracted with the V^{48}, the solution was acidified with HCl, 10 mg of Ca and Sc were added and precipitated from $1M$ Na_2CO_3. The supernatant containing the V^{48} was neutralized with $12N$ HCl and evaporated to dryness. The V activity was separated from most of the NaCl by extraction with approximately 5 ml of $12N$ HCl. The HCl solution containing the activity and milligram amounts of NaCl was evaporated to dryness and diluted with water to give an isotonic saline solution of carrier-free V^{48} which was used in biological tracer studies.

The V^{48} was identified by the assigned[3] 16-day half-life and by the 0.7-Mev positron and 1.33-Mev gamma-ray which have been reported.[1] Chemical separations with added Ca, Sc, Ti, and V carriers further identified the activity as V^{48}.

We are grateful to the staff of the 60-inch cyclotron for bombardments and to Professor G. T. Seaborg for his interest and helpful suggestions.

* This document is based on work performed under the auspices of the AEC.

† Lieutenant Colonel, U. S. Army, now stationed at Walter Reed Hospital, Washington, D. C.

[1] H. Walke, Phys. Rev. **52**, 777 (1937).
[2] G. T. Seaborg and I. Perlman, Rev. Mod. Phys. **20**, 585 (1948).
[3] W. C. Peacock and M. Deutsch, Phys. Rev. **69**, 306 (1946).

X-Ray Patterns of Soaps

A. J. Stosick
Department of Chemistry, University of Southern California, Los Angeles, California
February 27, 1950

THE x-ray diffraction patterns of solid soaps have been examined by many investigators using either single crystals or samples which have been described as powders. The single crystal patterns are not different in kind from those of other organic substances except for the fact that one of the unit cell axes is very long compared to the other two axes. Probably the most important difference is the appearance of a series of "long spacings" in the small angle region. These diffraction maxima can be called the (001) reflections if we label the long crystal axis a_3. The length of the long axis is related to the thickness of the micellar layer. This micellar layer consists of a central layer of metal ions, not necessarily in a single plane, and of two fatty acid ion layers with the acid ions extending outward on both sides from the metal ion layer. The hydrocarbon end groups form the outer surface of the micellar layer. The values obtained for the long spacing indicate that the chains are tipped rather than perpendicular to the median plane. Such micellar layers presumably form in solution, probably starting as ion pairs or triplets, and the solids consist of a stacking of such micellar layers. The forces leading to the coalescence of such layers are the weak van der Waals forces between hydrocarbon chain ends.

The more common type of diffraction diagram, referred to as a powder diagram, is notorious for its apparent variability. These patterns for a given sample sometimes change with time, they change if the sample is heated and then restored to its original temperature, and they depend on the method of preparing the soap. These diagrams show a series of (001) long spacings at small angles and a broad diffraction band, with no resolved *sharp* lines, in the region $2\theta \approx 20°$ (using copper x-rays). This broad band frequently shows broad sub-structure suggesting that it is the superposition of two or more broad peaks. Sometimes it is resolved into two or more broad peaks. Only very rarely are there additional broad peaks at larger scattering angles. Frequently there is a series of small narrow maxima extending out to $2\theta \approx 40°$.

It is possible to account for these diagrams in terms of a disordered structure in which the micellar layers are superimposed with stacking disorder, together with some physically reasonable assumptions concerning disorder within a micellar layer. The proposal that stacking disorder is present is certainly reasonable since the forces which would lead to an orderly arrangement are only the weak van der Waals forces of hydrocarbon chain ends. The central ion layers cannot exert strong interactions from one micellar layer to another.

The consequences of this proposal are that the (001) spectra are unaffected by the stacking disorder and are no different in sharpness or intensity from those given by a well-ordered layer sequence. An examination of published data and of unpublished data, very kindly provided by Professor R. D. Vold of this laboratory, shows that almost without exception all of the regular series of spacings past $2\theta \approx 20°$ can be identified as high orders of the (001) series. Previously these were called "side spacings."

On the other hand, when h and k are not both zero, then random stacking disorder causes the index 1 to become meaningless. The resulting (hkl) reflections become broad (hk) diffraction maxima of the two-dimensional lattice of the micellar layer. The present case differs from that discussed by Warren[1] for carbon black in that here the layers are many atoms thick. Elementary considerations concerning the Fourier transform from crystal space to reciprocal space shows that the (hk) maxima for thick distributions are narrower in scattering angle range than for thin layers. This is observed to be true for soaps as compared to carbon black, whose layers are presumed to be one atom thick.

Within a micellar layer the fatty acid ions must approximate a hexagonal array. This requires that there can be only three different (hk) pairs (and their negatives) which give diffraction maxima near $2\theta \approx 20°$. These are the (10), (01), and $(1\bar{1})$ maxima. The (11) maximum should occur at a value of $\sin\theta$ which is $\sqrt{3}$ times that of (10), and that for (20) should have a value of $\sin\theta$ twice that for (10). If the net is not exactly hexagonal the (10), (01), and $(1\bar{1})$ maxima occur at different but nearly equal angles, and the 20° peak may resolve.

If we assume that in a micellar layer the fatty acid ions are randomly oriented about their long axes, it can readily be shown that the only strong (hk) maxima should be (10), (01), and $(1\bar{1})$, i.e., those at $2\theta \approx 20°$.

These considerations permit a consistent and physically reasonable unification of the discordant observations. It is apparent that the great list of different diffraction patterns, which have been identified with different polymorphic forms, merely represent different conditions of ordering, and that probably only the single crystal specimens represent phases in the thermodynamic sense. A more complete report is in preparation.

[1] B. E. Warren, Phys. Rev. **59**, 693 (1941).

The Exchange of Water between Aqueous Chromic Ion and Solvent*

John P. Hunt† and Henry Taube
George Herbert Jones Laboratory, University of Chicago, Chicago, Illinois
March 10, 1950

A PROBLEM of interest in the chemistry of aqueous solutions is that of determining the formulas of the species which result upon the interaction of cations and water. With cations of one extreme type, including probably those of low charge and large radius, the complexes may be very labile, and the configuration even in the first sphere of coordination may be so indefinite, that it would be impossible to assign definite formulas to them. For other cations, of appropriate properties, it can be expected that a definite configuration with respect to water in the first sphere of coordination is maintained, and for these, in principle at least, meaningful formulas can be assigned to the complex consisting of the cation and directly bound water.

An indirect method which has been used to establish the coordination number of a cation for water in aqueous solution is to determine the maximum coordination number with respect to other ligands, the assumption being made that the coordination

TABLE I. Exchange of Cr_{aq}^{+++} with H_2O.

N expresses the mole fraction $\frac{H_2O^{18}}{H_2O^{18}+H_2O^{16}}$ *in the samples distilled from the solutions.* From these, values of N for zero and infinite time (N_0 exp. and N_∞ exp. respectively) are obtained by extrapolation. N_0^5, N_0^6, and N_0^7 are the calculated values of the mole fraction in the liquid for initial holdback by each Cr^{+++} of 5, 6, and 7 molecules of H_2O respectively. N_∞ calc. is the mole fraction calculated for random mixing in the liquid.

Experimental					
Time, hours		0.30	18.3	18.9	401.3
N		8.422	8.169	8.169	7.518
Calculated results					
N_0 exp.	N_0^5	N_0^6	N_0^7	N_∞ exp.	N_∞ calc.
8.427	8.307	8.474	8.653	7.517	7.582
$\frac{N_0 \text{ exp.}}{N_\infty \text{ exp.}}$	$\frac{N_0^6}{N_\infty \text{ calc.}}$		$\frac{N_0^7}{N_\infty \text{ calc.}}$	$\frac{N_0^6}{N_0 \text{ exp.}}$	$\frac{N_\infty \text{ calc.}}{N_\infty \text{ exp.}}$
1.1211	1.1177		1.1412	1.0056	1.0087

number will be the same for water.[1] Another indirect method is to carry out a variety of double decomposition reactions, analyzing the solid phases to learn whether a particular cation/water ratio recurs. This method involves the assumption that the configuration in the solid is retained in solution, and, unless the structure of the solid is known, an additional assumption about the disposition of the water molecules in the solid. A direct method of counting the positions occupied by water associated with a cation in water is based on studying the exchange of bound water with solvent water, using a tracer such as O^{18} for H_2O.[2] A condition for the success of this method is that the exchange be slow enough so as not to be completed by the time the first and succeeding samplings of the solvent are made. The fact that for some cations the rate of substitution of water by other ligands is measurably slow encouraged the hope that replacement of water by water would also prove slow enough in some cases to make the exchange method applicable. The present note reports some results which have been obtained with chromic ion,[3] a cation which does fulfill the condition of slow exchange of bound water for solvent water.

The experiments were conducted by mixing a known amount of solution of known composition containing $Cr(ClO_4)_3$ and $HClO_4$ dissolved in ordinary water with a known amount of water enriched in O^{18}. Aliquots were taken at intervals, a portion of the water removed by distillation, and the isotopic composition determined by equilibrating the distillate with CO_2, measuring the ratio O^{18}/O^{16} in CO_2 by means of a mass spectrometer. The results obtained using a solution 1.47 molal in $Cr(ClO_4)_3$ and 0.13 molal in $HClO_4$ at 25° are presented in Table I.

The data of Table I show that a slow exchange of water takes place in the system. In other experiments, we have found that there is no initial holdback (within a time of sampling even as short as 2 minutes) by H^+ or ClO_4^-; furthermore, that the exchange of H_2O with ClO_4^- or the glass containers is negligible under the conditions of these experiments. The exchange effects observed must therefore be attributed to Cr^{+++}. From the total change in N during the experiment, and the composition of the solution, the initial holdback per Cr^{+++} is calculated as 6.2 ± 0.2 (compare N_0 exp./N_∞ exp., N_0^6/N_∞ calc., N_0^7/N_∞ calc. in Table I). This value is based on the assumption that the mixing of H_2O^{16} and H_2O^{18} in the final solution is random. If allowance is made for the slight preference of the ions for H_2O^{18} over H_2O^{16} indicated by other results obtained in these studies, the holdback per Cr^{+++} is reduced by 0.1 to 0.2. The initial holdback per Cr^{+++} can also be obtained by comparing the values of N_0 exp. with the values of N_0 calculated from the composition for assumed values of the initial holdback. If the data are used in this way, allowance has to be made for the fractionation which takes place on the distillation of samples of water from the solution. N_0^6/N_0 exp. is 1.0056, which is very nearly the ratio of $N_{liq.}/N_{vap.}$ for a distillation under otherwise identical conditions using water. The second method leads to a value of 6.0 ± 0.2 as the initial holdback of H_2O for each chromic ion. If the initial holdback is interpreted as due to water held in the first sphere of coordination, the experiments show the coordination number of Cr^{+++} for H_2O in water to be 6. Other experiments under similar conditions not reported in detail support this value.

The half-life for the exchange of H_2O between $Cr(H_2O)_6^{+++}$ and water under the conditions of our experiments is *ca.* 40 hours. Further work on this exchange, and on the exchange of water with other hydrated cations, will be presented for publication later. A detailed account of experimental procedure, calculations, and further discussion is therefore deferred.

The authors wish to express their appreciation to Dr. Samuel Epstein for help in the analysis of samples, to Dr. Harold C. Urey for the use of his precise mass spectrometer, and to Dr. Lewis Friedman of the Brookhaven National Laboratories for making the mass-spectrometer analyses of preliminary samples.

* This work was supported in part by funds from the ONR under contract N6-ori-02026.

† AEC Predoctoral Fellow.

[1] N. Bjerrum (Zeits. f. anorg. allgem. Chemie **118**, 131 (1921)) has shown that the ions $Cr(CNS)_6^{---}$ can be formed in water solution. More recently, Hall and Eyring (Ph.D. Thesis "Isomers of chromic salts," 1948, University of Utah, Howard Tracy Hall) have used the reagent $(NH_4)_6Mo_7O_{24}\cdot4H_2O$ to count coordination positions unoccupied by other complex groups.

[2] H. W. Crandall, J. Chem. Phys. **17**, 602 (1949) using this method has shown that UO_2^{++} exists as a distinct species in water.

[3] Concurrently with, and independently of the work reported here, experiments on the Cr_{aq}^{+++}-H_2O exchange sponsored by F. A. Long have been in progress in the Department of Chemistry, Cornell University.

Raman Spectrum of Ethylene

P. TORKINGTON
British Rayon Research Association, Research Laboratories, Urmston, Lancashire, England

February 27, 1950

RECENTLY, a new assignment has been prepared for ethylene;[1,2] the following comments may be of interest.

(a) The Raman line at 3075 cm^{-1} is attributed to be a breakdown of selection rules in the liquid state, causing the appearance of the B_{2u} fundamental. The infra-red gas frequency of the latter is 3105 cm^{-1}. No liquid-vapor shift as large as 30 cm^{-1} has been reported previously, even in polar molecules (excepting hydrogen bonding*).

(b) The force constants for the two alternative assignments for the B_{1g} and B_{2u} bending modes, using unnormalized coordinates and factoring out the stretching modes, are as follows:

	(1)		(2)	
	B_{1g}	B_{2u}	B_{1g}	B_{2u}
δ	1050	995	1236	810.3 cm^{-1}
d	0.0993	0.1417	0.1376	0.0940×10^5 dynes/cm.

In (2), bending is more difficult in the B_{1g} than in the B_{2u} mode; no satisfactory physical explanation can be given for this, while repulsions between the non-bonded hydrogen atoms would account for the reverse order in (1). There is some evidence for an exaggerated repulsion of this type in tetra-chloro-ethylene.[3]

(c) The 995 cm^{-1} band seems too strong to be a Coriolis-perturbed fundamental of a normally inactive species; this is probably not true of the band centered at ~810 cm^{-1}.

It is also of interest that in both the combinations $B_{1g}(1)B_{2u}(2)$, $B_{1g}(2)B_{2u}(1)$ the force constants are practically the same in both modes; this would be so if the H···H forces were negligible (though the H···C forces could still be important). The first combination leaves 995 cm^{-1} to be explained, the second, 810 cm^{-1}; in view of (c) above, the first seems unlikely.

Finally, the Raman line at 1236 cm^{-1} can be accounted for by several triple combinations:

$$\begin{cases} 3019 - 949 - 825 = 1245(B_{1g}) \\ 1623 + 943 - 1342 = 1224(B_{2g}) \\ 3105 - 1050 - 825 = 1230(B_{3g}) \end{cases}$$

(using Herzberg's assignment). Since no separating Fermi reso-

nance occurs between these levels, it seems possible there might be a weak line in the region of 1230 cm^{-1}. If 1236 cm^{-1} is accepted as the B_{1g} frequency, then the most likely one for B_{2u} is still 995 cm^{-1}, leaving 810 cm^{-1} as the Coriolis-perturbed twisting mode again.

[1] Rank, Shull, and Axford, J. Chem. Phys. **18**, 116 (1950).
[2] R. L. Arnett and B. L. Crawford, Jr., J. Chem. Phys. **18**, 118 (1950).
[3] The existence of weak temporary induced dipoles has recently been suggested [D. H. Whiffen, Trans. Faraday Soc. **46**, 124 (1950)] as the explanation of the observed dielectric losses in the liquid microwave spectra of molecules having no permanent moment. Such temporary molecular asymmetry, for which there was previously no very definite evidence, would be the cause of any breakdown of selection rules in the liquid state.
The liquid-vapor shift in methyl mercaptan for νSH has recently been reported [H. W. Thompson and C. H. Miller, Trans. Faraday Soc. **46**, 22 (1950); cf. H. W. Thompson and N. P. Skerrett, Trans. Faraday Soc. **38**, 812 (1940)] as 2607 to 2572 cm^{-1}; there may well be weak hydrogen-bonding here.
[4] P. Torkington, Proc. Phys. Soc. (to be published).

Comment on "Thermodynamic Properties of the Surface of Magnesium Oxide"

G. L. Kington and J. A. Morrison
Division of Chemistry, National Research Laboratories, Ottawa, Canada
March 10, 1950

Recently Jura[1] has pointed out the possibility of the experimental determination of the thermodynamic properties of solid surfaces. While the method indicated is undoubtedly correct, the results depicted in Fig. 1 of the paper are thermodynamically inconsistent.

The relationship between γ and h is the well-known one

$$h=\gamma-T(\partial\gamma/\partial T)_\Sigma$$

from which it follows that if $(\partial\gamma/\partial T)_\Sigma$ is positive then γ must at all temperatures be greater than h, not less than h as indicated in Jura's Fig. 1.

However, there is evidence to suggest that $(\partial\gamma/\partial T)_\Sigma$ may indeed be negative for the particular solid system considered. Thermodynamics requires that

$$(\partial\gamma/\partial T)_\Sigma=-(\partial S/\partial\Sigma)_T,$$

where S is the total entropy of a body with a surface. The data concerning the difference in thermal properties of fine and coarse particles of magnesium oxide, considered by Giauque[2] require that $(\partial S/\partial\Sigma)_T$ be positive, from which it follows that $(\partial\gamma/\partial T)_\Sigma$ must be negative. It is, therefore, suggested that the positive value of $(\partial\gamma/\partial T)_\Sigma$ in Jura's Fig. 1 is incorrect.

Further, it should be noted that theoretical treatments exist which also lead to this conclusion. Several years ago Brager and Schuchowitzky[3] derived an explicit expression for the heat capacity of a solid taking into account the influence of the surface. They attempted to use this to evaluate the extent of surface of a solid. Huang and Wyllie[4] have evaluated the free surface energy of some metals, and have used in part the Brager and Schuchowitzky development.

[1] G. Jura, J. Chem. Phys. **17**, 1335 (1949).
[2] W. F. Giauque, J. Am. Chem. Soc. **71**, 3192 (1949).
[3] A. Brager and A. Schuchowitzky, Acta Physicochimica (URSS) **21**, 1001 (1946). A development along similar lines has been given by Montroll, J. Chem. Phys. **18**, 183 (1950).
[4] K. Huang and G. Wyllie, Proc. Phys. Soc. **A62**, 180 (1949).

The Hydrogen Exchange of Alkali Amides and Hydroxide with Deuterium Gas

Y. Claeys, J. Dayton, and W. K. Wilmarth
Department of Chemistry, University of Southern California, Los Angeles, California
March 13, 1950

Recently[1] two of us reported the catalytic conversion of parahydrogen by liquid ammonia solutions of the alkali metals; the detailed kinetics of this process will be reported in the near future. Since alkali metal solutions may contain amide ion impurity, it was necessary to show that the observed conversion was not due to amide impurities. This became especially important when it was discovered that ammonia solutions of potassium amide, even at −50°C, effect the conversion at rates comparable to those of the metal solutions. However, the amide solutions not only effect the ortho-parahydrogen conversion but also exchange with deuterium gas while the metal solutions show no such exchange, indicating the absence of amide. It would appear that the amide conversion, unlike the alkali metal process, proceeds through a chemical mechanism. In view of unpublished data, this difference is to be expected since the alkali-metal conversion appears to occur through a paramagnetic catalysis.

That amide should exchange at all with deuterium at these temperatures is somewhat unexpected in view of the fact that the thermal exchange with ammonia[2] cannot be conveniently studied much below 500°C and the exchange with hydroxide is difficult to measure below 90°.[3,4] Consequently, the exchange seemed of sufficient importance to justify a brief report although the experiments are being continued to include a general study of the exchange of deuterium gas with strong bases.

The rapidity with which this exchange proceeds is indicated by data from a typical experiment. A 0.001M solution of potassium amide has a half-life of less than one minute for the exchange in solution. The molar rate constant appears to increase with dilution, suggesting that the amide ion is the catalytic species. Most of the early measurements were studied using parahydrogen rather than deuterium because it simplified the analysis of the gas mixtures by the Pirani gauge technique.[5] We are still uncertain as to whether the hydrogen deuteride appears as an intermediate, but analyses using the mass spectrograph are under way to clarify this point.

The homogeneous nature of the hydroxide catalyzed exchange between deuterium oxide and hydrogen was first reported by Bonhoeffer.[3] Abe[4] later stated that the hydroxide solutions, if dialized or heated at 100°C for some time, lost their catalytic activity.

Our studies on the system deuterium, water and potassium hydroxide indicate that the reaction is not affected by either light or increase in glass surface, and, contrary to Abe's observations, that the catalytic activity cannot be destroyed. Abe attributed the activity to iron impurities, but this is unlikely since in our experiments, C.P. sodium hydroxide and potassium hydroxide, either C.P. or prepared from distilled metallic potassium, do not differ in activity.

The reaction is, within the limit of our experimental error, first order with respect to both deuterium gas and hydroxide ion. The process has a high temperature coefficient and the reported lack of reproducibility appears to arise from inadequate temperature control.

[1] Y. Claeys, C. Baes and W. Wilmarth, J. Chem. Phys. **16**, 425–6 (1948).
[2] A. Farkas, Trans. Faraday Soc. **32**, 416–27 (1936).
[3] K. Wirtz and K. F. Bonhoeffer, J. Physik. Chem. **177A**, 1–6 (1936).
[4] S. Abe, Sci. Papers, Inst. Phys. Chem. Research (Tokyo) **38**, 287–97 (1941).
[5] J. L. Bolland and H. W. Melville, Trans. Faraday Soc. **33**, 1316 (1937).

The Exchange of Water between Co^{+++}_{aq} and the Solvent and between Co^{++}_{aq} and the Solvent*

Harold L. Friedman,† Henry Taube, and John P. Hunt‡
George Herbert Jones Laboratory, University of Chicago, Chicago, Illinois
March 10, 1950

In a continuation of the experiments on the exchange of water between hydrated cations and the solvent, a study of the exchange with Co^{+++} was undertaken. This ion was chosen for early study since the rates of replacement of one ligand by another are slow in almost all of its complex ion reactions. It seemed probable, therefore, that the exchange of water coordinated to cobaltic ion with the solvent water would be slow enough to

permit the determination of the coordination number of the ion for water.

The exchange experiments with cobaltic ion are made difficult because this ion, particularly at high concentrations, oxidizes water fairly rapidly. Solutions of cobaltic perchlorate in perchloric acid were obtained by electrolytic oxidation of cobaltous perchlorate, and always contained cobaltous ion at concentrations about equal to that of cobaltic ion. The exchange experiments were conducted as described for Cr^{+++} with the difference that the various samples of water were obtained by successive distillations from a single sample of the solution in each experiment. Before the last water sample was taken, a portion of the solution was removed for analysis for Co^{+++} and then excess anhydrous hydrazine sulfate was added to the remainder of the solution to reduce the cobaltic ion to cobaltous ion. Separate experiments have shown that water is exchanged very rapidly between $Co^{++}{}_{aq}$ and solvent; hence the isotopic composition of water in the final reduced sample corresponds to complete exchange. The data obtained in three experiments on the cobaltic ion exchange are presented in Table I.

TABLE I. Exchange of water between aqueous cobaltic ion and the solvent.

(Part A describes the composition and handling of the solution; Part B, the results of the isotopic analysis on the samples of water removed at the indicated intervals. Concentration is expressed as molality, time in minutes. N is the ratio $O^{18}/(O^{16}+O^{18})$ in water. Temperature, 0±4°.)

Part A

Experiment No.	1	2	3
(Co^{+++})	0.510	0.430	0.406
(Total Co)	1.203	0.968	0.914
(H^+)	4.22	4.67	4.10
(ClO_4^-)	7.14	6.61	6.34
Expected decrease in 10^3N for slow exchange[a]	0.24	0.26	0.20
Time elapsed between mixing and final analysis	—	19.0	47.5
% decomposition of Co^{+++} in this interval	—	1.9	4.4
Fraction of total water removed by distillation	0.52	0.20	0.14

Part B

Experiment No. 1	Time	2.3	11.7	21.2	27.0	∞
	10^3N	5.818	5.827	5.856	5.879	5.828
Experiment No. 2	Time	2.7	9.2	15.2	∞	∞
	10^3N	6.313	6.327	6.330	6.356	6.370
Experiment No. 3	Time	2.2	14.4	30.1	43.3	∞
	10^3N	6.114	6.103	6.114	6.084	6.138

[a] This represents the total change in 10^3N expected if each Co^{+++} held back six molecules of water initially and then exchanged them during the course of the experiment.

The results show that the change in N, the isotopic composition, during each experiment is much smaller than that predicted on the basis of slow exchange of six water molecules per cobaltic ion. Indeed, the trend in N is in the opposite direction from that expected for slow exchange, and this trend has about the magnitude expected for that which would result from the fractionation of the water on repeated distillation (cf. the experiments with $Co^{++}{}_{aq}$). It may be concluded therefore that the exchange of water between aqueous cobaltic ion and the solvent is essentially complete under the conditions of our experiments by the time of the first sampling.

This result is surprising in view of the slow rates of substitution observed for Co(III) in all of the complex ions described for it. It is possible that the exchange of H_2O in this system does not proceed by direct substitution on Co^{+++}, but chooses an alternative path. If the electron exchange between aqueous cobaltous ion and cobaltic ion is rapid,[1] then $Co^{++}{}_{aq}$ will be an efficient catalyst for the $Co^{+++}{}_{aq}-H_2O$ exchange, since $Co^{++}{}_{aq}$ does exchange coordinated water rapidly with the solvent. Further experiments are being made to measure the $Co^{+++}{}_{aq}-H_2O$ exchange at much lower concentrations of $Co^{++}{}_{aq}$.

The observations on the exchange of H_2O between $Co^{++}{}_{aq}$ and the solvent are presented in Table II.

TABLE II. Exchange of H_2O between $Co_{aq}{}^{++}$ and solvent.

Experiment 1

$(Co^{++})=1.545$ molal; $(H^+)=3.00$ molal. Temperature 1°±1°.

Time, min.	2.0	12.2	1600[a]
10^3N	6.490	6.505	6.512

Experiment 2

$(Co^{++})=1.68$ molal; $(H^+)=1.68$ molal. Temperature 1°±1°.

Time, min.	2.5	34
10^3N	5.593	5.589

[a] The solution was allowed to warm up to room temperature in the interval between the end of the second distillation and the beginning of the third.

The data necessary for computing precise isotope balances in Experiment 2 were obtained. The value of N_∞ calculated for random mixing in the liquid is 5.660×10^{-3}, which agrees with the observed values of N within about the fractionation factor for distillation. The value of N_0 calculated for initial holdback of $6H_2O$ for each Co^{++} is 6.469×10^{-3}. For Experiment 1, N_∞ calc. and $N_0{}^6$ are *ca.* 6.52×10^{-3} and 7.43×10^{-3} respectively. The experiments prove that the exchange is complete within the time of the first sampling.

The isotope analyses were made in the laboratory of Professor Harold C. Urey of the Institute for Nuclear Studies, The University of Chicago, with the generous assistance of Dr. Samuel Epstein.

* This work was supported by funds from the ONR under Contract No. N6-ori-02026.

† Present address: Department of Chemistry, University of Southern California, Los Angeles, California.

‡ AEC Predoctoral Fellow.

[1] Hoshowsky, Holmes, and McCallum, Can. J. Research **27**, No. 4, 258 (1949), using various separation procedures, have observed complete electron exchange in this system within the time of separation of the ions.

Erratum: Photolysis of Methyl Iodide

[J. Chem. Phys. **18**, 194 (1950)]

ROBERT D. SCHULTZ AND H. AUSTIN TAYLOR

Department of Chemistry, New York University, New York and Department of Chemistry, Brookhaven National Laboratory, Upton, New York

THE sentence on page 195 pertaining to the infra-red analytical method should read: "CH_4 absorption at 7.7μ, C_2H_6 at 6.8μ, C_2H_4 at 10.6μ and $C_2H_2{}^4$ at 13.7μ were used for the analysis."

Ground State Splittings in the Iron Group, Particularly Cobaltous Ion. The Operation of Kramer's Rule

J. J. FRITZ

School of Chemistry and Physics, The Pennsylvania State College, State College, Pennsylvania

March 21, 1950

THE theoretical treatments of the susceptibility of paramagnetic salts, such as that of Schlapp and Penney[1] who have been quite successful with the rare earths and with many of the iron group salts, have met with little success in the interpretation of the data on those of cobalt. Bose,[2] in comparing his recent measurements on the principle susceptibilities of two double salts of cobaltous sulfate down to 80°K with the theory of Schlapp and Penney,[1] was able to choose between the two possibilities they suggested but was unable to get an over-all agreement between theory and experiment. Schlapp and Penney[1] had discarded as incorrect the hydrogen temperature data of Jackson,[3] which could not be made to fit the theory. Bose corrected Jackson's data for numerical errors, but was still unable to fit the theory to all of the low temperature data.

Recent measurements[4] on the magnetic susceptibility and heat capacity of powdered $CoSO_4 \cdot 7H_2O$ below 20°K suggest further difficulties with the theory and offer evidence of means for improving it. While the susceptibility of this salt is above the "spin-only" value even at 1°K, the deviations from Curie's law in this range are quite small. The intensity of magnetization in magnetic fields approximates that of an ideal paramagnetic material with $S=\frac{3}{2}$. Heat capacity data indicate that the over-all splitting of the four lowest levels is no more than 0.1 to 0.2 cm^{-1}.

In view of the present evidence, the theoretical treatment poses the following difficulties. First, it predicts an average susceptibility somewhat less than the "spin-only" value below 20°K, which is tantamount to the assumption of a splitting of the ground quartet much over 0.2 cm^{-1}. It predicts values which are too low near 20°K, but too high near room temperature. This evidence suggests that the theory has overestimated the effect of spin-orbit coupling in the splitting of the energy levels of the crystal and in increasing the magnetic susceptibility at higher temperatures.

For the average susceptibility we can obtain curves similar to those of Schlapp and Penney[1] by a very simple approximation. This involves considering a fourfold degenerate level with $L=0$ as the ground state and an upper fourfold level with $L=1$ and correspondingly higher J-values, without any interaction between the two. This scheme can be made to fit roughly the data of Bose,[2] and will improve the fit of data below 20°K, if the separation of the two levels is taken as 67 cm^{-1}. (The heat capacity data above 10°K indicate that a fourfold level could not be centered at any lesser distance above the ground state.) Somewhat better agreement could be obtained if these levels were split into two pairs with an appreciable spacing between.

This suggests that the lowest splitting assumed by Schlapp and Penney[1] (approx. 400 cm^{-1}) may be much too high, and the spin-orbit interaction consequently overestimated. It is possible that a revision of the theory taking direct account of a fourfold lowest level and lowering both splittings and spin-orbit interaction will provide a better explanation of the data. If the splitting is much below 400 cm^{-1}, as suggested, it should be possible to detect it from either absorption spectra or heat capacity measurements above 20°K.

An additional observation may be made by comparison of the helium temperature data for $CoSO_4 \cdot 7H_2O$[4], $NiSO_4 \cdot 7H_2O$,[5] and $FeSO_4 \cdot 7H_2O$.[6] The over-all ground state splittings for these three salts from heat capacity data are approximately 0.1 cm^{-1}, 5 cm^{-1}, and 20 cm^{-1}, respectively. Of the three Co^{++} is the only one which should show Kramer's degeneracy. The data suggest that the actual degeneracy in the crystalline field may be fourfold rather than the double degeneracy required by theory. The great difference in the ground state splitting raises the possibility that the orbital splittings may be much less for ions of even multiplicity than would be expected. It is important to note that most experimental and theoretical work on the iron-group salts has dealt with nearly ideal materials, where orbital splittings were taken so large that even major changes in them would not greatly affect the results.

The suggestions above are being examined more thoroughly and a more detailed treatment is in preparation.

[1] Schlapp and Penney, Phys. Rev. **42**, 667 (1932).
[2] Bose, Ind. J. Phys. **22**, 276 (1948).
[3] Jackson, Phil. Trans. Roy. Soc. (London) **A224**, 1 (1924).
[4] Fritz and Giauque, J. Am. Chem. Soc. **71**, 2168 (1949).
[5] Stout and Giauque, J. Am. Chem. Soc. **63**, 714 (1941).
[6] Lyon and Giauque, J. Am. Chem. Soc. **71**, 1647 (1949).

The Structure of the Carboxyl Group

ORVILLE THOMAS
The Edward Davies Chemical Laboratories, University College of Wales, Aberystwyth, Wales
March 21, 1950

THE data currently available on the geometrical structure of the carboxyl group show a marked inconsistency between the various methods of study; this is seen in the divergent values of the C—O "single" bond length.

With α as the angle between r_1 and r_2 whose values are in A units we have:

Model	r_1(C=O)	r_2(C—O)	α°
x-ray	1.24±0.04	1.30±0.04	125±2
e.d.	1.24±0.04	1.38±0.04	125±5
V.Z.W.	1.225	1.41	125
o.t.	1.27±0.01	1.34±0.01	126±1

The large uncertainties in r_1 and r_2 from the x-ray[1] and electron diffraction[2] data provide a fair summary of the results of many different authors for some fourteen acids. It must be remembered that while the e.d. data refer to the gaseous state, the x-ray results apply to the crystalline solid where, in some instances (e.g., oxalic acid dihydrate) special circumstances may give rise to somewhat "abnormal" values. The figure ±0.04A is about twice the uncertainty claimed in most individual estimates.

The third set shows the parameters arrived at by Van Zandt Williams from the rotational constants for formic acid[3] and its three deuterated derivatives (H·COOH, H·COOD, D·COOH, D·COOD). This interpertation of a considerable amount of quantitative spectroscopic data approximates to the e.d. values but is clearly incompatible with the large body of x-ray results.

The first feature of our reassessment of this data is the possible elimination of this important discrepancy. The fourth set of parameters, chosen as the result of a systematic trial, has been shown to be consistent with all the rotational fine structure constants for formic acid molecules to within the experimental accuracy. It is the only such set of parameters which approaches agreement with both x-ray and e.d. data.

The formate ion has $r(C{=}O)=1.27\pm0.02$.[4] Treating its vibrations as that of a symmetrical triatomic molecule ($m=13.018$) by the general methods of Torkington[5,6] with the assignment $\nu_1=1374$ cm^{-1}, $\nu_2=760$ cm^{-1}, $\nu_3=1678$ cm^{-1}, leads to principal force constants (units$\times10^5$ dynes/cm) in the ranges,

$$f(C{=}O)=10.4\pm1.0 : f\left(C\begin{matrix}O\\O\end{matrix}\right)=1.3\pm0.1.$$

A similar three-particle system treatment of the formic acid molecule with $\nu_1=1105$ cm^{-1}, $\nu_2=667$ cm^{-1}, $\nu_3=1770$ cm^{-1}, provides the following as probably the most significant set of valence force constants.*

$$f(C{=}O)=14.0 : f(C{-}O)=5.00 : f\left(C\begin{matrix}O\\OH\end{matrix}\right)=0.88.$$

$$f_{12}(\Delta r_1\Delta r_2)=1.8 : f_{13}(\Delta r_1\Delta\alpha)=0.6 : f_{23}(\Delta r_2\Delta\alpha)=0.6.$$

When a four-particle system treatment is carried out a significant change to 6.4 occurs in the value of f(C—O).

A full account of the present results and of a more extended treatment of the vibrational problem, including the assignment of the fundamental vibrations of formic acid and its deuterated derivatives is in course of preparation.

The author wishes to acknowledge his great debt to Dr. Mansel Davies for much helpful discussion and guidance, and to the Ministry of Education for a Research Grant.

[1] Wheland, *The Theory of Resonance and Its Applications to Organic Chemistry* (John Wiley and Sons, Inc., New York, 1947), appendix. Robertson *et al.*, J. Chem. Soc. (London) **142** (1947); *ibid.*, 980, 987, 993, 1001 (1949).
[2] L. O. Brockway, Rev. Mod. Phys. **8**, 231 (1936); J. Karle and L. O. Brockway, J. Am. Chem. Soc. **66**, 574 (1944).
[3] Van Zandt Williams, J. Chem. Phys. **15**, 232 (1947); S. H. Bauer and R. M. Badger, *ibid.* **5**, 852 (1937); H. W. Thompson, *ibid.* **7**, 453 (1939).
[4] W. H. Zachariasen, J. Am. Chem. Soc. **62**, 1011 (1940).
[5] P. Torkington, J. Chem. Phys. **17**, 357 (1949).
[6] P. Torkington, J. Chem. Phys. **17**, 1026 (1949).
* See footnote d of reference 6.

On the Molecular Structure of Uranium Hexafluoride

FAUSTO G. FUMI AND GILBERT W. CASTELLAN*
Department of Physics, University of Illinois, Urbana, Illinois
March 16, 1950

RECENTLY S. H. Bauer[1] studied the molecular structure of uranium hexafluoride by means of electron diffraction. The best agreement between calculated and observed intensities is given by Model A_4, obtained by distortion of a trigonal antiprism of symmetry C_{3v}, and by Model C_4, obtained by distortion of an octahedron of symmetry C_{2v}; however, the experimental precision† does not allow a selection to be made between models such as C_4 and C_3, the latter being a rhombic bipyramid of symmetry V_h.

Table I gives the polar coordinates of the bond vectors of the first two models; the bond numbers follow Bauer's enumeration. The configuration of Model C_3 is evident from Bauer's Table III.

All three models involve non-equivalent bonds. The symmetry group of the Model A_4 is C_{3v} and the symmetry group of the Model C_4 is C_2; in both these models the system of six fluorine atoms has a center of symmetry which, of course, does not coincide with the position of the uranium atom. Model C_3, on the other hand, has a center of symmetry.

The possible configurations of the valence electrons of the uranium atom in the models are obtained in Tables II–IV by group theory.

These configurations are:

For the Model A_4: $(sp, sd, pd)+(p^2d^2, d^4)$.
For the Model C_4: $(spd, sd^2, pd^2, d^3)+(pd^2, p^2d)$.
For the Model C_3: d^2sp^3.

Bauer's statement that the hybridization p^3d^3 can lead to a trigonal antiprism with the possibility of two unequal sets of three bonds is not proved in his paper nor included in Kimball's results.[2] Tables II and III show that the hybridization p^3d^3 which is compatible with a regular antiprism (D_{3d}) with all equivalent bonds[2] is also compatible with Models A_4 and C_4.

The hybridization d^3sp^2 is compatible with both the Models A_4 and C_4, while the hybridization d^5s is compatible with the Model A_4 and p^2d^4 with the Model C_4. d^3sp^2, d^5s, and p^2d^4 are the configurations of six valence electrons that Kimball[2] stated could not lead to arrangements with all equivalent bonds, without proving it rigorously since not all the possible arrangements of six equivalent bonds were considered in his paper. It is actually true that d^3sp^2, d^5s, and p^2d^4 necessarily lead to arrangements of coordination number six with some non-equivalent bonds since all the arrangements of six equivalent bonds, except the three considered by Kimball (octahedral O_h; trigonal prismatic D_{3h}; trigonal antiprismatic D_{3d}) and the trigonal trapezohedral $D_3[(s, d)+p+(p^2d^2, d^4)]$ require the use of f orbitals. However, it is interesting to note that d^3sp^2, d^5s, and p^2d^4 are compatible with arrangements which are not general "mixed type arrangements" in the sense implied by Kimball,[2] that is, formed of separate sets of equivalent bonds oriented arbitrarily with respect to one another, lacking any total symmetry. The arrangements with which d^3sp^2, d^5s, and p^2d^4 are compatible are particular mixed type arrangements, having a total symmetry, and thus lie within the scope of group theoretical treatment; they can properly be called "*arrangements with non-equivalent bonds*."

In general, group theory does not permit one to establish unambiguously the configuration to which a given hybridization will lead.‡ Consequently, it is impossible to state on purely group theoretical grounds which of the compatible hybridizations are operative in the Models A_4 and C_4. It is also impossible to eliminate Model C_3 as a covalent model on the ground that the hybridization d^2sp^3 is known[2] to lead to regular octahedra. Nevertheless, it seems reasonable to argue that the hybridizations d^3sp^2 and d^5s (Model A_4) and d^3sp^2, p^2d^4 (Model C_4) which *cannot* lead to arrangements having six equivalent bonds are more probable.

TABLE I. Polar coordinates of the bond vectors.

		Bond number	R(A)	θ	ϕ
Model A_4	First set	(1)	1.87	62° 46′	0°
		(2)	1.87	62° 46′	120°
		(3)	1.87	62° 46′	240°
	Second set	(4)	2.17	129° 59′	300°
		(5)	2.17	129° 59′	60°
		(6)	2.17	129° 59′	180°
Model C_4	First pair	(2)	1.87	90°	50° 36′
		(5)	1.87	90°	309° 24′
	Second pair	(3)	2.22	90°	139° 23′
		(4)	2.22	90°	220° 37′
	Third pair	(1)	2.12	7° 20′	158° 01′
		(6)	2.12	172° 40′	201° 59′

TABLE II. (Model A_4.)

C_{3v}	A_1	A_2	E
s	1	0	0
p	1	0	1
d	1	0	2
σ	2	0	2

TABLE III. (Model C_4.)

C_2	A	B
s	1	0
p	1	2
d	3	2
σ	3	3

TABLE IV. (Model C_3.)

V_h	A_{1g}	A_{1u}	B_{1g}	B_{1u}	B_{2g}	B_{2u}	B_{3g}	B_{3u}
s	1	0	0	0	0	0	0	0
p	0	0	0	1	0	1	0	1
d	2	0	1	0	1	0	1	0
σ	3	0	0	1	0	1	0	1

* AEC Postdoctoral Fellow.
[1] S. H. Bauer, J. Chem. Phys. **18**, 27 (1950).
† We are grateful to Professor Bauer for pointing this out to us.
‡ This point will be discussed in a forthcoming publication by F. G. Fumi.
[2] G. E. Kimball, J. Chem. Phys. **8**, 188 (1940).

The Kinetics of Hydrogen Evolution

J. O'M. BOCKRIS, ROGER PARSONS, AND H. ROSENBERG
Imperial College, London, England
February 27, 1950

CERTAIN conclusions reached by Van Rysselberghe in an interesting recent paper[1] are worthy of comment in the light of data, partly unpublished, obtained by the present authors and their co-workers.

(i) One of the most outstanding facts concerning hydrogen overpotential is its marked dependence on the cathode material most clearly expressed by the relation between overpotential and thermionic work function.[2] Van Rysselberghe suggests that the rate of the discharge of hydrogen ions is not dependent upon the immediate product of this reaction, i.e., whether it results in free atomic hydrogen, adsorbed atomic hydrogen or (by reaction with adsorbed hydrogen) adsorbed molecular hydrogen. The consequence of this view appears to be the prediction of a rate of discharge at high overpotentials (>0.1 v) which is independent of the cathode material, in contrast to the experimental evidence.

(ii) Van Rysselberghe also suggests on theoretical grounds the existence of several "Tafel regions." The experimental evidence for the existence of a different value of the coefficient b of the Tafel equations at low c.d.s. is unsatisfactory. The value of this coefficient for a mercury cathode in $N/10$ HCl was found to be constant at 0.119 v at 22°C from 3.10^{-8} to 10^{-3} amp./cm² by Levina and Sarinsky[3] whose results have been confirmed several times in both HCl and H_2SO_4 solutions at c.d.s. greater than 10^{-6} amp./cm².[4] These measurements are thus directly comparable with those of

Bowden and Grew[5] over the range $3.10^{-8}-10^{-6}$ amp./cm² in which range the results of the latter authors are approximately 0.1 v lower than those of Levina and Sarinsky. Consequently it appears more probable that the measurements of Bowden and Grew are vitiated by the extremely small traces of impurity effective at such low c.d.s. than that they represent a true variation in the coefficient b.

The more important correction to the experimental basis of this suggestion concerns the behavior at high c.d.s. ($>10^{-2}$ amp./cm²) where Van Rysselberghe presumably, mainly on the basis of the work of Hickling and Salt,[6] assumes that the coefficient b approaches zero. It has been shown by one of us[7] that this behavior is not due to errors in the commutator method used by Hickling and Salt. Recently we have observed using a mercury cathode that this effect is removed by extensive electrolytic purification of the solution but reappears on the addition of substances such as H_2S to this purified solution. We conclude that the previously reported approach of overpotential to a constant value at high c.d.s. is due to the presence of those impurities which like H_2S are adsorbed at the electrode only at potentials far from the electrocapillary maximum. In agreement with this Azzam[8] has found that for mercury and several other metals of high overpotential the Tafel equation is applicable to a c.d. of at least 150 amp./cm².

(iii) Van Rysselberghe's theory leads to the results that the overpotential is in the general case independent of hydrogen ion concentration, and in special cases dependent on it. Unpublished data obtained in the authors' laboratory[9] together with the scanty published data[3,10,11] obtained under satisfactory experimental conditions indicates that the reverse situation is observed. The overpotential is in fact independent of a pH only for high overpotential metals in solutions of pure acids at low and medium concentrations. For low overpotential metals in pure aqueous acids there is a variation of overpotential with pH even when the acid concentration is as low as $N/100$. In the presence of added salts, the overpotential appears to be a function of pH for both high and low overpotential metals.

[1] Van Rysselberghe, J. Chem. Phys. **17**, 1226 (1949).
[2] Bockris, Chem. Rev. **43**, 525 (1948).
[3] Levina and Sarinsky, Acta Physicochimica **6**, 491 (1937); *ibid.* **7**, 485 (1937).
[4] Agar and Llopis, Anal. fis y quin. **43**, 1087 (1947); Ruis and Llopis, *ibid.* **42**, 897 (1946); Béthune, J. Am. Chem. Soc. **71**, 1556 (1949).
[5] Bowden and Grew, Trans. Faraday Soc. Discussion **1**, 86 (1947).
[6] Hickling and Salt, Trans. Faraday Soc. **36**, 1226 (1940).
[7] Bockris, Trans. Faraday Soc. **43**, 417 (1947).
[8] Azzam, Thesis, London (1949).
[9] Conway, Thesis, London (1949); Potter (unpublished).
[10] Bockris and Parsons, Trans. Faraday Soc. **45**, 916 (1949).
[11] Lukovsev, Levina, and Frumkin, Acta Physicochimica **11**, 23 (1939); Legin and Levina, *ibid.* **12**, 251 (1940); Jofa, *ibid.* **10**, 391, 617, 903 (1939); Frumkin, Trans. Faraday Soc. Discussion **43**, 57 (1947).

Macroscopic Space Charge in Electrolytes during Electrolysis

WILLIAM SCHRIEVER
Physics Department, University of Oklahoma, Norman, Oklahoma
March 13, 1950

THIS is a reply to the Letter to the Editor, under the same title, by MacInnes, Shedlovsky, and Longworth[1] in which they claim to have shown that the work reported by Reed and Schriever[2] is faulty.

If significant changes in concentration near the current electrodes in our work had taken place, then the potential gradients should have increased as the cathode was approached. In five of the seven electrolytes investigated in the cathode half of the column, the gradients decreased; in the other two they first decreased to below average and then increased as the cathode was approached. Seven of the eight solutions exhibited a decrease in gradient as the anode was approached but one, $Al_2(SO_4)_3$, exhibited a large continuous increase through a distance of 5 cm. It is clear that ordinary concentration changes cannot account for our data. A more detailed explanation appeared in our original paper.[3]

If, as they claim, "erratically changing concentration differences" had developed then our data should have been erratic. Our data were reproducible and not erratic. This is illustrated by Table I in our original paper. During the 15 minutes that the current passed, in our work, an ion moved only one millimeter. If *all* the ions in a one-mm layer next to the cathode were swept out, and a full extra set were swept into the one-mm layer next to the anode, the densities of these layers would have changed by only 2 parts in 10,000. Actually, of course, the concentration changes would be much less than this and, in addition, these changes built up from zero to less than 2 parts in 10,000 during the 15 minute interval. Does it not seem a little unreasonable to expect appreciable "erratic" convection to be produced by such small density differences in such a short time?

They also claim that our electrodes were at fault. Again the reproducibility of our data indicates that our electrodes must have been quite satisfactory. Even if the indicated potential differences were in error, as far as absolute magnitude is concerned, such an error would have been the same for all points along the column of electrolyte. This constant error would cause no change in either the calculated potential gradients or in the calculated space-charges. If erratic changes had occurred we could not have achieved reproducibility of data. Any gradual changes in our electrodes were taken into account by the application of our "standard curve" procedure.[4]

Their "admittedly relatively crude" experiment would have been convincing if they had used one of the solutions for which data were reported in our paper, instead of KCl, and if they could have obtained *our* type of results with their tube horizontal, and *their* type of results with the tube vertical. They do not describe how they took their "three series of measurements"; if they did not measure their potential differences at all points along the column, for a constant time of current-flow, then their data are not comparable to ours.

It so happens that one of my students has been working since last November with a 0.0024 normal solution of KCl between platinum electrodes, and using the tip of a platinum wire as the exploring electrode. The apparatus and methods are essentially the same as those used by Reed. Our data are not yet complete but they do show that the potential gradient is remarkably constant for most of the length of the 40-cm column. Near the cathode end of the column a small negative space charge is indicated. The data in the anode half of the column are yet too few to make certain that we shall be able to detect a space charge effect there.

Therefore, my guess is that McInnes *et al.* would get essentially the same kind of results for KCl with their tube horizontal as they would with their tube vertical, if all measurements were carried out with care under exactly the same conditions. Their comments are very much appreciated.

[1] MacInnes, Shedlovsky, and Longworth, J. Chem. Phys. **18**, 233 (1950).
[2] C. A. Reed and W. Schriever, J. Chem. Phys. **17**, 935–944 (1949).
[3] See reference 2, p. 943.
[4] See reference 2, p. 939.

Further Studies of Hydrocarbon Flame Spectra*

GEORGE A. HORNBECK AND ROBERT C. HERMAN
Applied Physics Laboratory, The Johns Hopkins University, Silver Spring, Maryland
March 10, 1950

RECENTLY the authors reported some preliminary investigations of the spectra of stationary hydrocarbon flames, particularly those of ethylene and methane burning with oxygen at reduced pressures (~50 mm of Hg).[1,2] These investigations were carried out primarily to examine in greater detail the so-called hydrocarbon or ethylene flame bands. These bands, which

were first reported by Vaidya[3] on the basis of low dispersion spectra, lie in the spectral range 2500–4100A, appear degraded to the red, and have been assigned generally to the HCO radical.[4] Our studies of hydrocarbon flames, burning under a variety of conditions, reveal in this region of the spectrum the band systems of OH and CH, the Schumann-Runge band system of O_2, the Deslandres-D'Azambuja band system of C_2, and the CN bands when the fuel is mixed with air rather than oxygen. Various of these band systems are more prominent according to the conditions of burning. For example, the Schumann-Runge system is relatively stronger the higher the oxygen concentration in the fuel-oxygen mixture, the bands of C_2 becoming weaker.

As a continuation of this investigation we have examined the spectrum of the acetylene-oxygen flame burning the premixed gases in an ordinary acetylene torch at atmospheric pressure with carefully regulated gas flow control. The results mentioned above are also obtained with this source. The purpose of the present note is to report the spectral changes that occur when the fuel/oxygen ratio is increased considerably beyond that for stoichiometric proportions. Spectra were taken of the inner cone with an acetylene/oxygen ratio of about unity in the second order of a 21′10″ Jarrell-Ash grating spectrograph with a dispersion of about 2.4A/mm. Under this condition the Fox-Herzberg[5] system ($^3\Pi_g - {}^3\Pi_u$) of the C_2 molecule is found together with the bands of OH, CH, and all the other band systems of C_2.

Figure 1 is a densitometer tracing of the region ~3005–3064A which shows the (0−4) band of the Fox-Herzberg system mixed with many lines of OH. A portion of this band is labeled so as to identify the *R* and *P* triplets. The Fox-Herzberg bands degrade to the red, do not have pronounced heads, and are known to extend from 2378A (4−1) to 3283A (0−6).[5,6]

Our work would seem to indicate that hydrocarbon flames burning in different types of sources and under various conditions of pressure yield spectra which depend principally on the fuel/oxygen or fuel/air ratio. The spectra obtained appear to be the result of the overlapping of a large number of bands all of which degrade to the red except those of CN and some of the Deslandres-D'Azambuja system. It is not surprising that hydrocarbon flame spectra under low dispersion are difficult to interpret. It should be pointed out that at higher dispersion there still remains residual structure to be identified which, however, is weak in comparison to that already described. In any event we have as yet found no prominent structure which cannot be attributed to the various diatomic radicals and molecules.

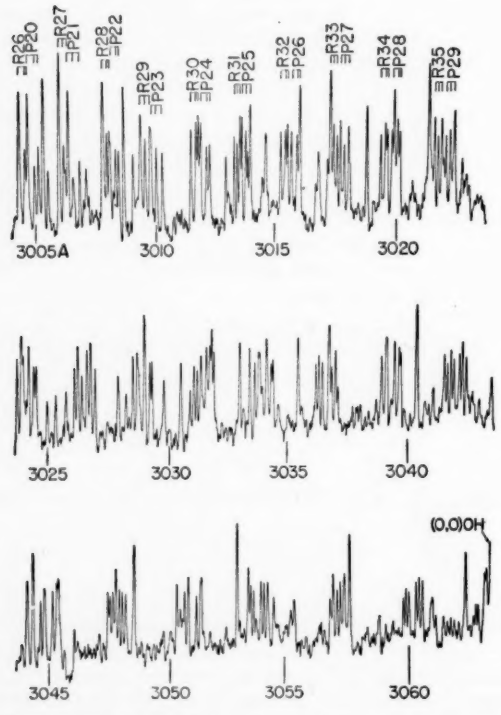

FIG. 1. Densitometer tracing of the spectrum of the acetylene-oxygen flame showing a portion of the (0−4) Fox-Herzberg band of C_2.

We wish to express our appreciation to Dr. G. Herzberg, National Research Council, Canada, and Dr. J. G. Phillips, Yerkes Observatory, University of Chicago, for their interest in our work.

* The work described herein was supported by the Bureau of Ordnance, U. S. Navy, under Contract NOrd-7386.

[1] G. A. Hornbeck and R. C. Herman, J. Chem. Phys. **17**, 842 (1949).
[2] R. C. Herman and G. A. Hornbeck, J. Chem. Phys. **17**, 1344 (1949).
[3] W. M. Vaidya, Proc. Roy. Soc. **A147**, 513 (1934).
[4] For example, see A. G. Gaydon, *Spectroscopy and Combustion Theory* (Chapman and Hall, Ltd., London, 1948).
[5] J. G. Fox and G. Herzberg, Phys. Rev. **52**, 638 (1937).
[6] J. G. Phillips, Astrophys. J. **110**, 73 (1949).

Exchange Reaction of Carbonate Ion with Carbonato-Tetrammine Cobaltic Ion

GORDON M. HARRIS
Chemistry Department, University of Melbourne, Melbourne, Australia
March 9, 1950

SOME recent studies of the cobalt complexes utilizing radioactive cobalt have indicated the relative inactivity of these systems toward exchange reactions involving the central cobalt ion of the complex.[1,2] It is desired to record here the results of a preliminary study of the system $[Co(NH_3)_4CO_3]^+ - CO_3^=$. In this work, exchange between complexed and uncomplexed carbonate ion was studied by means of radioactive carbon-14.

Aqueous solutions of carbonato-tetrammine cobaltic nitrate and sodium carbonate, the latter containing a small proportion of $Na_2C^{14}O_3$, were mixed in such proportions as to give a solution approximately 0.03*M* in the complex, and 0.01*M* in the carbonate. The reactant mixture was stored in the dark at 20°C, 1.5-ml samples being withdrawn for analysis at regular intervals. Free $CO_3^=$ ion was precipitated as $BaCO_3$, utilizing $BaCl_2$-NH_3 mixture 1*N* in each constituent. Separate tests showed that the complexed $CO_3^=$ ion remained unaffected by this reagent during several hours' standing at 20°C. The ~3-mg samples of $BaCO_3$ so obtained were counted in aluminium pans of 1 in. diameter according to standard radiochemical technique. The counts were of sufficient duration to give results with a standard deviation of within ±1 percent. Self-absorption corrections were unnecessary due to

TABLE I.

Duration of exchange (min.)	Weight of $BaCO_3$ sample (mg)	Net activity (A_t) of $BaCO_3$ sample (counts/mg/min.)	Fraction of exchange $f=\frac{A_0-A_t}{A_0-A_\infty}$	$(1-f)$
0	—	(109)[a]	0.00	1.00
10	2.87	107	0.03	0.97
62	2.97	100	0.11	0.89
120	2.89	94	0.19	0.81
246	2.82	84	0.32	0.68
425	2.86	71	0.48	0.52
660	2.88	56	0.67	0.33
1458	2.69	38	0.90	0.10
2892	3.08	30[b]	1.00	0.00

[a] Extrapolated value obtained from $\log A_t$ *vs.* *t* plot.
[b] Sample taken at end of about 7 "half-lives" of the exchange, so within one percent of exchange equilibrium. This value thus assumed for A_∞ in calculation of "*f*."

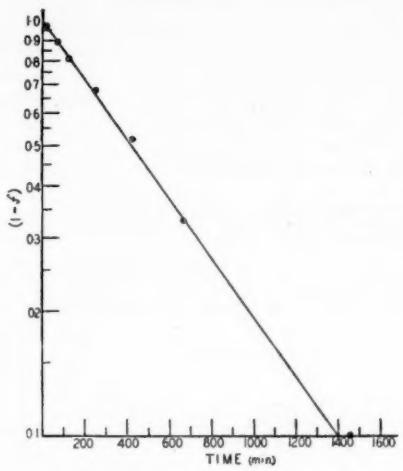

FIG. 1.

the thinness of the samples, and the fact that they were in any case closely comparable in weight. The data are summarized in Table I.

That the reaction appears to exhibit the conventional first-order characteristics of isotopic exchange[3] is illustrated by the $\log(1-f)$ *vs.* t plot of Fig. 1. It is seen from the latter that the half-time of exchange of about 7 hr. is rather unexpectedly long in view of the known instability of the carbonato-type of complex.[4] A detailed kinetic investigation of the reaction is now in progress in this laboratory, and a full report, including evidence as to the mechanism of the exchange, will be published at a later date.

[1] W. B. Lewis and C. D. Coryell, Brookhaven Conference Report BNL-C-8 (December, 1948).
[2] Hoshowsky, Holmes, and McCallum, Can. J. Research **27B**, 258 (1949).
[3] H. A. C. McKay, Nature **142**, 997 (1938).
[4] Abegg's *Handbuch der anorganischen Chemie* (Leipzig, 1935), Bd. IV, Abt. 3, Teil 3, Lief 2.

The Influence of the Shape of Molecules on the Thermodynamic Properties of Hydrocarbon Mixtures

I. PRIGOGINE AND V. MATHOT*
Faculté des Sciences de l'Université Libre de Bruxelles, Bruxelles, Belgium
March 7, 1950

IN recent experimental[1] and theoretical[2] work it has been shown to what extent the thermodynamic properties of solutions are affected by a *difference in size of the molecules* of the constituents.

The purpose of this investigation is to determine the influence of a *difference in shape or symmetry of the molecules.*

In order that the heat of mixing may be as small as possible, mixtures of saturated hydrocarbons have been chosen; the molecules of both constituents have practically the same size but they are either globular (more or less spherical) or chain-like as normal paraffins.

The total vapor pressure and the integral heat of mixing of the systems: cyclohexane-n-hexane at 20°C and tetraethylmethane (diethyl-3,3-pentane)-n-octane at 50°C have been measured.

The results have been calculated in terms of excess free energy g_e, excess entropy s_e, and excess enthalpy h_e related by the definitions

$$g_e = h_e - Ts_e$$
$$g_e = x_1 RT \lg f_1 + x_2 RT \lg f_2$$

(x_1, x_2 mole fractions; f_1, f_2 activity coefficients).

Figures 1 and 2 give these results, respectively, for cyclohexane-hexane and tetraethylmethane-octane, in calories per "mole" of solution against mole fraction. The accuracy is only about 10 percent, as the observed effects are very small.

It must be emphasized that both systems are far from regular. In the system tetraethylmethane-octane, there even appears a negative excess entropy and a negative excess enthalpy (*evolution* of heat while mixing), the excess free energy remaining positive. As far as the authors are aware, this is the only example of a system of saturated hydrocarbons with a negative enthalpy of mixing.

The influence of symmetry of isomer constituents of a solution has also been investigated theoretically. According to Guggenheim's theory,[2] any mixture of unbranched and branched chains, both occupying the same number of lattice sites, must be ideal in the athermal case. Using the Bethe-Chang method[3] we have calculated the combinatory factor for an assembly of linear rigid and right-angled triangular trimers on a two-dimensional lattice with square symmetry ($z=4$), assuming zero energy of mixing. This factor proved to be the same as for an ideal solution. Although there must be some effect with increasing size of the isomers, this seems to be zero or negligible for differences in shape met with in the more common hydrocarbon mixtures.

Therefore the origin of the entropy terms observed for both systems should be imputed to the enthalpies of mixing. Its effect would be to alter, not the combinatory factor—a contribution known to be very small and leading to negative excess entropy

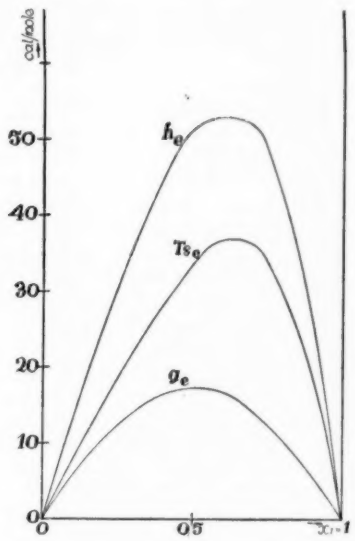

FIG. 1. Thermodynamic properties of cyclohexane-hexane solution (x_1 = mole fraction of cyclohexane).

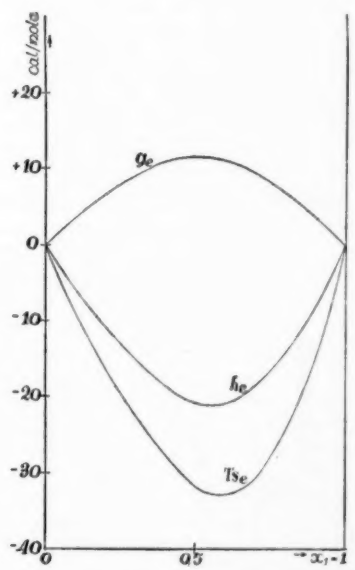

FIG 2. Thermodynamic properties of tetraethylmethane-octane solution (x_1 = mole fraction of tetraethylmethane).

anyway—but the internal partition functions. This assumption will be checked spectroscopically in this laboratory.

Further work is now in progress on other systems of the same kind.

A more detailed account will be published by one of us (V.M.) in Bull. Soc. Chim. Belg.

The calorimetric measurements have been performed at the University of Groningen (Netherlands) in Professor J. J. Hermans' laboratory with the collaboration of Dr. J. H. van der Waals. The vapor pressure has been measured in Professor J. Timmermans' laboratory at the University of Brussels. We are indebted to them for many interesting discussions.

* Aspirant du Fonds National Belge de la Recherche Scientifique.

[1] Bronsted and Koefoed, Kgl. Danske Vid. Sels. Mat.-fys. Medd. **XXII**, No. 17 (1946). J. H. van der Waals and J. J. Hermans, Rec. Trav. Chim. Pays Bas **68**, 181 (1949). H. Tompa, J. Chem. Phys. **16**, 292 (1948).

[2] E. A. Guggenheim, Proc. Roy. Soc. **A183**, 203 (1944). For further references see A. R. Miller, *The Theory of Solutions of High Polymers* (Oxford University Press, London, 1948).

[3] See T. S. Chang, Proc. Roy. Soc. **A169**, 512 (1939); A. R. Miller (reference 2).

Pressure Broadening Effects in Infra-Red Spectra: Ozone

M. Kent Wilson and Richard A. Ogg*
Mallinckrodt Chemical Laboratory, Harvard University, Cambridge, Massachusetts

February 27, 1950

THE recently observed effect[1] of foreign gases in altering the band envelope of the ν_3-fundamental of NO_2 is of simple physical origin, and hence to be expected for other molecular species.[2] For individual rotational lines of "natural" breadth at half-maximum, the absorption coefficient at the line center may be great enough to cause practically complete absorption in the experimental path length employed. In such case line broadening caused by addition of a foreign gas will lead to increased energy absorption, and hence to an apparent increase of the envelope intensity, as observed for the P and R branches of the ν_3-band of NO_2. If the separation of adjacent lines is comparable to the natural breadth, as is apparently the case for the Q branch of this band, further line broadening will result in only a minor increase in energy absorption and envelope intensity. The Q branch is thus *relatively* suppressed by the addition of considerable foreign gas.

From the above it is apparent why an unambiguous Q branch was not observed[3] in the 1043-cm^{-1} band of ozone, inasmuch as previous studies were made with ozone mixed with a large excess of oxygen. We have therefore repeated these studies, using pure ozone prepared by fractional distillation of ozonized oxygen. A Baird Associates infra-red recording spectrophotometer Model B was employed in this investigation. The gas cell was 4.0 cm in length and had NaCl windows. Figure 1 shows clearly the unequivocal Q branch in the band from pure ozone, and the practical suppression of it by the addition of a large excess of oxygen.

This observation of a Q branch in the 1043-cm^{-1} ozone band supports the assignment[3] of it as ν_3. Using pure ozone we have also observed the relatively weak ν_1-fundamental at 1110 cm^{-1} finding no indication of a Q branch in agreement with the previous observation.[3] The studies of Adel and Dennison[4] on the ν_2-fundamental at 705 cm^{-1} show it to be lacking a Q branch. An acute-angled model of ozone would require two of the fundamental bands to show Q branches, whereas the wide angle structure[5] requires one, in agreement with experimental observations. The present work thus offers further support for the obtuse model which is also indicated by the electron diffraction studies.[5]

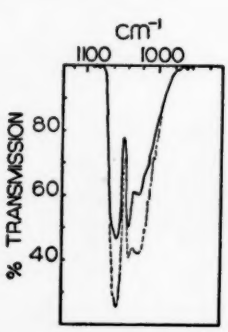

Fig. 1. Pressure broadening effect in the ν_3-band of ozone. Solid line denotes absorption by pure ozone at about 50 mm pressure. Dotted line represents absorption by same ozone with oxygen added to yield total pressure of one atmosphere.

* Currently on leave from Stanford University, California.

[1] Ogg, Richardson, and Wilson, J. Chem. Phys. **18**, 573 (1950).

[2] See, for example, E. von Bahr, Ann. d. Physik **29**, 780 (1909); **33**, 585 (1910).

[3] M. K. Wilson and R. M. Badger, J. Chem. Phys. **16**, 741 (1948).

[4] A. Adel and D. M. Dennison, J. Chem. Phys. **14**, 379 (1946).

[5] W. Shand and R. A. Spurr, J. Am. Chem. Soc. **65**, 179 (1943).

Synthesis of Cementite

L. J. E. Hofer and E. M. Cohn
Research and Development Branch, Office of Synthetic Liquid Fuels, Bureau of Mines, Bruceton, Pennsylvania

March 23, 1950

KNOWN methods of synthesis of cementite[1] suffer from the disadvantages that the product is formed in poor yield, is contaminated with free carbon, or is highly sintered. A new method has been found that overcomes these difficulties. It is based on the fact that in partly carburized iron containing either or both modifications of the iron carbide, Fe_2C,[2] the carbides will begin to react with the free iron at a relatively low temperature (above 260°C) and will have reacted completely below 500°C to form well-crystallized cementite. This reaction, $Fe_2C+Fe\rightarrow Fe_3C$, thus requires substantially lower temperatures than any other known series of reactions producing cementite uncontaminated by free carbon, and the synthesis is comparatively simple to carry out.

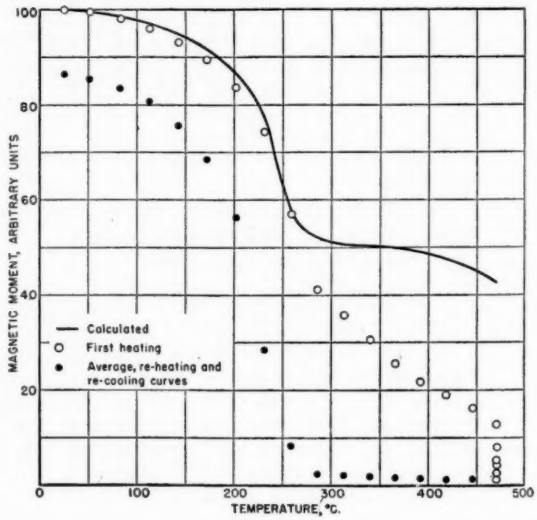

Fig. 1. Thermomagnetic curve showing the reaction Fe_2C-Hägg$+\alpha$-Fe$\rightarrow Fe_3C$.

The reaction was discovered when a thermomagnetic analysis was made of a mixture of about equal amounts of Fe_2C-Hägg and α-iron and it was observed that above 260°C the magnetic moment dropped more rapidly with increase in temperature than was expected. Upon cooling, the sample was only slightly magnetic until the Curie point of cementite was attained; by the time room temperature was reached, the sample had regained most of its initial magnetic moment. X-ray diffraction analysis of reactants and products from this and subsequent experiments substantiated the conclusions drawn from the magnetic changes. Figure 1 shows

the reaction as measured on a reduced and partly carburized synthetic-ammonia-type catalyst consisting initially of about 48 percent Fe_2C-Hägg and 52 percent α-iron. The curve is calculated for such a mixture, and the experimental points (circles) fit the curve fairly well up to just beyond the Curie point of Fe_2C-Hägg. The sample was kept at 470°C for 280 min., but the reaction was already complete after 150 min. After cooling, the sample was reheated and cooled (crosses represent average values) and found to be cementite plus a small amount of excess α-iron which had been present initially. A similar experiment was carried out with precipitated iron oxide containing 10 weight-percent copper and 0.32 weight-percent potassium (based on weight of iron), which consisted of about 48 percent hexagonal close-packed iron carbide, Fe_2C,[2] and 52 percent α-iron after reduction and partial carburization. In this case, the reaction was complete after 60 min.

[1] Arnold and Read, J. Chem. Soc. **65**, 788 (1895); Brill and Mark, Zeits. f. physik. Chemie **133**, 443 (1928); Hägg, Zeits. f. Krist. **89**, 92 (1934); Jack, Nature **158**, 60 (1946); Lipson and Petch, J. Iron Steel Inst. **142**, 95 (1940); Mittasch, Kuss, and Emert, Zeits. f. anorg. allgem. Chemie **170**, 193 (1928); Pingault, Ann. Chim. **20**, 371 (1933); Schenck and Stenkhoff, Zeits. f. anorg. allgem. Chemie **161**, 287 (1927).

[2] Hofer, Cohn, and Peebles, J. Am. Chem. Soc. **71**, 189 (1949).

Rate of the Rapid Gas Phase Reaction between NO, NO_2, and H_2O

LOWELL G. WAYNE* AND DON M. YOST
Gates and Crellin Laboratories of Chemistry, California Institute of Technology, Pasadena, California

March 24, 1950

FOLLOWING the successful application by Johnston and Yost[1] of the cathode-ray oscillograph to the study of the very rapid reaction between nitrogen dioxide and ozone, we have applied this technique to the following reaction, which

$$NO(g)+NO_2(g)+H_2O(g)=2HNO_2(g) \qquad (1)$$

is also probably involved in the atmosphere immediately after a lightning stroke, and which had been reported[2] to be practically instantaneous. In a trapped non-equilibrium mixture of the reacting gases the concentration of nitrogen dioxide was followed by photographing the screen of an oscilloscope which registered the output voltage of a multiplier photo-tube exposed to a chopped beam of blue light emergent from the reaction cell.

In experiments on dilution with nitrogen of mixture of NO and NO_2, such mixtures were found to attain equilibrium instantaneously (within the limits of observation of our apparatus). By using a constant large excess pressure of NO, namely 1 atmos. throughout, the ratio between the concentrations of the molecular species NO and N_2O_3 was kept constant at 2.1. The initial partial pressure of nitrogen dioxide was varied from about 0.005 to 0.03 atmos., and that of water vapor from about 0.09 to 0.025 atmos. The molecular ratio of NO_2 to H_2O was varied between 0.34 and 2.5. One hundred and twenty-three separate runs were made, all at temperatures of from 23° to 25°C.

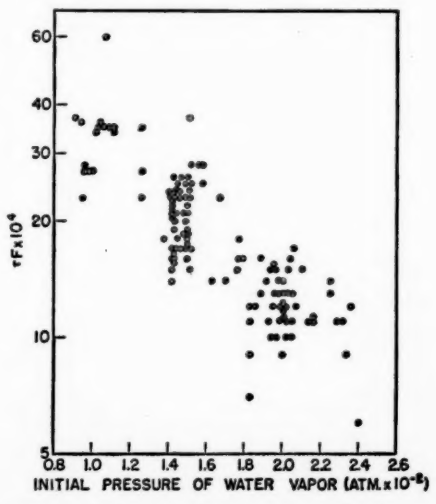

FIG. 1. Plot of τF of Eq. (3) against initial pressure of water vapor.

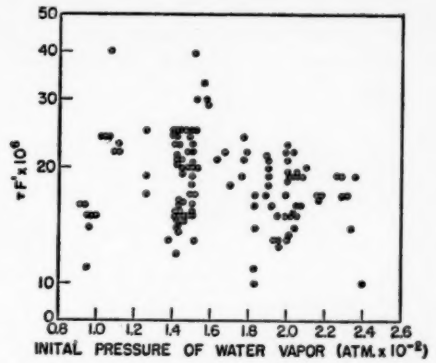

FIG. 2. Plot of $\tau F'$ against initial pressure of water vapor.

Calculations from thermodynamic data indicated that the reaction should reach an equilibrium with a substantial fraction of the reactants unconsumed, the equilibrium constant for reaction (1) being estimated as 1.65 atmos.$^{-1}$. Eleven of our photographs provided data from which this constant could be estimated; the resulting values ranged from 0.92 to 3.1 atmos.$^{-1}$, the log mean being 1.74, the median value 1.67.

Since the average age of the mixture in the light path at the instant of trapping was of the order of one centisecond, while the half-time of the reaction was in some cases as low as 1.4 centiseconds, it was considered more feasible to determine reaction rates on the basis of the rate of approach to equilibrium rather than on the "initial rate" approximation. The images on the photographic negatives were measured and relative displacement from position representing equilibrium were plotted on a logarithmic scale *vs.* time (linear scale). From such a plot an approximate half-time (i.e., time required for the system to proceed from any given state halfway to an equilibrium state) could be readily measured.

For a state of the system not too far from equilibrium, the general differential rate equation may be written

$$dx/kdt=Y[(a-x/2)(b-x/2)-x^2/K] \qquad (2)$$

where x denotes P_{HNO_2}, a and b are initial values of P_{NO_2} and P_{H_2O}, respectively, k is the rate constant of reaction (1) and K the appropriate equilibrium constant, Y being a factor (possibly variable) to represent any catalytic or inhibitory influences affecting the rate. If the reaction is first order with respect to both NO_2 and H_2O, i.e., Y is constant, a plot of the type described should give a hyperbolic tangent curve having the asymptotic slope $-Fk/2$, where

$$F=[(a-b)^2+16ab/K]. \qquad (3)$$

The half-time (τ) derived from this plot would then be inversely proportional to F; i.e., the product τF should be constant. Figure 1 shows a test of this constancy, in which τF (on a logarithmic scale) is plotted against initial pressure of water vapor, showing a distinct trend in the sense of inverse variation; a comparable plot of τF *vs.* the initial pressure of NO_2 displays no such trend. On the assumption that this indicates a higher order for the reaction with respect to water vapor, the product $\tau F'$ was plotted (Fig. 2), where F' is the product of F with the calculated pressure of water vapor in the equilibrium state. Values of $\tau F'$ show no significant trend with concentration of either reactant, and scatter noteworthily less than those of τF.

Based on the latter formulation, with $Y=b-x/2$, the rate constant k is estimated at 7.3×10^4 atmos.$^{-2}$ sec.$^{-1}$, or $\log k=4.86$ with a probable error in the log of 0.09, corresponding to a factor of 1.2.

We are indebted to Drs. Oliver Wulf and Norman Davidson for many helpful discussions. The work was supported by a grant from the Research Corporation for which we are very grateful.

* Present address: Mellon Institute of Industrial Research, Pittsburgh, Pennsylvania.

[1] H. S. Johnston and D. M. Yost, J. Chem. Phys. **17**, 386 (1949).

[2] E. H. Melvin and O. R. Wulf, J. Chem. Phys. **3**, 755 (1935).

Vibration-Frequency Correlations in the Paraffin Hydrocarbons

P. TORKINGTON
British Rayon Research Association, Urmston, Lancashire, England
March 16, 1950

THERE have been several attempts fairly recently to account at least partially for the vibration spectra of the paraffin hydrocarbons.[1] Barriol and Chapelle[2] concluded that few of the 700 to 1100 cm^{-1} bands could be C−C chain vibrations, contrary to previous views. A study of deuteropolythene with polarized infra-red radiation[3] disclosed that the 720 cm^{-1} band was due to a perpendicular CH_2 rocking mode. A recent normal coordinate analysis of N-paraffins[4] supports the view that CH bending modes make the greater contribution to the spectra. That this is so would be expected from the number of coordinates to be allocated to C−C stretching (one), and CH bending (four), in the unit link of the primary hydrocarbon chain. In a recent paper,[5] pairs of frequencies at 1145 and 1170 cm^{-1} and at 1200 and 1250 cm^{-1} are assigned to the vibrations of skeletons of systems X-$CHMe_2$ and X-CMe_3 respectively, force constant calculations on systems with X of infinite mass being said to confirm these assignments.† It is felt that they are incorrect, and that further work on these lines will lead to confusion. There is a fairly constant pair of frequencies at about 1135, 1180 cm^{-1} in the N-paraffins, and a very close pair of fairly strong bands at about 1147, 1155 cm^{-1} in 3-methyl paraffins. Again, a pair at about 1200–1210 cm^{-1} and 1250–1260 cm^{-1} can be found in the N-paraffins; in the 3-methyl compounds a pair at about 1200, 1280 cm^{-1} becomes evident with a primary chain longer than eight carbon atoms, appearing to arise from a single band at 1250 cm^{-1} in the shorter chains. There is thus no evidence for the assignments of 1145, 1170 cm^{-1} and 1200, 1250 cm^{-1} to skeletal vibrations of X-$CHMe_2$ and X-CMe_3 respectively. The former pair appears more likely to be due to methyl rocking; in polyisobutene there is rather an indefinite maximum at 1160 cm^{-1}, and there is a band in this region in hydro-rubber; also in crepe rubber, and, more intense, in methyl rubber.[6] The bands in the N-paraffins decrease in intensity with increasing chain-length. The region 1200–1300 cm^{-1} is the expected one for CH_2 bending parallel to the chain; in a long chain there is the one maximum at 1295 cm^{-1} and lower frequencies appear, first as shoulders to this band, as the chain-length decreases. The single strong sharp maximum in polyisobutene may perhaps be due to the CH_2 groups being non-adjacent in a chain with a preferred locked configuration.

The following argument should be considered. In a chain made up of N identical (repeated) units, if the vibrational displacement coordinates for any isolated link are Δ_1 to Δ_n, then the displacements in the chain are $\Delta_j e^{im\theta}$ ($j=1$ to n), for the mth unit ($m=1$ to N); $i^2=-1$ and θ is the phase difference between corresponding displacements in adjacent units. For stable (normal) vibrations, $0=\pi/N$. The secular equation for the vibrations can be reduced to order n[4,7] and the normal coordinates written

$$\eta_k=(\sum_{j=1}^{n} c_{kj}\Delta_j)e^{im\theta}.$$

Clearly, the allowed fundamentals in a chain of N units will be made up of the frequencies characteristic of lengths corresponding to all factors of N, plus frequencies first found in the N-chain (equal in number to the number of primes from 1 to N which are not factors of N, multiplied by the number of coordinates per chain-link, n). This argument is quite general. The exact result will never apply because of complications introduced with rotational isomerism. But it may be used to explain away the remarkable number of frequency-correlations found in the infra-red spectra of the paraffin hydrocarbons.

[1] The infra-red spectra are conveniently collected in the "Catalog of Infra-Red Spectrograms," American Petroleum Institute, Research Project 44. Raman frequencies are given by Kohlrausch, and there are other more recent data, e.g., reference 4.

[2] Barriol and Chapelle, J. Phys. Radium **8**, 8 (1947).

[3] G. B. B. M. Sutherland and N. Sheppard, Nature (London) **160**, 739 (1947).

[4] T. Simanouti and S. Mizushima, J. Chem. Phys. **17**, 1102 (1949).

[5] G. B. B. M. Sutherland and D. M. Simpson, Proc. Roy. Soc. **A199**, 169 (1949).

† The author carried out a frequency-prediction for the system X-CMe_3 ($m_X=\infty$), and found the following values: A_1: 1105, 603, 199 cm^{-1}; E: 1282, 425, and 310 cm^{-1}, with $k_{C-C}=4.65$, $f_{CCC}=0.45$, $\times 10^5$ dynes/cm. The characteristic frequencies for the system would be 1105 and 1282 cm^{-1}. This does not agree with Sutherland and Simpson (see reference 5).

[6] H. W. Thompson and P. Torkington, Proc. Roy. Soc. **A184**, 3 (1945); Trans. Faraday Soc. **41**, 246 (1945).

[7] E. Bartholome and E. Teller, Zeits. f. Physik. Chemie **B19**, 366 (1932); J. G. Kirkwood, J. Chem. Phys. **7**, 506 (1939); Whitcomb, Nielsen, and Thomas, J. Chem. Phys. **8**, 143 (1940).

Isothermal Rate of Solidification of Small Droplets of Mercury and Tin

D. TURNBULL
Research Laboratory, General Electric Company, Schenectady, New York
March 13, 1950

AGGREGATES of mercury droplets were prepared by agitating pure mercury and a 0.01 molar solution of stearic acid in white mineral or Cenco pump oil with a Waring blendor. The mean volume, v, of the droplets corresponded to a diameter of about 3.8 microns. After changing the medium of dispersion from oil to methyl cyclopentane (this had no detectable effect on the particle-size distribution) the solidification of aggregates of these droplets was followed dilatometrically.

In continuous cooling experiments (0.5°/min.) most of the droplets solidified between −98 and −102°. The progress of solidification with time was followed at four constant (±0.01°) temperatures in the range −98.5 to −100°.

After plotting the fraction solidified, X, against time, t, the slope dX/dt, was measured at various constant fractions of transformation between 0.30 and 0.45. If it is assumed that v equals the root-mean-square volume of the droplets that have not solidified the nucleation frequency, I cm^{-3} $sec.^{-1}$ can be written $I=dX/vdt(1-X)$. The absolute value of $\log I$ may be in error by as much as 0.3 because of the assumption, but the dependence of $\log I$ upon temperature is not affected by it provided I at the various temperatures is measured for a constant fraction transformed.

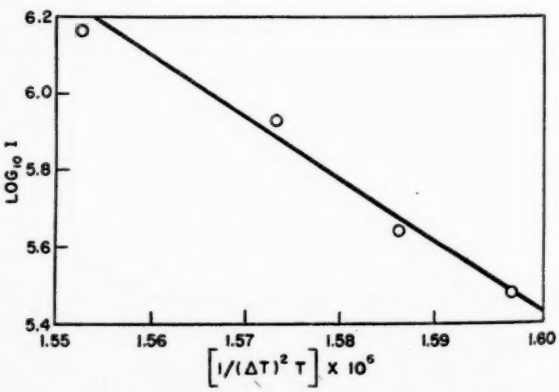

FIG. 1. Log$I$ *vs.* $1/(\Delta T)^2T$ for aggregate of mercury droplets at 40 percent solidification.

According to the theory of homogeneous nucleation for liquid-crystal reactions[1]

$$I=n(kT/h)\exp[-\Delta F_A/kT]\exp[-16\pi\sigma^3T_0^2/3\lambda^2(\Delta T)^2kT] \quad (1)$$

where n=number of atoms in the sample, ΔF_A=free energy of activation for transport across the liquid-solid interface, σ=interfacial energy between crystal nucleus and liquid, T_0=melting temperature °K, λ=heat of fusion/volume, and ΔT=supercooling. In the derivation of (1) it was assumed that the crystal nucleus is spherical and that the entropy of fusion is constant. Since the variation of $\exp(-\Delta F_A/kT)$ is small in the narrow temperature range, $\log_{10}I$ should be a linear function of $1/T(\Delta T)^2$. Straight lines having slopes that agree within experimental error are obtained for mercury when $\log I$ is plotted against $1/T(\Delta T)^2$ at constant fractions of solidification between 0.30 and 0.45. The line for 0.40 fraction solidified is shown in Fig. 1.

Isothermal rates of solidification of oxide-coated tin droplets measured by Vonnegut[2] were analyzed in the same way at $33\frac{1}{3}$ percent transformation. Within the experimental uncertainty $\log I$ was a linear function of $1/T(\Delta T)^2$.

The constants of Eq. (1) that reproduce the experimental results for tin and mercury at 0.40 transformation are given in Table I.

TABLE I.

Element	σ ergs/cm²	$B=(nkT/h)\exp(-\Delta F_A/kT)$ cm⁻³ sec.⁻¹ Observed	Calculated
Mercury	24.0	$10^{30.9}$	10^{33}
Tin	52.5	$10^{30.4}$	$10^{33.5}$

It is assumed that ΔF_A is identical to the free energy of activation for viscous flow so that $\exp[-\Delta F_A/kT]\approx 10^{-2}$.

Considering the experimental and theoretical uncertainties, the observed values of B are in satisfactory agreement with values calculated from nucleation theory.[1] A more complete description of the experiments and their analysis is to be published.

The writer gratefully acknowledges the valuable advice and assistance of B. Vonnegut in the preparation of the mercury dispersions and of Mr. E. F. Fullam in the particle-size determination. He also thanks Mr. W. A. Rocco for his assistance in the experiments.

[1] D. Turnbull and J. C. Fisher, J. Chem. Phys. 17, 71 (1949).
[2] B. Vonnegut, J. Colloid Sci. 3, 563 (1948).

Correlation of Liquid-Solid Interfacial Energies Calculated from Supercooling of Small Droplets

D. TURNBULL
Research Laboratory, General Electric Company, Schenectady, New York
March 13, 1950

IT has been shown[1] that the isothermal rates of solidification of mercury and tin droplets can be described approximately by an expression for the frequency of formation of crystal nuclei/volume, I, derived from homogeneous nucleation theory which is

$$I=n(kT/h)\exp[-\Delta F_A/kT]\exp[-16\pi\sigma^3T_0^2/3\lambda^2(\Delta T)^2kT]. \quad (1)$$

The symbols have been defined previously.[1] There are two unknown parameters in (1) the liquid-solid interfacial energy, σ and $\exp(-\Delta F_A/kT)$. However, for most metals $\exp(-\Delta F_A/kT)$ is of the order of 10^{-2}. Therefore, σ can be calculated from the value of I at one temperature.

The maximum supercooling, ΔT, at solidification of small droplets of several other metals have been measured by dilatometric and microscopic techniques.[2-5] Volumes of the droplets corresponded to a diameter of the order of 50 microns, and at a supercooling of ΔT given in Table I the nucleation frequency was $\approx 10^{-1\pm1}$ sec.$^{-1}$. Values of σ were calculated from these data and are listed in Table I. Because of the approximate agreement between theory and experiment and the uncertainty in the measured nucleation frequencies (excepting mercury and tin), it seems possible that

$$[nkT/Ih]\exp[-\Delta F_A/kT]=B/I$$

used in these calculations may be in error by a factor $\sim 10^4$. However, this degree of uncertainty in B/I can cause an error of only four percent in the calculated value of σ. For consistency, σ-values for mercury and tin given in Table I have been calculated from (1). The difference between these values and those calculated from the isothermal experiments[1] is small.

TABLE I.

Metal	ΔT^0	σ ergs/cm²	$\sigma_g/\Delta H_f$
Mercury[a]	58	24.4	0.53
Gallium[b]	76	56	0.44
Tin[c]	105	54.5	0.42
Bismuth[b]	90	54	0.33
Lead[b]	80	33	0.39
Antimony[d]	135	101	0.30
Germanium[d]	227	181	0.35
Silver[d]	227	126	0.46
Gold[d]	230	132	0.44
Copper[d]	236	177	0.44
Manganese[d]	308	206	0.48
Nickel[d]	319	255	0.44
Cobalt[d]	330	234	0.49
Iron[d]	295	204	0.45
Palladium[d]	332	209	0.45
Platinum[e]	370	240	0.46

[a] See reference 1.
[b] See reference 2.
[c] See reference 4.
[d] See reference 3.
[e] See reference 5.

By assuming arbitrarily that the liquid-nucleus interface is 1 atom thick "gram-atomic" interfacial energies, σ_g, have been calculated using the following relations:

$$\sigma_g=A\sigma=N^{\frac{1}{3}}V^{\frac{2}{3}}\sigma,$$

where A is the area of interface containing Avogadro's number of atoms and V is the gram-atomic volume of the crystal at the solidification temperature. A factor of the order of unity that depends on the packing in the interface has been neglected.

σ_g and the ratios $\sigma_g/\Delta H_f$, where ΔH_f is the gram-atomic heat of fusion, are given in Table I. $\sigma_g/\Delta H_f$ is nearly constant, 0.45, with a mean deviation of ± 0.02 for most of the metals. However, for antimony, bismuth, and germanium it is 0.33 ± 0.02.

An empirical correlation of the data equivalent to the $\sigma_g/\Delta H$ correlation is:

$$[(\Delta T/T_0)^2(T_0-\Delta T)/\Delta H_f]^{\frac{1}{3}}=\text{constant}. \quad (2)$$

A corollary of the experimental results and their interpretation is that the nucleation frequency in large continuous masses (e.g., 1 cc) of liquid metals completely free of nucleation catalysts and not subject to mechanical vibration should be the same as in 50 micron droplets at a supercooling of $\sim 0.85\Delta T$. The reason that large masses rarely supercool more than about $(1/10)\Delta T$ may be explained on the basis that the probability of finding a nucleation catalyst increases directly with the volume of the continuous mass.

It appears that the effect of the structure of the forming crystal upon the nucleation frequency is primarily a reflection of its effect upon the heat of fusion. To what extent the parameter σ can be identified with the interfacial energy of extensive liquid-crystal interfaces is considered in a more detailed article that is to be published.

[1] D. Turnbull, J. Chem. Phys. 18, 768 (1950).
[2] D. Turnbull (to be published).
[3] D. Turnbull and R. E. Cech (to be published).
[4] B. Vonnegut, J. Colloid Sci. 3, 563 (1948).
[5] C. E. Mendenhall and L. R. Ingersoll, Phil. Mag. 15, 205 (1908).

Sulfide in Zinc-Oxide Luminophors

S. MILTON THOMSEN
Radio Corporation of America, RCA Laboratories Division, Princeton, New Jersey
March 30, 1950

THE green luminescence emission observed in luminophors made by firing zinc oxide in hydrogen,[1] consisting of a characteristic broad band,[2] has been attributed to the presence of "excess" or "free" zinc[3] as an activator.

Two facts leave little doubt that the presence of a small amount of sulfide (zinc sulfide in solid solution), rather than free zinc, is necessary to obtain the observed green emission: (1) Reagent grades of zinc oxide contain approximately 0.01 percent zinc sulfate, which is reduced to zinc sulfide during the hydrogen-firing. The sulfide can be detected (by the plumbite-paper test) in the luminescent product. (2) Without the use of hydrogen or other reducing agent (to produce the postulated free zinc), zinc-oxide luminophors having this same green emission can be produced by mixing with zinc oxide a small amount of sulfide-introducing agent, such as zinc sulfide, sulfur, sodium thiosulfate or ammonium sulfide, and firing the mixture in a vessel with a close-fitting cover.

Further support is given by the fact that the substitution of zinc selenide for the small addition of zinc sulfide gives a zinc-oxide luminophor with an orange emission.

[1] E. Beutel and A. Kutzelnigg, Monatshefte f. Chemie **61**, 437 (1932).
[2] R. E. Shrader and H. W. Leverenz, J. Opt. Soc. Am. **37**, 939 (1947).
[3] A. Schleede, Angew. Chemie **50**, 1908 (1937).

Nitrogen Pentoxide Formation in the Oxygen-Nitric Oxide Reaction

RICHARD A. OGG, JR.*
Mallinckrodt Chemical Laboratory, Harvard University, Cambridge, Massachusetts
March 31, 1950

THE standard free energy change of the reaction

$$2NO+\tfrac{3}{2}O_2 \rightarrow N_2O_5 \qquad (I)$$

may be found from the well-known thermodynamic properties of NO and O_2, together with the heat of formation[1] of N_2O_5, and a reasonable estimate of the standard entropy of the latter as close to that of N_2O_4. This calculation indicates that at room temperature and partial pressures of the order of a few hundred millimeters of mercury the above reaction should proceed practically to completion. Extension of previous kinetic considerations[1-3] leads to the expectation that under proper conditions the rate of the above process may be such as to cause significant competition with the reaction

$$2NO+O_2 \rightarrow 2NO_2 \qquad (II)$$

hitherto considered the sole process in this reacting system.

The proposed mechanism for reaction (I) is as follows:

$$NO_2+O_2+NO \rightarrow NO_3+NO_2 \quad k_a \qquad (a)$$
$$NO_3+NO_2 \rightarrow N_2O_5 \quad k_b \qquad (b)$$
$$NO_3+NO \rightarrow 2NO_2 \quad k_c. \qquad (c)$$

Step (a) is seen to be the reverse of step (3) in the mechanism of nitrogen pentoxide decomposition,[1,2] whereas steps (b) and (c) are identical respectively with (2) and (4) of that mechanism. By familiar steady-state considerations the resulting rate expression is

$$\frac{d(N_2O_5)}{dt}=\frac{k_a(NO_2)(O_2)(NO)}{1+k_c(NO)/k_b(NO_2)}.$$

Comparison of this with the well-known termolecular rate expression for reaction (II) indicates that the conditions favorable to occurrence of reaction (I) involve a small concentration of NO and a large concentration of NO_2. A further point of importance concerns the quasi-bimolecular character[2] of step (b). In order to make the effective value of k_b as great as possible, the concentration of molecules effective for collisional deactivation should be large—it is desirable to add a chemically indifferent foreign gas in large quantity.

Experimental verification of the above predictions regarding formation of nitrogen pentoxide has been obtained, the characteristic infra-red absorption spectrum[3] being used for detection and quantitative estimation. The spectrometer and cells were the same as previously described.[3] Both the strong band at about 1350 cm^{-1} and a weaker one at about 860 cm^{-1} were used. The latter is completely resolved from bands of NO_2 and N_2O_4, even at the highest concentrations of the latter substances. The former is partially obscured by a neighboring N_2O_4 band, but use of a compensating cell filled with the proper amount of N_2O_4 and placed in the other beam of the spectrometer satisfactorily eliminates this interference. (A similar procedure was used to eliminate partial obscuring of the 860 cm^{-1} band by overlapping bands of SF_6.) The absorption cell was filled at room temperature with a mixture (in measured amounts) of NO, $NO_2-N_2O_4$ and either CO_2 or SF_6. A large reservoir space adjacent to the cell was then filled with pure oxygen at atmospheric pressure. By opening a large bore stopcock, oxygen was admitted as rapidly as possible to the gas mixture, the initial pressure being chosen so that oxygen was finally present in considerable stoichiometric excess. The chemical changes were completed in a few seconds. After closing the stopcock the infra-red spectrum was traced.

These studies have shown unequivocally that N_2O_5 is formed in significant amounts. In a typical case, the initial partial pressure of NO was 100 mm Hg, while those of N_2O_4 and SF_6, respectively, were some 100 mm and 300 mm Hg. After admission of oxygen to a total of one atmosphere pressure, the partial pressure of N_2O_5 proved to be some 10 mm Hg—a yield of 20 percent. Variation of yields with initial NO_2 concentration followed the general course predicted by the above rate expression. For otherwise constant conditions, the efficacy of added gases in promoting N_2O_5 formation increased sharply in the order O_2, CO_2, SF_6—the last being especially effective. This variation is excellent evidence for the quasi-bimolecular character of step (b). The high efficiency of SF_6 is expected in view of the large number of internal degrees of freedom available for collisional deactivation. Analysis of the yield data so far obtained indicate that the termolecular rate constant for step (a) cannot differ greatly in magnitude from that for the well-known reaction (II)—this comparison applying at some 300° Kelvin. The previous considerations[1] suggest that k_a has a nearly negligible temperature coefficient.

* Currently on leave from Stanford University, California.
[1] R. A. Ogg, Jr., J. Chem. Phys. **15**, 613 (1947).
[2] R. A. Ogg, Jr., J. Chem. Phys. **18**, 572 (1950).
[3] R. A. Ogg, Jr., W. S. Richardson, and M. K. Wilson, J. Chem. Phys. **18**, 573 (1950).

Influence of Molecular Structure of Ethylene Chloride on Ion-Association of Dissolved Salts

J. T. DENISON AND J. B. RAMSEY
Department of Chemistry, University of California, Los Angeles, California
March 31, 1950

BJERRUM[1] has derived an equation relating the thermodynamic dissociation constant, K, of an electrolyte to the temperature, the dielectric constant, D, of the solvent and the contact distance, a, of the two oppositely charged ions. A simple model is assumed in which the only force of interaction between

TABLE I.

Salt	$K\times10^5$ at 25°C In ethylene chloride	In ethylidene chloride
o-chloro	[a]3.92 ±0.12	0.414 ±0.010
o-methoxy	7.85 ±0.25	1.12 ±0.020
m-methoxy	3.89 ±0.12	0.415 ±0.010

[a] Recalculated from data of Ramsey and Colichman by use of method of least squares to establish more precisely the linear relation between the functions involved.

the ions is Coulombic and the ions are considered to be rigid unpolarizable spheres in a continuous medium of uniform dielectric constant equal to the macroscopic dielectric constant of the pure solvent. For a uni-univalent electrolyte, this equation takes the form

$$K^{-1}=\frac{4\pi N}{1000}\left(\frac{\epsilon^2}{DkT}\right)^3 Q(b),$$

in which

$$b=\frac{\epsilon^2}{aDkT} \quad \text{and} \quad Q(b)=\int_2^b e^y y^{-4}dy$$

where $y=\epsilon^2/(rDkT)$. Other symbols have their usual meaning.

That deviations from this equation will occur for systems which differ appreciably from the idealized model is expected. An apparent deviation has been reported by Ramsey and Colichman.[2] They found the dissociation constant at 25°C of *o*-chlorophenyltrimethylammonium perchlorate in ethylene chloride (1,2-dichloroethane) to be approximately tenfold greater than in ethylidene chloride (1,1-dichloroethane). Since the dielectric constants of these solvents at 25°C are approximately equal, 10.23 for ethylene chloride and 10.00[3] for ethylidene chloride, and since there is no apparent reason why the *a*-values of this salt should be appreciably different in these two very similar solvents, this large difference in *K*-values seems anomalous. The fact that the product, $\Lambda_0\eta$, of this salt has the same value within experimental error in these two solvents lends support to the conclusion that its *a*-values should be substantially the same.

In order to establish with certainty that a large difference in the *K*-values of a given salt in these two solvents exists, the *K*-value of the ortho-chloro salt in ethylidene chloride and those of the ortho-methoxy and meta-methoxy salts in ethylene chloride have been redetermined. In addition the *K*-values of the two methoxy salts were determined in ethylidene chloride. Shedlovsky's[4] modification of the Fuoss and Kraus[5] conductance equation was used in obtaining these *K*-values, given in Table I.

Since the *K*-values of each of these three salts is very much (from seven to ten times) larger in ethylene chloride than in ethylidene chloride, it seems probable that these differences should be attributable to certain fundamental differences in these two solvents which are not apparent from their macroscopic properties.

On the basis of the reasonable assumption that the *a*-value of each of the salts is the same in these solvents it follows from the above equation that the large difference in *K*-values may be due to a difference between the macroscopic dielectric constant of at least one of the solvents and its effective dielectric constant, that is, the dielectric constant which is effective in determining the stability of the associated ion-pair of an electrolyte in that solvent. The conclusion that such a difference does not exist in ethylidene chloride solution is justified by the fact that the molecules of this solvent are known to exist in but one form. However, the results of a number of investigations have established the existence of restricted rotation about the carbon-carbon bond in the molecules of ethylene chloride which consists of three potential minima, 120° apart, in one complete rotation about this bond axis. From a study of the relative intensities of certain Raman lines in the vapor and liquid phases of ethylene chloride, Mizushima *et al.*,[6] have estimated the equilibrium ratio of the number of molecules in the gauche forms (an angle of 60° between the C—Cl bonds viewed along the C—C bond axis) to the number in the *trans*-form (180° between the C—Cl bonds) to be 1.3:1 in liquid ethylene chloride at 25°C. They have also calculated the dipole moment of the gauche forms (one the mirror image of the other) to be 2.55×10^{-18} e.s.u. For comparison the dipole moment of ethylidene chloride molecules, determined by Ghosh *et al.*,[7] is 2.045×10^{-18} e.s.u.

The existence of these two isomers of ethylene chloride, the polar (the two gauche forms) and the non-polar (*trans*-) form leads to the conclusion that an ion in ethylene chloride will attract preferentially the gauche molecules and thereby produce an enhancement of the relative population of this form (N_g/N_t) in the near vicinity of the ion above the average in the pure solvent. This long-range ion-dipole interaction would make the effective dielectric constant in ethylene chloride greater than the macroscopic dielectric constant of this solvent and thus cause the measured *K*-value to be greater than that calculated by the above equation by use of the macroscopic dielectric constant and the correct *a*-value.

An independent method of determining the correct value of the parameter *a* to be used in the above equation is not in general available. However, the assumption that the *a*-value of a salt in ethylene chloride is the same as it is in ethylidene chloride provides, in this case, an independently determined *a*-value to be used for a given salt in ethylene chloride. The *a*-value found for each of the salts (in the order given in Table I) in ethylidene chloride are 3.50×10^{-8} cm, 3.85×10^{-8} cm and 3.50×10^{-8} cm, respectively. On substitution of the *a*-value, thus obtained, and the corresponding *K*-value, determined in ethylene chloride, the effective dielectric constant of ethylene chloride, consistent with these values, is evaluated by successive approximations. The average of the two values of the effective dielectric constant thus obtained is 11.9±0.1. The *K*-values of these three salts in ethylene chloride calculated by use of 11.9 for *D* are 3.82×10^{-5}, 8.18×10^{-5}, and 3.82×10^{-5}, respectively. These values are seen to agree within experimental error with those measured.

That the effective dielectric constant of ethylene chloride in the near vicinity of an ion may be as much as 1.7 units greater than its macroscopic dielectric constant (10.23) is indicated by the crude value of 15.5 (calculated) for the dielectric constant of the pure liquid gauche form by Onsager's equation, approximating its density and refractive index to be those of ethylene chloride.

[1] N. Bjerrum, Kgl. Danske Vidensk. Selskab. **7**, No. 9 (1926); see also R. M. Fuoss and C. A. Kraus, J. Am. Chem. Soc. **55**, 1019 (1933).
[2] J. B. Ramsey and E. L. Colichman, J. Am. Chem. Soc. **69**, 3041 (1947).
[3] Private communication from Arthur E. Martell, Chemical Laboratories, Clark University, Worcester, Massachusetts. Measured at Brown University, Providence, Rhode Island.
[4] T. Shedlovsky, J. Frank. Inst. **225**, 739 (1938).
[5] R. M. Fuoss and C. A. Kraus, J. Am. Chem. Soc. **55**, 476 (1933); R. M. Fuoss, *ibid.* **57**, 488 (1935).
[6] Mizushima, Morino, Watanabe, Simanouti, and Yamaguchi, J. Chem. Phys. **17**, 591 (1949).
[7] Ghosh, Mahauti, and Sen-Gupte, Zeits. f. Physik **54**, 711 (1929).

Calculation of the Heats of Formation of Alkali Halide Solid Solutions from Hildebrand's Equation

MORTON FINEMAN
Sprague Electric Company, North Adams, Massachusetts
March 27, 1950

HILDEBRAND[1] has derived the expression

$$\Delta H_f=\left(\frac{N_1V_1N_2V_2}{N_1V_1+N_2V_2}\right)\left[\left(\frac{\Delta E_1}{V_1}\right)^{\frac{1}{2}}-\left(\frac{\Delta E_2}{V_2}\right)^{\frac{1}{2}}\right]^2 \quad (1)$$

for the change in heat content on forming one mole of a solution from the pure liquids. ΔE, V, and N are the heat of vaporization, the molar volume and mole fraction, respectively, of the component liquids. In deriving the above equation the important

TABLE I. Heats of sublimation, molar volumes and solubility parameters of alkali halides.

Salt	ΔH_{sub}[a](cal./mole)	V^0(cm³/mole)	δ(cal./cm³)$^{\frac{1}{2}}$
NaCl	182,800	27.02[b]	82.25
NaBr	173,300	32.10[b]	73.48
KCl	164,400	37.52[c]	66.19
KBr	156,200	43.31[c]	60.05
RbCl	160,500	43.22[c]	60.94

[a] F. Seitz, *The Modern Theory of Solids* (McGraw-Hill Book Company, Inc., New York, 1940), p. 80.
[b] Nickels, Fineman, and Wallace, J. Phys. and Colloid Chem. **53**, 625 (1949).
[c] *International Critical Tables* (McGraw-Hill Book Company, Inc., New York, 1933).

TABLE II. Heats of formation of alkali halide solid solutions.

	ΔH_f (cal./mole of ion pairs)			
	Obs.	Calc. (Eq. (1))	Calc.[a] (Wallace)	Calc.[b] (Tobolsky)
		NaCl-NaBr		
Mole fraction NaCl				
0.75	257	442	440	
0.50	335	564	540	118
0.25	241	406	380	
		KCl-KBr		
Mole fraction KCl				
0.75	186	295	360	
0.50	232	379	450	94
0.25	163	274	300	
		RbCl-KCl		
Mole fraction				
0.50	203	277	400	83
		NaBr-KBr		
Mole fraction				
0.50	700	1660		480
		NaCl-KCl		
Mole fraction				
0.50	1050	2025		594

[a] See reference 2.
[b] See reference 7.

assumptions made are:[1] (1) the intermolecular forces are radially symmetrical, (2) the repulsive forces approach zero very rapidly with distance, (3) the constants of attraction between unlike molecules are the geometric mean between those for the like molecules and (4), thermal agitation maintains complete random mixing of the two components.

Equation (1) should apply not only to liquid solutions but solid solutions which fulfill the above conditions. There are now available in the literature[2] reliable data on the heats of formation of solid solutions of alkali halides as well as computed values from the older Born[3] and the newer Born-Mayer[4] model for ionic solids. It is of interest to calculate the ΔH_f of these same systems by Eq. (1) for comparison with experimental and computed values.

In the present model of ionic solids assumptions 1 and 2 above are made. However, in the case of solid solutions of ionic substances the assumptions concerning the constants of attraction cannot be rigorously justified but may be approximated by the geometric mean. As for the fourth assumption, it has often been assumed[5] that in ionic solid solutions in which the components are sufficiently alike, there is a random distribution of the particles over the lattice sites. This assumption has been verified by Eastman and Milner[6] for one case—a AgCl-AgBr solid solution.

To apply Eq. (1) to solid solutions of ionic substances, the various terms now refer to the pure component ionic solids. The ΔE term is no longer the heat of vaporization, but the heat of sublimation of the pure salt to an infinitely dilute gas of the ions. The values of ΔE and V as well as the solubility parameters $[\delta=(\Delta E/V)^{\frac{1}{2}}]$ for the alkali halides to be considered are listed in Table I.

Table II contains the experimental heats of formation for several solid solutions of alkali halides and the computed values from Eq. (1), as well as those computed by Wallace[2] and by Tobolsky.[7] The values obtained using the simple Hildebrand equation, although larger than the observed values, are of the same order of magnitude. It is of further interest to note that the computed values from Eq. (1) agree with experiment as well as those calculated from the more refined but tedious methods of Wallace and of Tobolsky.

[1] J. H. Hildebrand, *Solubility of Non-Electrolytes* (Rheinhold Publishing Corporation, New York, 1936).
[2] W. E. Wallace, J. Chem. Phys. **17**, 1095 (1949).
[3] *Handbuch der Physik*, XXIV/2, 623 (1933).
[4] M. Born and J. E. Mayer, Zeits. f. Physik **75**, 1 (1932).
[5] M. A. Fineman and W. E. Wallace, J. Am. Chem. Soc. **70**, 4165 (1948).
[6] E. D. Eastman and R. T. Milner, J. Chem. Phys. **1**, 444 (1933).
[7] A. V. Tobolsky, J. Chem. Phys. **10**, 187 (1942).

Passivation of Metals*

RUDOLPH SPEISER, F. H. BECK, M. G. FONTANA, AND E. N. LASSETTRE**
The Ohio State University, Columbus, Ohio
March 27, 1950

THE passivation of some metals by films of substances such as O_2 and the stability of these films in a corroding medium might be explained on the basis of the band theory of metals and surface thermodynamics.

It can be shown from the band theory of metals[1] that the consideration of a real crystal as a finite lattice leads to the existence of surface states. Shockley[2] has shown that the surface states occur near the overlapping bands of all metals. These surface states can be looked upon as residual valences of the metal. Saturated molecules such as N_2 and CO_2 are polarized by the surface of the metal and are held by van der Waals forces (physical adsorption). The heats of adsorption of these substances are relatively low and can be estimated by several theoretical[3] methods and directly measured.

Stronger interaction with the surface states is possible with molecules which have unpaired electrons such as O_2 and NO. (O_2, $^3\Sigma$ in the ground state is paramagnetic; NO has an odd number of electrons, is paramagnetic and behaves under many circumstances as a free radical.) Molecules of this type can be considered as having residual valences. The residual valences of the metal can be saturated by the residual valences of these molecules leading to much stronger bonds between the metal and O_2 and NO than is obtained between N_2 and CO_2. This increased bonding strength leads to the passivation† of certain metals by O_2 and NO films, whereas the films of saturated molecules such as N_2 and CO_2 are ineffective.

In general, it would be expected that the strongest bonding (due to these residual valences) would be exerted by the transition metals (due to contributions of the *d*-orbitals), hence metal alloys such as stainless steel are effectively passivated by O_2 and NO.

The behavior of passive films immersed in corroding media is readily explained by the thermodynamics of surface equilibria:

If γ_{so}†† is the interfacial tension between the metal and the passivating film. γ_{sc} the interfacial tension between the metal and the corroding medium and γ_{oc} the interfacial tension between the film and the corroding medium, then the following inequalities can be written:

If

$$\gamma_{sc} \geqslant \gamma_{so} + \gamma_{oc}, \tag{1}$$

then the passivating film is stable in presence of the corroding medium and the film is protective because the corroding medium has no tendency to wet the metal surface.

If

$$\gamma_{so} \geqslant \gamma_{sc} + \gamma_{oc}, \tag{2}$$

then the passivating film is unstable or metastable in the presence

of the corroding medium and the corroding medium has a tendency to wet the metal surface.

If the passivating film is metastable an activation process such as mechanical abrasion is necessary to cause the system to go to equilibrium, that is, to the state where the corroding medium wets the metal surface. When this occurs the metal surface becomes active. Under these conditions, failure of the film in one spot may lead to a nearly catastrophic replacement of the passivating film by the corroding medium.¶

Solutes can be added to the corroding medium that can either raise or lower the interfacial tension between the passivating film and the corroding medium and thus increase or decrease the stability of the passivating film. The Gibbs adsorption isotherm gives the relation between the change in surface tension and the positive or negative adsorption of a component of a solution at an interface.

$$d\gamma = -\Gamma RT \cdot dlna, \qquad (3)$$

where a is the activity of the solute in the solution, Γ the excess or deficiency of the solute in the interface over that in the solution. A deficiency of solute at the interface will lead to an increase in the surface tension. It follows from the nature of this phenomenon that a dissolved substance can lower the surface tension markedly but raise it only a slight degree.

The decrease in the protective property of a film with increasing temperature is simply explained by the decrease in stability of the film with increasing temperature and also by the more rapid decrease of surface tension of the corroding material than the surface tension of the protecting film.

* This work was done under contract between the ONR and The Ohio State University Research Foundation. (Contribution from the Department of Metallurgy.)

** Professor of Chemistry, Department of Chemistry.

[1] F. Seitz, *Modern Theory of Solids* (McGraw-Hill Book Company, Inc., New York, 1940), p. 320.

[2] W. Shockley, Phys. Rev. **56**, 317 (1939).

[3] S. Brunner, *The Adsorption of Gases and Vapors* (Princeton University Press, Princeton, 1943), Chapter VII.

† Experiments in this laboratory (to be published soon) show that pure NO and O_2 gases passivate stainless steel, whereas N_2, H_2, helium, and argon are ineffective.

†† For unit area of interface, γ_{so}, γ_{sc} and γ_{oc} are the free energies.

¶ This behavior is very much like the rapid crystallization of a supercooled liquid when seeded with a crystal.

The Cubic Secular Equation for Molecular Vibrations

P. TORKINGTON
British Rayon Research Association Laboratories, Urmston, Lancashire, England

March 30, 1950

SOME attention has been paid recently to the problem of solving the secular equation for molecular vibrations to give the force constants. It has been found possible to give an explicit solution which can, if desired, be used as a starting-point in the general case,[1] and complete solutions are now available for the second-degree equation.[2] In the present communication the solution of the cubic equation is approached from a point of view which may prove rather illuminating; it arose from a consideration of the potential function of tetrachloroethylene. This molecule has been treated several times. Early work suggested that the force constant of the C=C bond was abnormally low;[3,4] a later analysis of Duchesne[5] showed that if interactions between C=C stretching and C−Cl stretching, and between C=C stretching and Cl−C−Cl deformation were assumed to exist, then a range of values of the C=C stretching constant could be obtained by varying the interaction constants. For the C=C bond to be normal, the interaction constants had to be both positive, the first being quite large (of the order 1.5×10^5 dynes/cm); it is now known that there is some theoretical basis to this assumption, from an analysis of the electronic structure of conjugated systems.[6] Recently, a more complete normal coordinate analysis of tetrachloroethylene has been carried out.[7] In treating the A_g factor it was found that the solutions allowed to the three constants mentioned above lay on closed curves when the three pairs were plotted against each other. Thus in addition to the solutions given by Duchesne[5] there is another set; this corresponds to the interaction constants being both negative, that for $\Delta r_{C=C}\cdot\Delta r_{C-Cl}$ being much smaller than in the previous set ($\sim-0.2\times10^5$ dynes/cm). It is accepted that there is a negative constant for the interaction $\Delta r_{C=C}\cdot\Delta\theta_{CH_2}$ in ethylene;[8,9] a negative*,[10] constant for $\Delta r_{C=C}\cdot\Delta r_{C-H}$ interaction has also been reported for this molecule.[11] It may seem therefore more consistent to take the negative pair of constants for C_2Cl_4; otherwise it must be assumed that substitution of chlorine for hydrogen changes the sign of the interactions.

The above considerations are clearly quite general. For a cubic secular equation, if subscripts 1, 2, and 3 refer to the three coordinates, and if A and d are the matrices of the kinetic energy elements and force constants, then the following relations hold:

$$A_{11}d_{11}+A_{22}d_{22}+A_{33}d_{33}+2A_{12}d_{12}+2A_{13}d_{13}+2A_{23}d_{23}=\lambda_1+\lambda_2+\lambda_3 \qquad (1)$$

$$(|A|_{11})(|d|_{11})+(|A|_{22})(|d|_{22})+(|A|_{33})(|d|_{33})+2(|A|_{12})(|d|_{12})+2(|A|_{13})(|d|_{13})+2(|A|_{23})(|d|_{23})=\lambda_1\lambda_2+\lambda_1\lambda_3+\lambda_2\lambda_3 \qquad (2)$$

$$(|A|)(|d|)=\lambda_1\lambda_2\lambda_3 \qquad (3)$$

where $|A|_{ij}$ and $|d|_{ij}$ are minors of the determinants $|A|$ and $|d|$. If elements in the first row of d are taken as variables (in the case of C_2Cl_4 the remainder are carried over from the B_{3u} factor, Δ_1 being the C=C stretching coordinate), then elimination of d_{11} from (2) and (3) gives two simultaneous homogeneous second-degree equations in d_{12} and d_{13} for which the quantity $(ab-h^2)$ is respectively $\{(|A|_{22})(|A|_{33})-(|A|_{23})^2\}$ and $(d_{22}d_{33}-d_{23}^2)$. The first must necessarily be positive, being $A_{11}(|A|)$, and the second will be positive in all real cases (it must necessarily be positive here since it is from a second-degree factor). Both equations are therefore those of ellipses; allowed values of d_{22}, d_{33} and d_{23} will be those for which real intersection occurs, solutions of d_{12} and d_{13} being those for the points of intersection. Since real intersection of closed curves can only occur within a given field, the allowed solutions of d_{12} and d_{13}, and therefore of d_{11}, from (1), will also lie on closed curves when plotted against each other, in pairs.

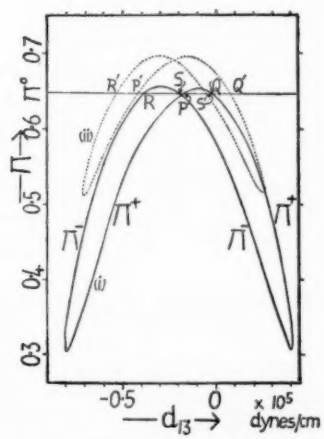

FIG. 1. Plots of the function Π ($\Pi^0=\lambda_1\lambda_2\lambda_3/|A|$), (i) With $d_{23}=1.193$, $d_{33}=0.07855$, $d_{23}=0.06922$; (ii) With $d_{23}=1.094$, $d_{33}=0.08431$, $d_{23}=0.05729$. $\times10^5$ dynes/cm. (These being values satisfying the B_{3u} factor, using unnormalized valence type symmetry coordinates.)

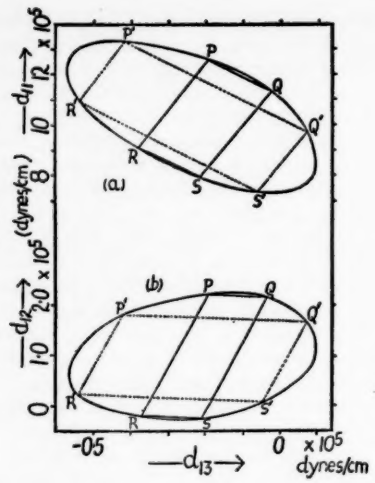

FIG. 2. The allowed solutions for (a) d_{11}, (b) d_{12}, plotted against the allowed solutions for d_{13}. (Δ_1, C=C stretching; Δ_2, C−Cl stretching; Δ_3, Cl−C−Cl deformation.)

An alternative approach may be of interest. For each set of constants d_{22}, d_{33}, d_{23}, (2) may be solved for the allowed values of d_{12} and d_{13} (d_{11} being eliminated with (1) as before). If these values are substituted in the left-hand side of (3), a closed curve is obtained characteristic of the set d_{22}, d_{33}, d_{23}. Two typical ones are shown in Fig. 1; Π^+ is the segment for the greater of the two allowed values of d_{11}, d_{12} for each value of d_{13} (taken here as the variable), and Π^- is the segment for the lesser values. Where this curve intersects the line $\Pi=\Pi^0$ (the value from the right-hand side of (3)), d_{13} satisfies all three equations. Change in d_{22}, d_{33}, d_{23} moves the curve vertically (and somewhat alters its shape). Intersections with $\Pi=\Pi^0$ are only allowed for a certain range of values of these constants. The final plots of d_{11} and d_{12} against d_{13} are shown in Fig. 2; the curves are not ellipses. The solutions for a given set d_{22}, d_{33}, d_{23} lie at the four corners of a parallelogram inscribed in the curve, all such parallelograms having mutually parallel sides, as indicated.

The author wishes to express his gratitude to Courtaulds Ltd. for making the present program of work possible.

[1] P. Torkington, J. Chem. Phys. **17**, 1026 (1949); Nature **162**, 370, 607 (1948).
[2] P. Torkington, J. Chem. Phys. **17**, 357 (1949).
[3] J. Duchesne, Nature (London) **139**, 288, 634 (1937).
[4] H. W. Thompson and J. W. Linnett, J. Chem. Soc., 1393 (1937).
[5] J. Duchesne, *Victor Henri Memorial Volume* (Desoer, Liége, 1948), where other references are given.
[6] C. A. Coulson and H. C. Longuet-Higgins, Proc. Roy. Soc. **A193**, 456 (1948).
[7] P. Torkington, Proc. Phys. Soc. (in press).
[8] H. W. Thompson and J. W. Linnett, J. Chem. Soc. (London), 1376 (1937).
[9] J. E. Kilpatrick and K. S. Pitzer, J. Research Nat. Bur. Stand. **38**, 191 (1947).
* It appears, from a more recent analysis of the author's (see reference 10) that the negative value obtained is to be ascribed to the use of 126° for the angle HCH. Using 120°, a small positive constant appears most probable. It still seems more consistent to take the negative range of d_{11} in C_2Cl_4 as being the more probable.
[10] P. Torkington, Proc. Phys. Soc. (in press).
[11] C. Manneback and A. Verleysen, Annales Soc. Sc. Bruxelles **56**, 349 (1936); Y. L. Tchang, *ibid.* **58**, 87 (1938).